Long Term Effects of Cyclic Loading on Suction Caisson Foundations

Master of Science Thesis

by
Cristina Lupea

August 2013

Support from:

Volker InfraDesign

SPT Offshore

Long Term Effects of Cyclic Loading on Suction Caisson Foundations

For obtaining the degree of Master of Science in Civil Engineering
at Technical University of Delft.
This thesis is **confidential until September 2015**.

by
Cristina Lupea

4187563

August 2013

Technical University of Delft
Faculty of Civil Engineering and Geosciences
Department of Geotechnical Engineering

Personal Information:

Author	:	**Cristina Lupea**
Electronic Mail	:	C.Lupea@student.TUDelft.nl lupea.cristina@gmail.com

Graduation Committee:

Technical University of Delft, Geotechnical Engineering:

prof. ir. A.F. van Tol	:	Chairman
dr. ir. R.B.J. Brinkgreve	:	Modelling specialist
ir. W.J. Karreman	:	Daily supervisor

Technical University of Delft, Structural Engineering:

ir. W.G. Versteijlen	:	Dynamic loading supervisor

Deltares:

ir. D. Luger	:	Geotechnical specialist

Volker InfraDesign:

ing. R. Thijssen	:	Daily supervisor

General Information:

Postal address	:	Technical University of Delft Geo-Engineering Section P.O. Box 5048 2600 GA, Delft The Netherlands
Telephone	:	(+31) 010-2182270 (+31) 015-2781880 (secretary)

ACKNOWLEDGEMENTS

This dissertation represents the final work carried out for the completion of my Master of Science studies at the faculty of Civil Engineering and Geosciences, Delft Univerisity of Technology.

The fulfillment of this work was possible due to the support, patience and guidance of several people to whom I owe my acknowledgement. First of all, my deepest gratitude is to prof. A.F. van Tol who agreed to undertake the supervision of my thesis, regardless of his numerous engagements and full agenda. His knowledge, support but also inquiry into my decissions inspired and motivated me to achieve higher standards.

Advice given by Dirk Luger and Pim Versteijlen were instrumental to the understanding of several aspects related to offshore engineering. I am particularly grateful for the time they have granted me and all my questions. I would like to also express great appreciation to dr. Ronald Brinkgreve whose guidance, support and patience made it possible to finalise the modelling and validation for this thesis. Moreover, his diligence and promptness, regardless of his crowded agenda, motivated me to strive for clarity and precision not just regarding modelling but also regarding my report.

I am particularly grateful for the assistance and encouragement given by Wouter Karreman and Rene Thijssen that have closely followed my progress and endeavour throughout these 9 months.

I would like to thank the following companies and institutions for their assistance with the collection of my data:

- EWEA (European Wind Energy Association);
- Deltares;
- Dong E&P (UK) Ltd.;
- NGI (Norwegian Geotechnical Institute);
- Oxford University;
- Plaxis;
- SPT Offshore;
- Volker InfraDesign.

My special thanks are extended to the staff of Volker InfraDesign that have so kindly received me within their collective and supported me throughout these nine months.

Last but not least, I would like to thank my family and friends for the patience, kindness, encouragement and support they have given me throughout this period.

August, 2013

Cristina Lupea

ABSTRACT

Significant financial investments are made in the offshore wind energy, in a race to reduce greenhouse gas emissions. The trend is to install larger capacity wind turbines in deeper waters, further from shore. DTI (2001) states that 30% of this investment is represented by the foundation costs. Senders (2008) and Byrne & Houlsby (2003) found suction caisson foundations within a multi-footing configuration to be a viable and more economically attractive solution. But, the available norms and standards provide insufficient guidance. It is the aim of this dissertation to provide an additional method to investigate the long term performance of these foundations for their usage as footings for large (6 MW) offshore wind turbines, embedded in sandy soil conditions.

Literature revealed significant research being undertaken to better understand the cyclic performance of different foundation types. Three main model types have been found: empirical (does not assess each individual cycle), constitutive (assess each individual cycle) and hybrid (a combination of the first two). The hypoplastic sand model with intergranular strain concept is employed, based on its ability to accurately assess the two main effects of cyclic loading on sand: pore pressure and strain accumulation, provided that a correct calibration is done.

This research looks at the usage of a centric three-leg jacket for an offshore wind turbine, located in the North Sea, with a soil profile characterised by medium dense sand. It is shown that suction caissons present a large advantage in lateral resistance. Due to their increased diameter, the problem is reduced to the assessment of vertical cyclic resistance, confirming the theory that multi-footings take the loads through a "push-pull" system. The loading conditions, defined by vertical mean load and cyclic amplitude, found within a certain range of the caisson capacity, produce no significant strain or pore pressure accumulation. The behaviour within the elliptically shaped boundary is dominantly hypoelastic. Outside of the boundary, hypoplastic strains and pore pressure build-up occur, with consequent strength and stiffness degradation.

Due to insufficient data for the calibration of the medium dense sand soil volume, an overestimation of the pore pressure occurs. Thus, no conclusion may be drawn regarding the behaviour outside of the defined boundary. Nonetheless, this boundary is conservatively constructed based on the chosen type of soil, medium dense sand that is more prone to pore pressure build-up than the denser sands found in-situ. The period of application of the load is conservatively chosen to be equal to the wave period, regardless of the observed larger values, closer to the wind period, which would allow for more consolidation time

This research provides a basis for the design of suction caisson foundations for offshore wind turbines. It provides a tool for the identification of loading conditions that are potentially dangerous for the long term performance of these foundations embedded in sand and subjected to vertical cyclic loading.

Contents

List of Figures

List of Tables

List of Symbols

$\dot{\mathrm{T}}$ represents the objective (Jaumann) stress rate in the hypoplastic model;

D represents Euler's stretching tensor in the hypoplastic model;

$\mathcal{L}$ is a fourth order constitutive tensor in the hypoplastic model;

$\mathcal{M}$ is a fourth order tangent stiffness tensor of the material in the hypoplastic model;

N is a second order constitutive tensor in the hypoplastic model;

α parameter controlling the dependency of peak friction angle on relative density in the hypoplastic model;

α is the wind shear exponent;

β parameter controlling the dependency of soil stiffness on relative density;

α_m, α_h association factors to account for stiffening in the radial force-displacement relationships within the flow rule of the hyperplastic model;

β_1, β_2 are shaping factors introduced to "round off" the pointed ends of the yield surface of the hyperplastic model on the V axis;

β_{12} is a function of β_1 and β_2 used in the hyperplastic model;

β_3, β_4 shaping factors for the flow rule function of the hyperplastic model;

β_r, χ control the rate of degradation of the stiffness with strain;

γ total unit weight of soil;

γ' is the effective unit weight of the soil;

γ_m is a material coefficient;

δ friction angle between the soil and the pile wall;

$\delta\varepsilon_{vc}$ plastic volumetric strain (densification) increment;

κ is the rate of increase of the undrained shear strength with depth;

Λ_1 is a wind turbulence scale parameter ;

ν is the ratio between the applied vertical load and the vertical capacity;

ν_u is the undrained Poissons' ratio;

$\nu_{c.ref}$ represents the reference current velocity;

φ is the undrained friction angle in the API = 0;

φ_{ij} represent the mobilised friction angles in the planes $x_i,\ x_j$ for the Matsuoka-Nakai critical stress criterion;

φ_c critical friction angle;

$\varphi'_{initial}$ the initial value of the friction angle, before the cyclic loading;

φ'_p effective peak friction angle;

φ_{rep} angle of repose of granular material;

φ'_{red} the reduced friction angle of the sand;

$\Delta\varepsilon_v$ variation of the volumetric strain;

ϑ model parameter to be determined from the curve N_l (number of cycles to liquefaction) vs. τ_c/σ'_{m0};

ρ_w represents the density of water;

ρ_s represents the density of solid particles;

$\sigma_{i,j}$ represent the principal stresses $(i, j = 1 - -3)$;

σ_k is the standard deviation of the k^{th} velocity component in the Kaimal wind spectrum;

σ' is the normal stress on the shear surface;

σ'_{m0} initial effective mean stress;

σ'_{v0} effective initial vertical stress;

$\Delta\sigma_d$ represents the change in deviatoric stress;

$\Delta\sigma_m$ represents the change in mean total stress;

ω represents the load frequency;

σ'_m change in effective mean stress;

τ_c cyclic shear stress;

a is the soil attraction;

A is a factor accounting for static or cyclic loading conditions for the API $p - y$ curves;

A represents the average vertical load;

A represents the sample cross sectional area of the constant head permeability test;

A_p is the gross end area of the pile;

A_s is the side surface area of the pile;

A' is the effective area of the foundation depending on load eccentricity;

B represents the amplitude of the vertical load, defined as amplitude in Table 3.9;

B' is the minimum effective lateral foundation dimension;

c is the soil cohesion;

c is undrained shear strength of the soil;

C is the compression index of the soil over the load range considered;

C is the scale coefficient in the Weibull distribution function;

C_c represents the secant compression index calculated from limit values of the calibration interval p_{s1} and p_{s2};

C_{c1}, C_{c2} can be estimated from loading steps proceeding and following p_{s1}, p_{s2};

C_1, C_2, C_3 are coefficients determined as function of the angle of internal friction of sand;

d_{ca} is a depth factor (see section 4.4.3.4 from DNV (1992));

$d_{\gamma,q}$ are depth factors (see sections 4.4.2.6–7 from DNV (1992));

D diameter of the foundation;

D is the average pile diameter from surface to depth;

D represents the soil skeleton bulk modulusin Zienkiewicz's model parameters;

D is the depth of embedment;

D represents the dilatancy parameter, to be defined from the stress path of undrained triaxial tests;

D_1 densification model paramter related to the pore pressure build-up during the first cycles;

D_2 densification model parameter that is inversely proportional to the volume strain;

D_r is the sample relative density;

e void ratio of the natural state of the soil;

e_0 initial void ratio;

$e_{max,min}$ maximum, repectively minimum index void ratio;

e_{p1}, e_{p2} are the void ratios corresponding to the stresses p_{s1}, p_{s2};

e_{c0} defines the position of the critical state line in the $\ln p$ vs. e space (critical void ratio);

e_{i0} controls the position of the isotropic compression line;

e_{d0} controls the position of the minimum void ratio line;

E_{res} residual stiffness;

E_s represents the soil Young's modulus in Zienkiewicz's model parameters;

f is the unit skin friction capacity;

f represents the wind frequency, measured in $[Hz]$;

f_s is a scalar factor expressing the influence of the stress level;

f_d is a scalar factor expressing the influence of density;

f_p is a dimensionless constant describing the limiting magnitude of vertical load as a proportion of V_{0m};

F is a correction factor, function of $\dfrac{\kappa \cdot B'}{s_{uo}}$;

F_i represents the resistance generated due to friction on the inside of the caisson walls;

F_o represents the resistance generated due to friction on the outside of the caisson walls;

$F(t)$ represents the vertical loading function, dependent on time (t);

g represents the gravitational acceleration;

G shear modulus;

G_0 initial shear modulus;

G_{90} is the initial shear stiffness after 90° change of strain path direction;

h is the layer thickness;

h is the height in Wortman's equation;

h_0 is the reference height in Wortman's equation;

h_2, h_3, m_2, m_3, q are factors used in the 3D formulation of the yield surface and depend on applied loads and bearing capacity;

H is the depth;

h_s controls the overall slope of the oedometric curve in the hypoplastic model;

Δh represents the constant pressure difference in the constant heat permeability test;

i_{ca} is a load inclination factor (see section 4.4.3.2 from DNV (1992));

$i_{\gamma,q}$ are load inclination factors (see section 4.4.2.4 from DNV (1992)).

I_D relative density;

I_R relative dilatancy index;

ΔI_D variation of relative density;

k represents permeability in Zienkiewicz's model parameters and in the constant head permeability tests;

k is the initial modulus of subgrade reaction, determined as a function of the internal friction angle;

k is the initial plastic stiffness in the hyperplastic model;

k is an index referring to the wind velocity component in the Kaimal spectrum(1—along the main wind direction, 2—to the left as seen along the main wind direction, 3—upwards);

k is the shape coefficient in the Weibull distribution function;

$k_1 \cdots k_5$ are dimensionless factors depending on the foundation geometry and Poisson's ratio;

K compression modulus of the soil skeleton;

K is the coefficient of lateral earth pressure (ratio of horizontal to vertical normal effective stress);

K_c is the correction factor that accounts for load inclination, footing shape, depth of embedment, inclination of base and inclination of the seafloor surface;

K_f represents the bulk modulus of the fluid in Zienkiewicz's model parameters;

K_q, K_γ are the correction factors that account for load inclination, footing shape, depth of embedment, inclination of base and inclination of the seafloor surface. The subscripts q, γ refer to the particular term in the equation;

L represents the drainage length in Zienkiewicz's model parameters;

L represents the height of the soil sample column;

L_k is the integral length scale parameter for the k^{th} velocity component and is a function of a turbulence scale parameter (Λ_1);

m_R is a parameter controlling the initial (very-small-strain) shear modulus upon 180° strain path reversal and the initial loading;

m_T is a parameter controlling the initial strain modulus upon 90° strain path reversal;

n is the soil porosity;

n controls the curvature of the oedometric curve in the hypoplastic model;

$(N_1)_{60-cs}$ is the equivalent clean sand blow count;

$(N_1)_{60}$ represents the equivalent penetration resistance at an effective overburden stress of 100 kPa;

N_γ, N_c, N_q represent bearing capacity factors;

$N_{l,liq}$ number of cycles to liquefaction;

ΔN increment of the number of cycles;

$\Delta(N_1)_{60}$ is a function of the percentage of fines—see Table 1 from Stark & Mesri (1992);

p_o is the effective overburden pressure at the point in question;

$p_{o,tip}$ is the effective overburden pressure at the pile tip;

p_s, e_p are the average limit values of p and e for the same interval in the hypoplastic model;

p_{s1}, p_{s2} are stresses calculated using Jáky's formula;

$p_{us,d}$ is the ultimate resistance, s=shallow, d=deep;

p_u is the ultimate bearing capacity at depth H;

p'_f mean effective stress at failure;

p'_o is the vertical effective stress at the base level (skirt tip level if skirts are used);

δp pore pressure increment;

P is the ultimate lateral resistance;

q is the unit end bearing capacity;

q_o is the initial effective vertical stress;

q_u is the ultimate bearing capacity;

Δq is the added effective vertical stress.

Q is the maximum vertical load at failure;

Q represents the volume of passing water in the constant head permeability test;

Q_d is the maximum total vertical load applied to the base of the footing at failure (excluding weight of the the soil) under undrained conditions, the ultimate axial capacity;;

Q'_d is the maximum total vertical load applied to the base of the footing at failure (excluding weight of the the soil) under drained conditions;

Q_f is skin friction resistance;

Q_p is the total end bearing;

Q_{tip} represents the tip end bearing resistance;

r represents the magnitude of the projection of the separation vector between the two considered points in the coherence function on a plane normal to the considered main wind direction;

R represents the radius of the circular foundation in the hyperplastic model;

R_c represents the installation resistance;

R_max represents the size of the elastic range (in the strain space) in the intergranular strain concept;

R_t represents the uplift resistance;

R_u ratio between the excess pore water pressure and the effective vertical stress;

$s_{\gamma,q}$ are shape factors (see section 4.4.2.5 from DNV (1992));

s_{ca} is a shape factor (see section 4.4.3.3 from DNV (1992));

$s_{u,crit}$ is the undrained critical shear strength (postliquefaction) at constant volume;

$s_{u,liq}$ is the undrained critical strength (postliquefaction) at constant volume;

s_{uo} is undrained shear strength of the soil;

$s_{u,res}$ the shear strength of the liquefied sand;

S is a factor introduced in the formulation of the yield surface of the hyperplastic model to ensure consistency of the sign of the yield function;

S_d represents the inclination of the stress path in a plot $\left(\frac{\Delta\sigma_d}{2}\ vs.\ \sigma_3\right)$;

S_k is the one sided spectrum for the k^{th} velocity component for the Kaimal wind spectrum;

S_{min} threshold shear stress ratio;

t represents the mobilised soil-pile adhesion;

t_{max} represents the maximum soil—pile adhesion or unit shaft friction;

t_{res} represents the residual soil—pile adhesion or unit shaft friction;

T represents the imposed period in Zienkiewicz's model parameters;

$\hat{T}$ represents the natural period of the system;

T_s is the period of the vertical load function;

Δt represents the time interval in the constant head permeability test;

u pore pressure;

u_v is the vertical settlement;

Δu represents the change in pore pressure;

V is the wind speed function of height;

V, H, M, T applied loads (vertical, horizontal, moment, torsion);

V_0 represents the vertical bearing capacity, or the maximum applied vertical load;

V_{0m} is the peak value of V_0;

V_{hub} is the mean velocity at hub height, measured in $[m/s]$;

V_m is the mean wind speed in the Weibull distribution function;

w_p is the vertical plastic penetration in the hyperplastic model;

z represents the pile axial defection;

z is the height of the considered point in the wind empirical exponential function;

z represents the depth of the point at which the current is calculated;

z_{pm} is the value of the plastic vertical penetration at the peak value V_{0m};

z_{ref} is the reference height—generally considered at hub level;

z_{res} represents the axial pile displacement at which the residual soil pile adhesion is reached;

z_w represents the water depth;

Chapter 1

INTRODUCTION

The first chapter of the current research project aims to introduce the reader to the topic of offshore wind energy, introduce the most commonly used foundation solutions for offshore wind turbines, state the aim of the research, presents all assumptions and limitations of this research, as well as an outline of the entire report.

Section 1.1 presents a brief history of the offshore wind energy. Moreover, it presents the trends with respect to increasing capacities and sizes of offshore wind turbines, increasing water depths at which they are installed, as well as in sizes of financial investments.

The second section (Section 1.2) of this chapter focuses on presenting the available foundation solutions and the design factors influencing the choice of these solutions.

The aim of this graduation project is presented in Section 1.3 and its assumptions and limitations are presented in Section 1.4.

Finally, the last section of this chapter, gives an outline of the entire report.

1.1 OFFSHORE WIND ENERGY

1.1.1 INTRODUCTION

Population growth, development of the civilised world, development of industry and technology are creating significant strains on the already tapped resources and on the planet as well. One of the most visible impacts of this is climate change (National Environment Research Council (2013)).

In 1997 the Kyoto Protocol was signed upon realising that global action needs to be taken in order to limit the increase in global average temperatures and consequently climate change. Presently there are 195 parties involved. This protocol legally binds the developed countries to strive for reduction of greenhouse gas (GHG) emissions. It was instated in 2005, and its first commitment period has ended last year (2012).

The protocol emphasized the need for renewable energy on a world-wide scale and has caused significant investment in technological advances within this field: solar, wind, currents and waves. From all the mentioned renewable energy sources, wind energy seems to have the largest potential. Wind power is based on the conversion of the wind energy into electrical energy with the aid of wind turbine generators.

Reasons such as noise and aesthetical pollution caused by wind turbines have made the general public to oppose to their construction onshore. Constructing them offshore would avoid such opposition, but also higher wind power at sea can be tapped in—see Figures 1.3 and 1.4 on page 3.

On a global scale, Europe is the leader in cumulative offshore wind energy capacity—see Figure 1.1 and 80% of the installations in 2012 can be found in the North Sea basin—see Figure 1.2, which is also chosen as location for this graduation topic.

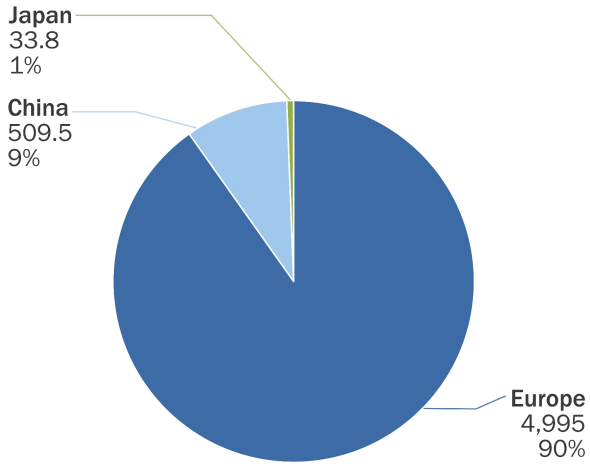

Figure 1.1: Global cumulative offshore wind energy capacity. Source EWEA (2012)

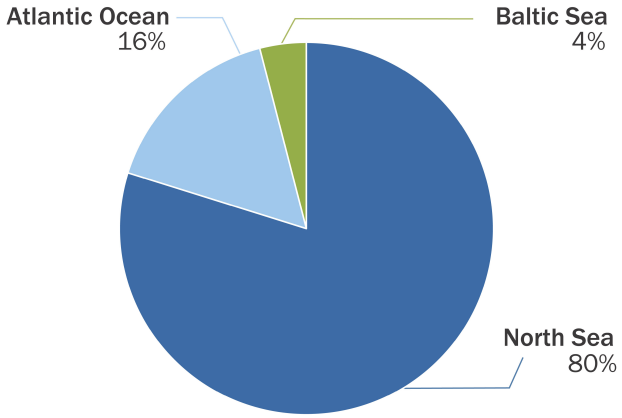

Figure 1.2: Sea basin share of 2012 annual installations. Source EWEA (2012)

1.1.2 TRENDS IN OFFSHORE WIND ENERGY

It becomes clear from the above statistics that the European countries are currently leaders of the offshore market as installed capacity. Additionally in other statistics provided by EWEA (2011) and EWEA (2012) one will notice that European based enterprises are dominating the market of offshore wind turbine generators' production, installation, including vessels, substructures and electrical infrastructure.

Additionally, when following the evolution of the offshore capacity in the past decade—see Figure 1.3, and the positioning of the offshore wind projects—see Figure 1.4, one can clearly observe an increasing trend for both.

In Figure 1.4 there exists a clear trend towards moving further from the shore and into deeper waters. Following the development of the turbine capacities and rotors, one can see in Figure 1.5 that also the sizes of the wind turbines have been increasing in the past years.

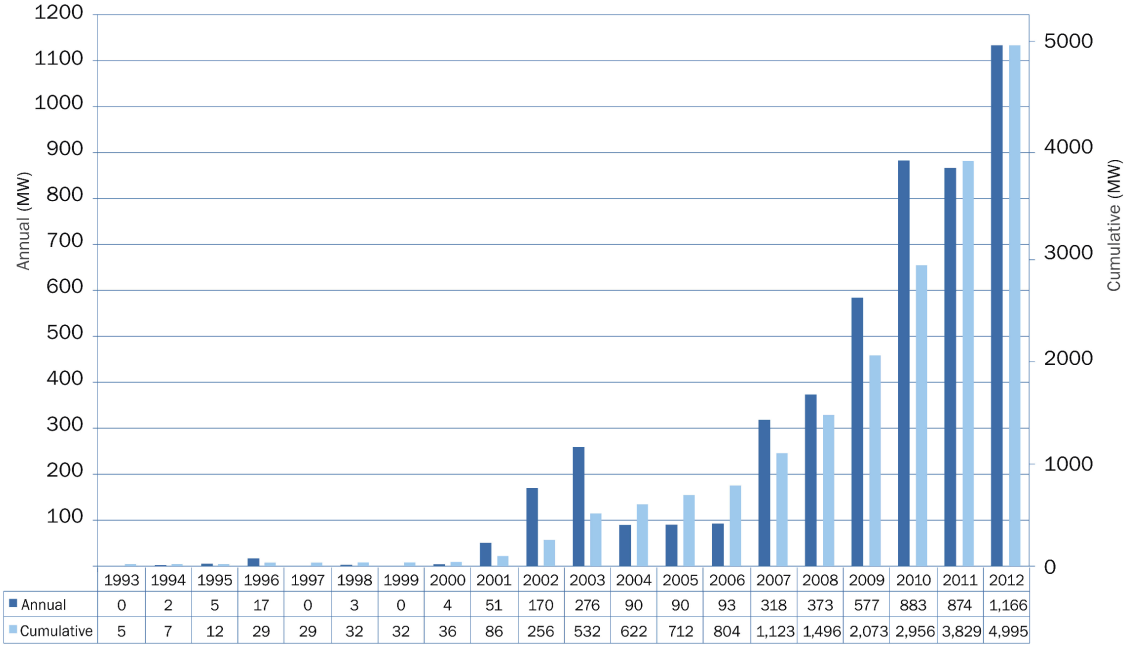

	1993	1994	1995	1996	1997	1998	1999	2000	2001	2002	2003	2004	2005	2006	2007	2008	2009	2010	2011	2012
Annual	0	2	5	17	0	3	0	4	51	170	276	90	90	93	318	373	577	883	874	1,166
Cumulative	5	7	12	29	29	32	32	36	86	256	532	622	712	804	1,123	1,496	2,073	2,956	3,829	4,995

Figure 1.3: Evolution of offshore wind turbine capacity 2000-2012. Source EWEA (2011)

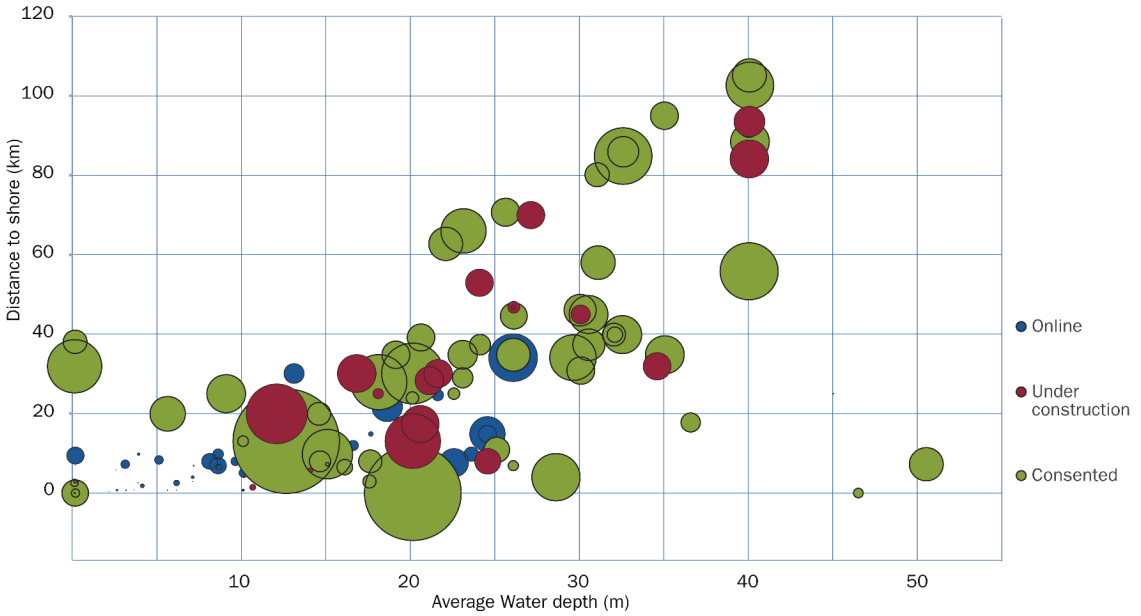

Figure 1.4: Evolution of offshore wind turbine distance from shore and water depth. Source EWEA (2012)

As the size of the offshore wind turbines and installed capacity has been increasing, so has the needed financial investment—see Figure 1.6. These investments are generally based on local government subsidies (Senders (2008)), but an important aspect for their continuity is optimising the costs versus the power output. DTI (2001) states that 30% of this investment is represented by the foundation costs. Therefore, special attention must be given to the chosen foundation type and its installation method.

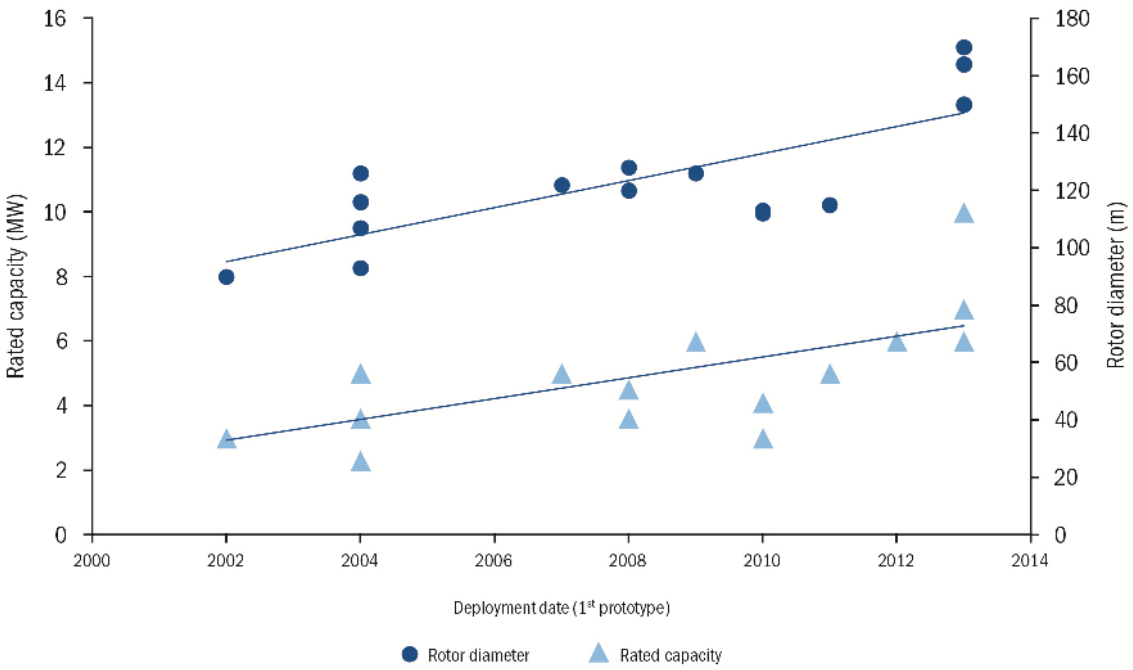

Figure 1.5: Growth trends of rated capacity and rotor diameter for offshore wind turbines. Source EWEA (2012)

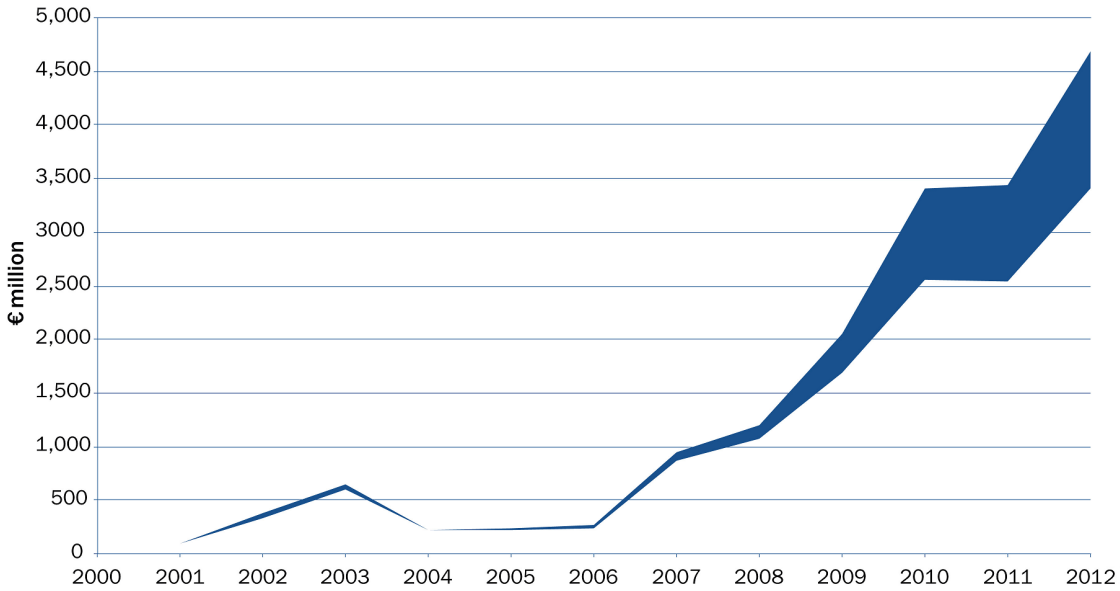

Figure 1.6: Investments in offshore wind power 2000-2012. Source EWEA (2012)

According to Senders (2008) following from the projects Horns Rev. and OWEZ (Offshore Wind Park Egmond aan Zee) significant costs during installation of the wind turbines were caused by the bad weather conditions. These caused stand-by periods during which no operations could be performed offshore. Therefore, decreasing the number of needed offshore operations will bring significant reductions in the installation costs. Two potential solutions are increasing the output of each wind turbine and simplifying the foundation installation.

1.1.3 CONCLUSIONS OFFSHORE WIND ENERGY

To conclude this section, due to a wish to reduce the amount of GHGs, for the past decade a significant interest into renewable energies has appeared. One of the most promising alternatives, benefiting from large financial investments, is the offshore wind energy.

The general tendency is to move further from the shore, into deeper waters and use larger wind turbine generators in order to optimise the output. Meanwhile, a balance between costs and generated power is still to be found. Presently considered solutions for optimising the costs with respect to generated power are related limiting the amount of offshore operations, in order to avoid too much stand-by time. This is considered to be possible through increasing the individual wind turbine capacity, and consequently the size of the turbine itself and of its support structure. A second solution is related to simplifying the foundation installation process.

The following section presents the available types and trends for offshore wind turbine foundations.

1.2 OFFSHORE WIND TURBINE FOUNDATIONS

1.2.1 GENERAL

Foundations have the role of transferring the loads from the superstructure to the supporting soil. They vary in size and depth depending on the magnitude of the loads and the soil's bearing capacity.

Design of offshore wind turbines foundations are governed by two limit state requirements: ultimate (related to collapse) and serviceability (related to long term operability). They must be strong enough to withstand the applied maximum forces and not fail or cause collapse of the structure under ultimate loading conditions.

Additionally, under long term loading conditions, the serviceability of the wind turbine must be ensured, which is generally related to the tilting of the superstructure due to foundation settlements or rotations. This latter requirement has been found to be the dominating one in the design of offshore wind turbine foundations (Safinus *et al.* (2011), Jardine *et al.* (2012)). The most important design factors are briefly discussed in the following section.

1.2.2 DESIGN FACTORS

The design of offshore wind turbine foundations depends on several factors, as found by Feld (2004): "soil condition, water depth, possible erosion, size and type of wind turbine and environmental actions (wave height, current, ice etc.) [...] the selection of the concept is highly influenced by a keen desire to achieve the lowest cost development ...". In the following paragraphs each of these factors will be briefly discussed and it will become clear that they are strongly related to each other.

Soil Conditions & Possible Erosion The soil conditions determine the bearing capacity of the foundation and also its installation method. The most commonly encountered marine soil types are sand and clay. This dissertation will assess the properties of a foundation embedded in sand. A denser sand will determine a higher bearing capacity, but may also be more challenging during installation through driving.

Whenever possible, a common practice in the design phases is the uniformization of soil conditions. This is done in order to be able obtain one foundation type suitable for the entire area, which would save costs by mass production and facilitate the installation process. Nonetheless, the uniformization must be done taking into account the soil variability, as it will inevitably influence the individual behaviour of each foundation from the project.

In sandy soils, erosion may occur around the pile, this process is also known as scour. In such cases scour protection may need to be applied.

Water Depth The water depth will determine the magnitude of the hydrodynamic loading on the wind turbine and consequently on the foundations. A larger water depth will lead to an increase in foundation size. As it can be seen in Figure 1.7, the planned offshore wind turbines are in deeper waters and further from the shore.

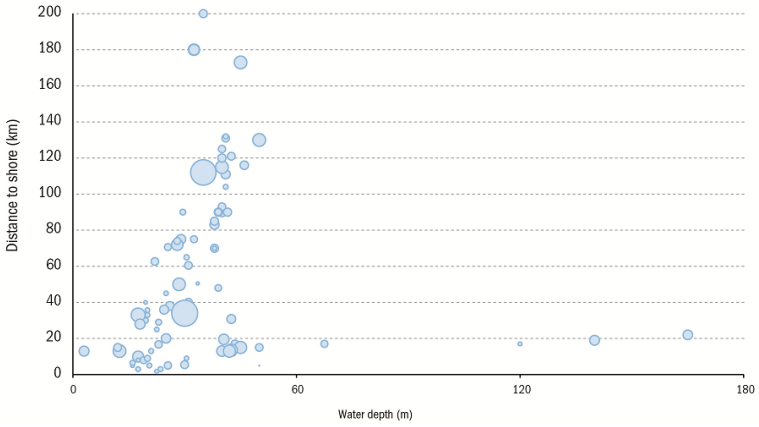

Figure 1.7: Distance and depth of planned offshore wind farms. Source EWEA (2011)

Wind Turbine The size and type of wind turbine will determine the dead load applied to the foundation, but also the aerodynamic load based on the system employed to capture the wind energy. In Figure 1.5, on page 4 one can clearly observe a tendency of increasing the energy output and rotor size of wind turbines for the upcoming years.

Environmental Actions Environmental actions such as wind, wave and current will determine the loads and their dynamic character when transmitted to the foundation. This topic is more thoroughly assessed in Chapter 3 of this report.

Cost Development As already mentioned, within an offshore wind farm project, 30% of the costs are due to the foundation costs. In Figure 1.6, on page 4 it is clearly visible that the size of the financial investments has been increasing considerably and will continue to do so in the following years. Therefore, a reduction of foundation costs would make a considerable difference in the overall project cost. Nonetheless, a choice regarding the size of the investment in the design phase versus the one during operation and maintenance is necessary.

1.2.3 FOUNDATION TYPES

There are several foundation types currently being used for offshore wind turbines. These foundations may be classified in two ways (see Figure 1.8:

- according to the number of footings:
  - mono-footings;
  - multi-footings: braced or jacket structure;
- according to the embedment ratio ($\lambda = L/D$—Embedded Length/Diameter) of the footing:
  - shallow foundations (gravity based foundations) $\lambda < 1$ (API & ISO19901-4 (2000));

  - "intermediate" foundations (caissons) $1 \leq \lambda \leq 10$ — proposed by Fugro to API & ISO19901-4 (2000);
  - deep foundations (piles) $\lambda > 10$ (API & ISO19901-4 (2000)).

GRAVITY BASED FOUNDATIONS

Gravity based foundations are designed on the principle that the dead load provided by the foundation itself is sufficient to prevent failure through uplift, tilting, sliding, but must not exceed the bearing capacity of the underlying soil.

Even though the costs of such a foundation are relatively low (low material costs and can be floated to the location), the following issues might prove problematic:

- soft soil deposits may endanger the stability of the foundation;
- it is vulnerable to erosion and scour;
- seabed preparation is needed prior to installation;
- at large water depths the foundation size increases considerably, making it not economically feasible—only feasible at shallower water depths (2–10 m);

More information related to the design consideration for gravity based foundations can be found in Chapter 2.

CAISSON FOUNDATIONS

This type of foundation uses caissons that are installed by applying suction. Suction caissons are also known as bucket foundations or skirted foundations. They are used in both mono- and multi-footing configurations. At large water depths monopods may prove to be uneconomical due to increasing dimensions to undertake the large overturning moments. But, the multi-footing (braced or jacket structures) were proven to be highly effective in undertaking the large overturning moments through a "push-pull" system as indicated by Byrne & Houlsby (2002), Kelly *et al.* (2006b).

Suction caissons are more often used within the offshore industry, e.g. as anchors, as foundations for offshore oil and gas platforms, or for steel jackets. There are several economical reasons that support this technology, such as material savings, savings in installation equipment, savings in time, as well the possibility of removal of the foundation after decommissioning. Moreover, recent developments in offshore wind turbine installation regulations require more frequent use of significant noise mitigating measures for offshore pile driving. Therefore, suction pile foundations could also be an environmentally adequate foundation alternative for offshore wind turbines.

Upon designing suction caisson foundations for an offshore wind turbine there are several aspects that need to be considered:

- Installation:
  - Gravity penetration;
  - Suction;
- Long term performance under drained or undrained loading conditions (compression, tension and/or combined—vertical, horizontal, moment and torsion—VHMT):

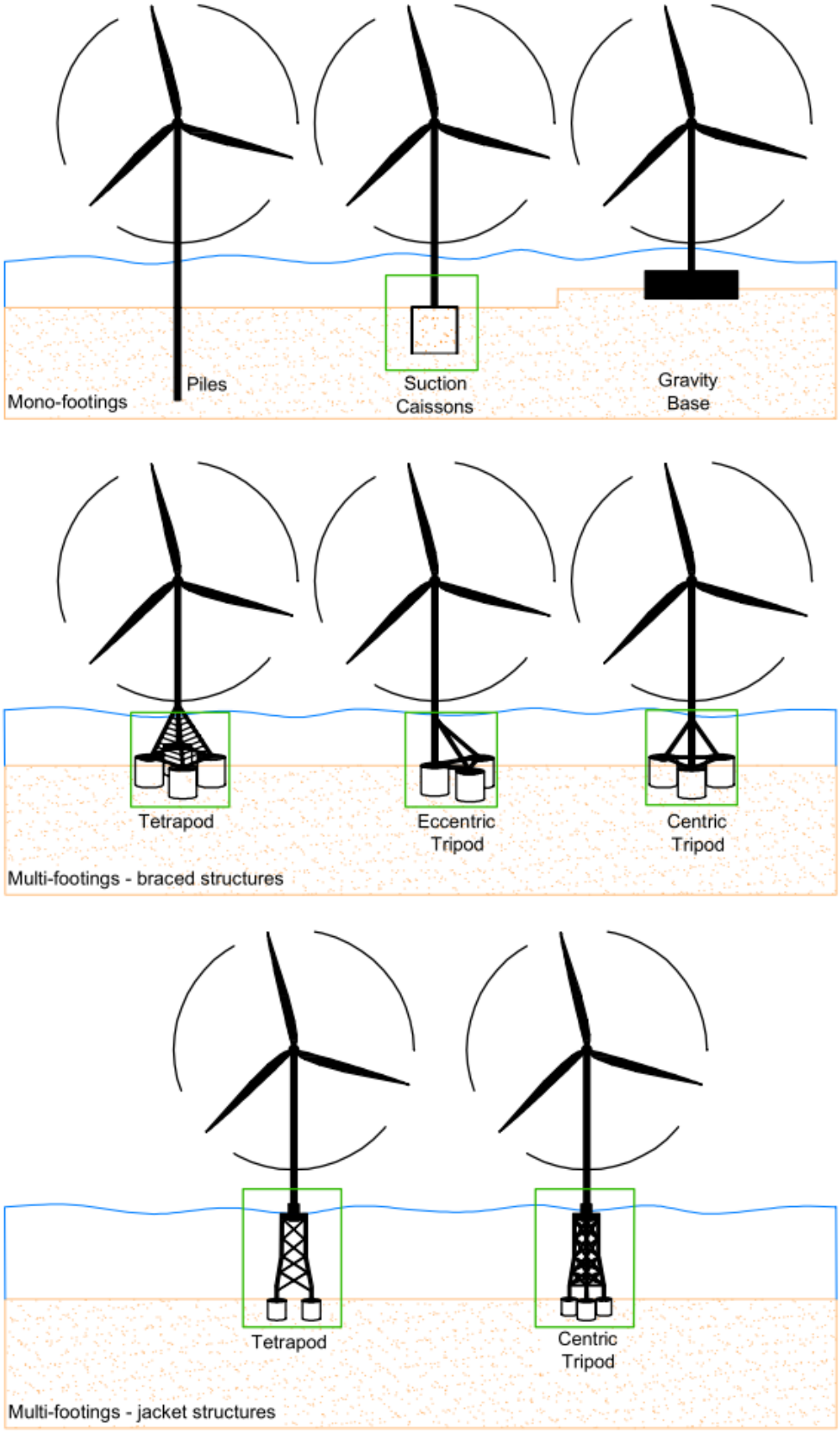

Figure 1.8: Sketch of offshore wind turbine foundation types (marked in green rectangles are the types that the proposed model addresses)

  - Static conditions;
  - Cyclic conditions;

- Removal.

Almost all the previously mentioned issues have more or less satisfactory developed design methods. Nonetheless, for performance of suction pile foundations under long term cyclic loading there is almost no data available that can provide design guidance. An overview of the available literature is given in Chapter 2. The design of the foundation of an offshore wind turbine is governed by stability and operability during the design life time as reported by Safinus *et al.* (2011), Jardine *et al.* (2012). Therefore the need to establish a method to assess its behaviour under these conditions is highly important.

More information about suction caissons can be found in Chapters 2 and 4 of this thesis.

PILE FOUNDATIONS

Similarly to suction caissons, piles can be used both in a monofooting and multifooting configuration. According to statistics provided by EWEA (European Wind Energy Association) in Figure 1.9, the monopile foundation has been dominating the choice of foundation type in the past year.

Monopile foundations consist of large diameter steel piles. The connection between the monopile and the turbine is made through a transition piece. The load transmitted from the superstructure is transferred to the foundation soil by lateral earth pressure. The required lateral resistance governs the needed penetration depth (varies between 20–30 m). The installation method can be done with the aid of a hydraulic hammer (driven), a vibratory hammer (vibrated) or drilled into the seabed. For monopiles, the following issues are generally encountered:

- at large water depths (25 m) the turbine structure together with the monopile may become flexible, thus decreasing the natural frequency of the structure (Liingaard (2006));
- if the soil conditions present large boulders, this foundation type is not suitable;
- in sandy locations scour protection may be needed;
- the size of the installation hammers may prove problematic for piles with diameters larger than 5-6 m for large water depths.

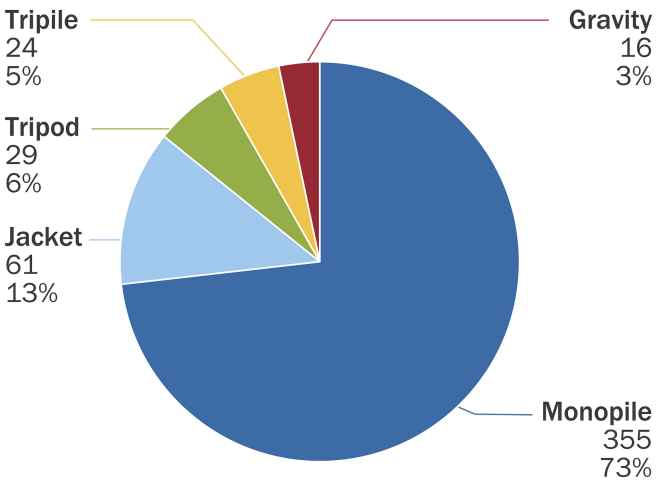

Figure 1.9: Foundation types share of 2012 annual market. Source EWEA (2012)

Multi-pile foundations such as tripods or tetrapods, using as footings piles have been often used in the offshore oil and gas industry. Contrary to monopiles, the design of these piles is governed by axial bearing capacity. The substructure creates a "push-pull" action on the foundation piles. This foundation type may also be used at larger water depths.

More information related to the design consideration for pile foundations can be found in Chapter 2 and Annex A.

1.2.4 CONCLUSIONS OFFSHORE WIND TURBINE FOUNDATIONS

Following from the above sections, it can be concluded that both structurally and financially the choice of foundation for offshore wind turbines has a significant impact.

According to statistics provided by EWEA (European Wind Energy Association) in Figure 1.9, one can notice that the monopile foundation has been dominating the choice of foundation type in the past year, followed by the piles supporting jacket structures and tripods.

Currently the offshore wind turbines (OWTs) are installed on large diameter (i.e. 4 to 6 m) monopiles. Jacket type structures are founded on slender piles and gravity base foundations are not used very often. Presently, the costs of the foundations of an offshore wind farm may raise up to 30% of the total costs (DTI (2001)). With the trend leading towards larger wind turbines, larger distances from shore and deeper waters, the size of the foundations will also increase to sustain these loads. Therefore, other types of foundations should be considered that may provide sufficient strength and stiffness with reduced sizes and less financial investment.

Senders (2008) and Byrne & Houlsby (2003) have found suction caisson foundations within a multi-footing configuration to be a viable and economically attractive solution. The subject of the current research will look at the long term performance of suction caisson foundations under a centric three-leg jacket structure for an offshore wind turbine of 6 MW. The economical aspect of this solution does not represent an interest for this research.

1.3 AIM OF RESEARCH

The current graduation project aims to provide answers regarding long term performance of suction caisson foundations, embedded in medium dense sand, under cyclic loading in the context of:

- *loss of stability due to the reduction of subsoil bearing capacity as a consequence of pore pressure build-up;*
- *loss of serviceability due to the accumulation of differential settlements (strains).*

Firstly, it presents the status-quo of the available guidelines and research on cyclic loading of foundations and show its applicability to suction caissons. Furthermore, it proposes a new method of assessing the long term performance of suction caissons under cyclic loading conditions with the help of the hypoplastic sand model with intergranular strain concept integrated.

This document gives insight into the dominant loading conditions for a three-leg jacket structure with suction caissons, proving that the dominant loading condition is vertical cyclic loading, while horizontal loading proves to be negligible. Furthermore, it proves that the dominant operational loading cases, representing approximately 70% of the life-time of an offshore wind turbine are not causing damage, and the behaviour of the predesigned foundation is within an elastic range. Therefore, the extreme conditions corresponding to storm events are the ones that will endanger the serviceability and structural stability of the wind turbine. Thus,

characteristics such as changes in mean load and cyclic amplitude are investigated.

Moreover, it gives insight into the proposed model: the general procedure, the different discretisation between operational and extreme conditions, the calibration against laboratory data, parameter sensitivity and extrapolation for in-situ conditions.

Finally, it will compare the adequacy of the methods recommended by the API (2011) and the DNV (1992) for assessing suction caisson capacity under vertical cyclic loading and provide an answer regarding long term performance, keeping in mind the taken assumptions and limitations of this thesis.

The appendices of the report will provide results supporting the conclusions drawn throughout the document.

1.4 ASSUMPTIONS AND LIMITATIONS

In this section of the report a gathering of all the assumptions used within the course of this research project and the limitations following from it is presented.

1.4.1 ASSUMPTIONS

The current research is based on the following assumptions regarding the status-quo of the offshore wind industry:

- there exists a clear trend towards increasing sizes of offshore wind turbines and the water depths at which they are installed, and a clear trend in increasing the size of financial investment for offshore wind turbine farm projects;
- 30% of costs are due to the foundation costs, the choice of foundation solution is also highly dominated by economical aspects;
- there are several foundation solutions for offshore wind turbines, and their viability also depends on the water depth at the project location.

The assumptions made to determine the level of relevance for the operational loading cases are based on:

- a higher number of occurrences increases the relevance of the case and/or subcase;
- assuming the same frequency, a higher cyclic amplitude is expected to create more damage than a lower cyclic amplitude;
- as long as the behaviour is in the compressive range, a higher mean compressive load is expected to cause more displacement than a lower one;
- loading in the tensile region is critical—in practice it is avoided through applying ballast and thus increasing the weight so that loading remains in the compressive region.

With respect to the chosen foundation solution: three-leg jacket structure, with suction caissons as footings, the following assumptions are made:

- suction caissons are economically viable options for offshore wind turbines, due to reduced installation costs and possibility of recovering materials;
- suction caissons are more environmentally friendly due to decreased noise levels in the installation process and possibility of removal of the foundation upon decommissioning;
- for the chosen water depth (40 m) monopods were not a viable option (due to increased dimensions);

- the capacity of the predesigned foundation is assumed to ensure sufficient safety in the case of a static application of the extreme loads.

The geotechnical modelling presented in this research project is based on the following assumptions:

- the model calibration is based on the calibration of the soil model against laboratory test data and extrapolation of certain parameters for in-situ conditions;
- the soil volume in which the caisson is embedded is considered to be uniform medium dense sand;
- the top plate of the suction caisson is considered infinitely stiff, as a consequence of the usage of stiffeners in reality and as well to ensure that the loads are transmitted to the caisson shell;
- even though the distance between the designed caissons under the jacket structure is limited, no interaction effects shall be considered as it is outside the scope of the current research;
- it is assumed that under cyclic loading conditions pore pressure build-up and strain accumulation will occur, and consequently changes in strength and stiffness (degradation or densification);
- it is assumed that between the installation of the offshore wind turbine, until its actual operational condition there is one month of consolidation for the soil;
- the applied loading conditions are divided between operational and extreme, being applied in a quasi-static manner with 2 phases of instant load application, each followed by a short consolidation period, equivalent to half of the loading period;
- the period assumed for the applied loading conditions is considered to be equal to the period of the associated wave, therefore smaller than in reality (the period of the vertical load is in between the associated wind and wave period).

1.4.2 LIMITATIONS

The current research and the conclusions following from it, should not be generalised outside of the below limitations:

- the presented solution refers to a three-leg jacket structure with suction caissons as footings;
- the predesigned caisson is overdimensioned with respect to the extreme values of vertical compressive forces, as it was designed also for tension;
- the predesign of the suction caisson does not account for effects of cyclic loading;
- in the predesign for installation and removal of the caisson only rough estimations are provided and no buckling analysis for the skirts of the caisson is done as it is outside the scope of the present research;
- the applied loading conditions, as given by Dong and roughly checked by the author, are limited to the chosen foundation solution;
- the period assumed for the applied loading conditions is considered to be equal to the period of the associated wave, therefore smaller than in reality (the period of the vertical load is in between the associated wind and wave period);
- the resulting cyclic loads are applied in a quasi-static manner and not dynamically;
- the results presented in this thesis refer to medium dense sandy soil conditions;
- the method of analysis is a numerical model, thus careful consideration in the interpretation of these results must be given;

- the soil considered in the geotechnical modelling is uniform, there is no account of variability with respect to depth, nor horizontally—this is highly unrealistic due to the size of the foundations but also of the offshore wind farms that sometimes extend over tens of square kilometers;
- the sand considered is medium dense, as only for this sample sufficient information existed for calibration, within the North Sea dense and very dense sand conditions are more common, thus the analysis represents a more unfavourable case;
- effects of preshearing within the soil mass are not considered;
- in order to calibrate the soil model the minimal laboratory testing that should be carried out includes: one isotropically consolidated undrained triaxial test, one constant head permeability test, three undrained cyclic direct simple shear tests (or three undrained cyclic triaxial tests), out of which at least one test should provide strain results for the small strain range;
- the model is calibrated against laboratory data which is not fully suitable for the in-situ conditions: the tests were performed in a medium strain range. Therefore, one must remain critical with respect to the parameters reflecting small strain stiffness, and the extrapolations required to adjust some of these parameters;
- there is insufficient data for an accurate calibration of the parameters influencing the behaviour in the small strain range ($m_R,\ R_{max}$)—the calibration is made for medium strain range;
- the chosen hypoplastic model has a tendency to overestimate the pore pressure build-up;
- the hypoplastic model does not account for densification effects, this may be observed in the calibration procedure, where the resulting stress state in the model remains equal to the applied stress, while in the laboratory sample a damping of the measured stress can be observed;
- the non-symmetry of the mesh plays a significant role in the generation of non-symmetric "plastic" failure mechanisms, even though the load is symmetrically applied at boundary value problem level;
- there is no model test data available to be used in order to validate the results and the chosen model.

1.5 OUTLINE OF THESIS

This report can be seen as having two main parts: one presenting the status-quo related to the available knowledge of offshore wind turbine foundations and a second presenting the propsed model and its outcomes for the assessment of long term performance of suction caisson foundations embedded in sand under vertical cyclic loading.

This first chapter of the report aims to introduce the reader to the offshore wind energy, foundations for offshore wind turbines (OWTs), the existing trends of increasing the sizes, capacities and water depth for installation of the OWTs and consequently the foundation dimensions and financial investments. Moreover, within this chapter a gathering of all assumptions and limitations of the present research is made.

The second chapter provides an overview of the outcomes of literature research conducted for this thesis. It aims to summarise the methods currently being used in the industry, the available research and its development trend. Differences between the different methods, their limitations but also their advantages are revealed in the context of long term effects of cyclic loading on suction caissons within a multi-footing configuration embedded in sand. The methods presented are the basis of the model proposed through this graduation project.

Chapter 3 presents a more detailed view on the way the loads are considered to act on the foundation considered

in this thesis. The data are provided by Dong E&P(UK) Ltd. and represent the simulation results for a three leg jacket for UK Round 3, with 6 MW wind turbine generators with a design life of 25 years. As the main purpose of the current research is to assess the soil behaviour under cyclic loading, the manner in which the loads are obtained plays a secondary role—these are generally given by the structural engineer. Therefore, only an overview of the theory behind the different actions is given, while the processing of the final vertical loading data into a cyclic load represents the main focus.

Chapter 4 focuses on suction caisson foundations. It aims to present the results of applying some of the existing design principles from Chapter 2 in the predesign of the suction caisson that is further used in the analyses. The in-place capacity, installation and retrieval resistances are assessed for the medium dense sand sample, but also compared to a very dense sand sample.

Chapter 5 aims to give insight into the model used to assess the long term cyclic behaviour of suction caisson foundations, embedded in medium dense sand. It presents the overall structure of the model with the considered assumptions and corresponding limitations. Moreover, it presents the way the problem was discretised, the basis for calibration and sensitivity to a few factors is proposed to be investigated through several scenarios.

The sixth chapter of this report presents the results obtained from the analyses carried out by following the steps described in Chapter 5. Conclusions related to caisson behaviour under operational and extreme conditions are drawn. Moreover, aspects such as sensitivity to changes in mean load, cyclic amplitude and period are discussed. Finally, the author discusses the adequacy of the existing guidelines for the problem at hand.

The seventh chapter and final of this dissertation presents the main conclusions following from the current research and provides further recommendations regarding future potential research to be carried out in the hope to gain more clarity.

The appendices of this thesis aim to provide insight into the most important obtained results. All results of the carried analyses and digital information connected to this thesis are to be found on a hard-drive that is property of Volker InfraDesign.

Chapter 2

LITERATURE REVIEW

This chapter provides an overview of the outcomes of the literature research carried out for the current graduation project. It aims to summarise the methods being used in the industry, the available research and development trend. Differences between the existing methods, their limitations but also their advantages are revealed.

Section 2.1 gives an overview of the general literature available for the design of offshore foundations. It shall focus on the relevance of this information for the problem at hand: long term effects of cyclic loading on suction caissons within a multi-footing configuration embedded in sand.

Section 2.2 presents the relevant literature with respect to the assessment of the loading conditions for offshore wind turbine structures. This will construct the basis for Chapter 3.

Sections 2.4 and 2.5 summarise the behaviour of suction caisson foundations to the corresponding loading conditions and the available methods to assess it. Finally, the last section of this chapter will sum up the relevant conclusions.

The presented methods will construct the basis of the model proposed through the current graduation project. Therefore, the following chapters of the thesis aim to present the chosen alternative approach for dealing with long term effects of cyclic loading on suction caissons. The proposed method shall be presented in the context of its application for an offshore wind farm project.

2.1 AVAILABLE LITERATURE

The available literature with respect to foundations for offshore structures dates back to the 1970s. This is within the time frame of construction of the first oil and gas platforms in the North Sea, but many years after the "first primitive attempts of offshore oil recovery" in the United States of America in the 1880s (Smith (2011)). As the industry moved further from the shore and in deeper waters in the search for resources, the interest in the effects of cyclic loading due to waves also increased. Typical foundations for oil and gas platforms were either slender pipe piles or gravity base foundations, embedded in typical offshore soils: clays and/or sands. This was the logical step considering the significant amount of onshore experience for both foundation types.

In the past two decades, the interest in renewable energy increased in the race to reduce CO_2 emissions. One of the most promising alternatives has been found to be the offshore wind energy. Significant investments have been made and are still planned within this field—see Figure 1.6 on page 4. Thus, also the amount of research regarding offshore loading conditions and foundation response has highly increased within the last decades as it can be seen in the below subsections.

2.1.1 EXISTING NORMS AND STANDARDS

With respect to norms or regulations providing support in the design of offshore structures in marine soils, there are three main guidelines currently being used internationally:

- the Recommended Practices from the American Petroleum Institute API (2011) and API & ISO19901-4 (2000) generally preferred for the design of long pipe piles;
- Det Norske Veritas DNV (1992) and DNV (2004) which are generally preferred for the design of gravity base foundations;
- the Norwegian Standard for offshore industry NORSOK (2002) presents in detail the design of structural elements. But for foundation design it refers to ISO 19900.

Except for DNV (2004), the other guidelines present guidance for the design of foundations for offshore platforms and not offshore wind turbines. Even DNV (2004) bases its foundation design recommendation on the existing guidelines for offshore platforms. The only novelty lies with the recommendation to consider in design the loads transferred from the wind turbine. The difference between the design of foundations for offshore platforms to wind turbines is represented by the magnitude of the loads transmitted by the superstructure to the substructure. The vertical loads imposed by the wind turbine are not as high as in the case of a platform. On the other hand, the horizontal loads and overturning moment associated to wind turbines are much larger (Byrne *et al.* (2002)).

In addition to the difference in magnitudes of loading conditions between offshore platforms and wind turbines, one important aspect that is insufficiently treated in standards, refers to assessment of the effects of cyclic loading on the foundation. The guidance is significant for the steel components of the structural elements and their fatigue analysis. But for foundation design to cyclic loading, in sand, it is limited to a correction factor (API & ISO19901-4 (2000), DNV (2004)) applied to the pile $p-y$ (load-displacement) curves and an effective stress analysis for cohesionless soils with respect to the shear strength and pore pressure build-up due to cyclic wave loading in undrained conditions. Nonetheless, all these guidelines admit to the fact that significant consequences related to stability and serviceability of the structure may occur and that the engineers should take it into account. However, no assessment method is proposed. It is recommended to "seek specialist advice".

In general the above mentioned guidelines provide support in the design of either slender pipe pile foundations or gravity base foundations. Limited support is provided for caisson foundations. More details regarding the methods provided by the API & ISO19901-4 (2000) and DNV (1992) will be presented in Section 2.5.

2.1.2 AVAILABLE RESEARCH

In order to provide a bridge over the gaps from the existing norms and standards, research has been conducted in the past decade to investigate the effects of cyclic loading on offshore foundations. There exist six main groups dominating the research: the Norwegian Geotechnical Institute (NGI), the Imperial College of London (ICL), Oxford University, Aalborg University, Karlsruhe Institute of Technology and University of Western Australia. This research is spread over:

- experimental or numerical assessment of in place or installation behaviour;
- two main soil types: clayey and sandy soils;
- various loading regimes: cyclic axial/vertical, cyclic lateral, cyclic combined lateral and moment, cyclic combined lateral and moment with monotonic vertical load or simply static components;
- various foundation types: gravity base (shallow) foundations, pile (deep) foundations or caisson (intermediate) foundations as mono-footings or multiple-footings;
- a few installation methods: driving or suction.

The conducted research has proven that the dominant loading conditions for the design of offshore wind turbine foundations is related to structural stability and serviceability over the design life of 20–25 years rather than ultimate limit states (Safinus *et al.* (2011), LeBlanc *et al.* (2010), Byrne & Houlsby (2000)). Therefore, the need of investigation of long term behaviour is justified.

Experiments and numerical modelling of the behaviour of foundations in clayey soils are dominated by the research groups at NGI and ICL. The focus is mostly on the determination of the accumulated displacements and decrease in stiffness, as it can be observed in publications by Briaud & Felio (1986a), Pestana *et al.* (2000), Karlsrud *et al.* (2005), Jardine *et al.* (2012). Bond & Jardine (1990) discovered that measurement of pore pressures and local stresses for clays is meaningful only if very stiff cells close to the pile surface are used, but does not dominate the behaviour of cohesive soils.

Generally the results of the investigations conducted so far on clayey soils indicate that cyclic loading may induce a degradation or an increase in shaft and bearing resistance and soil modulus depending on soil properties such as plasticity, overconsolidation ratio (or yield stress ratio) or loading rate. The general approach is based on a shear strain contour diagrams constructed from the considerable database developed by NGI (Nowacki *et al.* (1993), Karlsrud *et al.* (2005)). As clayey soils are not the main focus of the current research, more attention will be given to the chosen sandy soils.

Similar to clayey soils, both experimental and numerical assessment of the foundation embedded in sandy soils was pursued. Within this field the dominating groups are the ones of the Oxford University and University of Western Australia. For sandy soils the research focused on the following aspects: strain accumulation, pore pressure build-up and drainage behaviour.

The investigations cover the different foundation types mentioned above and a wide variety of loading regimes. The research programme at Oxford University is a consequence of the existing interest in the UK to identify a more economical foundation solution. Therefore, the Department of Trade and Industry (DTI (2001)) provided funding for the investigation of applicability in-service and installation of suction caissons for offshore wind turbine foundations. The outcome of this research was that suction caissons (as monopods or tripods/tetrapods) are a viable and economic foundation solution.

From the reviewed literature the behaviour of the foundation is dominated by the considered drainage behaviour: undrained behaviour is generally considered as being the safest, but also the most conservative approach for design. Cassidy & Houlsby (1999) found that drained behaviour may be considered if the applied loads have a sufficiently slow rate and amplitude. While in reality the behaviour is partially drained, as proven by Kelly *et al.* (2006a), Thijssen *et al.* (2011). Assessment of the drainage behaviour is proposed by Zienkiewicz *et al.* (1980) as a function of the soil permeability, drainage length, soil modulus and porosity. More details about this can be found in Chapter 4.

Following the chosen drainage behaviour, the pore pressure build-up might dominate the behaviour of the foundation under the cyclic loading in terms of strength and stiffness reduction as well as strain accumulation. For pore pressure assessment there are two main approaches: pore pressure models (Song (1990)) and strain accumulation models. For the latter there are two main directions: elasto-plastic modelling (Houlsby (2003)) and hypoplastic modelling (P.A. von Wolffersdorff (1996)). More details regarding these approaches will be given in Section 2.5.

Researchers at Oxford conducted laboratory testing of combined (vertical, horizontal, moment—VHM) loading. Their results did not provide evidence of increased stiffness or strength degradation as long as the loading occurred within the compression range—the degradation remained within a stable region. Although, once tensile loading is applied, significant deformation is needed (approximately 10% of caisson diameter, with an embedment ratio of approximately 0.65) in order to fully mobilise the tensile capacity (Houlsby *et al.* (2006), Kelly *et al.* (2006c)). This phenomenon may be occurring due to reverse end bearing and/or partial drainage. Additionally, the secant stiffness significantly decreased as the hysteresis loops increased. Therefore, the authors reinforce the recommendation of completely avoiding tensile loading with the use of mitigating measures (e.g. ballasting).

The same group of researchers have found that the permanent displacement increases with increasing loading amplitude, in the case of vertical transient loading (Byrne & Houlsby (2002), Kelly *et al.* (2006c)) and as well for combined cyclic HM under constant V loads (Byrne & Houlsby (2000)).

One more aspect related to caisson foundations refers to installation effects, research shows a tendency of the sand within to loosen (Jostad *et al.* (1997), Kelly *et al.* (2006b)). Therefore, in cases when loosening and heave of the sand within the caisson occurs it is recommendable to consider already in the design phases the occurrence of a gap between the top plate and the mud line. The top plate bearing gives a significant contribution to overall capacity and minimises displacements, grouting of this gap is needed when the applied load exceeds the capacity provided by the shaft friction and tip end bearing.

From the above paragraphs it becomes obvious that the behaviour of offshore foundations embedded in sand is highly complex. Furthermore, most of the attempted testing procedures and numerical modelling is limited to just a few hundreds or thousands of cycles, which are not representative for the full design life of an offshore wind turbine of 20–25 years.

The researchers from Karlsruhe University seem to be the leading group with respect to numerical modelling of larger number of cycles (100 000). Such attempts were made by Wichtmann *et al.* (2011) and Safinus *et al.* (2011) with the aid of the "High cycle accumulation (HCA) model" proposed by Niemunis (2003). The authors used the HCA within an implicit calculation procedure to ensure accuracy through initial and control steps. Additionally they used empirical formulas to create a bridge over the large number of cycles through an explicit calculation procedure. This type of approach seems to be the only one capable to assess the required number of cycles in order to investigate the serviceability and structural stability over the wind turbine's design life. Thus, extrapolation procedures are needed, but these may introduce uncertainties with respect to the long term

accuracy.

The following sections present into depth the available methods in literature to assess the loads on offshore wind turbines, as well as how to assess the response of the foundation to the corresponding loading conditions.

2.2 LOADS ON OFFSHORE WIND TURBINES

An essential aspect in the design of the foundation of an offshore wind turbine foundation is understanding the loads acting on the superstructure and substructure and the manner through which these loads are carried by the foundation elements. Considering this aspect, it becomes obvious that a good cooperation between the structural and geotechnical engineers is very important for an optimal design (Senders (2005)).

As design is dominated by serviceability requirements and not ultimate capacity, the loads used should be unfactored (Byrne & Houlsby (2000)) in order to provide a more accurate view of the response stiffness. Unfortunately, the available literature does not always clearly state whether the loads considered use partial safety factors or not. For consistency and accuracy of results, within the current document, loads used for operational conditions are unfactored.

According to DNV (2004) and NORSOK (2002) the following classification of loads may be considered:

- permanent actions—include weight of the full structure (superstructure and substructure—i.e. braced, jacket type or transition piece) and weight of the permanent equipment on it;
- variable actions—include e.g. personnel, transient loads, crane operational loads;
- environmental actions—include aerodynamic loads, hydrodynamic loads, earthquake loads, braking loads, ice loads;
- accidental actions—due to fires or explosions, impact loads;
- deformation actions—due to changes in temperature or settlement of foundations.

The load cases will be constructed in such a manner that the relevant design situations and corresponding actions are considered. According to DNV (2004) the governing design action for wind turbines is caused by different wind conditions—see Table 4-1 from DNV (2004).

The loads that will be considered within the current graduation project will focus on normal operation conditions for the wind turbine. More explicitly:

- self weight of the super- and sub- structure, as permanent vertical and axial loads;
- aerodynamic loads due to wind action and aerodynamic loads on the turbine blades, as environmental horizontal loads;
- hydrodynamic loads due to waves and current, as environmental horizontal loads.

Therefore, braking or ice loads, earthquakes or accidental loads shall not be considered.

The loads used within this thesis will be provided by Dong E&P(UK) Ltd. for a three leg jacket for UK Round 3, with 6 MW (or more) wind turbine generators. The data is considered to represent typical loading data, for a lifetime of 25 years. More details with respect to the considered loading conditions will be given in Chapter 3.

Within the industry commercial software such as Bladed and Flex5 are used to assess wind turbine performance and loading. The University of Western Australia has also developed their own software SOS3D-WIND (Senders (2008)) to calculate the loads on the wind turbine. Additionally a force resultant model ISIS, based on Model C by Cassidy & Houlsby (1999) was integrated to be able to asses the foundation response.

2.2.1 SELF WEIGHT

Generally the reviewed literature presents the self weight of an offshore wind turbine to include the weight of the following elements: blades, nacelle, superstructure (i.e. turbine tower) and substructure (i.e. braced, jacket type structure or transition piece).

The weight is generally calculated by considering the volume of the used steel, its relative mass density with respect to air and water and the gravitational acceleration. It is considered to act in a vertical downward direction and is constant in time (Senders (2008)).

2.2.2 AERODYNAMIC LOADS

The reason for which it is not called simply wind loading is related to the fact that there are two different components to be considered:

- the load on the wind turbine rotor;
- the loads on the support structure.

The loads on the support structure are directly caused by wind action. Yet, the load on the turbine rotor depends on the angle of the blades. In order to produce optimal output, but also to ensure structural stability, a pitch-control system is used to change the angle of the turbine's blades. In simpler terms, the blades are turned in order to catch more or less wind for optimal power output.

The determining factor for both loads is the wind speed variation as a function of height and time. The methods to analyse wind speed are well documented in the mentioned codes and norms, as DNV (2004), NORSOK (2002), API (2011).

In the following paragraphs an outline of the methods used is presented, without too many details at this moment. More information can be found in Chapter 3, dedicated to loads.

The variation of wind speed with height, also known as wind shear, is assessed by using a logarithmic function of the wind profile, by Wortman (1983), depending on the average or reference wind speed, surface roughness length and reference height.

The variation of wind speed within its typical climate period is generally assessed with the aid of power spectral density functions as described by Kármán & Lin (1951) or Kaimal (1972). Both methods consider the frequency of the wind and average wind speed at the reference height (hub level).

According to Petersen *et al.* (1998) the Von Kármán spectrum gives a good description for wind turbulence, but the Kaimal spectrum fits better the empirical observations and is currently recommended within IEC61400-3 (2005) as one of the standard practices.

The determination of transient wind speed, shear and direction IEC61400-3 (2005) is currently being used in the industry as standard for safe design. The wind speed may be transformed into the two equivalent time-dependent horizontal loads on the rotor and support structure.

The reviewed literature showed that the maximum force on the rotor will not occur at maximum wind speed, but actually at optimum power output (Senders (2005)). Additionally, Senders (2008) considered in his analysis only one operational loading condition with constant pitch angle as the wind gust passes. This simplification in analysis was considered reasonable as the time period for a wind gust is 14 s according to IEC61400-3 (2005) and the likeliness of the automatic pitch angle adjustment is low for this time frame.

2.2.3 HYDRODYNAMIC LOADS

Hydrodynamic loads are caused by the water particle velocities and accelerations from waves and current. The resulting velocities and accelerations will vary in space and time.

The methods to analyse wave and current velocities are documented in the mentioned codes and norms DNV (2004), NORSOK (2002), API (2011). In the following paragraphs an outline of the methods used is presented, without going too much into detail at this moment. More information can be found in Chapter 3.

Current speed may be assessed with the aid of a power law profile as described by Soulsby (1997).

For the assessment of the energy and wave height at a certain location, there are two recommended standard formulations: the Pierson-Moskowitz wave spectrum and the JONSWAP (Joint North Sea Wave Project) wave spectrum. The first one is for fully developed seas assuming steady wind blows for long time periods and large areas. Whereas the latter is a fetch limited version of the Pierson-Moskowitz spectrum assuming a continuous non-linear interaction between waves over a long period of time. Both are described with the aid of the significant wave height (H_s) and the mean zero-crossing wave period (T_z). Upon determining the fluid field characteristics, based on the realtion between the significant wave height and period with the wave velocities and accelerations, the Morison equation is used to calculate the wave loading on the substructure.

The current graduation project uses as reference the North Sea for soil conditions and sea states. Thus, the JONSWAP spectrum will be presented into more detail in Chapter 3, describing the loading conditions.

2.2.4 CONCLUSIONS REGARDING LOADS

A sketch of all the above mentioned loads can be seen in Figure 2.1.

Within literature, researchers show that both aerodynamic and hydrodynamic loading have a significant contribution in the assessment of long term effects on the foundation. And that the transmitted load to the foundation should be assessed at least as a cyclic load (dynamic analyses are highly laborious and currently there is insufficient information) in order to correctly assess long term behaviour.

The method through which the loading conditions are considered within this graduation project will be presented in Chapter 3.

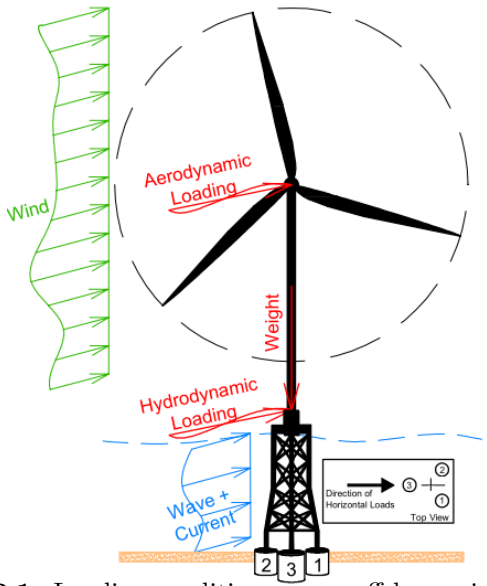

Figure 2.1: Loading conditions on an offshore wind turbine

2.3 SUCTION CAISSON FOUNDATIONS

The different types of foundations for offshore wind turbines have been presented in Chapter 1 of the current report, as well as a description of suction caisson foundations. The current section will focus on the available information to assess its behaviour and adequacy for offshore conditions.

Byrne & Houlsby (2003) have proven that suction caissons are a viable option for offshore wind turbine foundations. Moreover, it is also mentioned that additional research is needed in order to better understand their long-term behaviour. Most of the current available knowledge is related to three main aspects: predicting the installation and uplift resistance of suction caissons, and their static bearing capacity.

The research groups at Oxford, Aalborg, NGI and University of Western Australia are currently conducting investigations to assess the cyclic bearing capacity of these foundations. Also, the purpose of this graduation project is to assess the long term behaviour of suction caisson foundations under vertical cyclic loading in sand. The topic of cyclic bearing capacity is presented in section 2.4.

The following subsections will present the outlines for each of the three previously mentioned design aspects related to suction caissons as they have been discovered in the course of the literature review.

2.3.1 PREDICTION OF INSTALLATION RESISTANCE

Generally the installation resistance is assessed based on the inner and outer friction along the caisson walls and the tip end bearing.

$$R_c = F_i + F_o + Q_{tip} \tag{2.1}$$

where:

R_c represents the installation resistance;

F_i represents the resistance generated due to friction on the inside of the caisson walls;

F_o represents the resistance generated due to friction on the outside of the caisson walls;

Q_{tip} represents the tip end bearing resistance.

The main differences refer to the three factors considered in the assessment of the installation resistance.

The API & ISO19901-4 (2000) do not mention specifically a method to assess penetration resistance for suction caissons in sand, guidance is provided for push-in resistance of pile foundations in cohesionless soils based on the above mentioned principle. Additionally, they mention in one paragraph the need to ensure that full penetration has occurred for skirted foundations, but no more guidance is given

A similar approach, but specifically developed for suction caissons, by the Oxford group (Houlsby & Byrne (2005)) includes a reduction in the internal friction and end bearing and an increase in outer friction. The authors assume that the influence of the suction pressure on the stress conditions on the inside and outside of the skirt is linear with depth, while for the tip they use the difference between the inner and the outer pressures.

The DNV (1992) proposes the usage of two dimensionless reduction coefficients (k_f and k_p) in order to relate the unit friction and unit end bearing to the cone penetration resistance. The values of these factors for North Sea conditions may be found in Table 6.1 from DNV (1992).

The NGI (Jostad *et al.* (1997)) proposes a method similar to the one in the DNV (1992) for the push-in

resistance ("no flow"). In order to account for the influence of suction installation they propose a method to assess the resistance in "no flow" and "flow" conditions based on a critical suction boundary, that depends on the permeability ratio and penetration depth (see Figure 4 from Jostad *et al.* (1997)).

To conclude this section, in order to assess suction penetration of caissons in sand, it is important to assess the influence of the suction pressure on the three components of the penetration resistance: inner and outer friction and tip end bearing of the penetrating skirt. Additionally, a thorough overview of all the available methods for prediction of installation resistance can be found in Senders (2008).

2.3.2 PREDICTION OF UPLIFT RESISTANCE

The prediction of uplift resistance (R_t) is based on the friction resistance on the inner and outer walls of the caisson.

$$R_t = F_i + F_o \tag{2.2}$$

The differenceS between the methods for the uplift resistance are based on the assessment of its two frictional components.

The API & ISO19901-4 (2000) do not mention specifically a method to assess uplift resistance for suction caissons in sand, but guidance is provided for pile foundations in cohesionless soils based on the above mentioned principle.

The Oxford group (Houlsby *et al.* (2005b)) propose a similar method to assess extraction capacity by considering the effects of the excess pressure under the caisson lid. The authors identify four possible scenarios that may occur based on the extraction speed, potential cavitation and liquefaction—details are to be found in the referenced article.

Another approach is proposed in CUR (2001) for tensile capacity of piles driven in sand. A frictional capacity is considered under fully drained conditions or slow extraction by connecting the inner and outer friction to the cone resistance.

To conclude this section, the uplift or extraction capacity for suction installed caissons is based on the friction on the inner and outer skirts and the applied pressure. A thorough overview of all the available methods for prediction of uplift resistance can be found in Senders (2008).

2.3.3 PREDICTION OF STATIC BEARING CAPACITY

The prediction of static bearing capacity of suction caissons is generally based on the design principles of piles. Following formulas for vertical bearing capacity for piles from API & ISO19901-4 (2000), the vertical static bearing capacity of suction caissons can be assessed by considering the shaft friction and plug end bearing capacity.

Similarly from pile design, the lateral bearing capacity may be assessed by considering the ultimate lateral pressure resistance and soil shear resistance at the base of the pile.

More details regarding the static bearing capacity assessment are given in Appendix A.

2.3.4 CONCLUSIONS REGARDING SUCTION CAISSON FOUNDATIONS

Firstly, Byrne & Houlsby (2003) have proven that suction caissons are a viable option for offshore wind turbine foundations. Yet, as it was observed from the previous sections, the current norms (API & ISO19901-4 (2000), DNV (1992)) provide no information regarding the design of suction installed caisson foundations. The currently researched design guidelines (Houlsby & Byrne (2005), Jostad *et al.* (1997), Houlsby *et al.* (2005b)) for suction installed caissons are based on the experience from pile design and take into account the influence of the applied suction pressure on the frictional and end bearing capacities.

2.4 FOUNDATION RESPONSE TO LOADING CONDITIONS

The previous section presented the loads applied to a wind turbine and which will consequently be transferred to the foundation.

Experiments and research have shown that in the case of mono-footings the dominating loads are a combination of horizontal, vertical and moment, with dominant effects from cyclic horizontal and moment loading. For multi-footings, the substructure transmits to the foundations the bending moment and horizontal loads through a "push-pull" system. Therefore, the behaviour will be dominated by cyclic axial loading with critical behaviour due to tensile components (Byrne & Houlsby (2003), Byrne & Houlsby (2004) and Kelly *et al.* (2006a)). As the current research investigates multi-footings, vertical or axial cyclic loading will constitute the main focus. Moreover, it is considered by the same researchers that fulfilling the axial design requirements, then the lateral capacity is also ensured.

The following subsections will look more closely at the fundamentals of behaviour of the foundation and foundation soil under various loading regimes. The way through which these are modelled can be found in section 2.5.

2.4.1 ELASTIC BEHAVIOUR

Upon loading under the yielding limit (as defined within the hyperplasticity theory) the behaviour of the soil may be characterised as being elastic. Elastic behaviour implies that the deformations occurring within these boundaries are recoverable and that the soil is considered to return to its previous state.

For a 6 degree of freedom problem the following relationship by Doherty *et al.* (2005) is defined between the loads and the corresponding displacements:

$$\begin{bmatrix} V/(4GR^2) \\ H_2/(4GR^2) \\ H_3/(4GR^2) \\ T/(8GR^3) \\ M_2/(8GR^3) \\ M_3/(8GR^3) \end{bmatrix} = \begin{bmatrix} k_1 & 0 & 0 & 0 & 0 & 0 \\ 0 & k_3 & 0 & 0 & 0 & -k_4 \\ 0 & 0 & k_3 & 0 & k_4 & 0 \\ 0 & 0 & 0 & k_5 & 0 & 0 \\ 0 & 0 & k_4 & 0 & k_2 & 0 \\ 0 & -k_4 & 0 & 0 & 0 & k_2 \end{bmatrix} \begin{bmatrix} w/(2R) \\ u_2/(2R) \\ u_3/(2R) \\ \omega \\ \theta_2 \\ \theta_3 \end{bmatrix} \tag{2.3}$$

where:

$k_1 \dots k_5$ are dimensionless factors depending on the foundation geometry and Poisson's ratio;

G shear modulus;

V, H, M, T applied loads (vertical, horizontal, moment, torsion);

R represents the radius of the circular foundation in the hyperplastic model;

Within their research Doherty *et al.* (2005) and Doherty & Deeks (2006) present a thorough assessment of the elastic behaviour of a caisson. For this they used a technique called "scaled boundary finite-element method" in order to evaluate the load-displacement response of a skirted foundation embedded in a non-homogeneous elastic half-space subjected to HVMT (horizontal, vertical, moment and torsion) loads. The authors use the factor k_4 to couple the pure horizontal load and the pure moment for the determination of the horizontal movement and rotation, which is not considered in the API (2011).

However, it is well known that to fully describe soil behaviour, elasticity is certainly insufficient. It is needed to also account for permanent, long term deformations, which are generally described as plastic behaviour—described in the following section.

2.4.2 PLASTIC BEHAVIOUR

As mentioned earlier, plastic behaviour is characterised by the fact that the occurring deformations are irreversible. Within the hyperplasticity theory, plastic deformations occur once the yield surface is reached. The same theory also uses a flow rule in order to realistically predict these displacements.

The bounding limit regarding accumulation of permanent strain is defined by a failure criterion. Nonetheless, in the case of serviceability design, failure will not refer to the ultimate loss of capacity of the soil, but rather to a limit set by the engineer in order to ensure the safe operational conditions of the structure.

More details regarding the implementation of plastic behaviour will be given in section 2.5.

2.4.3 BEHAVIOUR UNDER CYCLIC LOADS

Behaviour of soils under cyclic loading has been investigated significantly in the past decades. Initial interest on the effects of cyclic loading arose within earthquake engineering when investigating the problem of sand liquefaction.

Liquefaction "is the act or process of transforming any substance into a liquid" by de Groot *et al.* (2006).

In a civil engineering context, applied to soils, liquefaction is defined as the state in which the pore pressure becomes equal to or larger than the initial effective stress. In simpler terms, the pressure exerted by the water particles on the soil particles is large enough to break the contact bonds within the soil structure and the soil transforms into a liquid state.

In reality, it is not needed that the soil reaches a state of liquefaction in order to cause stability problems, the existence of excess pore pressure which leads to the reduction of shear strength may already endanger foundation stability as indicated by Safinus *et al.* (2011). According to the available norms DNV (1992), DNV (2004), API (2011) and API & ISO19901-4 (2000) the impact of cyclic loading on the capacity of the foundation is significant: "The effect of cyclic loading on shear strength should always be considered. Cyclic loading may lead to a build-up of pore pressures leading to a reduction of shear strength" (DNV (1992)) and similar phrases can be found as well in the other norms.

The conducted literature review revealed the following effects of cyclic loading as being the most significant with respect to foundation capacity:

- pore pressure build-up (drainage behaviour during cyclic loading);
- strength or stiffness degradation;
- accumulation of strains, displacements;

- initial shear stress prior to cyclic loading (preshearing).

The above mentioned effects are strongly connected to the characteristics of the applied cyclic loading, i.e. number of cycles, average cyclic shear stress, amplitude of cyclic shear stress, direction of loading. In the following paragraphs more information regarding the above effects and a brief overview of the methods to assess them are presented. More details regarding the steps of the different approaches can be found in Section 2.5.

PORE PRESSURE BUILD-UP

In the case of sandy soils the behaviour under cyclic loading is dominated by the accumulation of pore pressures. An increase in pore pressure as the effective stresses decrease means that the defined failure envelope will be reached faster. Consequences of this are that strength or stiffness are reduced compared to their static values, but also a more pronounced accumulation of strains.

The assessment of the pore pressure build-up is fully connected to the characteristics of the applied cyclic loading and the assessment of the drainage behaviour during cyclic loading.

The accumulation of pore pressures depends on the number of applied cycles—see Figure 2.2. Unless drainage occurs, the pore pressure will tend to accumulate with the number of cycles until liquefaction is reached.

Thus, a correct assessment of the drainage behaviour under the given loading conditions will determine the soil behaviour: undrained, partially drained or drained—see Figure 2.3.

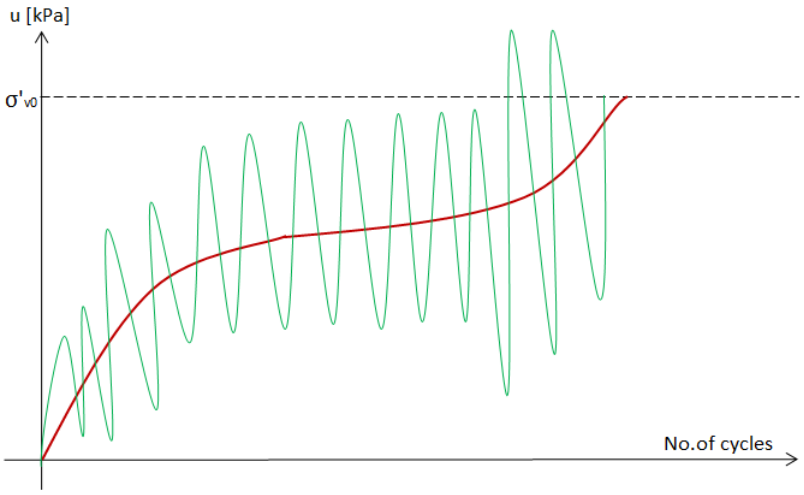

Figure 2.2: Sketch representing the accumulation of residual pore pressure under undrained conditions with increasing number of cycles–red line

On one hand if the loading does not allow for water to seep away (undrained behaviour), the pore pressure will increase as a result of hindering of the contraction tendency. Further the effective stresses will decrease. Finally, when the pore pressure increases sufficiently to carry all the load (pore pressure ratio $R_u = u/\sigma'_{v0} = 1$), the soil liquefies as the pore pressure pushes the soil particles away from each other.

On the other hand, if (partial) drainage is allowed the amount of accumulated pore pressure might reach a stable state, or even slowly dissipate as compaction of the soil occurs. According to experimental work by de Groot *et al.* (2006) and Kelly *et al.* (2006b) partial drainage is present as the measured pore pressures were smaller than expected.

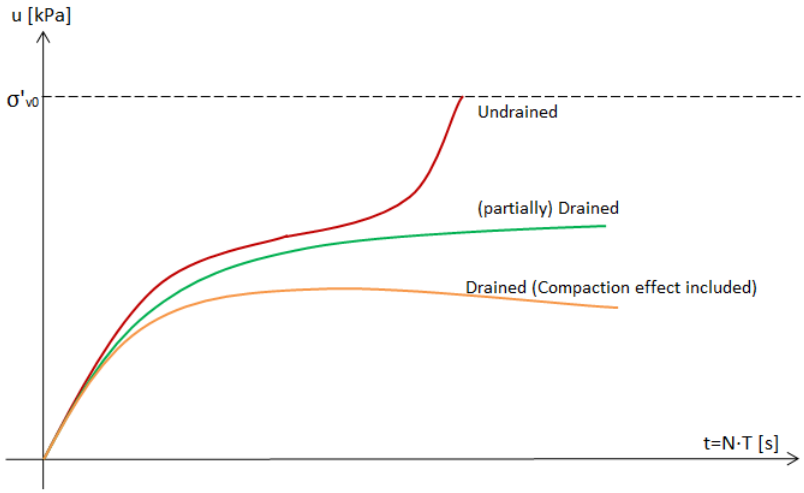

Figure 2.3: Sketch representing the variation of pore pressure build-up depending on the considered effects

In order to assess drainage behaviour the method described by Zienkiewicz *et al.* (1980) may be used:

$$\Pi_1 \begin{cases} < 10^{-2} & undrained \\ \in [10^{-2}; 10^{+2}] & partially\ drained \\ > 10^{+2} & drained \end{cases} \tag{2.4}$$

and

$$\Pi_1 = \frac{2k}{\rho_w/\rho_s \cdot \pi \cdot g} \cdot \frac{T}{\hat{T}^2} \tag{2.5}$$

where the meaning of the parameters can be found in Table 2.1.

Parameter	Description	Unit of measurement
k	permeability	m/s
ρ_w	density of water	kg/m^3
ρ_s	density of solid particles	kg/m^3
g	gravitational acceleration	m/s^2
T	imposed period	s
$\hat{T} = \frac{2L}{\sqrt{\frac{D + K_f/n}{\rho_s}}}$	natural period of the system	m/s^2
L	drainage length	m
$D = \frac{E_s}{3 \cdot (1 - 2 \cdot \nu)}$	soil skeleton bulk modulus	kPa
E_s	the soil Young's modulus	kPa
ν	Poisson's ratio	–
K_f	bulk modulus of the fluid	kPa
n	porosity	–

Table 2.1: Parameters needed to calculate Π_1 Zienkiewicz *et al.* (1980)

Within the API & ISO19901-4 (2000) the pore pressure is considered only for clays undergoing active consolidation (with excess pore pressure) in the determination of the unit shaft friction ($f = \alpha \cdot s_u$, s_u is the undrained shear strength of the soil), when the dimensionless shaft friction factor for clays $\alpha = 1$. But there is no guidance in reference to the value of the dimensionless shaft friction factor (β) for sands that may account for existence of pore pressure.

The DNV (1992) recommends the usage of soil specific pore pressure contour diagrams derived from undrained cyclic tests and a few formulas for low to moderate stress levels and transient undrained loading.

The hyperplastic formulation proposed by Houlsby (2003) does not look specifically at the pore pressure build-up but rather at the changes in stiffness due to the changes in load amplitude. Moreover, the author assumes that except for a few extreme events the loading will stay within the yield surface and thus dominated by elastic behaviour—recoverable displacements. A suggestion is made for the development of the "continuous hyperplastic" model as future work to better estimate these effects.

Within hypoplastic formulation the pore pressure build-up is assessed through its rate type of equation that considers the stress rate as a function of the strain rate, void ratio and current stress state with barotropic (stress level dependent) properties.

Densification models assess pore pressure build-up through the change in plastic volumetric strains and the shear stress ratio.

STRENGTH OR STIFFNESS DEGRADATION

As previously mentioned, pore pressure build-up may cause a reduction of the soil strength and stiffness. Additionally, according to Jardine *et al.* (2012) a two-dimensional cyclic loading will produce halving of the bearing capacity within a smaller number of cycles. In the following paragraphs, cyclic loading will refer to a uni-directional loading.

The API & ISO19901-4 (2000) do not provide an elaborate method for the assessment of the strength or stiffness degradation, but acknowledges their existence: "Repetitive loads can cause a temporary or permanent decrease in resistance and/or accumulation of deformation" and recommends the usage of a cyclic loading factor $A = 0.9$ for the calculation of the lateral soil resistance.

In DNV (1992) for soils subjected to cyclic loading it is recommended the usage of one of the following:

- the reduced static shear strength for the effect of cyclic loads;
- the cyclic shear strength—the sum of static and cyclic stress that causes failure for a given number of cycles.

In geotechnical earthquake engineering, based on the pore pressure build-up, a method of reducing the strength of the soil is often used (equation 2.6, originally from Srbulov (2008)).

$$R_u = 1 - \frac{\tan \varphi'_{red}}{\tan \varphi'_{initial}} \tag{2.6}$$

From which the following relation can be deduced:

$$\varphi'_{red} = \arctan\left((1 - R_u) \cdot \tan \varphi'_{initial}\right) \tag{2.7}$$

where:

R_u ratio between the excess pore water pressure and the effective vertical stress;

φ'_{red} the reduced friction angle of the sand;

$\varphi'_{initial}$ the initial value of the friction angle, before the cyclic loading.

If liquefaction is reached ($R_u = 1$) then the shear strength of the liquefied sand may be reduced to 5—20% of the effective stress—see Equation 2.8, according to Stark & Mesri (1992) and Olson (2001) or Equation 2.9, according to Olson & Stark (2003).

$$s_{u,crit} = 0.0055 \cdot (N_1)_{60-cs} \cdot \sigma'_{v0} \tag{2.8}$$

$$s_{u,liq} = [0.03 + 0.0075 \cdot (N_1)_{60} \pm 0.03] \cdot \sigma'_{v0} \tag{2.9}$$

where:

$s_{u,crit}$ is the undrained critical shear strength (post-liquefaction) at constant volume;

$s_{u,liq}$ is the undrained liquefied shear strength;

$(N_1)_{60-cs}$ is the equivalent clean sand blow-count, with the following formula
$(N_1)_{60-cs} = (N_1)_{60} + \Delta(N_1)_{60} = 44 \cdot D_r + \Delta(N_1)_{60}$;

$(N_1)_{60}$ represents the equivalent penetration resistance at an effective overburden stress of 100 kPa, the samples considered by Stark & Mesri (1992) had $(N_1)_{60} \leq 12$;

$\Delta(N_1)_{60}$ is a function of the percentage of fines—see Table 1 from Stark & Mesri (1992);

D_r is the sample relative density;

σ'_{v0} is the vertical effective stress.

An important factor to be mentioned is that both formulas investigate loose to medium dense sands. In his presentation, Youd (2011) mentions that there is no data above blow-count values of 16, because there is no case record of liquefaction induced failure in granular materials. The potential for liquefaction of dense to very dense sands is therefore very low.

In Figure 2.4 the two proposed formulas are shown as function of the sand relative density, also extended above the prescribed limit ($(N_1)_{60} \leq 12$) by Stark & Mesri (1992) and Olson & Stark (2003).

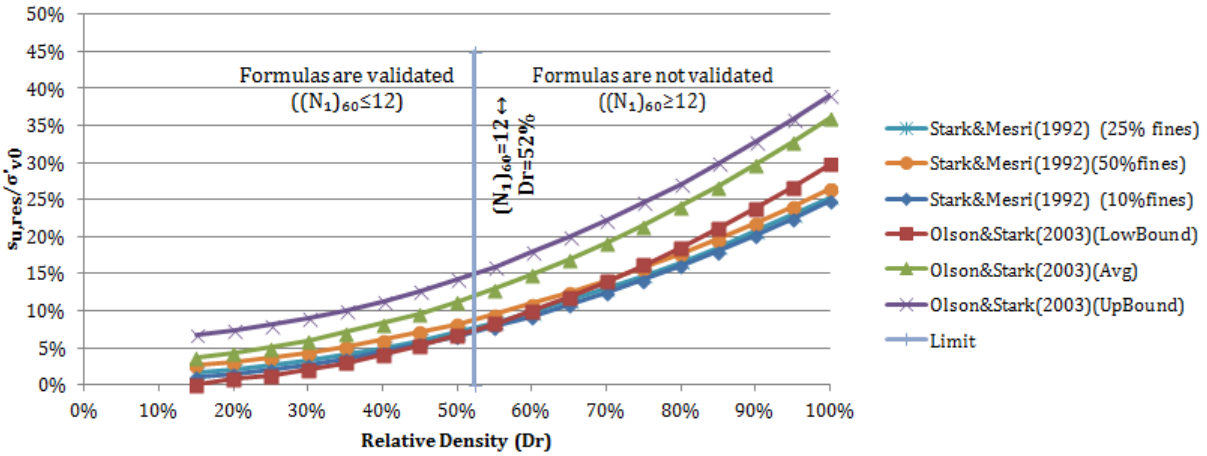

Figure 2.4: Influence of density on post-liquefaction shear strength

In the transition state towards liquefaction, the stiffness of the sand layer will also be significantly reduced. The method through which this is assessed within this model uses the shear modulus G, measured through

cyclic loading tests and it translates it into residual stiffness (E_{res})—see Equation 2.10 (where ν_u—undrained Poisson's ratio ($= 0.5$)).

$$E_{res} = 2 \cdot (1 + \nu_u) \cdot G \tag{2.10}$$

It may lead to reductions in stiffness of over 90%.

Within the hyperplasticity framework, the assessment of the stiffness of the response is based on the chosen yield surface and hardening law Houlsby (2003).

Within hypoplastic formulation the change in stiffness is assessed through its rate type of equation that defines the stress rate as a function of the strain rate, void ratio and current stress state with pyknotropic (density dependent) properties.

In pore pressure build-up models or densification models the hardening effect can be described by a negative exponential function of accumulated plastic volumetric strain (according to densification test data Song (1990)).

An additional factor that needs to be considered in the assessment of the stiffness of the response to cyclic loading is related as well to the Cyclic Shear Stress Ratio ($CSSR = \Delta\tau/\sigma'_{v0}$, $\Delta\tau$—the mobilised shear strength, σ'_{v0}—initial effective vertical stress), the number of cycles to liquefaction and the relative density. In Figure 2.5 it can clearly be seen that as more shear strength is mobilised, the number of cycles needed to reach liquefaction is reduced de Groot *et al.* (2006).

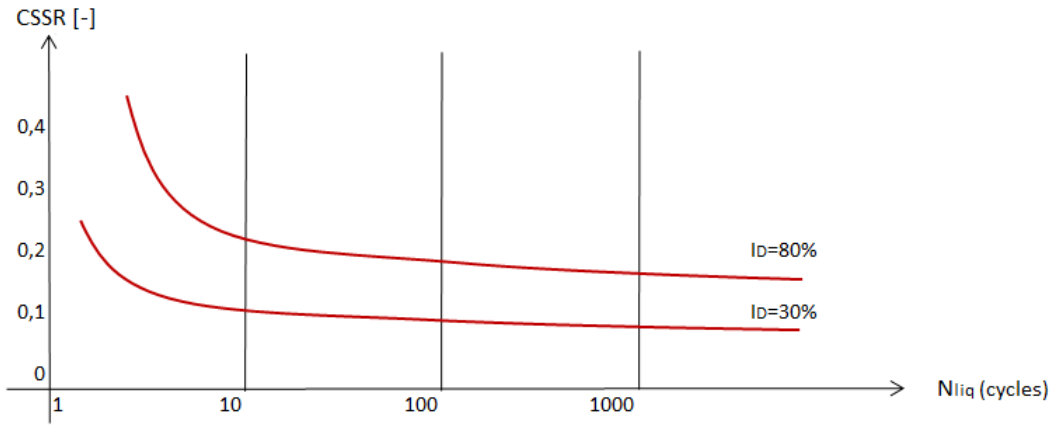

Figure 2.5: Relation between $CSSR$, I_D and N_{liq} (de Groot *et al.* (2006))

ACCUMULATION OF STRAINS, DISPLACEMENTS

Due to cyclic loading, accumulation of strains occurs and it is significantly influenced by the pore pressure build-up and the number of applied cycles. The accumulation may occur due to dissipation of pore pressures, but also due to the amplitude of the cyclic shearing.

It has been observed by Houlsby *et al.* (2005a) that large amplitudes determine larger strain accumulations and that the strain accumulation rate does not seem to have a convergence tendency even at large numbers of cycles (Wichtmann *et al.* (2011)). According to Poblete *et al.* (2011) the rate of strain accumulation ($\Delta\varepsilon_{acc}$) is approximately proportional to the square of the rate of the strain amplitude ($(\varepsilon^{ampl})^2$) for one dimensional strain loops.

According to DNV (1992) the full assessment of "total and differential settlement and displacements during

the design life of the structure shall include:. . . cyclically induced permanent settlements and deformations; . . . ”

They identify two mechanisms causing cyclic settlements: undrained shear deformations and consolidation of pore pressures due to cyclic loading. In order to estimate these settlements they recommend the usage of analytical methods that use soil models with the ability to assess average shear stresses and cyclic shear stress history in all soil elements. But no further guidance is given.

According to API (2011): “Repetitive loads can cause a temporary or permanent decrease in resistance and/or accumulation of deformation” and it is recommended the usage of a cyclic loading factor $A = 0.9$ for the calculation of the lateral soil resistance, but which does not account for any cyclic loading characteristic, nor the number of applied load cycles. Further only static formulas are provided for the assessment.

Within the framework of hyperplasticity, the chosen flow rule will determine the relationship between the plastic multiaxial displacement components (Houlsby (2003)).

The hypoplastic model assesses the total strains through two components:

- an intergranular strain (δ) representing the deformation of interface layers at intergranular contacts. It is linear with respect to the strain rate and occurs in reverse and neutral loading (hypoelastic behaviour);

- a component related to the rearrangement of the soil skeleton. It is non-linear with respect to strain rate and occurs together with the first under continuous loading conditions (hypoplastic behaviour).

In densification models, only the plastic volume strain increment is considered and an increase in the densification will lead to a decrease in the potential for further densification (Song (1990)).

PRESHEARING

Preshearing may determine an increase in cyclic shear strength and may have an important effect on relative density. However, no clear trend was identified through testing up to this point. But it may also determine a decrease in cyclic shear strength, if preshearing causes large shear strains that may break down the structure (Andersen (2009)). Therefore, no positive nor negative consequence is generally considered to occur due to the initial shear stress prior to cyclic loading due to the fact that no clear trend in the behaviour has been observed.

2.4.4 CONCLUSIONS REGARDING THE FOUNDATION RESPONSE

From the above paragraphs it becomes clear that the behaviour under cyclic loading may have significant consequences even if the ultimate state of liquefaction is not reached. Cyclic loading is characterised by the number of cycles, average shear stress, amplitude and direction of loading. Each of these characteristics influence aspects of soil behaviour such as changes in pore pressure, strength, stiffness or strains and displacements.

2.5 MODELLING APPROACHES

In the previous sections the methods available to assess foundations of offshore structures under cyclic or quasi-static conditions were only briefly mentioned. The current section aims to present in more detail these methods and their applicability for the assessment of long term performance of suction caisson foundations under vertical cyclic loading, embedded in sand. In Figure 2.6 an overview of the different types of models is given.

Model Type	Dominant Characteristic	Applied cyclic loading	Behaviour under cyclic loading	Foundation types	Examples
Empirical models	based on test data, reflects "real behaviour", does not assess each individual cycle	quasi-static, sometimes cyclic (the actual number of cycles is not always considered)(VHM)	considers reduced shear strength due to pore pressure build-up (not always connected to the cyclic loading characteristics)	Slender pipe piles, Gravity Base Foundations (GBS)	API, DNV
Constitutive soil models	based on analytical formulas to assess each individual cycle, simulates accurately "real behaviour"	cyclic loading (VHM) (number of applied cycles may be limited to 10^2 cycles, due to numerical instability of the model)	strain accumulation and/or pore pressure build-up strongly connected to cyclic characteristics of the applied load (e.g. average value, cyclic amplitude, number of cycles, frequency ...)	GBS, suction caissons	Strain accumulation models (Hyperplastic, Hypoplastic)
Hybrids	uses a combiantion of steps that individually model each cycle, together with steps that assess cyclic behaviour without modelling each individual cycle	cyclic loading (VHM) (may assess larger numbers of cycles $>10^3$ cycles)	generally assess the full range of the behaviour: accumulation of pore pressures and strains, as well as degradation of strength and stiffness based on the cyclic loading characteristics (e.g. average value, cyclic amplitude, number of cycles, frequency ...)	GBS	High Cyclic Strain Accumulation Model (implicit steps based on the hypoplastic model, explicit steps based on extrapolations and empirical formulas) or pore pressure build-up models (densification)

Figure 2.6: Overview and classification of the existing models/approaches

In the following subsections, some of the examples in Figure 2.6 are presented in more detail. This is done in order to investigate the models' adequacy to assess long term effects of cyclic loading on offshore foundations.

2.5.1 THE API APPROACH

The current section will present the guidance given through API (2011) and API & ISO19901-4 (2000) for the design of offshore foundations. The considered superstructure of these foundations is generally an offshore oil and gas production platform.

LOADING CONDITIONS

An important aspect to be mentioned is related to the fact that the cyclic or transient actions will be considered as quasi-static loads on the foundation according to API & ISO19901-4 (2000).

Within API (2011) a considerable section is addressed to the static assessment of waves. The analysis starts by considering wave and current kinematics but is finally reduced to a series of local forces applied on each element that sum up to a global force. A dynamic analysis is recommended for guyed towers and tension leg platforms which must include the stiffness of the structures and reflect the structure/foundation interaction.

The assessment of the wind loading should be dynamic "when the wind field contains energy at the frequencies near the natural frequencies of the platform" API (2011).

FAILURE DEFINITIONS

Within API & ISO19901-4 (2000) they define two types of failure:

Bearing failure "any failure mode that could result in excessive combinations of vertical displacement, lateral displacement, or overturning rotation of the foundation";

Pure sliding/Torsional failure "failure mode where the foundation translates or twists in a horizontal plane".

SHALLOW FOUNDATIONS

The API (2011) recommends the derivation of loading envelopes that capture the ultimate capacity of the foundation under various loading conditions.

Bearing capacity
Formulas for bearing capacity for drained and undrained conditions may be found in the Appendix A. The formulas do not consider cyclic loading conditions.

Displacements and settlements
The response to loading is assessed through the short term displacements for undrained loading conditions (equations 6.14.1-1–4 from API (2011)) and long term displacements or primary settlements (equation 6.14.2-1 from API & ISO19901-4 (2000), also below).

$$u_v = \left(\frac{h \cdot C}{1 + e_0}\right) \lg \frac{q_o + \Delta q}{q_o} \tag{2.11}$$

where:

u_v is the vertical settlement;

h is the layer thickness;

e_0 is the initial void ratio;

C is the compression index of the soil over the load range considered;

q_o is the initial effective vertical stress;

Δq is the added effective vertical stress.

Cyclic behaviour
The API (2011) recommends the investigation of the influence of dynamic loads imposed by current, waves, ice, wind and earthquakes on the structure-foundation system. Additionally, "the influence of the foundation on the structural response and the integrity of the foundation itself should be considered" (API (2011)). But no specific guidance is given.

PILE FOUNDATIONS

The API (2011) recommends that the pile foundation design should ensure that the foundation carries "static, cyclic and transient loads without excessive deformations or vibrations in the platform". They specifically refer to steel cylindrical (pipe) pile foundations.

Ultimate capacity
The formulas for the ultimate axial and lateral capacity of piles defined in API & ISO19901-4 (2000) and API (2011) can be found in the Appendix A. These formulas correspond to static loading conditions.

Displacements and settlements
The response to axial loading is assessed through the relationship between the mobilised soil-pile shear transfer and local pile deflection through $t - z$ curves—see Figure 2.7.
where:

z represents the pile axial defection;

D represents the pile outer diameter;

t represents the mobilised soil-pile adhesion;

t_{max} represents the maximum soil pile adhesion or unit shaft friction;

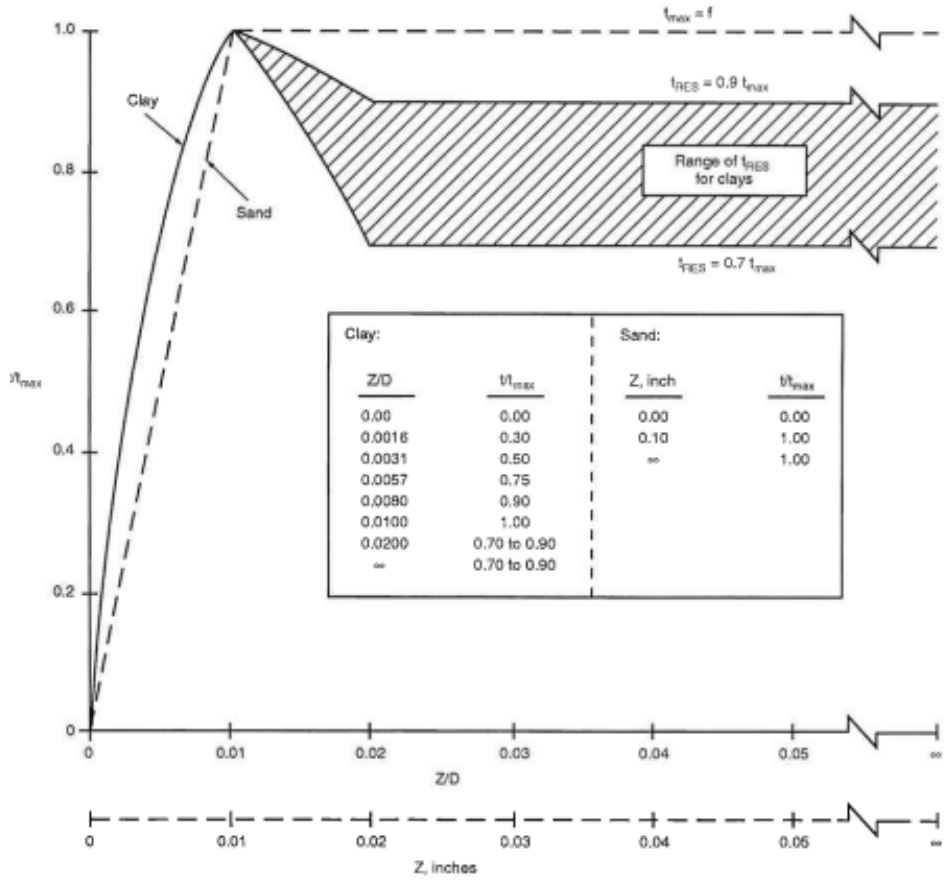

Figure 2.7: Typical axial pile load transfer-displacement $(t - z)$ curves. Source API (2011)

t_{res} represents the residual soil-pile adhesion or unit shaft friction;

z_{res} represents the axial pile displacement at which the residual soil pile adhesion is reached.

The response to lateral loading is assessed through lateral soil resistance-deflection $(p - y)$ relationships for sands:

$$P = A \cdot p_u \cdot \tanh\left[\frac{k \cdot H}{A \cdot p_u} \cdot y\right] \tag{2.12}$$

where:

P is the ultimate lateral resistance;

A is a factor accounting for static or cyclic loading conditions: $A = 0.9$ for cyclic loading and $A = (3.0 - 0.8 \cdot H/D) \geq 0.9$ for static loading;

H is the depth;

D is the average pile diameter from surface to depth;

p_u is the ultimate bearing capacity at depth H;

k is the initial modulus of subgrade reaction, determined as a function of the internal friction angle.

Cyclic behaviour
The API (2011) mentions the following with respect to the axial pile performance subjected to cyclic loading:

"Cyclic loadings (including inertial loadings) developed by environmental conditions such as storm waves and earthquakes can have two potentially counteractive effects on the static axial capacity. Repetitive loadings can cause a temporary or permanent decrease in load-carrying resistance, and/or an accumulation of deformation. Rapidly applied loadings can cause an increase in load-carrying resistance and/or stiffness of the pile.

The resulting influence of cyclic loading will be a function of the combined effects, magnitudes, cycles, and rates of applied loads, the structural characteristics of the pile, the types of soils, and the factors of safety used in design of piles."

Nonetheless, no guidance related to its assessment is given.

The ultimate lateral resistance may be assessed by considering cyclic loading through the specific $A = 0.9$ value. This value is independent of any cyclic loading characteristics (average cyclic shear, cyclic amplitude, number of cycles, etc...) which implies significant uncertainty with regard to its applicability.

CONCLUSIONS API METHOD

From the previous paragraphs, it becomes clear that the proposed assessment method for cyclic loading of the two types of offshore foundations is limited to either vague recommendations, or the usage of a reduction factor for the lateral resistance in the case of piles that does not account for any cyclic loading characteristics. It does not even satisfy their own recommendation for the axial pile performance subjected to cyclic loading. Additionally, the proposed formulas assess either fully undrained or drained behaviour; the possibility of partially drained behaviour is not even mentioned.

With respect to caissons, or skirted foundations, there are no design guidelines, only a few comments related to the benefits of their usage (e.g. potential increase in the ability to sustain short term tensile total stresses).

To conclude, even though this approach has a high simplicity with respect to the required parameters, it does not provide sufficient support to assess long term effects of vertical cyclic loading on suction caisson foundations embedded in sand.

2.5.2 THE DNV APPROACH

The current section will present the guidance given through DNV (1992) and DNV (2004) for the design of offshore foundations.

Within DNV (1992) the considered superstructure of these foundations is an offshore oil and gas production platform. This standard provides a thorough approach in the assessment of gravity base foundations, but a similar method to the API (2011), API & ISO19901-4 (2000) for pile design.

The DNV (2004) specifically addresses offshore wind turbines. Unfortunately, it does not provide additional guidance for any type foundation design other than the API (2011), API & ISO19901-4 (2000), nor DNV (1992).

Therefore, this section shall focus on the approach proposed within DNV (1992) for gravity base foundations.

LOADING CONDITIONS

It is important to mention that DNV (2004) presents a very thorough assessment of the external conditions. It even provides a comparison between the usage of IEC61400-3 (2005) or Kaimal (1972) methods of assessing the power spectral densities for wind actions and procedures for the calculation of the aerodynamic loads due to the blades rotating.

The DNV (1992) considers cyclic loading due to wave action as the considered structures are typically offshore gravity base platforms.

FAILURE DEFINITIONS

Within DNV (1992) failure is defined in terms of the ultimate limit state (ULS) condition: "Foundation failure should be defined as a situation when the deformations of the soil becomes so large that damage may occur to the structure or vital equipment...".

For effective stress analyses, local failure is defined by reaching the shear stress state described by:

$$\tau = \frac{\sigma' \tan \varphi'}{\gamma_m} \tag{2.13}$$

where:

σ' is the normal stress on the shear surface;

φ' is the friction angle at failure;

γ_m is a material coefficient.

Additionally, Figure 4.7 from DNV (1992) gives examples of possible failure modes (i.e. sliding at skirt tips, along soft layer, localised failure, deep-seated bearing capacity failure or moment imbalance).

SHALLOW FOUNDATIONS

The DNV (1992) recommends the effective stress analysis in case of cyclic loading, as pore pressure must be accounted for.

Bearing capacity

The formulas for the static drained or undrained bearing capacity of gravity base foundations defined in DNV (1992) can be found in the Appendix A. These formulas correspond to static loading conditions.

Effects on bearing capacity due to cyclic loading are considered through the assessment of the undrained shear strength within the effective stress analysis that will be presented in the paragraph dedicated to cyclic behaviour.

Additionally, the DNV (1992) provides a thorough assessment of the foundation dynamic stiffness, through the assessment of spring and damping coefficients for different modes of vibration—see Table 7.2.3.4 from DNV (1992).

Displacements and settlements

The assessment of "immediate and consolidation settlements" according to DNV (1992) can be either with the classical theory of elasticity (see section 5.3.2 from DNV (1992)), or Janbu's method (see section 5.3.4 from DNV (1992)). In these cases, settlements are caused by application of static loads.

Settlements due to cyclic loading are also recommended to be assessed. Two mechanisms are identified as their source: undrained shear deformations and consolidation of pore pressures due to cyclic loading. In order to estimate these settlements they recommend the usage of analytical methods that use soil models with the ability to assess average shear stresses and cyclic shear stress history in all soil elements. But no further guidance is given.

Cyclic behaviour

For the assessment of the effects of cyclic loading an effective stress analysis is proposed by DNV (1992). As effective stresses are considered, all pore pressure contributions must be included in the analysis:

- "initial in-situ pore pressures;
- pore pressures due to installation;
- pore pressures due to cyclic loading;
- pore pressures due to transient loading."

In order to determine pore pressure build-up they recommend the usage of pore pressure contour diagrams derived from undrained cyclic testing—see Figure 2.8.

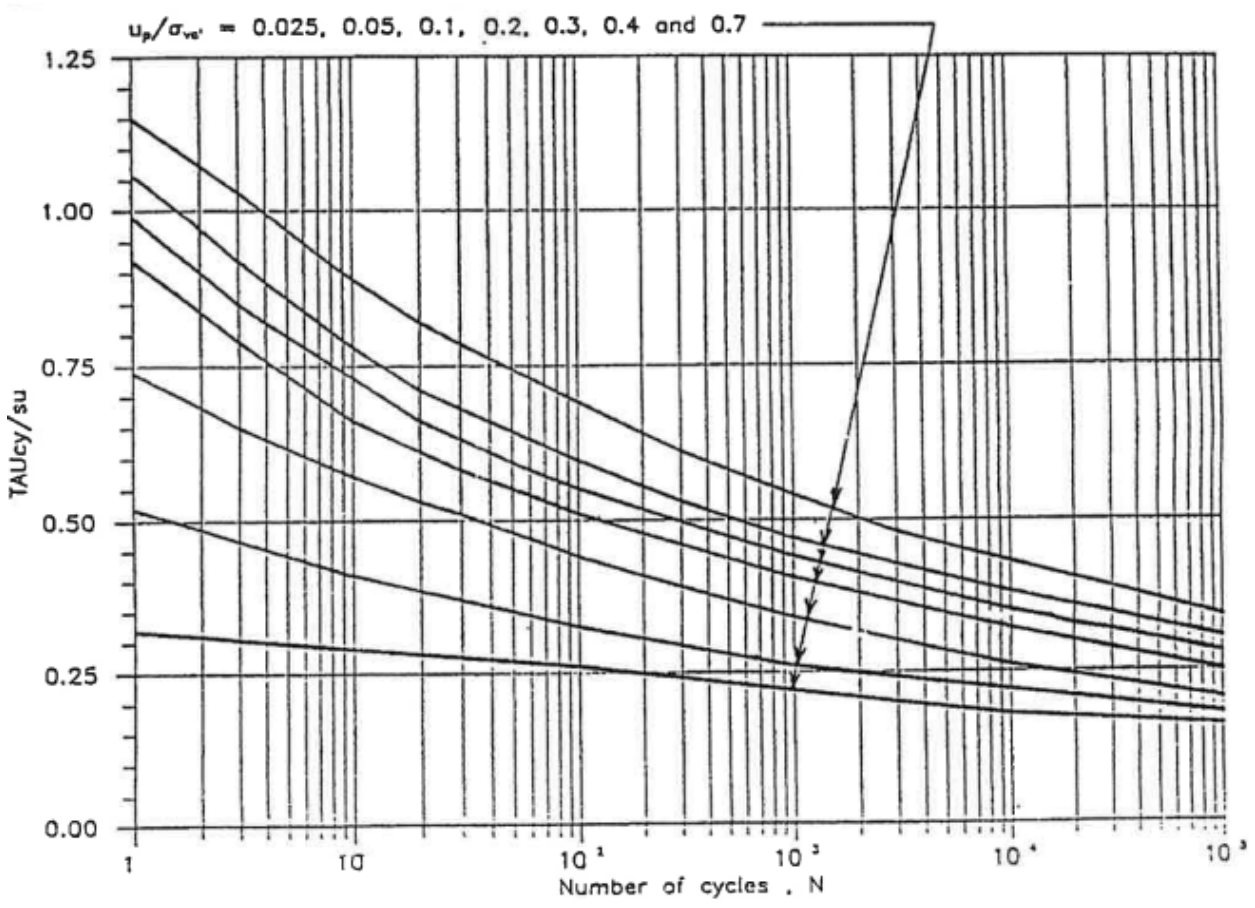

Figure 2.8: Example of pore pressure contour diagram. Source DNV (1992)—Figure 4.4

In the case of low to moderate stress levels they recommend the following assessment for the pore pressure response:

$$R_u = \Delta\sigma_d \frac{dN}{du} \tag{2.14}$$

where:

R_u represents the cumulative pore pressure resistance against repeated loading $R_u = r_u \cdot N$;

N represents the number of cycles at stress level $\Delta\sigma_d$;

r_u is to be determined from laboratory tests;

$\Delta\sigma_d$ represents the change in deviatoric stress, $\Delta\sigma_d = \Delta\sigma_1 - \Delta\sigma_3$;

Therefore the change in pore pressure (Δu) may be written from equation 2.14 as follows:

$$\Delta u = \frac{\Delta\sigma_d}{r_u} \cdot \ln N \tag{2.15}$$

For the change in pore pressure due to transient loading, according to DNV (1992) the equation below is proposed:

$$\Delta u = \Delta\sigma_m - D \cdot \Delta\sigma_d \tag{2.16}$$

where:

Δu represents the change in pore pressure;

$\Delta\sigma_m$ represents the change in mean total stress $\Delta\sigma_m = 1/3 \cdot (\Delta\sigma_1 + \Delta\sigma_2 + \Delta\sigma_3)$;

$\sigma_{1,2,3}$ represent the major, intermediate and minor principal stresses;

$\Delta\sigma_d$ represents the change in deviatoric stress, $\Delta\sigma_d = \Delta\sigma_1 - \Delta\sigma_3$;

D represents the dilatancy parameter, to be defined from the stress path of undrained triaxial tests
$D = 1/3 + 1/(2 \cdot S_d)$;

S_d represents the inclination of the stress path in a plot $\left(\frac{\Delta\sigma_d}{2}\ vs.\ \sigma_3\right)$, $S_d = \frac{\Delta\sigma_1 - \Delta\sigma_3}{2 \cdot \Delta\sigma_3}$.

Additionally, the DNV also recommends including pore pressure dissipation, but without giving any guidelines related to the implementation.

CONCLUSIONS DNV METHOD

The DNV (2004) brings support to the load assessment method, while DNV (1992) provides a method of assessing changes in pore pressure based on the number of cycles and the cyclic shear strength. The method is fully dependent on the development and accuracy of the pore pressure contour diagrams, which would require significant amounts of laboratory testing as the databases for sand are not as developed as for clays.

To conclude, even though this method identifies key aspects related to cyclic behaviour, from pore pressure build-up to cyclic settlements, the required amount of laboratory testing to develop the necessary pore pressure contour diagrams make it less likely to be used within the industry.

The following sections will present three other models that have been used for the assessment of this problem: densification model, hyperplastic model and hypoplastic model.

2.5.3 DENSIFICATION MODEL

INTRODUCTION

Offshore structures and implicitly their foundations are subjected to cyclic load, which makes it essential to know the behaviour of the founding soil under these conditions:

Drained conditions the loose granular soil will tend to densify, compact.

Undrained or partially drained conditions pore pressure will tend to build-up, causing strength and stiffness reduction.

Densification the plastic volume change due to cyclic loading, by Song (1990).

In order to analyse the pore pressure build-up in the soil beneath a foundation Song (1990) created a densification model.

The initial stress ratio within this model is estimated through an elasto-plastic analysis and the storage equation estimates the pore pressure build-up. The author considers the soil underneath the foundation of an offshore structure during a complete storm, including thousands of waves.

The processes occurring during each loading cycle are highly complex. Each of the cycles will cause further densification until a very dense sand state is reached. The densification and liquefaction of the soil is mainly controlled by the cyclic shear strain amplitude (Silver & Seed (1971), Youd (1972)). In practical work, the amount of densification is generally quantified with the aid of the cyclic shear stress ratio ($CSSR$).

THE DENSIFICATION MODEL

Song (1990) proposed a model based on undrained liquefaction tests, thus aiming to model the undrained and partially drained soil behaviour. For deformations due to monotonic loading an elastic model is used.

The following assumptions are made for the creation of this model:

- In an undrained test the total stress remains the same after one cycle;
- In undrained conditions the total volume strain increment is very small and may be neglected compared to the plastic volume strain increment;
- An average value for the compression modulus of the soil skeleton is used for simplification (this will decrease the accuracy of the densification, but the pore pressure build-up is believed to be modelled properly Song (1990));
- An increase of pore pressure will determine an increase in shear stress ratio, thus accelerating the build-up of pore pressure;
- The increase of densification leads to a decrease in the potential for further densification (hardening effect);
- The hardening effect can be described by a negative exponential function of accumulated plastic volumetric strain (according to densification test data).

Following from the above assumptions the model equations are:

$$\delta p = K \delta \varepsilon_{vc} \tag{2.17}$$

$$\delta\varepsilon_{vc} = D_1 \left(\frac{\tau_c}{\sigma'_m} - S_{min} \right)^{1/2} \cdot \left(\frac{\tau_c}{\sigma'_m} \right)^{\vartheta} \exp(-D_2 \varepsilon_{vc}) \cdot \Delta N \tag{2.18}$$

where:

δp pore pressure increment;

K compression modulus of the soil skeleton;

$\delta\varepsilon_{vc}$ plastic volumetric strain (densification) increment;

D_1 model parameter related to the pore pressure build-up during the first cycles;

τ_c cyclic shear stress;

σ'_m change in effective mean stress;

S_{min} threshold shear stress ratio;

ϑ model parameter to be determined from the curve N_l (number of cycles to liquefaction) vs. τ_c/σ'_{m0}

D_2 model parameter that is inversely proportional to the volume strain;

ΔN increment of the number of cycles.

DETERMINATION OF DENSIFICATION MODEL PARAMETERS

Cyclic shear stress ratio

From earthquake engineering, the cyclic shear stress ratio is the cyclic shear stress on the horizontal plane over the initial vertical stress and can be simulated by simple shear tests. However, in practical foundation problems the stress conditions are much more complicated. Therefore, a new definition is given by replacing the vertical effective stress by the present isotropic stress, which changes cyclically.

The author, Song (1990), defines the cyclic shear stress with the aid of the second invariant of the deviator stress induced by the cyclic load, which for triaxial tests is reduced to and can be used directly as:

$$\tau_c = \frac{1}{2}(\sigma_1^c - \sigma_3^c) \tag{2.19}$$

where:

σ_1^c, σ_3^c represent the principal stresses.

Special attention is required if direct simple shear test data are used: the stress ratio should be multiplied by 1.25 from the original value (Song (1990)) as the formula is constructed considering triaxial stress states.

Static shear

Static shear stress has a significant effect on the pore pressure build-up in the soil: pore pressure build-up is limited if the static shear stress is large enough so that no reversal occurs during cyclic loading (Finn *et al.* (1978), Vaird & Chern (1983)).

From Vaird & Chern (1983) in Figure 2.9 the influence of the static shear is represented by the means of the effective stress ratio ($K_c = \sigma'_1/\sigma'_3$) can be seen.

The current model approximates the effect of static shear stress: densification is reduced when the failure

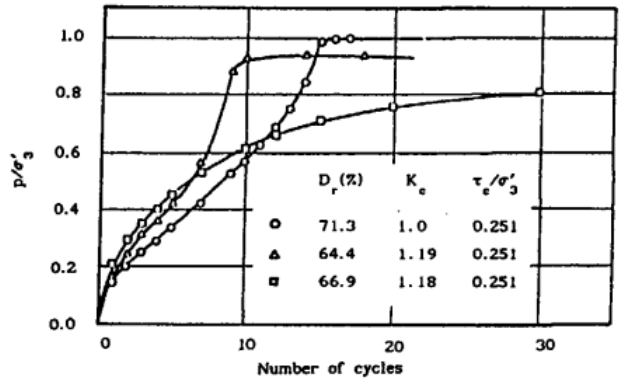

Figure 2.9: Cyclic loading behaviour of dense sand with and without static shear stress by Vaird & Chern (1983)

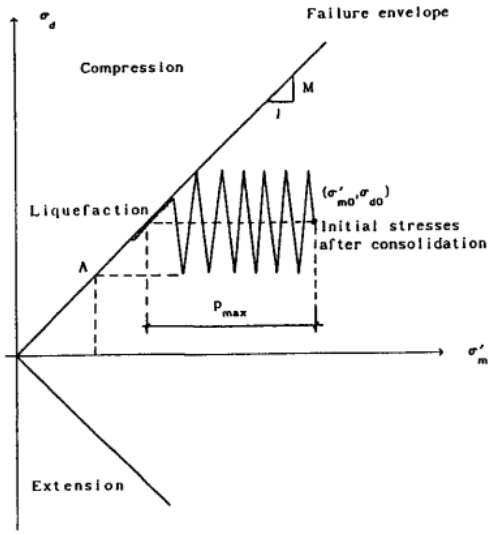

Figure 2.10: Limiting value of pore pressure in the soil under anisotropic conditions. Source Song (1990)

line is approached. The failure line is defined by the slope of the critical state line—see Figure 2.10 and Equation 2.20.

$$M = \frac{6 \sin \varphi_c}{3 - \sin \varphi_c} \tag{2.20}$$

where:

φ_c is the critical state friction angle.

Parameter ϑ

The model parameter ϑ can be determined from the curve N_l (number of cycles to liquefaction) vs. τ_c/σ'_{m0}—see Figure 2.11. From the same figure the relation in Equation 2.21 is deduced through curve fitting.

$$N_l = A \left(\frac{\tau_c}{\sigma'_{m0}} - S_{min} \right)^{-1/2} \cdot \left(\frac{\sigma'_{m0}}{\tau_c} \right) \tag{2.21}$$

where:

N_l number of cycles to liquefaction;

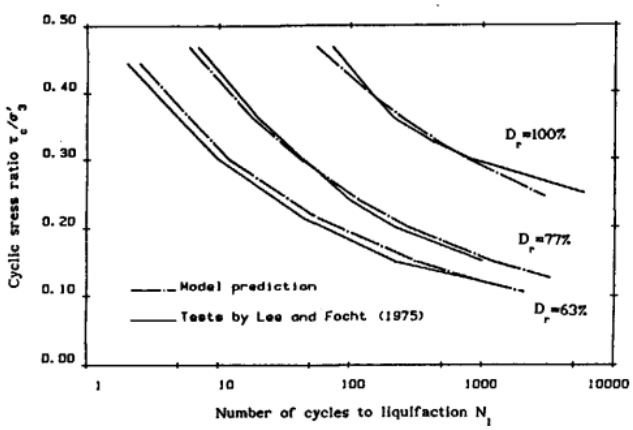

Figure 2.11: Cyclic loading strength from undrained triaxial tests. Source Song (1990)

A is a constant;

τ_c cyclic shear stress;

σ'_{m0} initial effective mean stress;

S_{min} threshold shear stress ratio;

ϑ model parameter to be determined using Figure 2.11.

Parameter D_1
The model parameter D_1 can be determined from the pore pressure build-up during the first cycles, using equation 2.22

$$D_1 = \frac{D_1^* \sigma'_{m0}}{K} \tag{2.22}$$

where:

D_1^* can be determined with equation 2.23:

$$D_1^* = 1.5/A \tag{2.23}$$

A is a constant;

K compression modulus of the soil skeleton;

σ'_{m0} initial effective mean stress.

Parameter D_2
After determining the parameters D_1 and ϑ, the model parameter D_2 can be determined by simulating undrained tests. The parameter shall be calibrated by attempting to determine the number of cycles to liquefaction. Based on the Figure 2.11 the author recommends equation 2.24:

$$D_2 = D_2^* K / \sigma'_{m0} \tag{2.24}$$

Where all the parameters have been explained in the previous subsections.

D_r	ϑ	D_1^*	D_2^*	S_{min}
63%	4.0	26.0	7.5	0.10
77%	4.0	7.6	7.5	0.12
100%	5.0	1.8	9.0	0.22

Table 2.2: Densification model parameters, by Song (1990)

CONCLUSIONS REGARDING THE DENSIFICATION MODEL

For the data given in Figure 2.11 the values of the calibrated parameters are given in Table 2.2.

The author of the model, Song (1990) compares the prediction of his model with Seed's pore pressure model in Figure 2.12.

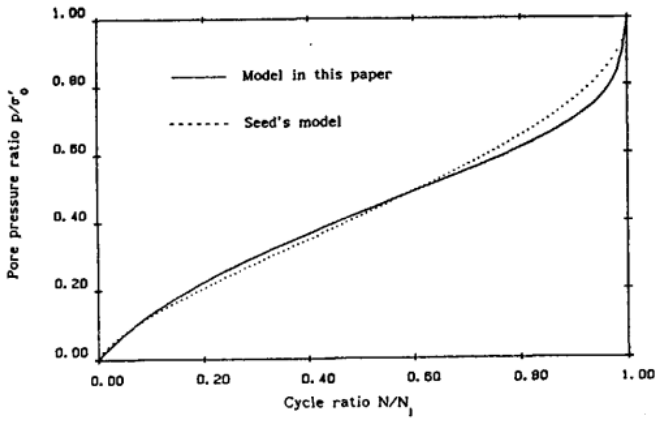

Figure 2.12: Comparison of pore pressure build-up. Source Song (1990)

The test data needed for the determination of the densification model parameters includes:

- Cyclic triaxial undrained test data to determine and calibrate most of the model parameters;
- Monotonic triaxial undrained test data to determine the limiting pore pressure and the critical state parameters.

The most important limitation regarding the usage of this model during the tender phase of offshore projects is the fact that the required data for the parameter determination and calibration is generally not available and correlation formulas may lead to large errors. Moreover, some of the parameters do not have a direct physical meaning which makes the understanding of the model not accessible. In addition to this several assumptions were made to simplify the calculations, but their impact on the final result was not assessed.

Additionally, Song (1990) also presents the application of this model for the Ekofisk tank problem, where concrete gravity structures were placed in the North Sea. The tank was 90 m high and had a footprint of 7360 m^2, with a submerged weight of 1900 MN. The soil conditions underneath the tank were considered to be 16 m of fine dense sand ($D_r = 100\%$), underlain by 2 m of hard clay. The water depth was 70 m

The loading scheme considered can be seen in Figure 2.13 and corresponds to the wave parameters of a 100 year design storm, as reported in a paper by Bjerrum (1973).

The important aspect to be noted from the two figures 2.13 and 2.14 is the fact that the pore pressure accumulates towards its peak which coincides with the collision of the maximum wave. Afterward it starts to dissipate. Secondly, the pore pressure underneath the structure at the centre shall be higher than at the edge,

where faster dissipation may occur.
The pore pressure response to the loading in Figure 2.13 can be found in Figure 2.14.

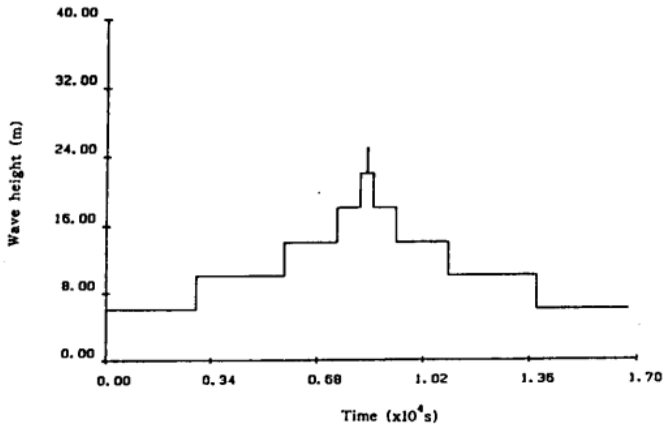

Figure 2.13: The wave loading sequence. Source Song (1990)

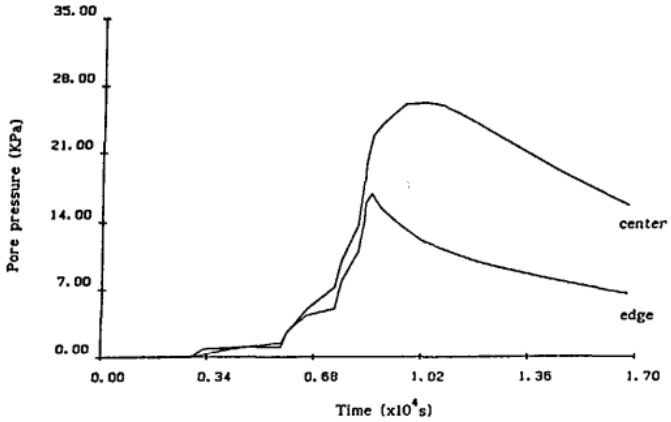

Figure 2.14: Pore pressure build-up beneath the Ekofisk tank Song (1990)

Even though the author provides an example of application of his model on a real case, the above mentioned reasons (test data availability, lack of physical meaning of certain parameters, unknown impact of the chosen simplifications) render the model not easily applicable in tender phases of projects.

2.5.4 CONTINUOUS HYPERPLASTIC MODEL

INTRODUCTION

Research at the Oxford University has been conducted in order to model the behaviour of shallow offshore foundations by using numerical modelling (Cassidy & Bienen (2002), Cassidy *et al.* (2004), Houlsby (2003)). Further this research has also been used for the modelling of suction caisson foundations for offshore wind turbines by Senders (2005).

They developed a "force resultant" model that captures the soil behaviour surrounding an offshore soil foundation: it considers the foundation as being rigid, but the interaction with the soil is expressed with non-linear relationships between the force resultants applied to the foundation and the displacements. The model is based on four components:

- a yield surface;

- a hardening law;
- a flow rule;
- definition of elastic behaviour inside the yield surface.

In the development of the expressions for each component the authors have used both theoretical and empirical formulas obtained through model tests.

YIELD SURFACE

A familiar concept in geotechnical engineering is the bearing capacity analysis: failure of the foundation under a certain load. A more in depth view of this concept is that below the bearing capacity limit the behaviour is elastic (recoverable deformations occur), while above this limit the behaviour is plastic (permanent displacements occur). Thus, the bearing capacity limit may be seen as a "yield point" from the plasticity theory.

For any combination of certain proportions of vertical, horizontal and moment loading there will be a value (yield point) below which the behaviour is elastic, but upon reaching it plastic deformations will occur.

In a general form the yield surface for a 3 dimensional case is:

$$f = h_2^2 + h_3^2 + q^2 + m_2^2 + m_3^2 + 2 \cdot a \cdot (h_2 \cdot m_3 - h_3 \cdot m_2) - \beta_{12}^2 \cdot S(\nu^2)^{\beta_1} \cdot \left((1-\nu)^2\right)^{\beta_2} = 0 \tag{2.25}$$

where,

S is introduced to ensure consistency of the sign of the yield function, $S = sgn\,(\nu_1 \cdot (1 - \nu_2))$;

$\beta_{12} = (\beta_1 + \beta_2)^{(\beta_1+\beta_2)} \cdot \beta_1^{-\beta_1} \cdot \beta_2^{-\beta_2}$;

β_1, β_2 are introduced to "round off" the pointed ends of the yield surface on the V axis and are smaller than 1.0;

$\nu = V/V_0$;

$q = \dfrac{Q}{2 \cdot R \cdot q_0 \cdot V_0}$;

$h_2 = \dfrac{H_2}{h_0 \cdot V_0}$ and analogously for h_3, m_2, m_3.

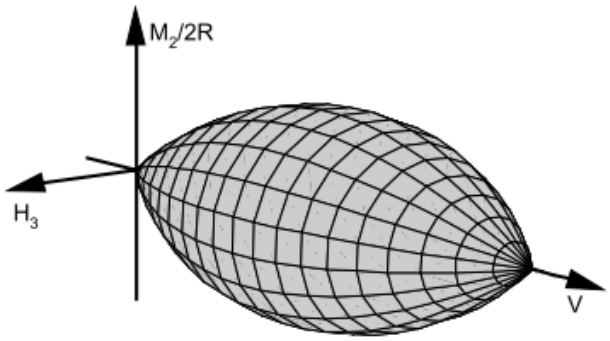

Figure 2.15: Yield surface for in-plane loading by Houlsby (2003)

For in plane loading ($H_2 = Q = M_3 = 0$) the yield surface would look as in Figure 2.15. The apex of the defined yield envelope on the V-axis represents in fact the bearing capacity under pure vertical loading. The authors have confirmed the appropriateness of the form for the planar loading of the yield surface by model testing with a 3 degree of freedom loading rig. Their work is currently extended to a 6 degree of freedom loading apparatus.

HARDENING LAW

According to the bearing capacity theory, the value of the bearing capacity limit is considered fixed, regardless of the amount of deformation occurring. In reality, as deformation occurs and the foundation is pushed further into the ground, the capacity increases. Therefore, the size of the yield surface is not fixed, but it increases with the occurrence of plastic deformations. The hardening law determines the stiffness of the response.

The authors consider a reasonable assumption that the capacity increases only due to further embedment of the foundation in the ground. Thus, vertical bearing capacity may be written as a function of the vertical plastic penetration (w_p):

$$V_0 = \pi \cdot R^2 \cdot (\gamma \cdot R \cdot N_\gamma + \gamma \cdot N_q \cdot w_p) \tag{2.26}$$

where:

V_0 represents the vertical bearing capacity or the maximum applied vertical load;

R represents the radius of the circular foundation;

γ represents the specific unit weight of the soil;

N_γ, N_q represent bearing capacity factors;

w_p vertical plastic penetration of the foundation in the ground.

In practice models may be implemented through curves of bearing capacity with respect to plastic deformation (w_p, V_0) or by using empirical fitting on observed data. According to Cassidy & Houlsby (1999) the following formulation is suggested:

$$V_0 = \frac{kz_p + \left(\frac{f_p}{1-f_p}\right)\left(\frac{z_p}{z_p m}\right)^2 V_{0m}}{1 + \left(\frac{kz_{pm}}{V_{0m}} - 2\right)\left(\frac{z_p}{z_{pm}}\right) + \left(\frac{1}{1-f_p}\right)\left(\frac{z_p}{z_{pm}}\right)} \tag{2.27}$$

where:

k is the initial plastic stiffness;

V_{0m} is the peak value of V_0;

z_{pm} is the value of the plastic vertical penetration at the peak value V_{0m};

f_p is a dimensionless constant describing the limiting magnitude of vertical load as a proportion of V_{0m};

The values of the parameters were determined from experimental data.

FLOW RULE

When multiaxial loading is applied, the flow rule determines the ratios between the plastic displacement components.

If the flow rule is associated to the yield surface, then yield surface determines as well the plastic potential. This format is more simple as no additional relation needs to be specified and reasonable results are given for horizontal displacements and rotations. Unfortunately, it is insufficiently accurate in the prediction of vertical movements. Therefore, the usage of a non-associative flow rule is required.

In their research, Cassidy & Houlsby (1999), found the behaviour of sands to be highly complex: a plastic

potential surface with a similar mathematical formulation as the yield surface and additional relations accounting for the history of movement were created for this model.

$$g = \left(\frac{H}{\alpha_h h_0 V_0}\right)^2 + \left(\frac{M/D}{\alpha_m m_0 V_0}\right)^2 - 2a\left(\frac{HM/D}{\alpha_h \alpha_m h_0 m_0 V_0^2}\right)^2 - \\ - \left[\frac{(\beta_3+\beta_4)^{(\beta_3+\beta_4)}}{\beta_3^{\beta_3}\cdot\beta_4^{\beta_4}}\right]^2 \left(\frac{V}{V_0}\right)^{2\beta_3}\left(1-\frac{V}{V_0}\right) = 0 \quad (2.28)$$

where:

α_m, α_h association factors to account for stiffening in the radial force-displacement relationships;

β_3, β_4 shaping factors for the flow rule function;

D diameter of the foundation;

H, V, M applied loads (vertical, horizontal, moment);

V_0 represents the vertical bearing capacity or the maximum applied vertical load.

ELASTIC BEHAVIOUR

As previously mentioned in the above sections, within the yield surface the soil behaviour is elastic and recoverable deformations occur. For a 6 degree of freedom problem the same equation 2.3 on page 24 given by Doherty *et al.* (2005) defines the relationship between the loads and the corresponding displacements.

In this first development of the model by Houlsby (2003) it is assumed that except for a few extreme events, the cyclic loading will remain inside the yield surface and will be dominated by the elastic behaviour—recoverable displacements are assumed to occur. The author mentions future work on a "continuous hyperplastic model" that would be able to follow better the effects of cyclic loading.

CONCLUSIONS HYPERPLASTIC MODEL

The proposed hyperplastic model represents an alternative for assessing the behaviour of an offshore foundation subjected to cyclic loading.

Unfortunately, the large number of parameters (over 30) required to calibrate the model may cause significant difficulty in its usage. Moreover the assumption of the model that the cyclic loading will remain within the elastic response range still requires confirmation.

2.5.5 HYPOPLASTIC MODEL

INTRODUCTION

For a better understanding of the model, a definition of hypoplasticity must be given:

Hypoplasticity is a constitutive law of the rate type. It is a relation which associates the strain rate to the stress rate. The mechanical behaviour characteristics of granular material are expressed in one single tensorial equation (Kolymbas (2000)).

The hypoplastic model is a particular incremental non-linear constitutive model that can be used to predict soil behaviour. The model does not decompose the strain rate into elastic or plastic parts, as in elasto-plastic theory. Nor does it explicitely use the notion of the yield surface and plastic potential surface. Regardless of this, the hypoplastic model is able to predict important aspects of soil behaviour: critical state, dependency of

peak strength on soil density, non-linear behaviour in the small and large strain range etc ...

Hypoplastic sand model

The hypoplastic model is based on the modified equation by Gudehus (1996) including the influence of the stress level (barotropy) and the influence of density (pyknotropy):

$$\dot{\mathrm{T}} = f_s \mathcal{L} : \mathrm{D} + f_s f_d \mathrm{N} \|\mathrm{D}\| \tag{2.29}$$

where:

$\dot{\mathrm{T}}$ represents the objective (Jaumann) stress rate;

D represents Euler's stretching tensor;

$\mathcal{L}$ is a fourth order constitutive tensor;

N is a second order constitutive tensor;

f_s is a scalar factor expressing the influence of the stress level;

f_d is a scalar factor expressing the influence of density.

The hypoplastic model for sand is based on the model propsed by Gudehus (1996) (see equation 2.29) with the Matsuoka-Nakai critical stress state condition—see Figure 2.16, encorporated by von Wolffersdorff (1996). Which is presently considered as the standard hypoplastic model for sands.

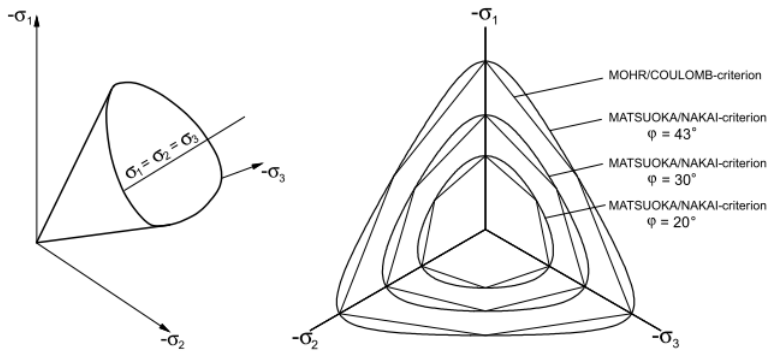

Figure 2.16: Matsuoka-Nakai limiting surface. Source Marcher *et al.* (1999)

The hypoplastic model as defined by equation 2.29 is able to successfully predict the behaviour in the medium to large strain range (as defined by principal strains).

Intergranular strain concept

Niemunis & Herle (1997) created an extension to Von Wolffersdorff's model by including "intergranular strain"; thus accounting for high quasi-elastic soil stiffness in the small strain range, upon cyclic loading.

The rate formulation from the enhanced model by Niemunis & Herle (1997) is:

$$\dot{\mathrm{T}} = \mathcal{M} : \mathrm{D} \tag{2.30}$$

where:

$\dot{\mathrm{T}}$ represents the objective (Jaumann) stress rate;

D represents Euler's stretching tensor;

$\mathcal{M}$ is a fourth order tangent stiffness tensor of the material;

The total strain is considered the sum of two components (Mašín (2012)):

1. Intergranular strain tensor (δ) representing the deformation of interface layers at intergranular contacts;
2. Component related to the rearrangement of the soil skeleton.

In reverse and neutral loading conditions the observed overall strain is related only to the first component (hypoelastic behaviour), whilst in continuous loading conditions both components contribute (hypoplastic behaviour).

HYPOPLASTIC SAND MODEL PARAMETERS

Von Wolffersdorff's model requires 8 material parameters—see Table 2.3:

Symbol	**Description**
φ_c	critical state friction angle
h_s and n	parameters controlling the shape of the limiting void ratio curves (normal compression lines and critical state line)
e_{d0} , e_{c0} , e_{i0}	reference void ratios specifying positions of limiting void ratios
α	parameter controlling the dependency of peak friction angle on relative density
β	parameter controlling the dependency of soil stiffness on relative density

Table 2.3: Overview of the parameters of the sand hypoplastic model

The calibration procedure for each of the parameters in Table 2.3 can be found in Herle & Gudehus (1999). Further in the following subsections each of the parameters will be briefly discussed.

Critical state friction angle

Critical state is assumed to be reached during monotonic shearing as stress rate reduces to null values and deformation becomes infinite. The problem is reduced to localising the deformation into shear bands.

Following from this logic, it was concluded by Miura *et al.* (1997) that it is suitable to determine φ_c by measuring the angle of repose φ_{rep} for materials with a grain size larger than 0.1 mm. Considerable agreement was found by Herle & Gudehus (1999) between the angle of repose and the values of critical state angle measured in shear tests—see Table 2.4. The method is not suitable for materials with the grain size smaller than 0.1 mm due to a potential increase of φ_{rep} because of capillarity effects; in such cases laboratory shear experiments are required.

Material	φ_{rep} [°]	φ_c [°] **(shear test)**	**Test Type**
Hochstetten gravel	35.7	36.5	ds
Hochstetten sand	34.0	34.0	txd, ds
Hostun RF sand	32.0	32.0	txd
Karlsruhe sand	29.1	30.0	txd
Lausitz sand	33.0	32.2	txd
Toyoura sand	30.4	30.9	txu
Zbraslav sand	30.8	29.7	ds

Table 2.4: Correspondence between φ_{rep} and φ_c [°] (shear tests: direct shear-ds, triaxial drained-txd, triaxial undrained-txu) by Herle & Gudehus (1999)

Often the critical friction angle is not available, but only the peak friction angle (φ'_p) is known and the mean effective stress at failure (p'_f) which is common in the tender phase of the projects. Then the relative dilatancy

index may be determined (I_R) and consequently the critical friction angle with the following formulas (see Equations 2.31, 2.32—for plane strain, 2.33—for triaxial strain) recommended by Bolton (1986):

$$I_R = I_D \cdot (10 - \ln(p'_f)) - 1 \tag{2.31}$$

$$\varphi'_p - \varphi_c = 5 \cdot I_R \tag{2.32}$$

$$\varphi'_p - \varphi_c = 3 \cdot I_R \tag{2.33}$$

where:

I_R relative dilatancy index;

I_D relative density;

φ'_p effective peak friction angle;

φ_c critical friction angle;

p'_f mean effective stress at failure.

Parameters h_s and n
The parameters h_s and n influence the shape of the compression curve (see Figure 2.17) can be determined directly from oedometric loading curves and Bauer (1996)'s formula by time-differentiation:

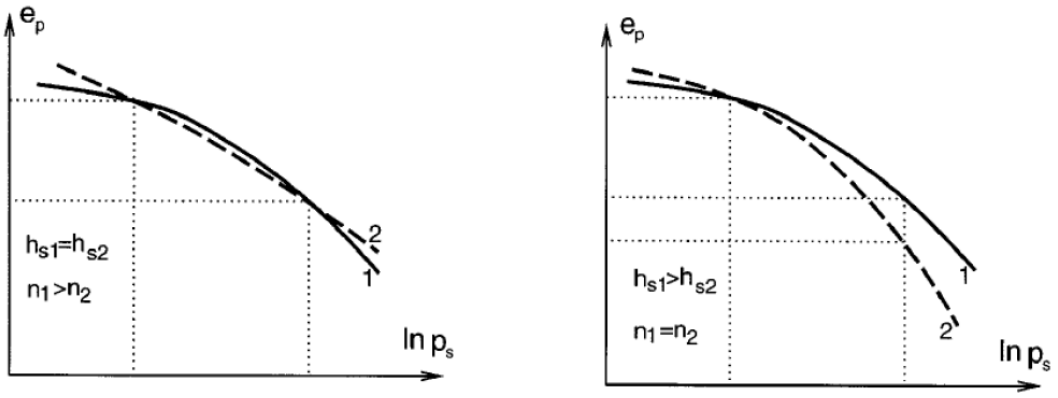

Figure 2.17: Influence of h_s and n on the shape of the compression curve

h_s controls the overall slope of the oedometric curve—see Equation 2.34:

$$h_s = 3p_s \left(\frac{ne_p}{C_c}\right)^{\frac{1}{n}} \tag{2.34}$$

where:

C_c represents the secant compression index calculated from limit values of the calibration interval p_{s1} and p_{s2};

p_s, e_p are the average limit values of p and e for the same interval.

n controls the curvature of the oedometric curve—see Equation 2.35:

$$n = \frac{\ln \frac{e_{p1} C_{c2}}{e_{p2} C_{c1}}}{\ln \frac{p_{s2}}{p_{s1}}} \tag{2.35}$$

where:

p_{s1}, p_{s2} are to be calculated using Jáky's formula:

$$K_0 = 1 - \sin \varphi_c \tag{2.36}$$

e_{p1}, e_{p2} are the void ratios corresponding to the stresses p_{s1}, p_{s2};

C_{c1},C_{c2} can be estimated from loading steps proceeding and following p_{s1}, p_{s2}—see Figure 2.18.

The limiting void ratios and the relation between the parameters e_{c0}, e_{i0} and e_{d0} can be seen in Figure 2.19.

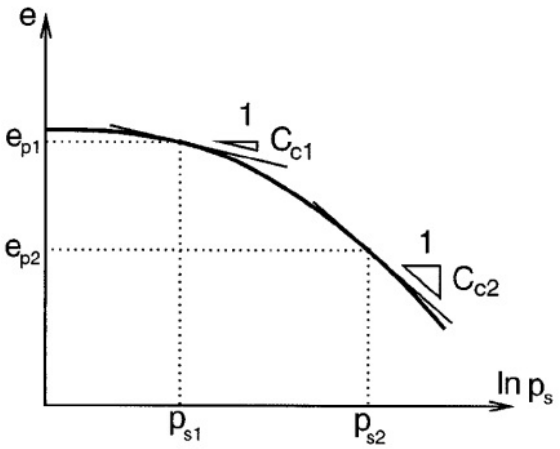

Figure 2.18: Determination of the parameters C_{c1},C_{c2} based on the loading steps and following p_{s1}, p_{s2} by Herle & Gudehus (1999)

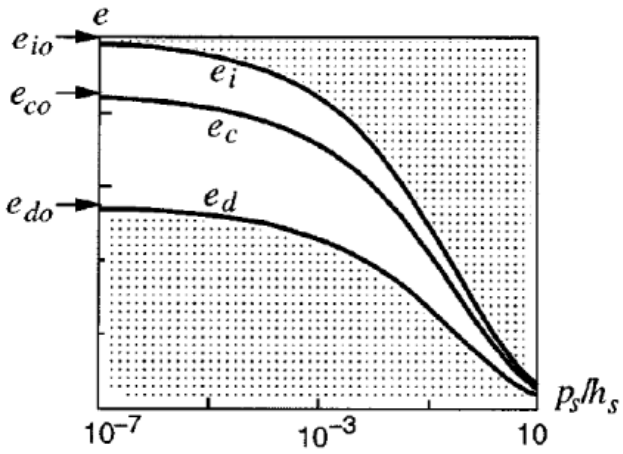

Figure 2.19: The dependence of the reference void ratios e_{c0}, e_{i0} and e_{d0} on the mean stress and granular hardness, by Herle & Gudehus (1999)

Parameter e_{c0}

e_{c0} defines the position of the critical state line in the $\ln p$ vs. e space, according to Bauer (1996)'s equation:

$$e_c = e_{c0} \exp \left[\left(\frac{3p}{h_s} \right)^n \right] \tag{2.37}$$

The simplest way for determining e_{c0} is based on the assumption that the sand mass during the evaluation of the angle of repose is close to the critical state. The soil for the oedometric test performed for determining h_s and n is also aimed at the loosest state. Therefore, the initial void ratio of the oedometric test on a loose sand can be considered as an appropriate estimate of e_{c0}.

Parameter e_{i0}

e_{i0} controls the position of the isotropic compression line. For the given mean stress, e_i represents the theoretical loosest possible state.

During isotropic compression, the compression line converges towards the ideal normal compression line (NCL) very slowly. Thus, e_i represents the theoretical e_{max} in gravity free-space. Upon studying the idealised loosest packing of spherical particles, Herle & Gudehus (1999) proposed $e_{i0} = 1.2 \cdot e_{c0}$.

Parameter e_{d0}

e_{d0} controls the position of the minimum void ratio line. The best densification can be obtained by means of small amplitude cyclic shearing at constant pressure.

An alternative empirical approach is suggested by Herle & Gudehus (1999) upon evaluating e_{d0} and e_{c0} on seven different granular soils: the ratio e_{d0}/e_{c0} varies between the range 0.52–0.64. The lower bound of the range ensures that the state $e < e_d$ is not allowed. In absence of the minimum void ratio, the following estimate can be used: e_{d0}=0.5e_{c0}.

Parameter α

α controls the dependency of the peak friction angle φ_p on the relative void ratio:

$$r_e = \frac{e - e_d}{e_c - e_d} \tag{2.38}$$

The calibration is done by means of single element simulation of triaxial shear test on a soil with $r_e < 1$ (see Figure 2.20).

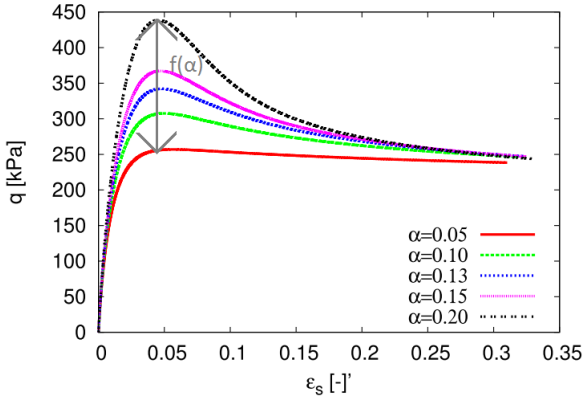

Figure 2.20: Calibration of parameter α by David Mašín (2012).

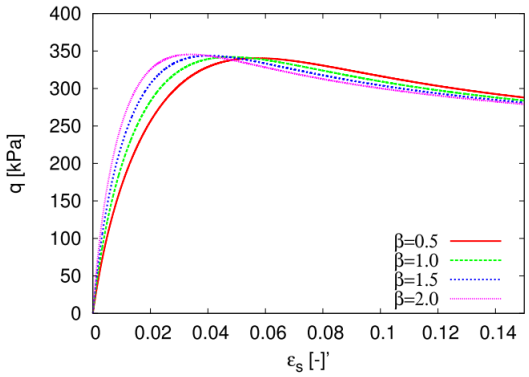

Figure 2.21: Calibration of parameter β by David Mašín (2012).

Parameter β

β influences the size of the response envelope (both bulk and shear stiffness). It is best calibrated by means of fitting shear strain in triaxial shear test—see Figure 2.21.

Conclusions regarding hypoplastic sand model parameters

Following from the above sections, one may conclude that the minimum needed experimental program, in order to use P.A. von Wolffersdorff (1996)'s hypoplastic model for sand, includes:

- **Angle of repose test**—Resulting parameter: φ_c or **Shear test** to determine φ_p and through empirical formulas φ_c;
- **Oedometric test** (at least one on initially loose sample)—Resulting parameters: h_s, n, e_{c0} and empirically e_{d0}, e_{i0};
- **Drained triaxial test** (at least one on initially dense sample)—Resulting parameters: α and β.

From Herle & Gudehus (1999), Table 2.5 gives an overview of the evaluated model soil parameters for seven different granular soils:

INTERGRANULAR STRAIN CONCEPT PARAMETERS

In order to be able to model small strain stiffness effects in hypoplasticity, Niemunis & Herle (1997) developed the intergranular strain concept. It requires 5 additional parameters:

Material Name	φ_c [°]	h_s [GPa]	n [−]	e_{d0} [−]	e_{c0} [−]	e_{i0} [−]	α [−]	β [−]
Hochstetten gravel	36	32	0.18	0.26	0.45	0.5	0.1	1.9
Hochstetten sand	33	1.5	0.28	0.55	0.95	1.05	0.25	1.5
Hostun RF sand	31	1.0	0.29	0.61	0.96	1.09	0.13	2
Karlsruhe sand	30	5.8	0.28	0.53	0.84	1	0.13	1
Lausitz sand	33	1.6	0.19	0.44	0.85	1	0.25	1
Toyoura sand	30	2.6	0.27	0.61	0.98	1.1	0.18	1.1
Zbraslav sand	31	5.7	0.25	0.52	0.82	0.95	0.13	1
min. sand	**30**	**1.0**	**0.19**	**0.44**	**0.82**	**0.95**	**0.13**	**1.0**
max. sand	**33**	**5.8**	**0.29**	**0.61**	**0.98**	**1.1**	**0.25**	**2.0**

Table 2.5: Hypoplastic sand model parameters evaluated by Herle & Gudehus (1999)

m_R is a parameter controlling the initial (very-small-strain) shear modulus upon 180° strain path reversal and the initial loading;

m_T is a parameter controlling the initial strain modulus upon 90° strain path reversal;

R represents the size of the elastic range (in the strain space);

β_r, χ control the rate of degradation of the stiffness with strain.

Parameter m_R

m_R controls the initial shear modulus (G_0). When considering P.A. von Wolffersdorff (1996) hypoplasticity, G_0 is proportional to:

$$G_0 \approx p^{(1-n)} \tag{2.39}$$

G_0 may be measured by means of the velocity of propagation of shear waves (e.g. by means of bender element soil tests). And m_R is a proportionality constant which can be calibrated by a parametric study (see Figure 2.22).

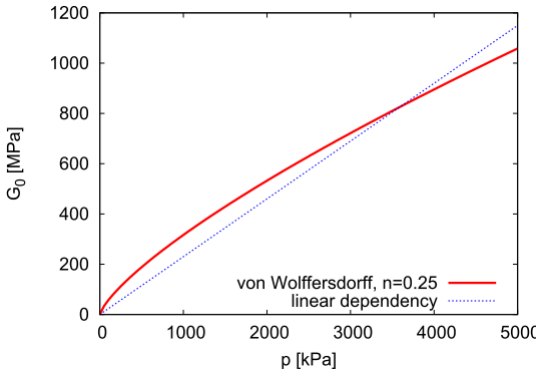

Figure 2.22: Calibration of parameter m_R by David Mašín (2012).

Parameter m_T

m_T is difficult to calibrate, but $m_R/m_T = G_0/G_{90}$, where G_{90} is the initial shear stiffness after 90° change of strain path direction. But, G_{90} cannot be measured using bender element tests, accurate strain measurements using strain transducers are needed. Therefore, the estimation of G_0/G_{90} remains difficult.

Experiments conducted by Richardson (1988) and Atkinson *et al.* (1990) indicate that $m_T \approx 0.5 m_R$.

Parameter R

R determines the size of the elastic range—see Figure 2.23.

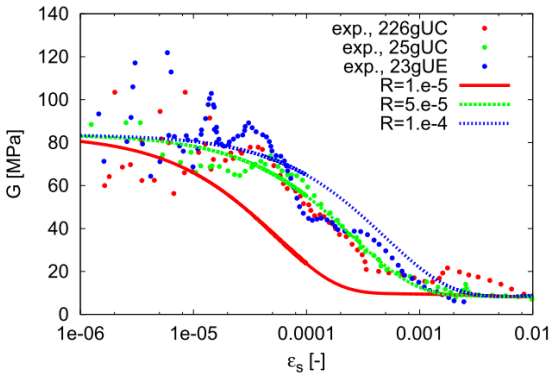

Figure 2.23: Influence of R by David Mašín (2012).

Parameters β_r and χ

β_r and χ control the shape of the stiffness degradation curves—see Figure 2.24.

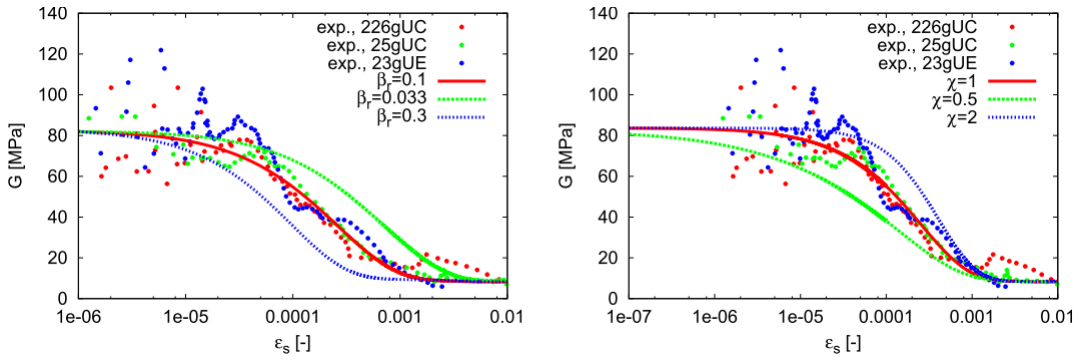

Figure 2.24: Influence of β_r and χ by David Mašín (2012).

From Figures 2.23 and 2.24 it was seen that R has a similar influence as β_r on the stiffness curve. Therefore, Mašín (2012) recommends to take R as an independent material constant $R = 10^{-4}$, and for controlling the stiffness curve to only use the parameter β_r and take $\chi = 1$ as a material constant.

Parameter calibration for cyclic loading

As previously mentioned, the intergranular strain concept allows the modelling the effects of cyclic loading. When simulating it, it is recommendable to calibrate the parameters against relevant cyclic test data. The usage of this type of data may create difficulties to distinguish between the influence of the individual parameters—see Figures 2.25 and 2.26. From the same figures it can be seen that β_r and χ have the same influence as m_R on the cyclic behaviour.

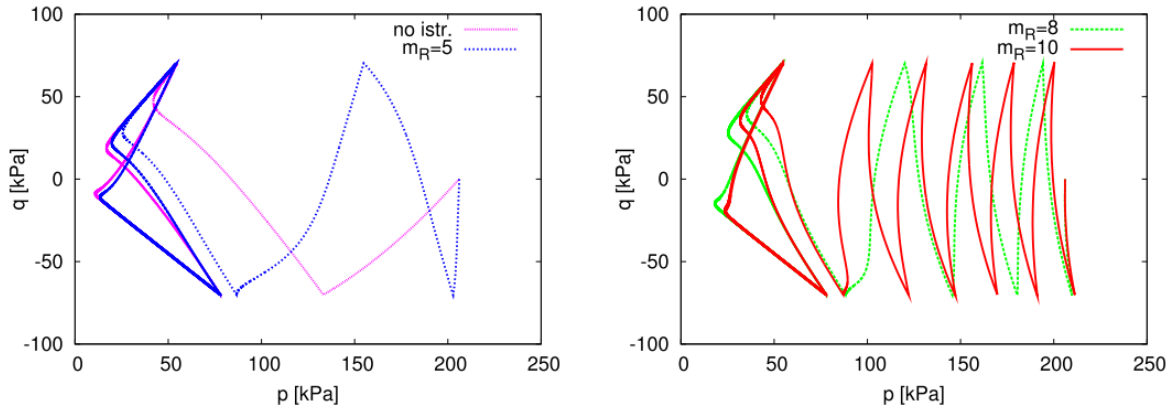

Figure 2.25: Calibration of m_R by David Mašín (2012).

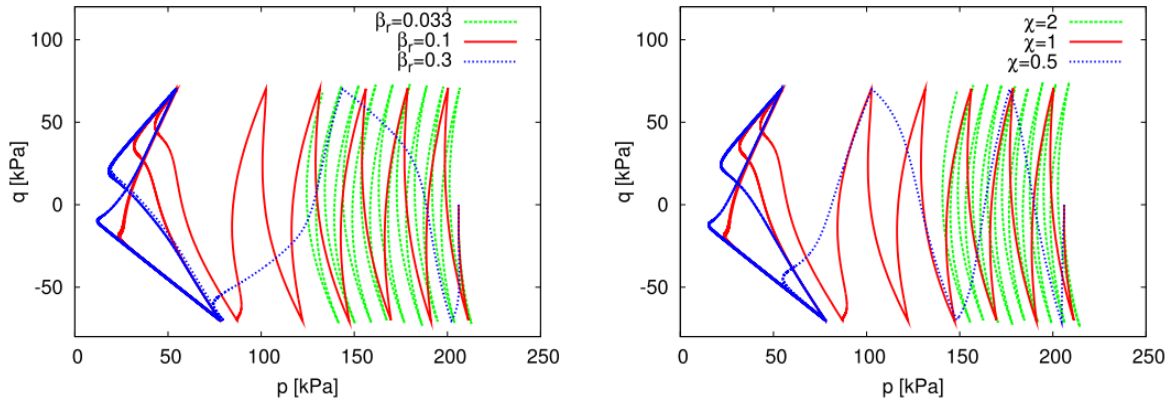

Figure 2.26: Calibration of β_r and χ by David Mašín (2012).

Conclusions regarding intergranular strain concept

Following from the descriptions and calibration of the intergranular strain concept parameters, a simplification to calibrate the model is proposed Mašín (2012):

- R and χ can be treated as independent material constants ($R = 10^{-4}$ and $\chi = 1$)—the values may still need slight calibration for the "best fit";
- m_R can be calibrated using bender element tests or G/G_{max} degradation curves from literature or SHAKE-91 software package created at University of California, Berkeley (SHAKE website of University of California, Berkeley);
- m_T can be approximated by $m_T \approx 0.5 m_R$;
- β_r is the only parameter used to control the cyclic behaviour.

Two examples of parameter sets for sand are given in Table 2.6

Material Name	R [−]	m_R [−]	m_T [−]	β_r [−]	χ [−]
Hochstetten sand	$1 \cdot 10^{-4}$	5	2	0.5	6
Karlsruhe sand	$5 \cdot 10^{-5}$	6.7–12 (pressure dependent)	-	0.3	1

Table 2.6: Intergranular strain concept parameters evaluated by Niemunis & Herle (1997)

Based on the hypoplastic model, the "High Cyclic Accumulation (HCA) Model" was developed by Niemunis (2003) and further used for the assessment of foundations for offshore structures within hybrid models

by Wichtmann *et al.* (2005), Wichtmann *et al.* (2011) and Safinus *et al.* (2011). These hybrid models use the high accuracy of the integrated constitutive model as the implicit procedure (each cycle is individually assessed), to ensure accuracy for the estimated behavioural trends within an explicit empirically based procedure (the cycles are not individually assessed). The results of the finite element modelling were in agreement with centrifuge test data, no field test data was available for verification.

These models are currently the only ones able to assess foundation behaviour to over 10^5 cycles and ensure a certain accuracy of the given results. Therefore, making them the optimum method to assess long term behaviour of foundations to cyclic loads.

CONCLUSION MODELLING APPROACHES

To conclude this section of the second chapter, a comparison between the chosen examples of each of the modelling approaches is shown in Figure 2.27.

Type of Literature / Criteria	Norms, Standards and/or Guidelines			Other Literature, Research	
	API/ISO	DNV	NORSOK	Strain accumulation models	Pore pressure build-up models
Model Type	Empirical	Empirical	focus - steel structure	Hybrid/Constitutive	Hybrid
Foundation Type	Long pipe piles	GBS	Piles	Any	Any - case study on GBS
Soil Type	Sand	Sand	Not mentioned	Sand	Sand
Cyclic loading	-/+	+	-/+	++	++
Displacements/Strain Accumulation	only due to static loading	only due to static loading	-	++	+
Strength and/or Capacity	+	+/-	-	+	+
Stiffness/ Relative density	-	-	-	+	++
Stresses/ Pore pressures	-	+	-	++	++
Limitations	cyclic load "=" quasi-static	effective stress methods - all contributions to pore pressures must be included	Focus - steel components and not soil. Selected criteria ref. steel.(ISO 19901-4 for geotechnical design)	Iterative process - error generation (explicit + control steps). Large number of parameters, soil data for calibration.	Iterative process -error generation (explicit + control steps). Large number of parameters with unclear physical meaning, calibration based on laboratory tests.

Figure 2.27: Comparison of the modelling capabilities of the chosen approaches

2.6 CONCLUSIONS

The literature review revealed that the current standards and norms offer limited guidance with respect to the foundation design for cyclic loading. In order to bridge this gap a significant amount of research has been conducted in the past decades. The leading groups in this research are the Norwegian Geotechnical Institute (NGI), Imperial College of London (ICL), Oxford University, Aalborg University , Karlsruhe Institute of Technology and University of Western Australia. They attempt to provide experimental data and numerical models for the assessment of the effects of long term exposure of foundations to cyclic loading.

The reviewed literature showed that the cyclic loads on an offshore wind turbine are caused by the aerodynamic action of the wind and the automatic pitch angle adjustment for optimum output; and the hydrodynamic action of the waves. There are several methods through which these actions may be assessed, and they have been presented briefly in section 2.2. Chapter 3 of the current document shall focus on the manner through which the provided loading data is assessed.

Research conducted by Byrne & Houlsby (2003) has proven that suction caissons are a viable option as foundations for offshore wind turbines. The main aspects that have been investigated particularly for suction installed caissons refer to penetration and uplift resistance, but which are based on the design of piles (see section 2.3). Additionally, research by Safinus *et al.* (2011), LeBlanc *et al.* (2010) and Byrne & Houlsby (2000) has shown that the design of foundations for offshore wind turbines is generally dominated by serviceability requirements over the 25 year design life and not ultimate limit states.

The foundation response to the applied loading conditions is highly complex. The characteristics of the cyclic actions (e.g. number of applied cycles, average shear stress, cyclic shear amplitude...) have a significant effect on the pore pressure and strain accumulation, strength and stiffness degradation. Each of these phenomena have been presented in section 2.4, whilst the methods of assessing them are more thoroughly presented in section 2.5. Another important aspect is related to the fact that the available research addressing suction caissons within a multi-footing configuration recommends to approximate the cyclic loading to its vertical component due to the "push-pull" effect.

In section 2.5, it becomes obvious that the methods proposed by the API and the DNV are not fully adequate either for cyclic loading, nor for suction installed caissons. Models based on hyperplasticity, hypoplasticity or densification theories give better and more accurate predictions of strain and pore pressure accumulation, respectively strength and stiffness degradation.

In Wichtmann *et al.* (2011) and Wichtmann *et al.* (2005) the High Cyclic strain Accumulation model (HCA), based on the hypoplasticity, has been successfully used to model 10^5 loading cycles for a shallow foundation in sand. The results of the finite element modelling were in agreement with centrifuge test data, as no field test data was available.

Therefore, from the last three mentioned models, the hypoplasticity is the only one that has been used within a structure capable of assessing large numbers of cycles to simulate offshore conditions. Taking this into account, the hypoplastic model is the most adequate one for the assessment of the research topic: "Long term effects of cyclic loading on suction caisson foundations".

The proposed model is thoroughly presented in Chapter 5. The obtained results and their interpretation are available in Chapter 6. Additionally, within the sixth chapter a comparison is made between the obtained results and the methods proposed by the available norms.

Chapter 3

LOADS ON THE WIND TURBINE FOUNDATION

In the second chapter, in sections 2.2 a short overview is provided regarding the applied loads on a wind turbine—see Figure 3.4. The current chapter will provide a more detailed view on the way the loads are considered to act on the foundation within this graduation project. The data are provided by Dong E&P(UK) Ltd. and represents the simulation result for a three leg jacket for UK Round 3, with 6 MW (or more) wind turbine generators with a design life of 25 years.

As the main purpose of the current research is to assess the soil behaviour under cyclic loading and no detailed insight was provided for the determination of the cyclic loads, it will be assumed that they are an adequate representation of the loading history of an offshore wind turbine throughout its design life. Therefore, a brief check of the data and an overview of the theory behind the different actions is given, while the processing of the received vertical loading data into a cyclic load represents the main focus.

Section 3.1 provides insight into how the dead load is calculated.

Section 3.2 shows how the impact of the wind load on the overall structure is assessed. While, Section 3.3 shows how the loads due to waves and current are assessed.

Section 3.4 explains the manner in which all the previously presented loads are transferred as a cyclic load to the individual footings under the jacket structure.

Finally, Section 3.5 draws the conclusions with respect to the loading on the wind turbine foundation considered for this graduation project.

3.1 DEAD LOAD

The dead load of an offshore wind turbine comes from the summation of the structural mass of the individual components, multiplied by the gravitational acceleration, as was already presented in the previous chapter, includes the weight of the following elements—see also Figure 3.1:

- RNA(Rotor Nacelle Assembly), including:
  - rotor, including the hub and the blades;
  - nacelle;
  - top tower adapter;
- superstructure (i.e. turbine tower);
- substructure—in the present case a jacket type structure.

Each of the above elements include also miscellaneous components (e.g. tower internals, secondary steel due to boat-landing etc. . .) which were included in the final mass used by Dong in their calculations. It is considered that the dead load acts in a vertical downward direction and is constant in time.

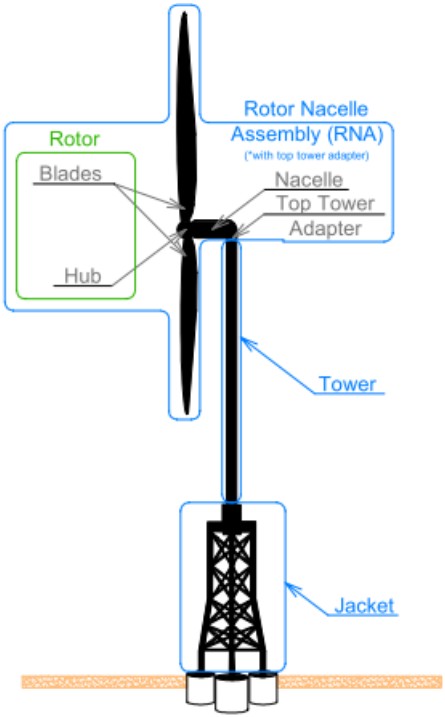

Figure 3.1: Sketch representing the components of the considered offshore wind turbine

Within this thesis, the weight the following components is considered—see Table 3.1.

Structural Element	**Unit of Measurement**	**Mass Value**
(1) Blade	metric ton	25.4
Hub (fully instrumented)	metric ton	76.0
Nacelle mass (excluding top adapter)	metric ton	207
Rotor Nacelle Assembly	metric ton	**360**
Tower	metric ton	**346**
Jacket (submerged)	metric ton	**505**

Table 3.1: Mass of components considered in the calculation of the self weight

3.2 AERODYNAMIC LOADS

As it has already been explained in the previous chapter, the wind conditions have a significant effect on the wind turbine. It is very important to distinguish between two different effects due to wind action:

- the load on the wind turbine rotor—function also of the pitch angle of the blades for optimal output and structural stability;
- the loads on the support structure—due to the direct pressure, suction and possible vortex shedding effects of the wind on the tower shell.

The determining factor for both loads is the wind speed variation and turbulence as a function of height and time. The wind conditions will represent one of the input parameters for the code developed at the Technical University of Denmark "Flex5". The code has incorporated a dynamic wake model that allows for a realistic prediction of the pitch angle changes, and consequently, a full realistic response to wind action.

The following subsections focus on how the assessment of the wind conditions occurs.

3.2.1 WIND MODELLING

A simplified wind assessment considers a uniform, constant wind velocity, i.e. each point of the rotor is acted upon by the same wind velocity. However, a more accurate analysis will consider the spatial and temporal variation of the wind speed and its direction, including turbulence.

Three steady-state spatial characteristics define a wind field:

- Wind shear—represents the variation with height of the wind speed;
- Tower shadow—represents the distortion of the wind flow because of the wind turbine's tower;
- Turbine wake effect—caused by full or partial immersion of the turbine rotor in the wake of another upwind located operating turbine—see Figure 3.2

Figure 3.2: Turbine wake clouds at Horns Rev Wind Farm. Source: Emeis (2010), owned by Vattenfall, photographer Christian Steiness

WIND SHEAR

The variation of wind speed with height, may be assessed with various formulas. For example, in his doctoral thesis, Senders (2008), uses a logarithmic function of the wind profile, by Wortman (1983), depending on the average or reference wind speed, surface roughness length and reference height.

In the loading data provided by Dong, a steady state is assumed and an empirical exponential function is used for the wind profile (Bianchi *et al.* (2007)):

$$V_m(z) = V_m(z_{ref}) \cdot \left(\frac{z}{z_{ref}}\right)^{\alpha} \tag{3.1}$$

where,

V_m is the mean wind speed function of height;

z is the height of the considered point;

z_{ref} is the reference height—generally considered at hub level;

α is the wind shear exponent (surface roughness, terrain dependent).

3D TURBULENCE MODEL

Wind turbulence refers to "all wind speed fluctuations with frequencies above the spectral graph", by Bianchi *et al.* (2007). Generally, wind turbulence has a minor effect on the annual energy output, but major impact on the aerodynamic loads (Bianchi *et al.* (2007)).

Wind turbulence is assessed by means of its power spectrum. As was already mentioned in Section 2.2, Petersen *et al.* (1998) state that the Von Kármán spectrum gives a good description of wind turbulence, but the Kaimal spectrum fits better with the empirical observations and is presently recommended within IEC61400-3 (2005) as one of the standard practices.

For the assessment of wind turbulence, Dong uses in the given data the Kaimal spectrum together with an exponential coherence function.

The Kaimal (1972) spectrum is defined as:

$$\frac{f \cdot S_k(f)}{\sigma_k^2} = \frac{4 \cdot f \cdot L_k/V_{hub}}{(1 + 6 \cdot f \cdot L_k/V_{hub})^{5/3}} \tag{3.2}$$

where:

f represents the frequency, measured in $[Hz]$;

k is an index referring to the wind velocity component (1—along the main wind direction, 2—to the left as seen along the main wind direction, 3—upwards);

S_k is the one sided spectrum for the k^{th} velocity component;

σ_k is the standard deviation of the k^{th} velocity component;

$$\sigma_k^2 = \int_0^{\infty} S_k(f) df \tag{3.3}$$

L_k is the integral length scale parameter for the k^{th} velocity component and is a function of a turbulence scale parameter (Λ_1);

V_{hub} is the mean velocity at hub height, measured in $[m/s]$.

In order to account for spatial correlation of the velocity along the main wind direction, Dong uses an exponential coherence model together with the Kaimal spectrum:

$$Coh(r,f) = \exp\left[-12\left(\left(\frac{f\cdot r}{V_{hub}}\right)^2 + \left(0.12\cdot\frac{r}{L_1}\right)^2\right)\right] \tag{3.4}$$

where:

r represents the magnitude of the projection of the separation vector between the two considered points in the coherence function on a plane normal to the considered main wind direction.

IEC TRANSIENTS

In order to assess the variation of the speed, shear and direction of the wind, Dong uses the definition of the transient states according to IEC61400-3 (2005). The final given vertical load data includes the simulation of transient changes in wind speed, direction, horizontal and vertical shear.

For the operational conditions of the wind turbine, a two-parameter Weibull distribution of the wind speed is assumed—see equation 3.5, source Bianchi *et al.* (2007). The Weibull distribution is a probability density function which reveals that mean wind speeds of large magnitude rarely occur, while moderate ones have a higher frequency.

$$p(V_m) = \frac{k}{C}\left(\frac{V_m}{C}\right)^{k-1}\cdot e^{-(V_m/C)^k} \tag{3.5}$$

where:

V_m is the mean wind speed;

k is the shape coefficient;

C is the scale coefficient.

The coefficients k and C are adjusted to match the particular wind data characteristic for the considered site.

3.2.2 AERODYNAMIC LOADS ON THE BLADES

The aerodynamic loads within the FLEX5 code are calculated using the Blade-Element-Momentum theory (BEM), modified so that it includes a dynamic wake model. Wake effects may be seen in Figure 3.2 on page 61. Therefore, a more realistic prediction of the response due to the changes of the pitch angle is obtained.

The BEM theory is used to derive the expressions for the captured power, developed torque and axial thrust force. The captured energy is dependent on the developed torque. Torque develops due to the tangential components of the lift (F_L) and drag forces (F_D) acting on the turbine blades.

The lift force is perpendicular to the local wind direction and the drag force follows the local wind flow direction—see Figure 3.3. And both depend on the relative wind velocity (V_{rel}) and the angle of the blade with respect to the wind direction, also known as pitch angle. It must be kept in mind that higher wind speeds generate more energy (Bianchi *et al.* (2007)) but may also determine a change in pitch angle.

Finally, the thrust force is composed of the axial components of the lift and drag forces. The thrust force can be the source of large overturning moments at foundation level Houlsby *et al.* (2005b).

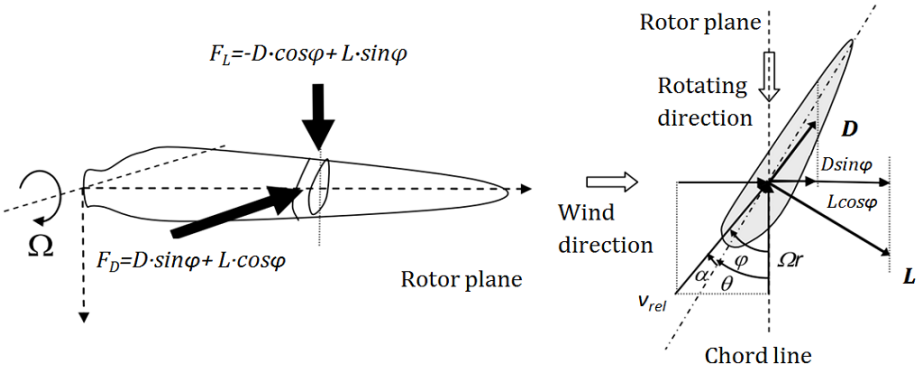

Figure 3.3: Lift and drag forces on the turbine blade. Source: Senders (2008)

3.2.3 CONCLUSIONS AERODYNAMIC LOADS

To conclude this section regarding aerodynamic loads it is important to remember that the source is the wind action. But, the aerodynamic loading has two components: the thrust force, due to aerodynamic loads on the blades and the force resulting from the direct wind action on the tower shell. The wind speed and direction are determining factors particularly for the magnitude of the thrust force, while the wind direction does not play a significant role for the tower shell itself, due to symmetry.

The wind speed varies in space and time. The variation of wind speed with height is called wind shear and is assessed in the given data with an exponential empirical function. The fluctuations of the wind above the spectral graph are called wind turbulence and are analysed by using a Kaimal spectrum and a coherence function in order to account for spatial correlation of the velocity along the main wind direction. For operational conditions over the design life of 25 years a Weibull distribution is assumed for the wind speed and energy variation.

Finally, in order to assess the variation of the speed, shear and direction of the wind, for the given data the transient states according to IEC61400-3 (2005) were used. The given vertical load data include the simulation of transient changes in wind speed, direction, horizontal and vertical shear over a design life of 25 years.

3.3 HYDRODYNAMIC LOADS

As already mentioned in section 2.2, hydrodynamic loads are due to the resulting water particle velocities and accelerations caused by waves and water current. The resulting velocities and accelerations will vary in space and time. The methods to analyse wave and current velocities are also highly documented in the mentioned codes and norms DNV (2004), NORSOK (2002), API (2011). In the following sections the basis of the considerations taken by Dong to assess the hydrodynamic loading is presented.

3.3.1 CURRENT

Water currents are caused by temperature differences within the water mass and include also tidal waves caused by the force of the moon and sun. In the case of offshore wind turbines, it is the surface currents (up to 400 m deep) that play a major role. They vary in space and time, but the scale of this variation is very large when compared to the spatial and temporal dimensions considered for an offshore wind turbine. Therefore, it is often assumed that the current is a horizontal uniform flow field of water, where the velocity is a function of the vertical coordinate and there is no acceleration.

For the assessment of current speed, a power law profile as described by Soulsby (1997) is often used—see equation 3.6.

$$\nu_{cur}(z) = \begin{cases} \nu_{c.ref} \left(\dfrac{z}{0.32 \cdot z_w} \right)^{1/7} & for\ 0 < z \leq 0.5 \cdot z_w \\ 1.07 \cdot \nu_{c.ref} & for\ 0.5 \cdot z_w < z \leq z_w \end{cases} \tag{3.6}$$

where:

z represents the depth of the point at which the current velocity is calculated;

z_w represents the distance from the mudline to the water surface;

$\nu_{c.ref}$ represents the reference current velocity at the water surface (z_w).

Within the given data, all currents were applied in line with the wave propagation and superimposed on the wave kinematics. The considered current at sea surface for all sea states analysed was 0.5 m/s. While for the extreme events, a depth averaged current of 1.1 m/s was used.

The following section will present how the wave spectra were assessed.

3.3.2 WAVES

Ocean waves are of the Rayleigh surface type, where water particles move in an orbital motion due to the action of the wind. Stronger winds will determine higher waves as the friction force between the air and water particles increases. In design, wave spectra are considered which according to Michel (1968) represent the distribution of the total energy of the sea with respect to the frequencies of the various wave components . Which are defined for a specific location and climate, considering the statistical properties to remain constant over a period of three hours. For the assessment of wave spectra, there are two recommended standard formulations: the Pierson-Moskowitz wave spectrum and the JONSWAP (Joint North Sea Wave Project) wave spectrum. Both are described with the aid of the significant wave height (H_s) and the mean zero-crossing wave period (T_z).

The Pierson-Moskowitz spectrum is for fully developed seas assuming steady wind blows for long time periods and large areas.

The JONSWAP (Joint North Sea Wave Project) wave spectrum is a fetch limited version of the Pierson-Moskowitz spectrum assuming a continuous non-linear interaction between waves over a long period of time. It is based on wave measurements conducted in 1968–1969 during the Joint North Sea Wave Project. Thus, fully adapted to the North Sea conditions. Based on the wave spectrum a relation of the wave height to wave velocity and acceleration is determined. Having determined the fluid field, Morison's equation (Journée & Massie (2001)) is used to approximate the wave loads on a slender body using wave kinematics: the undisturbed fluid velocity (U), and the acceleration of the fluid (dU/dt):

$$F = \frac{1}{2} C_d |U| U + C_m \rho \frac{\pi D^2}{4} \frac{dU}{dt} \tag{3.7}$$

In the above equation the wave force has two components: the drag component, introduced by the drag coefficient (C_d) and the inertia part, introduced by the inertia coefficient(C_m). Where, ρ is the water density and D is the diameter of the cylinder.

A JONSWAP spectra with 500 wave components was considered for operational and extreme conditions by Dong E&P (UK) Ltd. for UK Round 3. The specific values can be found in Table 3.2 and 3.3.

Wind speed $[m/s]$	**Significant wave height** (H_s $[m]$)	**Period** (T_p $[s]$)
(0–3)		
4(3–5)	0.79	5.6
6(5–7)	0.9	5.79
8(7–9)	1.07	6.06
10(9–11)	1.3	6.42
12(11–13)	1.59	6.84
14(13–15)	1.93	7.32
16(15–17)	2.34	7.84
18(17–19)	2.8	8.4
20(19–21)	3.32	8.99
22(21–23)	3.9	9.61
24(23–25)	4.54	10.25

Table 3.2: Operational wave loads for fatigue assessment, by Dong E&P (UK) Ltd. for UK Round 3

Water Depth LAT	40 m
50 year water level	43.1 m
$H_{max,50yr}$	14.4 m
$H_{s,50yr}$	7.5 m
$T_{p,50yr}$	12.6 s

Table 3.3: Characteristics of the 50 year storm wave load conditions considered by Dong E&P (UK) Ltd. for UK Round 3

The above mentioned characteristics were implemented in the computer program “Flex5” for the determination of data received from Dong E&P (UK) Ltd. for UK Round 3.

3.3.3 CONCLUSIONS HYDRODYNAMIC LOADING

To conclude this section regarding hydrodynamic loading it is important to remember that there are two main components: the action of the current and waves. Both of the two components vary in space and time. But as the domain of variation for the current is much larger than that of the considered problem, it shall only be considered to vary with water depth. Therefore it will not have a significant role in the cyclic loading of the wind turbine foundation. In the given data, all currents have been applied in the same propagation direction as the waves.

The variation of waves is directly linked to the variation of wind—see Table 3.2. The analysis of the wave spectra in both operational and extreme conditions is done with the aid of the JONSWAP spectrum, based on wave measurements carried out in the North Sea. Waves will have a major influence on the period of the cyclic loading applied to the turbine foundation.

Finally, the given vertical load data results from considering both waves and current over the design life of 25 years. But, when processing this data, the waves will have a significant role in determining the period of the cyclic loading.

3.4 LOADING CHARACTERISTICS

This section presents first the given data by Dong E&P, as a result of the above mentioned analysis and considerations. Finally, it shows the method used to assess this data and transform it into the applied load on the suction caissons.

3.4.1 GIVEN DATA

In the previous sections the principles used to calculate the provided data were presented. In the following paragraphs, the results of the simulations carried out by Dong E&P (UK) Ltd. are presented. This data was provided in numerical form containing the mean vertical load, the range between which it varied and how many occurrences were counted throughout 25 years.

In a simplified manner one can see in Figure 3.4 all the considered loads acting on a wind turbine and the considered arrangement of the suction caissons with respect to the direction of loading. The given load data is considered to be at the connection of the jacket leg with the corresponding caisson (at seabed level).

Sorted by increasing order of the vertical mean load, the data can be seen in Figures B.1, B.2 and B.2, respectively for the horizontal load in Figures B.4, B.5 and B.5 in Appendix B. In these figures it can be assumed that the extremes represent the loading resulting from extreme conditions, such as the 50 year design storm.

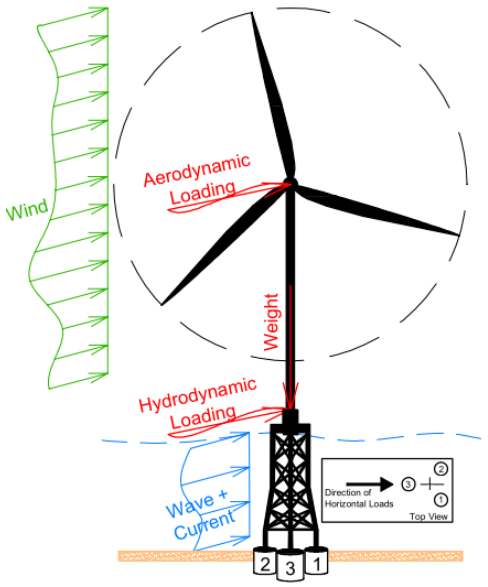

Figure 3.4: Sketch of loading conditions on an OWT and positioning of caissons with respect to the direction of loading

3.4.2 DATA ANALYSES

Upon analysing the given numerical data in more detail the following observations were made with respect to the number of occurrences :

- 97.5% of the mean compressive vertical loads can be found in the interval 2700–6600 kN (see Figure 3.5), values exceeding this range may be assumed to correspond to extreme conditions;
- 47.5% of the mean vertical loads for caisson 3 are in tension (negative values — see Figure 3.5);
- 97.5% of the ranges of variation of the mean vertical load (2· Amplitude) are bellow 3400 kN (see Figure 3.6), values exceeding this range may be assumed to correspond to extreme conditions;

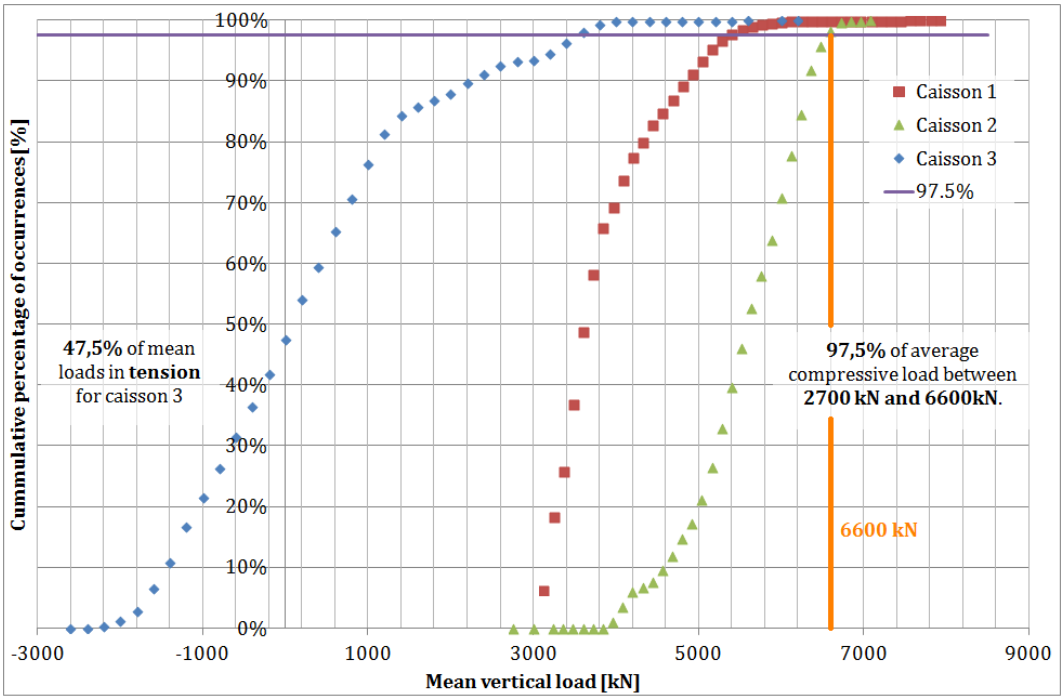

Figure 3.5: Distribution function of vertical mean loads for caissons 1, 2 and 3

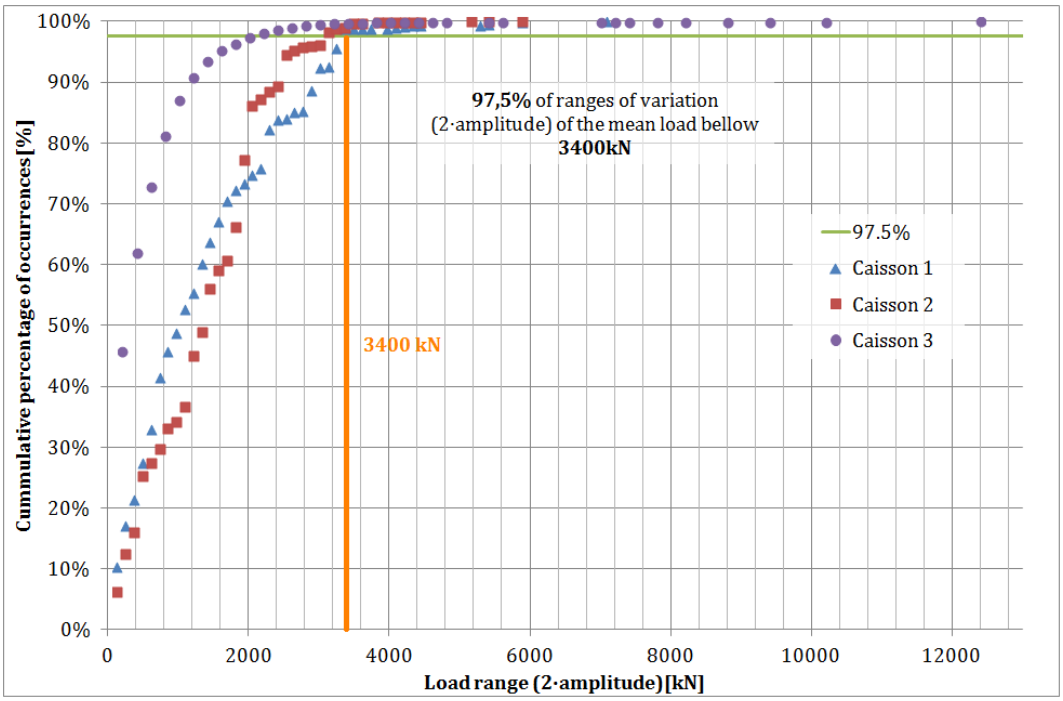

Figure 3.6: Distribution function of the ranges of variation for the vertical mean loads for caissons 1, 2 and 3

- 97.5% of the horizontal loads can be found in the interval 0–360 kN (see Figure 3.7), values exceeding this range may be assumed to correspond to extreme conditions.

The following sections shall present the considered extreme and operational loads and the manner through which they will be used within the following phases of the project.

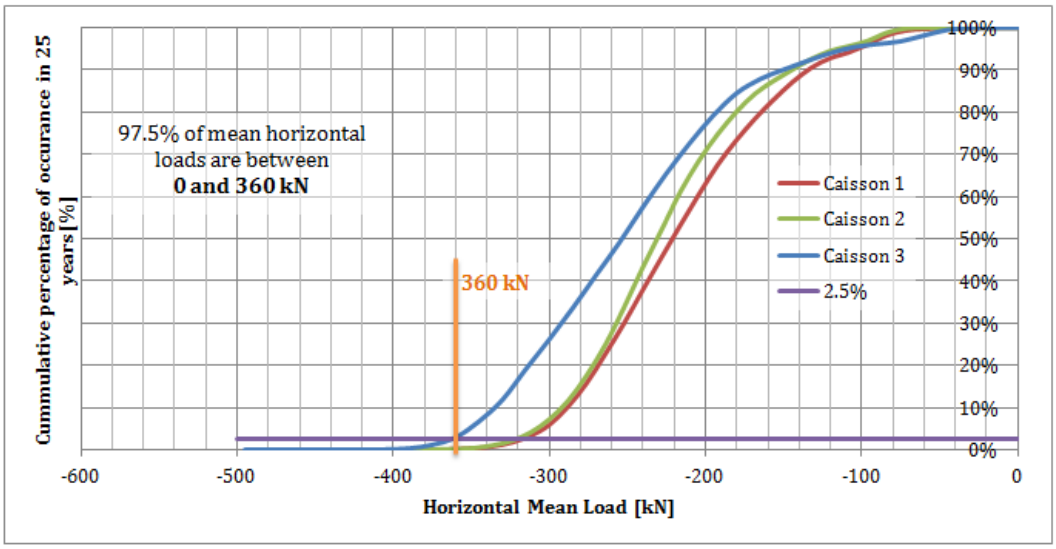

Figure 3.7: Distribution function of horizontal mean loads for caissons 1, 2 and 3

3.4.3 EXTREME CONDITIONS

For extreme conditions, the representative event is considered to be the 50 year design storm as required by DNV (2004). This is generally done by using the Hansteen distribution—see Table 3.4 (*only the first half is presented due to symmetry reasons). This distribution ensures the build-up to the "monster wave" that dominates the 50 year design storm.

The extreme loads provided by Dong E&P are based on the absolute maximum loads, with a partial safety factor of 1.35, and they have generally a very short time period, typically below 1 second. These extreme loads (see Table 3.5) will be considered in designing the caisson.

Step [-]	**Number of waves** [-]	**Loading percentage** [%]
1	900	20
2	500	37
3	200	49
4	90	58
5	50	64
6	30	70
7	15	77
8	8	82
9	4	89
10	2	96
11	1	100

Table 3.4: Hansteen distribution for a 6 hour storm

Vertical Compression $[kN]$	**Vertical Tension** $[kN]$	**Horizontal** $[kN]$
24600	20200	3300

Table 3.5: Maxima of extreme loads (see Figures B.11, B.12 and B.13) including safety factors

In Chapter 4 of this thesis it will become clear that the horizontal load is not significant when compared to the

lateral capacity of the caisson, as the design will be dominated by the vertical loads rather than the horizontal ones.

3.4.4 OPERATIONAL CONDITIONS

For the determination of the operational loading conditions the following two steps were taken: a clustering of the given data for vertical and horizontal loading and a procedure for the determination of the period corresponding to these loads.

DATA CLUSTERING

Following the results presented in the section 3.4.2, a clustering analysis was done in order to concentrate the loading data into a data set that is more easily implemented within the model. For each caisson, based on the number of occurrences four large cases were created based on the clustering of the mean loads. Furthermore, for each vertical mean load case, subcases clustering the amplitudes were also created. For all cases and subcases the percentage of occurrence was calculated:

- for a case X: $P(case.X) = \frac{N_{occurrences.X}}{N_{total}}$ [%];
- for a subcase Y of case X: , $P(subcase.Y) = \frac{N_{occurrences.Y}}{N_{occurrences.X}}$ [%].

These results can be found in Appendix B, for vertical loads in Figure B.7, Figure B.8 and Figure B.9, respectively in Figure B.10 for the horizontal loads of all three caissons. In chapter 4 it will become clear that the horizontal loads are significantly smaller than the actual caisson capacity and their influence on the caisson capacity may be disregarded.

The assumptions made to determine the level of relevance for each case are based on:

- a higher number of occurrences increases the relevance of the case and/or subcase;
- assuming the same frequency, a higher cyclic amplitude is expected to create more damage than a lower cyclic amplitude;
- as long as the behaviour is in the compressive range, a higher mean compressive load is expected to cause more displacement than a lower one;
- loading in the tensile region is critical—in practice it is avoided through applying ballast and thus increasing the weight so that loading remains in the compressive region.

Therefore, the representative cases for operational conditions for caisson 1 can be found in Table 3.6, for caisson 2 in Table 3.7 and for caisson 3 in Table 3.8.

Case ID (Percentage of	occurrence[%])	**Mean load [kN]**	**Average Amplitude [kN]** (Percentage of occurrence[%])
A	3		270 (46.4%)
(65.86%)	9	3744	1350 (33.9%)
B	3		270 (55.7%)
(30.85%)	6	5148	750 (34.2%)

Table 3.6: Load cases for caisson 1, operational conditions

Following from Tables 3.6, 3.7 and 3.8, it is not just the individual caisson foundation capacity, but also based on similarities of the percentages of occurrence, one may consider a first operational loading case (including subcases A, G, J) and a second one (B, F, I) that allow for the estimation of the tilt angle based on the differential settlements of each foundation.

Case ID (Percentage of	occurrence[%])	**Mean load [kN]**	**Average Amplitude [kN]** (Percentage of occurrence[%])
F	3		270 (49.4%)
(21.12%)	6	4914	750 (32.3%)
G	3		270 (55.7%)
(74.71%)	6	6318	750 (34.2%)

Table 3.7: Load cases for caisson 2, operational conditions

Case ID (Percentage of	occurrence[%])	**Mean load [kN]**	**Average Amplitude [kN]** (Percentage of occurrence[%])
I	3		550 (99.4%)
(6.52%)	2 (max)	-2535	1000(99.4%)
J	3		650 (98.6%)
(70.53%)	2 (max)	0	1200 (98.6%)

Table 3.8: Load cases for caisson 3, operational conditions

PERIOD OF CYCLIC LOADING

The given data by Dong E&P (UK) Ltd. contained only the information in Table 3.2 relating the wind and wave loads to their period. For the given numerical data, it was not disclosed which loading conditions were assumed for each specific state. Therefore, no direct information exists with respect to the period or frequency of the vertical loads in operational conditions. In storm conditions, the frequency of the vertical load is considered to be 0.3 Hz, as it was disclosed during follow-up communication.

In order to provide a realistic estimate of the period for the loads in operational conditions, the public meteo files provided by the NoordzeeWind joint venture (`http://www.noordzeewind.nl/en/knowledge/reportsdata/`) from the years 2007–2008 were used. Noordzee Wind has been carrying out measurements as part of the Offshore Windpark Egmond aan Zee (OWEZ) project, containing 36 wind turbines of 3 MW each. The project is located 10–18 km from the coast at Egmond aan Zee, The Netherlands. The measurement devices are placed on a 116 m meteorological mast at three heights: 21 m, 70 m, 116 m (Eecen *et al.* (2006)).

The height of the measurement mast is smaller than the height of the considered 6 MW turbine and the location is more north. Nonetheless, upon checking the variation of the wind speed with height (Eecen *et al.* (2006)), it was observed that no significant increase in wind speed occurred from the measurement device at 70 m to the one at 116 m. Thus, it will be assumed that these measurements may be extrapolated to the present case. A summary of the percentages of occurrences from the measuring devices at 116 m, per wind speed interval, throughout the months of the years 2007 and 2008 can be found in Figure 3.8. Unfortunately, the measurements from the years 2009–2010 are not reliable due to malfunctioning of the measurement device. From the Figure 3.8 one can observe that the wind speeds with the highest occurrence percentage are up to 15–17 m/s. Keeping in mind these percentages and the ones related to the number of occurrences of the mean loads in Tables 3.6, 3.7 and 3.8 one can make an assumption of the correspondence between the vertical loads and their associated wind speeds.

Table 3.2 shows the associated significant wave height and period for each wind speed interval. It was disclosed that under operational conditions, for the vertical load, the associated period is a value between the wind and wave period. In absence of more information, a conservative assumption will be taken: the period of the vertical load will be considered to be equivalent to the wave period. Therefore, the assumed period will be shorter than its actual period: the wind period is quite large (minimum of 30–50 s return period) compared to

2007	Wind Speed Intervals [m/s]												
	0-3	3-5	5-7	7-9	9-11	11-13	13-15	15-17	17-19	19-21	21-23	23-25	Total
January	1,73%	4,67%	7,44%	10,49%	13,03%	18,37%	16,71%	16,25%	7,46%	1,90%	1,09%	0,86%	100,00%
February	6,26%	11,46%	18,64%	27,13%	19,45%	10,33%	4,76%	1,79%	0,18%	0,00%	0,00%	0,00%	100,00%
March	5,53%	9,13%	18,37%	21,87%	16,08%	12,10%	8,93%	4,36%	3,29%	0,33%	0,00%	0,00%	100,00%
April	4,78%	23,12%	33,57%	21,32%	12,57%	4,53%	0,12%	0,00%	0,00%	0,00%	0,00%	0,00%	100,00%
May	12,20%	14,04%	17,47%	18,86%	16,69%	12,68%	6,75%	1,23%	0,09%	0,00%	0,00%	0,00%	100,00%
June	11,36%	21,50%	25,28%	21,47%	10,18%	5,29%	2,70%	1,85%	0,37%	0,00%	0,00%	0,00%	100,00%
July	6,28%	10,72%	16,55%	21,29%	17,66%	15,94%	8,00%	2,54%	0,85%	0,12%	0,06%	0,00%	100,00%
August	11,15%	16,47%	26,83%	20,10%	14,37%	5,09%	4,27%	1,72%	0,00%	0,00%	0,00%	0,00%	100,00%
September	6,70%	10,07%	11,71%	18,00%	18,75%	17,07%	13,21%	3,93%	0,52%	0,04%	0,00%	0,00%	100,00%
October	10,91%	16,18%	28,15%	22,27%	11,08%	6,84%	2,70%	1,88%	0,00%	0,00%	0,00%	0,00%	100,00%
November	3,34%	9,51%	15,58%	16,50%	16,96%	15,89%	12,36%	6,26%	3,08%	0,42%	0,09%	0,00%	100,00%
December	7,61%	12,24%	15,80%	10,09%	9,53%	13,95%	16,96%	7,33%	5,65%	0,76%	0,07%	0,00%	100,00%
Average/Year	7,32%	13,26%	19,62%	19,11%	14,70%	11,51%	8,12%	4,10%	1,79%	0,30%	0,11%	0,07%	
Cummulative	7,32%	20,58%	40,19%	59,31%	74,01%	85,51%	93,64%	97,73%	99,52%	99,82%	99,93%	100,00%	
2008	Wind Speed Intervals [m/s]												
	0-3	3-5	5-7	7-9	9-11	11-13	13-15	15-17	17-19	19-21	21-23	23-25	
January	0,17%	3,03%	5,55%	12,02%	21,94%	22,66%	17,57%	10,89%	3,87%	2,31%	0,00%	0,00%	100,00%
February	7,81%	15,97%	10,90%	10,61%	9,16%	8,62%	11,66%	9,24%	7,55%	5,37%	2,55%	0,56%	100,00%
March	5,34%	8,09%	10,77%	15,72%	18,54%	16,13%	12,86%	6,81%	2,96%	1,79%	0,94%	0,07%	100,00%
April	9,95%	17,51%	24,74%	24,05%	13,14%	8,93%	1,42%	0,26%	0,00%	0,00%	0,00%	0,00%	100,00%
May	4,19%	19,38%	31,97%	26,07%	11,54%	4,73%	2,01%	0,11%	0,00%	0,00%	0,00%	0,00%	100,00%
June	12,43%	26,54%	21,39%	15,40%	15,18%	4,51%	3,24%	1,22%	0,10%	0,00%	0,00%	0,00%	100,00%
July	10,97%	19,67%	20,10%	22,42%	12,82%	7,47%	3,70%	2,61%	0,24%	0,00%	0,00%	0,00%	100,00%
August	4,35%	12,85%	19,96%	17,15%	19,64%	12,76%	5,55%	5,27%	1,61%	0,69%	0,16%	0,00%	100,00%
September	10,22%	19,29%	18,49%	19,02%	8,88%	10,37%	8,32%	4,71%	0,71%	0,00%	0,00%	0,00%	100,00%
October	5,75%	10,18%	14,41%	22,22%	18,54%	10,13%	8,04%	6,84%	1,98%	0,68%	1,18%	0,05%	100,00%
November	4,86%	11,34%	13,21%	20,76%	20,79%	10,21%	10,58%	5,19%	1,66%	1,06%	0,20%	0,13%	100,00%
December	5,05%	14,62%	18,05%	20,24%	23,72%	10,60%	4,39%	2,11%	1,23%	0,00%	0,00%	0,00%	100,00%
Average/Year	6,76%	14,87%	17,46%	18,81%	16,16%	10,59%	7,44%	4,60%	1,82%	0,99%	0,42%	0,07%	
Cummulative	6,76%	21,63%	39,09%	57,90%	74,06%	84,65%	92,09%	96,70%	98,52%	99,51%	99,93%	100,00%	

Figure 3.8: Percentages of measured wind speeds from the public meteo files provided by the NoordzeeWind joint venture (`http://www.noordzeewind.nl/en/knowledge/reportsdata/`) from the years 2007–2008

the period of the waves (5–12 s). To conclude, a combination of the two will certainly result in a period larger than the wave period.

Therefore, for the cases defined in the Tables 3.6, 3.7 and 3.8, the associated wind speed and period can be seen in Table 3.9.

Case ID (Percentage of	occurrence[%])	**Mean load [kN]**	**Amplitude [kN]** (Percentage of occurrence[%])	**Wind speed [m/s]**	**Associated period [s]**
A	3 (avg)		270 (46.4%)	13–15	7.32
(68.5%)	9 (avg)	3744	1350 (33.9%)	13–15	7.32
B	3 (avg)		270 (55.7%)	15–17	7.84
(30.85%)	6 (avg)	5148	750 (34.2%)	15–17	7.84
F	3 (avg)		270 (49.4%)	15–17	7.84
(21.12%)	6 (avg)	4914	750 (32.3%)	15–17	7.84
G	3 (avg)		270 (55.7%)	13–15	7.32
(74.71%)	6 (avg)	6318	750 (34.2%)	13–15	7.32
I	3 (avg)		550 (99.4%)	17–19	8.4
(10.83%)	2 (max)	-2535	1000(99.4%)	17–19	8.4
J	3 (avg)		650 (98.6%)	13–15	7.84
(70.53%)	2 (max)	0	1200 (98.6%)	13–15	7.84
K	3 (avg)		700 (98.9%)	15–17	7.84
(18%)	2 (max)	3705	1300 (98.9%)	15–17	7.84

Table 3.9: Load cases and characteristics, operational conditions

Additionally, samples of 300 s duration for the harmonic loading functions can be seen in the Figures B.14, B.15 and B.16 in Appendix B. These were created with the following formula: $F(t) = A + B \cdot \sin(\omega \cdot t)$. Where:

$F(t)$ represents the vertical loading function, dependent on time (t); A is the average vertical load, defined as mean in Table 3.9; B is the amplitude of the vertical load, defined as amplitude in Table 3.9; ω is the load frequency, be computed as $\omega = 2 \cdot \pi / T_s$, where T_s is the period defined in Table 3.9.

LOAD CHECK

In order to verify the values of the given loads, a rough check was made considering the 6 MW wind turbine and a wind speed of 16 m/s. Simplifying structural assumptions were made; such that the foundations are infinitely stiff and reducing the three-legged jacket to a two foundation system where one is in tension (representing caisson 3) and the other in compression (representing caissons 1 and 2).

The applied loading conditions (as presented in Figure 3.4) were considered for the 16 m/s wind speed, 2.34 m significant wave height with a period $T_p = 7.84\ s$. These conditions resulted in two overturning moments redistributing the weight of the turbine as follows:

- caissons 1 and 2 have a vertical reaction force varying between 3800–5900 kN;
- caisson 3 between 100–4000kN.

These values are similar to the ones identified in Table 3.9 and corresponding to the same wind speed (16 m/s): for caisson 1–case B (3960–5280 kN); caisson 2–case F (3960–5040 kN); caisson 3–case K (1400–3800 kN). The reasons for having the interval boundaries larger can be due to the simplifications made in the calculation.

Additionally, this rough verification of the loads confirmed that the variation of the overturning moment due to the variation of the wind speed in time, has a more significant contribution to the period of the vertical reactions on the caissons, than the overturning moment due to waves (see Figures 3.9 and 3.10).

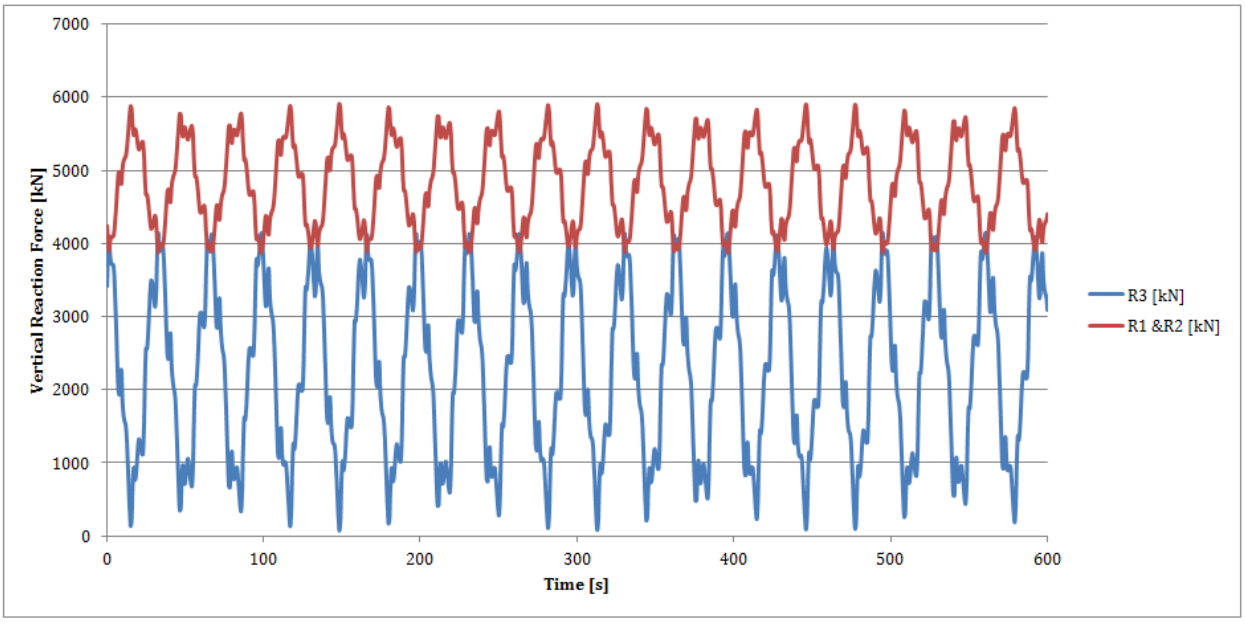

Figure 3.9: Rough verification of vertical reaction forces corresponding to a 16m/s wind

3.5 CONCLUSIONS

To conclude this section it is important to know that the loading data was provided by Dong E&P (UK) Ltd. and the first three sections of this chapter give a rough overview of the principles and methods used to obtain this data. The last section presents the method through which this data is analysed and transformed to fit the

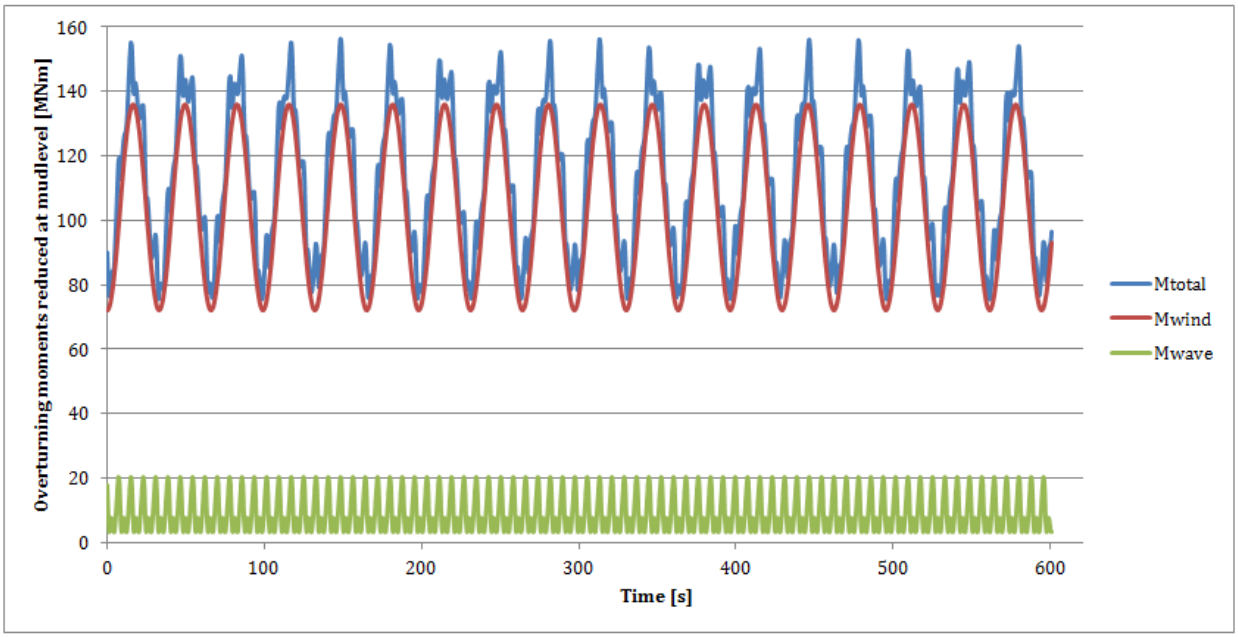

Figure 3.10: Rough estimation of overturning moments due to wind and wave loading

purpose of this research.

The loads acting on the wind turbine and transmitted to the foundation are the dead load, the aerodynamic loading and the hydrodynamic loading. The dead load of an offshore wind turbine comes from the self weight of the structure itself, as described in section 3.1.

The source of the aerodynamic load is the wind action. But, the aerodynamic loading has two components: the thrust force, due to aerodynamic loads on the blades and the force resulting from the direct wind action on the tower shell. In the analysis of wind speed, one must assess the wind shear and wind turbulence. The given vertical load data include the simulation of transient changes in wind speed, direction, horizontal and vertical shear over a design life of 25 years.

There are two main components of hydrodynamic loading: the action of the current and waves. Both components vary in space and time. But as the domain of variation for the current is much larger than that of the considered problem, it shall only be considered to vary with water depth. The variation of waves is directly linked to the variation of wind—see Table 3.2. The analysis of the wave spectra in both operational and extreme conditions is done with the aid of the JONSWAP spectrum.

The given data by Dong E&P (UK) Ltd. was analysed based on the number of occurrences and the following remarks were made:

- 97.5% of the mean compressive loads can be found in the interval 2700–6600 kN (see Figure 3.5), values exceeding this range may be assumed to correspond to extreme conditions;
- 47.5% of the mean loads for caisson 3 are in tension (negative values — see Figure 3.5);
- 97.5% of the ranges of variation of the mean load (2· Amplitude) are bellow 3400 kN (see Figure 3.6), values exceeding this range may be assumed to correspond to extreme conditions;
- 97.5% of the horizontal loads can be found in the interval 0–440 kN (see Figure 3.7), values exceeding this range may be assumed to correspond to extreme conditions.

Following from these statistics, the data was clustered into several groups and the results can be found in Appendix B, for caisson 1 in Figure B.7, caisson 2 in Figure B.8 and caisson 3 in Figure B.9, and for the horizontal loads in Figure B.10.

For extreme conditions it was found that the caissons must be designed to withstand a maximum compressive vertical force of 24600 kN, tensile vertical force of 20200 $kN$and a maximum horizontal load of 3300 kN. Generally storm conditions are analysed using a Hansteen storm distribution.

For operational conditions, based on the probabilities of occurrence of these cases, the most representative ones were chosen to be further used in analyses. The associated wind speeds for these cases were determined based on a correlation between probabilities of occurrence of measured wind data from the NoordzeeWind project and the loads' probabilities. Under these conditions, for the vertical load, the associated period is a combination of the wind and wave period, which was confirmed within a rough load assessment. Yet, in absence of more information, a conservative assumption was taken: the period of the vertical load is considered to be equivalent to the wave period. The assumed period will be shorter than its actual period, allowing for less pore pressure dissipation within the sand mass, causing a potentially faster development towards failure.

Case ID (Percentage of occurrence[%])	**Mean load [kN]**	**Amplitude [kN]**	**Wind speed [m/s]**	**Associated period [s]**
OP 1 (68.5%)	3744	800	13–15	7.32
OP 2 (74.7%)	6318	500	13–15	7.32
OP 3 (70.5%)	0	650	13–15	7.32

Table 3.10: Representative case for operational loading conditions

Considering the limited amount of time for performing the analyses, the final operational representative load case is considered to be the one in Table 3.10. The method through which these loads will be applied in the model will be presented in Chapter 5 of the report. Additionally, several other loading scenarios will be presented in Chapter 5. The aim of those scenarios will be to investigate the model and foundation sensitivity to changes in mean load, cyclic amplitude, period of the cyclic loading or consolidation coefficient.

Chapter 4

SUCTION CAISSON FOUNDATIONS

This chapter provides more information related to suction caisson foundations. A preliminary design of a suction caisson is made with the use of the existing design standards. This design is further used in the analyses carried out through this thesis. Even though the very dense sand sample shall not be analysed using the proposed model due to insufficient data, estimations for the capacity of the caisson embedded within it are made in order to draw a parallel with respect to the medium dense sand.

Section 4.1 gives a review of the previously presented information related to suction caissons, the available types of suction caissons, typical geometrical characteristics, and a brief review of the applied loading conditions.

Section 4.2 is the largest part of this chapter, presenting the principles on which the design of suction caissons is based: in-place capacity, installation and retrieval analyses. The results of applying these design principles to the current case are also given in this section.

Finally, Section 4.3 closes the chapter and presents the main conclusions of the fourth chapter.

4.1 INTRODUCTION

In Chapter 1, section 1.2 of this thesis an overview of the presently used offshore wind turbine foundations is given. The most important design factors are presented, as found by Feld (2004): "soil condition, water depth, possible erosion, size and type of wind turbine and environmental actions (wave height, current, ice etc.) [...] the selection of the concept is highly influenced by a keen desire to achieve the lowest cost development ...".

Within the same section, caisson foundations are classified as intermediate foundations due to their embedment ratio ($\lambda = L_{emb}/D$) which is between the one for shallow foundations ($\lambda < 1$) and pile foundations ($\lambda > 10$).

In Chapter 1 the aspects to be considered in designing suction caisson foundations for an offshore wind turbine are mentioned: installation, long term performance under static and/or cyclic loading conditions and removal. Almost all the previously mentioned issues have more or less satisfactorily developed design methods, except for long term performance. However, Safinus *et al.* (2011) and Jardine *et al.* (2012) emphasize that the design of the foundation of an offshore wind turbine is governed by stability and operability during the design life time. An overview of the available literature on these design principles is given in Chapter 2.

Argumentation that supports suction caisson technology may be of economical nature (as mentioned in Chapter 1) such as material savings or savings in installation equipment, in time as well as removal of the foundation after decommissioning. Moreover, recent developments in offshore wind turbine installation regulations require more frequent use of significant noise mitigating measures for offshore pile driving. Therefore suction pile foundations may also be an environmentally adequate foundation alternative for offshore wind turbines.

The following sections will present the different types of suction caisson foundations, their main geometrical characteristics, the applied loading conditions and the foundation response to these conditions.

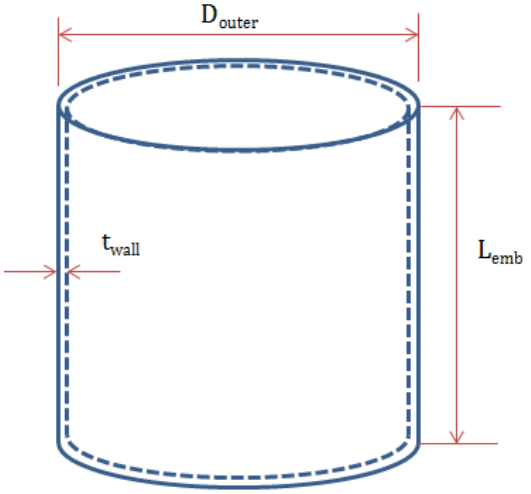

Figure 4.1: Main geometrical characteristics of suction caissons

4.1.1 TYPES OF SUCTION CAISSON FOUNDATIONS

The different types of suction caisson foundations may be classified on the number of footings used (see Figure 1.8 on page 8): mono-footings and multi-footings: braced or jacket structure.

Suction caissons have been used in both mono- and multi-footing configurations. Although, at large water depths monopods may prove to be uneconomical due to increasing dimensions to undertake the large overturning moments, the multi-footing braced or jacket structures were proven to be highly effective in undertaking the large overturning moments through a "push-pull" system (Byrne & Houlsby (2002), Kelly *et al.* (2006b)). This thesis investigates the behaviour of the suction caissons under a three leg jacket structure.

4.1.2 GEOMETRICAL CHARACTERISTICS

There are three dominant geometrical characteristics of suction caissons: the outer diameter, the embedment length and the wall thickness (see Figure 4.1). Generally, the outer diameter and embedment length are determined based on in-place capacity requirements.

The outer diameter has an important role in the horizontal capacity, while the embedment length ensures the vertical capacity. This shall be presented in the section dedicated to the foundation response to the applied loading. The wall thickness of the caisson has a significant role in the buckling analysis during installation, but this shall not be presented in this thesis.

Typical geometrical characteristics of suction caissons in sand, have proven to have a ratio around 1:1 between caisson diameter and embedment length. Larger ratios embedment lengths are used in the case of clayey soils. Further information regarding clayey soil conditions may be found in Chapter 2 and the respective mentioned references. The conducted research focuses on sandy soil conditions, therefore this shall be further presented.

4.2 FOUNDATION RESPONSE TO LOADING

In Chapters 2 and 3 of the present report the applied loading conditions are presented. In the case of monopods, VHM resistance envelopes (see Figure 4.2) are created as proposed by Kay & Palix (2011).

In the present case, as the vertical load dominates the loading conditions, the focus shall be put on the vertical compressive and tensile capacity. It will also be observed below, that ensuring a sufficient safety factor for the vertical capacity, actually determines a very high safety factor for the horizontal capacity . Consequently, the existing horizontal loads shall have a negligible role—see Figures 4.4 and 4.6.

The following subsections will focus on presenting the results of the foundation design for the two available soil samples of medium and very dense sand.

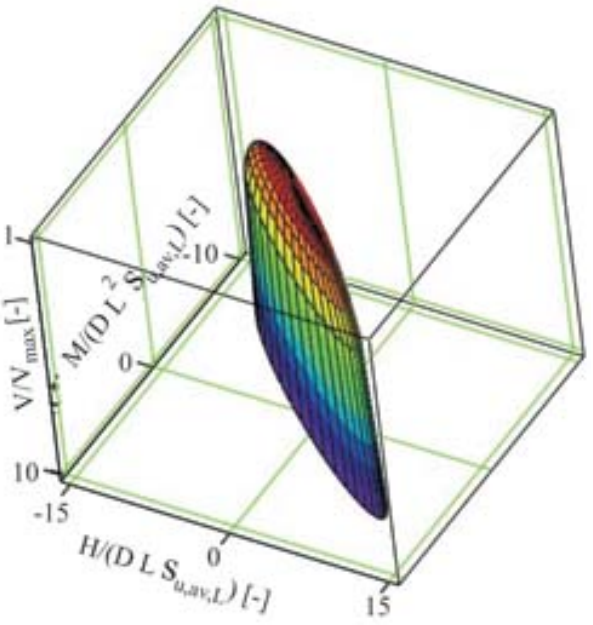

Figure 4.2: VHM resistance envelope for suction caissons (by Kay & Palix (2011))

4.2.1 IN-PLACE CAPACITY

The in-place capacity of the caisson has been determined based on the guidance given by API (2011) and DNV (2004). The considered loads represent the extreme loads presented in Table 3.5 on page 69.

As one of the caissons is subjected to tension, the goal of the design is to also ensure sufficient tensile capacity through inner and outer friction, with a factor of safety higher than 2.5 in tension. It is known that normally in design and in practice tension is avoided by putting ballast on top of the caisson so that no tension occurs. It is the choice of the author to investigate the behaviour of the caisson under tensile loading in order to check the model behaviour as well as draw conclusions with respect to the avoidance of this loading. Therefore, the designed caisson is overdimensioned for compression.

In Figure 4.3 the in-place capacity for the medium dense sand sample is calculated and for the very dense sand in Figure 4.5. It is clear that for the same caisson dimensions, the capacity in very dense sand is higher than in medium dense sand, as expected. The vertical stiffness in the two figures is determined considering the guidance given in Chapter 2 and by Randolph & Wroth (1978).

Input Data

OD [m]	15	N [-]	7.8
L_{emb} [m]	16	K	3.3
t_{wall} [m]	0.05		
A_{tot} [m^2]	176.7	C_1	2.5
A_{in} [m^2]	174.4	C_2	3.1
$A_{skirt,tip}$ [m^2]	2.3	C_3	40
γ'[kN/m^3]	12.75		
$\sigma'_{v,0,tip}$	204	α	0.37
φ' [°]	32.5	f_i	48
$s_{uDSS,tip}$ (z) [kN/m^2]	130.0	q_c [kN]	8.86E+03
$s_{uC,tip}$ (z) [kN/m^2]	77.9		
$s_{uT,tip}$ (z) [kN/m^2]	71.3	A	0.9
$s_{u,Av,tip}$ (z) [kN/m^2]	74.6	K_{zz} [kN/m]	1.42E+06

Lateral Pile Capacity

Lateral soil resistance-Displacement (API)			
H_{tip} [kN]	22966.2		
p_u [kPa]	377631.7		
y [m]	0.15	$H_{d,max}$ [kN]	3300
$H_{r,max,tip}$ [kN]	339869	**FoS**	**103.0**
Soil shear resistance at pile tip (DNV)			
p_{us} [kN]	17646.0		
p_{ud} [kPa]	122400.0		
p_u [kN]	17646.0		
$H_{r,max,tip}$ [kN]	264690.0	**FoS**	**80.2**

Vertical Pile Capacity

Tensile Capacity			
Outter shaft friction [kN]	36256		
Inner shaft friction [kN]	13325	$V_{d,t,max}$ [kN]	20200
Weight of soil plug [kN]	35571	$V_{d,c,max}$ [kN]	24600
$V_{r,tens}$ [kN]	49581	**FoS**	**2.5**
$V_{r,compr}$ [kN]	70379	**FoS**	**2.9**

Figure 4.3: In-place design of the caisson for the medium dense sand, based on API (2011) and DNV (1992)

From Figures 4.3 and 4.5, it also becomes clear that the horizontal capacity of the caisson is much larger than the actual applied horizontal load. In order to investigate the influence of the horizontal load on the vertical capacity, the failure envelopes for the two soil samples are constructed based on the formula suggested by Bang *et al.* (2011) for the inclined loading capacity of suction piles in sand and the formula suggested by Supachawarote *et al.* (2004) for the pull-out capacity of suction caissons in clay. The latter formula can be used as the undrained shear strength of sand was extrapolated using formulas recommended within the DNV.

$$\left(\frac{H}{H_{r,max}}\right)^{\left(0.5+\frac{L_{embd}}{OD}\right)} + \left(\frac{V}{V_{r,compr,max}}\right)^{\left(4.5-\frac{L_{embd}}{3\cdot OD}\right)} = 1 \tag{4.1}$$

.

$$\left(\frac{V}{V_{r,max}}\right) = \frac{H}{H_{r,max}} \cdot \tan\left(\frac{H_{r,max}}{V_{r,max}} \cdot \tan\theta\right) \tag{4.2}$$

In the formula by Bang *et al.* (2011) the angle θ represents the load inclination angle with respect to the horizontal direction ($\theta = \arctan(V/H)$). The results of applying these formulax and the failure envelopes for the two soils can be found in Figure 4.4 for the medium dense sand, respectively in Figure 4.6 for the very dense sand. Obviously, for the same dimensions, the foundation embedded in the very dense sand has a higher capacity.

From the two figures it becomes even more obvious that even under extreme conditions, the horizontal load has very little impact on the vertical foundation capacity.

Therefore, in the following analyses carried out within this research the horizontal load component shall not be considered as its effects are insignificant.

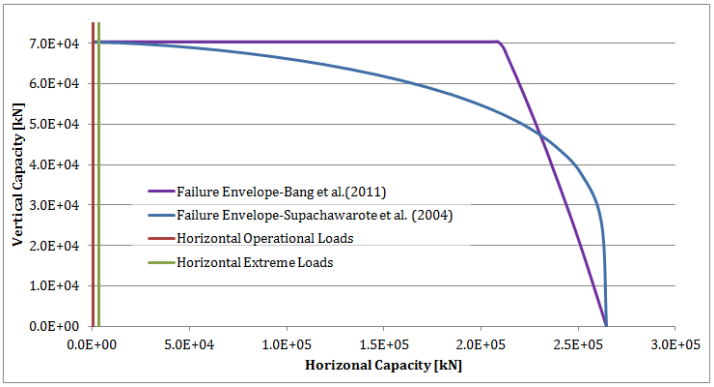

Figure 4.4: Failure envelope for the medium dense sand

Input Data

OD [m]	15	N [-]	7.8
L_{emb} [m]	16	K	3.6901723
t_{wall} [m]	0.05		
A_{tot} [m^2]	176.7	C_1	3
A_{in} [m^2]	174.4	C_2	3.5
$A_{skirt,tip}$ [m^2]	2.3	C_3	56
γ'[kN/m^3]	13.25		
$\sigma'_{v,0,tip}$	212	α	0.37
φ' [°]	35	f_i	55
$s_{uDSS,tip}$ (z) [kN/m^2]	148.4	q_c [kN]	1.52E+04
$s_{uC,tip}$ (z) [kN/m^2]	79.5		
$s_{uT,tip}$ (z) [kN/m^2]	77.3	A	0.9
$s_{u,Av,tip}$ (z) [kN/m^2]	78.4	K_{zz} [kN/m]	2.56E+06

Lateral Pile Capacity

Lateral soil resistance-Displacement (API)			
H_{tip} [kN]	26232.2		
p_u [kPa]	436016.7		
y [m]	0.15	$H_{d,max}$ [kN]	3300
$H_{r,max,tip}$ [kN]	392415.1	FoS	**118.9**
Soil shear resistance at pile tip (DNV)			
p_{us} [kN]	21306.0		
p_{ud} [kPa]	178080.0		
p_u [kN]	21306.0		
$H_{r,max,tip}$ [kN]	319590.0	FoS	**96.8**

Vertical Pile Capacity

Tensile Capacity			
Outter shaft friction [kN]	41412		
Inner shaft friction [kN]	15220	$V_{d,t,max}$ [kN]	20200
Weight of soil plug [kN]	36966	$V_{d,c,max}$ [kN]	24600
$V_{r,tens}$ [kN]	56632	FoS	**2.8**
$V_{r,compr}$ [kN]	92334	FoS	**3.8**

Figure 4.5: In-place design of the caisson for the very dense sand based on API (2011) and DNV (1992)

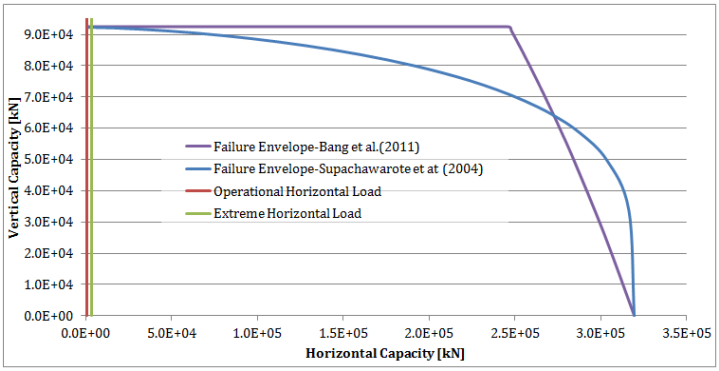

Figure 4.6: Failure envelope for the very dense sand

Based on the estimated stiffness of the caisson, and by knowing the applied loading conditions in the operational load cases ($F_z = K_{zz} \cdot u_z$), the following vertical displacements are estimated in Tables 4.1 and 4.2.

Case ID		**Applied load** [kN]	**Vertical stiffness** [kN/m]	**Estimated displacement** [m]
OP 1	(average)	3744	$1.42 \cdot 10^6$	0.0026
	(max)	4544	$1.42 \cdot 10^6$	0.0032
OP 2	(average)	6318	$1.42 \cdot 10^6$	0.0045
	(max)	6818	$1.42 \cdot 10^6$	0.0048

Table 4.1: Estimated vertical displacement for medium dense sand in operational conditions

Case ID		**Applied load** [kN]	**Vertical stiffness** [kN/m]	**Estimated displacement** [m]
OP 1	(average)	3744	$2.56 \cdot 10^6$	0.0015
	(max)	4544	$2.56 \cdot 10^6$	0.0018
OP 2	(average)	6318	$2.56 \cdot 10^6$	0.0025
	(max)	6818	$2.56 \cdot 10^6$	0.0027

Table 4.2: Estimated vertical displacement for very dense sand in operational conditions

It is observed from Tables 4.1 and 4.2 that the operational loading conditions do not cause a significant displacement. Which shall also be later confirmed by the analyses carried out with the proposed model on the medium dense sand. Yet, larger displacements are expected for the extreme conditions (see Table 4.3). In the table it can be seen that the displacements increase almost 5 times more, even when considering this static calculation formula and no effects of stiffness degradation. Therefore, these results are optimistic as no effects of the cyclic loading are considered.

Case ID		**Applied load** [kN]	**Vertical stiffness** [kN/m]	**Estimated displacement** [m]
EX - medium dense sand	(average)	35189 (50% capacity)	$1.42 \cdot 10^6$	0.0248
	(max)	26392 (75% capacity)	$1.42 \cdot 10^6$	0.0186
EX - very dense sand	(average)	35189 (50% capacity)	$1.42 \cdot 10^6$	0.0138
	(max)	26392 (75% capacity)	$1.42 \cdot 10^6$	0.0103

Table 4.3: Estimated vertical displacement in extreme conditions

4.2.2 INSTALLATION AND REMOVAL RESISTANCE

In Chapter 2 of this thesis, it is presented how the installation (see section 2.3.1) and removal resistance (see section 2.3.2) are calculated. Based on these calculations one may determine the needed suction pressure ($p_s = (Resistance - Weight)/Area_{to\ be\ embedded}$) in order to ensure that the embedment length is reached. It must be kept in mind that the weight of caisson, jacket, pump and miscellaneous have a favorable effect in the case of penetration, and unfavorable for removal. In the case of multi-footings, the suction is applied simultaneously on all footings as they are connected to the substructure.

The limitations to be considered in this case are based on the maximum applied suction pressure due to the pump of approximately 5 bar and due to the water depth of 40 m, respectively 4 bar.

The results of the rough analysis carried out for the medium dense sand can be seen in Figure 4.7, and in Figure 4.8 for the very dense sand. An analysis for the self weight penetration is not included, as the soil mass is considered uniform, which is not realistic as in-situ conditions are normally characterised by layered soils with softer sediments on top. Additionally, a buckling analysis for the caisson walls has not been carried out, this might influence the thickness of the caisson walls, reducing it closer to the skirt tip.

Input		
W_{suct} [kN]	1407	
W_{struct} [kN]	505	
$W_{pump\&misc}$ [kN]	5,5	
OD [m]	15	
L_{emb} [m]	16	
t_{wall} [m]	0,05	
$A_{skirt,\ tip}$ [m^2]	2,35	
$A_{lateral,\ inner\&outer}$[$m^2$]	478,4	
$A_{top,plate}$ [m^2]	174,37	
q_c [kPa]	1,00E+04	
DNV coefficients [-]	**Most prob**	**High Exp**
kp	0,3	0,6
kf	0,001	0,003
Output		
q_{tip} [kPa]	3000	6000
R_{tip} [kN]	7045	14090
f [kPa]	10	30
R_f[kN]	4784	14352
$R_{tot}=R_{tip}+R_f$ [kN]	11829	28442
Installation	**Most prob**	**High Exp**
p_{suct}[kPa]	57	152
p_{suct}[bar]	0,57	1,52
Removal	**Most prob**	**High Exp**
p_r[kPa]	40	98
p_r[bar]	0,40	0,98

Figure 4.7: Rough analysis of required installation pressure for the caisson in medium dense sand

Input		
Wsuct [kN]	1407	
Wstruct [kN]	505	
$W_{pump\&misc}$ [kN]	5,5	
OD [m]	15	
L_{emb} [m]	16	
t_{wall} [m]	0,05	
$A_{skirt,\ tip}$ [m^2]	2,35	
$A_{lateral,\ inner\&outer}$[$m^2$]	478,4	
$A_{top,plate}$ [m^2]	174,37	
q_c [kPa]	1,75E+04	
	Most prob	**High Exp**
kp	0,3	0,6
kf	0,001	0,003
Output		
q_{tip} [kPa]	5250	10500
R_{tip} [kN]	12329	24658
f [kPa]	18	53
R_f[kN]	8372	25116
$R_{tot}=R_{tip}+R_f$ [kN]	20701	49774
Installation	**Most prob**	**High Exp**
p_{suct}[kPa]	108	274
p_{suct}[bar]	1,08	2,74
Removal	**Most prob**	**High Exp**
p_r[kPa]	62	163
p_r[bar]	0,62	1,63

Figure 4.8: Rough analysis of required installation pressure for the caisson in very dense sand

Following from the results of this rough analysis, it can be said that as the suction and removal pressures do not exceed the limiting pressures mentioned above, the installation of the caisson is possible.

4.3 CONCLUSIONS

The design of foundations for offshore wind turbines depends on several factors as presented in Section 4.1, based on these factors the most adequate foundation system is chosen. It was already shown in Chapter 2 that the solution used in this thesis, a three leg jacket structure with suction caissons as footings, is an economically viable option and that the applied loading in this case is simplified to a "push-pull" system. Within this chapter, it is confirmed that the existing horizontal loads, even under extreme conditions have little influence on the overall vertical capacity and are thus not considered in further analyses.

The designed caisson is over-dimensioned for vertical compression (see Figures 4.3 and 4.5), as it was chosen to ensure a sufficient factor of safety even for tension. The obtained outer diameter (15 m) and embedment length (16 m) were determined based on in-place resistance requirements, following the guidance given by API (2011) and DNV (2004) for slender pipe piles. The capacity of the caisson is larger in very dense sand than in the medium dense sand as expected.

The wall thickness is chosen to be 5 cm based on in-house experience and references from literature. This value may be prone to change upon conducting a buckling analysis for the caisson's skirt upon installation, but this has not been done researched in this thesis. A rough installation and removal resistance analysis is carried out, and based on the limiting pressures due to pump capacity and water depth, the caisson can be installed in both uniform medium and very dense sand.

To conclude, the designed suction caisson has more than sufficient capacity to carry out the extreme loads on vertical and horizontal directions under static conditions, and the chosen dimensions allow for its installation and removal. Therefore, the designed caisson will be used in the following analyses.

Chapter 5

GEOTECHNICAL MODELLING

The fifth chapter aims to give insight into the model used to assess the long term cyclic behaviour of suction caisson foundations, embedded in sand. It presents the overall structure of the model with the considered assumptions and corresponding limitations. Moreover, it presents the way the problem was discretised, the basis for calibration and sensitivity to a few factors are suggested through several proposed scenarios.

Section 5.1 presents the main principles behind the model proposed to investigate the long term cyclic behaviour of suction caisson foundations, embedded in sand. The proposal is a hybrid model including two different procedures: implicit and explicit. The model uses the implicit procedure for an accurate assessment of the initial loading steps and control step. Whilst the explicit procedure is used to bridge over the large number of cycles that characterise the life time of an offshore wind turbine.

Section 5.2 reveals how the problem was discretised from a geometrical point of view, as well as initial, boundary and loading conditions.

Section 5.3 shows the principles governing the model calibration in a step-wise procedure that includes also the required laboratory tests. The considered assumptions and limitations of the model are summarised in section 5.4.

Section 5.6 presents the additional scenarios that will be considered in order to investigate the model's sensitivity to factors such as: changes in applied mean vertical load, the load's amplitude, the period.

Finally, section 5.7 closes this chapter and presents the main conclusions resulting from the previously mentioned sections.

5.1 MODEL PROPOSAL

5.1.1 GENERAL PRINCIPLES

INTRODUCTION

The design of offshore foundations for OWT shallow foundations in a granular subsoil is not governed by ultimate limit state, but actually by serviceability and stability requirements as defined by Safinus *et al.* (2011):

loss of stability large reductions of the subsoil bearing capacity due to accumulated pore water pressure;

loss of serviceability tilting of the foundation caused by uneven accumulation of settlements.

The soil conditions for the embedment of a foundation for an OWT are generally characterised by sandy soils, clayey soils or a layered structure of the two. Within the time span available for this graduation project, only the sandy soil conditions are assessed as they are considered the typical soil conditions for the necessary embedment of suction caissons in the Dutch part of the North Sea. Compared to clayey soils pore pressure build-up may play a significant role in the behaviour of sandy soils.

OWTs may be subjected to several hours of cyclic loading during storm conditions. For cohesionless, loosely packed soils, under cyclic shear a tendency to densify in drained conditions is common. However, when drainage is not permitted within the time frame of the loading (undrained or partially drained conditions) pore pressure build-up will occur. This latter phenomenon may cause strength and stiffness reduction of the foundation soil. Therefore it is essential to provide an estimation of its magnitude.

An important characteristic of the long term performance of the foundation of an OWT, is that during the design life of 20–25 years it is subjected to approximately 10^8 cycles of varying cyclic amplitudes. Therefore, it is needed to develop a model that has the capacity to estimate in a sufficiently accurate manner this behaviour for a large numbers of cycles.

The current engineering practice is based on the API (2011) for long pipe piles and on DNV (1992) for gravity base foundations. Neither of these two approaches consider caisson foundations explicitly. In addition to this, the approach towards cyclic loading of offshore foundations has been found to be insufficiently accurate and insufficient guidance is provided when looking at large numbers of cycles (Jardine *et al.* (2012)). Academic research has attempted to bridge this gap and several methods are proposed. An overview of these methods may be found in Chapter 2 of this thesis. For sand, there are two main approaches: strain accumulation models and pore pressure build-up models. These type of models are generally integrated within a hybrid model as implicit procedures. The span over the large number of cycles is bridged with the help of explicit procedures.

Implicit models are very well known for high accuracy as long as the number of cycles simulated is under 100. Above this limit they tend to become numerically unstable. On the other hand, explicit models are well known for large calculation capacities, but with potentially significant error propagation.

The proposed model incorporates the benefits of these two calculation procedures. It is based on a hypoplastic soil model for the implicit calculations and for the explicit calculations on empirical formulas for the estimation of pore pressure build-up during cyclic loading. Finally using the pore pressure build-up, one may estimate the strength and stiffness characteristics of the soil and consequently the resulting deformations and stability.

Essentially, the model has three main components:

- implicit calculation steps (the number of cycles assessed at a time must be lower than 100) to generate the initial state at the beginning of each cyclic loading package and for control steps with the aid of a hypoplastic soil model.;

- explicit calculation steps to extrapolate the pore pressure build-up and strain accumulation for each loading package through empirical formulas developed through curve fitting;
- reactualization of strength and stiffness parameters with the aid of empirical formulas based on pore pressure build-up.

The reasons for choosing the hypoplastic model over other models (continuous hyperplasticity or pore pressure build-up model—presented in Chapter 2) lie not only in its good prediction capacities for a limited number of cycles, but also in a relatively simple determination of the parameters and calibration of the soil model itself—see Figure 2.27 from Chapter 2, for more details on the comparison criteria. A sketch of the principles behind the model may be seen in Figure 5.1. A similar sequence may be considered for strain accumulation.

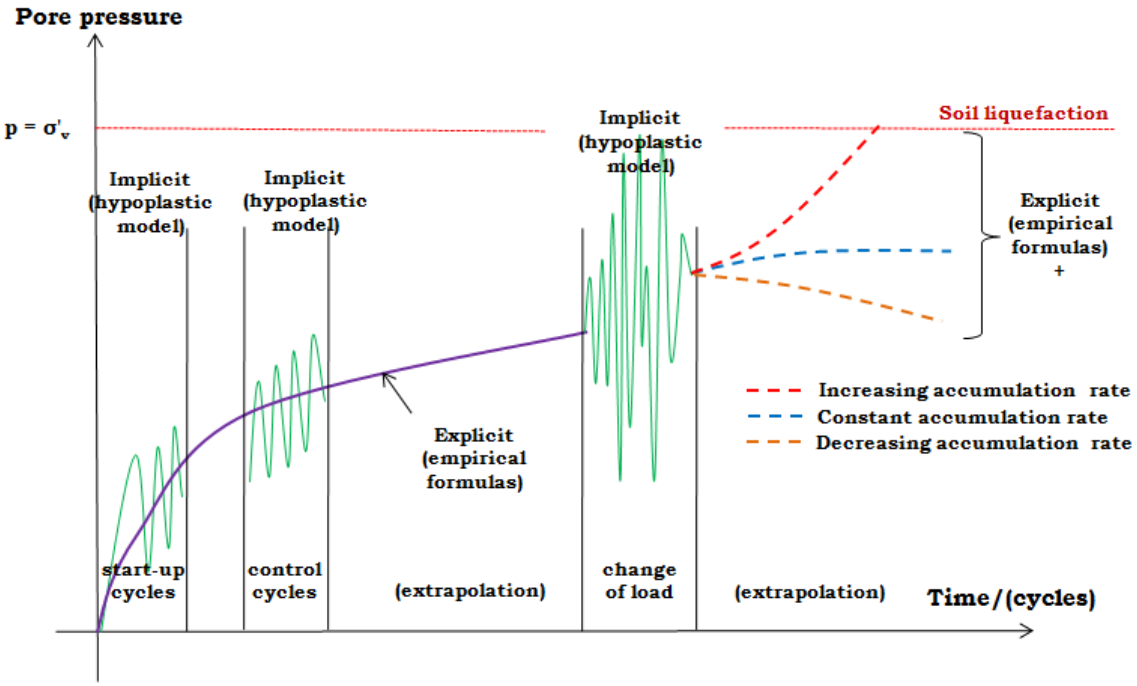

Figure 5.1: Schematic representation of the steps to analyse pore pressure development (exaggeration)

There are several important factors to be considered and will be briefly treated in the following subsections:

- definition of the loading conditions;
- definition of failure;
- definition of considered stress state due to the loading.

FAILURE DEFINITION

Ultimate limit state failure corresponds to the exceeding of load-carrying capacities of the foundation. While in service limit state failure corresponds to user defined damage levels depending on the intended purpose of the structure. As previously mentioned the two main mechanisms to dominate the design of an OWT foundation are the fulfillment of stability and serviceability requirements (Safinus *et al.* (2011), Byrne & Houlsby (2004)). In the case of an OWT the serviceability limit is considered to be a rotation of the entire structure with 4° according to LeBlanc *et al.* (2010). A more conservative limit shall be considered of 0.5° as it is considered standard within the industry (it would represent a deflection of approximately 1.4 m for a wind turbine with the hub level at 160 m above mudline).

In order to cause stability and serviceability problems, the subsoil does not need to reach liquefaction, the accumulation of pore pressure may lead to stiffness and shear strength reduction and accumulation of strains (API (2011), Safinus *et al.* (2011), Briaud & Felio (1986a)). Therefore causing differential settlement between the 3 caissons of the jacket structure and a subsequent 0.5° rotation of the entire structure.

Additionally, the soil behaviour for the analysis of this problem shall be done with the aid of the hypoplastic soil model, presented in Chapter 2 of this dissertation. This soil model incorporates a Matsuoka-Nakai (see Figure 2.16 on page 48) critical state stress condition in the formulation by P.A. von Wolffersdorff (1996). It can be observed that the projection in the deviatoric plane is not circular, but it is rounded and incorporates all the corners of the Mohr-Coulomb hexagon. This is justified by the fact that the Matsuoka-Nakai behaviour is described with the aid of the Lode angle and considers the "Spatially mobilised plane (SMP)". And can be considered a "smoothened Mohr-Coulomb" Maïolino & Luong (2009); which uses one equation (instead of six as in the Mohr-Coulomb) to describe the failure criterion—see Equation 5.1 Darve *et al.* (2004).

$$\tan^2 \varphi_{12} + \tan^2 \varphi_{13} + \tan^2 \varphi_{23} = const \tag{5.1}$$

where,

$$\varphi_{ij} = \sin^{-1} \frac{\sigma_i - \sigma_j}{\sigma_i + \sigma_j} \tag{5.2}$$

i, j take values between 1 and 3;

$\sigma_{i,j}$ represent the principal stresses;

φ_{ij} represent the mobilised friction angles in the planes x_i, x_j.

STRESS STATE

According to the applied loads three stress states may be considered to surround the suction caisson during eccentric loading: direct simple shear, triaxial compression and extension—see Figure 5.2.

For higher accuracy, it would be required to consider for each of the regions the corresponding shear strength. In order to simplify the analysis, while remaining conservative, for all points surrounding the caisson the cyclic shear strength that will be assumed is the one obtained through direct cyclic shear tests. The cyclic shear strength obtained through direct simple shear represents an average between the triaxial compression and extension.

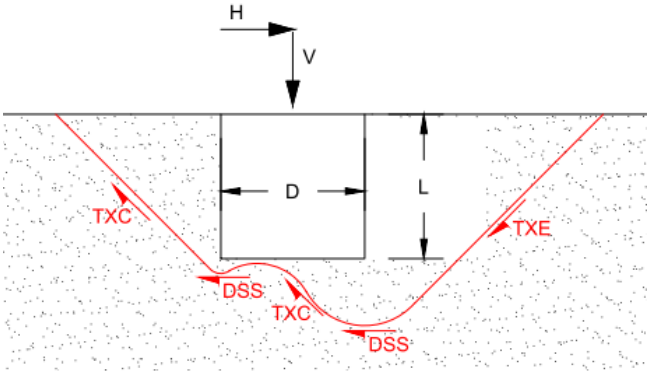

Figure 5.2: Stress states surrounding a suction caisson (TXE—Triaxial Extension, DSS—Direct Simple Shear, TXC—Triaxial Compression)

In case triaxial cyclic tests are carried out, the confining pressure may provide additional strength to the sample. Therefore the obtained cyclic shear strength will be multiplied with a correction factor varying between 0.6–1.0 (Seed & Rahman (1978) and Song (1990)). It is recommended that the relevant model parameters are to calibrated against direct cyclic shear test data.

5.1.2 IMPLICIT PROCEDURE

As previously mentioned, in order to adequately assess the long term behaviour of the suction caisson foundation it is needed to use several implicit calculation steps which can ensure the accuracy of the model. But due

to numerical instability of implicit numerical models it is not recommended to assess more than 100 cycles at a time.

The implicit numerical model that will be used for pore pressure build-up and strain accumulation is the hypoplastic model with the intergranular strain concept integrated for the assessment of cyclic loads. This subsection will provide a review of the information provided in Chapter 2.

For a better understanding of the model, the definition of hypoplasticity is repeated (it can also be found in Chapter 2):

Hypoplasticity is a constitutive law of the rate type. It is a relation which associates the strain rate to the stress rate. The mechanical behaviour characteristics of granular material are expressed in one single tensorial equation.

The hypoplastic model is a particular incremental non-linear constitutive model that can be used to predict soil behaviour. The model does not decompose the strain rate into elastic or plastic parts, as in elasto-plastic theory. Nor does it use explicitly the notion of the yield surface and plastic potential surface. Regardless of this, the hypoplastic model is able to predict important aspects of soil behaviour: critical state, dependency of peak strength on soil density, non-linear behaviour in the small and large strain range etc ...

5.1.3 HYPOPLASTIC SAND MODEL

The hypoplastic model is based on the modified equation by Gudehus (1996) (see equation 2.29) including the influence of the stress level (barotropy) and the influence of density (pyknotropy)—see equation 2.29 in Chapter 2. It includes the Matsuoka-Nakai critical stress state condition—see Figure 2.16, incorporated by von Wolffersdorff (1996). Which is presently considered as the standard hypoplastic model for sands.

The hypoplastic model as defined by equation 2.29 is able to successfully predict the behaviour in the medium to large strain range (as defined by principal strains).

5.1.4 INTERGRANULAR STRAIN CONCEPT

Niemunis & Herle (1997) created an extension to P.A. von Wolffersdorff (1996)'s model by including "intergranular strain"; thus accounting for high quasi-elastic soil stiffness in the small strain range, upon cyclic loading—see equation 2.30 in Chapter 2.

Finally, the total strain is considered the sum of two components (Mašín (2012)):

1. Intergranular strain tensor (δ) representing the deformation of interface layers at intergranular contacts;

2. Component related to the rearrangement of the soil skeleton.

In reverse and neutral loading conditions the observed overall strain is related only to the first component (hypoelastic behaviour), whilst in continuous loading conditions both components contribute (hypoplastic behaviour).

Through the simple incremental non-linear stress-strain formulation and the fact that the state of the material at any point is described by the stress and its void ratio, the hypoplastic model is considered suitable for the implicit analysis (initial and control steps).

5.1.5 EXPLICIT PROCEDURE

As the implicit model cannot assess large number of cycles, empirical formulas are to be used in order to be able to cover the full design life of an OWT. The explicit procedure shall evaluate two aspects:

- pore pressure build-up due to cyclic loading;
- strain accumulation.

Considering the parameters of the hypoplastic model well calibrated, it can be assumed that the given pore pressure build-up diagrams are accurate within the initial and control cycles. Through curve fitting an estimation of the residual pore pressure may be expressed—see Figure 5.1. The estimated values for the pore pressure build-up will be checked through the control cycles.

Following from the pore pressure build-up, the pore pressure ratio (R_u) may be calculated:

$$R_u = \frac{u}{\sigma'_{v0}} \tag{5.3}$$

where:

R_u pore pressure ratio;

u pore pressure;

σ'_{v0} effective initial vertical stress.

The pore pressure ratio is an indication when liquefaction occurs ($R_u = 1$ the grains are pushed apart by the water pressure and become suspended) and also regarding the reduction of strength and stiffness—which will be further discussed in the next section.

Using the variation of the volumetric strain and void ratio, one can determine the change in void ratio from Equations 5.4 and 5.5:

$$\Delta\varepsilon_v = \Delta I_D \cdot \frac{(e_{min} - e_{max})}{(1 + e_0)} \tag{5.4}$$

$$\Delta I_D = I_D - I_{D,0} = \frac{\Delta e}{e_{max} - e_{min}} \tag{5.5}$$

$$\Delta e = \Delta\varepsilon \cdot (1 + e_0) \tag{5.6}$$

where:

$\Delta\varepsilon_v$ variation of the volumetric strain;

ΔI_D variation of relative density;

I_D relative density $\left(I_D = \frac{e_{max} - e}{e_{max} - e_{min}}\right)$;

$e_{max,min}$ maximum, receptively minimum index void ratio;

e_0 initial void ratio;

e current void ratio of the natural state of the soil.

By knowing the variation of void ratio, one may update the value of the initial void ratio and carry out a new set of cyclic loading with the hypoplastic model. This procedure may prove to be valuable for the first analysis phases until an adequate calibration of the model is achieved.

Finally, with the aid of the estimations of pore pressure and change in strains an assessment of the reduced strength and stiffness of the foundation soil can be made; as well as for the expected displacements under long term cyclic loading.

5.1.6 "UPDATE" OF STRENGTH AND STIFFNESS

Knowing the values for the pore pressure build-up and as well the pore pressure ratio, one may determine the strength and stiffness as a consequence of the long term cyclic loading.

In order to simulate the effects of pore pressure build-up, in geotechnical earthquake engineering the method of reducing the strength of the soil is often used (see Equation 2.6). This method is employed within this model as well through Equation 2.7.

If liquefaction is reached ($R_u = 1$) then the shear strength of the liquefied sand may be reduced to 5—20% of the effective stress—see Equation 2.8, according to Stark & Mesri (1992) and Olson (2001) or Equation 2.9, according to Olson & Stark (2003). More details regarding this can be found in Chapter 2 on page 29.

In the transition state towards liquefaction, the stiffness of the sand layer will also be significantly reduced. The method through which this is assessed within this model uses the shear modulus G, measured through cyclic loading tests and it translates it into residual stiffness (E_{res})—see Equation 2.10 on page 30.

5.1.7 CONCLUSIONS

To conclude this section of the Model Proposal, the current model is expected to be able to assess the long term behaviour under cyclic loading of the suction caisson foundations under a jacket structure through a combination of implicit and explicit numerical analysis. Where the cyclic loads have been defined as the hydrodynamic and aerodynamic loads translated through a push-pull system of cyclically varying vertical load.

The obtained results shall be considered in the frame of ensuring serviceability and stability of the overall system (OWT with its foundation structure). One important aspect to be remembered is that all loads and material properties shall be unfactored. This is done in order to obtain the best estimate values for the actual soil behaviour and an overall factor of safety will be required on bearing capacity. It should not be forgotten that a conservative assumption is taken regarding the stress state in the soil which is considered to be equivalent to direct shearing.

The following sections shall focus on presenting the problem discretisation, the model calibration, the considered assumptions, limitations and further analysis scenarios.

5.2 PROBLEM DISCRETISATION

The following subsections present the method through which the problem analysed within this report is discretised from a geometrical point of view, the considered initial and boundary conditions as well as the considered loading conditions.

5.2.1 GEOMETRICAL DISCRETISATION

Even though the overall thesis considers three suction caissons, within each analysis only one suction caisson is considered at a time, with the corresponding vertical loading applied. This suction caisson shall be considered embedded within a soil volume as shown in Figure 5.3 for operational conditions and Figure 5.4 for extreme conditions. The initial and boundary conditions shall be presented in the following sections.

The expected failure mechanisms around the caisson have been discussed in the previous section on page 88. It is concluded that the soil volume will be calibrated against cyclic direct simple shear test data, which is a conservative assumption. The generated mesh is constructed in such a manner that it is finer in the vicinity of the caisson (the chosen fineness is 0.5) and it becomes coarser with the increasing distance from the caisson.

OPERATIONAL CONDITIONS

Under operational conditions the problem shall be analysed in three dimensions, considering a rectangular soil volume (see Figure 5.3) extending 45 m around the caisson that can be found in its middle.

The distance from the caisson to the soil volume boundary, equals six diameters, has been chosen in order to avoid that the boundary itself influences the results. The boundary conditions of the soil volume are explained in the respective section.

The method through which the points of application of the loads are chosen shall be explained in the following sections. The water depth is set to 40 m.

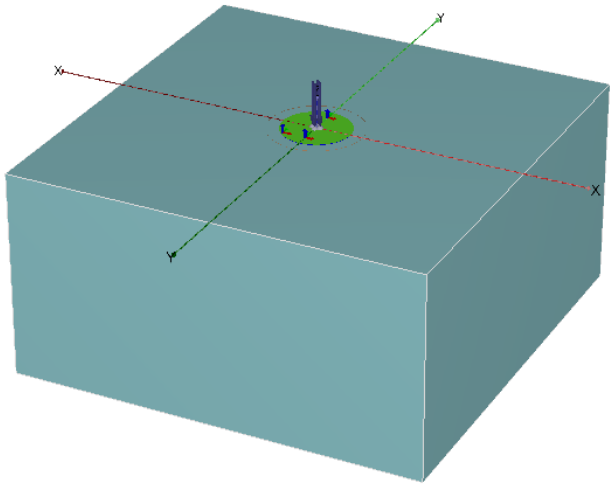

Figure 5.3: Problem geometry in operational conditions

EXTREME CONDITIONS

Under extreme conditions the problem shall also be analysed in three dimensions, considering a rectangular soil volume (see Figure 5.4). Initially, an attempt to analyse the problem as presented for the operational loading conditions was made.

As the results obtained presented significant irregularities (see Figure 5.5), it became clear that even though the problem is symmetric at a boundary value problem level, the non-symmetry at stress point level (asymmetric mesh) causes the development of non-symmetric failure mechanisms (see Figure 5.5). Moreover, within the three dimensional environment, issues regarding the computational accuracy may appear from difficulties in an accurate integration of stresses on curved surfaces and unbalance in pore pressures caused by the high water depth. An unbalance between the pore water pressures inside and outside of

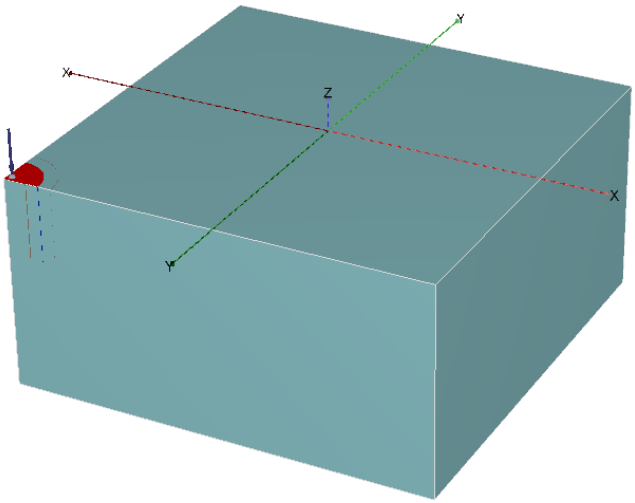

Figure 5.4: Problem geometry in extreme conditions

the caisson may be present, which will finally result in an unbalanced force within the model.

In order to reduce this effect, and keeping in mind that the problem is symmetric in the X and Y planes, only a quarter of the problem is further analysed: the caisson is placed on the corner of the soil volume previously considered (see Figure 5.4). The boundary conditions in this case are not the same as in the operational conditions and they will be explained in the following section.

The method through which the points of application of the loads are chosen are explained in the section dedicated to the loading conditions. The water depth is set to the prescribed 40 m.

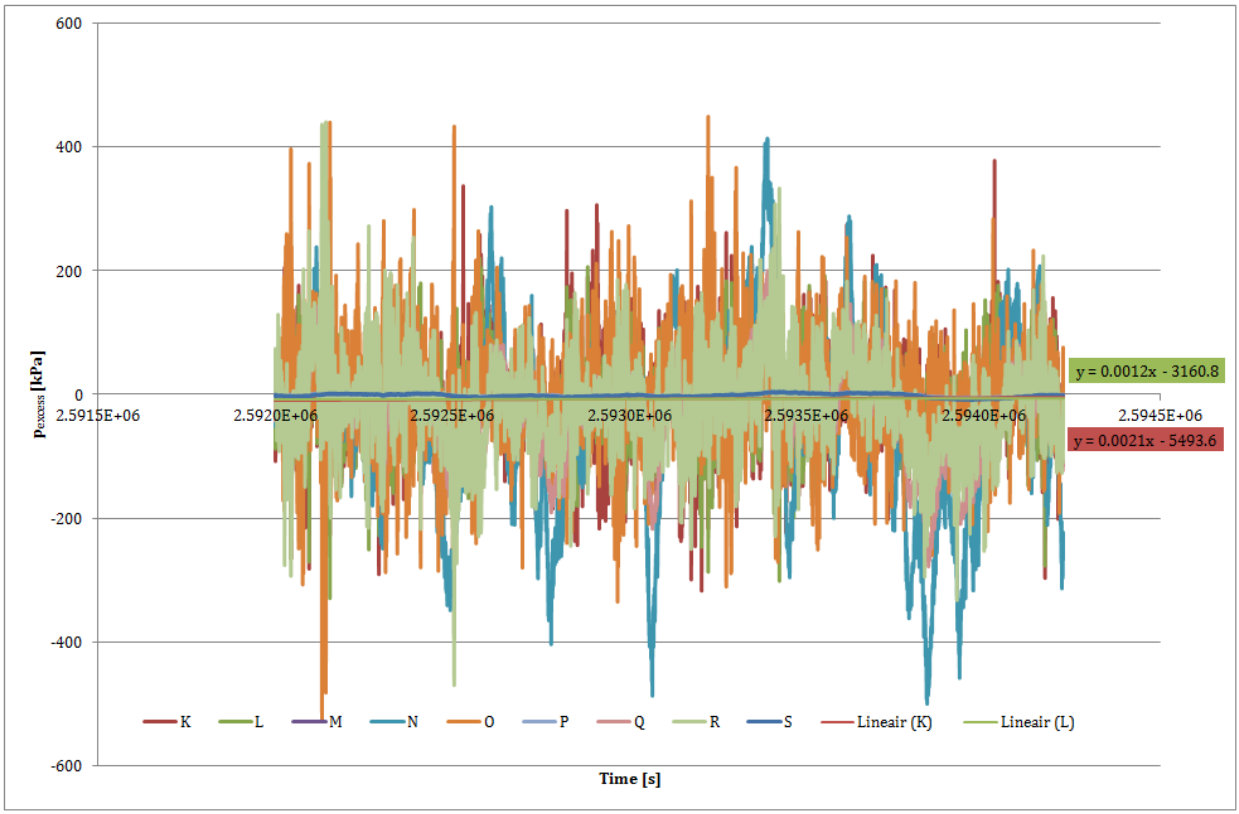

Figure 5.5: Excess pore pressure development under extreme conditions, considering the full problem geometry

5.2.2 INITIAL CONDITIONS

The soil conditions are considered to be uniform throughout the entire soil mass being analysed. Therefore, all three caissons of the jacket structure are considered to be embedded within the same uniform soil mass. This is an unrealistic assumption, as it is very well known that variety with respect to depth may influence the installation procedure of the caisson and of course its bearing capacity.

Moreover, considering that the centre to centre distance between the three caissons is 23 m, variability also on a horizontal direction is normally expected, though at a smaller scale than vertical. Nonetheless, the dimensions of offshore wind farms extend over tens of square kilometers, therefore horizontal variability may play a significant role in the design of the foundations for wind turbines positioned at different points within the wind farm.

It is assumed that there is one month between the installation of the offshore wind turbine on top of the foundation and is in operation. Therefore, before the cyclic loading is applied a one month consolidation period

of the soil underneath the weight of the super- and sub- structure. It was considered safe to assume that the load is applied statically undrained, as installation of wind turbines does not occur during storm weather conditions. Thus, the loading due to both aerodynamic and hydrodynamic actions should not have a significant influence within this time frame.

Additionally, it shall be considered that the settlement occurring during this period is uniformly distributed.

5.2.3 BOUNDARY CONDITIONS

In the subsection presenting the geometrical discretisation it is mentioned that the boundary conditions from operational to extreme conditions change.

OPERATIONAL CONDITIONS

The suction caisson is placed at the top of the considered soil volume in a central position, far from the soil volume boundaries. As the considered soil is sand, all boundaries of the soil volume are considered drained in this case.

EXTREME CONDITIONS

The quarter of the suction caisson is placed at the top of the considered soil volume in a corner position, on the soil volume boundaries. Therefore, for the soil volume boundaries adjacent to the suction caisson are considered undrained (in accordance to the new problem geometry). While for the rest of the boundaries, are considered drained.

5.2.4 LOADING CONDITIONS

This section briefly presents the loading conditions, as they have been obtained in Chapter 3. Furthermore, it shall present the method through which they will be applied in time and space.

OPERATIONAL LOADING CONDITIONS

Chapter 3 of this thesis presents how the loading conditions were calculated and considered by Dong E&P (UK). After a statistical analysis, the data was clustered into one dominant operational case for each caisson for approximately 70% of life-time, as can be seen in Table 5.1.

Case ID (Occurrence [%])	**Mean load** [kN]	**Amplitude** [kN]	**Wind speed** [m/s]	**Associated period** [s]	**Mean/ Capacity**	**Max/ Capacity**
OP 1 (68.5%)	3744	800	13–15	7.32	5.3 [%]	6.5 [%]
OP 2 (74.7%)	6318	500	13–15	7.32	9.0 [%]	9.7 [%]
OP 3 (70.5%)	0	650	13–15	7.32	0.0 [%]	0.2 [%]

Table 5.1: Representative case for operational loading conditions and comparison to caisson capacity

As the applied loading conditions are much lower compared to the capacity, less than 10%, and the soil conditions are represented by medium to very dense sand, it is expected that the occurring degradation may be negligible. Therefore, in order to gain more clarity regarding aspects such as sensitivity to changes in mean load, cycling amplitude, period of the load several scenarios are prepared and presented in section 5.6.

EXTREME LOADING CONDITIONS

Chapter 3, subsection 3.4.3 of this dissertation presents the values of the extreme loading conditions and their assessment method by using the Hansteen distribution. The extreme loading conditions considered in the

current research, will be based on percentages of the caisson capacity and are further presented in section 5.6 (see Figure 5.27), dedicated to the model scenarios used to investigate the effects of changes in mean load and amplitude.

LOADING CHARACTERISTICS

There are two main aspects that need to be considered regarding the loading characteristics: their distribution in time and points of application in space. The two aspects are thoroughly presented in the following two subsections.

Temporal Charateristics

As presented in Chapter 3, the loading conditions resulting from the aerodynamic and hydrodynamic loading can be represented by a cyclic function in time with the characteristics given in Table 5.1. One must keep in mind that the eigen frequency of the structure is determined within the structural model, thus the given loads include amplification effects.

Furthermore, in operational conditions the frequency of the suction caisson (even when taken as the frequency of the wave) is outside of the natural frequency of the structure. Thus, allowing the application of the load in a quasi-static manner (see Figure 5.6). This method of applying the loads does not interfere with the fact that the soil behaviour is undrained, as the allowed consolidation time is insignificant ($T/t_{90} = 2.9\%$). The analyses were done using the theory presented by Zienkiewicz *et al.* (1980). The results of these analyses can be found in Annex C.

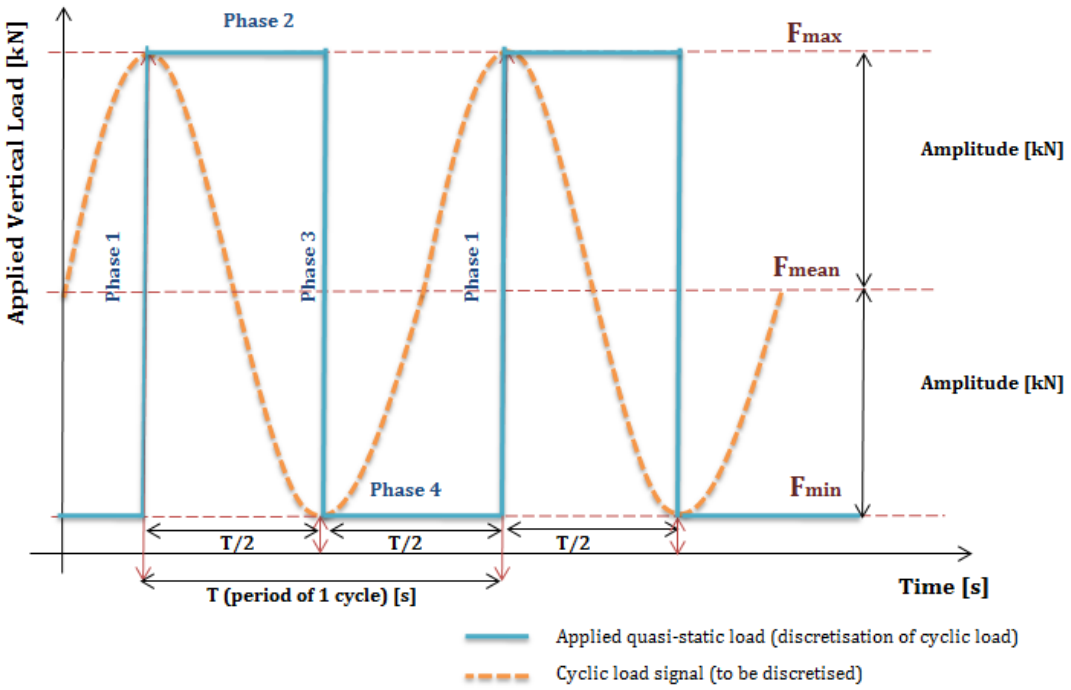

Figure 5.6: Sketch of discretised cyclic load signal in four phases

In Figure 5.6 one can see that the method through which one cycle of the applied load is considered has 4 phases:

- Phase 1—the maximum vertical component ($F_{max} = F_{avg} + Amplitude$) is applied instantaneously, in an undrained manner;
- Phase 2—under the applied F_{max} a consolidation phase is considered, with a time interval equal to half the cyclic loading period. This phase allows for a slight pore pressure dissipation of the previous phase;

- Phase 3—the minimum vertical component ($F_{min} = F_{avg} - Amplitude$) is applied instantaneously, in an undrained manner;

- Phase 4—under the applied F_{min} a consolidation phase is considered, with a time interval equal to half the cyclic loading period. This phase allows for a slight pore pressure dissipation of the previous phase.

Each of the above phases, uses as initial pore pressure, the pore pressure from the end of its previous phase.

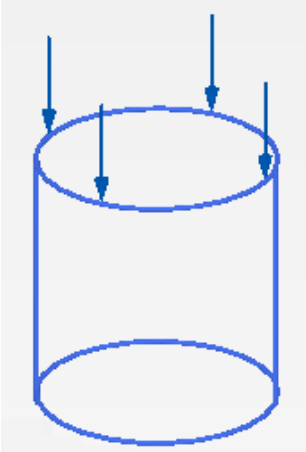

Figure 5.7: Screen-shot from PLAXIS of initially considered distribution of the loads—four points on the caisson's rim

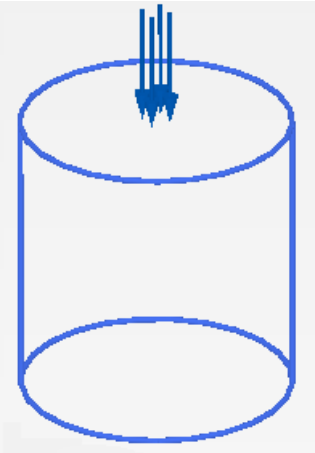

Figure 5.8: Screen-shot from PLAXIS of chosen distribution of the loads—four points closer to the caisson—jacket connection

Spatial Characteristics

From a structural point of view the load is undertaken uniformly by the rim of the caisson. Therefore, as an initial assumption the load was distributed in 4 points on the top of the rim. Yet, due to the repeated phases within the analysis, a severe and not realistic degradation of the soil surrounding the caisson was observed. In Figure 5.10 one can see that point B has a strong accumulation of displacements, which linearly extrapolated to 25 years gave displacements in the order of meters. This may be caused by the deformation of the mesh and shifting of the application point of the load which is at the interface of the caisson rim and surrounding soil.

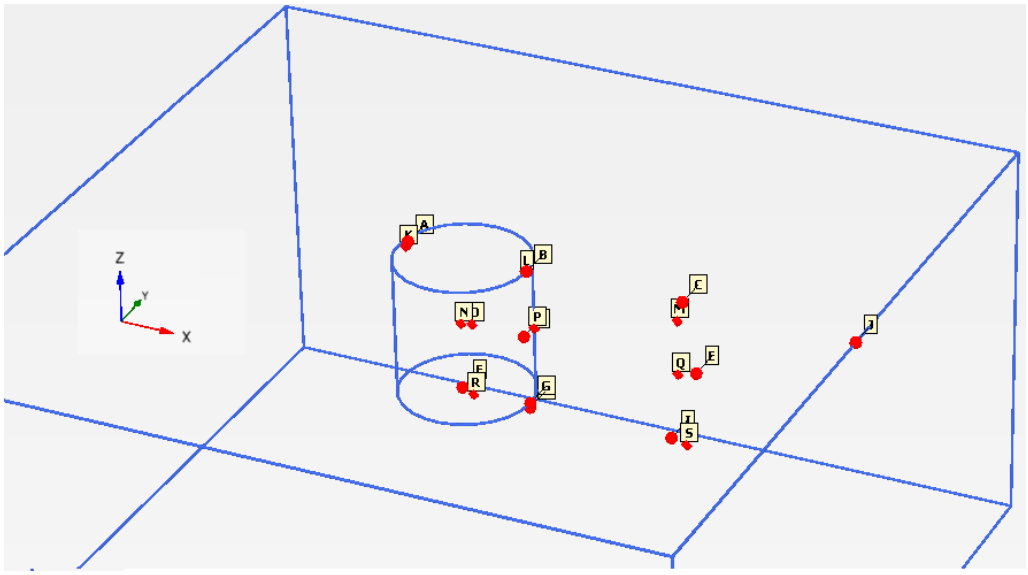

Figure 5.9: Screen-shot of the locations of the chosen nodes and stress points for the full problem

It was thus concluded that distributing the load in four points closer to the centre, where the jacket leg would be connected will provide more accurate results (see Figure 5.8). In reality stiffeners are used, in order to ensure that the loads are uniformly transmitted to the rim of the caisson, therefore a larger stiffness for the top plate was chosen. In this manner the focus also remains on the soil behaviour rather than the behaviour of the caisson's top plate.

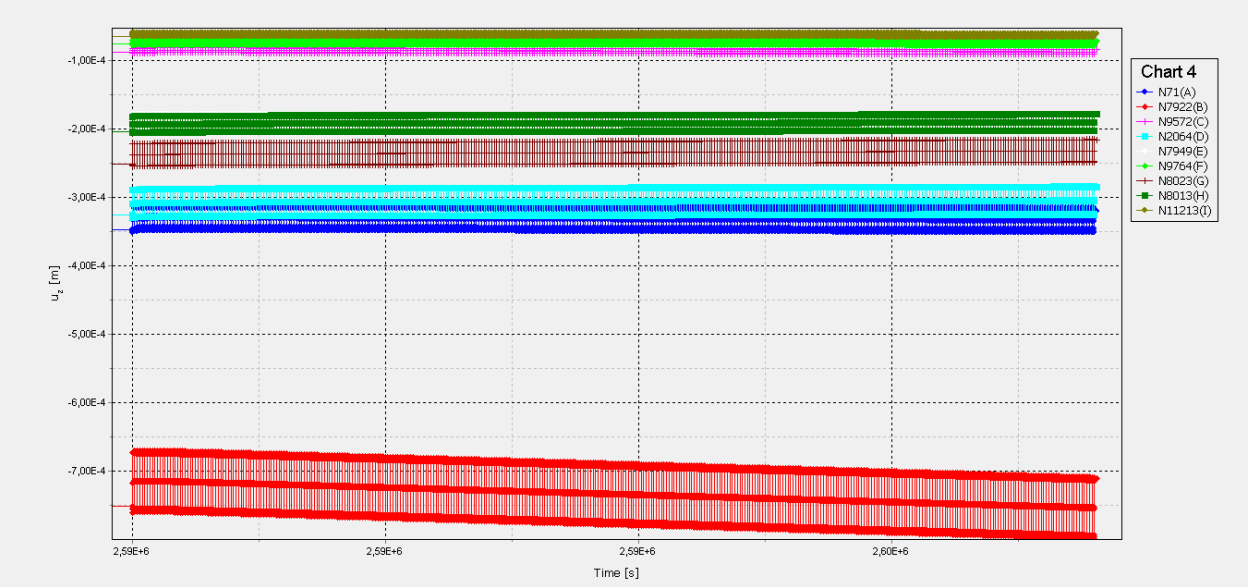

Figure 5.10: Screen-shot of vertical displacements during 520 loading cycles in medium dense sand—loads are applied on the rim (locations of the selected points can be found in Figure 5.9)

5.3 MODEL CALIBRATION

The calibration of the model will be based on the soil behaviour under cyclic loading. More specifically, the sand modelled in the analyses is calibrated against undrained triaxial compression and undrained cyclic triaxial and cyclic direct simple shear tests, all samples are isotropically consolidated:

- the very dense sand sample (with a relative density of 75%) is calibrated using an undrained triaxial compression test and an undrained cyclic triaxial test;
- the medium dense sand sample (with a relative density of 50%) is calibrated using an undrained triaxial compression test and an undrained cyclic direct simple shear test;

The following subsections will present the needed step-wise procedure for the soil calibration.

STEP 1: PREPARATION

The first step in the calibration procedure should be an assessment of the Cyclic Shear Stress Ratio (CSSR) following from the application of the expected in-situ loads on the soil conditions resulting from in-situ tests (CPTs, boreholes). The cyclic testing should be based on the expected mobilised shear strength and corresponding CSSR values. For a good calibration, it is very important to have at least one test at small CSSR values in order to be able to calibrate the parameters influencing the small strain stiffness.

In this case, this procedure was done only for the extreme loading conditions and not for operational. Thus, the first step becomes the reading of the laboratory data and understanding the results of these tests and the behaviour of the soil following from them. The laboratory data provided by Deltares and used in this thesis include:

- cyclic undrained triaxial tests with varying Cyclic Shear Stress Ratio (CSSR);
- cyclic direct simple shear tests with varying CSSR;
- isotropically consolidated undrained triaxial tests;
- constant head permeability tests.

The samples used in these tests were reconstituted at a density index (I_D) of 50% for the medium dense sand and 75% for the dense to very dense sand sample. The sand samples were retrieved from in-situ boreholes.

Constant Head Permeability Tests
The constant head permeability test is a common laboratory testing method used to determine the permeability of granular soils like sands and gravels. The test involves water flow through a column of cylindrical saturated soil sample under the constant pressure difference.

Knowing the height of the soil sample column (L), the sample cross sectional area (A), and the constant pressure difference (Δh), the volume of passing water (Q), and the time interval (Δt), one can calculate the vertical permeability (k) of the sample as:

$$k = \frac{Q \cdot L}{(A \cdot \Delta h \cdot \Delta t)} \tag{5.7}$$

The results of these tests are summarised in Table 5.2 and will be used as permeability values of the considered soil conditions. The tests were conducted according to CEN-ISO/TS17892-11 (2004).

Sample I_D [%]	**Minimum Permeability** $[m/s]$	**Average Permeability Permeability** $[m/s]$	**Maximum permeability Permeability** $[m/s]$	**Initial Void Ratio** $[-]$
75%	$1.3 \cdot 10^{-5}$	$1.9 \cdot 10^{-5}$	$2.5 \cdot 10^{-5}$	0.45
50%	$1.9 \cdot 10^{-5}$	$2.5 \cdot 10^{-5}$	$3.2 \cdot 10^{-5}$	0.54

Table 5.2: Summary of the results of the permeability tests conducted by Deltares

Isotropically Consolidated Undrained Triaxial Tests
Consolidated undrained triaxial tests are performed in order to determine the undrained shear strength of the sample. The tests were performed according to CEN-ISO/TS17892-9 (2004), on reconstituted samples as follows (the results of these tests may be found in Appendix D):

- for the very dense sand sample, with a density index of 80% and isotropically consolidated at 50 kPa;
- for the medium dense sand sample, with a density 50% and isotropically consolidated at 75 kPa.

An important aspect regarding the understanding of the soil behaviour is understanding the stress path resulting from the given test results of the isotropically consolidated undrained triaxial tests on the two samples (see Figures D.1 and D.4).

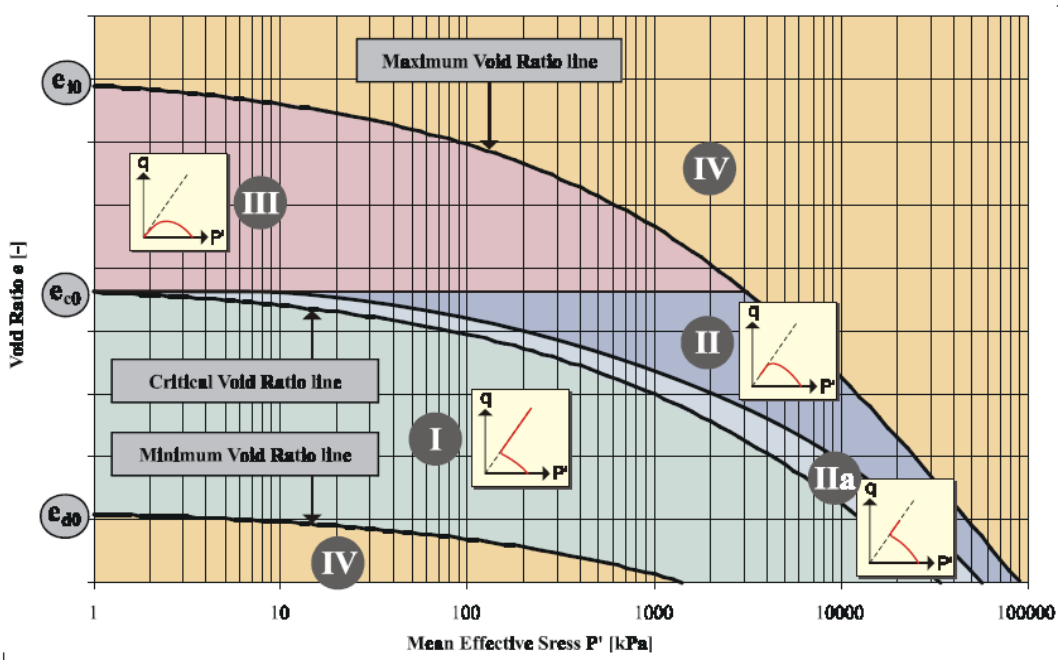

Figure 5.11: Different types of soil behaviour considered by the constitutive hypoplastic equation, by Vanden Berghe (2001)

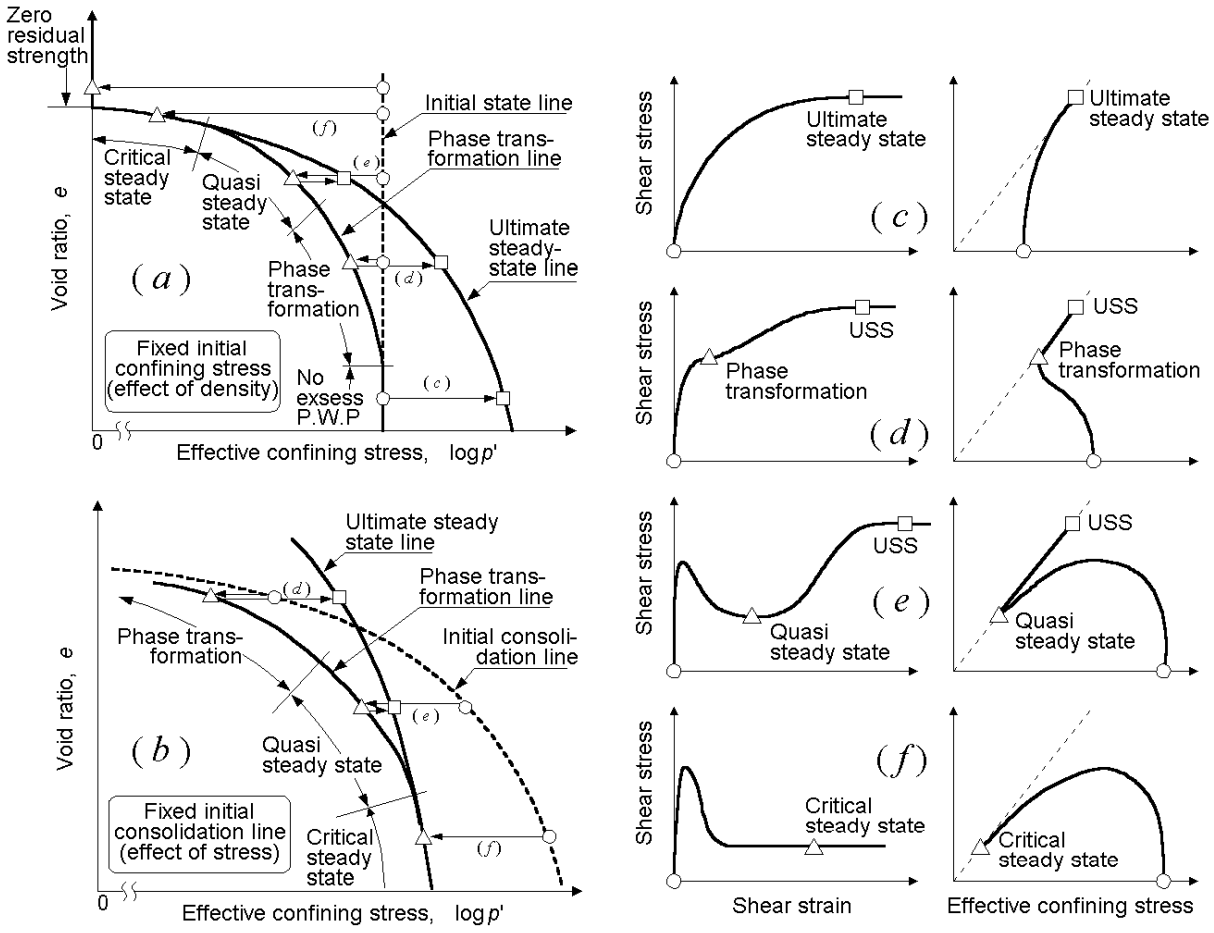

Figure 5.12: General undrained shear behaviour of sand under large deformation by Yoshimine & Ishihara (1998)

The stress path of the medium dense sand (see Figure D.1) indicates that the sample has an initially dilative behaviour as the stress path commences to curve towards the right, followed by contractive behaviour as the stress path curves to the left and finally dilative behaviour with the critical mean stress lower than the initial mean stress, which is characterised by Vanden Berghe (2001) as being in zone I (see Figure 5.11). While for the very dense sample (see Figure D.4), the path curves immediately to the right until it reaches the critical state line, thus also zone I.

This observation is important in the choice of values for e_{c0}, e_{d0} and e_{i0} for both samples. The final dilative behaviour shows that the critical void ratio has a higher value than the initial void ratio. For the medium dense sample, the contractive behaviour shows that the sample densifies before reaching the critical state path ($e_{d0} < e_0$). Whereas the very dense sample is already in its densest state and directly dilates to reach the critical state ($e_{d0} \approx e_0$).

Following the theory of sand flow potential by Yoshimine & Ishihara (1998), the medium dense sample goes through phase transformation before reaching the ultimate steady state, corresponding to case (d) from Figure 5.12, while the very dense sample dilates directly towards the ultimate steady state, case (c) from Figure 5.12. Moreover, it is also confirmed that the two samples have a very low flow potential.

Cyclic Direct Simple Shear Tests with Varying CSSR

Simple shear testing is used to investigate the stress-strain-strength relationships for a range of soil types. In the present case the reconstituted medium dense sand sample ($I_D = 50\%$) was subjected first to a first phase of consolidation at 80 kPa followed by a series of shear stress controlled cycles at varying CSSR values of 0.10, 0.075 and 0.05, under undrained conditions, at a frequency of 0.1 Hz. A schematic representation of the cyclic direct simple shear test can be seen in Figure 5.13.

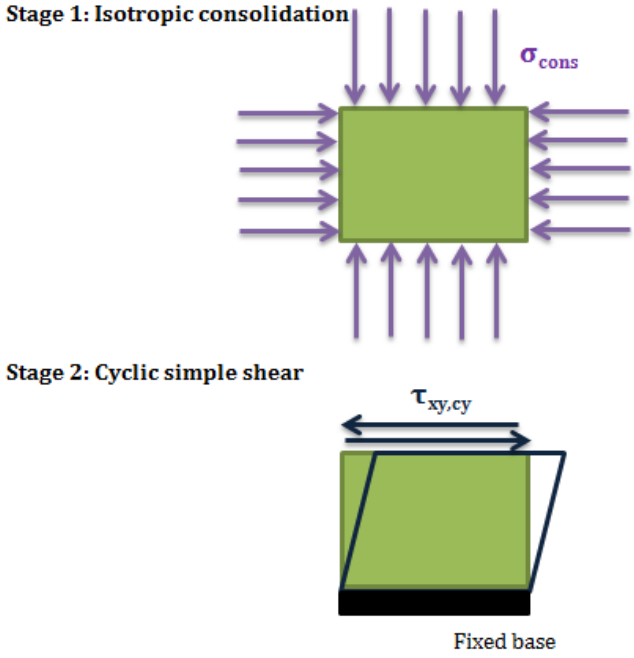

Figure 5.13: Schematic representation of a cyclic direct simple shear test (stress controlled)

The results of these tests can be found in Appendix D. An important aspect to be observed from these tests is the fact that the strain range resulting from these tests (Figures D.24, D.36 and D.30) can be characterised as a medium strain range, as it can be observed in Figure 5.15 by Ishihara (1996). This fact will influence the selection of the m_R parameter, which controls the initial (very-small-strain) shear modulus upon 180° strain path reversal and the initial loading.

Furthermore, in Figures D.20, D.32 and D.26, one could observe that as the sample approaches failure, the measured shear stress undergone by the sample decreased. One more obvious conclusion from the tests is the fact that the larger the CSSR value used in the test, the faster failure occurred.

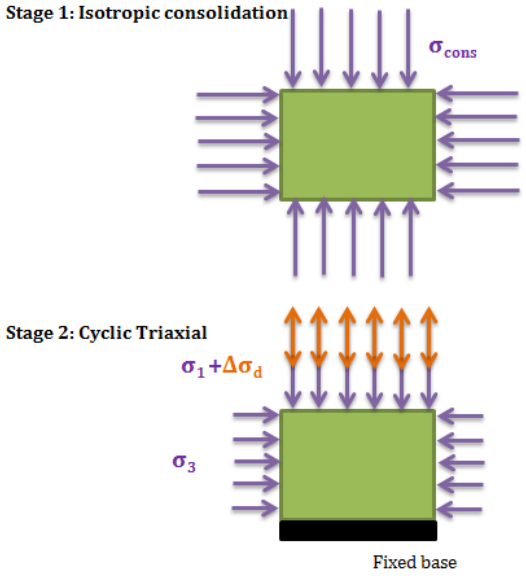

Figure 5.14: Schematic representation of a cyclic undrained triaxial test (stress controlled)

Cyclic Undrained Triaxial Tests with Varying CSSR

Cyclic undrained triaxial tests are used also for investigation of the stress-strain-strength relationships of various soil types. In the current case, the reconstituted very dense sand sample ($I_D = 75\%$) was subjected first to a first phase of consolidation at 40 kPa followed by a series of vertical stress controlled cycles at varying CSSR values of 0.15 and 0.20, under undrained conditions, at a frequency of 0.1 Hz. A schematic representation of the cyclic undrained triaxial test can be seen in Figure 5.14.

The results of these tests can be found in Appendix D. An important aspect to be observed from these tests is the fact that the strain range resulting from these tests (Figures D.12 and D.18) can be characterised as a small to medium strain range, as it can be deduced from Figure 5.15 by Ishihara (1996). This fact will influence the selection of the m_R parameter controlling the initial (very-small-strain) shear modulus upon 180° strain path reversal and the initial loading.

Furthermore, in Figures D.8 and D.14, one could observe that as the sample approaches failure, the measured shear stress undertaken by the sample decreased. One more obvious conclusion from the tests is the fact that the larger the CSSR value used in the test, the faster failure occurred. Yet, in the case of the cyclic undrained triaxial tests, even though the CSSR values were higher than in the case of the cyclic direct simple shear tests, the number of cycles required to reach liquefaction is much higher. This is most certainly a consequence of the fact that the sample is denser, but it also shows the influence of the trixial cell on the sample strength.

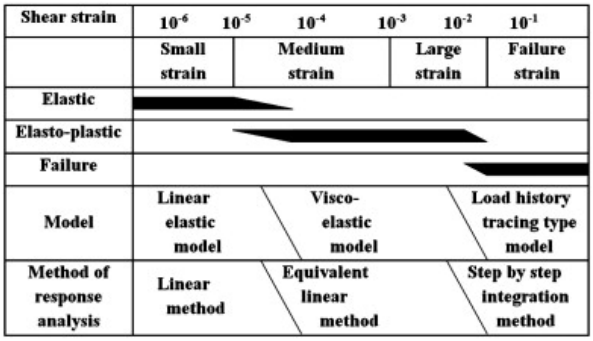

Figure 5.15: Modeling of soil behaviour in compliance with strain-dependent deformation characteristics by Ishihara (1996)

The following two steps will present in detail the way through which the parameters of the hypoplastic sand model with intergranular strain concept integrated are used in order to obtain the best fit between the model and the above mentioned laboratory data. Moreover, the individual influence of the parameters with respect to soil behaviour will also be presented.

STEP 2: DETERMINATION AND CALIBRATION OF HYPOPLASTIC SAND MODEL PARAMETERS

The hypoplastic sand model parameters were thoroughly presented in Chapter 2, in section 2.5.5. They are calibrated using the isotropically consolidated undrained triaxial test results, while keeping the values of the intergranular strain concept parameters null.

Critical friction angle (φ'_c)

In this first calibration phase, the critical state friction angle (φ'_c) is kept equal to the value obtained from the tests in order to ensure that the same failure state is reached (see Table 5.3). This value shall be revised in Step 3 (see Figure 5.16).

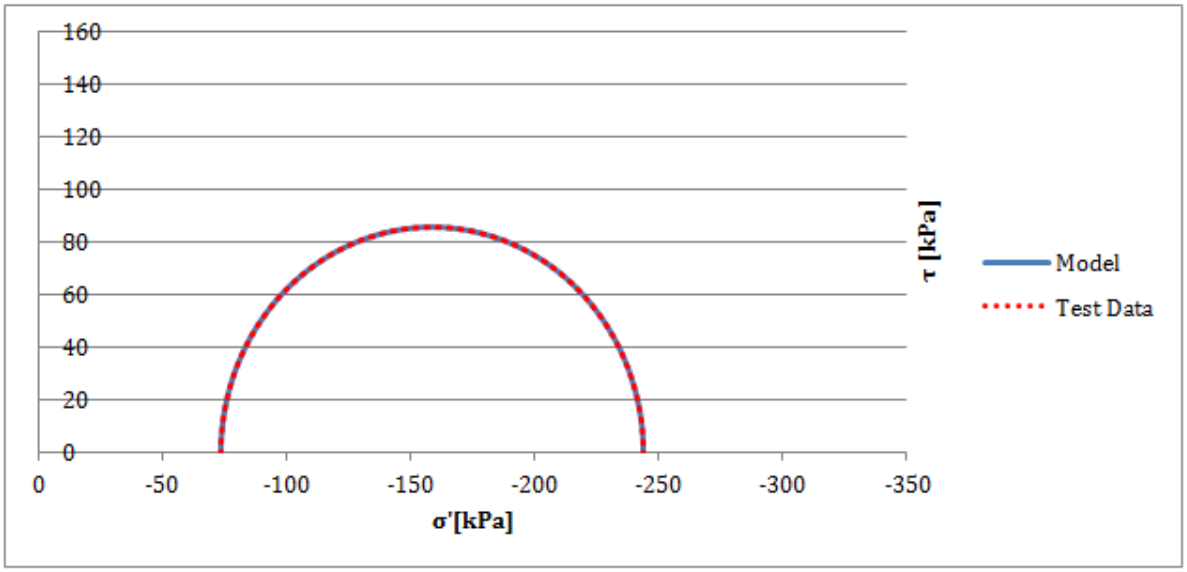

Figure 5.16: Stress state within the model and the sample

Soil Type	φ'_c
Medium dense sand	32.5°
Very dense sand	39.9°

Table 5.3: Initial values of the critical state friction angle (φ'_c)

Reference void ratios (e_{c0}, e_{d0} and e_{i0})

The reference void ratios are determined based on the interpretation of the soil behaviour from Step 1, while the initial void ratio was deduced from the constant head permeability tests (Table 5.2). Following those observations, the corresponding values are in Table 5.4.

Soil Type	e_0	e_{c0}	e_{d0}	e_{i0}
Medium dense sand	0.54	0.55	0.40	0.85
Very dense sand	0.45	0.52	0.40	1.00

Table 5.4: Values for the reference void ratios

The following parameters are calibrated by using the Soil Testing facility in Plaxis and modelling a isotropically consolidated undrained triaxial test, following the test description as given in Step 1: the very dense sand sample, with a density index of 80% was isotropically consolidated at 50 kPa and the medium dense sand sample, with a density 50%, was isotropically consolidated at 75 kPa. Further, the sample was loaded until the principal strain became equal to 20%.

Parameter h_s—Granular hardness

The granular hardness (h_s) parameter controls the stiffness of the sample, more specifically it changes the slope of the deviatoric stress with respect to the axial strain (smaller h_s steeper slope). The results of the calibration of h_s can be seen in Figures E.1 and E.2. The granular hardness also influences the pressure at which the failure line is reached, a smaller h_s determines failure at smaller confining pressures (see Figure 5.17).

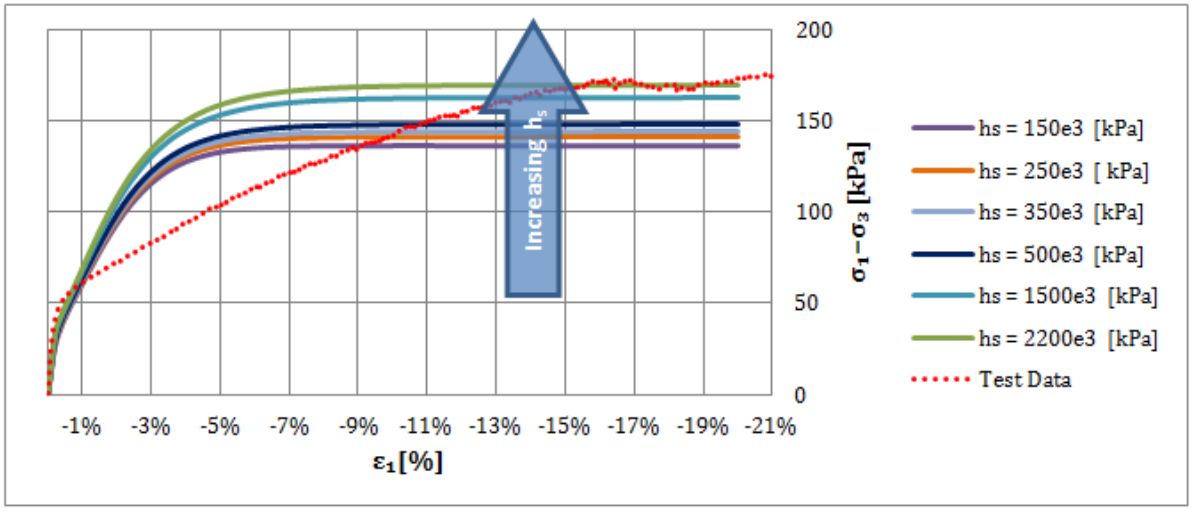

Figure 5.17: Influence of h_s on deviatoric stress ($I_D = 50\%$)

Additionally one can notice that it also determines the amount of generated excess pore pressure, its peak value and the slope of the dissipation curve, a higher h_s seems to determine a higher maximum pore pressure.

Parameter n—Exponent of the compression law

The exponent of the compression law (n) also controls the stiffness of the sample, more specifically it influences the curvature of the deviatoric stress with respect to the axial strain. The results of its calibration can be found in Appendix E, Figures E.3 and E.4. This can be observed both in the curvature of the deviatoric stress with respect to the axial strain and in the curvature of the dissipation path of the excess pore pressure (smaller n—larger curvature). A clear connection between the values of n and the maximum deviatoric stress cannot be fully extrapolated. Its influence should be investigated more.

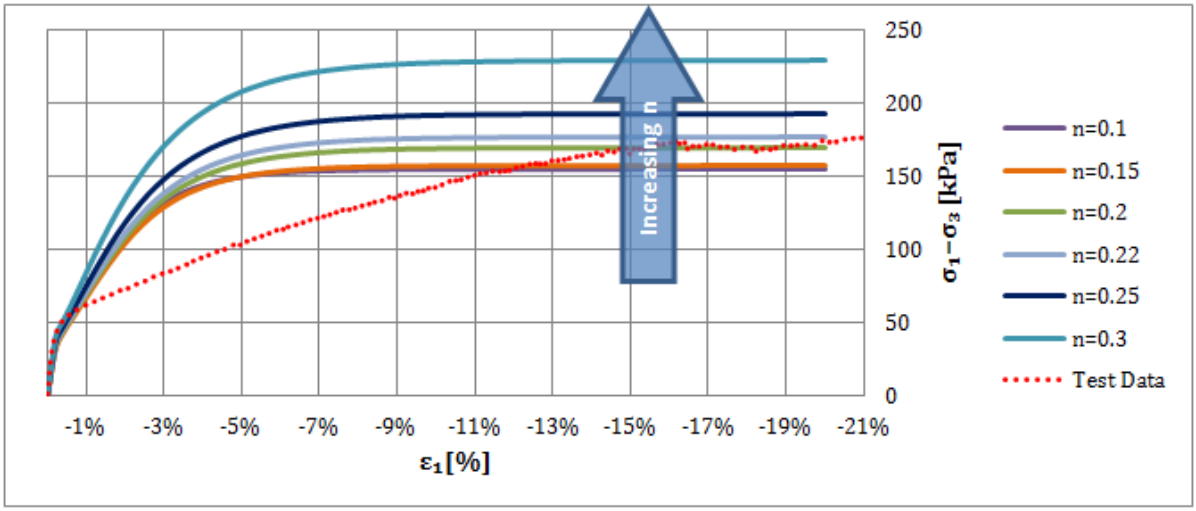

Figure 5.18: Influence of n on deviatoric stress ($I_D = 50\%$)

Parameter α—Pyknotropy factor

Parameter α is one of the two pyknotropy factors of the hypoplastic sand model. The results of its calibration

can be found in Appendix E in Figures E.5 and E.6. α influences the peak friction angle, and controls the mean and deviatoric stresses at failure, as well as the peak pore pressure and the slope of the dissipation curve.

Parameter β—Pyknotropy factor

Parameter β is the second of the two pyknotropy factors of the hypoplastic sand model, it controls the shear stiffness of the response, which can be seen in the curvature of the deviatoric stress with respect to axial strain. The results of the calibration can be found in Appendix E in Figures E.7 and E.8. It has little influence over the mean and deviatoric stresses at failure, but it does influence the curvature of the pore pressure dissipation path (larger β values give steeper pore pressure dissipation curves).

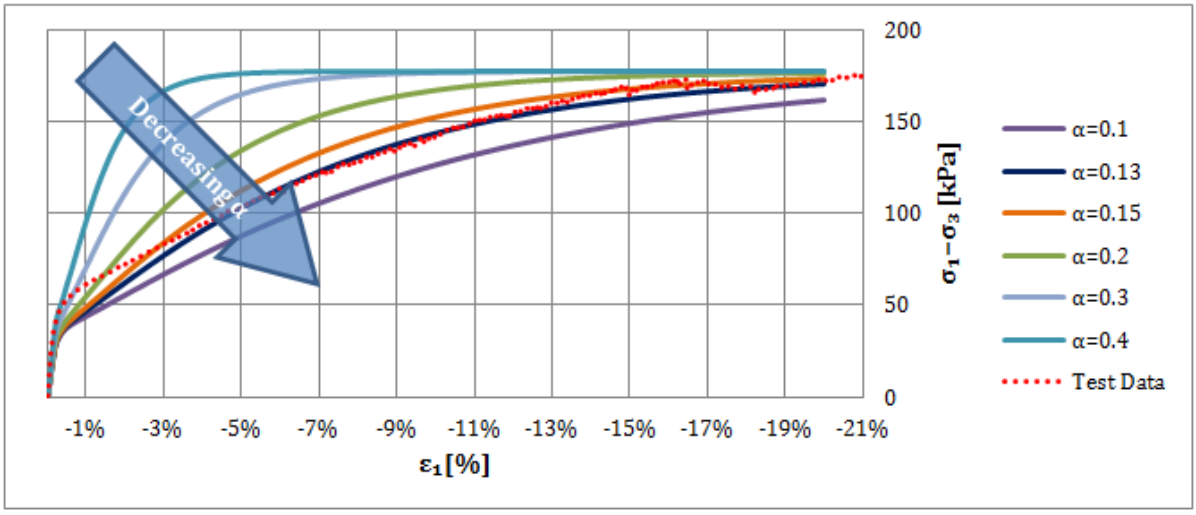

Figure 5.19: Influence of α on deviatoric stress ($I_D = 50\%$)

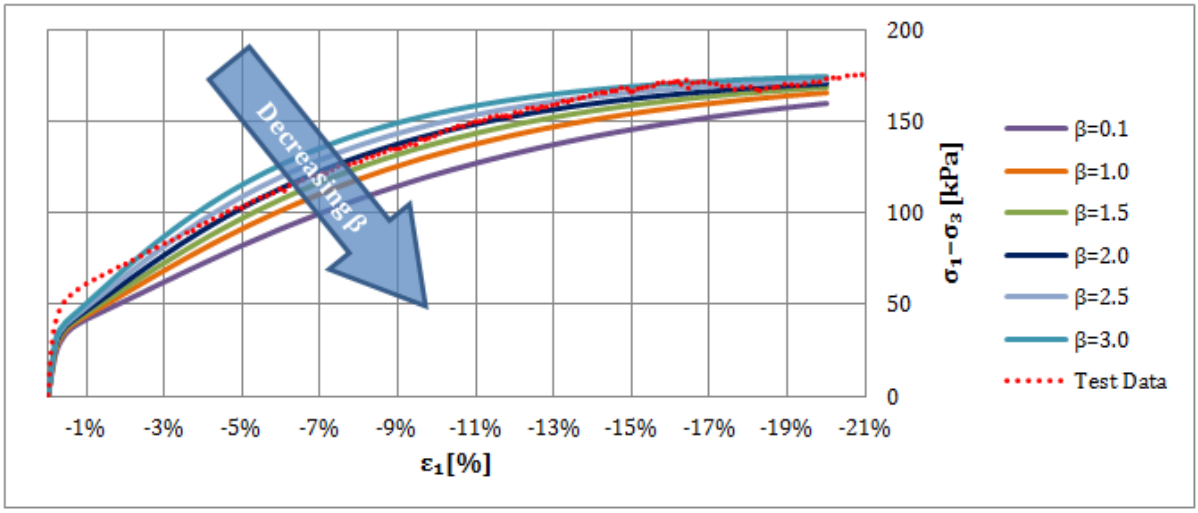

Figure 5.20: Influence of β on σ_3' ($I_D = 50\%$)

Conclusions

The outcomes of the calibration procedures may be found in Appendix E in Figures E.9 and E.10. Additionally the final chosen values for all parameters may be found in Table 5.5. Two important limitations of the model can be mentioned at this moment: the model does not account for densification effects (no softening, nor hardening of the measured stress can be observed), and it has a tendency to generate extra pore pressure.
From the above paragraphs, the following conclusions regarding the influence of the hypoplastic sand model parameters can be drawn—see Figure 5.21.

Material Name	φ_c [°]	h_s [GPa]	n [−]	e_{d0} [−]	e_{c0} [−]	e_{i0} [−]	α [−]	β [−]
Medium dense sand	32.5	2.2	0.22	0.40	0.55	0.85	0.13	1.5
Very dense sand	39.9	1.0	0.17	0.40	0.52	1.00	0.25	2.0

Table 5.5: Outcome of calibration of the hypoplastic sand model parameters

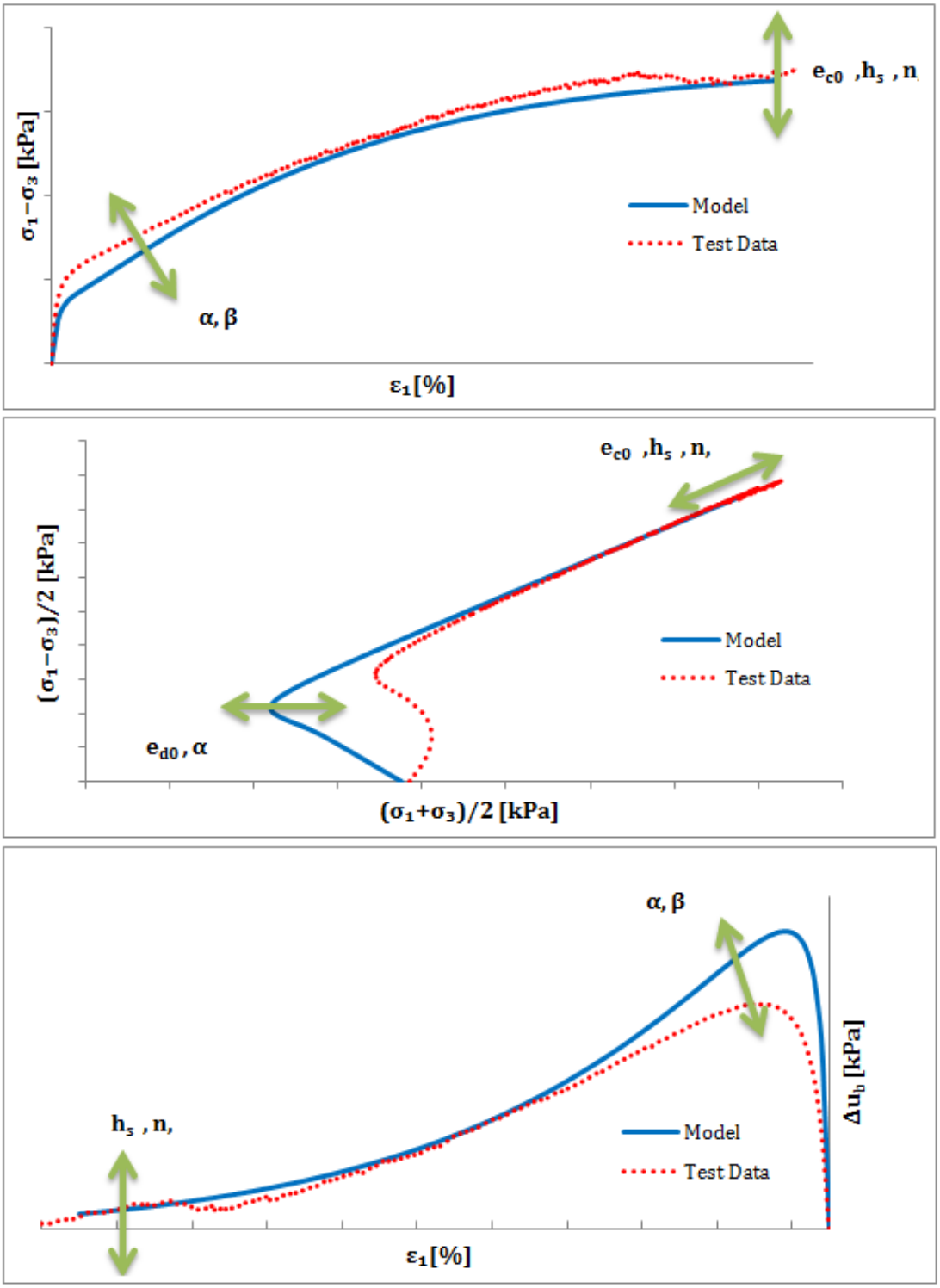

Figure 5.21: Influence of the hypoplastic sand parameters on model behaviour ($I_D = 50\%$)

STEP 3: DETERMINATION AND CALIBRATION OF INTERGRANULAR STRAIN MODEL PARAMETERS

The intergranular strain concept parameters are calibrated using the results of the cyclic loading tests (cyclic direct simple shear, undrained cyclic triaxial tests). These tests were modeled using the soil testing facility in Plaxis 2D. For the cyclic direct simple shear test an initial phase of isotropic consolidation of the medium dense sand sample at 80 kPa was created in order to follow closely the laboratory procedure. In the following phases, the shear stress (τ_{xy}) was varied with the corresponding amplitude depending on the CSSR of the test being simulated (see Figure 5.13). The undrained cyclic triaxial test also included an initial phase of isotropic consolidation of the very dense sand at 40 kPa, further a deviator stress was applied as shown in Figure 5.14, the values depending on the CSSR corresponding to each test simulated.

Critical friction angle (φ'_c)

Finally, the critical state friction angle (φ'_c) is determined based the theory presented in Chapter 2, subsection 2.5.5. The resulting values can be found in Table 5.6.

Soil Type	φ'_c
Medium dense sand	28°
Very dense sand	30°

Table 5.6: Final values of the critical state friction angle (φ'_c)

Parameter m_R—Stiffness multiplier

m_R is a stiffness multiplier for initial and reverse loading, controlling the stiffness increase for a 90° load reversal. The results of the calibration of m_R can be found in Appendix E in Figures E.11, E.12, E.13, E.28 and E.29. As it can be observed from these images, it controls the stiffness of the initial response: larger values give stiffer responses. Therefore, in order to calibrate m_R one will strive to obtain the best fit for the stiffness degradation curve of the first cycle (see Figure 5.22 bellow, and Figures E.14, E.15 and E.16 in Appendix E).

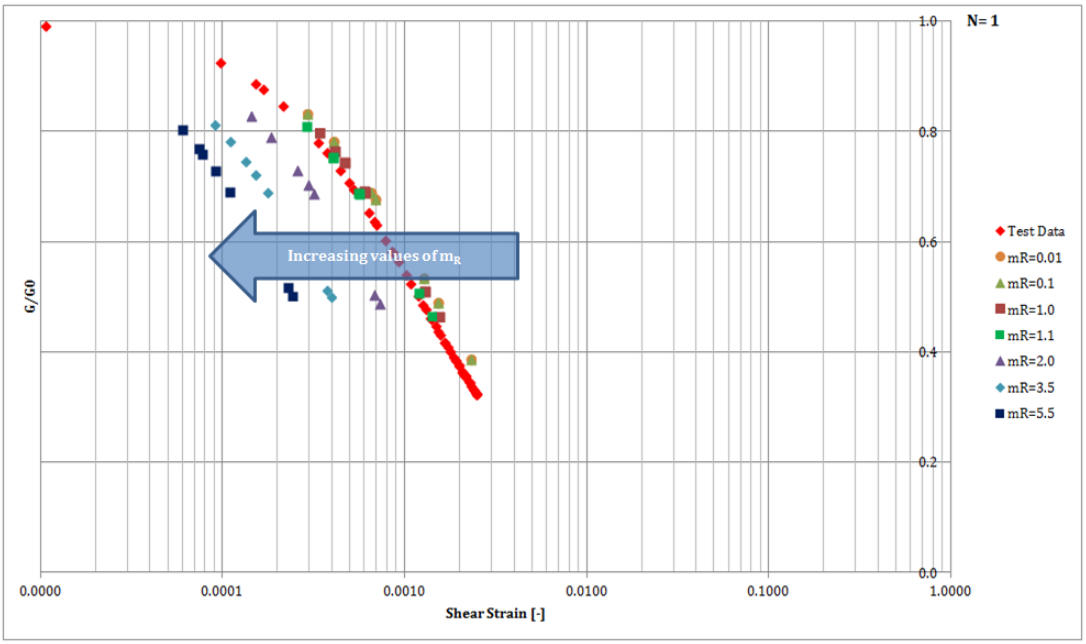

Figure 5.22: Calibration of m_R ($I_D = 50\%$, $CSSR = 0.10$)

In Figures E.11, E.12, E.13, E.28 and E.29 it can be seen that m_R has an influence on the amplitude of the cyclic shear strains and their accumulation rate, but it is very important not to calibrated based on this data, but on the stiffness degradation curves. Nonetheless, the value of m_R must not be lower than unity. In these cases, lower values for m_R were found to give a better fit, and this may be due to the fact that the strains from

the tests are mostly in the medium range (Ishihara (1996)).

Parameter m_T—Stiffness multiplier

m_T is a stiffness multiplier for neutral loading, controlling the stiffness increase for a 180° load reversal. The results of the calibration of m_T can be found in Appendix E in Figures E.17 and E.30. It was observed during the calibration procedure that no significant influence could be observed within the range around $0.5 \cdot m_R$ proposed by Richardson (1988) and Atkinson *et al.* (1990). Yet, the chosen value should not be lower than unity.

Parameter R_{max}—Small strain stiffness limit

R_{max} is the small strain stiffness limit and controls the radius of elastic range. According to Mašín (2012) it may be considered as a material constant, equal to 10^{-4}. For the current samples other values were found to be more adequate due to the fact that the test results used for calibration were in the medium strain range. The results of the calibration of R_{max} can be found in Appendix E in Figures E.18, E.19, E.31 and E.32. As it can be observed from these figures, it determines the amount of elastic response of the sample and this should be considered as main calibration requirement (see Figure 5.23).

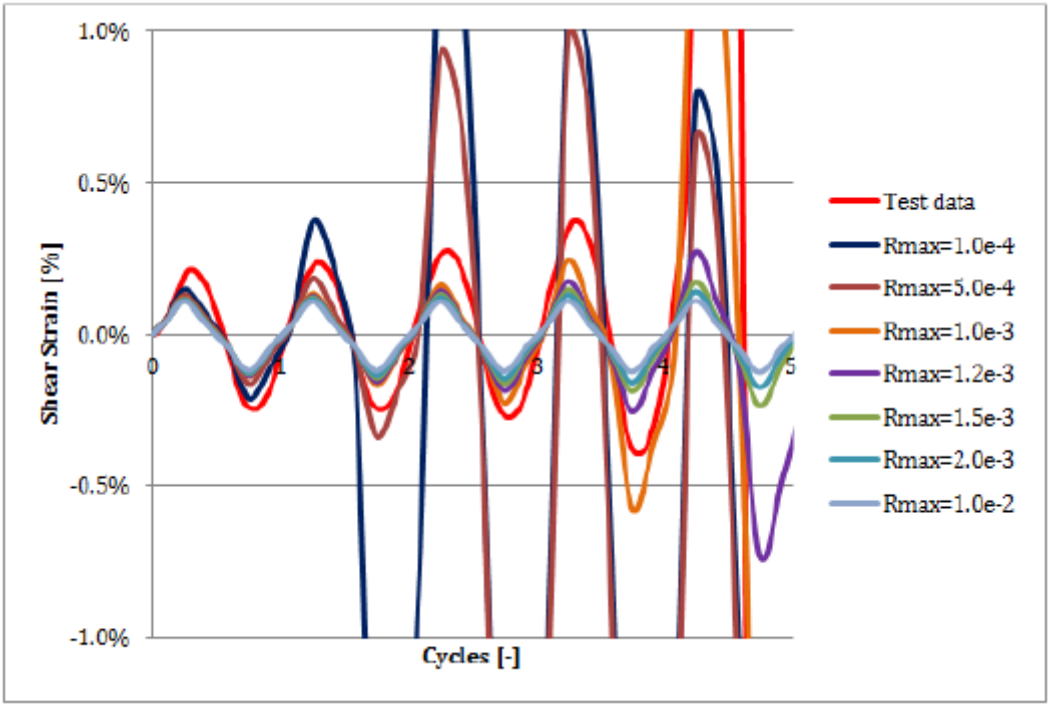

Figure 5.23: Calibration of $R_{max}(I_D = 50\%, CSSR = 0.10)$—shear strain amplitude

Parameter β_r

β_r is a parameter adjusting stiffness reduction curve slope and is the main parameter for the cyclic calibration. The results of the calibration of β_r can be found in Appendix E in Figures E.20, E.21, E.22, E.33 and E.34. From these images it can be concluded that smaller β_r values determine less accumulation of pore pressure and strain, as well as smaller strain amplitudes, while larger β_r values may cause earlier failure and model instability. Furthermore, there is a strong correlation between β_r and the $CSSR$ considered in the load application—see Figure 5.24 below, and Figure E.26 from Appendix E, connecting β_R with $CSSR$ and the number of cycles needed to reach liquefaction.

From Figures 5.24 and E.26 once can conclude that β_r plays a significant role in the extrapolation of the soil calibration from laboratory data to in-situ conditions.

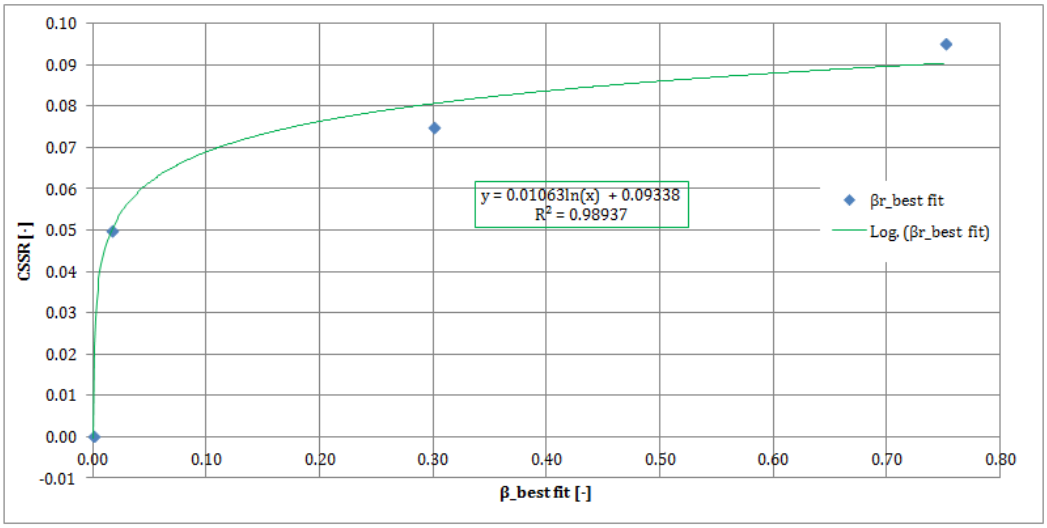

Figure 5.24: Calibration of β_r for different $CSSR$ values ($I_D = 50\%$)

Parameter χ

χ is a parameter adjusting stiffness reduction curve slope, but its influence is similar to the one of β_r (see Figures E.27 and E.37) it is taken as a material constant = 1.

Conclusions

From the above paragraphs, it becomes clear that significant attention must be given to the parameter calibration procedure and that each parameter has to be calibrated keeping in mind its main influential characteristic on the model behaviour, as their influence in certain aspects may overlap.

Finally, the values chosen after the calibration procedure for the intergranular strain concept parameters may be found in Table 5.7.

Material Name	R_{max} [–]	m_R [–]	m_T [–]	β_r [–]	χ [–]
Medium dense sand	$1 * 10^{-4}$	1.1	1	0.016–0.75 ($CSSR$ dependent)	1
Very dense sand	10^{-3}	5	2.5	0.9—0.975 ($CSSR$ dependent)	1

Table 5.7: Values of intergranular strain parameters after the calibration procedure

STEP 4: FROM LABORATORY TO IN-SITU

In order to be able to move from the laboratory conditions to the in-situ conditions, the values of the $CSSR$ used in testing are compared to the ones corresponding to the in-situ conditions (see Figures 5.25). One may observe from this figure that the in-situ conditions corresponding to the operational loads are much smaller than the ones used in the laboratory testing, where 0.05 (5%) was the smallest considered value.
From Figure 5.25 and Figure 5.15 one realizes that the smaller CSSR values will shift the behaviour of the soil from the medium strain level into the very small to small strain ranges where even a linear elastic model would be suitable for the analysis (Ishihara (1996)). Thus, the calibration of the m_R parameter is not adequate for in-situ conditions.

Finally, an extrapolation procedure is used for β_r following the trend shown in Figure 5.24 for the medium dense sand sample. Unfortunately, as only two samples were available for the very dense sample, an extrapolation could not be made. Thus, the very dense sand sample is not further analysed within the model.

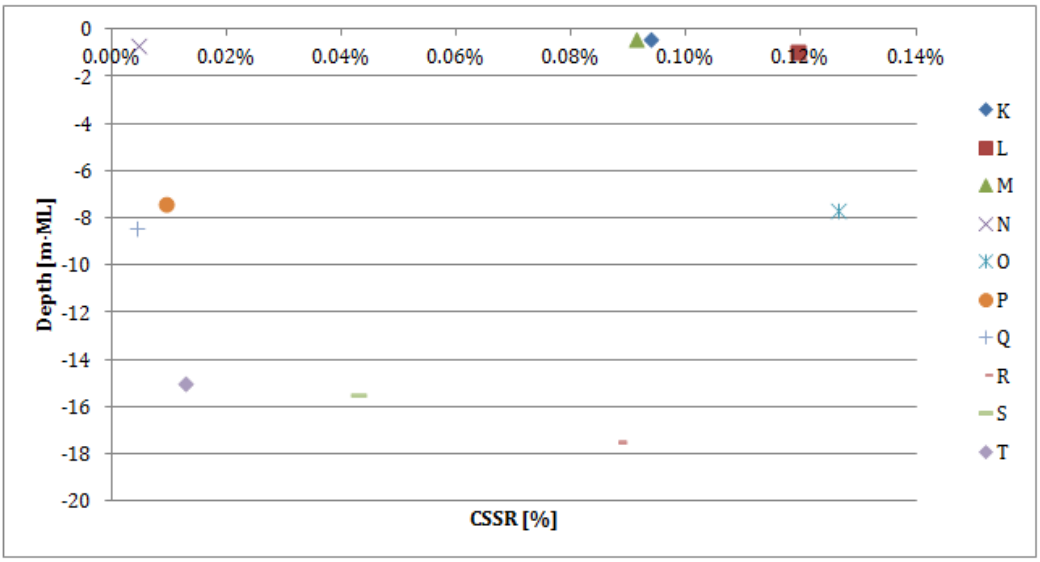

Figure 5.25: *CSSR* values corresponding to operational conditions from OP2 in the medium dense sand sample

CONCLUSIONS

To conclude the section related to the model calibration, the following aspects are important to remember:

- a complete understanding of the given laboratory data is needed before any calibration procedure may start;
- each parameter must be calibrated keeping in mind the main feature that it is expected to change, as there exists a slight overlapping between the influence of each parameter;
- each parameter and their influence on the soil behaviour has been presented thoroughly in the above paragraphs;
- the sensitivity of each parameter was briefly checked with respect to model behaviour, yet the interaction between the changes in one parameter with respect to the others has not been checked;
- the laboratory data is not representative for the operational loading conditions;
- there is insufficient data for an accurate calibration of the parameters influencing the behaviour in the small strain range (m_R, R_{max})—the calibration is made for medium strain range;
- a check between the $CSSR$ values from in-situ and laboratory must be made, and extrapolation of the β_r parameter should be done;
- a minimum of three cyclic tests at different $CSSR$ values are needed in order to be able to extrapolate the β_r parameter for minimal accuracy; and at least one of those tests should be performed so that the strain results are in the small strain range;
- it is assumed that calibrating the soil against the laboratory data and extrapolating this data for in-situ conditions ensures the model calibration;
- the calibrated soil volume tends to overestimate the peak pore pressure and parameters controlling the small strain stiffness are calibrated for medium strain levels—thus a more severe response than in reality.

5.4 ASSUMPTIONS AND LIMITATIONS

The following two subsections will present the relevant assumptions and limitation resulting from the geotechnical modelling. They have also been incorporated in Chapter 1, together with the rest of the assumptions and limitations of this research.

5.4.1 ASSUMPTIONS

The geotechnical modelling of this research project is based on the following assumptions:

- the model calibration is based on laboratory test data and extrapolation of certain parameters for in-situ conditions;
- the soil volume in which the caisson is embedded is considered to be uniform medium dense sand;
- the top plate of the suction caisson is considered infinitely stiff, as a consequence of the usage of stiffeners in reality and as well to ensure that the loads are transmitted to the caisson rim;
- even though the distance between the designed caissons under the jacket structure is limited, no interaction effects shall be considered as it is outside the scope of the current research;
- it is assumed that under cyclic loading conditions pore pressure build-up and strain accumulation will occur, and consequently strength and stiffness degradation;
- it is assumed that between the installation of the offshore wind turbine, until its actual operational condition there is one month of consolidation for the soil;
- it is assumed that the eigen frequency of the structure is determined from the structural model and loads are thus inclusive of amplification effects;
- the applied loading conditions are divided between operational and extreme and applied in a quasi-static manner with 2 phases of instant load application, each followed by a short consolidation period, equivalent to half of the loading period;
- the period assumed for the applied loading conditions is considered to be equal to the period of the associated wave, therefore smaller than in reality (the period of the vertical load is in between the associated wind and wave period).

5.4.2 LIMITATIONS

It is important to know that this thesis and its conclusions are limited with respect to the following issues:

- the solution presented in the current research refers to a three-leg jacket structure with suction caissons as footings;
- the predesigned caisson is overdimensioned with respect to the extreme values of vertical compressive forces, as it was designed also for tension;
- the predesign of the suction caisson does not account for effects of cyclic loading;
- in the predesign for installation and removal of the caisson only rough estimations are provided and no buckling analysis for the skirts of the caisson is done as it is outside the scope of this research;
- the applied loading conditions, as given by Dong and roughly checked by the author, are limited to the chosen foundation solution;

- the period assumed for the applied loading conditions is considered to be equal to the period of the associated wave, therefore smaller than in reality (the period of the vertical load is in between the associated wind and wave period);
- the resulting cyclic loads are applied in a quasi-static manner and not dynamically;
- the results of this thesis refer to sandy soil conditions;
- the method of analysis is a numerical model, thus careful consideration in the interpretation of these results must be given;
- the soil considered in the geotechnical modelling is uniform, there is no account of variability with respect to depth, nor horizontally—this is highly unrealistic due to the size of the foundations but also of the offshore wind farms that extend over tens of square kilometers sometimes;
- the sand considered is medium dense sand, as only for this sample there existed sufficient information for calibration, within the North Sea dense and very dense sand conditions are more common, thus the analysis is more conservative;
- effects of preshearing within the soil mass are not considered;
- in order to calibrate the soil model the minimal laboratory testing that should be carried out includes: one isotropically consolidated undrained triaxial test, one constant head permeability test, three undrained cyclic direct simple shear tests (or three undrained cyclic triaxial tests), out of which at least one test should provide give strain results for the small strain range;
- the model is calibrated against laboratory data which is not fully suitable for the in-situ conditions: the tests were performed in a medium strain range. Therefore, one must remain critical with respect to the parameters reflecting small strain stiffness, and the extrapolations required to adjust some of these parameters;
- there is insufficient data for an accurate calibration of the parameters influencing the behaviour in the small strain range (m_R, R_{max})—the calibration is made for medium strain range;
- the chosen hypoplastic model has a tendency to overestimate the pore pressure build-up;
- the hypoplastic model does not account for densification effects, this may be observed in the calibration procedure, where the resulting stress state in the model remains equal to the applied stress, while in the laboratory sample a damping of the measured stress can be observed;
- the non-symmetry of the mesh plays a significant role in the generation of non-symmetric “plastic” failure mechanisms, even though the load is symmetrically applied at boundary value problem level;
- there is no model test data available to be used in order to validate the chosen model.

5.5 MODEL VALIDATION

The best way to validate the model would imply performing either model or full scale tests of suction caissons embedded in sand and subjected to vertical cyclic loading. Moreover, the sand must be previously tested as described in the model calibration procedure.

Unfortunately such data could not be found. Within his thesis, Senders (2008) performed vertical cyclic loading of the model caisson, but as he mentions “the very small displacement were elastic” and therefore do not constitute a sufficient base for validation. Furthermore, Byrne & Houlsby (2000) and Byrne & Houlsby

(2002) performed also model tests of suction caissons embedded in sand, but the sand used was not previously subjected to any laboratory cyclic load testing, thus not providing any basis for calibration. Even though an extensive database for cyclic testing of sand can be found within the NGI database, their model testing included suction anchors in clay and also suction caissons in sand, the later could not be acquired in order to fulfill the time constraints of this research.

As no adequate data was found for validation, the problem was analysed using axisymmetry within Plaxis 2D, in order to check whether 3D calculations are required. The reason for which axisymmetric analyses are possible is connected to the cylindrical shape of the suction caisson and the applied loading which is purely vertical, with no horizontal components. This method was not chosen from the very beginning due to the increased manual work needed to create the cycles for the analyses. As it has already been mentioned in the section related to the geometrical discretisation within the three dimensional environment, issues regarding the computational accuracy may appear from difficulties in an accurate integration of stresses on curved surfaces and unbalance in pore pressures caused by the high water depth. These issues would be avoided by using the hypoplastic model within the axisymmetric environment, which is better suited for the analysis of cylindrical shaped problems.

The Plaxis 3D version allows for an expert mode in which commands may be used in order to generate the different phases for calculation in a semi-automatic manner. The commercially available Plaxis 2D version, does not yet have the expert mode available, but a newer version is presently being developed that incorporates this possibility. Therefore, a few analyses were carried out using this unreleased version. These analyses were carried out using the data from the extreme case EX 1ii (see Figure 5.27). A few "bugs" were identified and reported during this process. The results of these analyses may be found in Appendix H.

Four analyses were carried out, focusing mostly on the effects of the pore pressure build-up, rather than strains:

- Case A: The load was applied using 4 consolidation phases, basically the 2 plastic phases were replaced by 2 consolidation phases with a duration of 0.1 s. The analyses were stopped at the seventh cycle when the maximum pore pressure exceeded the maximum allowed effective vertical stress (approx. 450 kPa);
- Case B: The load was applied in 4 phases as described in subsection 5.2.4, 2 plastic phases of instantaneous loading each followed by a very short consolidation phase. The analyses were stopped at the first cycle when the maximum pore pressure exceeded the maximum allowed effective vertical stress (approx. 450 kPa);
- Case C: The load was applied using 4 consolidation phases, the 2 plastic phases were replaced by 2 consolidation phases with a duration of 0.01 s. The analyses were stopped at the first cycle when the maximum pore pressure exceeded the maximum effective vertical stress;
- Case D: The load was applied using 4 consolidation phases, the 2 plastic phases were replaced by 2 consolidation phases with a duration of 0.05 s. The analyses were stopped at the first cycle when the maximum pore pressure exceeded the maximum effective vertical stress;

The first thing that one notices in the results from Appendix H and Appendix G for the results of case EX 1ii is that there exists less instability in the obtained results, particularly in the cases using all consolidation phases. One also observes that as the time for the consolidation phase, used to activate and apply the new load, decreases the generated pore pressure increases—see Table 5.8.
Based on the results from Table 5.8 one may conclude that the results obtained throughout the course of this thesis represent a conservative boundary, as the generated excess pore pressures and strains are larger than in the validation cases.

Case [−]	Cycle and phase [−]	Duration of load application [s]	Maximum pore pressure [kPa]
EX1 ii (3D)	1.1	0	-297.7
A (Axisymm.)	1.1	0.1	-213.3
B (Axisymm.)	1.1	0	-224.9
C (Axisymm.)	1.1	0.01	-253.4
D (Axisymm.)	1.1	0.05	-234.6

Table 5.8: Values of generated pore pressures for validation and original cases

5.6 MODEL SCENARIOS

Within the course of this thesis, several scenarios are considered in order in order to check the sensitivity of the model to changes related to applied loading conditions such as changes in mean load, amplitude of loading and period.

5.6.1 SENSITIVITY TO APPLIED LOADING CONDITIONS

The loading sensitivity is related to the three main characteristics of cyclic loading:

- mean load;
- cyclic amplitude;
- period of the cyclic load;

OPERATIONAL LOAD SCENARIOS

The operational load scenarios (see Figure 5.26) represent 60–70% of the loading that occurs within the life time of an offshore wind turbine. It can be noticed that the applied loading in these cases does not represent more than 10% of the caisson capacity. Therefore, from these load cases one can expect very little deformations and pore pressure build-up.

Operational cases					Mean/ Capacity	Max/ Capacity
Case	Period	Caisson	Mean Load	Amplitude		
[-]	[s]	[-]	[kN]	[kN]	[%]	[%]
OP	7.32	1 (65.86%)	-3744	800	5.3%	6.5%
		2 (74,71%)	-6318	500	9.0%	9.7%
		3 (70.5%)	0	650	0.00%	0.2%

Figure 5.26: Characteristics of operational load scenarios

EXTREME LOAD SCENARIOS

The extreme loading scenarios as defined in Figure 5.27 have the purpose to investigate the caisson behaviour under extreme loads approaching and even surpassing caisson capacity. These were not derived from the actual loading conditions as provided by Dong. In these cases one expects to observe significant accumulation of strains and pore pressure, and thus significant damage. Based on the results of these analyses one may be able to draw conclusions related to the model's sensitivity to changes in mean load and amplitude.

Extreme cases					Mean/	Max/
Case	Period	Caisson	Mean Load	Amplitude	Capacity	Capacity
[-]	[s]	[-]	[kN]	[kN]	[%]	[%]
EX 1	7.32	1 or 2	-35189	8797	50.0%	62.5%
				17595		75.0%
				35189		100.0%
EX 2	7.32	1 or 2	-24600	500	35%	35.7%
				5000		42.1%
				1500		37.1%
EX 3	7.32	3	20200	500	40.7%	41.7%
				5000		50.8%
				10000		60.9%

Figure 5.27: Characteristics of extreme load scenarios (negative values represent compressive forces and positive values represent tensile forces)

An investigation should be carried out regarding the influence of increasing the load period, currently equal to the period of the operational associated wave, to the period of the extreme 50 year storm wave of 12.6 seconds, and further to 30 seconds. The latter value is based on typical measurements of the thrust force on a 6 MW offshore wind turbine at a wind speed of 16 m/s (see Figure 5.28). Such an investigation should reveal the beneficial effects of the increased period on the pore pressure dissipation and consolidation allowed within Phases 2 and 4 of each quasi-statically applied load cycle.

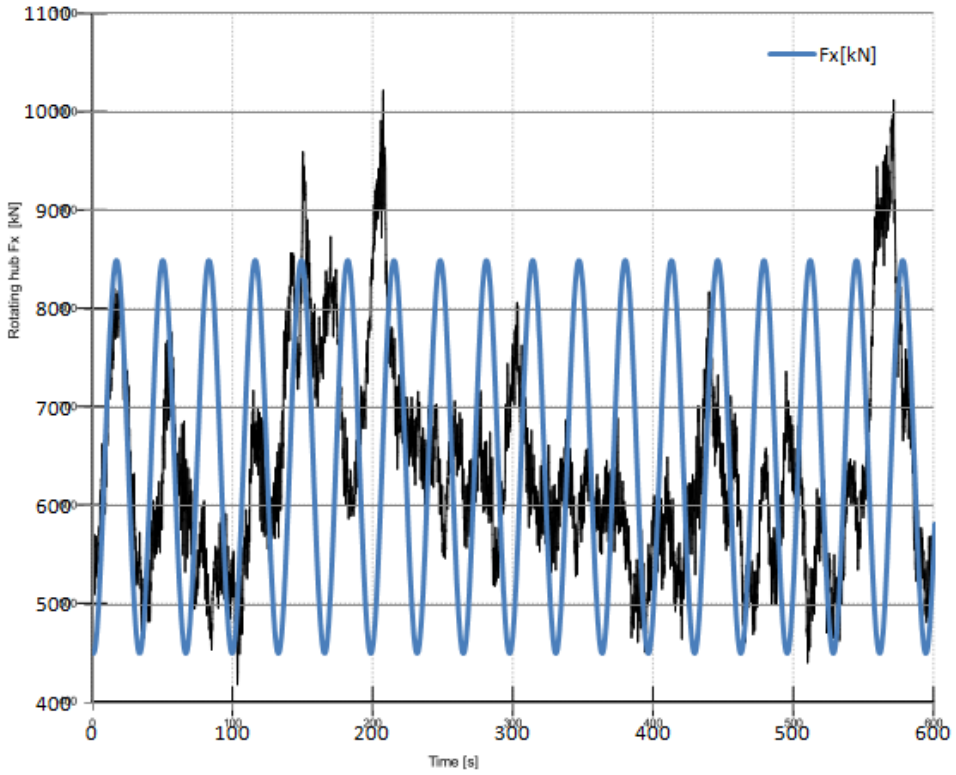

Figure 5.28: Typical measurements of the thrust force on a 6 MW offshore wind turbine at a wind speed of 16 m/s

5.7 CONCLUSIONS

The present chapter aimed to present the model proposed for the analysis of long term cyclic loading of suction caisson foundations, the manner through which the problem is discretised, the assumptions made and subsequent limitations, as well as present the scenarios to be considered.

The proposed model (see Figure 5.1) has three main components: an implicit procedure, based on the hypoplastic sand model with intergranular strain concept integrated and aiming to ensure accuracy; an explicit procedure based on extrapolations, in order to provide a bridge for the large number of cycles to be considered; and a step of reactualization for strength and stiffness of the considered soil volume. More details can be found in section 5.1.

The problem is discretised from a geometrical point of view differently for operational conditions than for extreme conditions, where only a quarter of the problem is analysed, and thus different boundary conditions will also be used. The reason for this is that when larger loads are applied the non-symmetry of the automatically generated mesh determines the formation of non-symmetric "plastic" failure mechanisms.

The initial conditions consider that there exists a one month period between the installation of the wind turbine to its actual start of operation, allowing for a full dissipation of the excess pore pressures. Therefore, allowing for a one month consolidation period. Furthermore, it is presented within the same section the manner through which the load is applied in a quasi-static manner. More details can be found in section 5.2.

An important aspect modelling is the model calibration (see section 5.3), which is based on the calibration of the soil from the provided laboratory data (see Appendix D) and further extrapolated to reflect the in-situ conditions. For the calibration of the hypoplastic model parameters a sensitivity analysis was performed in order to determine the influence of the parameters on the soil behaviour. The results of the soil calibration may be found in Appendix E. More details can be found in section 5.3.

Some of the most important outcomes of the soil calibration refer to the laboratory testing that should be carried out: isotropically consolidated undrained triaxial tests, constant head permeability tests, undrained cyclic direct simple shear tests (or undrained cyclic triaxial tests), out of which at least one test should provide results for the small strain range. Furthermore, the calibrated soil volume will tend to overestimate the pore pressure build-up and is not fully adequately calibrated for the small strain range. These latter two aspects will lead to a conservative design.

Based on the proposed model, several assumptions are considered, such as a uniform soil volume, no variability in soil properties are considered, within which the caissons are embedded; even though the distance between the caissons is limited and interaction is possible, this is not analysed within this thesis as it exceeds the scope. Most importantly it is considered that the calibration of the model based on the calibration of the soil to laboratory data and further extrapolated to in-situ conditions, is representative for the current problem.

Additional to the assumptions made, several limitations must be kept in mind: the results obtained are representative for the chosen three-leg jacket structure with suction caissons as footings embedded in a uniformly medium dense sand volume; spatial variability of soil conditions is not considered; the chosen loading period is conservatively chosen to be equal to the wave period; the available laboratory data used in the calibration is not completely suitable for the in-situ loading conditions and extrapolation is needed; and most importantly there are no model tests available to validate the results. All the assumptions and limitations may be found in section 5.4 of this report.

As this is a numerical model, a series of scenarios are suggested in section 5.6 to check its sensitivity to changes in mean load, cycling amplitude, loading period and coefficient of consolidation.

In order to provide a clearer view regarding the actions needed to be followed to analyse this problem, a stepwise procedure was created based on the experience of this research—see Figure 5.29.

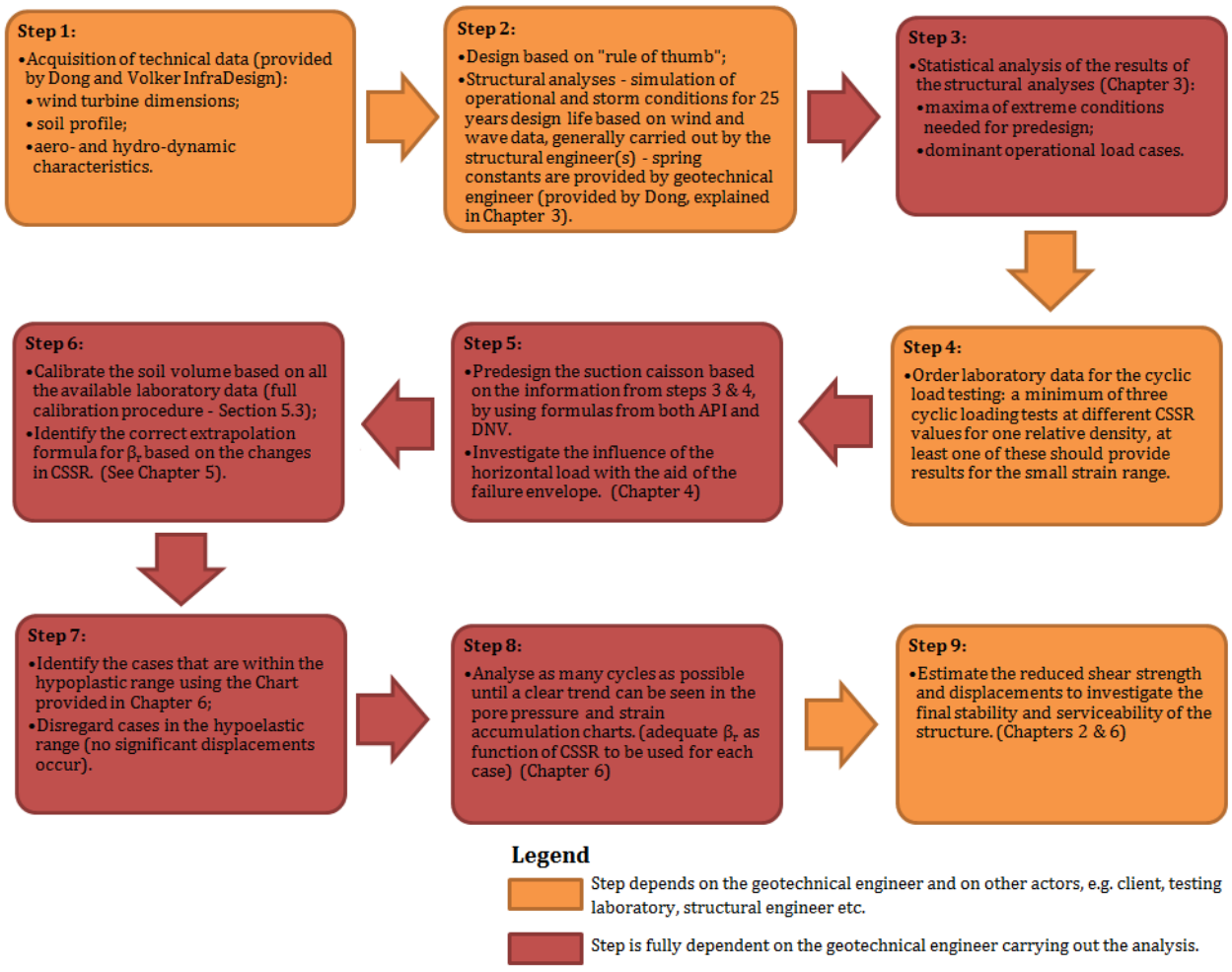

Figure 5.29: Step-wise procedure in order to investigate long term effects of cyclic loading on suction caissons

The following chapter shall present the results of the analyses conducted in order to determine the effects of vertical long term cyclic loading on suction caisson foundations embedded in a uniform medium dense sand volume.

Chapter 6

RESULTS OF GEOTECHNICAL MODELLING

The sixth chapter of this report presents the results obtained from the analyses carried out by following the steps described in Chapter 5. Conclusions related to caisson behaviour under operational and extreme conditions are drawn. Moreover, aspects such as sensitivity to changes in mean load and cyclic amplitude are discussed. Finally, the author discusses the adequacy of the existing guidelines for the problem at hand.

The first section of this chapter presents and interprets the results of the analyses carried out using the operational cases defined in Figure 5.26 in Chapter 5, that represent approximately 70% of the loading conditions within the design life of 25 years of an offshore wind turbine. All the results of the operational load cases may be found in Appendix F.

Section 6.2 shows the results of the analyses carried out using the extreme loading conditions as defined in Figure 5.27 from Chapter 5. The adequacy of the full proposed model is discussed within this section. The results of these analyses may also be found in Appendix G.

Section 6.3 shows the implementation of the suggested explicit procedure.

Section 6.4 presents the main outcomes regarding the influence of the changes in mean load and cycling amplitude, finally providing a plot of these changes with respect to the foundation's capacity.

Section 6.5 aims to compare the used model to the guidelines given by API (2011) and DNV (1992), as described in the second chapter of this report and implemented in the fourth for the predesign of suction caissons as foundations for offshore wind turbines.

Finally, the section dedicated to the conclusions sums up the main outcomes of all the carried out analyses.

6.1 OPERATIONAL CONDITIONS

For the operational conditions 520 cycles were analysed in sequences of approximately 25 cycles (100 phases) at a time, the outcomes of these analyses can be found in Appendix F. When looking at these results one notices that the response to the applied loading conditions (Figure 5.26) is almost symmetric and that the accumulation trends are almost insignificant within the 520 cycles. These results are not unexpected as the applied loading in all cases is less than 10% of the caisson's capacity, and from the literature review follows that for axial cyclic loading conditions on piles in clay under 50% of the ultimate foundation capacity the produced displacements were not significant (Briaud & Felio (1986b)), no information was found for sand.

In this case it can be concluded that the event causing the largest amount of deformation is the period between the installation and commence of operation of the turbine. Upon analysing closely the excess pore pressure (see Figures F.3, F.9 and F.15) and the axial strain charts (see Figures F.5, F.11 and F.17) one may conclude that the behaviour corresponds mostly to the hypoelastic range and little hypoplastic behaviour actually occurs.

Based on the obtained results for the volumetric strain (see Figures F.6, F.12 and F.18) and to simplify calculations linear accumulation over the number of cycles is assumed. This is done instead of the logarithmic trend expected due to reaching a stable state based on convergence of the results. The assessment of the changes in void ratio due to operational loads is presented in Figure 6.1. It is noticed from these calculations that a number of cycles larger than 10^6 is needed to be analysed in order to obtain sufficient change within the volumetric strain so that a significant change in void ratio occurs, where the rate of accumulation of the volumetric strain is assumed to increase linearly instead of logarithmically, thus overestimated. Due to the increased computational time needed to analyse 10^6 cycles in order to obtain a potential sufficient change in void ratio one shall not proceed further with these cases as they do not produce significant changes.

Case ID	**OP1 (for caisson 1, Fmean = -3744 kN, Ampl = 800 kN)**								
		Cycle(s) - N	**ε_v**	**$\Delta\varepsilon_v$**	**$\Delta\varepsilon_v$/N**	**e_{520}**	**N**	**$\Delta\varepsilon_v$**	**e_{1E06}**
Point 1	L	0	-1.50E-05						
		520	-2.20E-05	-7.00E-06	-1.3E-08	0.540000	1.00E+06	-0.01344	0.523743
Point 2	M	0	-4.40E-05						
		520	-4.75E-05	-3.50E-06	-6.7E-09	0.540000		-0.00672	0.529655
Case ID	**OP2 (for caisson 2, Fmean = -6318 kN, Ampl = 500 kN)**								
		Cycle(s) - N	**ε_v**	**$\Delta\varepsilon_v$**	**$\Delta\varepsilon_v$/N**	**e_{520}**	**N**	**$\Delta\varepsilon_v$**	**e_{1E06}**
Point 1	L	0	-5.50E-06						
		520	-1.10E-05	-5.50E-06	-1.1E-08	0.540000	1.00E+06	-1.06E-02	0.52374
Point 2	M	0	-4.40E-05						
		520	-4.75E-05	-3.50E-06	-6.7E-09	0.540000		-6.72E-03	0.52965
Case ID	**OP3 (for caisson 3, F mean =0 kN, Ampl = 650 kN)**								
		Cycle(s) - N	**ε_v**	**$\Delta\varepsilon_v$**	**$\Delta\varepsilon_v$/N**	**e_{520}**	**N**	**$\Delta\varepsilon_v$**	**e_{1E06}**
Point 1	L	0	-1.25E-05						
		520	-1.52E-05	2.70E-06	5.2E-09	0.540000	1.00E+06	5.18E-03	0.54798
Point 2	M	0	-1.28E-05						
		520	-1.62E-05	3.45E-06	6.6E-09	0.540000		6.62E-03	0.55020

Figure 6.1: Assessment of changes in void ratio (see equation 5.6) due to operational loads based on the change in volumetric strain at the top of the caisson (locations of the points can be seen in Figure 5.9)

A rough estimation of the anticipated tilt angle of the structure is made based on the theory of determination of the angle between two vectors normal to the initial and tilted plane. The outcomes of this calculation can be seen in Figure 6.2. The tilt angle of the structure is calculated using the displacements caused by the operational case OP1 on caisson 1, OP2 on caisson 2, respectively OP3 on caisson 3.

Geometry		
C-C	23	[m]
Radius	13.28	[m]
Height	19.92	[m]

Initial [m]			
Points	X	Y	Z
1	6.64	11.5	0.00
2	6.64	-11.5	0.00
3	-9.9593	0	0.00
Determination of vector normal to the caissons' plane			
	i	j	k
Vector 0-1	6.64	11.50	0.00
Vector 0-3	-9.96	0.00	0.00
Normal vector	0.0	0.0	114.5

After Installation [m]			
Points	X	Y	Z
1	6.64	11.5	-0.00020
2	6.64	-11.5	-0.00030
3	-9.9593	0	-0.00005
Determination of vector normal to the caissons' plane			
	i	j	k
Vector 0-1	6.64	11.50	-0.00020
Vector 0-3	-9.96	0.00	-0.00005
Normal vector	-0.0006	-0.0023	114.5

Tilt	0.0012	[°]

Figure 6.2: Assessment of the tilt angle of the structure due to operational loads, the three points are considered at the centre of the top plate

Following from the above calculations, it can be concluded that for the operational loading scenarios of axial loads applied cyclically at lower levels than 10% of the caisson's capacity no significant changes within the soil mass occur. Consequently, no significant changes in capacity, nor significant displacements occur. Therefore, it is safe to assume that higher levels of cyclic loading, corresponding to storm-like events have a main role in producing significant changes in the strength and generating higher levels of displacement.

Furthermore, an analysis was carried out based on the dominant statistics regarding the loading conditions ($F_{mean} = 6600\ kN$, $Amplitude = 1700\ kN$, $F_{max} < 11.8\%$ of capacity):

- 97.5% of the mean compressive loads can be found in the interval 2700–6600 kN (see Figure 3.5), values exceeding this range are assumed to correspond to extreme conditions;
- 97.5% of the ranges of variation of the mean load (2· Amplitude) are below 3400 kN (see Figure 3.6), values exceeding this range may be assumed to correspond to extreme conditions;

The response following from this analysis showed the same trend as the operational load cases 1 and 2. Therefore, it can be concluded that 97.5% of the loading occurring during the lifetime of the considered offshore wind turbine, is presently lower than 12% of the capacity and determines a mainly hypoelastic response of the foundation. Thus, the events causing large displacements and higher pore pressure build-up are due to storm conditions, which are analysed in the following section.

6.2 EXTREME CONDITIONS

The considered extreme conditions can be found in Figure 5.27, and the results of these analyses are available in Appendix G.

6.2.1 EXTREME COMPRESSIVE LOADS

As expected due to the extreme loading conditions one can observe significant pore pressure and strain accumulation (see Figures G.3, G.12, G.6, G.15). From the same figures, one realises that the pore pressure is significantly overestimated, considering the expected effective vertical stress is around 450 kPa. The overestimation of the pore pressure was expected from the soil calibration, but it also becomes clear that above the

boundary of 450 kPa the results are erroneous. A soil calibration including the missing data for loading at small CSSR values and with more small strain measurements might potentially avoid this effect.

The images presenting the changes in void ratio—see Figures G.17, G.18, G.19, G.20, G.21 confirm that the sand densifies within the first cycles until it reaches its densest state, followed by localised loosening under the caisson top plate and centre. One can assume based on the pore pressure graphs and the void ratio images that for these analyses some of the sand particles found in the central area within the caisson become suspended, reaching liquefaction within the first two cycles, while closer to the rim the sand continues to densify.

The extreme loading conditions from the cases with the identifications EX1 are even more severe than the ones presented within the Dong loading data. The distribution of the loading data obtained from Dong (see Figures B.7, B.8 and B.9) shows clearly that for high mean loading values, the corresponding amplitude is much smaller: for the maximum mean compressive loads, the corresponding amplitude intervals are below 500 kN (0.71% of capacity).

The results of the analyses show significant damage (high pore pressure and strain accumulations), which was expected considering the applied mean load was at 50% of capacity and with amplitudes of 12.5%, 25% and 50% of the capacity. It also becomes clear that as the amplitude increases, the more severe the response of the model is: higher excess pore pressures, higher strains and displacements. Unfortunately, the generated values are overestimated and potentially erroneous, as explained already in Section 5.5.

Following the trend of the data provided by Dong, case EX 2i was created in order to investigate the behaviour under conditions resembling storm conditions. In Figures G.28 and G.29 one will notice that the response to loading similar to the characteristics of the "monster wave" as found by Dong (high mean load, but low cyclic amplitude) will give a hypoelastic response. Therefore, one concludes that it is a combination of mean load and cyclic amplitude that will determine higher pore pressure build-up and strain accumulation. This aspect is more thoroughly presented in Section 6.4.

6.2.2 EXTREME TENSILE LOADS

From the operational loading case for the third caisson, one notices that loading occurring at a zero average between tension and compression with a 650 kN amplitude renders a hypoelastic response. For this reason, the extreme cases from Figure 5.27 with the identification EX 3 were suggested. The results from these analyses can be found in Appendix G.

In Figures G.32 and G.31 it can be observed that at a mean tensile load of approximately 40% of the tensile capacity, but with a small amplitude, less than 2% of the tensile capacity, the caisson behaviour is dominantly hypoelastic—no strain accumulation can be observed. But, as the cyclic amplitude of the applied load increased to 5000 kN (approximately 10% of the tensile capacity) strain accumulation occurs, even though no significant effect on the pore pressure can be seen. Therefore, one can conclude that as long as the tensile loads are applied within certain boundaries, the caisson can undertake tensile loading. Further details regarding this shall be provided in Section 6.4.

6.3 EXPLICIT PROCEDURE

As in the operational loading cases the response of the foundation was within the hypoelastic range and extrapolations were not possible, the check for the viability of the extrapolation procedure is done on the extreme loading case identified as EX 1 ii. The reason for this choice is that the change in void ratio is significant even during the first 25 cycles—see Figure 6.3. From Figures 6.3 and 6.4 one may notice that the estimation with

Case ID		EX1ii							
		Cycle(s) - N	ε_v	$\Delta\varepsilon_v$	$\Delta\varepsilon_v/N$	e_{10}	N	$\Delta\varepsilon_v$	e_{25}
Point 1	K	0	-2.97E-04						
		10	-6.17E-03	-5.87E-03	-5.9E-04	0.530957	25	-1.5E-02	0.52
Point 2	S	0	-3.42E-04						
		10	-2.74E-03	-2.40E-03	-2.4E-04	0.536303		-6.0E-03	0.53

Case ID		EX1ii							
		Cycle(s) - N	ε_v	$\Delta\varepsilon_v$	$\Delta\varepsilon_v/N$	e_{10}	N	$\Delta\varepsilon_v$	e_{25}
Point 1	O	0	-1.72E-04						
		10	-4.11E-03	-3.94E-03	-3.9E-04	0.533936	25	-9.8E-03	0.52
Point 2	Q	0	-1.23E-04						
		10	-1.71E-03	-1.59E-03	-1.6E-04	0.537556		-4.0E-03	0.53
								$e_{25,avg}$	**0.525**

Figure 6.3: Assessment of changes in void ratio (see equation 5.6) due to extreme load case EX 1 ii based on the change in volumetric strain at the top of the caisson (locations of the points can be seen in Figure G.2)

the empirical formula over 15 cycles (from cycles 10 to 25) seems to give accurate results.

In order to check whether the change in void ratio within the model renders the same results the soil volume within the caisson was assigned the new void ratio of $e_0 = 0.525$ reflecting the new densified state.

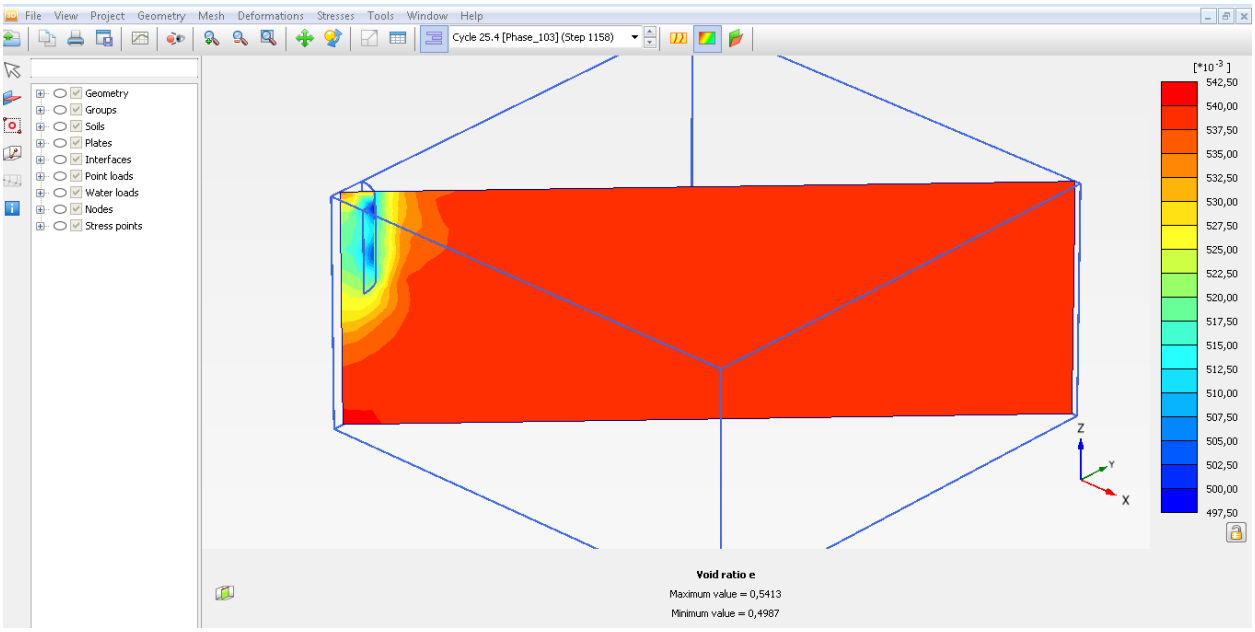

Figure 6.4: Changes void ratio from EX 1 ii, 25^{th} cycle

Unfortunately, as it can be seen in Figure 6.5 the results are not equivalent to the initial analysis. The direct usage of a denser sand ($I_D \approx 54\%$) gives results showing less strain accumulation and pore pressure build-up. Therefore, it becomes obvious that the loading history plays a significant role in the response of the foundation.

Additionally, it becomes clear that the denser the initial sand is, the less pore pressure and strain accumulation occurs. The attempt to extrapolate by using the change in void ratio is therefore not a viable option, as the new considered soil does not have the same development and stress history.

Therefore, the suggested method for extrapolation based on the change in volumetric strain determining a new soil profile cannot be implemented for these extreme conditions where the history of loading, also known

as preshearing has such a significant effect. While for loading conditions within the hypoelastic region, the changes in volumetric strain are not sufficient to justify the usage of the extrapolation formula. Nonetheless, the implicit part of the model provides valuable information regarding the response of the foundation with respect to the applied mean load and its cyclic amplitude as it will be shown in the following section.

Figure 6.5: Volumetric strain development after change of void ratio, 1–95 cycles

6.4 INFLUENCE OF CHANGES IN MEAN LOAD AND CYCLIC AMPLITUDE

From the conclusions drawn related to the behaviour of the foundation under the defined operational cases, it became clear that when the applied load is below 10% of the capacity the behaviour of the foundation corresponds to the hypoelastic region of the model. Further investigation has shown that for a mean load below 25% of the compressive capacity and an amplitude of 5%, the behaviour remains within the elastic region, but as the amplitude increased to 6.25% plastic failure mechanisms were formed. Even a mean load at 50% of the compressive capacity but with an amplitude under 1% also determined no strain nor pore pressure accumulation, the response generally reaching a value at which it stabilises. Similar effects were found with respect to tensile loading and tensile capacity.

Therefore, it is concluded that a combination of the mean load and cyclic amplitude determines the foundation response to the applied loading. In Figure 6.6 the results from several analyses are plotted with respect to the dominant soil response: hypoelastic (no strain accumulation within the generated number of cycles) or hypoplastic. Following from this distinction between the two responses, one may draw a boundary under which the hypoplastic strains occurring are not significant.

Based on Figure 6.6 one may design a caisson for which the response would remain within the boundaries of no significant strain or pore pressure accumulation. But, in practice a balance must be found also with respect to the costs involved. It is the belief of the author that with accurate calibration of the sand used within the model, a more realistic response to the extreme loading conditions can be obtained. However, before any final conclusion with respect to the accuracy of the results can be made, model testing and actual measurements should become available in order to be able to provide the ultimate validation of these results.

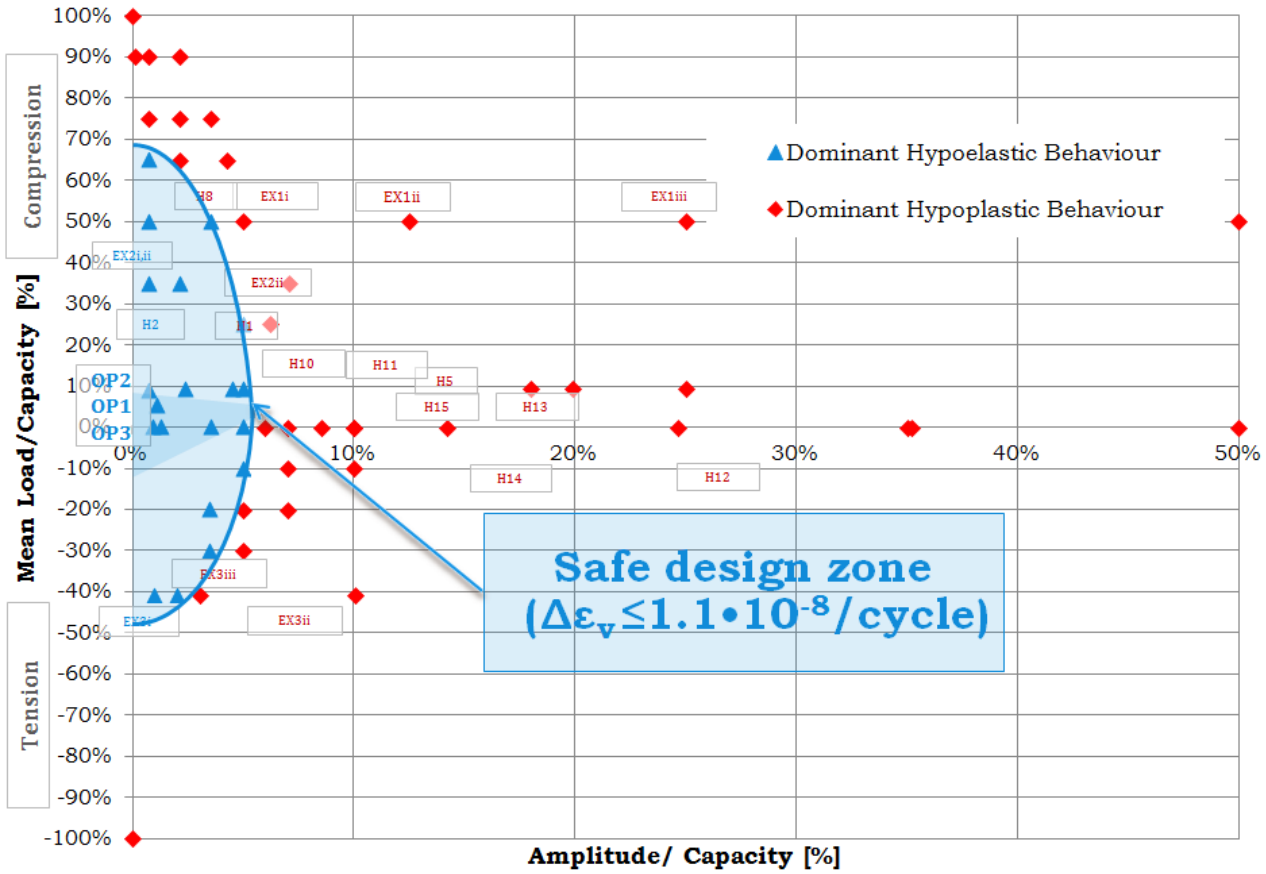

Figure 6.6: Impact of the change in mean load and cyclic amplitude with respect to caisson tensile and compressive capacity and soil behaviour (characteristics and results may be found in Appendix I)

6.5 MODEL COMPARISON

In Section 6.1, it becomes clear that the dominant operational condition as defined in Figure 5.26 do not produce significant change in void ratio and that the behaviour is within an "elastic" range for the dimensions chosen in Chapter 4. This is mainly due to the chosen caisson dimensions. Furthermore, as long as the ratio between the applied loading conditions and caisson capacity stays within the boundaries defined in Figure 6.6, the foundation response remains within the elastic region.

Therefore, regarding the adequacy of the standards API & ISO19901-4 (2000) and DNV (1992) for the design of suction caisson foundations, the author can only conclude that it is highly dependent also on the safety imposed by the designing engineer. As in the current case the imposed safety margins were considerably high due to the wish to investigate the foundation response in the tensile region, the predesign proved to be more than sufficient. Most certainly, within the defined boundaries in Figure 6.6 the standards are valid. But outside of these boundaries, the ability to adequately capture the foundation behaviour is doubtful. Even the obtained results with this model must be critically analysed as there are no field measurements to validate them.

To conclude, in order to be able to provide an answer with respect to the adequacy of the existing standards, but also for the proposed model, one must carry out scale tests and/or field measurements and compare the outcomes.

6.6 CONCLUSIONS

The analyses conducted for the operational load cases have proven that 70% of the life time of the wind turbine determines loading conditions that are below 10% of the caisson's predesigned capacity and render a hypoelastic response of the foundation. Further analyses have proven that the foundation response depends on a combination of the mean load with the cyclic amplitude. As long as the applied loading conditions are within the boundaries defined in Figure 6.6 the behaviour can be characterised as hypoelastic, with no significant strain accumulation, nor pore pressure build-up. Outside of these boundaries, strains accumulate and also pore pressures. Due to uncertainties following from the soil calibration and extrapolations, one cannot be fully certain that the obtained results are valid. It is the recommendation of the author that model tests need to be carried out in order to validate these results.

Unfortunately, the proposed extrapolations within the explicit procedure presented in Chapter 5 of the present report have proven to be inadequate, as they were too simplistic. One cannot just take the soil as being in a denser state and expect that under the same loading conditions the results will finally converge towards previous ones. The reason for this inadequacy is related to the fact that the stress and strain history of the soil plays a significant role on the response to loading and cannot be neglected. On the other hand, the implementation of the denser soil conditions have proven that even a slightly denser sand in which the foundation is embedded determined that less strain and pore pressure accumulation occurred.

Under extreme loading conditions two main phases in behaviour could be identified: the first in which the soil within the caisson and in its vicinity reaches a common denser state, followed by a second phase where in the top centre of the caisson localised failure due to high pore pressures starts to occur, while the sand closer to the rim continues to densify. An expansion of the localised failure zones may be problematic as they will reduce the friction on the inner side of the caisson. Unfortunately, with respect to the pore pressure build-up in the extreme cases, it became clear that the expected overestimation of pore pressure from the calibration phase determines erroneous results, as it was already explained in the section dedicated to the model calibration. A better calibration of the model, using data also covering the small strain range might avoid such errors in the future. Nonetheless, model tests should be carried out for a full model validation.

Finally, the current model allowed for the definition of an area within which the strain accumulation and pore pressure build-up are insignificant for the used medium dense sand, under quasi-statically applied loading conditions, with a period of approximately 7 s. The defined boundary is conservative as normally the period of the vertical loading should be larger, somewhere in between the period of the thrust force and the period of the waves. Furthermore, as mentioned, the analysed soil conditions represent medium dense sand, while the North Sea seabed is most often characterised by dense to very dense sand. Unfortunately, due to limited data for calibration, one cannot provide conclusive affirmations related to the behaviour outside of this region. It can be seen that pore pressure build-up can be very problematic and cause localised liquefaction within the sand found in the caisson itself for the analysed medium dense sand. Effects from pore pressure build-up are most probably not expected to occur in denser sands.

Chapter 7

CONCLUSIONS AND RECOMMENDATIONS

This final chapter of this thesis presents the main conclusions following from the current research and provides further recommendations regarding future potential research to be carried out.

7.1 CONCLUSIONS

The main problem analysed during the course of this research refers to the long term performance of suction caissons under cyclic loading. This was investigated in order to clarify the adequacy of suction caissons as foundations for large (6 MW) offshore wind turbines. Literature study has shown that the most important design criteria are based on serviceability and long term stability of the structure over the course of 25 years. Moreover, it showed that a gap exists in the method to tackle this issue within the existing norms and standards. This gap is presently being bridged by researchers at Aalborg University, Imperial College of London, Karlsruhe Institute of Technology, NGI, Oxford University and University of Western Australia and now also Delft Technical University.

An important aspect that has been discovered and proven with this investigation is that for a three leg jacket structure, the suction caissons have a significant advantage in horizontal resistance: due to the specific geometry of the problem and the large diameter of the suction caissons, the horizontal resistance is much larger than the applied horizontal loads, having no significant impact on the vertical capacity. Thus, the problem can be reduced to the behaviour of the suction caisson under vertical cyclic loading.

The model proposed by the current graduation dissertation to analyse the behaviour under vertical cyclic loading is based on the hypoplastic sand model with intergranular strain concept integrated. It has proven to be a good tool for the prediction of the foundation's behaviour for several hundreds of cycles for specific loading ranges. The proposed solution for the extrapolation of the results to larger numbers of cycles proved to be ineffective, but emphasized the need to investigate preshearing effects in sand. Nonetheless, the model is considered to be a viable option for the investigation of limited numbers of cycles for any loading range, provided that an adequate soil calibration is performed. In order to be able to perform realistic extrapolations of this data, more knowledge is needed regarding the influence of the loading history on sand.

The soil condition under investigation is represented by sand, as one of the most commonly encountered soil profiles within the North Sea. The literature review showed that in the case of cyclic loading of sand, aspects such as pore pressure build-up, resulting in strength and stiffness degradation as well as strain accumulation are the main issues of concern and were also observed within the results of the conducted analyses. The medium dense sand ($I_D = 50\%$) used for the calibration of the soil mass, represents a conservative case, as the encountered sand within the offshore soil investigations in the North Sea is generally dense to very dense. These latter two are less prone to liquefaction, and as it was also discovered by Andersen (2009), the cyclic shear strength of sand increases with density, especially for sands with $I_D \geq 65\%$. In the performed analyses under extreme conditions it could be observed that the medium dense sand initially densified within the caisson. As the cyclic loading continued, localised loosening due to increased pore pressure build-up under the caisson top plate and centre occurred. Yet, these effects are not expected to be significant in a denser sand.

For the obtained results the overestimation of pore pressure, from the soil calibration phase, proves to be problematic in certifying the accuracy of the obtained results. Nonetheless, the alternative approach, using axisymmetry, proved that the results presented in Figure 6.6 represents a conservative boundary for when hypoplastic strains accumulate at larger, potentially damaging rates. Nonetheless, the boundary found between the dominant hypoelastic and dominant hypoplastic behaviour provides a guideline for a safe foundation design, though it might not always prove economic. This boundary is also an indication of which cyclic loads need to be further investigated in order to assess long term damages. The same figure also confirms that the foundation can resist tensile loads, but that capacity decreases significantly as tensile cyclic loading components appear.

Finally, it can be concluded that within the enclosed boundary in Figure 6.6 the long term behaviour of suction caissons under vertical cyclic loading is dominantly hypoelastic and will not result in significant strain

accumulation nor high pore pressure build-up and consequently no significant strength nor stiffness degradation. But, outside this boundary a thorough investigation of these effects has to be carried out in order to achieve a more economic design. The proposed hypoplastic sand model with intergranular strain concept integrated can be an adequate method, provided that all criteria for calibration are met. More detailed conclusions can be found at the end of each chapter of this dissertation.

7.2 RECOMMENDATIONS

Upon finalising this research, a few recommendations are made by the author in the hope of a future better understanding of this research topic.

The first recommendations refers to a need of developing a coordinated research related to the response of sand to cyclic loading. This research should include sands at different relative densities and be subjected to both undrained cyclic triaxial tests as well as cyclic direct simple shear tests with varying CSSR values and pre-shear stresses. The outcomes of this research should present a clearer view on the accumulation of pore pressure and shear strain, but also degradation of the friction angle and stiffness with respect to the applied loading conditions. Conclusions regarding the impact of the applied mean load and cyclic amplitude on the above mentioned characteristics would provide a great aid in the understanding of foundations' behaviour in offshore conditions characterised by sandy soils. Furthermore, conclusions regarding the impact of the loading history on the behaviour of sand under cyclic loading could aid the development of empirical formulas. Moreover, a good experimental basis would provide the needed foundation for the fine-tuning of the available numerical models and possibly even development of new ones.

A second recommendation states the need of validation of the current model. This may be done by performing model or full scale tests. Placement of measurement devices is required in order to record data related to pore pressures and strains within the caisson and on its outer rim.

The third recommendation addresses the need for an extensive research and potential investment in processing field measurements and simulations of offshore loading conditions. The present research has proven that 97.5% of these loading conditions cause an "elastic" foundation response, as they are below 12% of the predesigned foundation's capacity. It is the belief of the author that a detailed statistical analysis of the loading conditions on an offshore wind turbine during its lifetime could prove to reduce the uncertainty regarding the foundation design itself. An important role in this matter will be played by the collaboration between structural and geotechnical engineers in the iterations of soil spring stiffness versus the loading reactions.

The fourth recommendation refers to the need to investigate the sensitivity of the hypoplastic sand model parameters to each other. This thesis only looked at their influence on the soil behaviour, and only briefly mentioned that their influence seems to overlap. An investigation of the influence of the parameters on each other would lead to a more accurate calibration of the soil.

A fifth recommendation refers to the need to investigate the influence that actually exists between the caissons under the three-leg jacket structure, as the distance between them is small. Furthermore, in offshore conditions a new aspect appears: for a three-leg structure two footings are loaded in compression, yet the third is potentially loaded into tension. An investigation regarding the effect on the suction caisson group capacity should also be carried out.

The final recommendation represents in fact a set of suggested improvements to be made in Plaxis, the software used for these analyses. These have been provided already via email and live communication to Plaxis.

Appendix A

API & DNV STATIC BEARING CAPACITY FORMULAS

The current appendix is a supplement for the information provided in Chapter 2 - Section 2.5. The bearing capacity formulas proposed by API & ISO19901-4 (2000) and DNV (1992) will be further presented in the next sections.

A.1 THE API APPROACH

The current section will present the guidance given through API (2011) and API & ISO19901-4 (2000) for the static bearing capacity assessment for offshore foundations. The considered superstructure of these foundations is generally an offshore oil and gas production platform.

A.1.1 SHALLOW FOUNDATIONS

The undrained bearing capacity, when constant shear strength may be assumed, is defined in API & ISO19901-4 (2000) and API (2011) as:

$$Q = (c \cdot N_c \cdot K_c + \gamma \cdot D) \cdot A' \tag{A.1}$$

where:

Q is the maximum vertical load at failure;

c is undrained shear strength of the soil;

N_c is a dimensionless constant equal to 5.14 for $\varphi = 0$;

φ is the undrained friction angle = 0;

γ total unit weight of soil;

D is the depth of embedment;

A' is the effective area of the foundation depending on load eccentricity;

K_c is the correction factor that accounts for load inclination, footing shape, depth of embedment, inclination of base and inclination of the seafloor surface.

The undrained bearing capacity, when linearly increasing shear strength may be assumed, is defined in API & ISO19901-4 (2000) and API (2011) as:

$$Q_d = F \cdot \left(s_{uo} \cdot N_c + \frac{\kappa \cdot B'}{4} \right) \cdot K_c \cdot A' \tag{A.2}$$

where:

Q_d is the maximum total vertical load applied to the base of the footing at failure (excluding weight of the the soil) under undrained conditions;

F is a correction factor, function of $\dfrac{\kappa \cdot B'}{s_{uo}}$;

κ is the rate of increase of the undrained shear strength with depth;

s_{uo} is undrained shear strength of the soil;

N_c is a dimensionless constant equal to 5.14;

B' is the minimum effective lateral foundation dimension;

A' is the effective area of the foundation depending on load eccentricity;

K_c is the correction factor that accounts for load inclination, footing shape, depth of embedment, inclination of base and inclination of the seafloor surface.

The drained bearing capacity is defined in API & ISO19901-4 (2000) and API (2011) as:

$$Q'_d = [p'_o\,(N_q - 1) \cdot K_q + 0.5 \cdot \gamma' \cdot B' \cdot N_\gamma \cdot K_\gamma] \cdot A' \tag{A.3}$$

Q'_d is the maximum total vertical load applied to the base of the footing at failure (excluding weight of the the soil) under drained conditions;

N_q is a dimensionless function of φ', $N_q = e^{(\pi \cdot \tan \varphi')} \cdot \tan^2 (45° \varphi'/2)$

N_γ is an empirical dimensionless function of φ', $N_\gamma = 1.5 \cdot (N_q - 1) \cdot \tan \varphi'$;

φ' is the effective friction angle of the Mohr envelope;

γ' is the effective unit weight of the soil;

p'_o is the vertical effective stress at the base level (skirt tip level if skirts are used);

B' is the minimum effective lateral foundation dimension;

A' is the effective area of the foundation depending on load eccentricity;

K_q, K_γ are the correction factors that account for load inclination, footing shape, depth of embedment, inclination of base and inclination of the seafloor surface. The subscripts q, γ refer to the particular term in the equation.

A.1.2 PILE FOUNDATIONS

The ultimate axial capacity of piles is defined in API & ISO19901-4 (2000) and API (2011) as:

$$Q_d = Q_f + Q_p = f \cdot A_s + q \cdot A_p \tag{A.4}$$

where:

Q_d is the ultimate axial capacity;

Q_f is skin friction resistance;

Q_p is the total end bearing;

f is the unit skin friction capacity, $f = K \cdot p_o \tan \delta$;

K is the coefficient of lateral earth pressure (ratio of horizontal to vertical normal effective stress);

p_o is the effective overburden pressure at the point in question;

δ friction angle between the soil and the pile wall;

A_s is the side surface area of the pile;

q is the unit end bearing capacity, $q = p_{o,tip} \cdot N_q$;

$p_{o,tip}$ is the effective overburden pressure at the pile tip;

N_q dimensionless bearing capacity factor;

A_p is the gross end area of the pile.

Limiting values for the above parameters are given in Table 6.4.3-1 from API (2011). It can be observed that no effects of pore pressure build-up are considered in the values of the parameters.

The pile capacity for axial pull-out loads may be equal or less than the skin friction resistance (Q_f).

The ultimate lateral capacity for piles in sand varies in values for shallow or deep depths—between the two values, the smallest should be chosen:

$$p_{us} = (C_1 \cdot f + C_2 \cdot D) \cdot \gamma' \cdot H \tag{A.5}$$

$$p_{ud} = C_3 \cdot D \cdot \gamma' \cdot H \tag{A.6}$$

where:

$p_{us,d}$ is the ultimate resistance, s=shallow, d=deep;

γ' is the effective soil weight;

H is the depth;

f is the unit skin friction capacity, $f = K \cdot p_o \tan\delta$;

$C_1,\ C_2,\ C_3$ are coefficients determined as function of the angle of internal friction of sand;

D is the average pile diameter from surface to depth.

A.2 THE DNV APPROACH

The current section will present the guidance given through DNV (1992) and DNV (2004) for the static bearing capacity assessment for gravity base offshore foundations. The bearing capacity of piles will not be mentioned as the approach is the same as in the API (2011).

The considered superstructure of these foundations is generally an offshore oil and gas production platform.

The undrained bearing capacity, when constant shear strength may be assumed, is defined in DNV (1992) as:

$$q_u = N_c \cdot s_u \,(1 + s_{ca} + d_{ca} - i_{ca}) + p'_o \tag{A.7}$$

where:

q_u is the ultimate bearing capacity;

p'_o is the effective overburden pressure at base level;

N_c is a dimensionless constant equal to 5.14 for $\varphi = 0$;

φ is the undrained friction angle = 0;

s_u is the undrained shear strength;

s_{ca} is a shape factor (see section 4.4.3.3 from DNV (1992));

d_{ca} is a depth factor (see section 4.4.3.4 from DNV (1992));

i_{ca} is a load inclination factor (see section 4.4.3.2 from DNV (1992)).

The undrained bearing capacity, when linearly increasing shear strength may be assumed, is defined in DNV (1992) as:

$$q_u = F \cdot \left(s_{uo} \cdot N_c + \frac{\kappa \cdot B'}{4} \right) \cdot (1 + s_{ca} + d_{ca} - i_{ca}) \tag{A.8}$$

where:

q_u is the ultimate bearing capacity;;

F is a correction factor, function of $\dfrac{\kappa \cdot B'}{s_{uo}}$;

s_{uo} is undrained shear strength of the soil;

N_c is a dimensionless constant equal to 5.14;

κ is the rate of increase of the undrained shear strength with depth;

B' is the minimum effective lateral foundation dimension;

s_{ca} is a shape factor (see section 4.4.4.3 from DNV (1992));

d_{ca} is a depth factor (see section 4.4.4.4 from DNV (1992));

i_{ca} is a load inclination factor (see section 4.4.4.2 from DNV (1992)).

The drained bearing capacity is defined in DNV (1992) as:

$$q_u = 0.5 \cdot \gamma' \cdot B' \cdot N_\gamma \cdot s_\gamma \cdot d_\gamma \cdot i_\gamma + (p'_o + a) \cdot N_q \cdot s_q \cdot d_q \cdot i_q \tag{A.9}$$

q_u is the ultimate bearing capacity;

p'_o is the effective overburden pressure at base level;

B' is the minimum effective lateral foundation dimension;

a is the soil attraction;

$N_{\gamma,q}$ are bearing capacity factors (see sections 4.4.2.2–3 from DNV (1992));

$s_{\gamma,q}$ are shape factors (see section 4.4.2.5 from DNV (1992));

$d_{\gamma,q}$ are depth factors (see sections 4.4.2.6–7 from DNV (1992));

$i_{\gamma,q}$ are load inclination factors (see sectin 4.4.2.4 from DNV (1992)).

Appendix B

LOAD ASSESSMENT

This appendix will present the given data over a life time of 25 years, sorted in the increasing order of the vertical, respectively horizontal mean load can be seen in Figures B.1, B.2 and B.3, respectively B.4, B.5 and B.6 .

These loads on the 3 caissons were clustered according to mean load values and their percentages of occurance; amplitudes and their percentages of occurance. A "traffic light colour" system is used to reflect the relevance for each set: red—(very) low; yellow—medium; green—high. The relevance of each set increases as the percentage of occurrence increases, as well as the assumption that a higher absolute magnitude is more damaging and thus more relevant.

The clustering of the vertical loads can be found in Figures B.7, B.8 and B.9. And the clustering of the horizontal loads can be found in Figure B.10.

Finally a sample of the resulting load signals will be shown in Figures B.14, B.15 and B.16.

B.1 DATA PROCESSING

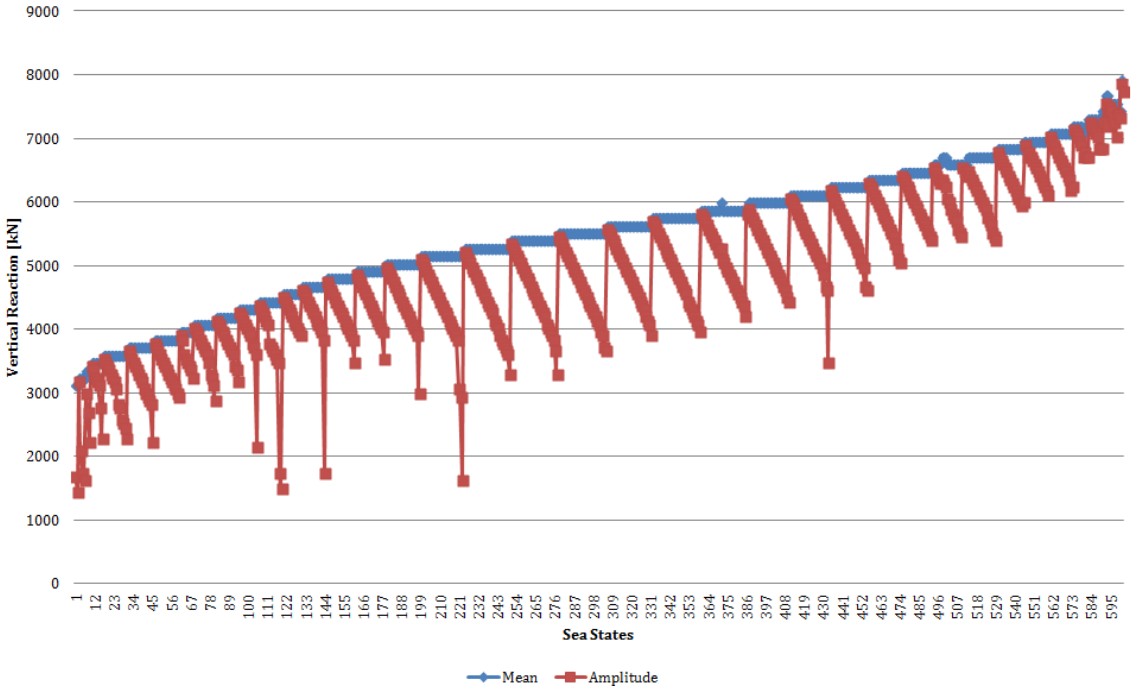

Figure B.1: Vertical load reactions on caisson 1 at different sea states over 25 years design life

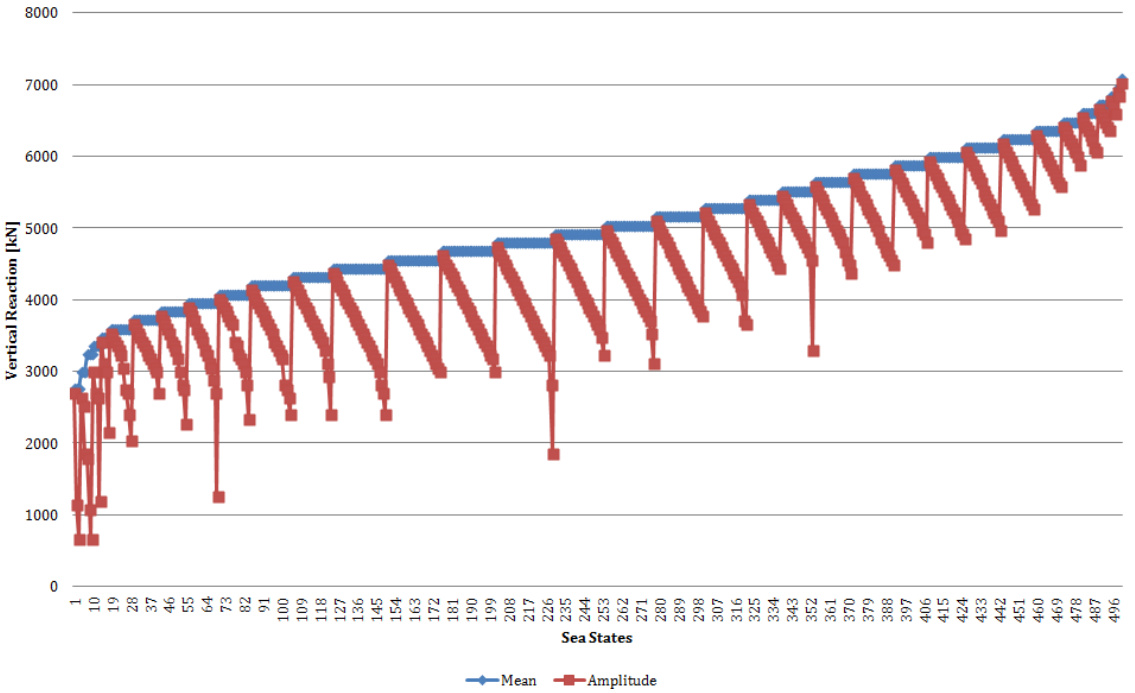

Figure B.2: Vertical load reactions on caisson 2 at different sea states over 25 years design life

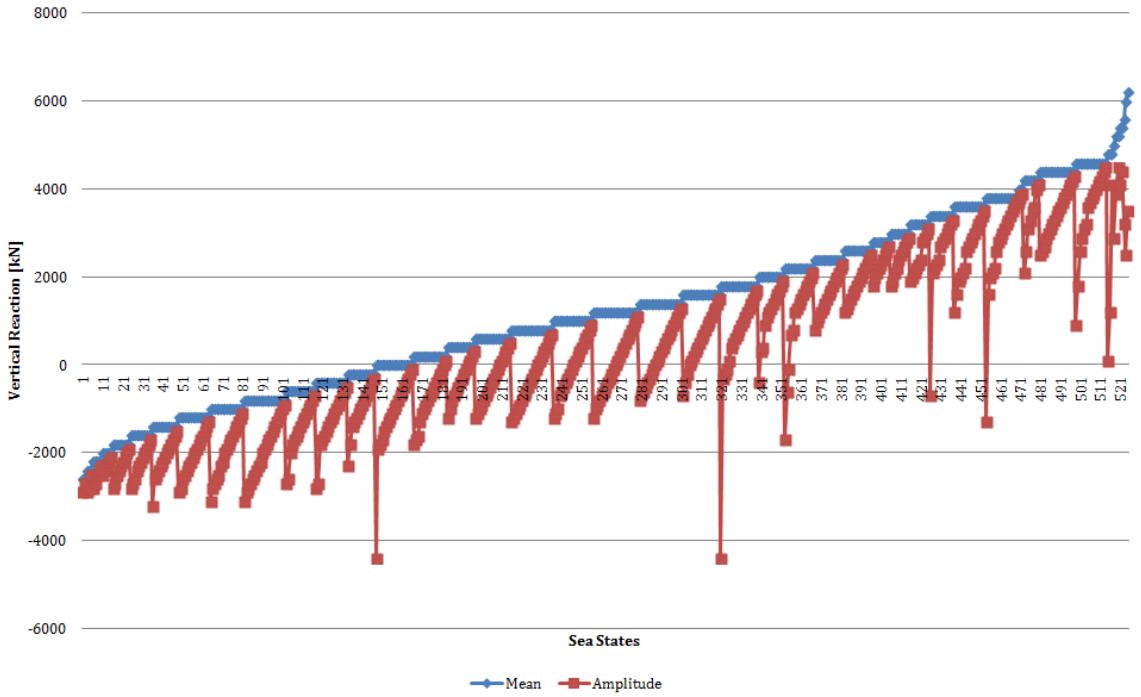

Figure B.3: Vertical load reactions on caisson 3 at different sea states over 25 years design life

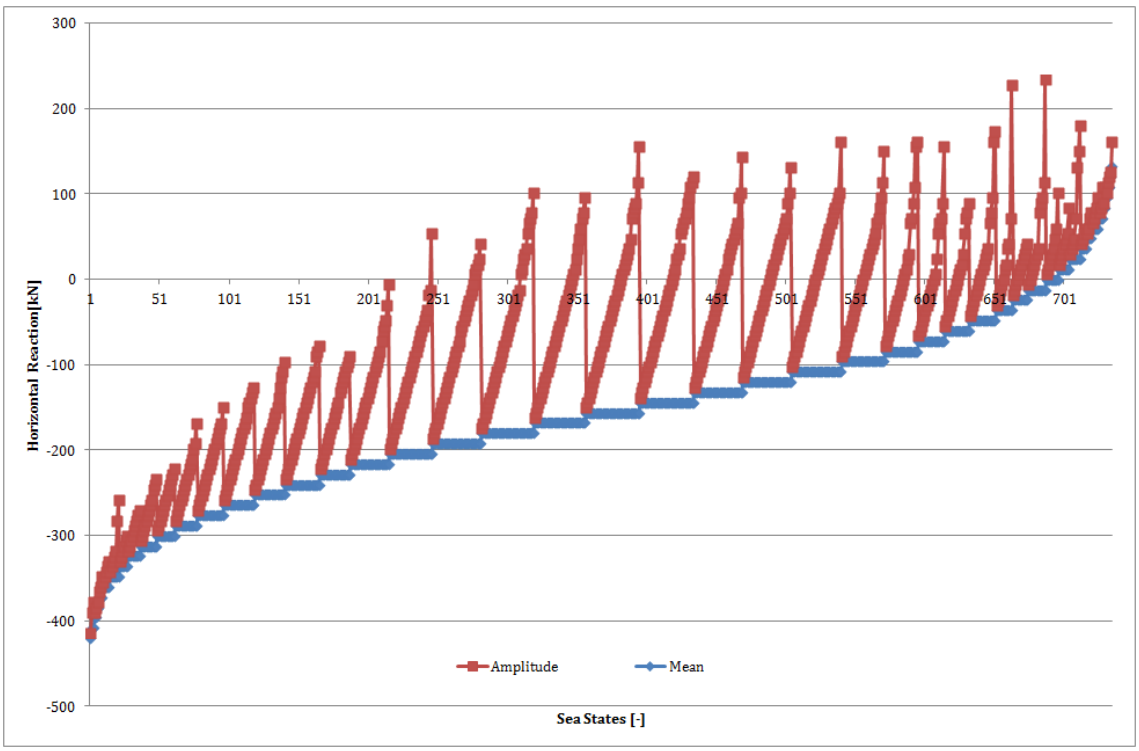

Figure B.4: Horizontal load reactions on caisson 1 at different sea states over 25 years design life

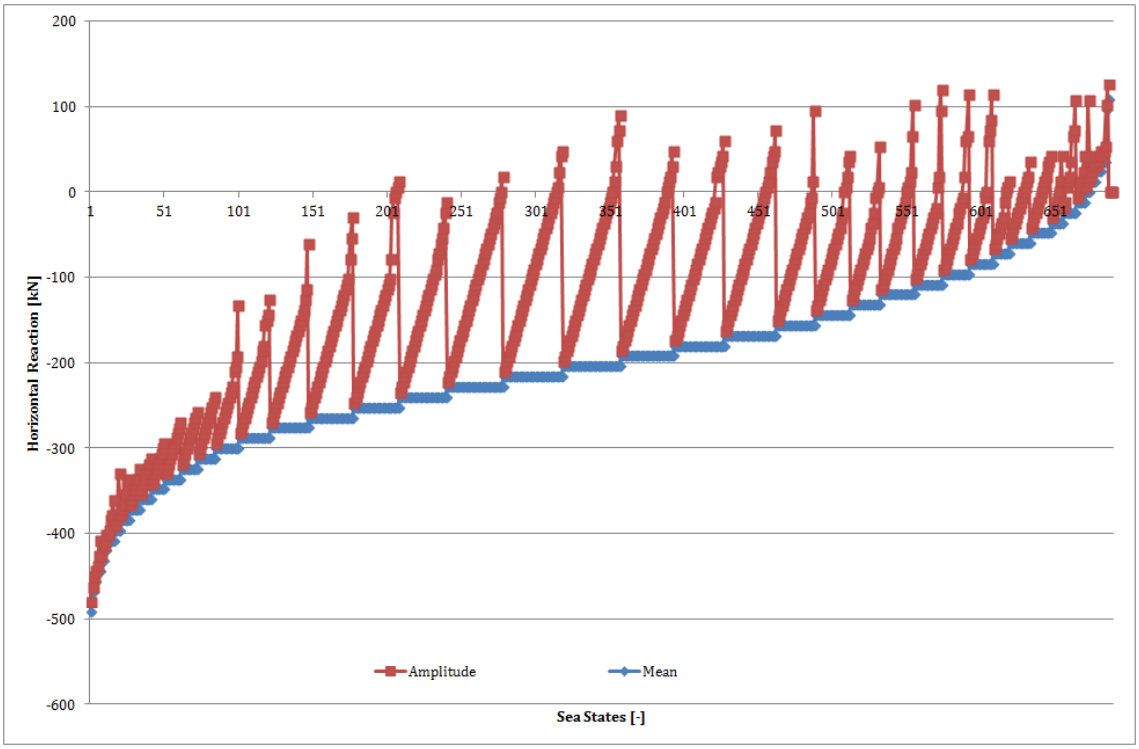

Figure B.5: Horizontal load reactions on caisson 2 at different sea states over 25 years design life

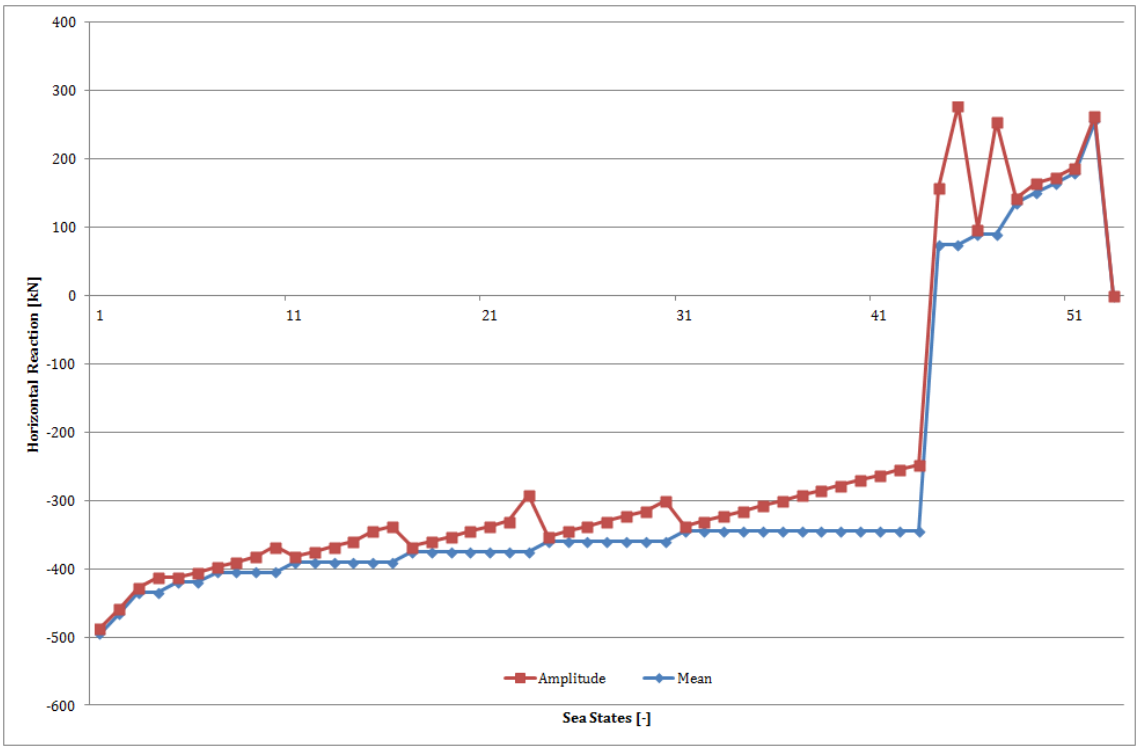

Figure B.6: Horizontal load reactions on caisson 3 at different sea states over 25 years design life

Case ID and probability of occurence		Mean [kN]	Number of occurences in 25 years	Amplitude [kN] and probability of occurence	
	1	Min		60 min	
	2	3120		480 max	
	3			270 avg	46.4%
	4			540 min	
	5			960 max	
A	6			750 avg	19.7%
	7	3744	3.07E+08	1020 min	
	8			1680 max	
	9			1350 avg	33.9%
	10			1740 min	
	11	Max		3540 max	
65.86%	12	3840		2310 avg	0.0%
	1	Min		60 min	
	2	3960		480 max	
	3			270 avg	55.7%
	4			540 min	
	5			960 max	
B	6			750 avg	34.2%
	7	5148	1.44E+08	1020 min	
	8			1680 max	
	9			1350 avg	6.5%
	10			1740 min	
	11	Max		3540 max	
30.85%	12	5280		2310 avg	3.5%
	1	Min		60 min	
	2	5400		480 max	
	3			270 avg	34.0%
	4			540 min	
	5			960 max	
C	6			750 avg	30.3%
	7	6084	1.51E+07	1020 min	
	8			1680 max	
	9			1350 avg	31.5%
	10			1740 min	
	11	Max		3540 max	
3.25%	12	6240		2310 avg	4.2%
	1	Min		60 min	
	2	6360		480 max	
	3			270 avg	52.0%
	4			540 min	
	5			960 max	
D	6			750 avg	34.6%
	7	7722	2.02E+05	1020 min	
	8			1680 max	
	9			1350 avg	13.4%
	10			1740 min	
	11	Max		3540 max	
0.04%	12	7920		2310 avg	0.0%

Figure B.7: Vertical load cases and characteristics on caisson 1 clustered according to mean load values and percentages of occurance

Case ID and probability of occurence		Mean [kN]	Number of occurences in 25 years	Amplitude [kN] and probability of occurence	
	1	Min		60 min	
	2	2760		480 max	
	3			270 avg	11.4%
	4			540 min	
	5			960 max	
E	6			750 avg	83.7%
	7	3744	2.20E+05	1020 min	
	8			1680 max	
	9			1350 avg	0.9%
	10			1740 min	
	11	Max		2940 max	
0.05%	12	3840		2198 avg	4.0%
	1	Min		60 min	
	2	3960		480 max	
	3			270 avg	49.4%
	4			540 min	
	5			960 max	
F	6			750 avg	32.3%
	7	4914	9.92E+07	1020 min	
	8			1680 max	
	9			1350 avg	17.4%
	10			1740 min	
	11	Max		2940 max	
21.12%	12	5040		2198 avg	0.9%
	1	Min		60 min	
	2	5160		480 max	
	3			270 avg	27.5%
	4			540 min	
	5			960 max	
G	6			750 avg	47.7%
	7	6318	3.51E+08	1020 min	
	8			1680 max	
	9			1350 avg	23.7%
	10			1740 min	
	11	Max		2940 max	
74.71%	12	6480		2198 avg	1.1%
	1	Min		60 min	
	2	6600		480 max	
	3			270 avg	77.6%
	4			540 min	
	5			960 max	
H	6			750 avg	13.5%
	7	6903	1.94E+07	1020 min	
	8			1680 max	
	9			1350 avg	8.9%
	10			1740 min	
	11	Max		2940 max	
4.13%	12	7080		2198 avg	0.0%

Figure B.8: Vertical load cases and characteristics on caisson 2 clustered according to mean load values and percentages of occurance

Case ID and probability of occurence		Mean [kN]	Number of occurences in 25 years	Amplitude [kN] and probability of occurence	
	1	Min		100 min	
	2	-2600		1000 max	
	3			550 avg	99.4%
	4			1100 min	
I	5	-2535	3.35E+08	1800 max	
	6			1450 avg	0.6%
	7			1900 min	
	8	Max		6200 max	
10.83%	9	-1400		3388 avg	0.0%
	1	Min		100 min	
	2	-1200		1200 max	
	3			650 avg	98.6%
	4			1300 min	
J	5	0	8.55E+07	2100 max	
	6			1700 avg	1.3%
	7			700 min	
	8	Max		1800 max	
70.53%	9	1200		1250 avg	0.0%
	1	Min		100 min	
	2	1400		1300 max	
	3			700 avg	98.9%
	4			1400 min	
K	5	3705	3.11E+06	2100 max	
	6			1750 avg	1.0%
	7			2200 min	
	8	Max		6200 max	
17.99%	9	3800		3686 avg	0.1%
	1	Min		100 min	
	2	4000		300 max	
L	3	6045	3.11E+06	200 avg	99.5%
	4			400 min	
	5	Max		6200 max	
0.65%	6	6200		2316 avg	0.5%

Figure B.9: Vertical load cases and characteristics on caisson 3 clustered according to mean load values and percentages of occurance

Caisson 1				
Interval		Avg.	% of occurence	No.of occurences
Min	Max			
-420	-300	-360	12.4%	5.77E+07
-300	-108	-204	88.3%	8.65E+08
-108	0.00	-54	5.8%	5.71E+07
0.00	132	66	0.0%	2.88E+05

Caisson 2				
Interval		Avg.	% of occurence	No. Of occurrences
Min	Max			
-492	-300	-396	15.377%	7.76E+07
-300	-156	-228	80.32%	8.66E+08
-156	-12.00	-84	12.49%	1.35E+08
-12.00	0	-6	0.00%	2.75E+04

Caisson 3				
Interval		Avg.	% of occurence	No. of occurences
Min	Max			
-495	-345	-420	6.750%	6.41E+07
-345	-150	-247.5	83.35%	7.92E+08
-150	0.00	-75	9.89%	9.39E+07
0.00	255	127.5	0.02%	1.60E+05

Figure B.10: Horizontal load cases and characteristics on the three caissons clustered according to mean load values and percentages of occurance

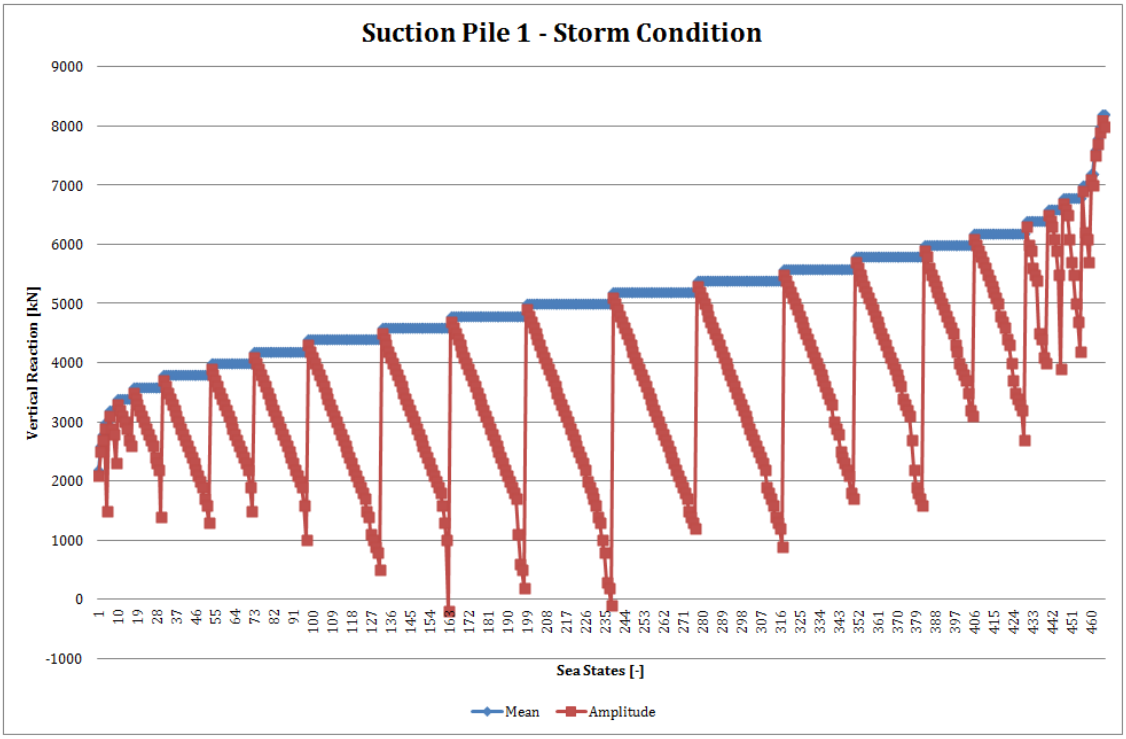

Figure B.11: Vertical load reactions on caisson 1 at different sea states under storm conditions–not factored

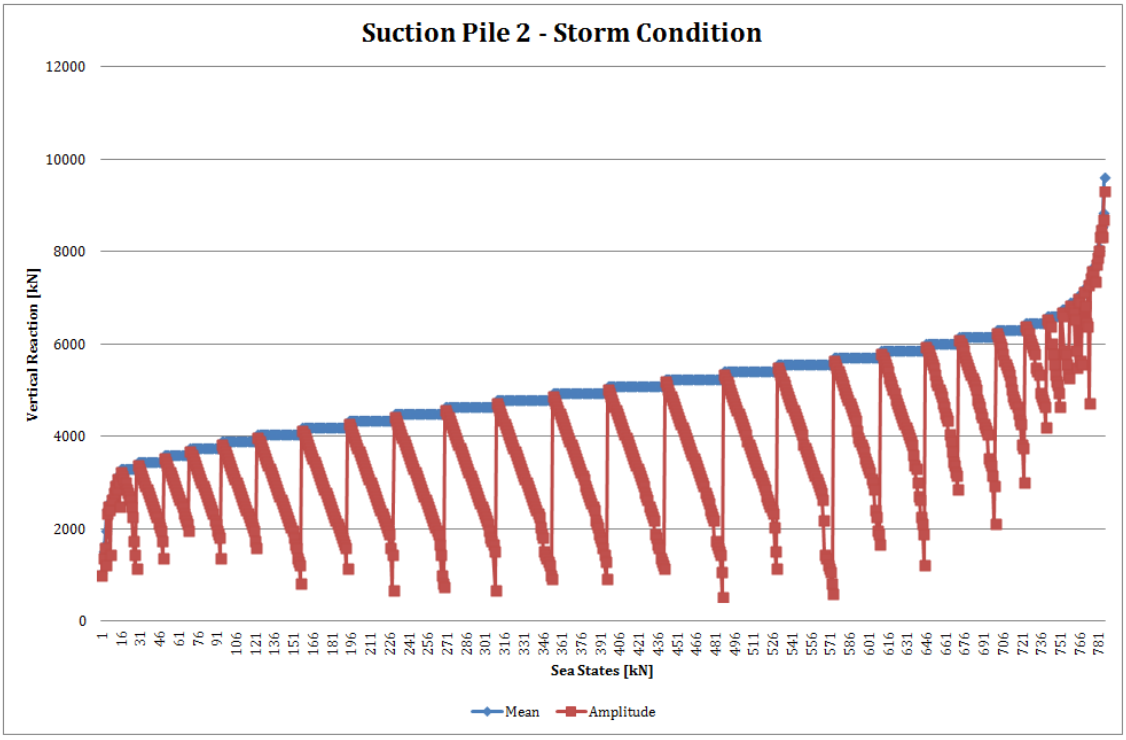

Figure B.12: Vertical load reactions on caisson 2 at different sea states under storm conditions–not factored

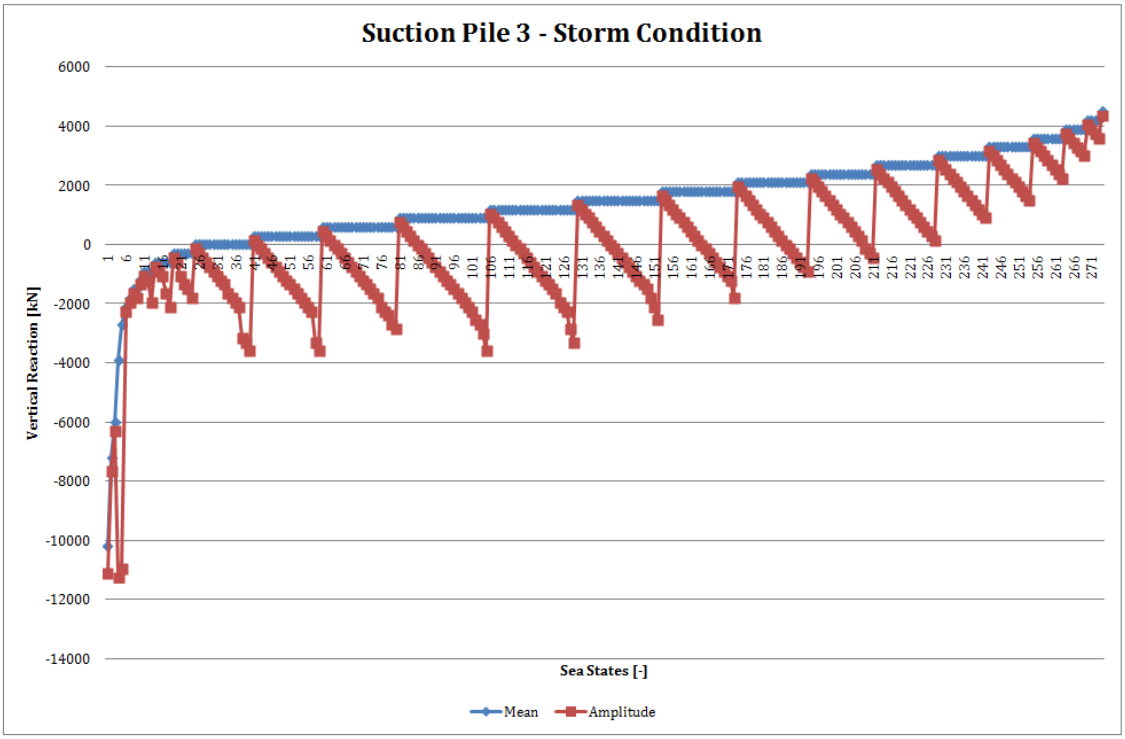

Figure B.13: Vertical load reactions on caisson 3 at different sea states under storm conditions–not factored

B.2 RESULTING LOAD SIGNAL

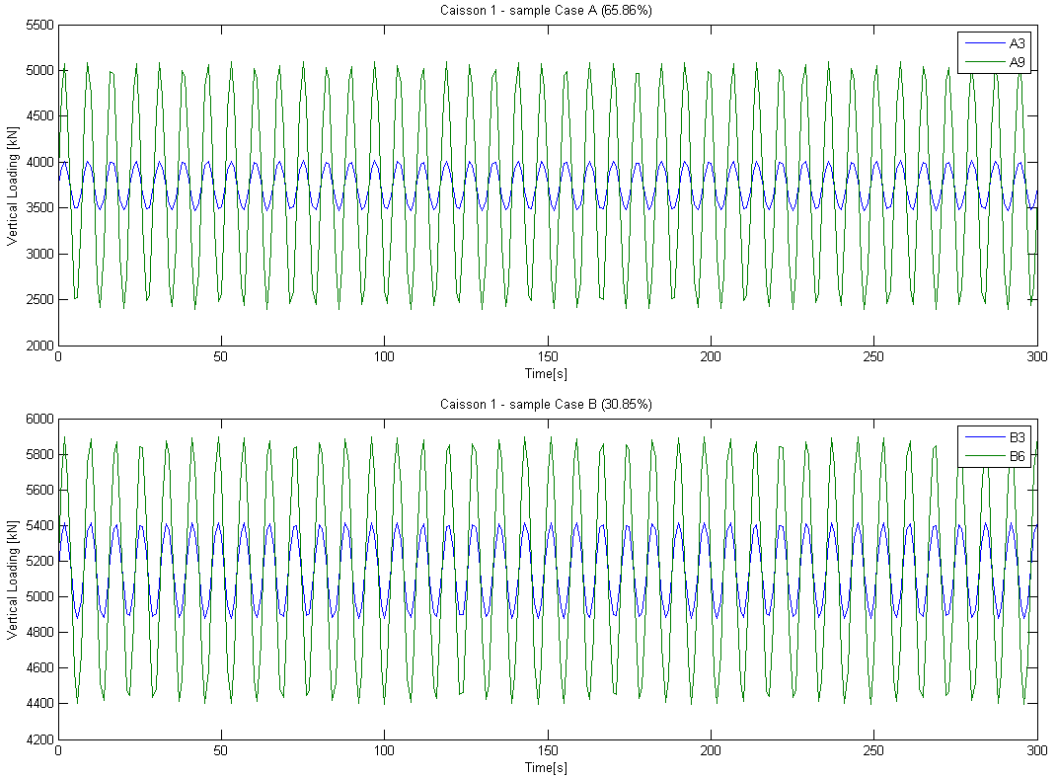

Figure B.14: Sample vertical load characteristics on caisson 1

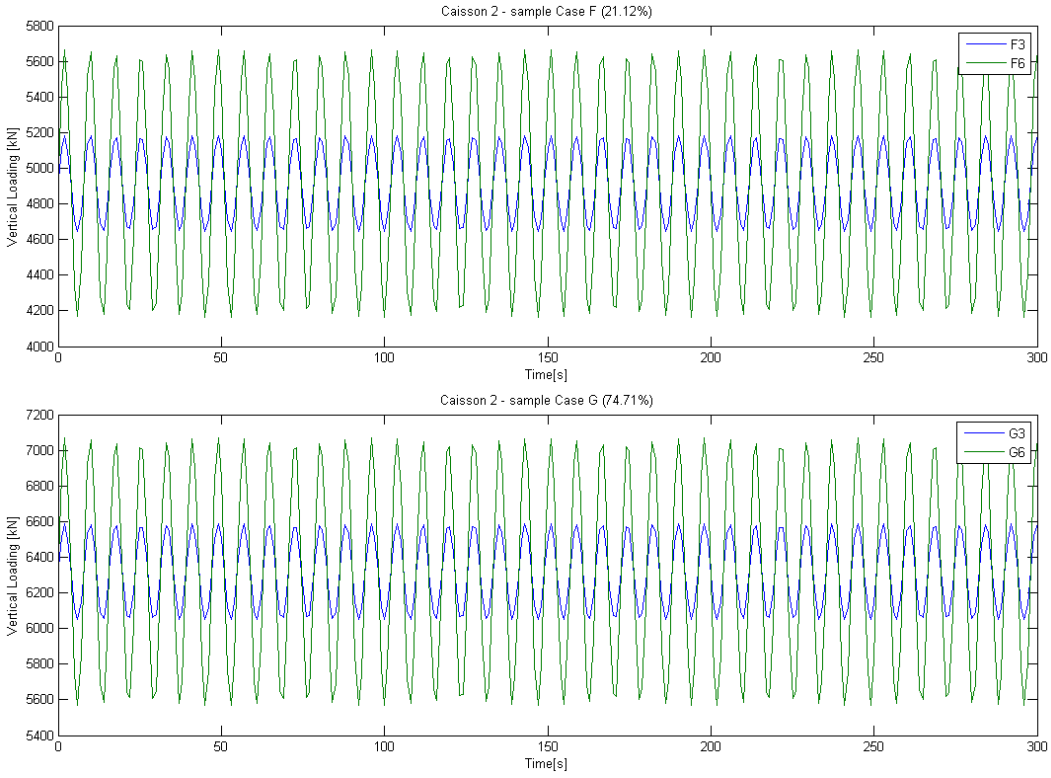

Figure B.15: Sample vertical load characteristics on caisson 2

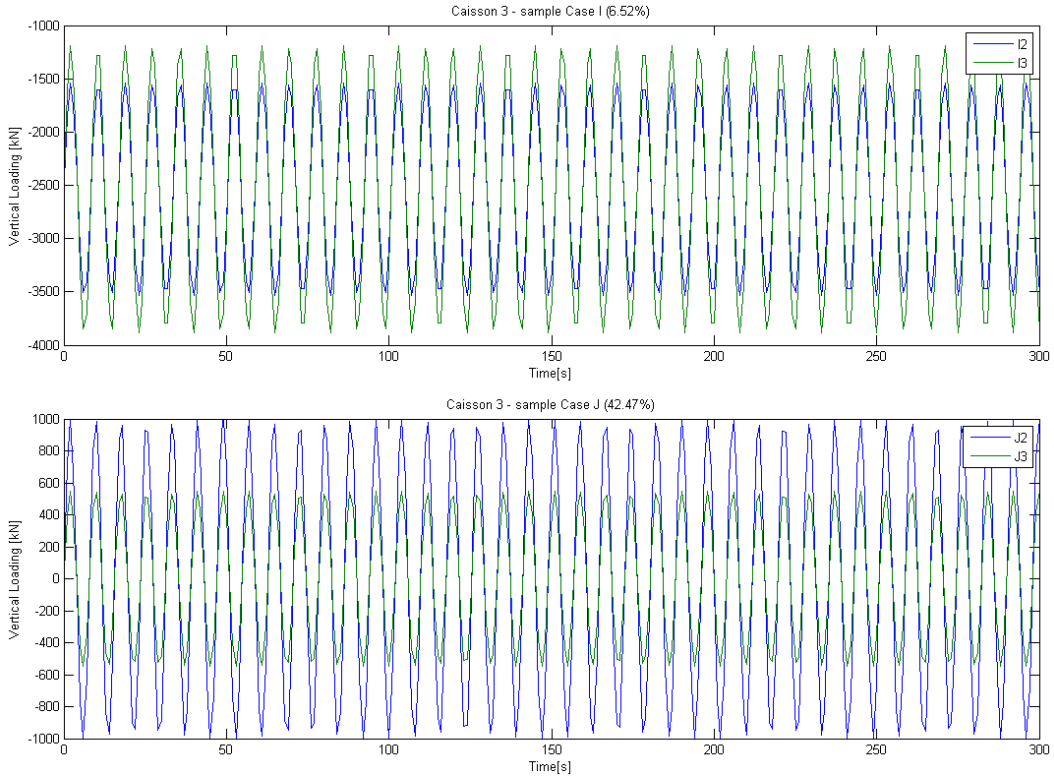

Figure B.16: Sample vertical load characteristics on caisson 3

Appendix C

ASSESSMENT OF DRAINAGE BEHAVIOUR

The current appendix provides a short theoretical background of the drainage behaviour analyses done on the two sand samples and the results of these analyses. More details regarding the importance of the drainage behaviour with respect to pore pressure build-up may be found in Chapter 2 of the current report.

C.1 THEORETICAL BACKGROUND

In order to assess drainage behaviour the method described by Zienkiewicz *et al.* (1980) is used:

$$\Pi_1 \begin{cases} < 10^{-2} & undrained \\ \in [10^{-2}; 10^{+2}] & partially\ drained \\ > 10^{+2} & drained \end{cases} \tag{C.1}$$

and

$$\Pi_1 = \frac{2k}{\rho_w/\rho_s \cdot \pi \cdot g} \cdot \frac{T}{\hat{T}^2} \tag{C.2}$$

where the meaning of the parameters can be found in Table C.1.

Parameter	Description	Unit of measurement
k	permeability	m/s
ρ_w	density of water	kg/m^3
ρ_s	density of solid particles	kg/m^3
g	gravitational acceleration	m/s^2
T	imposed period	s
$\hat{T} = \frac{2L}{\sqrt{\frac{D + K_f/n}{\rho_s}}}$	natural period of the system	m/s^2
L	drainage length	m
$D = \frac{E_s}{3 \cdot (1 - 2 \cdot \nu)}$	soil skeleton bulk modulus	kPa
E_s	the soil Young's modulus	kPa
ν	Poisson's ratio	–
K_f	bulk modulus of the fluid	kPa
n	porosity	–

Table C.1: Parameters needed to calculate Π_1 Zienkiewicz *et al.* (1980)

More information regarding the importance of drainge behaviour of the considered soil can be found in Chapter 2, under the section regarding pore pressure build-up (2.4.3

C.2 RESULTS FOR MEDIUM DENSE SAND ANALYSIS

The table bellow presents the results of the drainage behaviour analysis performed on the medium dense sand sample. The formulas used for the determination of the parameters are presented in the section dedicated to the theoretical background.

Input	Description	U.M.	Value
e_0	void ratio	[-]	0.54
n	In-situ porosity	[-]	0.35
ν	Poisson's ratio	[-]	0.30
k	Vertical permeability	[m/s]	2.5E-05
E_s	Young's modulus	[kPa]	3.1E+04
g	gravitational acceleration	[m/s^2]	9.81
ρ_{water}	density of water	[kg/m^3]	1025
ρ_{soil}	density of solid particles	[kg/m^3]	2097
OD	outter diameter of caisson	[m]	15
L_{embd}	embedment length	[m]	16
L_d	Drainage length	[m]	7.5
T	Imposed period	[s]	7.32
Kf	Bulk modulus of fluid	[kPa]	2.3E+06
D	Soil skeleton bulk modulus	[kPa]	2.6E+04
Output	**Description**	**U.M.**	**Value**
$\breve{T}$	Natural period of the system	[s]	2.7E-01
Π_1	Zienkiewicz's dimensionless parameter	[-]	3.4E-04
Behaviour		[-]	**undrained**

Figure C.1: Drainage behaviour analysis for the medium dense sand

C.3 RESULTS FOR VERY DENSE SAND ANALYSIS

The table bellow presents the results of the drainage behaviour analysis performed on the very dense sand sample. The formulas used for the determination of the parameters are presented in the section dedicated to the theoretical background.

Input	Description	U.M.	Value
e_0	void ratio	[-]	0.45
n	In-situ porosity	[-]	0.31
ν	Poisson's ratio	[-]	0.30
k	Vertical permeability	[m/s]	1.90E-05
E_s	Young's modulus	[kPa]	5.58E+04
g	gravitational acceleration	[m/s^2]	9.81
ρ_{water}	density of water	[kg/m^3]	1025
ρ_{soil}	density of solid particles	[kg/m^3]	2140
OD	outter diameter of caisson	[m]	15
L_{embd}	embedment length	[m]	16
L_d	Drainage length	[m]	7.5
T	Imposed period	[s]	7.32
Kf	Bulk modulus of fluid	[kPa]	2.34E+06
D	Soil skeleton bulk modulus	[kPa]	4.65E+04
Output	**Description**	**U.M.**	**Value**
$\check{T}$	Natural period of the system	[s]	2.52E-01
Π_1	Zienkiewicz's dimensionless parameter	[-]	2.97E-04
Behaviour		[-]	**undrained**

Figure C.2: Drainage behaviour analysis for the very dense sand

Appendix D

LABORATORY TEST RESULTS

The following laboratory tests were conducted by Deltares: constant head permeability tests, isotropically consolidated undrained (CIU) triaxial tests; cyclic undrained triaxial tests with varying Cyclic Shear Stress Ratio (CSSR); cyclic direct simple shear tests with varying CSSR. The results from the latter three mentioned tests are plotted in the following sections and represent the results which the model's output should simulate after calibration. These plots are the result of processing of the actual laboratory measurements provided by Deltares in numerical format.

D.1 ISOTROPICALLY CONSOLIDATED UNDRAINED TRIAXIAL TEST RESULTS

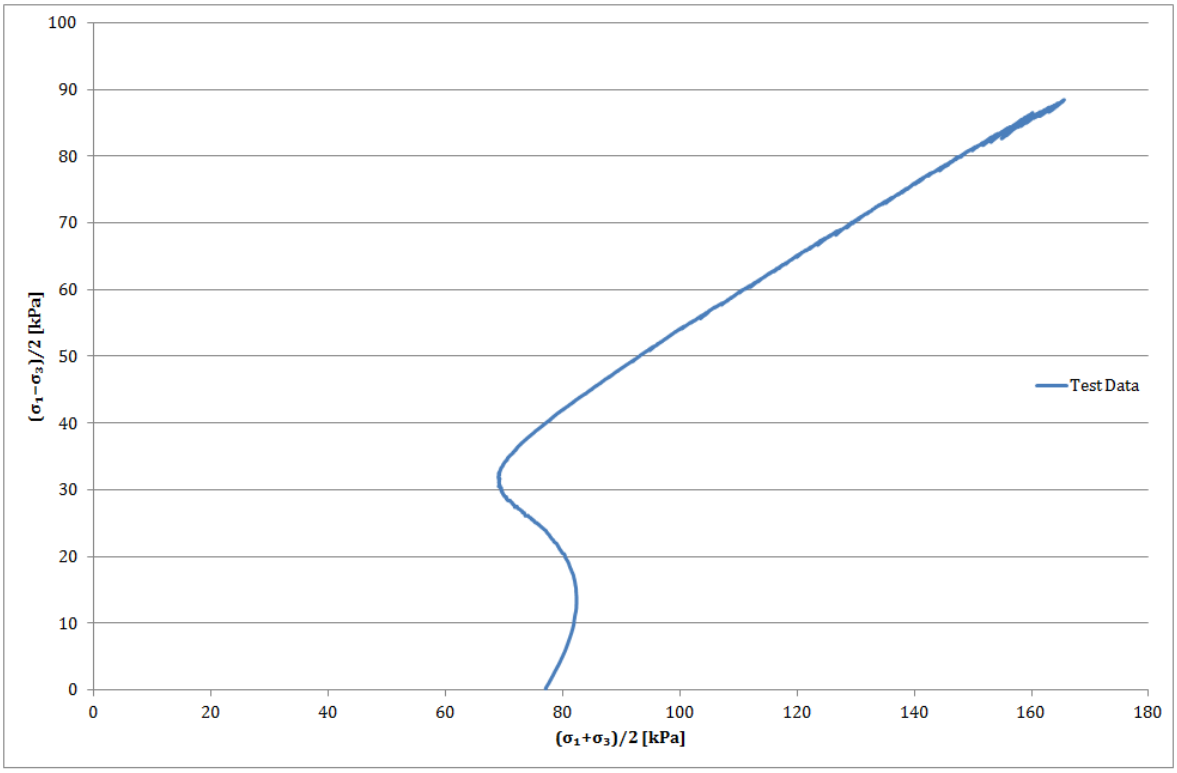

Figure D.1: CIU triaxial test results ($I_D = 50\%$)—stress path

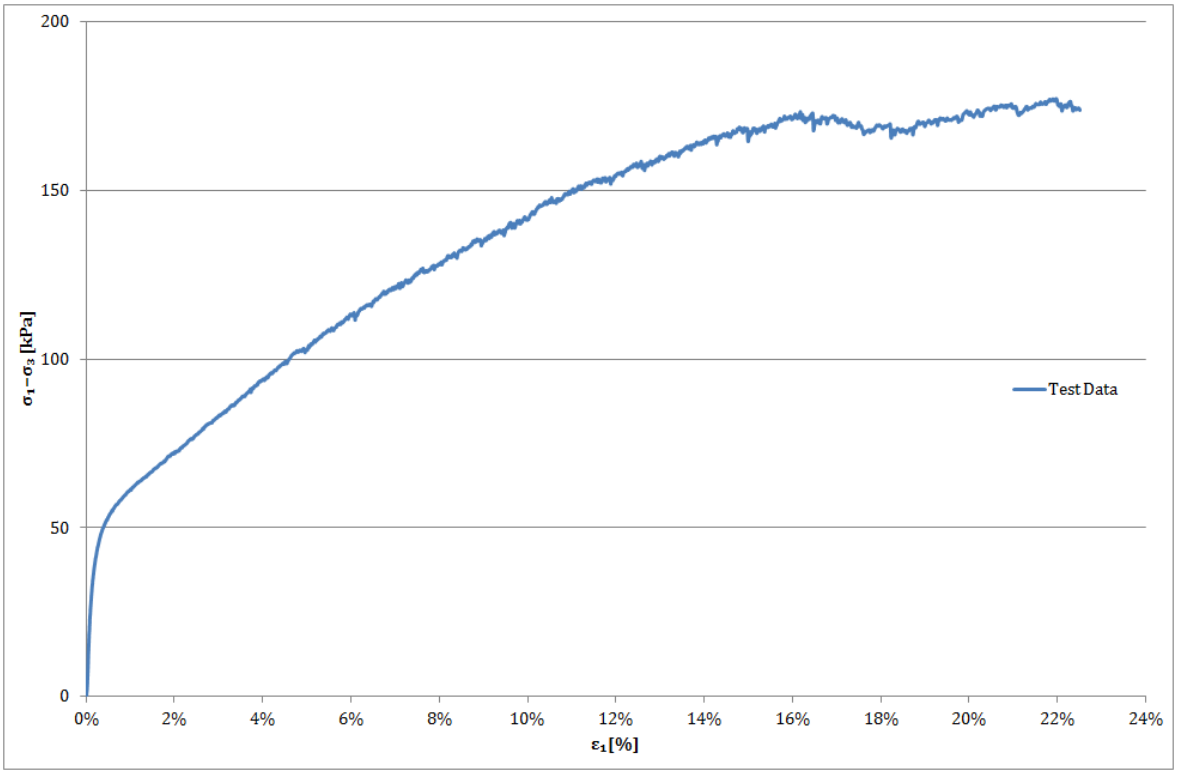

Figure D.2: CIU triaxial test results ($I_D = 50\%$)—axial strain vs. deviatoric stress

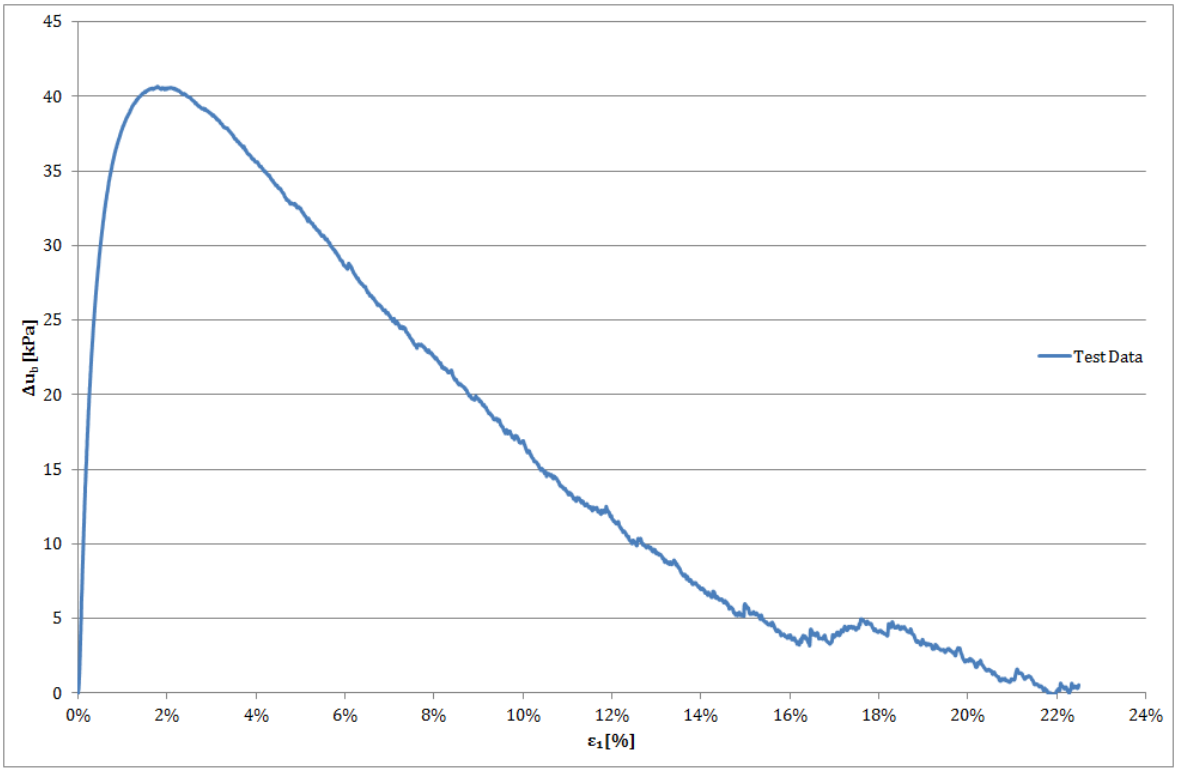

Figure D.3: CIU triaxial test results ($I_D = 50\%$)—axial strain vs. pore pressure

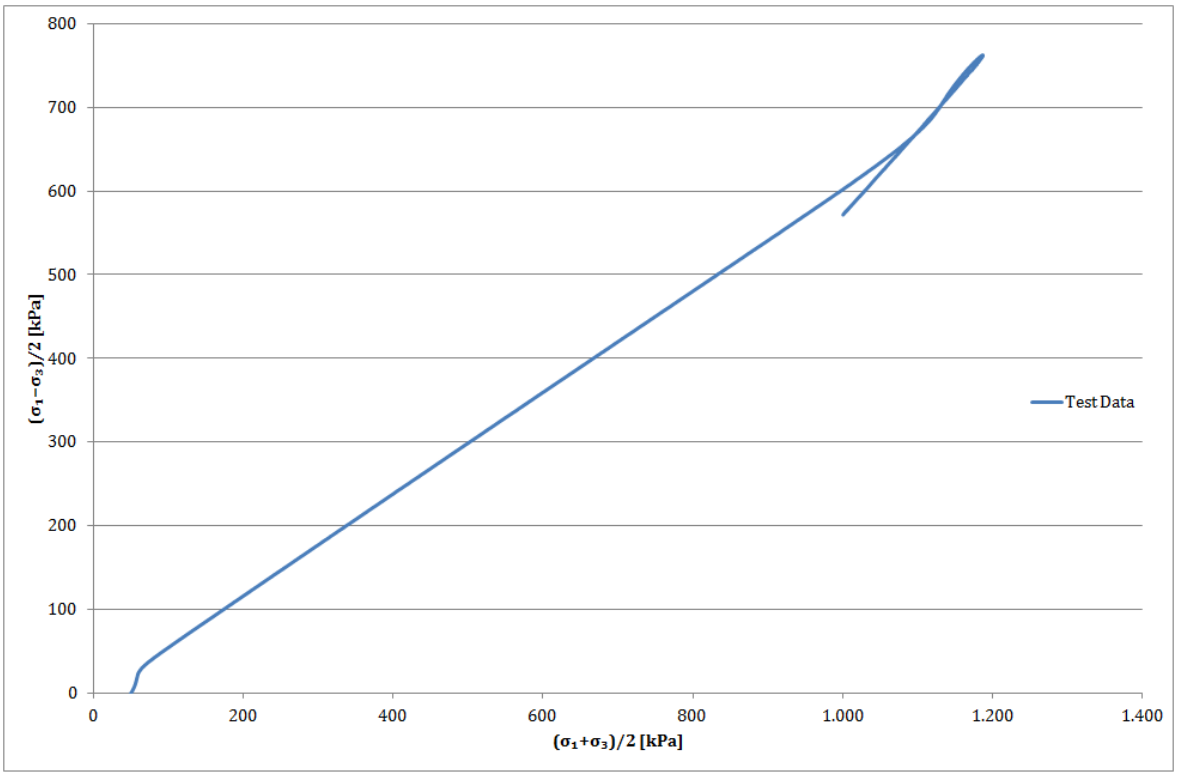

Figure D.4: CIU triaxial test results ($I_D = 75\%$)—stress path

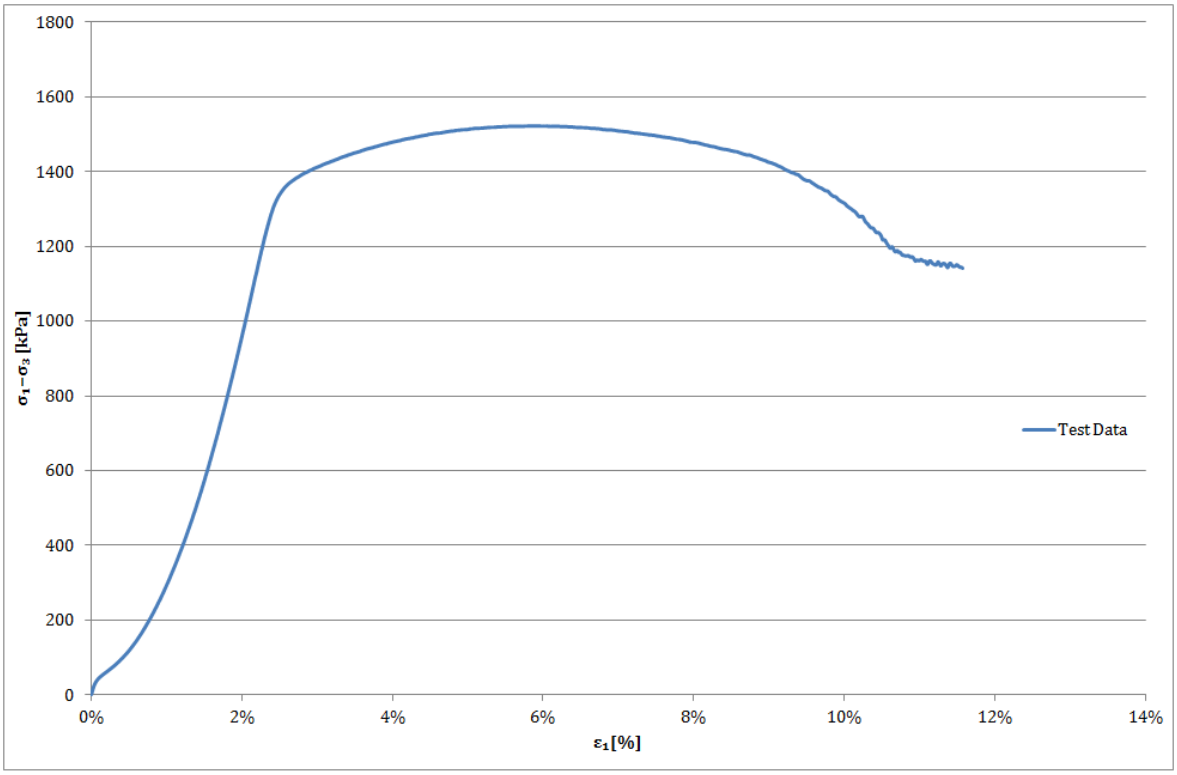

Figure D.5: CIU triaxial test results ($I_D = 75\%$)—axial strain vs. deviatoric stress

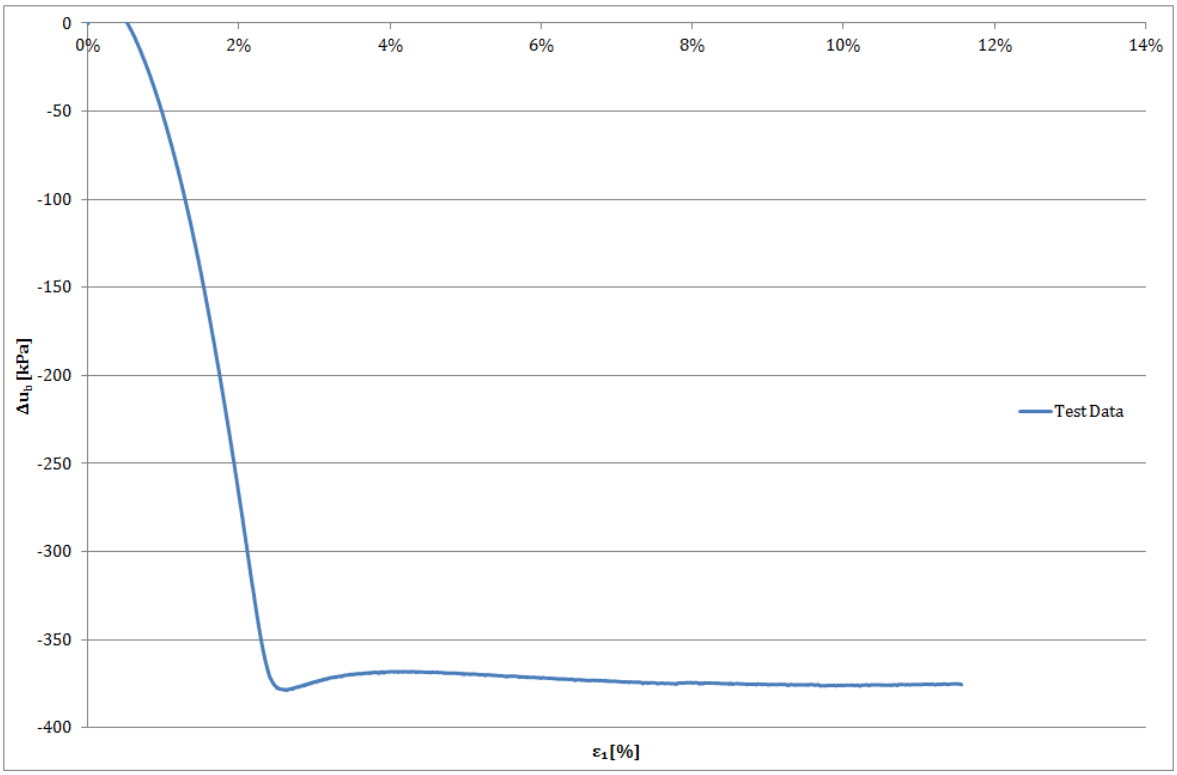

Figure D.6: CIU triaxial test results ($I_D = 75\%$)—axial strain vs. pore pressure

D.2 CYCLIC UNDRAINED TRIAXIAL TESTS WITH VARYING CSSR

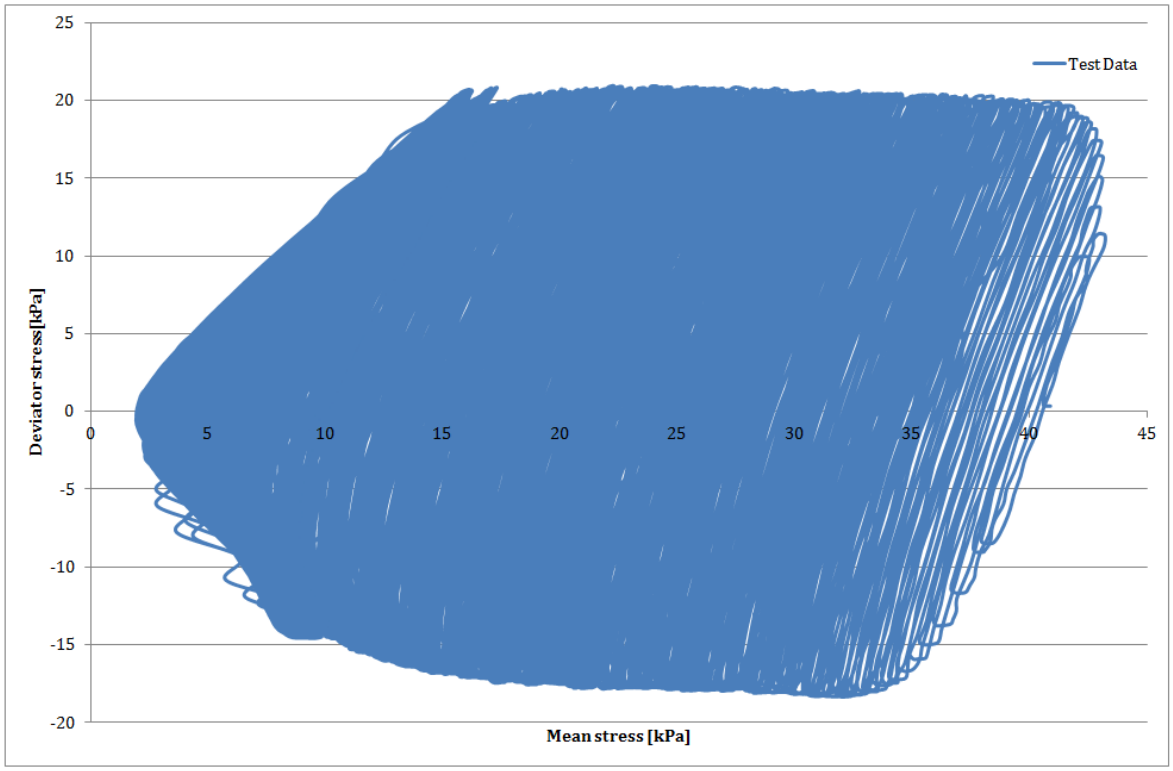

Figure D.7: Cyclic undrained triaxial test results ($CSSR = 0.15$, $I_D = 75\%$)—stress path

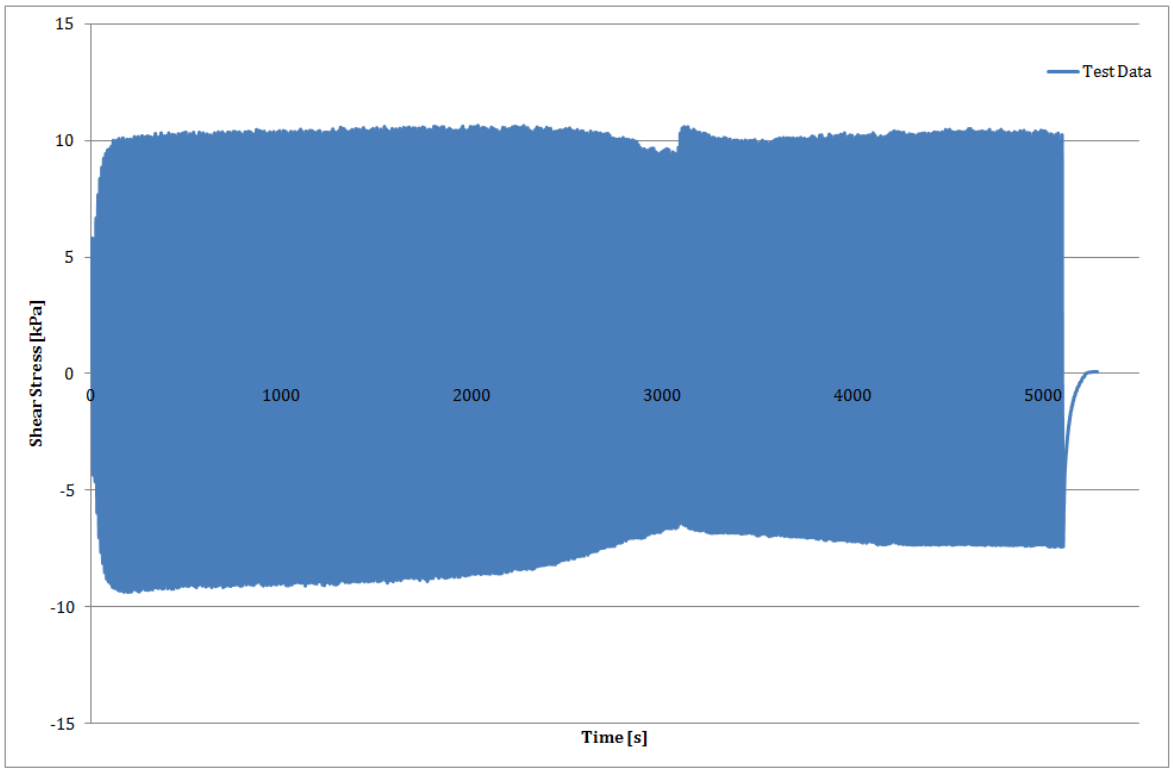

Figure D.8: Cyclic undrained triaxial test results ($CSSR = 0.15$, $I_D = 75\%$)—shear stress in time

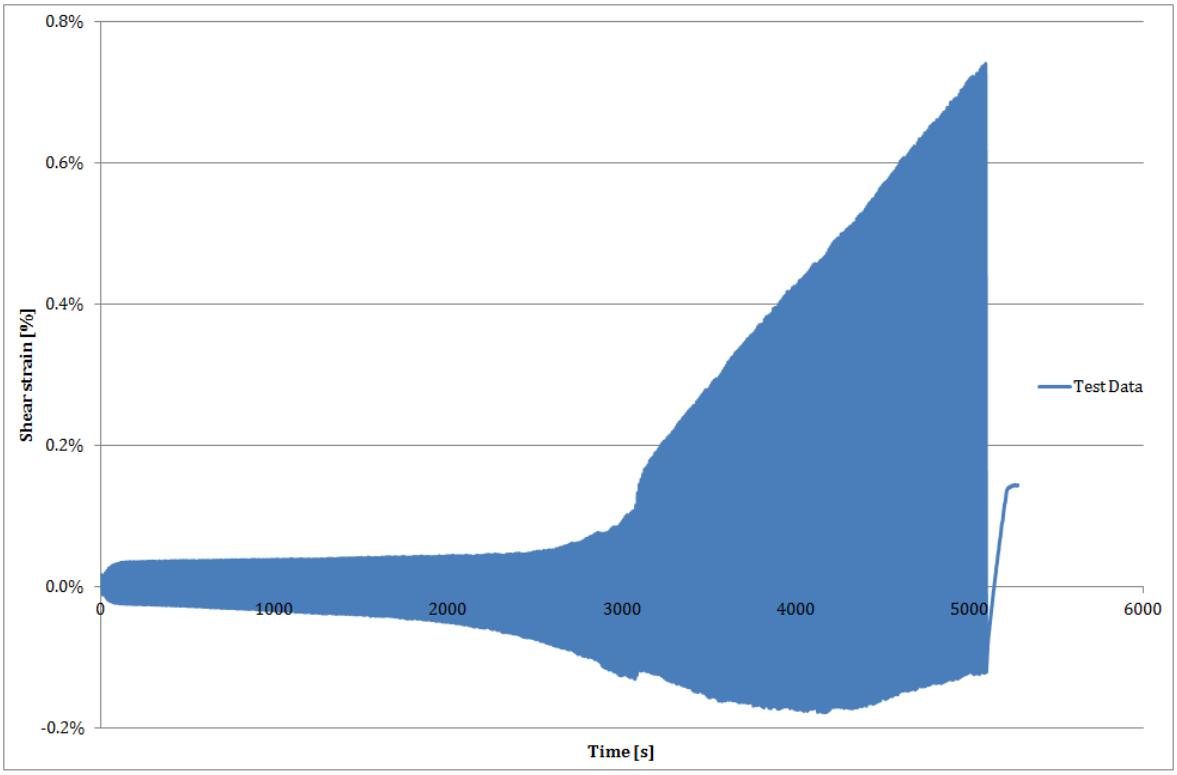

Figure D.9: Cyclic undrained triaxial test results ($CSSR = 0.15$, $I_D = 75\%$)—shear strain in time

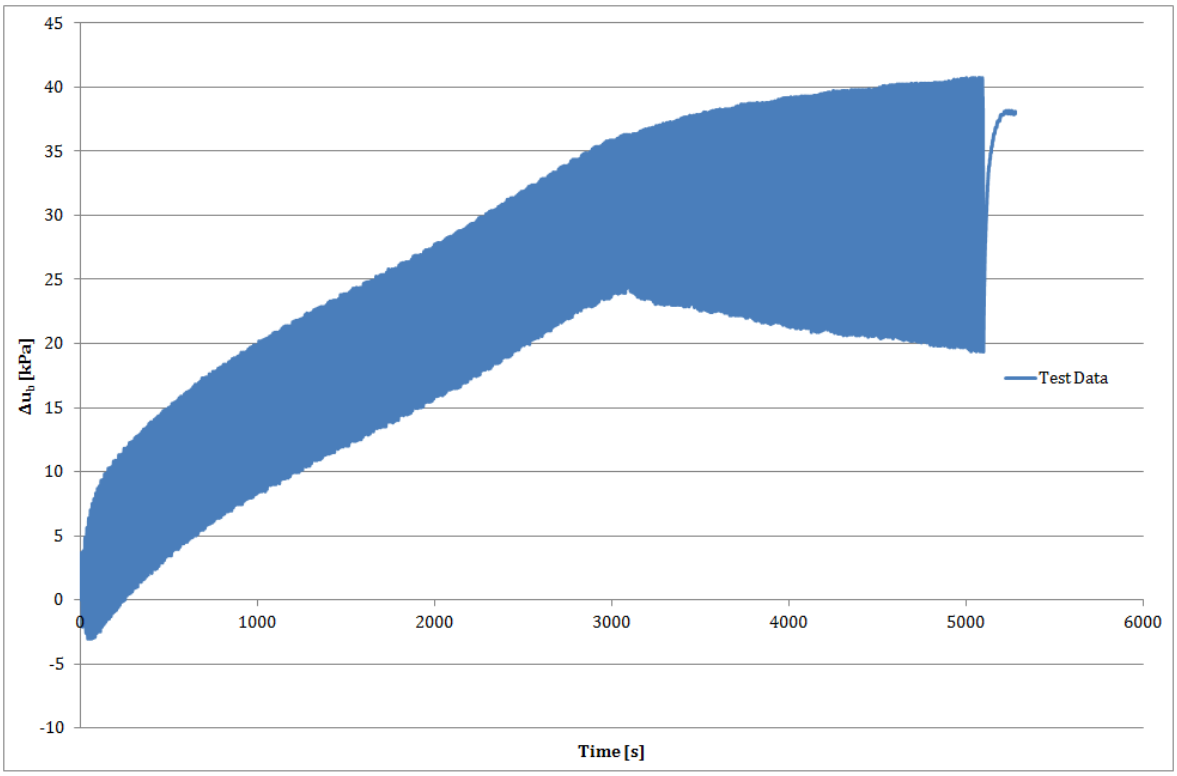

Figure D.10: Cyclic undrained triaxial test results ($CSSR = 0.15$, $I_D = 75\%$)—pore pressure in time

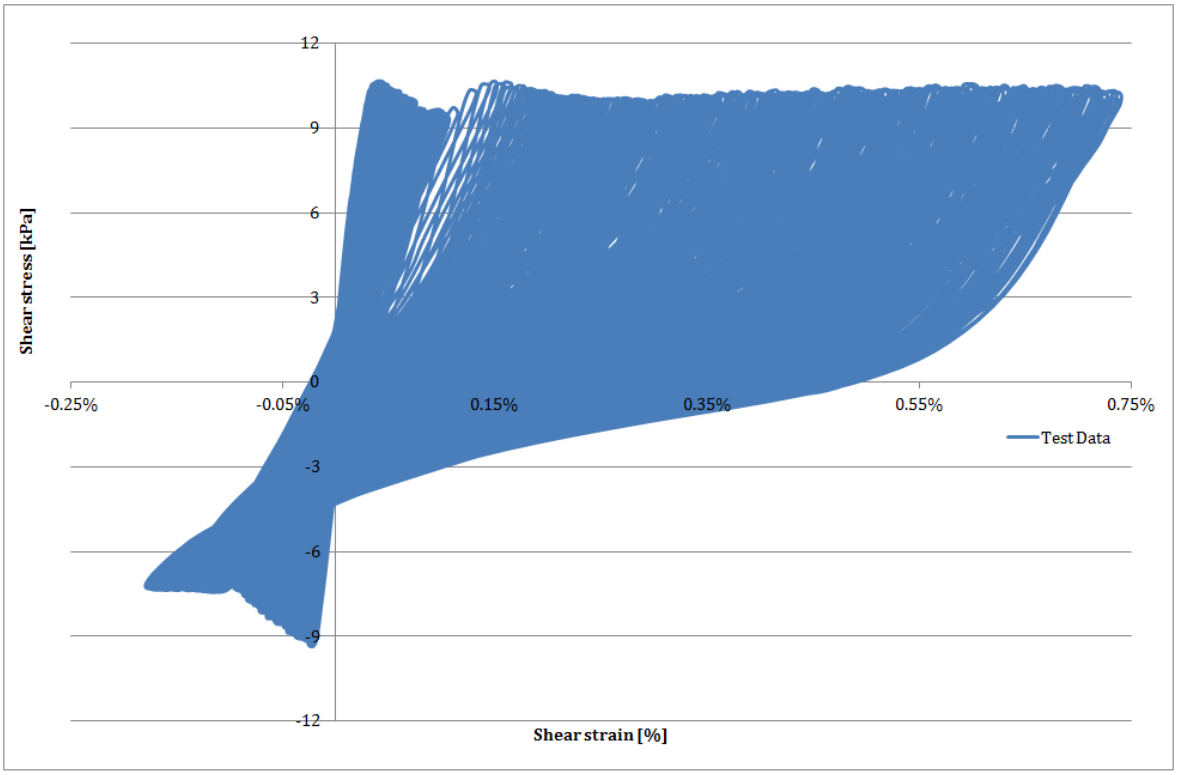

Figure D.11: Cyclic undrained triaxial test results ($CSSR = 0.15$, $I_D = 75\%$)—shear strain vs. shear stress

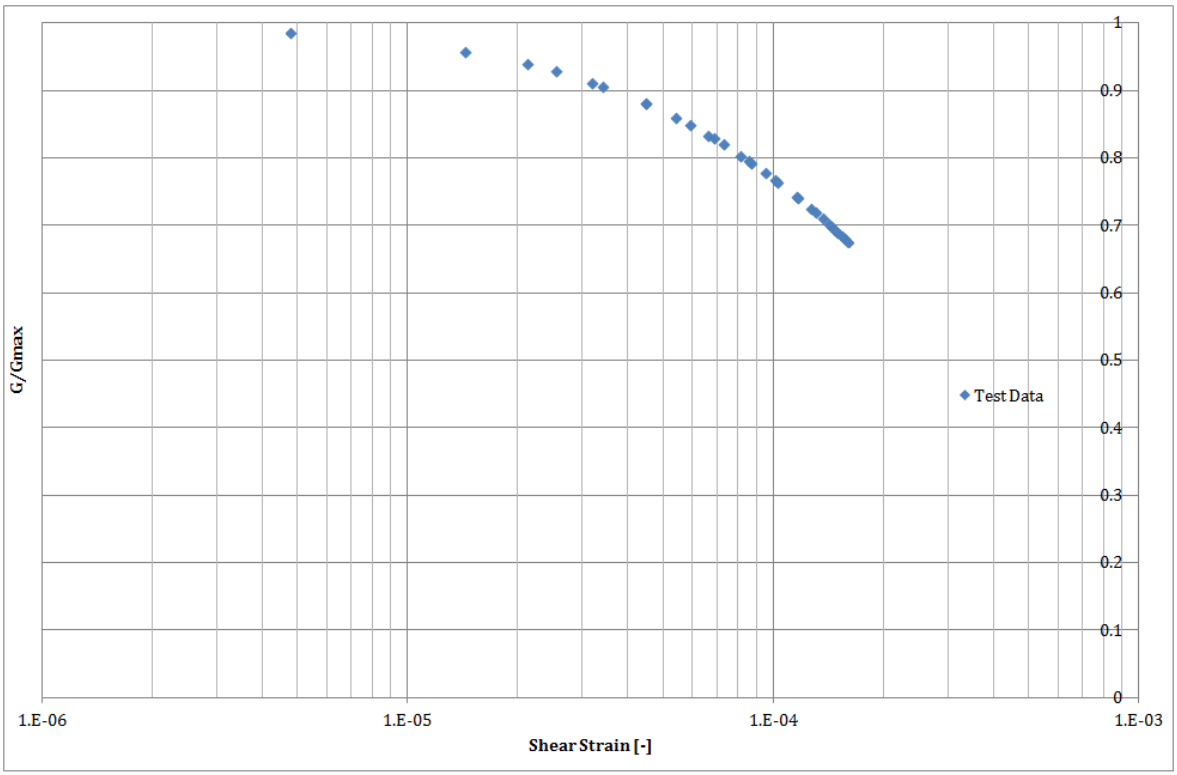

Figure D.12: Cyclic undrained triaxial test results ($CSSR = 0.15$, $I_D = 75\%$)—stiffness degradation curve

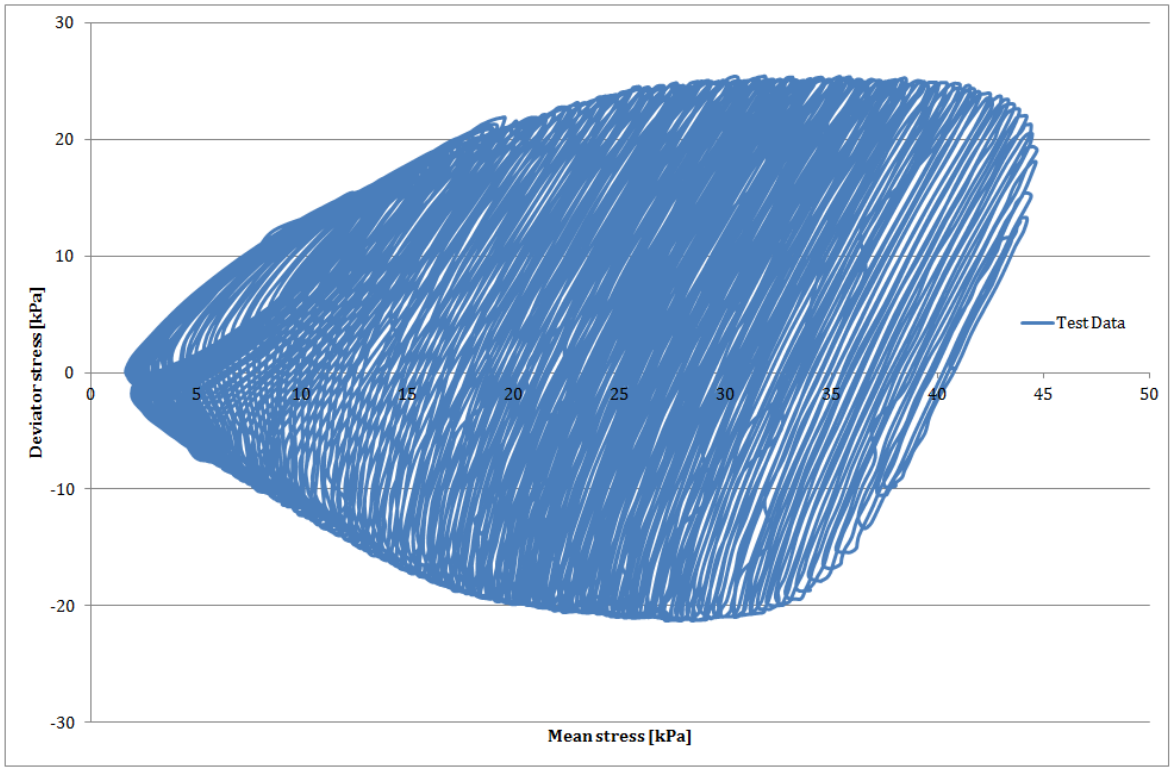

Figure D.13: Cyclic undrained triaxial test results ($CSSR = 0.20$, $I_D = 75\%$)—stress path

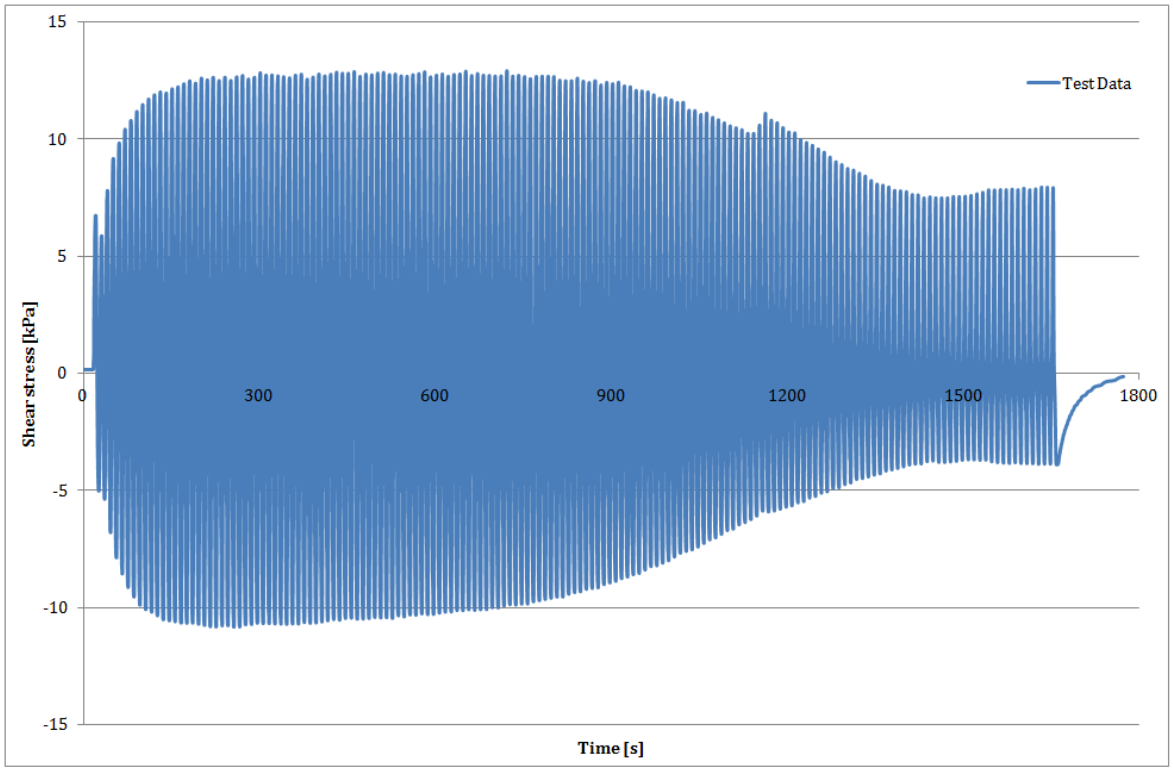

Figure D.14: Cyclic undrained triaxial test results ($CSSR = 0.20$, $I_D = 75\%$)—shear stress in time

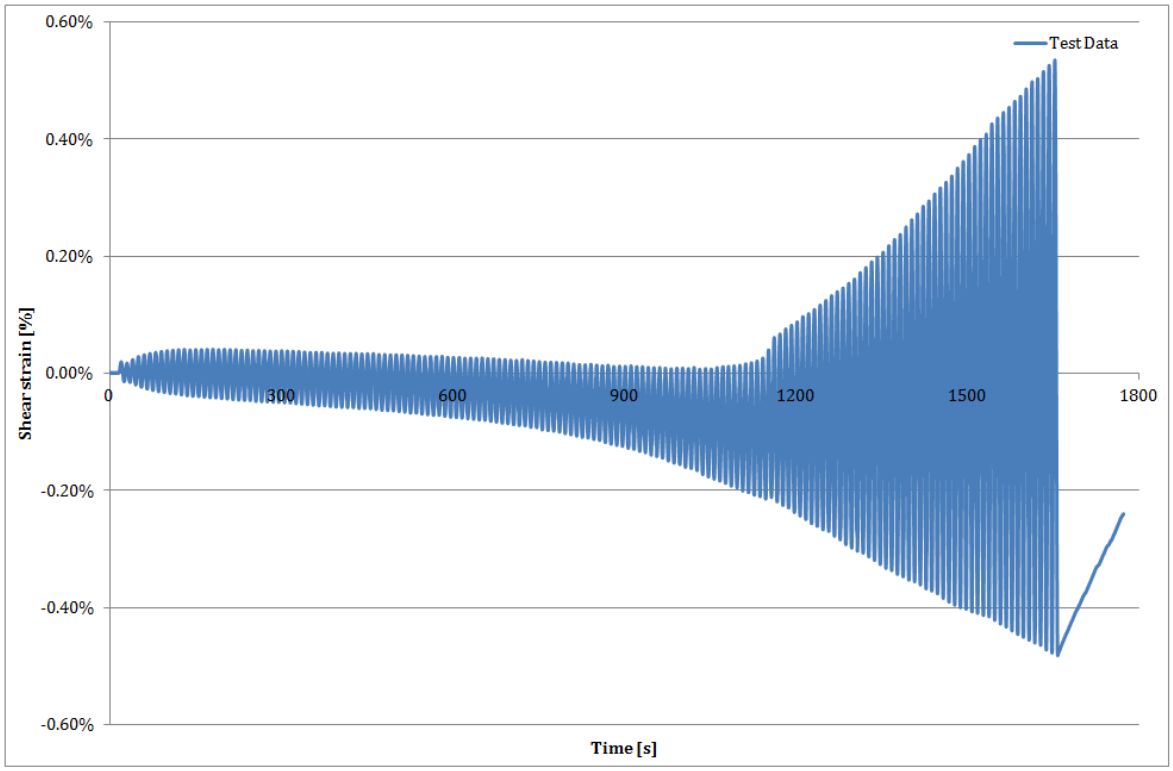

Figure D.15: Cyclic undrained triaxial test results ($CSSR = 0.20$, $I_D = 75\%$)—shear strain in time

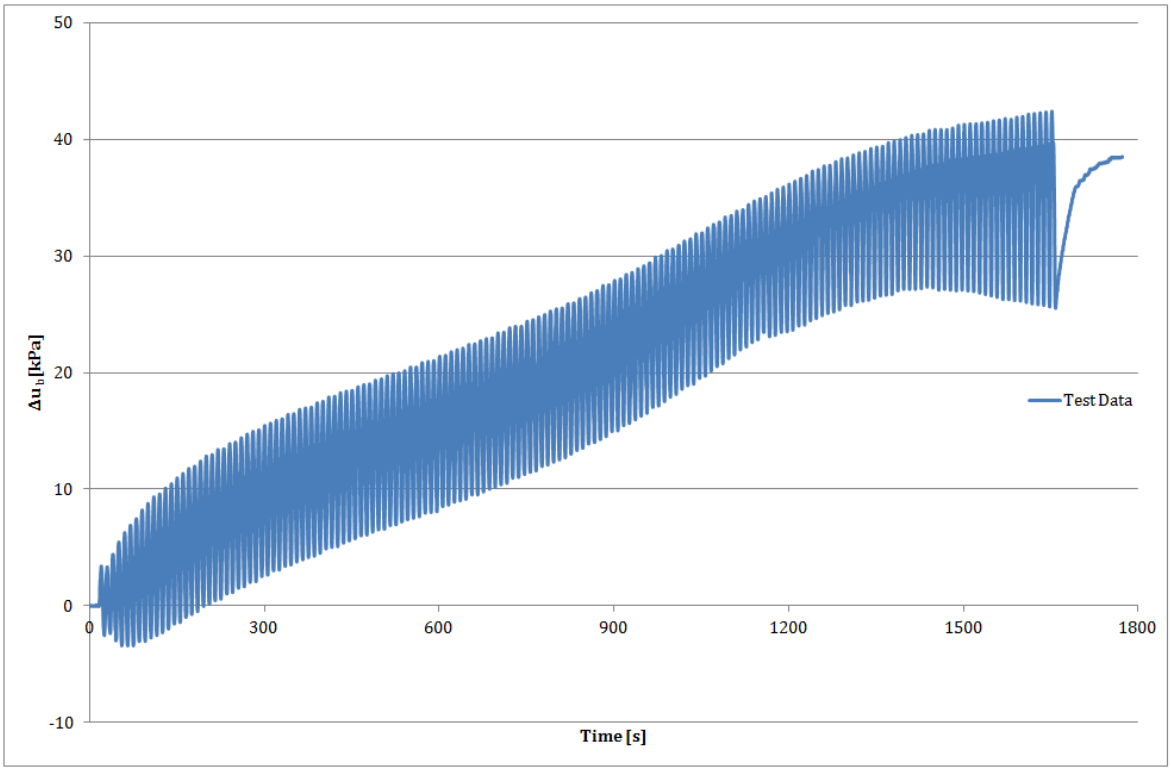

Figure D.16: Cyclic undrained triaxial test results ($CSSR = 0.20$, $I_D = 75\%$)—pore pressure in time

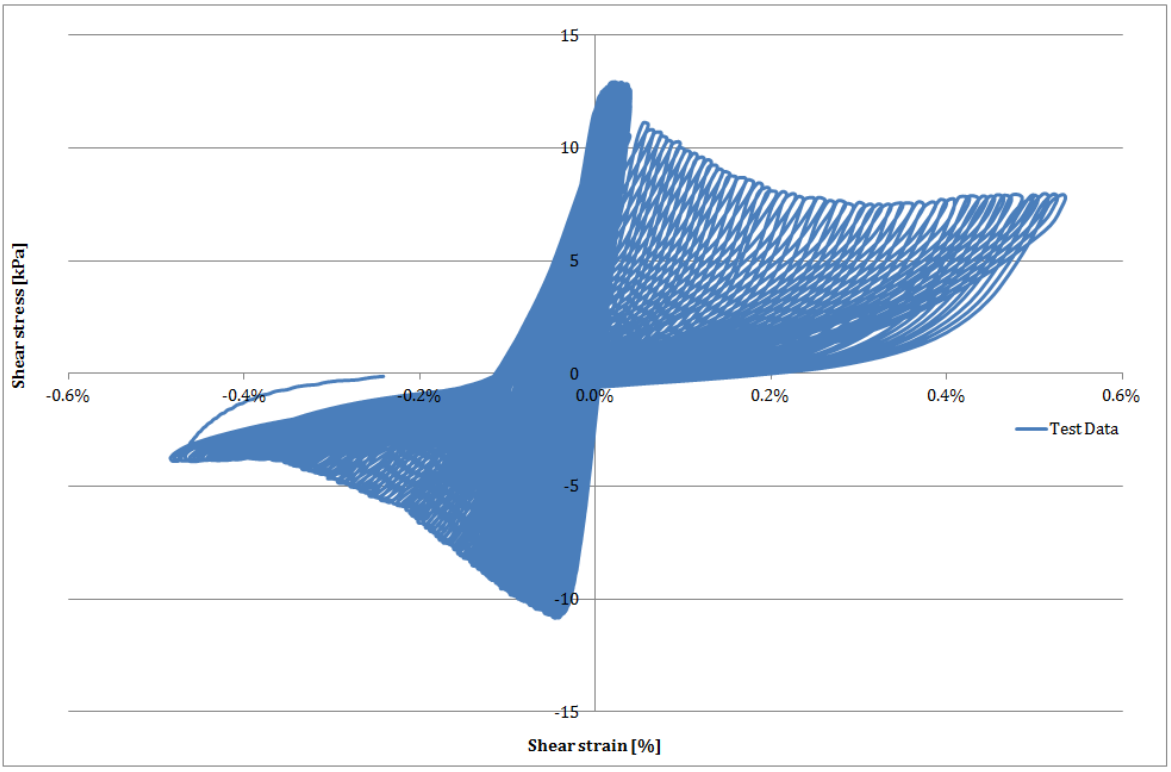

Figure D.17: Cyclic undrained triaxial test results ($CSSR = 0.20$, $I_D = 75\%$)—shear strain vs. shear stress

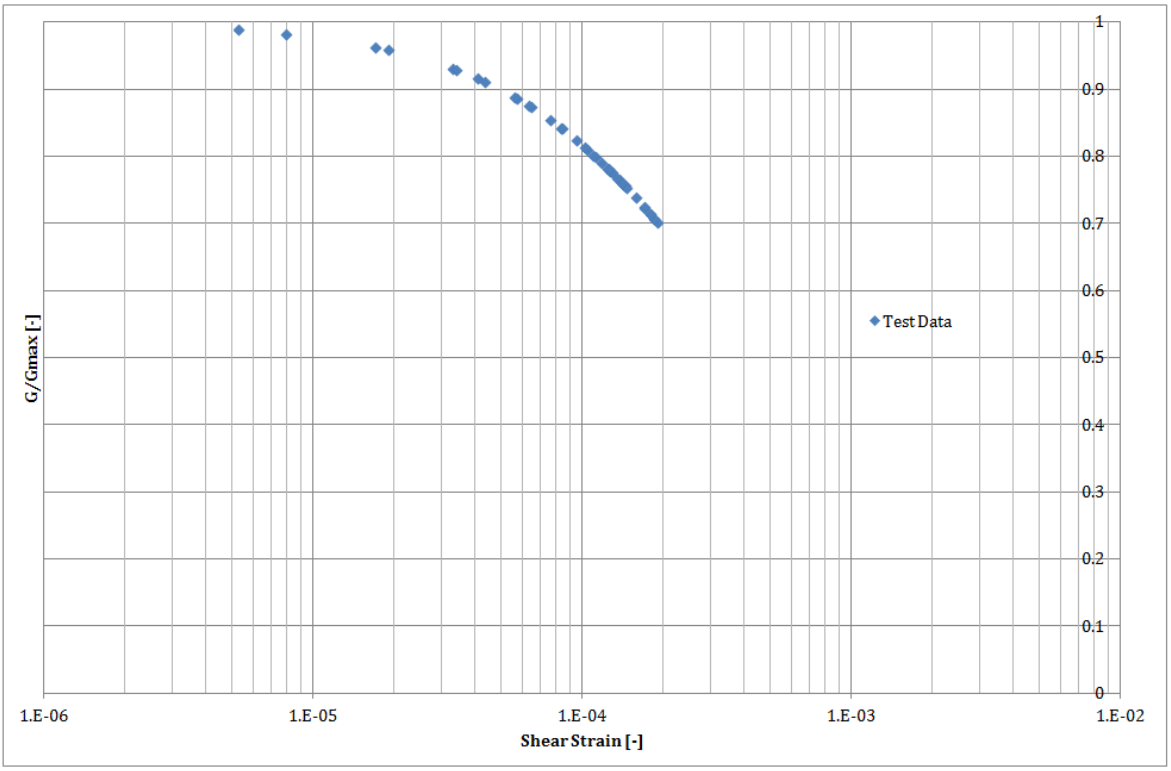

Figure D.18: Cyclic undrained triaxial test results ($CSSR = 0.20$, $I_D = 75\%$)—stiffness degradation curve

D.3 CYCLIC DIRECT SIMPLE SHEAR TESTS WITH VARYING CSSR

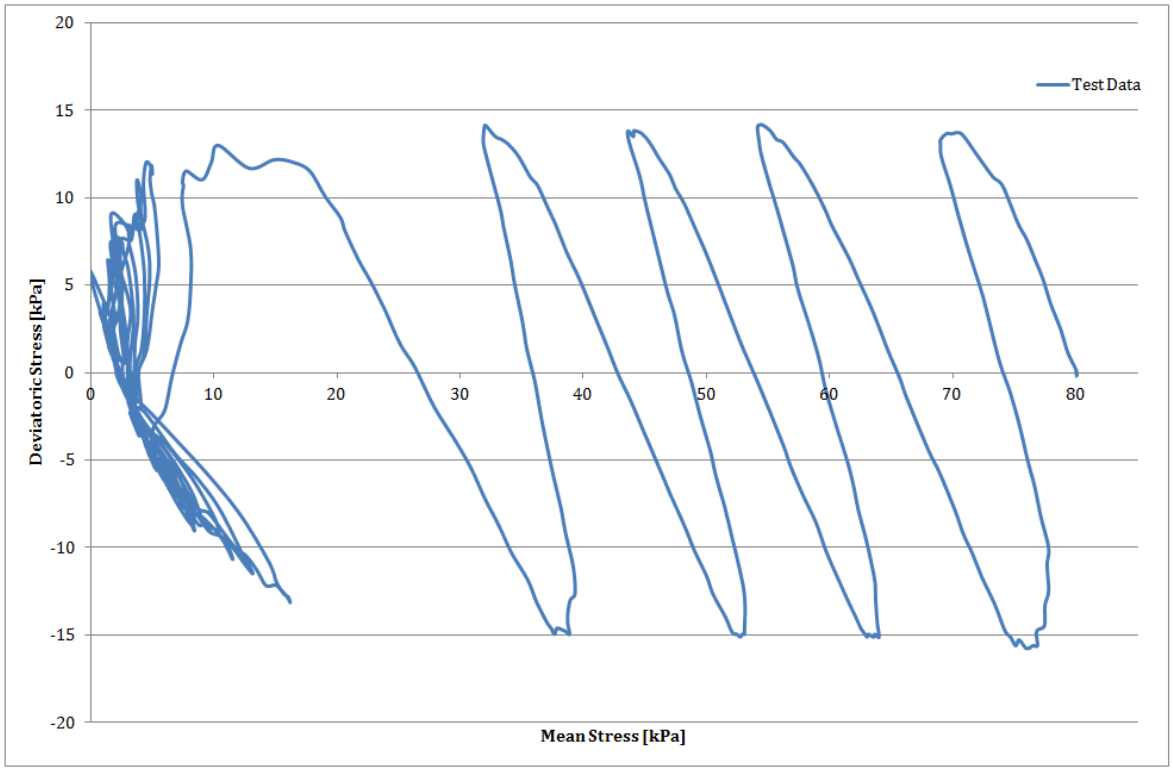

Figure D.19: Cyclic direct simple shear test results ($CSSR = 0.10$, $I_D = 50\%$)—stress path

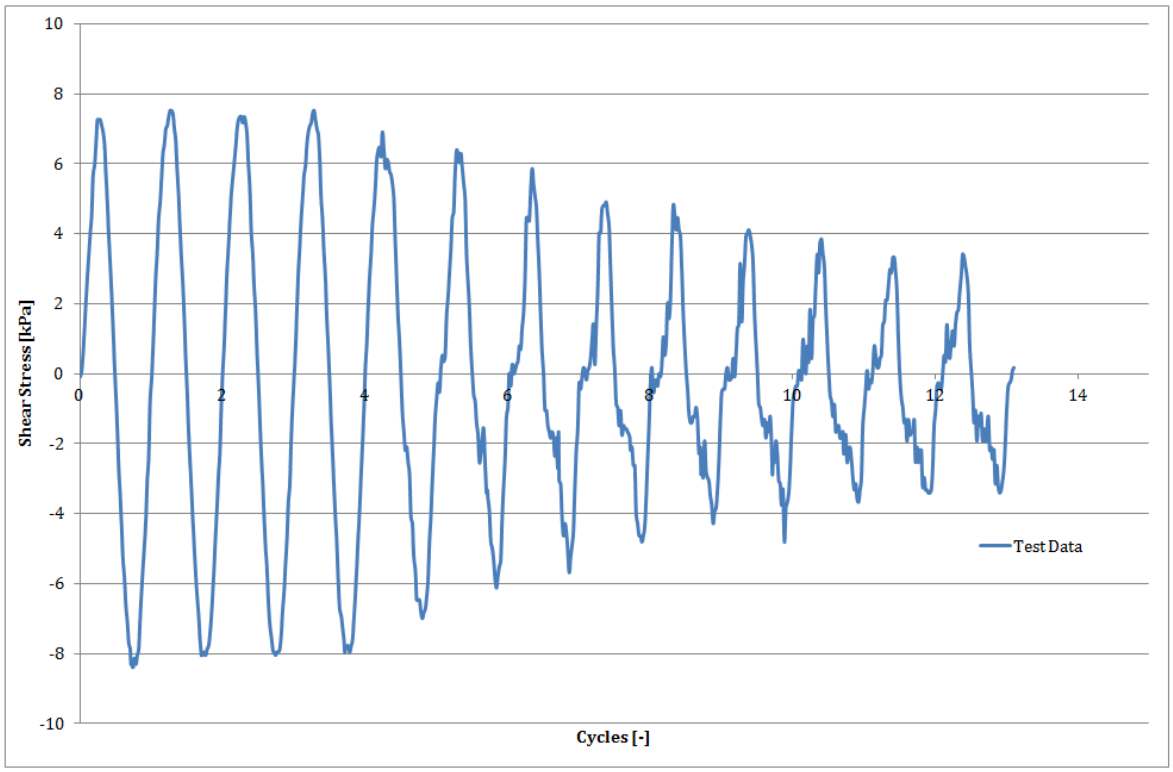

Figure D.20: Cyclic direct simple shear test results ($CSSR = 0.10$, $I_D = 50\%$)—shear stress with respect to the number of cycles

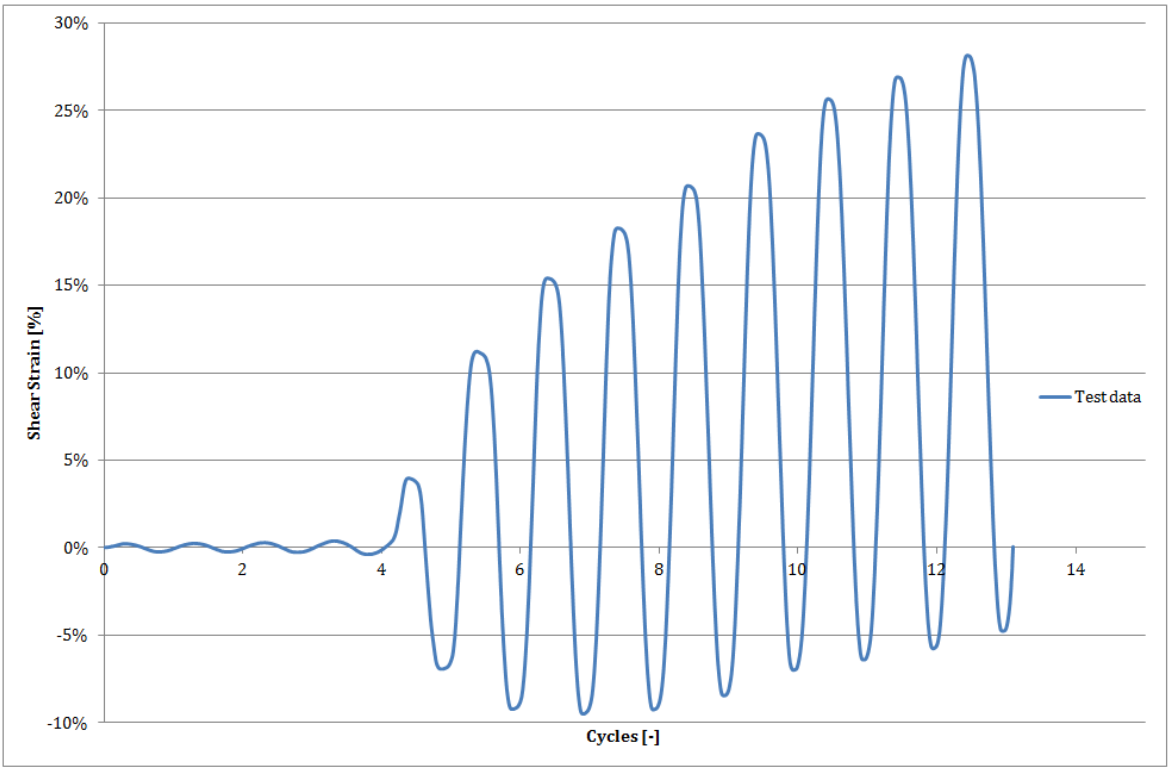

Figure D.21: Cyclic direct simple shear test results ($CSSR = 0.10$, $I_D = 50\%$)—shear strain with respect to the number of cycles

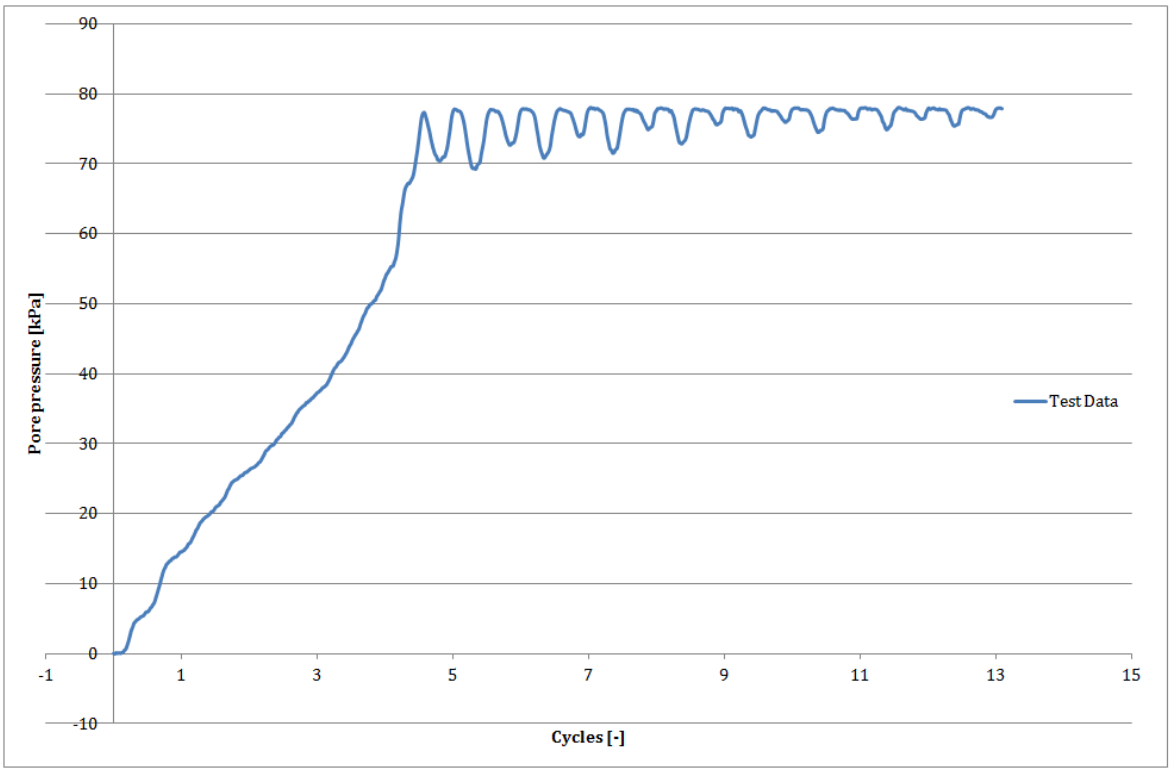

Figure D.22: Cyclic direct simple shear test results ($CSSR = 0.10$, $I_D = 50\%$)—pore pressure with respect to the number of cycles

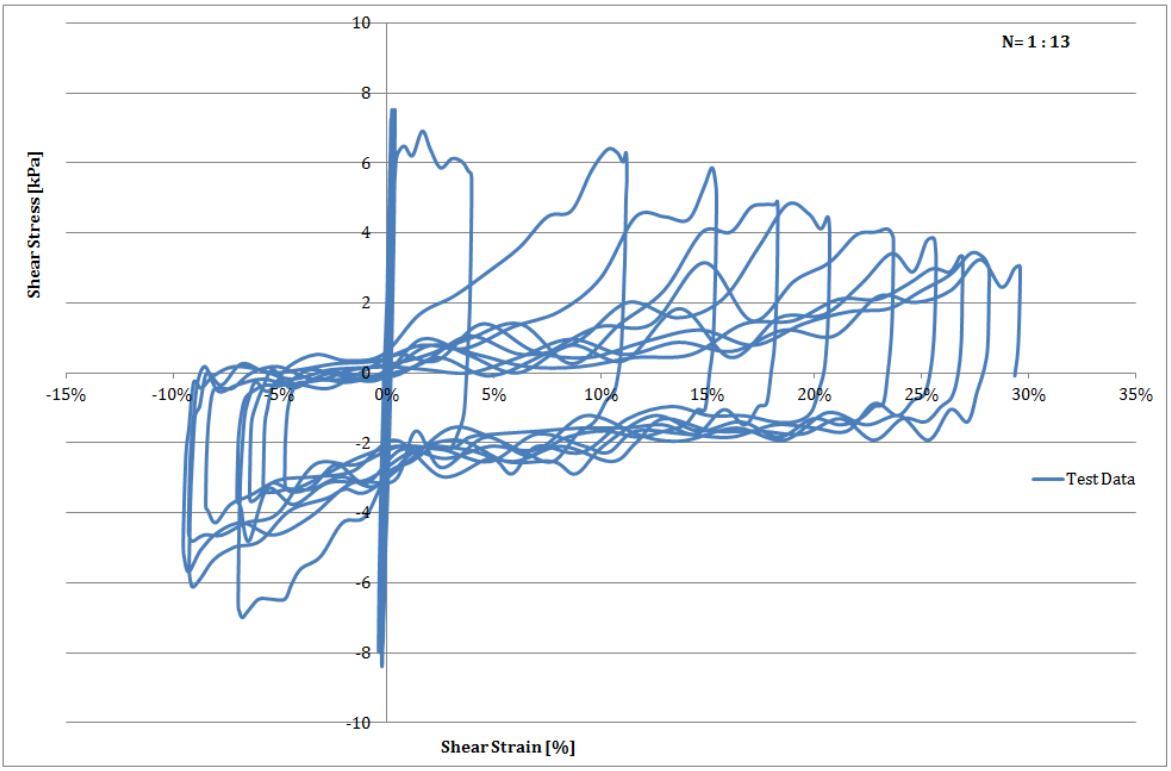

Figure D.23: Cyclic direct simple shear test results ($CSSR = 0.10$, $I_D = 50\%$)—shear strain vs. shear stress

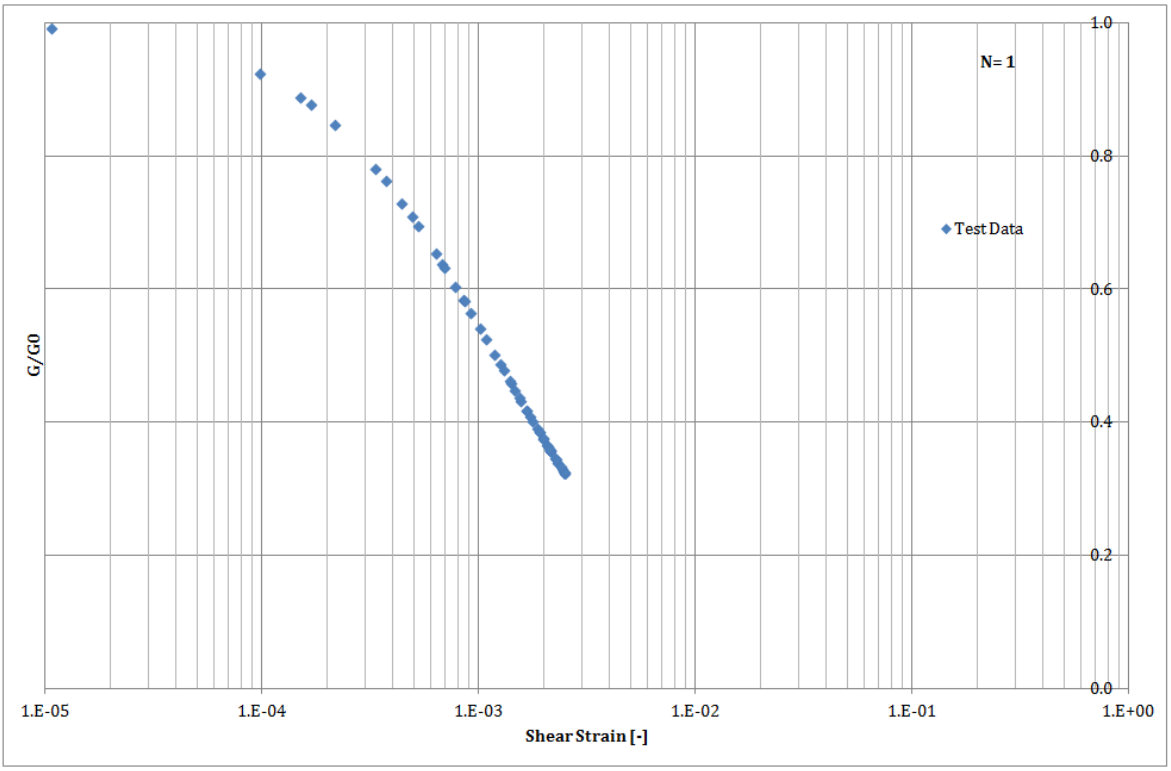

Figure D.24: Cyclic direct simple shear test results ($CSSR = 0.10$, $I_D = 50\%$)—stiffness degradation curve

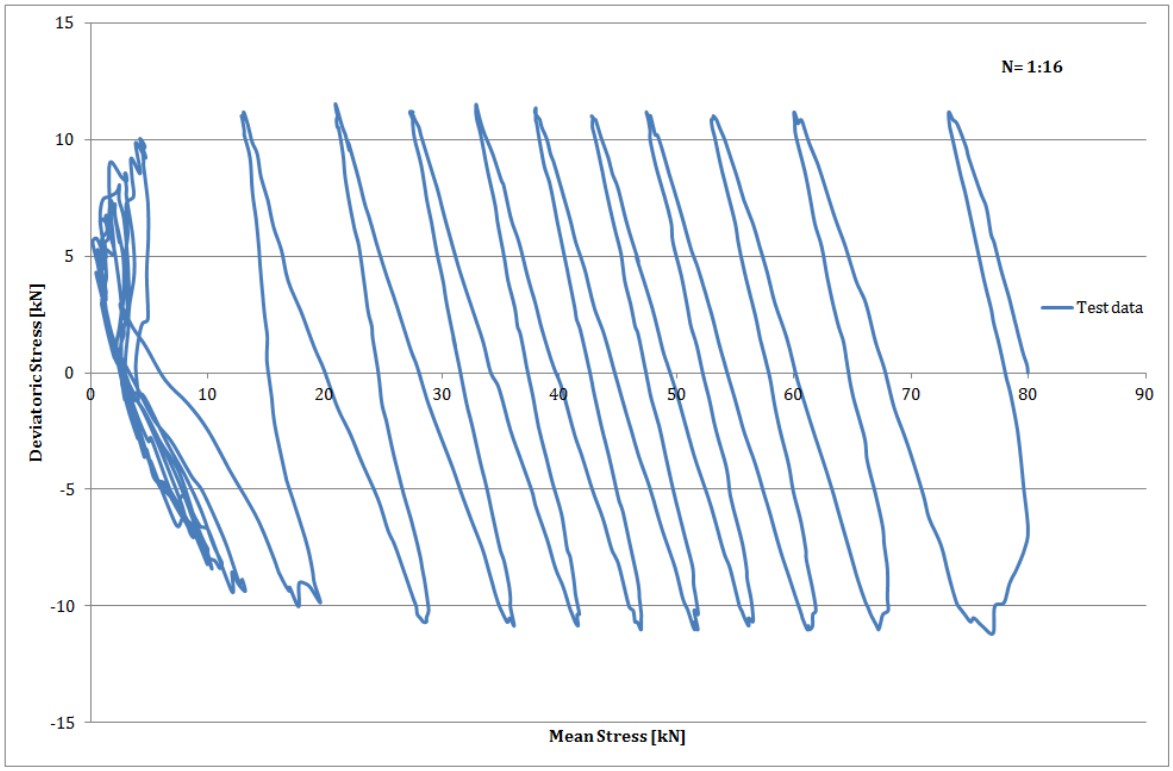

Figure D.25: Cyclic direct simple shear test results ($CSSR = 0.075$, $I_D = 50\%$)—stress path

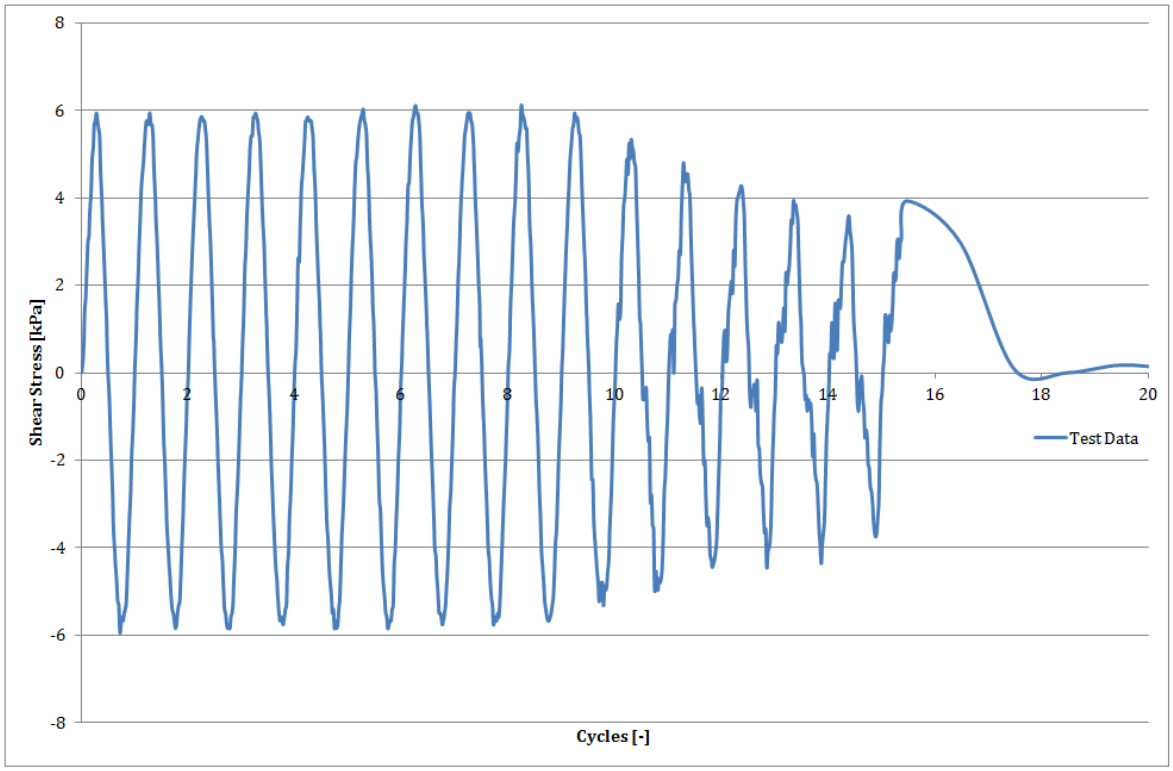

Figure D.26: Cyclic direct simple shear test results ($CSSR = 0.075$, $I_D = 50\%$)—shear stress with respect to the number of cycles

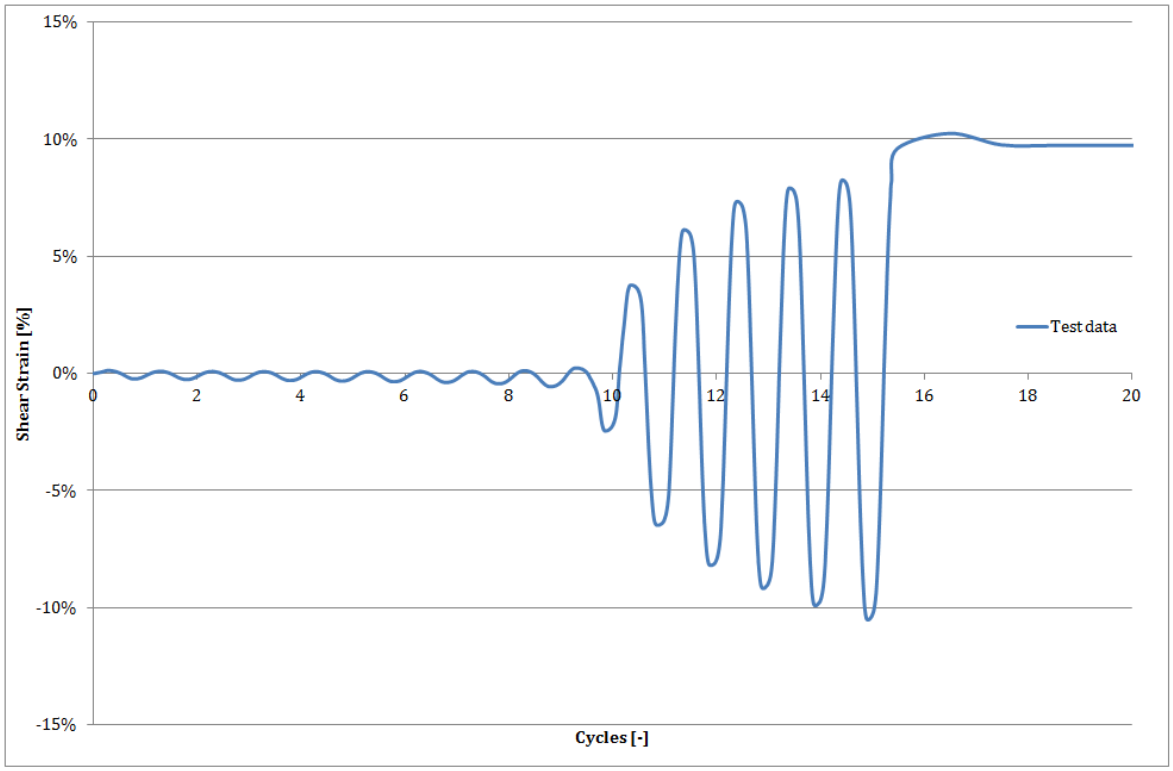

Figure D.27: Cyclic direct simple shear test results ($CSSR = 0.075$, $I_D = 50\%$)—shear strain with respect to the number of cycles

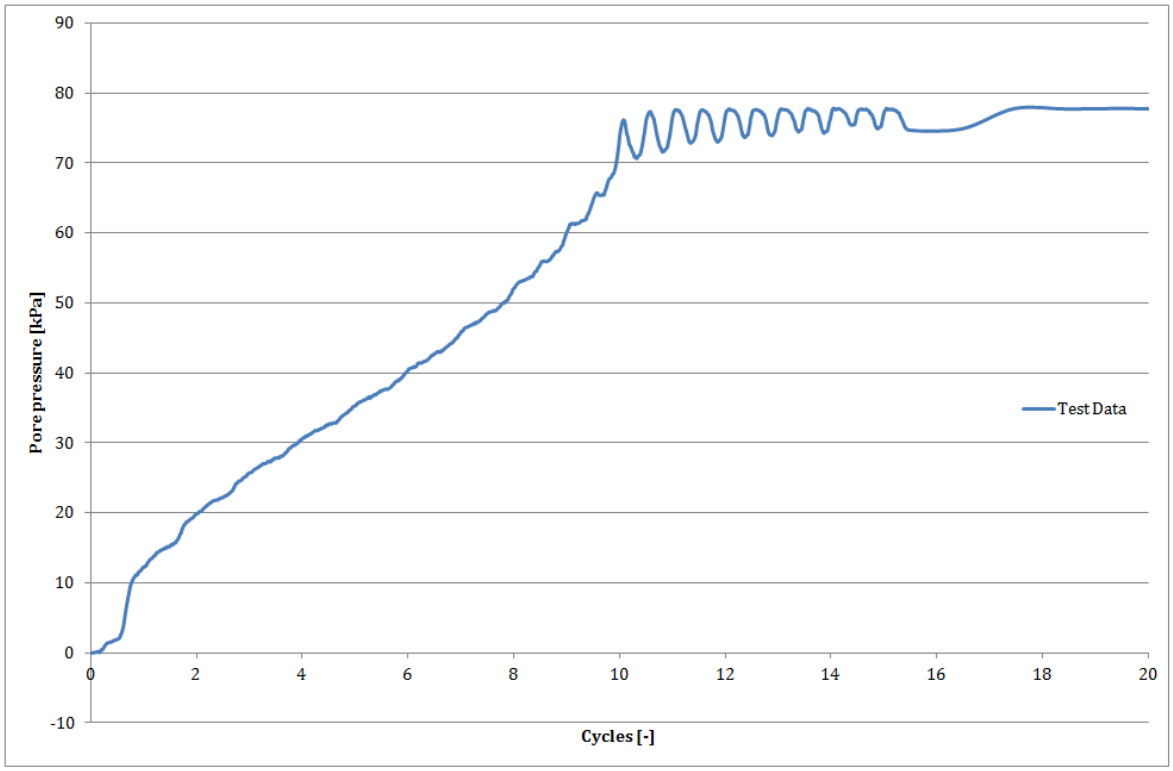

Figure D.28: Cyclic direct simple shear test results ($CSSR = 0.075$, $I_D = 50\%$)—pore pressure with respect to the number of cycles

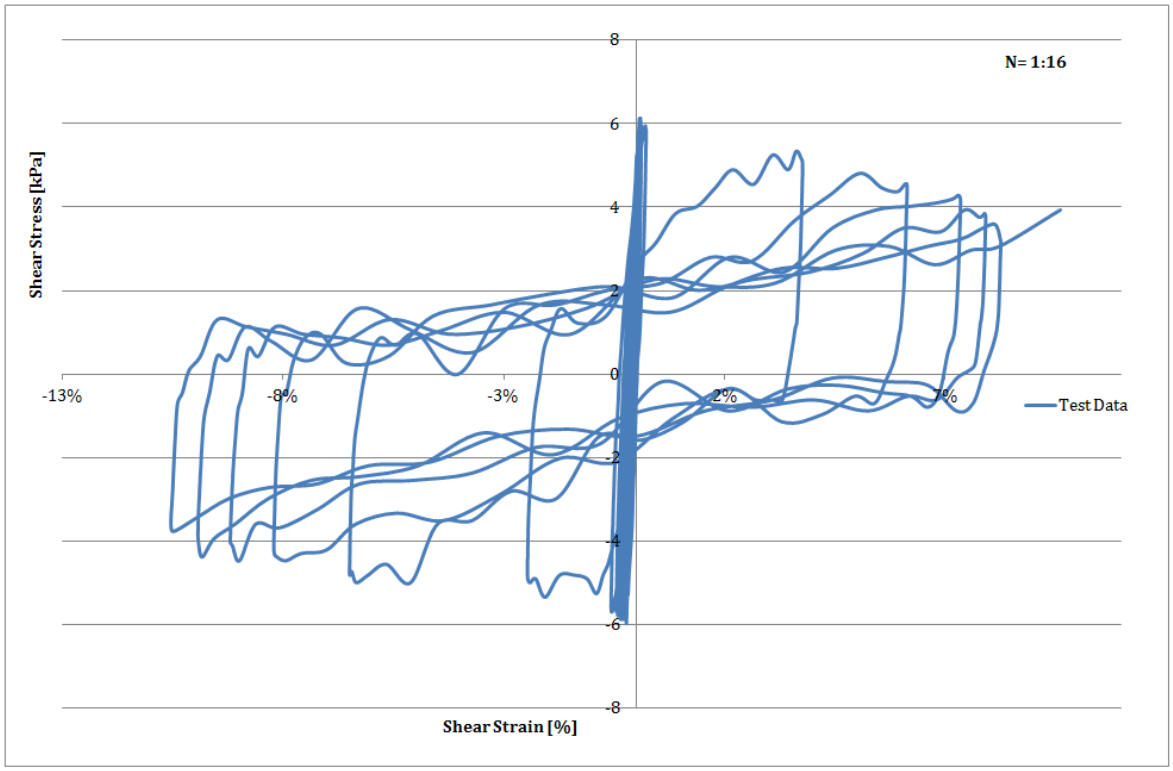

Figure D.29: Cyclic direct simple shear test results ($CSSR = 0.075$, $I_D = 50\%$)—shear strain vs. shear stress

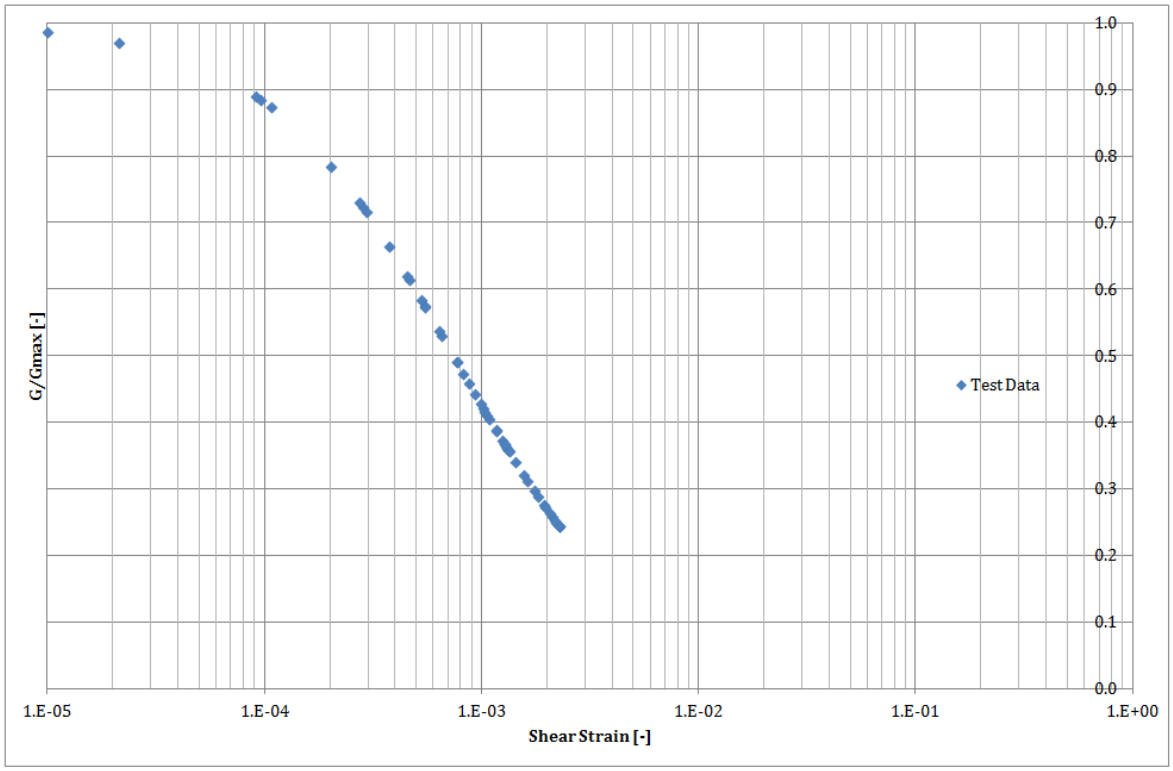

Figure D.30: Cyclic direct simple shear test results ($CSSR = 0.075$, $I_D = 50\%$)—stiffness degradation curve

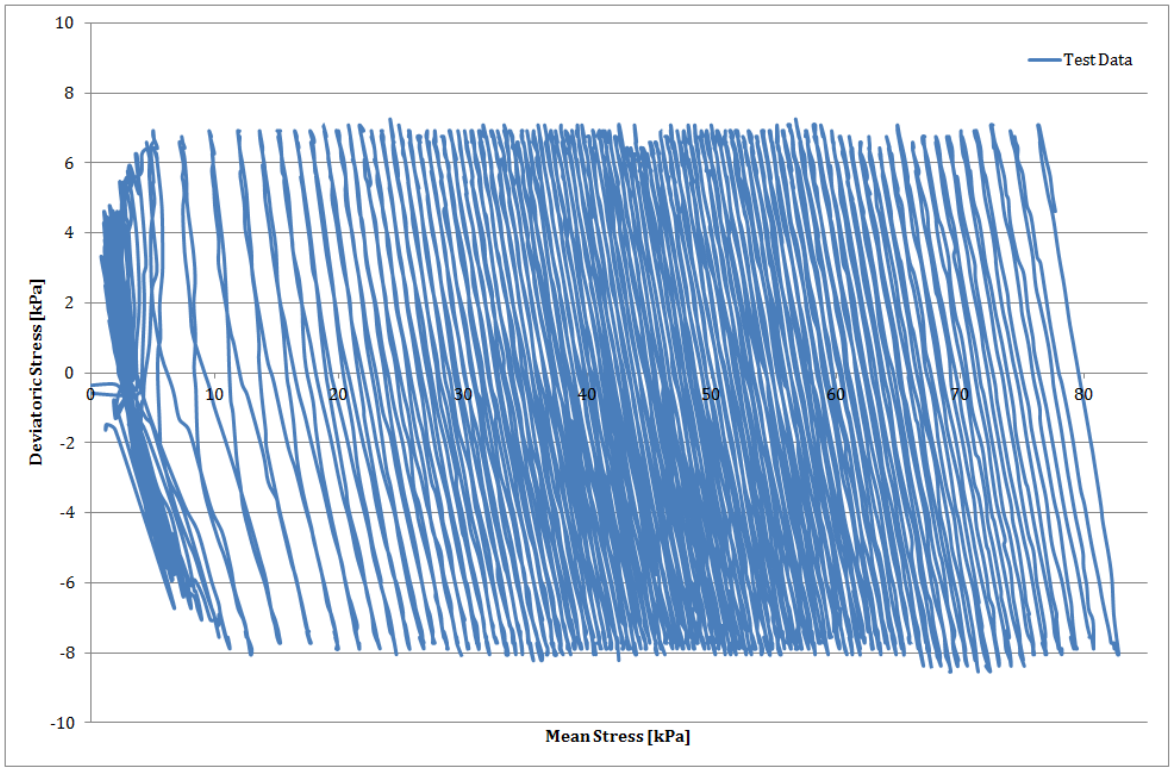

Figure D.31: Cyclic direct simple shear test results ($CSSR = 0.05$, $I_D = 50\%$)—stress path

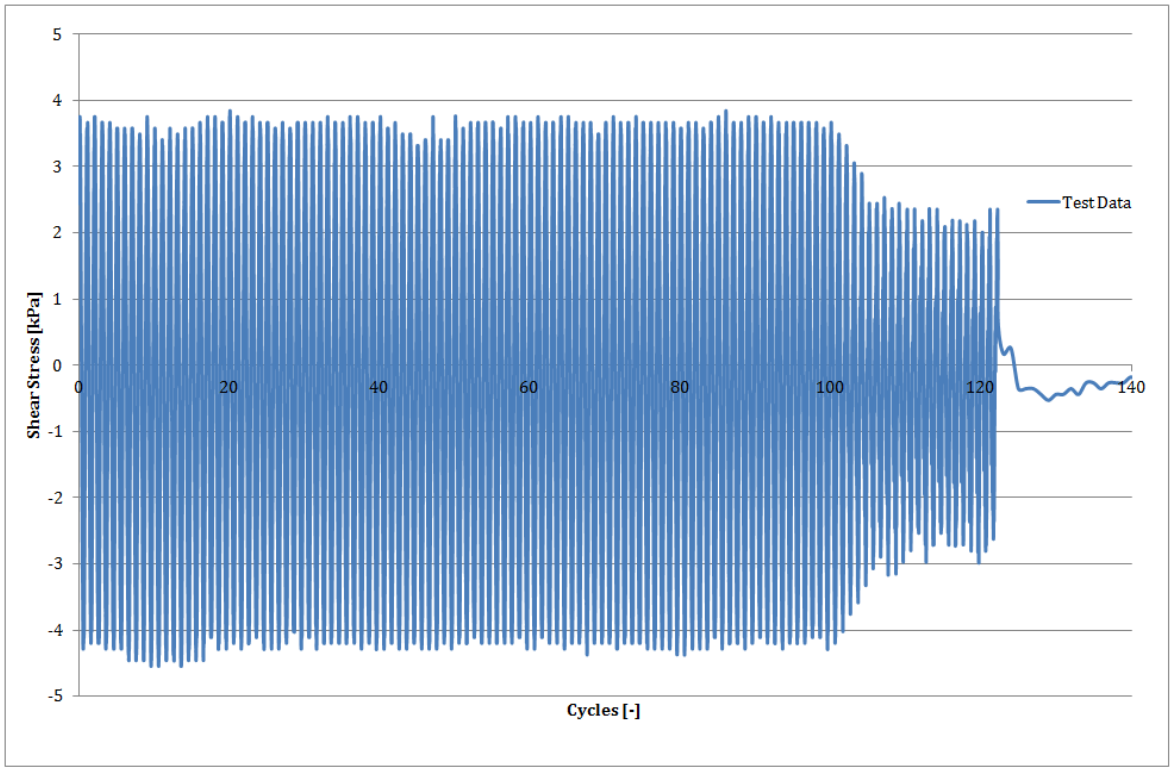

Figure D.32: Cyclic direct simple shear test results ($CSSR = 0.05$, $I_D = 50\%$)—shear stress with respect to the number of cycles

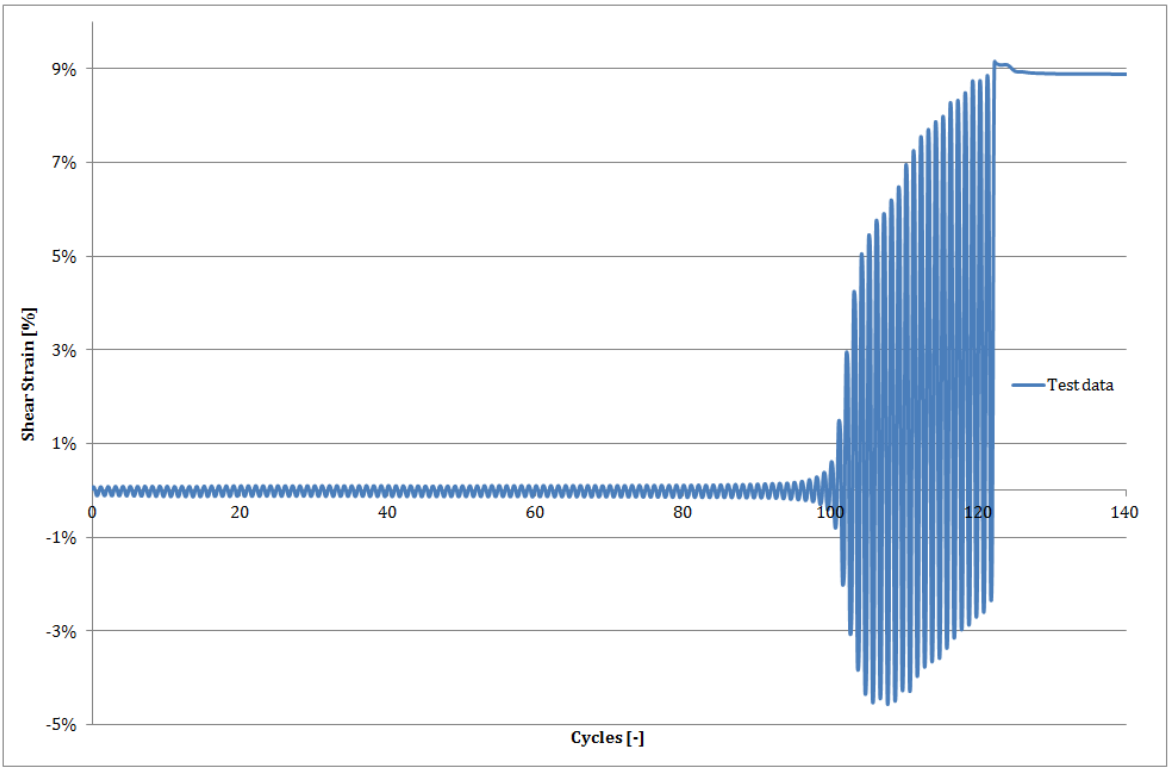

Figure D.33: Cyclic direct simple shear test results ($CSSR = 0.05$, $I_D = 50\%$)—shear strain with respect to the number of cycles

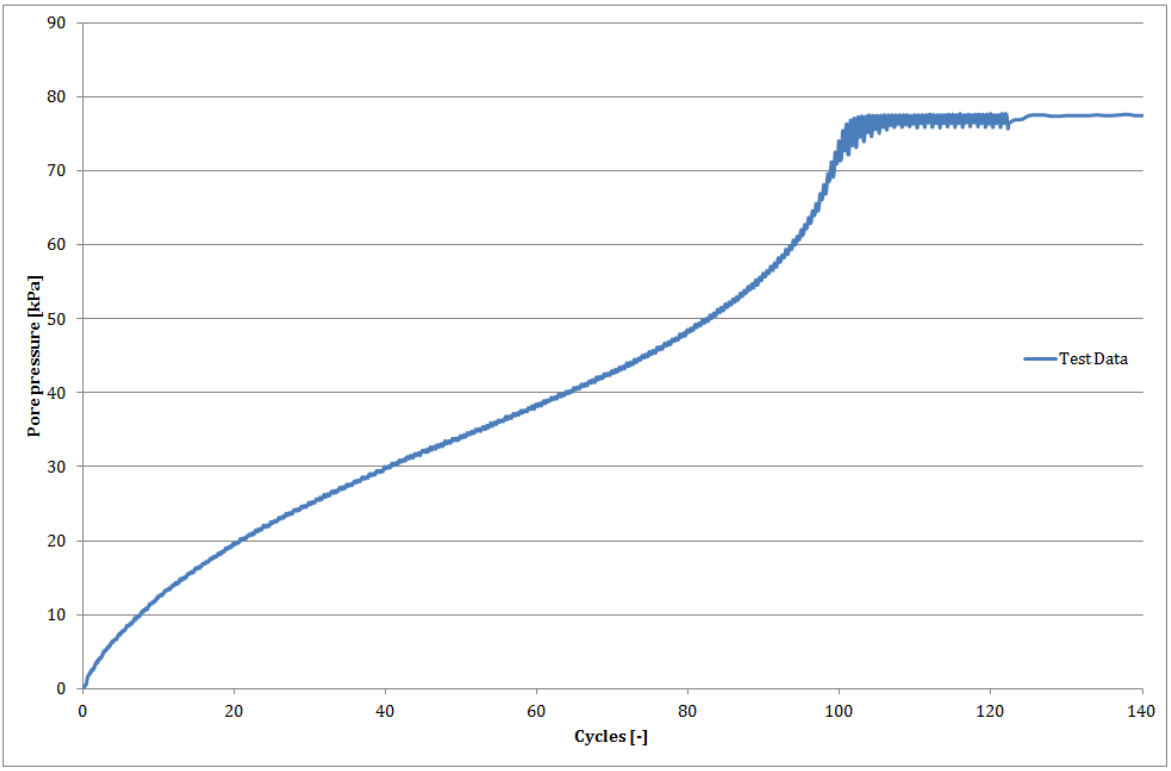

Figure D.34: Cyclic direct simple shear test results ($CSSR = 0.05$, $I_D = 50\%$)—pore pressure with respect to the number of cycles

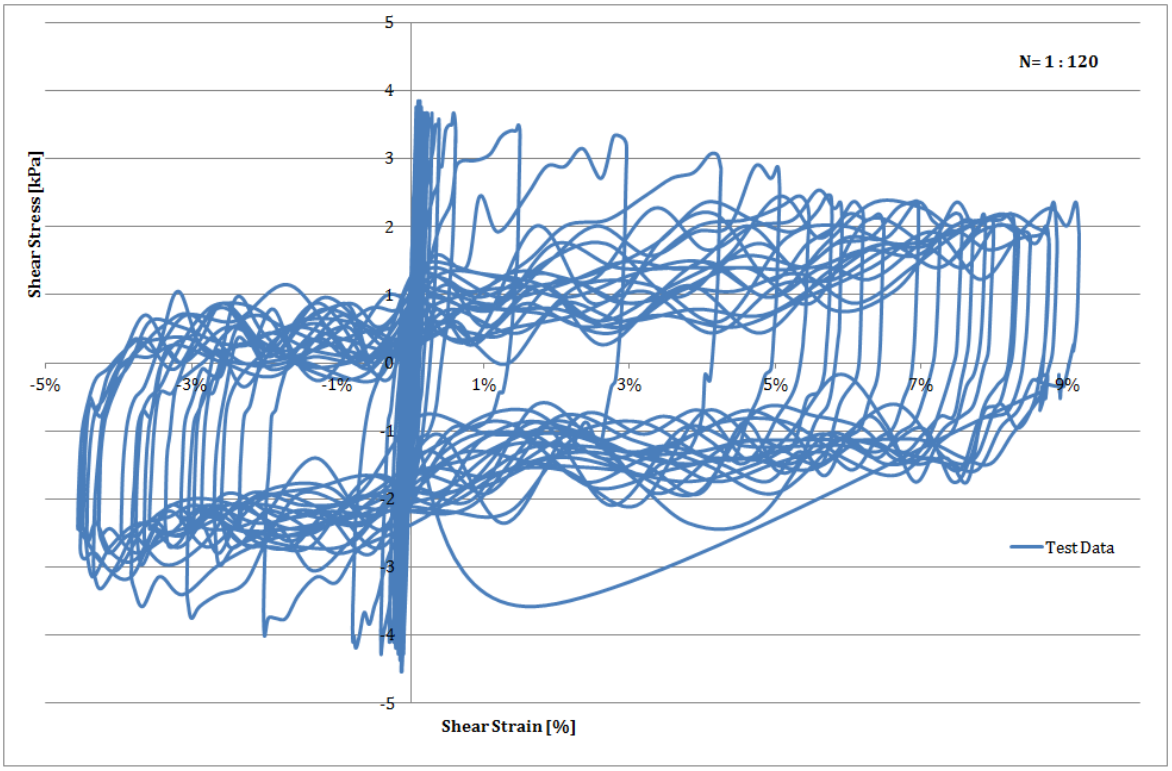

Figure D.35: Cyclic direct simple shear test results ($CSSR = 0.05$, $I_D = 50\%$)—shear strain vs. shear stress

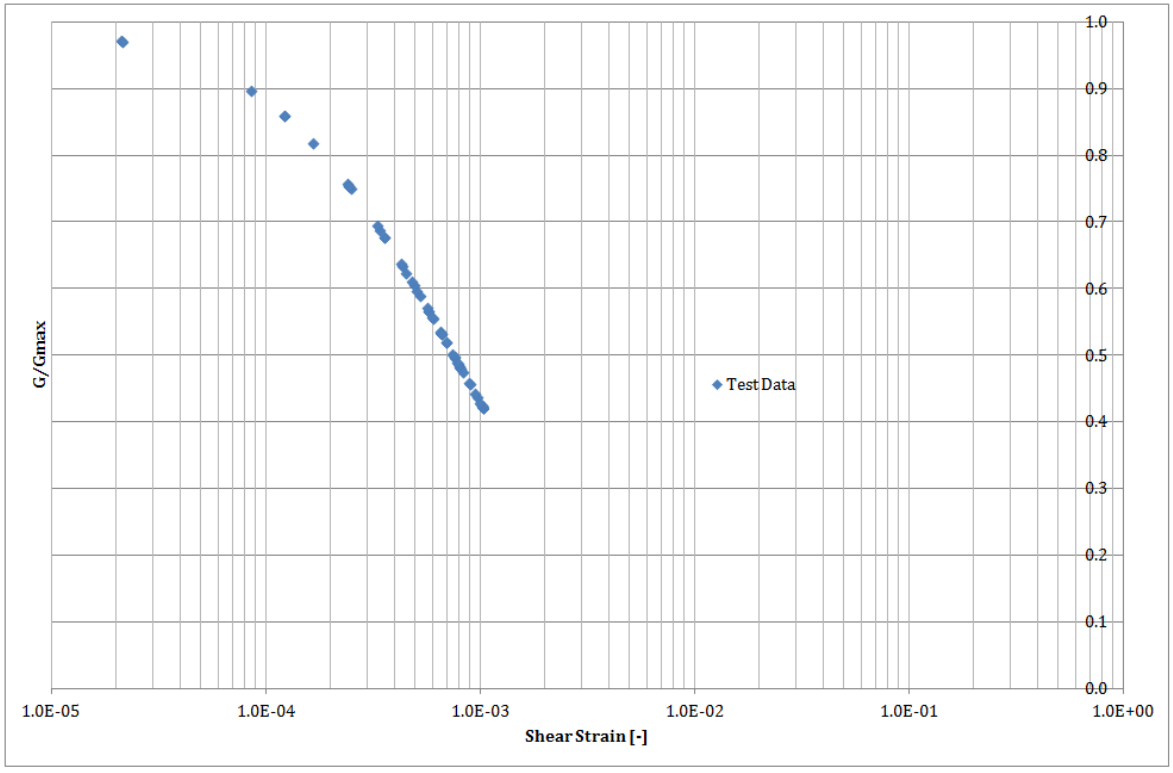

Figure D.36: Cyclic direct simple shear test results ($CSSR = 0.05$, $I_D = 50\%$)—stiffness degradation curve

Appendix E

CALIBRATION RESULTS

The current appendix shows the results of the calibration procedure for the hypoplastic sand model with intergranular strain concept.

E.1 CALIBRATION OF THE HYPOPLASTIC SAND MODEL PARAMETERS FROM ICTxU

ICTXu represents the abreviation for Isotropically Consolidated Undrained Triaxial tests.

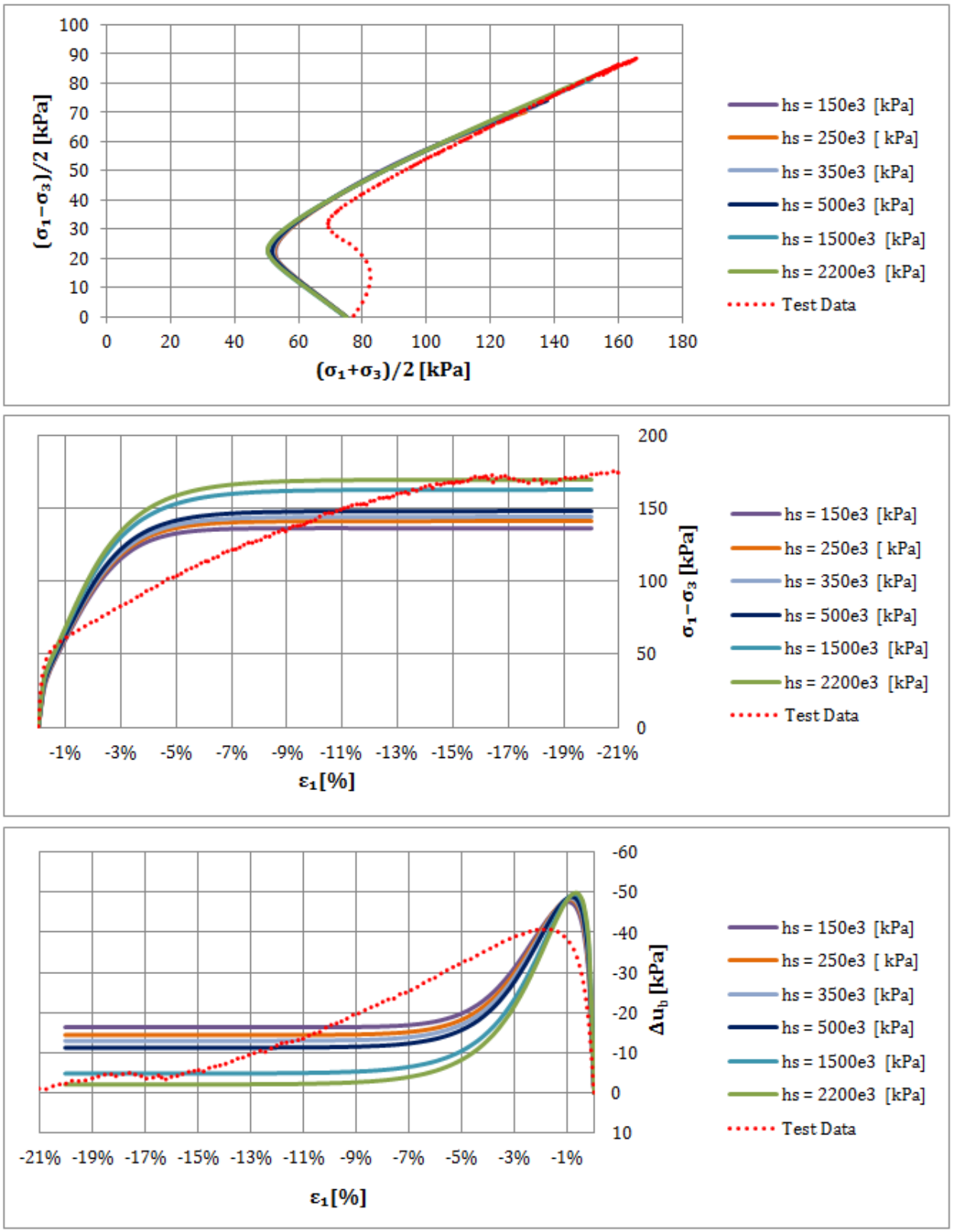

Figure E.1: Calibration of h_s ($I_D = 50\%$)

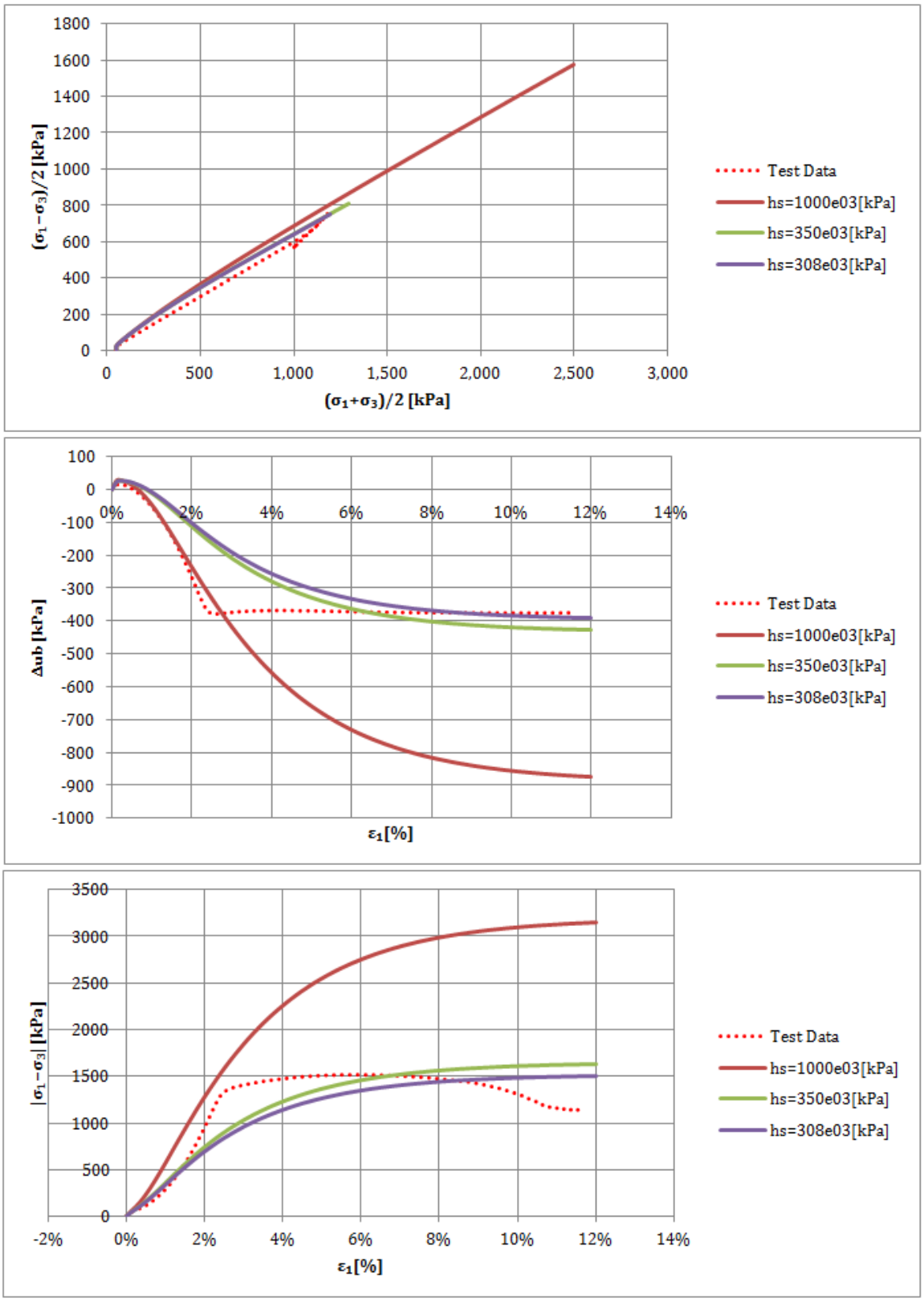

Figure E.2: Calibration of h_s ($I_D = 80\%$)

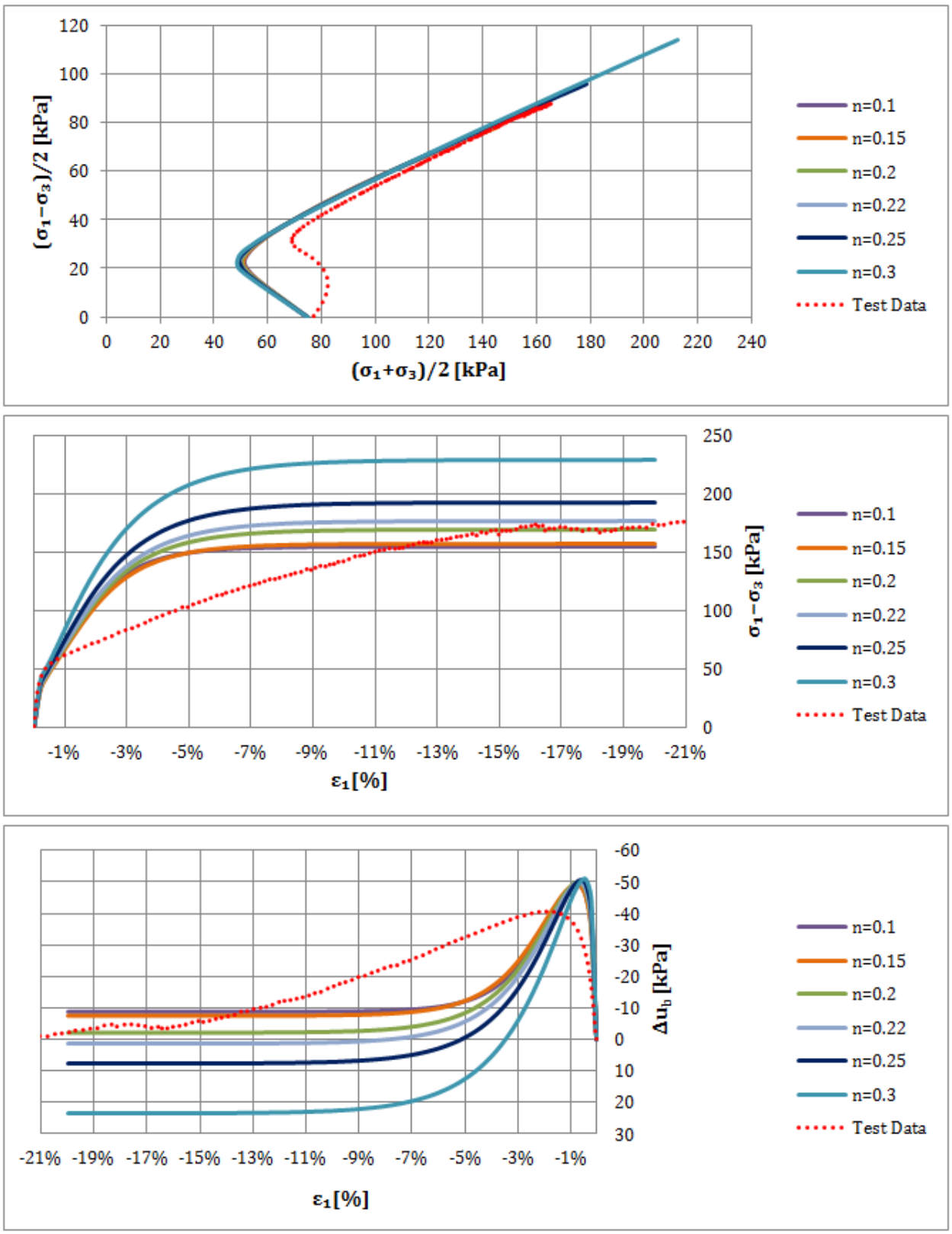

Figure E.3: Calibration of n ($I_D = 50\%$)

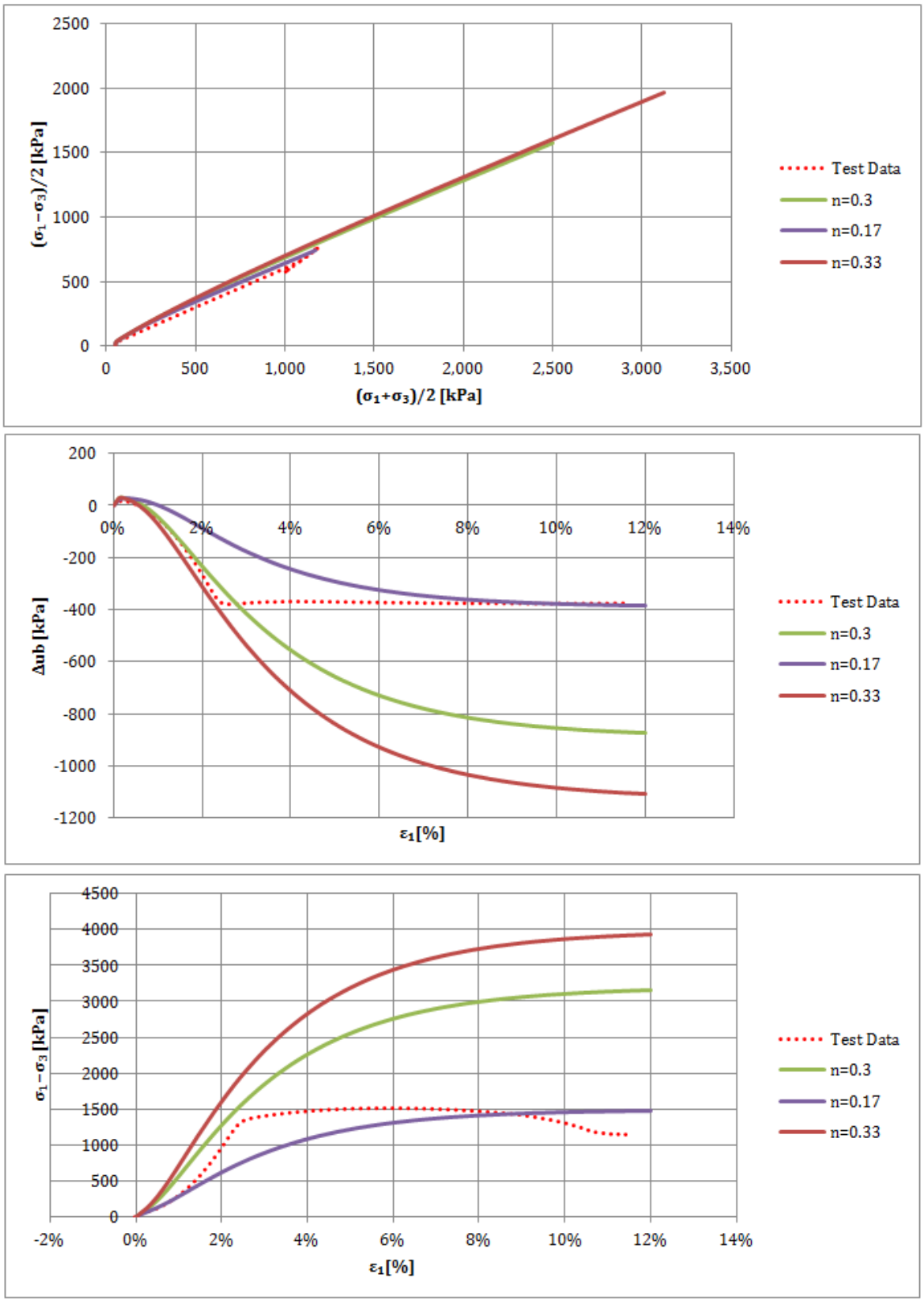

Figure E.4: Calibration of n ($I_D = 80\%$)

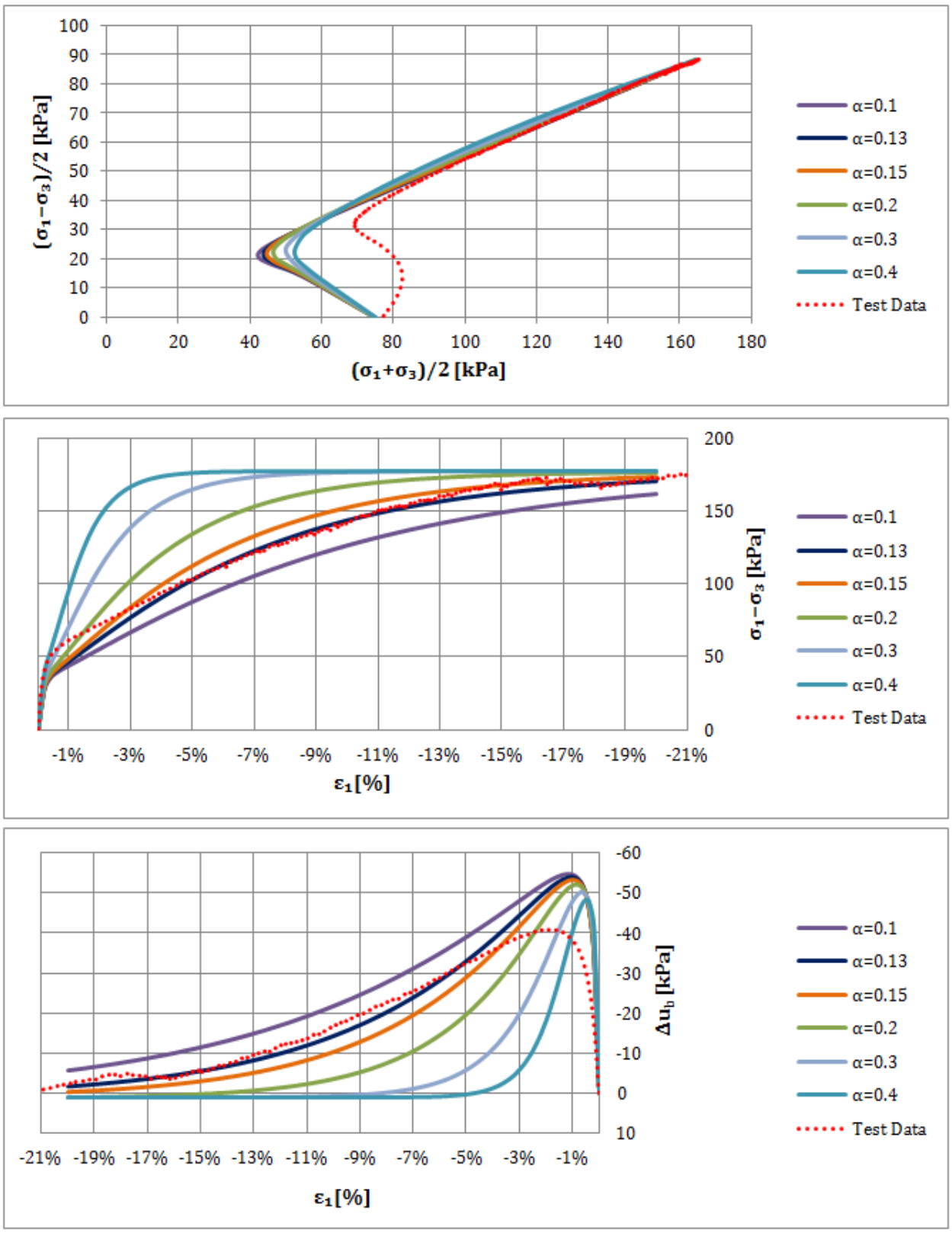

Figure E.5: Calibration of α ($I_D = 50\%$)

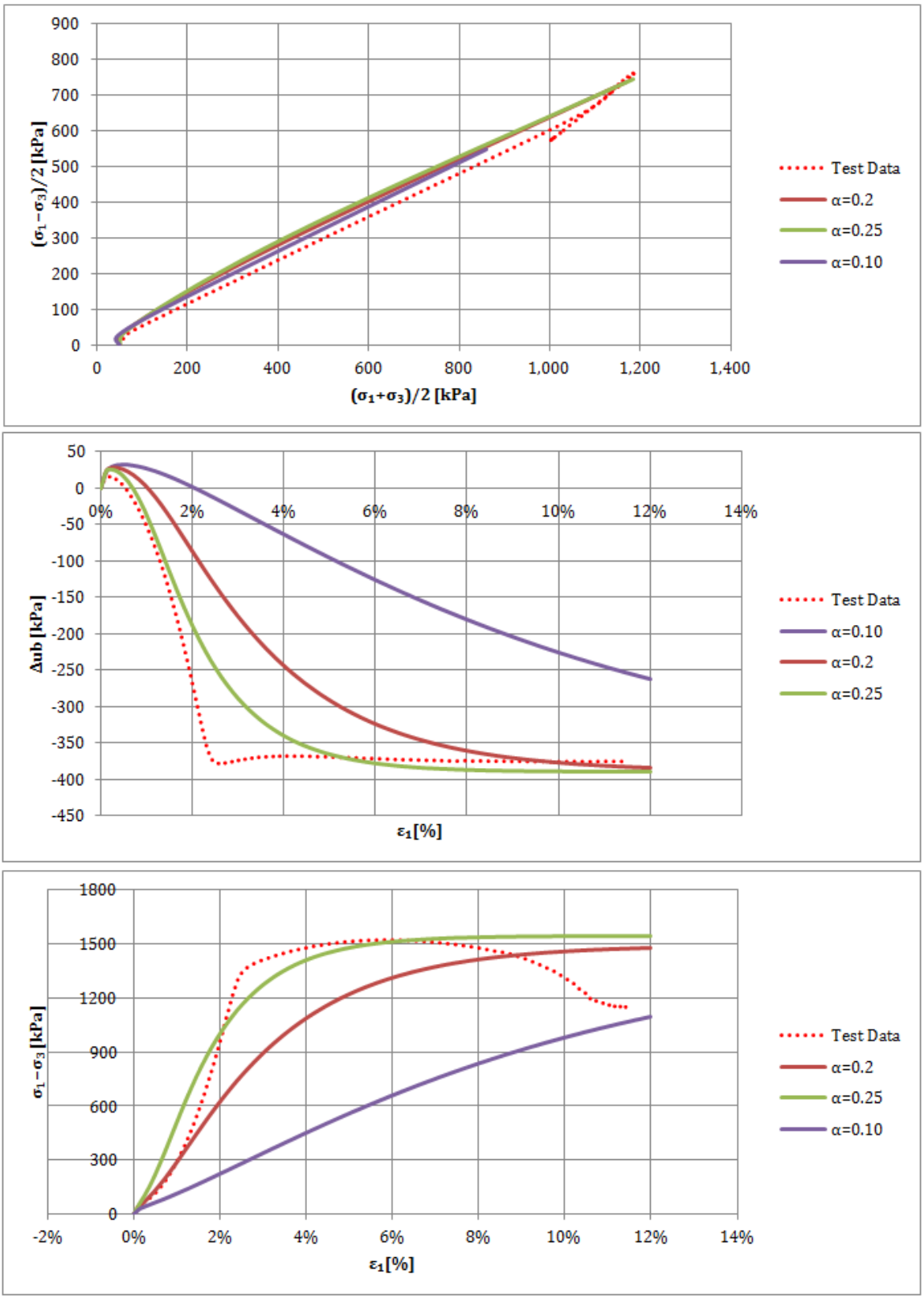

Figure E.6: Calibration of α ($I_D = 80\%$)

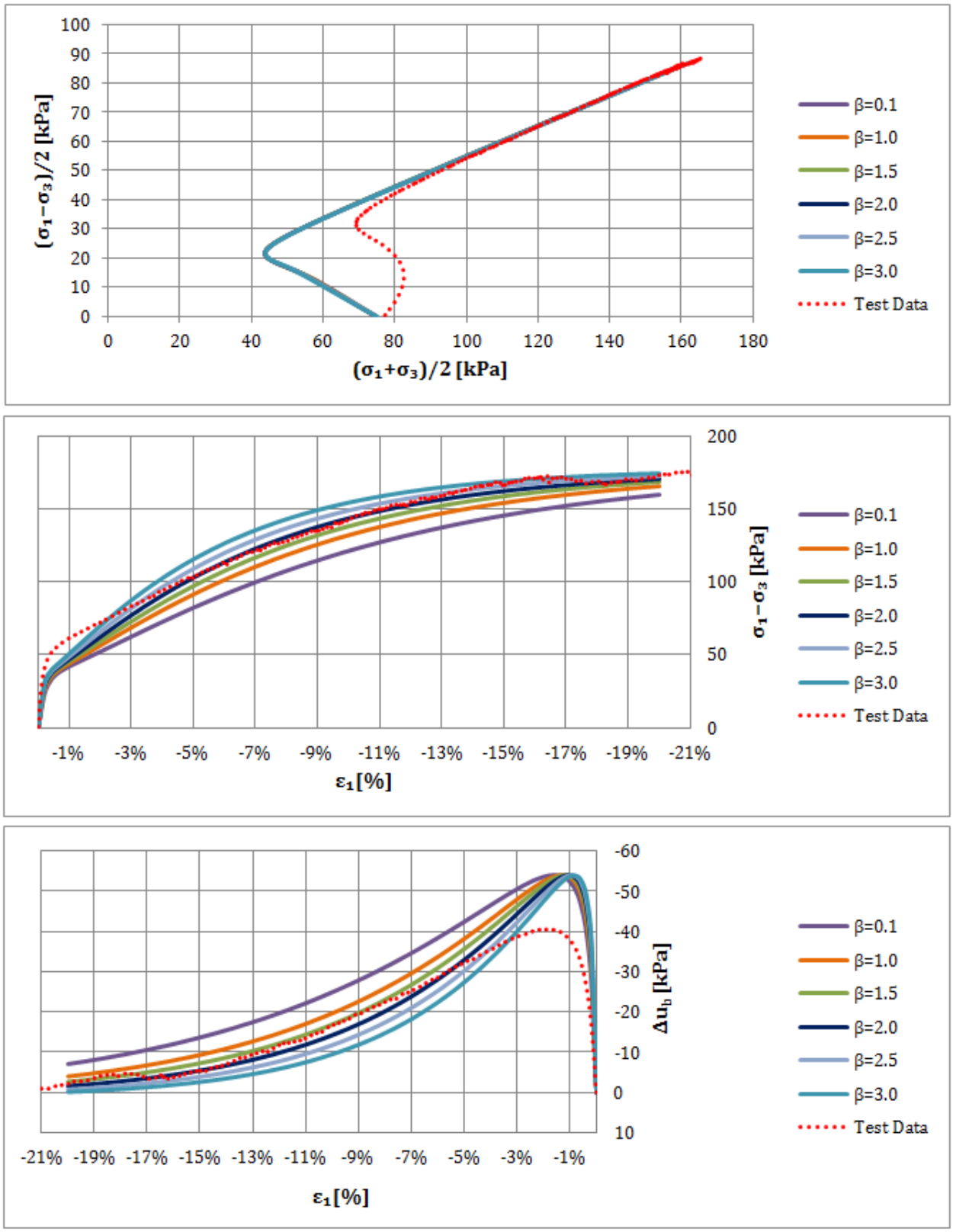

Figure E.7: Calibration of β ($I_D = 50\%$)

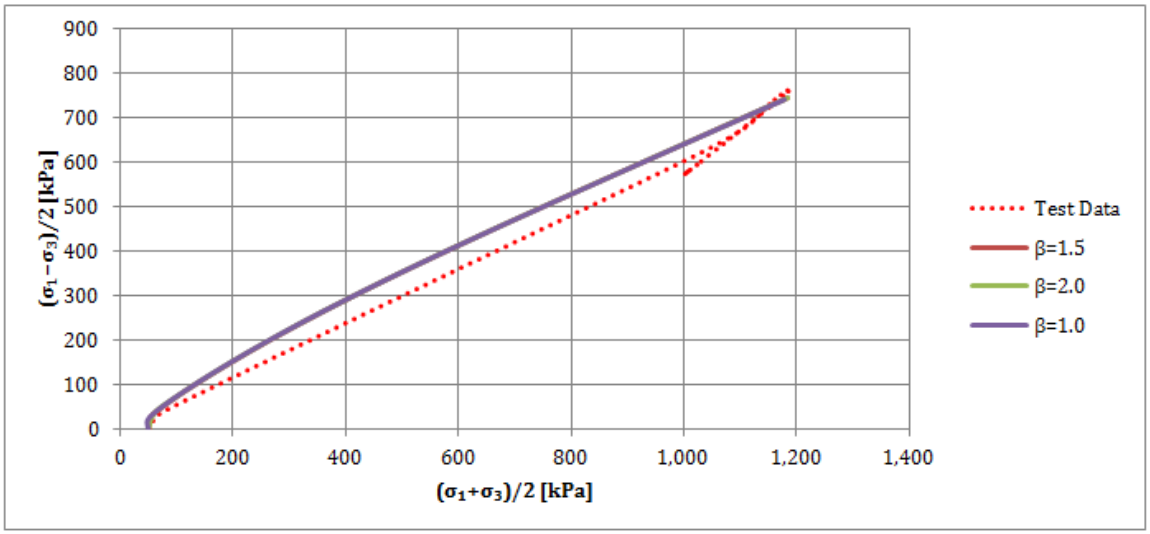

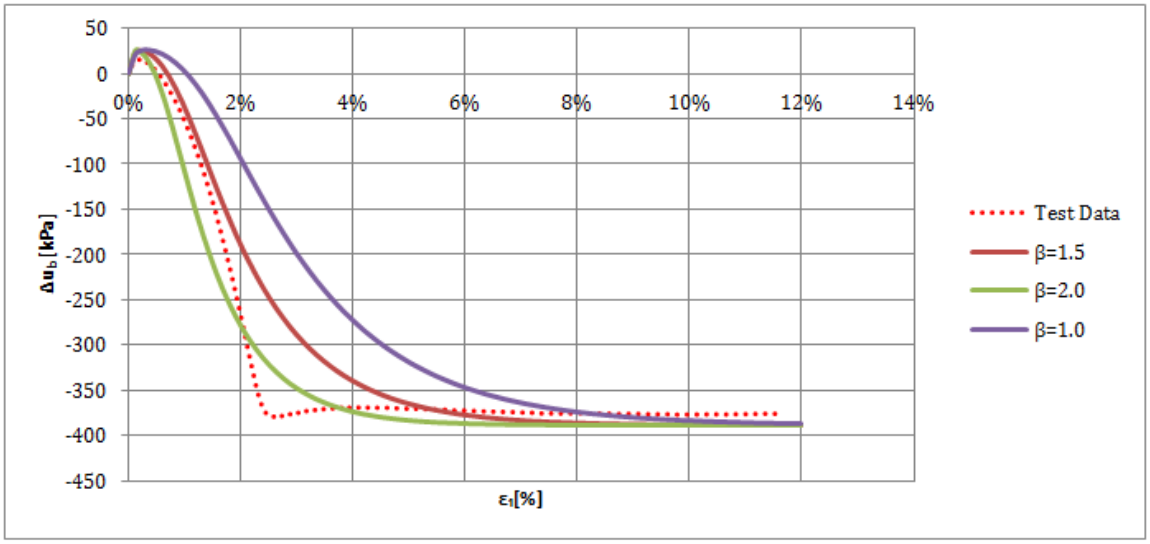

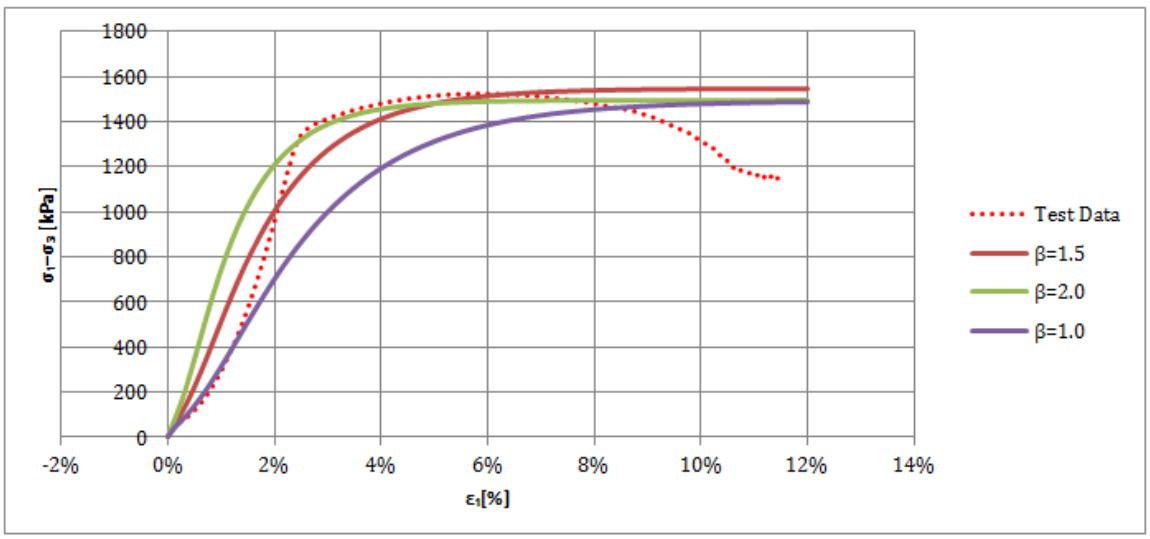

Figure E.8: Calibration of β ($I_D = 80\%$)

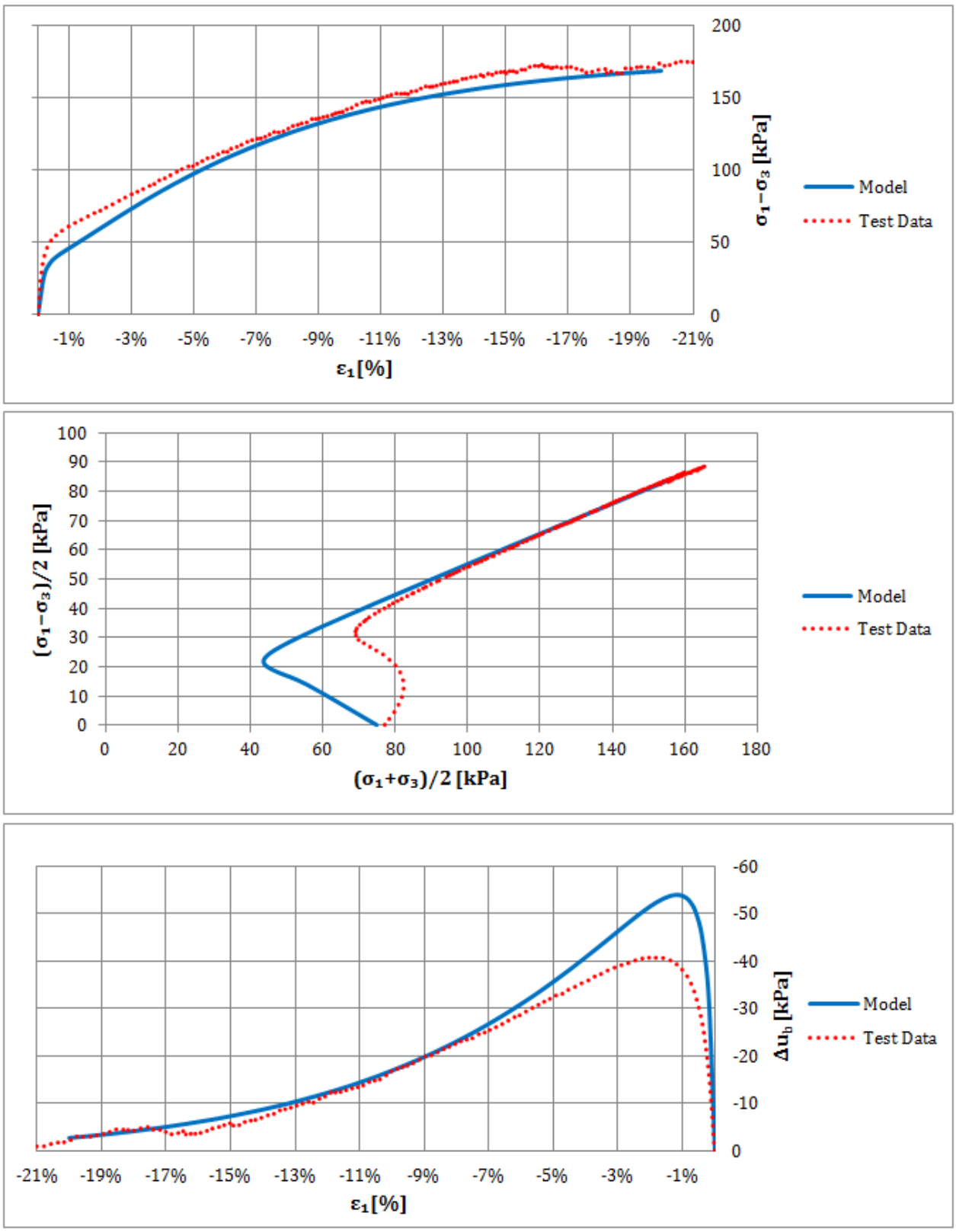

Figure E.9: Outcome of the calibration of the hypoplastic sand model parameters ($I_D = 50\%$)

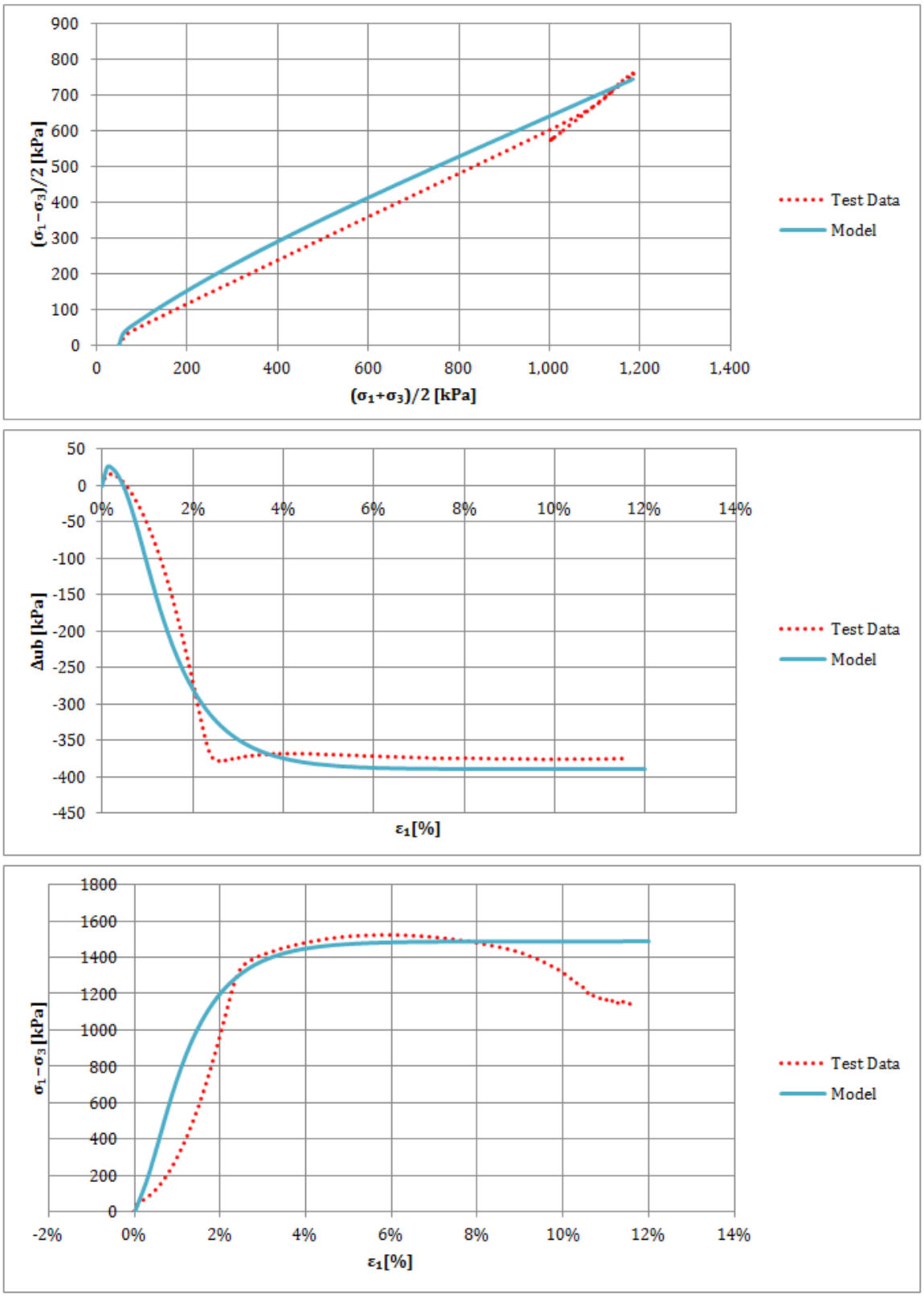

Figure E.10: Outcome of the calibration of the hypoplastic sand model parameters ($I_D = 80\%$)

E.2 CALIBRATION OF THE INTERGRANULAR STRAIN CONCEPT PARAMETERS

E.2.1 FROM CYCLIC DIRECT SIMPLE SHEAR TESTS

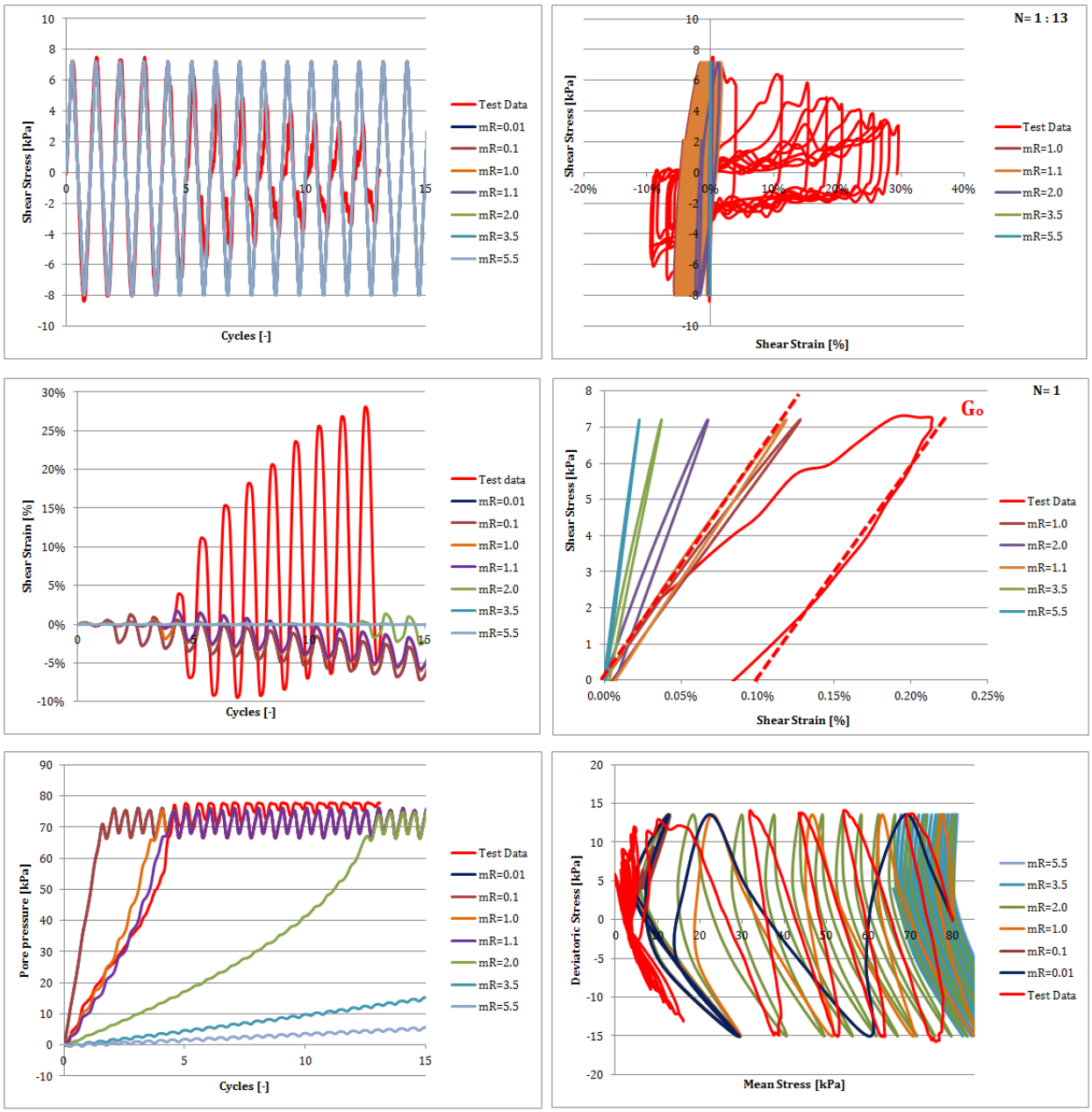

Figure E.11: Calibration of m_R ($I_D = 50\%$, $CSSR = 0.10$)

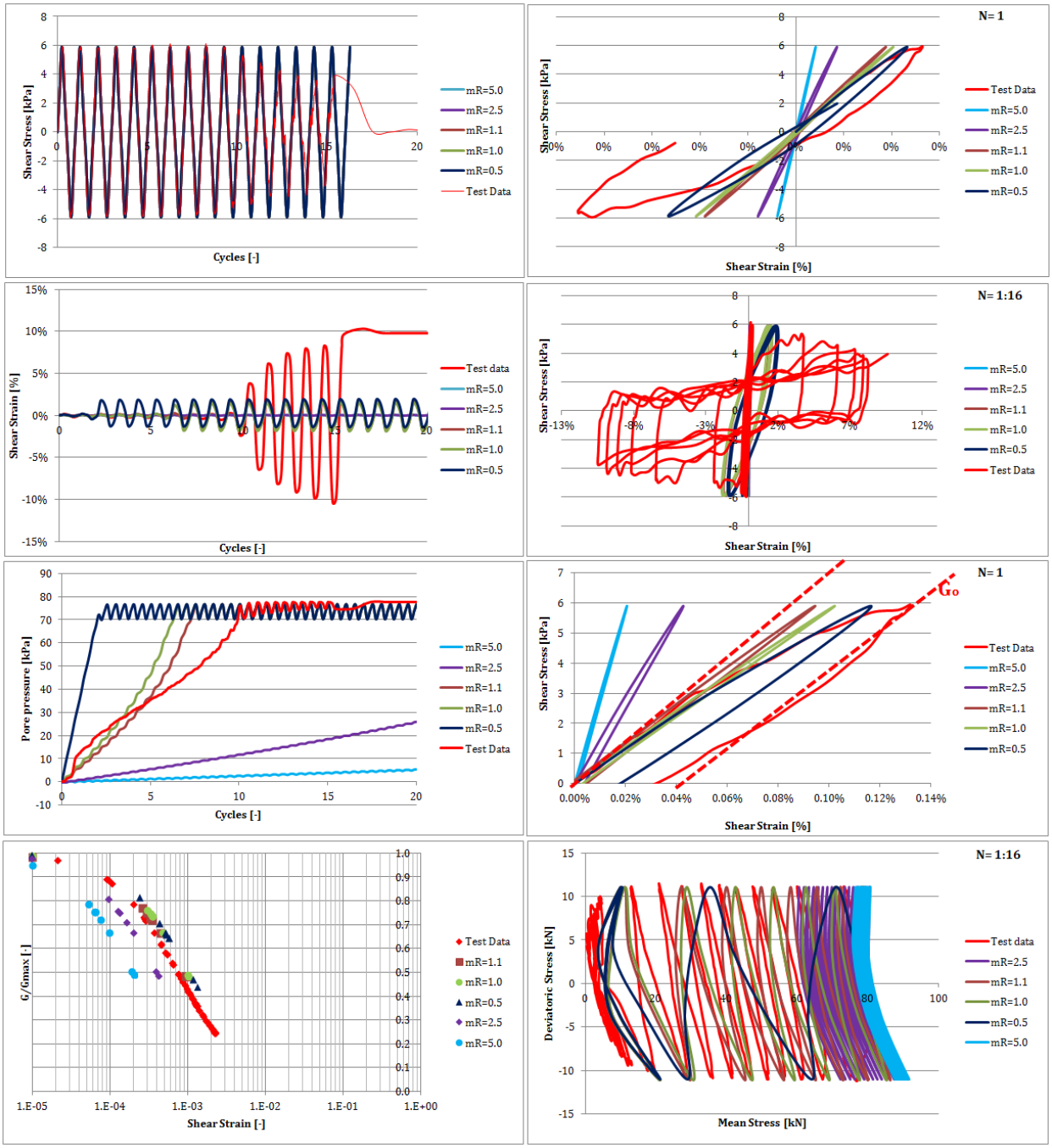

Figure E.12: Calibration of m_R ($I_D = 50\%$, $CSSR = 0.075$)

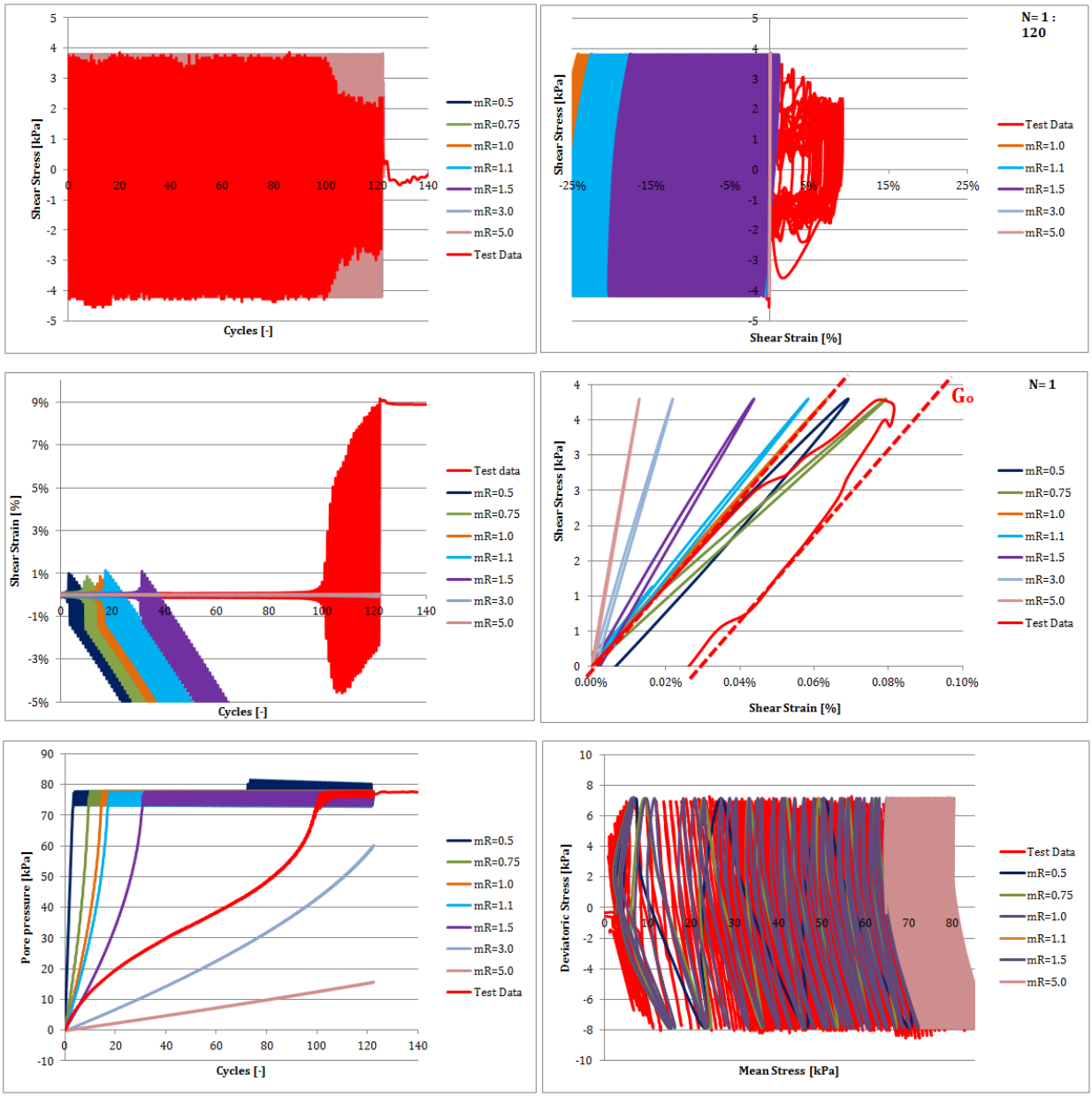

Figure E.13: Calibration of m_R ($I_D = 50\%$, $CSSR = 0.05$)

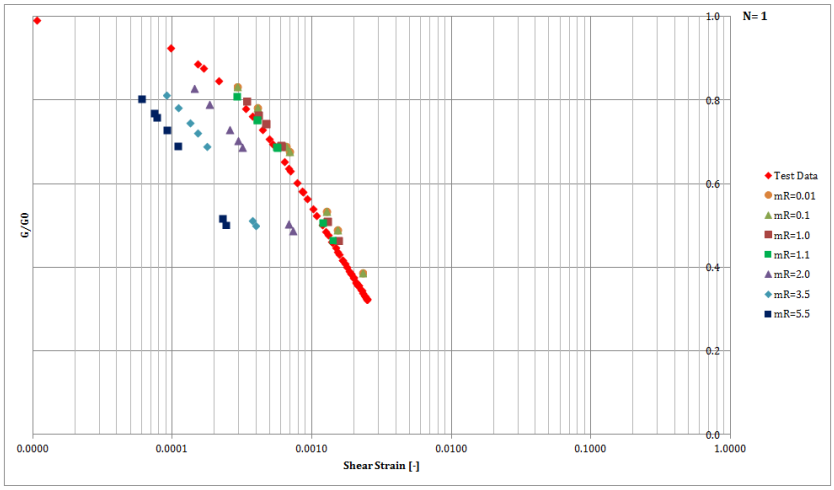

Figure E.14: Calibration of m_R ($I_D = 50\%$, $CSSR = 0.10$)

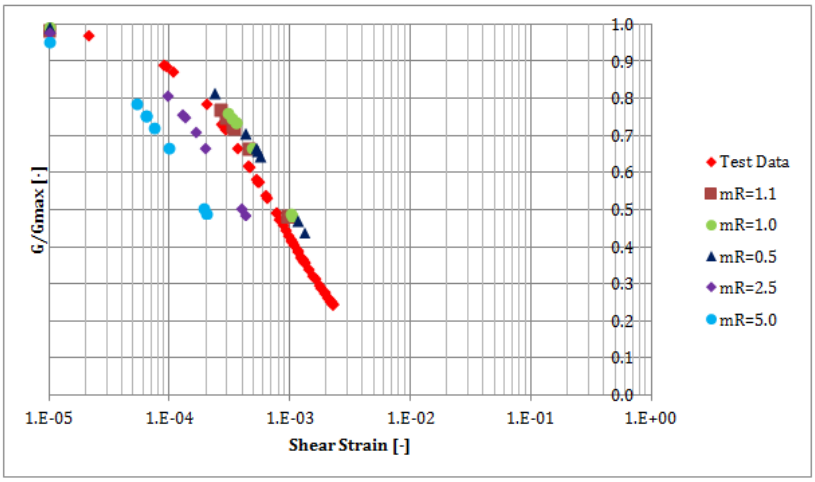

Figure E.15: Calibration of m_R ($I_D = 50\%$, $CSSR = 0.075$)

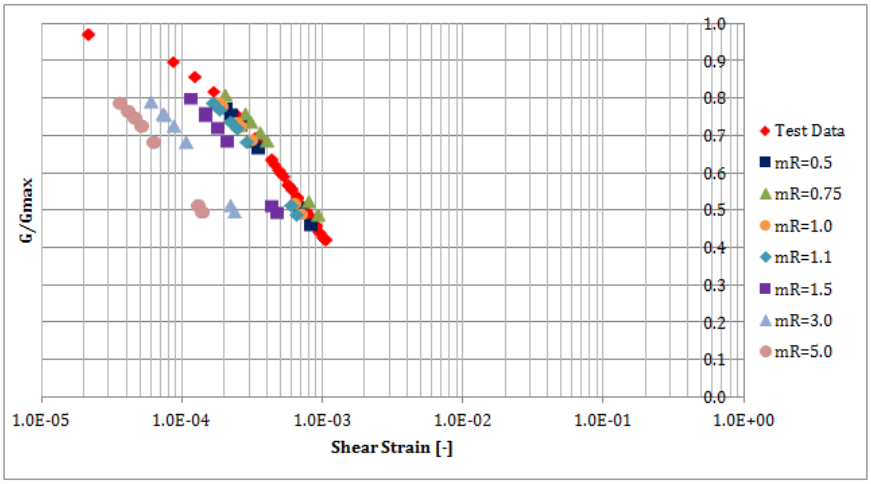

Figure E.16: Calibration of m_R ($I_D = 50\%$, $CSSR = 0.05$)

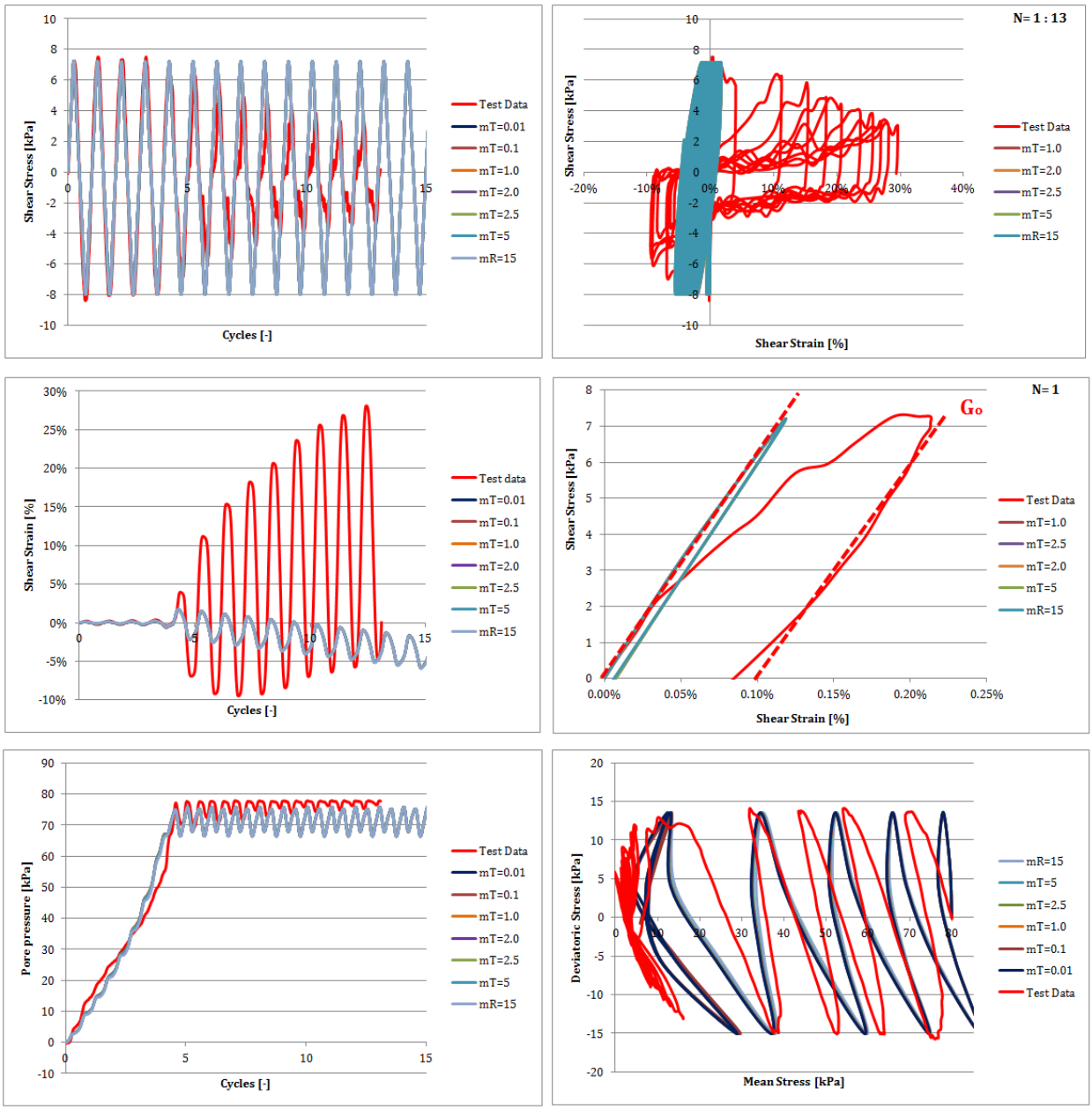

Figure E.17: Calibration of m_T ($I_D = 50\%$, $CSSR = 0.10$)

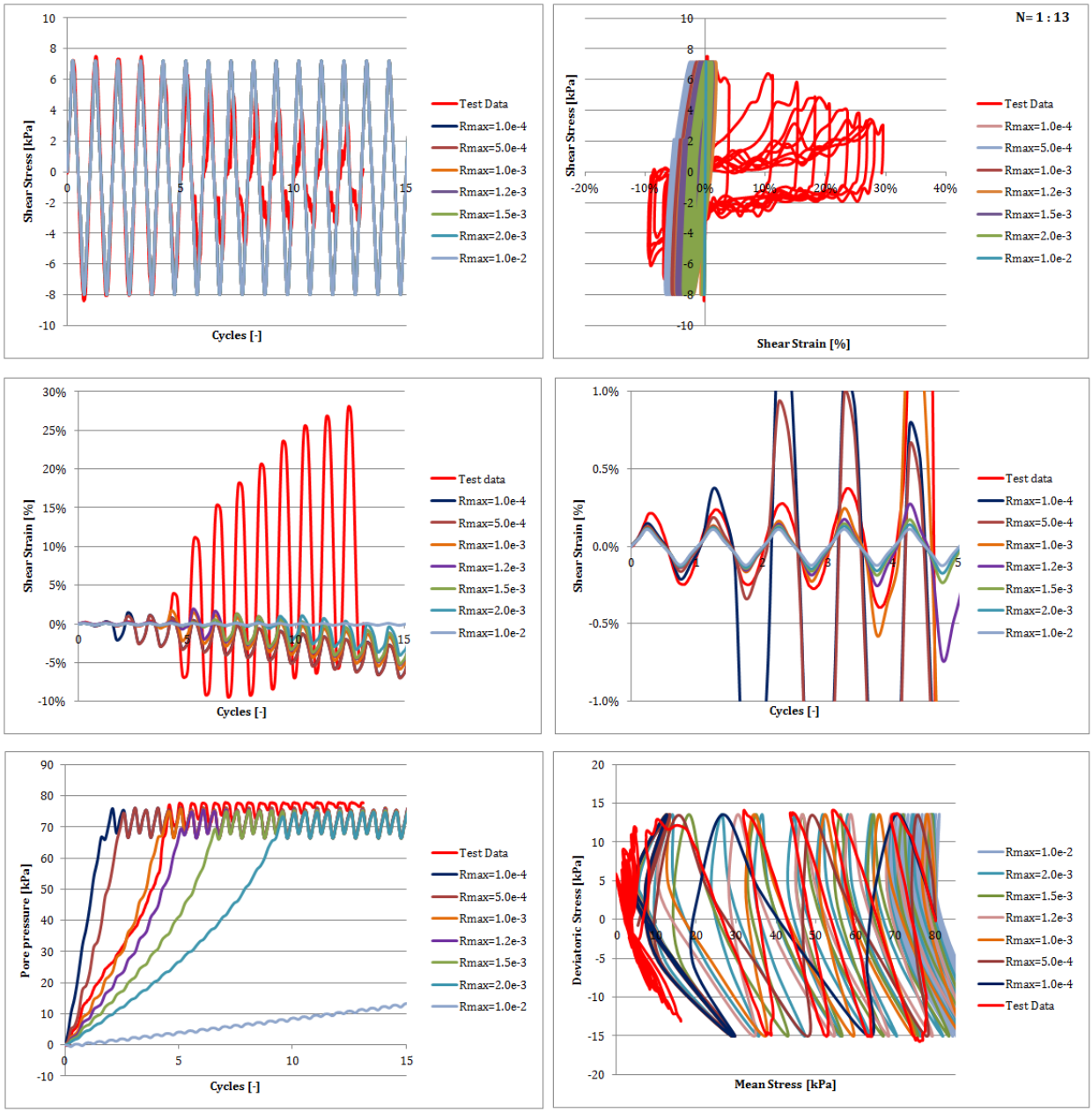

Figure E.18: Calibration of R_{max} ($I_D = 50\%$, $CSSR = 0.10$)

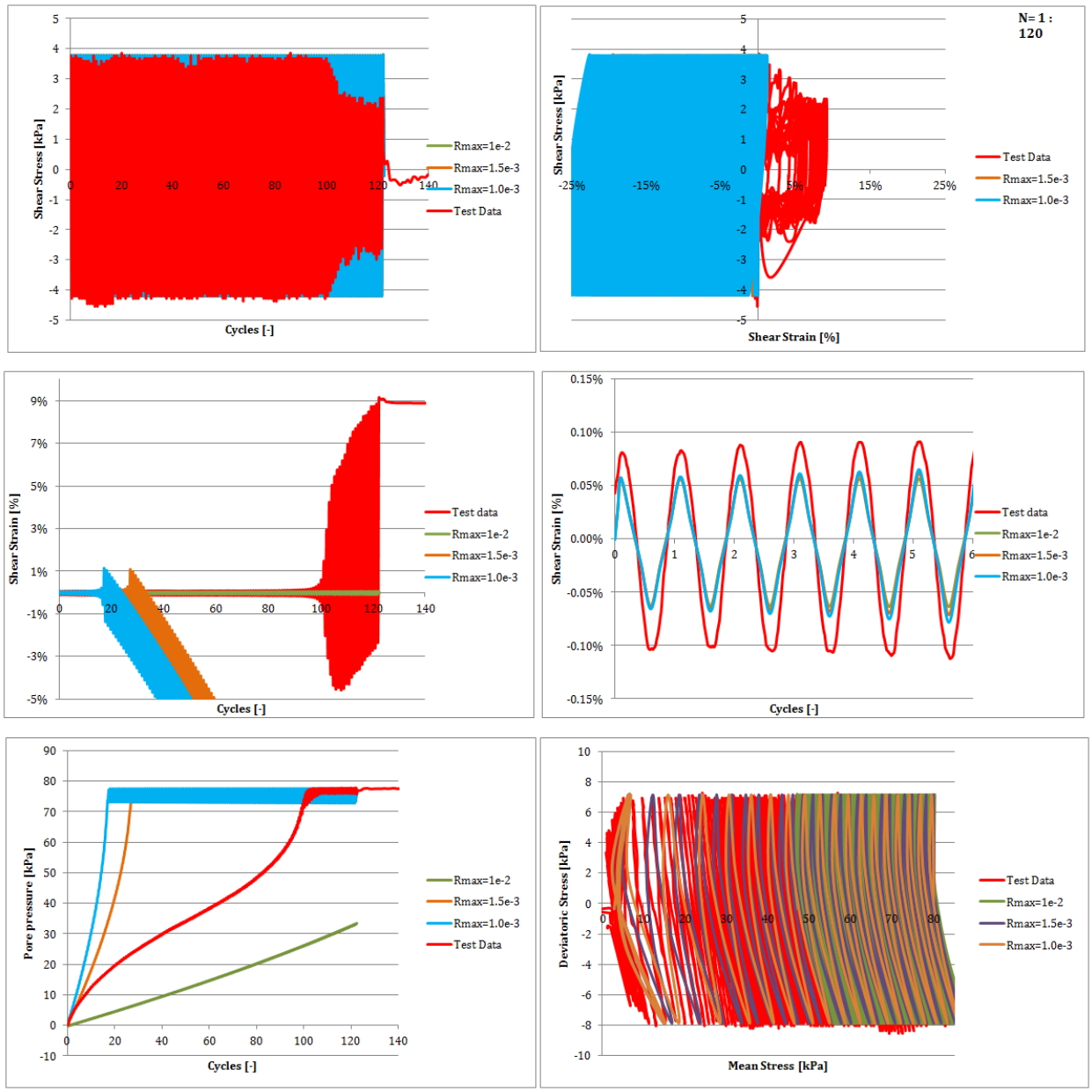

Figure E.19: Calibration of R_{max} ($I_D = 50\%$, $CSSR = 0.05$)

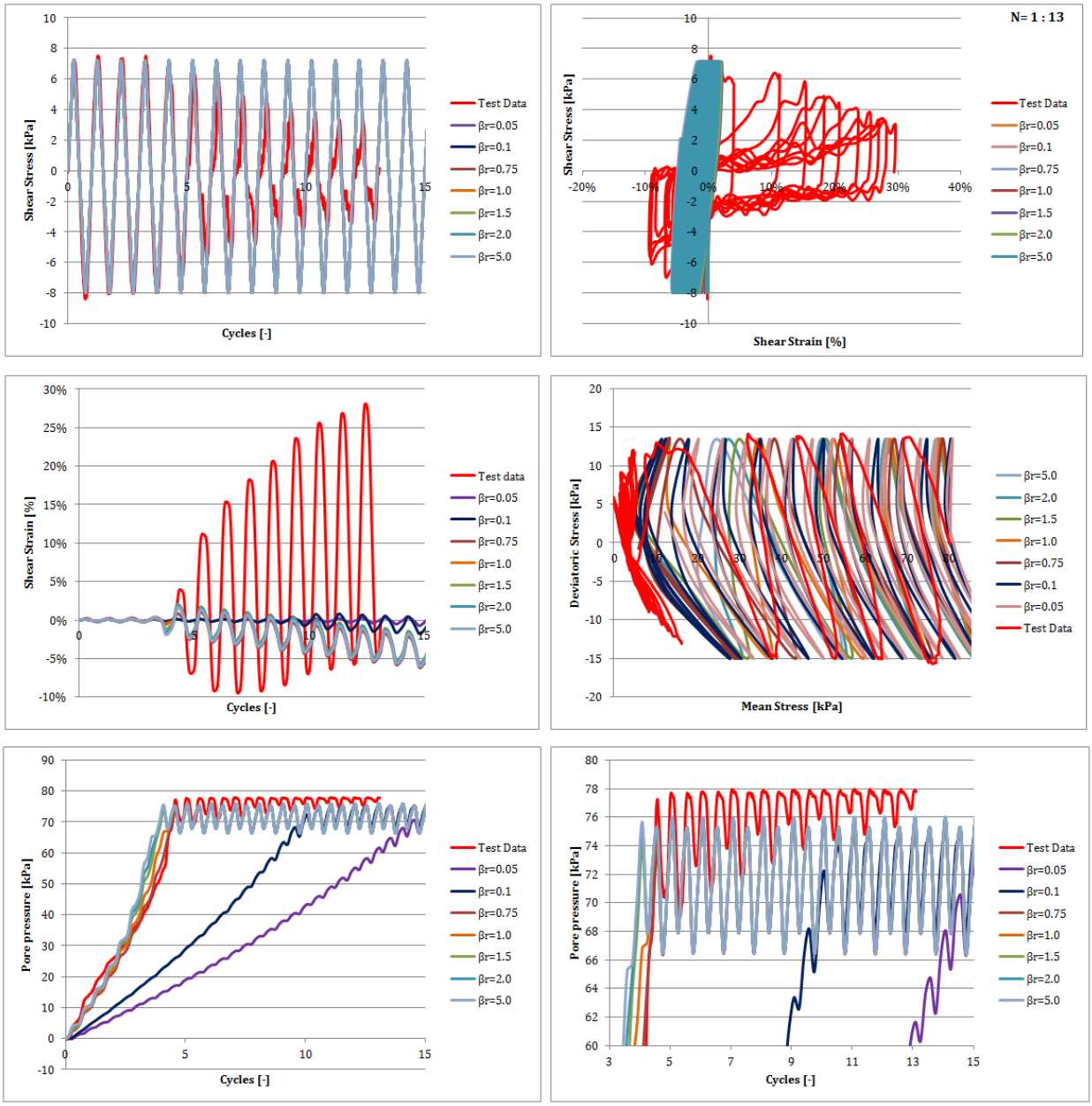

Figure E.20: Calibration of β_r ($I_D = 50\%$, $CSSR = 0.10$)

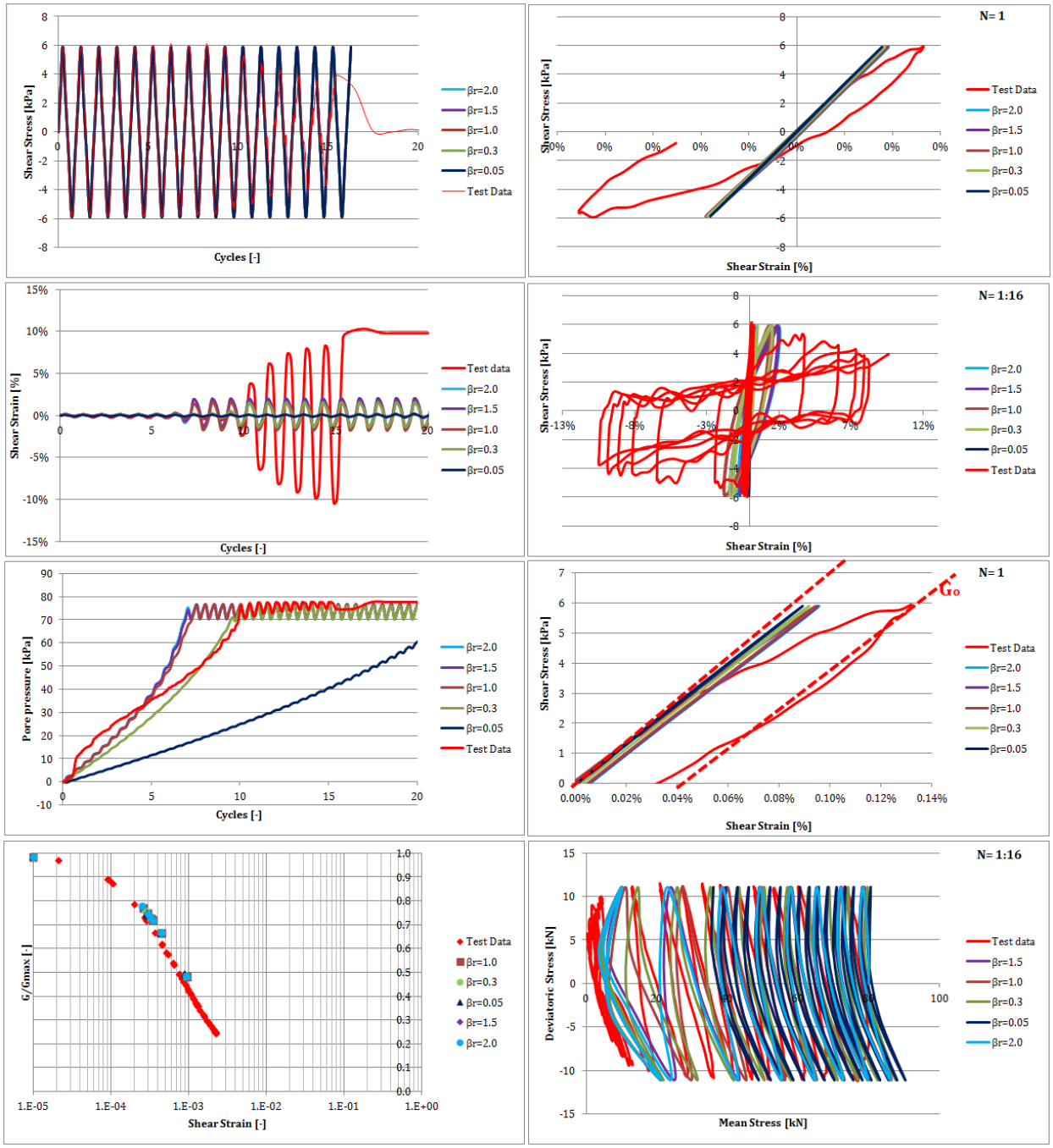

Figure E.21: Calibration of β_r ($I_D = 50\%$, $CSSR = 0.075$)

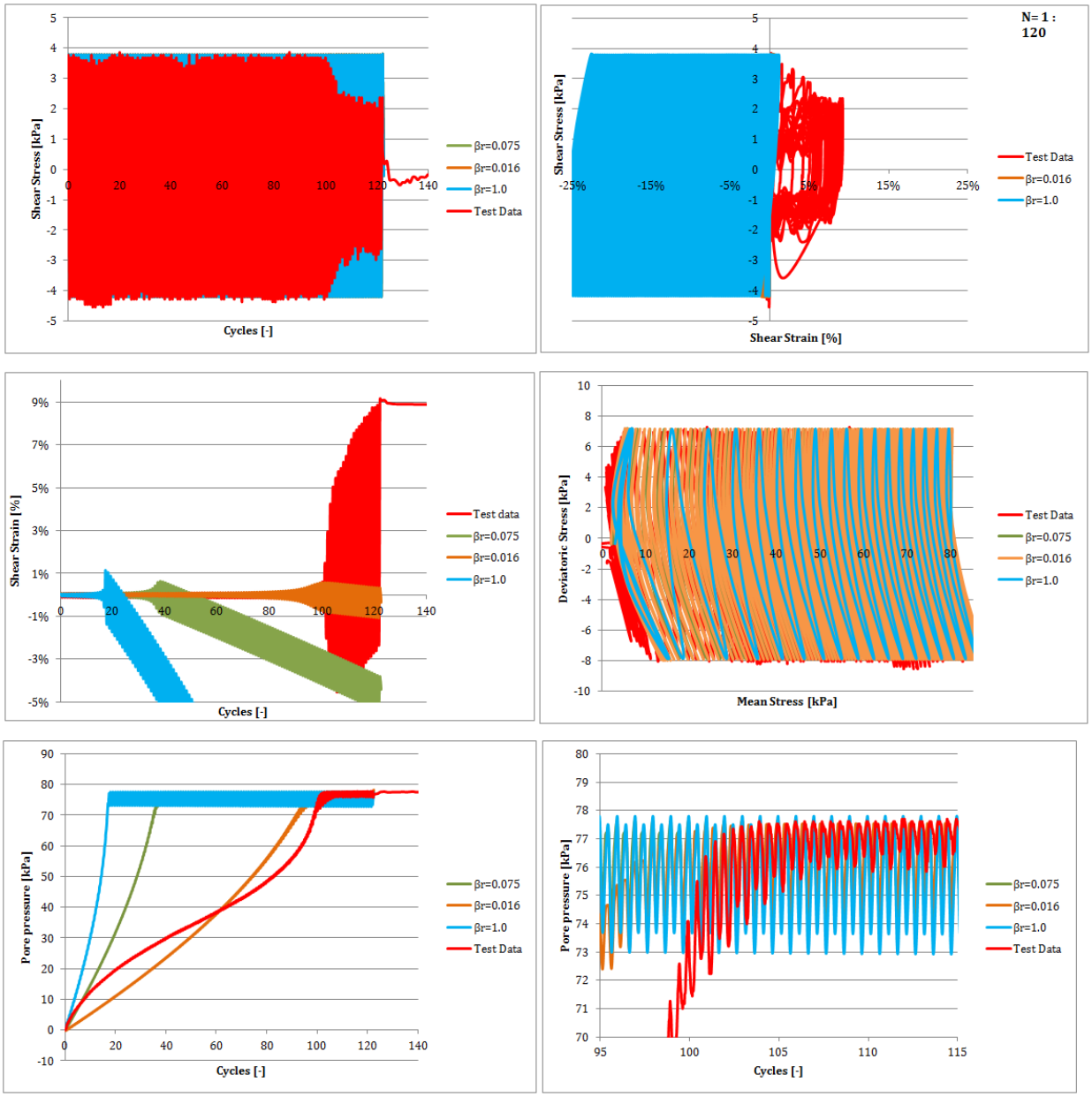

Figure E.22: Calibration of β_r ($I_D = 50\%$, $CSSR = 0.05$)

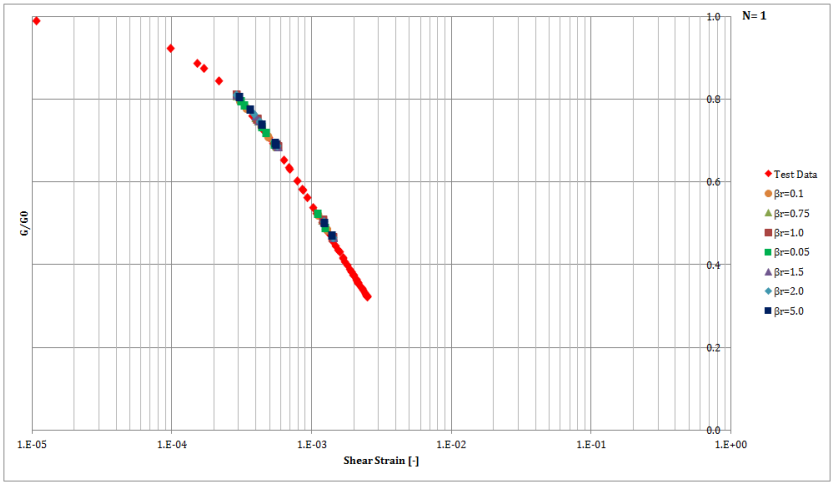

Figure E.23: Calibration of β_r ($I_D = 50\%$, $CSSR = 0.10$)

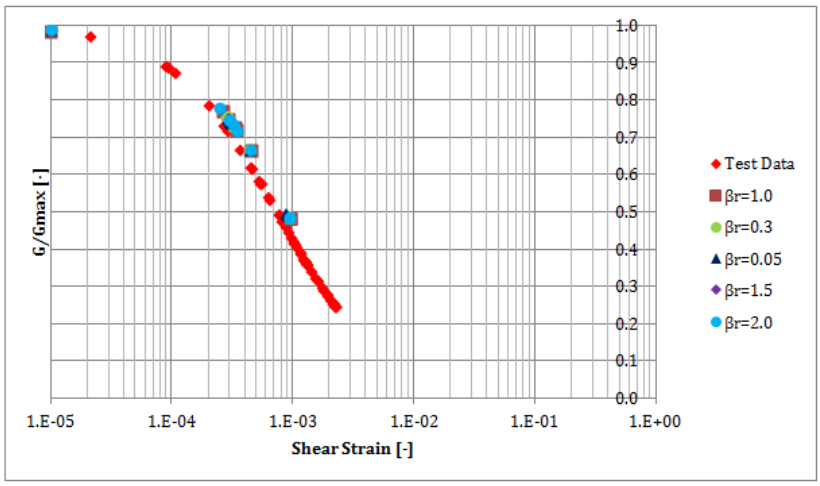

Figure E.24: Calibration of β_r ($I_D = 50\%$, $CSSR = 0.075$)

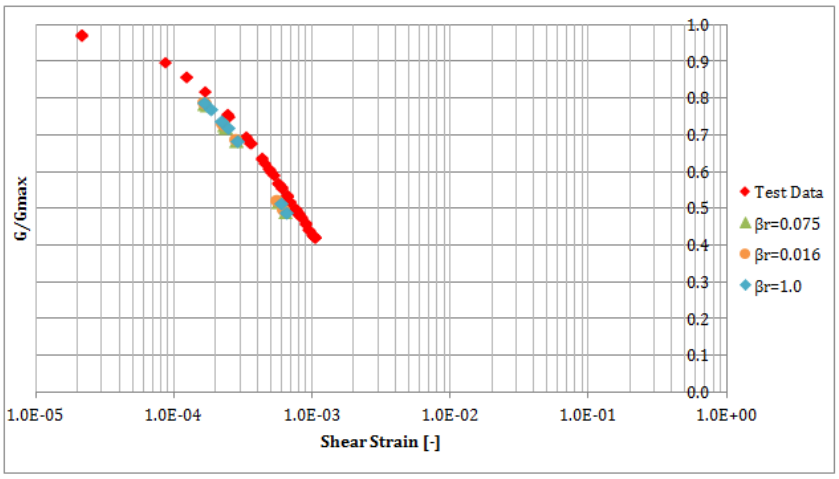

Figure E.25: Calibration of β_r ($I_D = 50\%$, $CSSR = 0.05$)

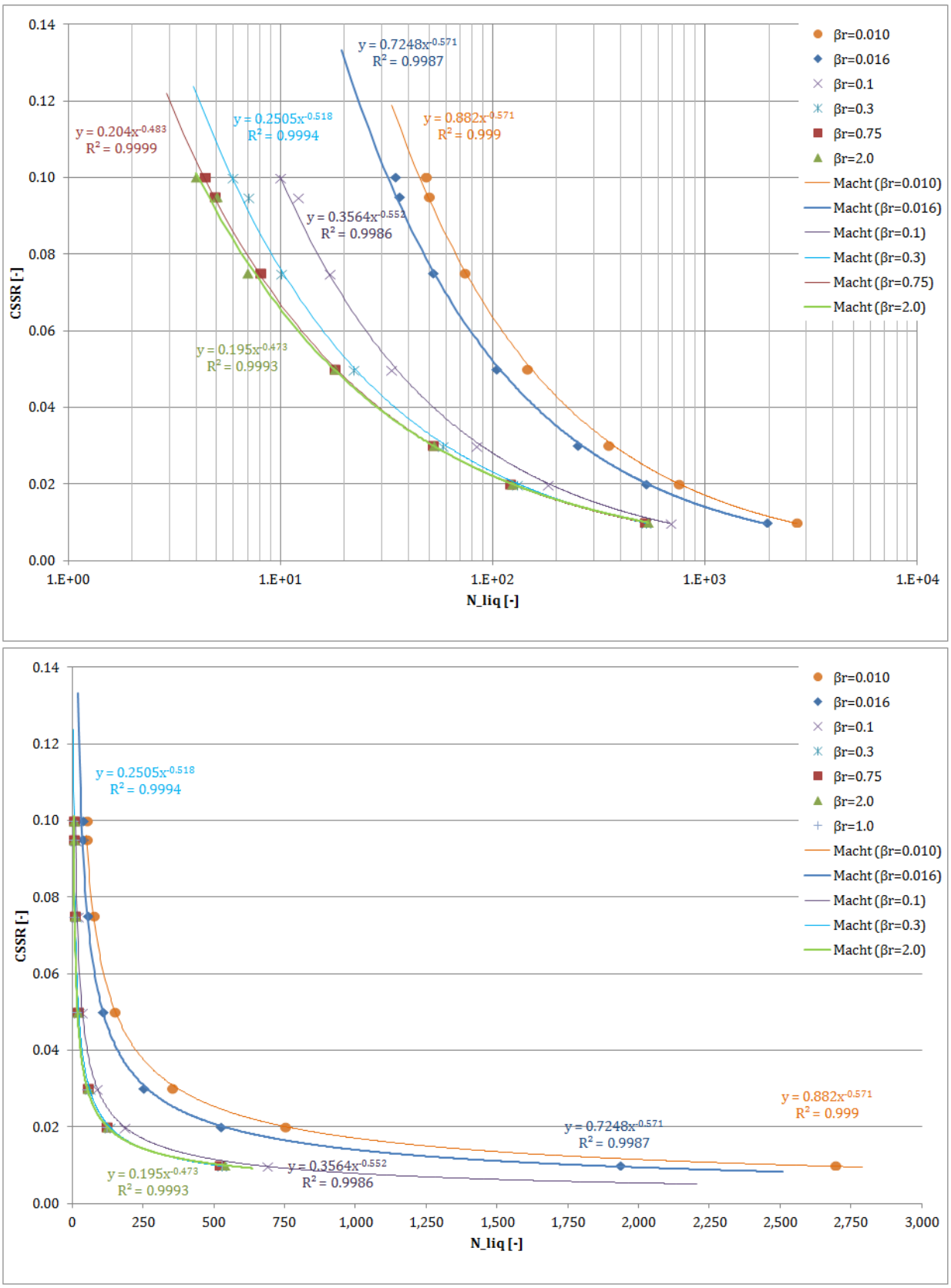

Figure E.26: Impact of β_r on the $CSSR$ and N_{liq} ($I_D = 50\%$)

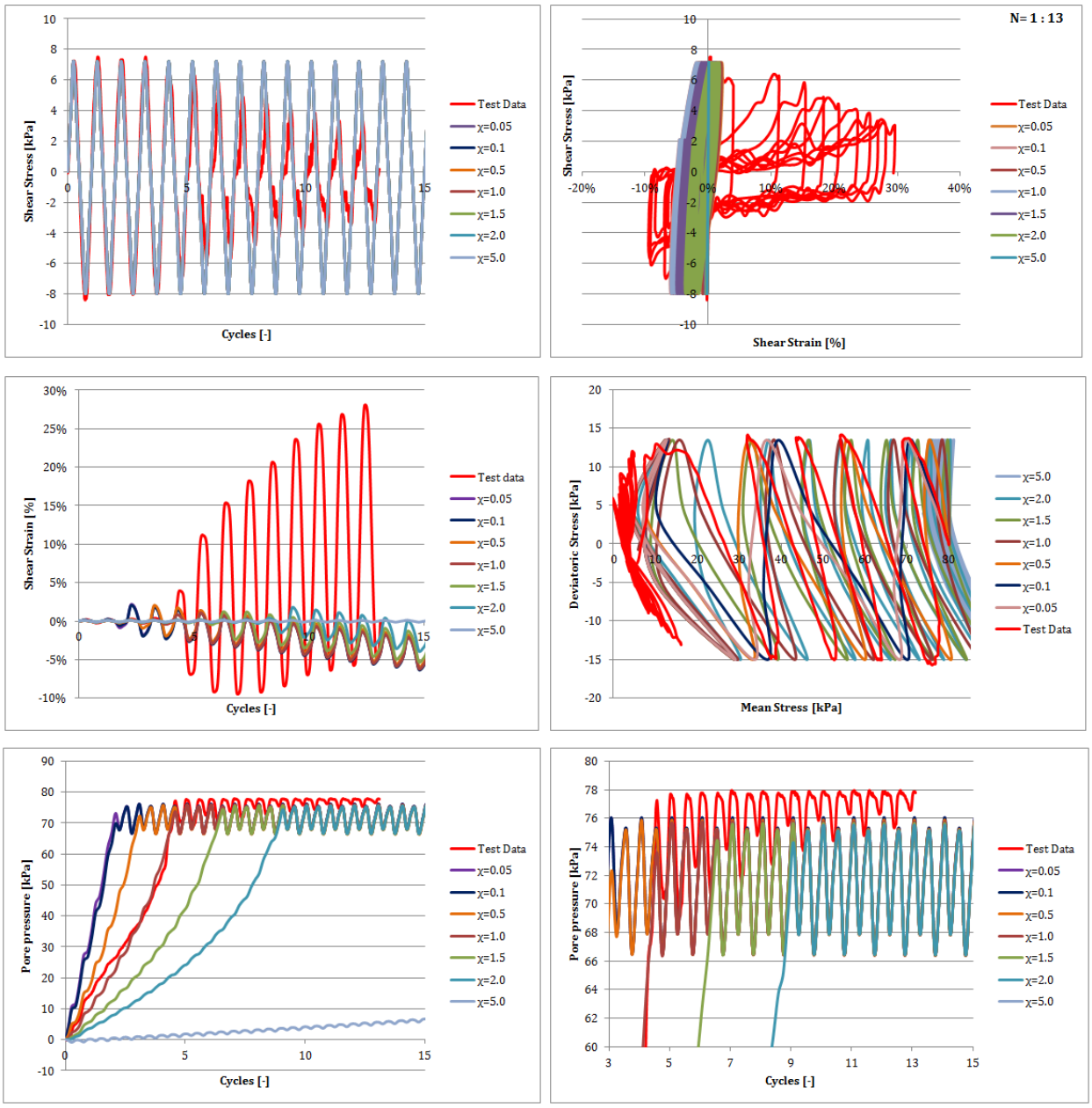

Figure E.27: Calibration of χ ($I_D = 50\%$, $CSSR = 0.10$)

E.2.2 FROM UNDRAINED CYCLIC TRIAXIAL TESTS

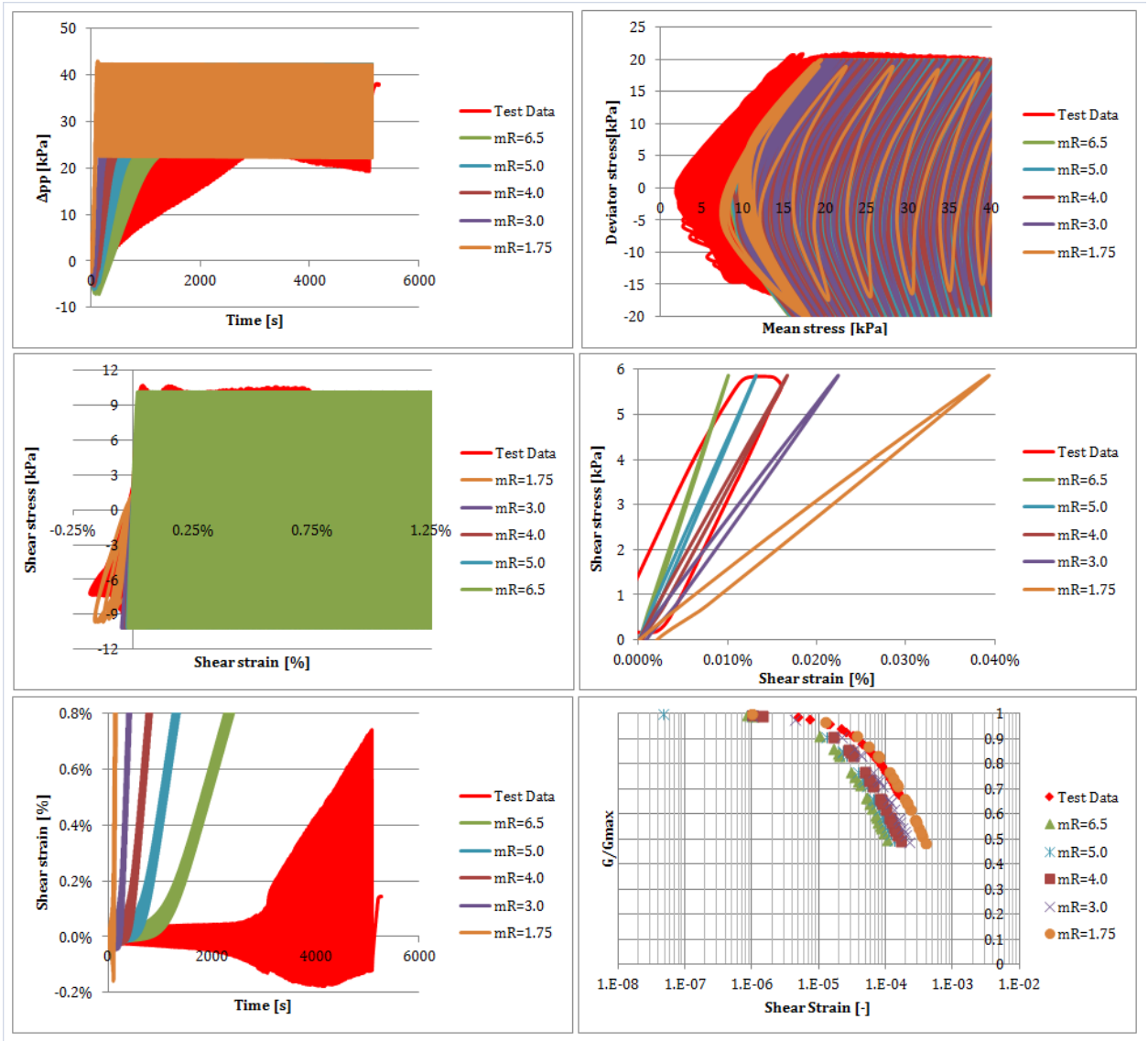

Figure E.28: Calibration of m_R ($I_D = 75\%$, $CSSR = 0.15$)

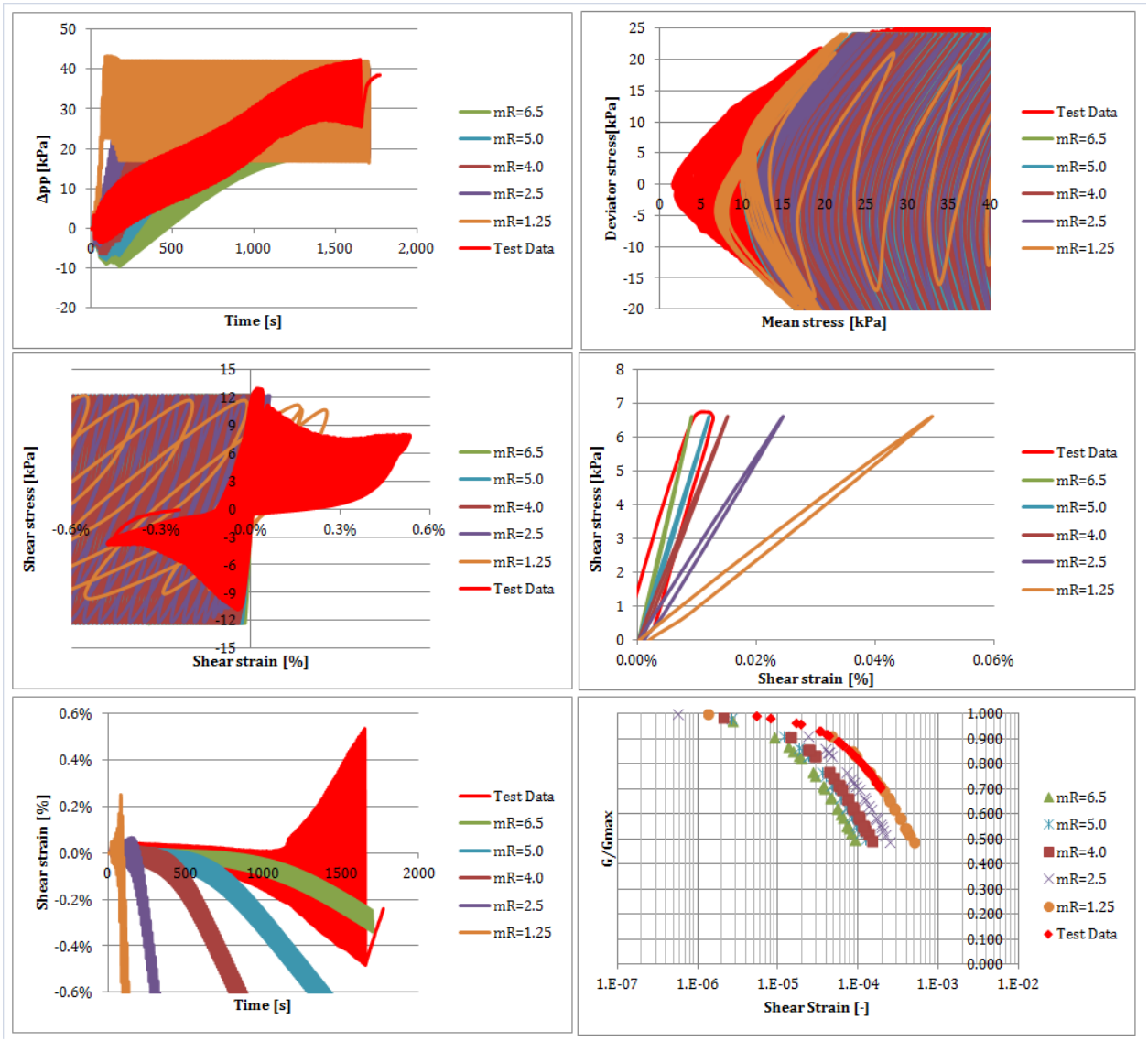

Figure E.29: Calibration of m_R ($I_D = 75\%$, $CSSR = 0.20$)

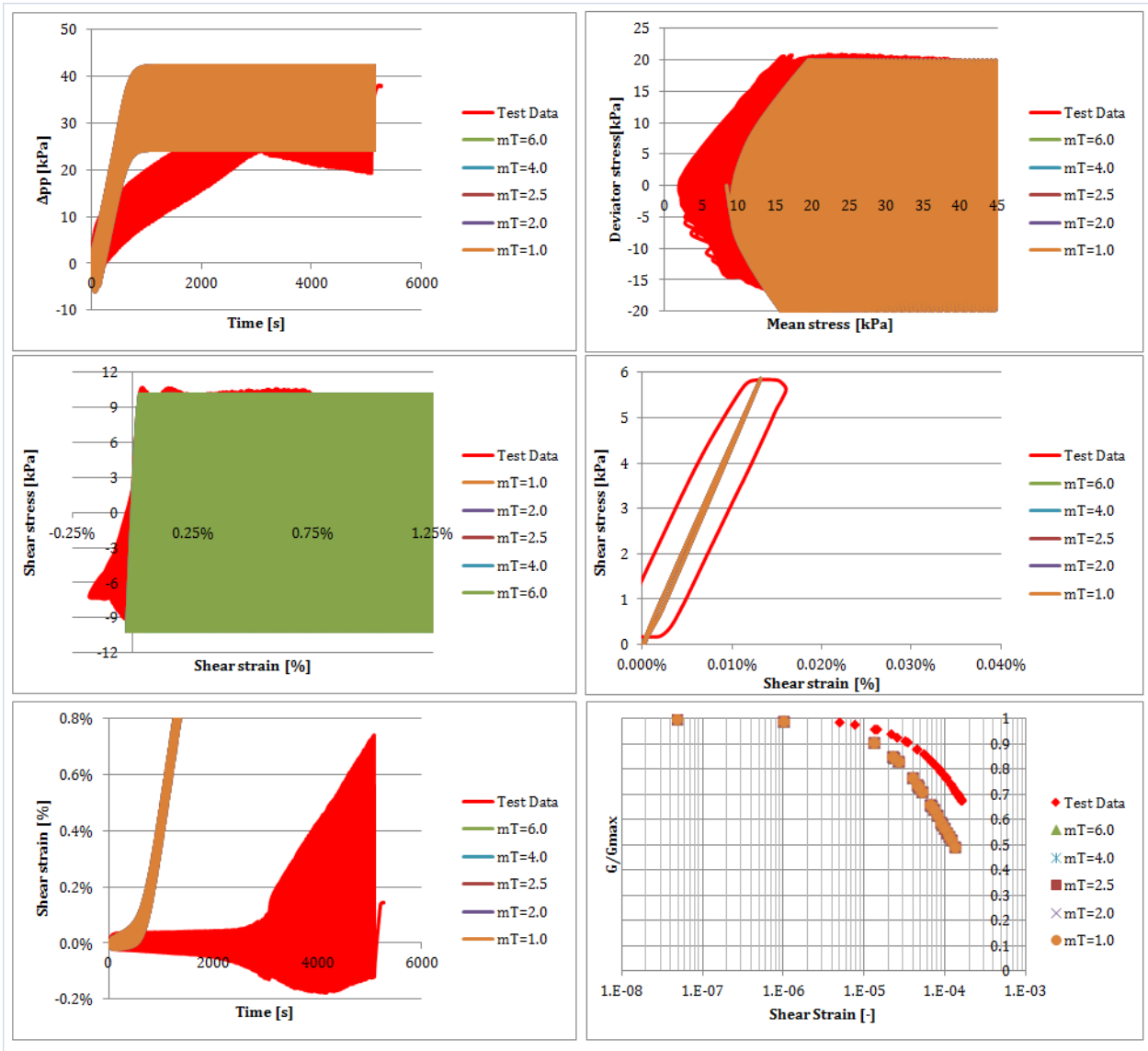

Figure E.30: Calibration of m_T ($I_D = 75\%$, $CSSR = 0.15$)

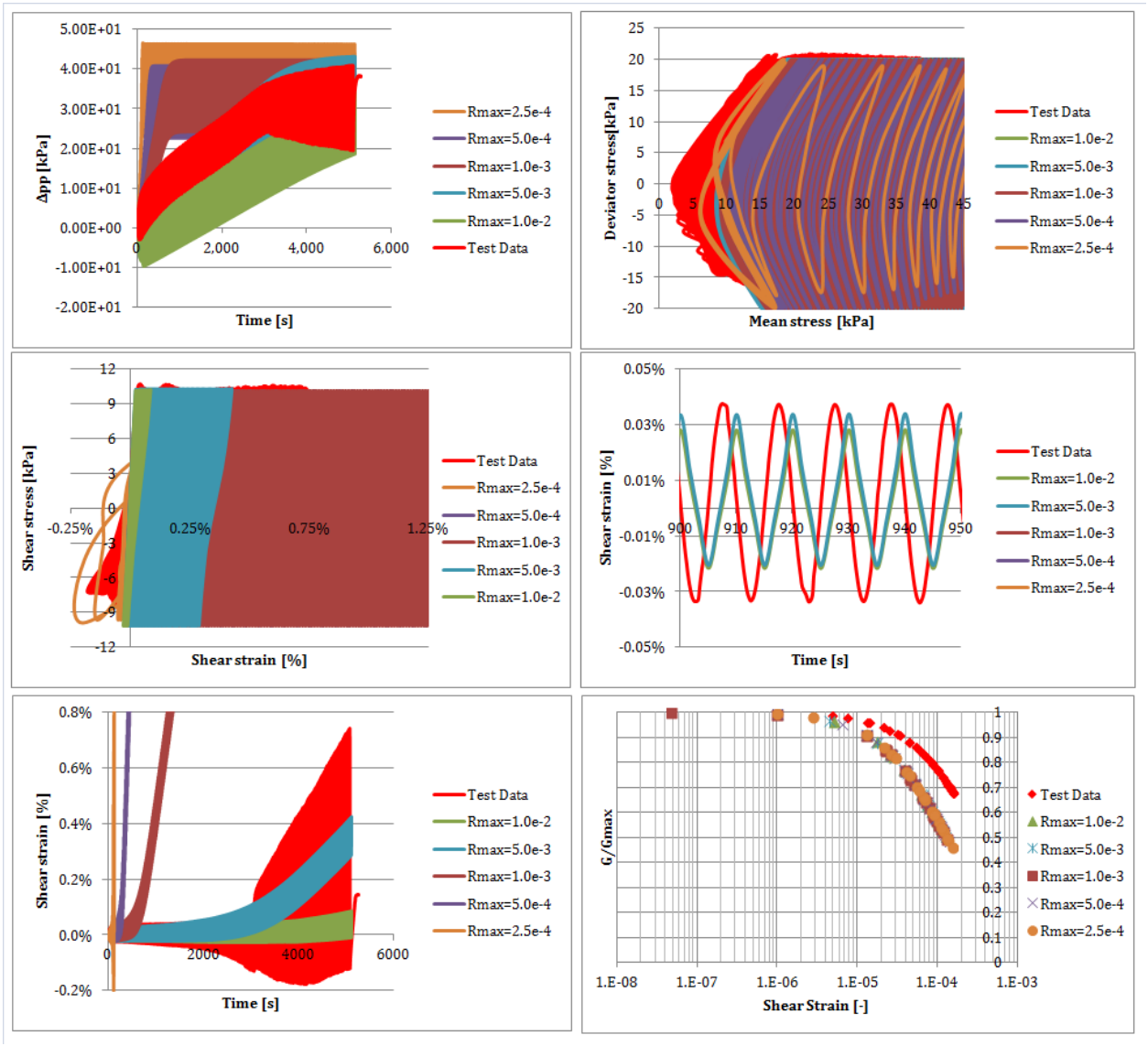

Figure E.31: Calibration of R_{max} ($I_D = 75\%$, $CSSR = 0.15$)

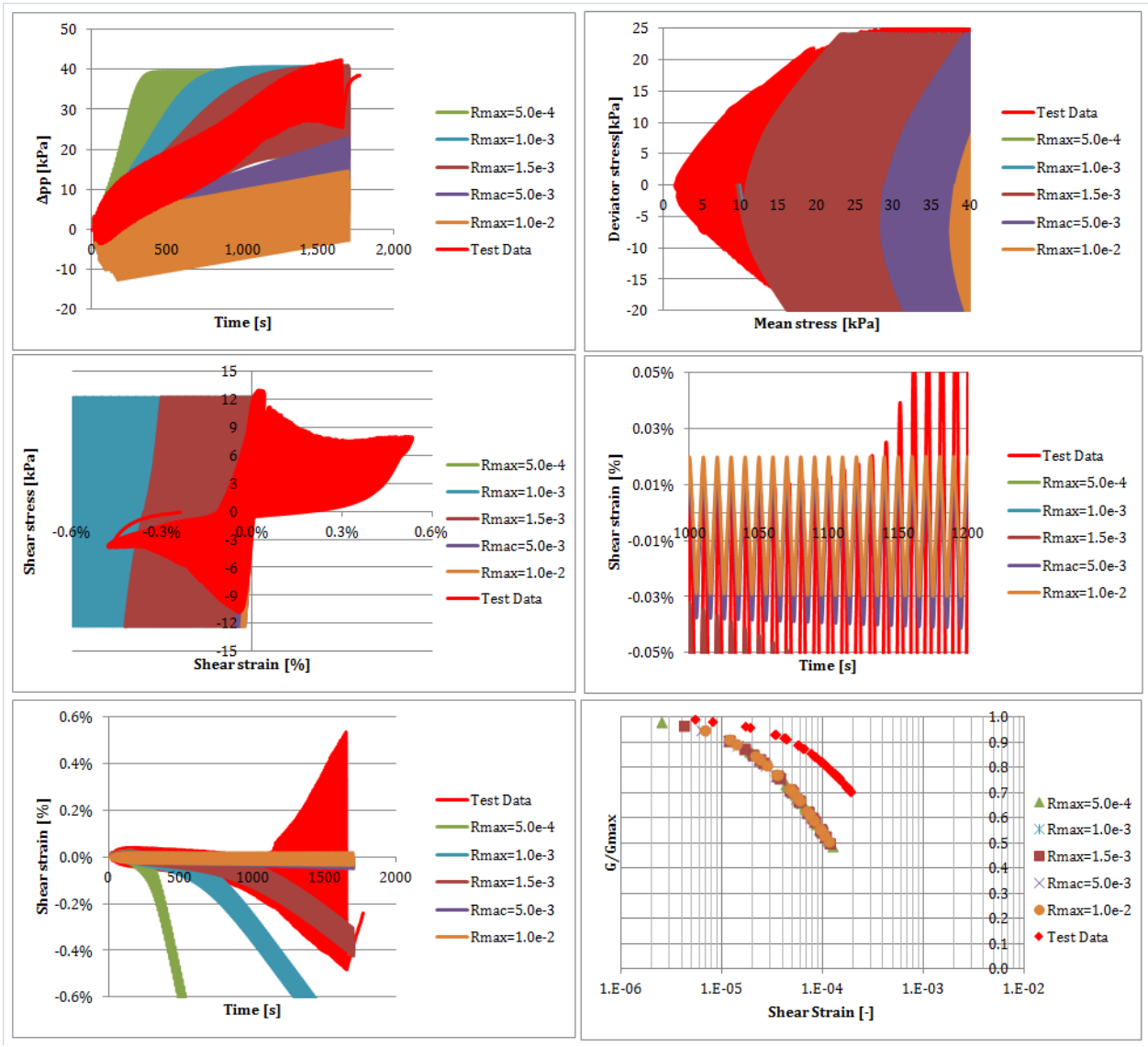

Figure E.32: Calibration of R_{max} ($I_D = 75\%$, $CSSR = 0.20$)

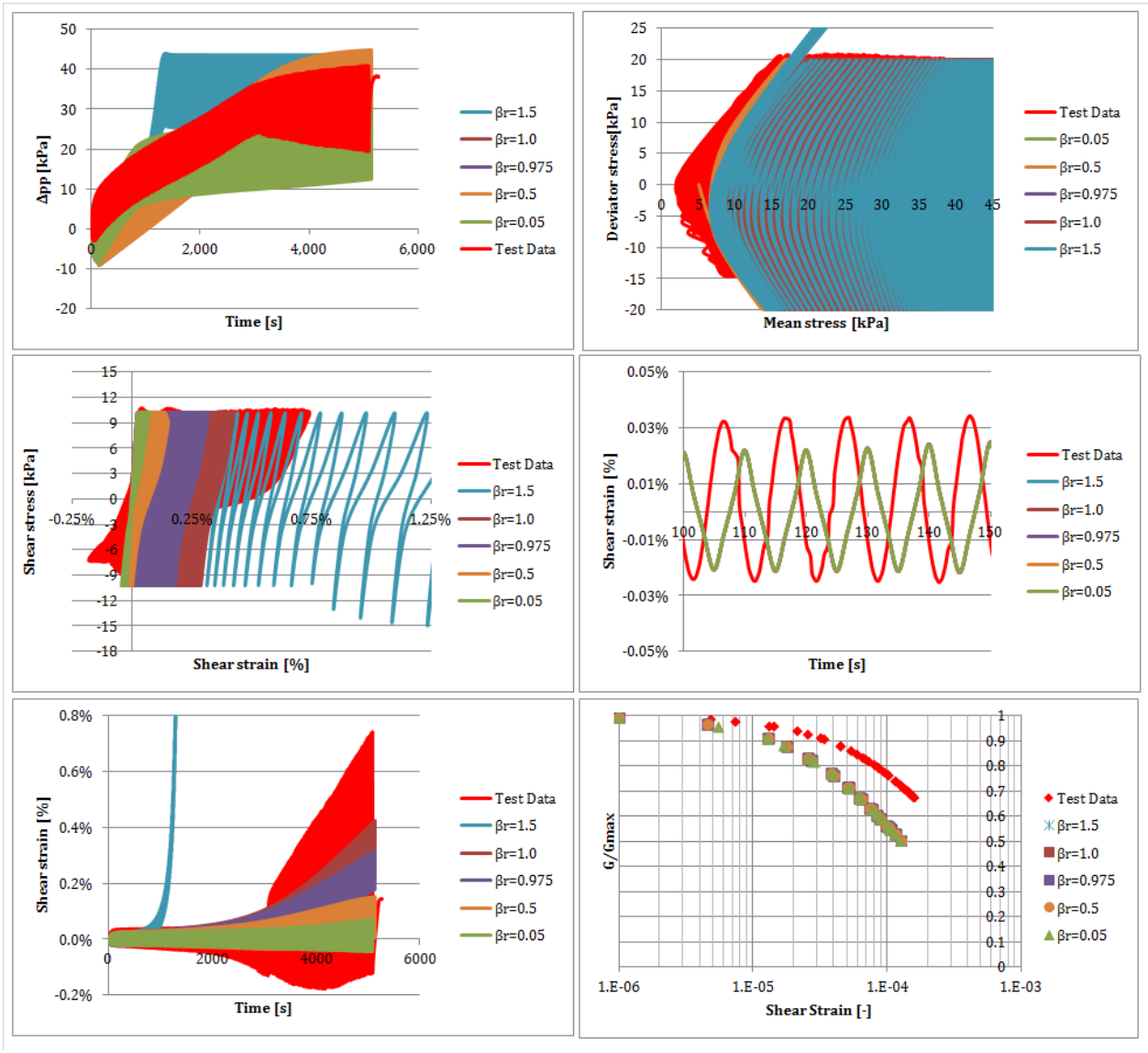

Figure E.33: Calibration of β_r ($I_D = 75\%$, $CSSR = 0.15$)

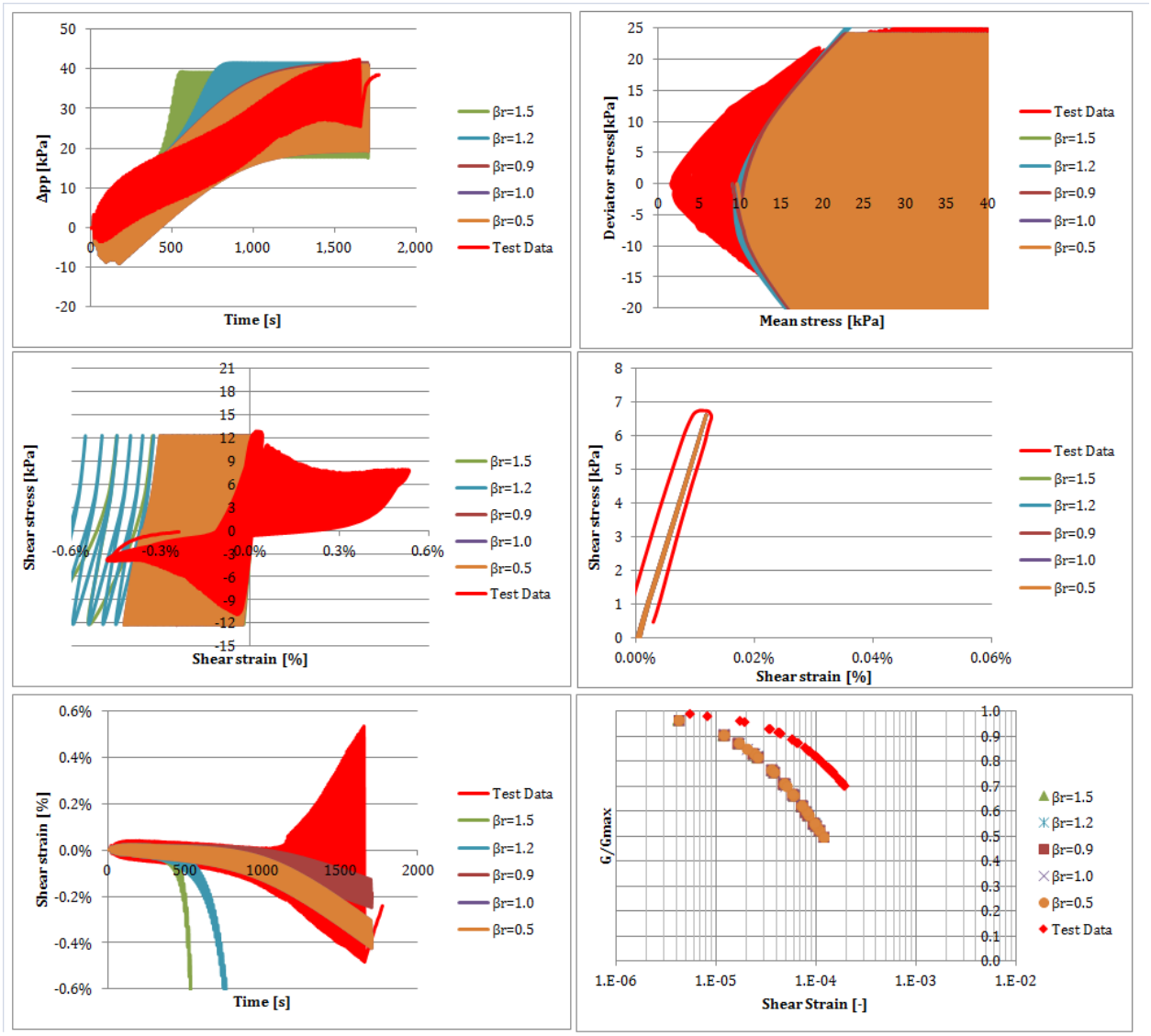

Figure E.34: Calibration of β_r ($I_D = 75\%$, $CSSR = 0.20$)

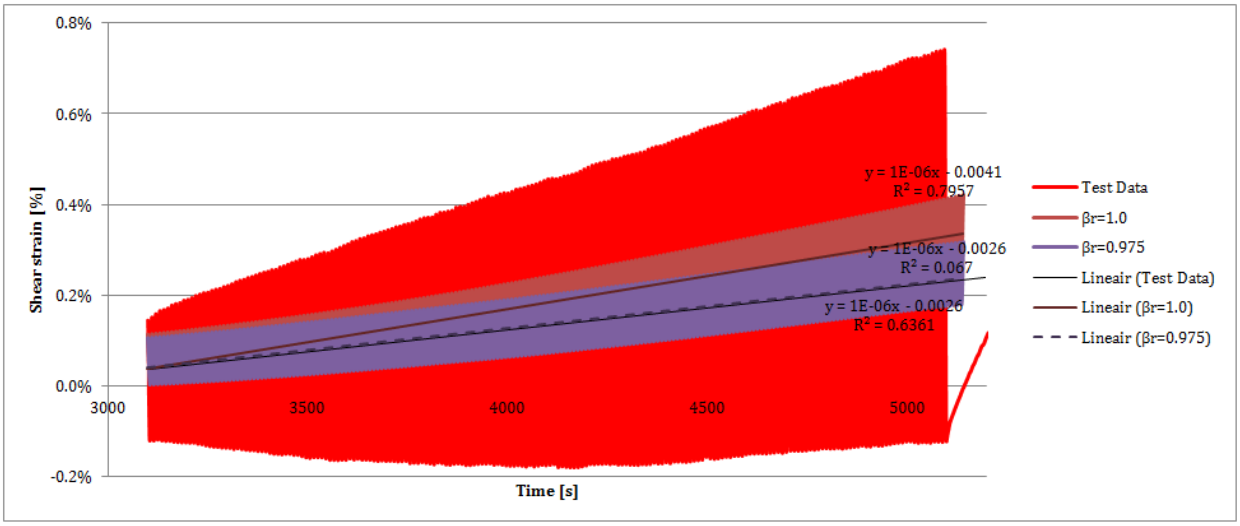

Figure E.35: Calibration of β_r ($I_D = 75\%$, $CSSR = 0.15$)—strain accumulation trends

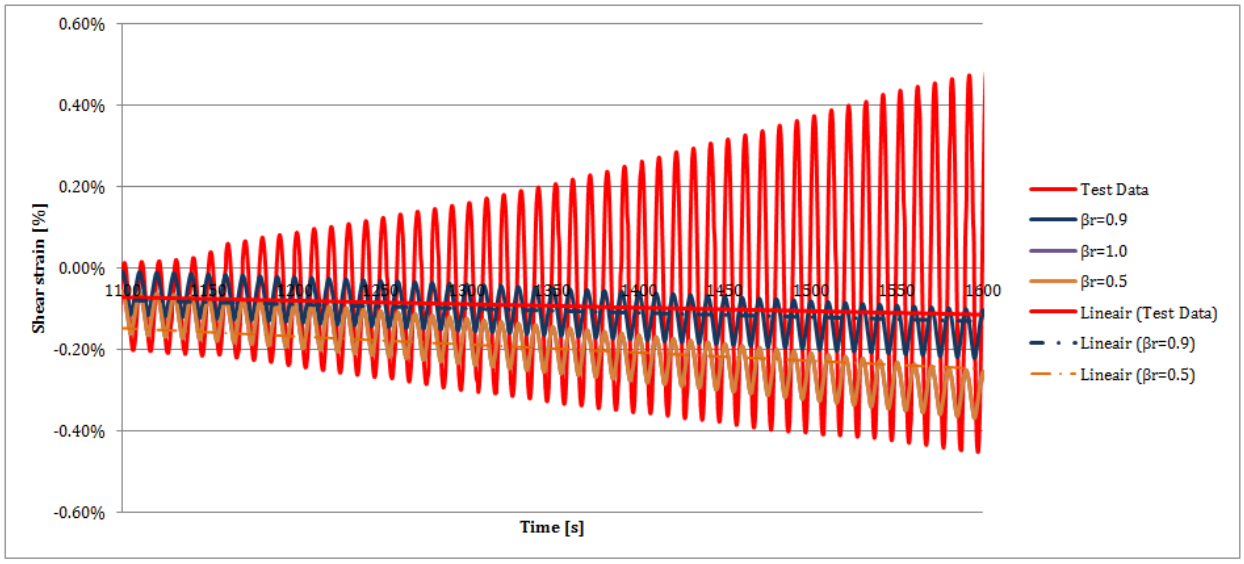

Figure E.36: Calibration of β_r ($I_D = 75\%$, $CSSR = 0.20$)—strain accumulation trends

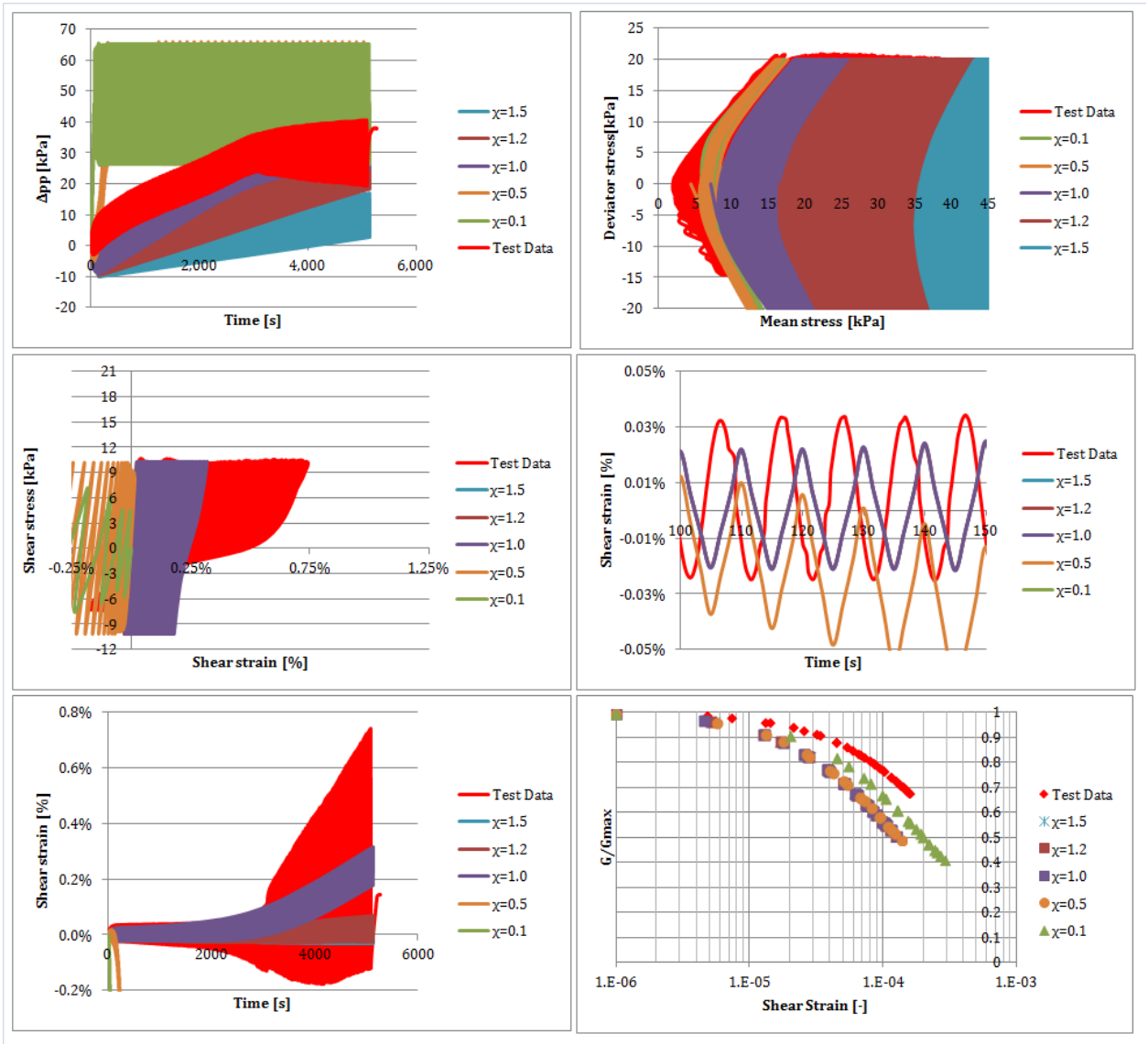

Figure E.37: Calibration of χ ($I_D = 75\%$, $CSSR = 0.15$)

Appendix F

RESULTS OF OPERATIONAL CONDITIONS

The current appendix presents the results obtained from applying the operational load cases as defined in Table F.1.

Case ID (Occurrence [%])	**Mean load** [kN]	**Amplitude** [kN]	**Wind speed** [m/s]	**Associated period** [s]	**Mean/ Capacity**	**Max/ Capacity**
OP 1 (68.5%)	3744	800	13–15	7.32	5.3 [%]	6.5 [%]
OP 2 (74.7%)	6318	500	13–15	7.32	9.0 [%]	9.7 [%]
OP 3 (70.5%)	0	650	13–15	7.32	0.0 [%]	0.2 [%]

Table F.1: Representative case for operational loading conditions and comparison to caisson capacity

Generally the positioning of the selected stress points and nodes is as in Figure F.1

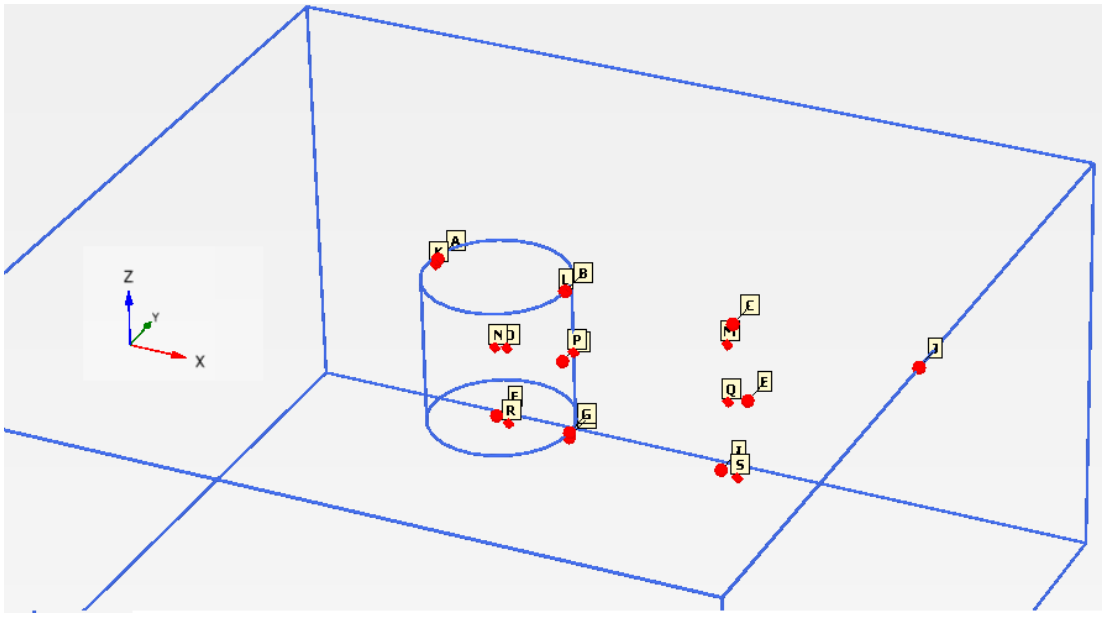

Figure F.1: Screen-shot of the locations of the chosen nodes and stress points for the full problem

F.1 CASE OP1

Name	X	Y	Z
A	-7,44	0,94	0,00
B	7,50	0,00	0,00
C	25,21	0,58	0,00
D	-1,04	0,13	-8,18
E	7,50	0,00	-7,71
F	26,92	0,47	-8,36
G	-0,60	0,08	-16,00
H	7,50	0,00	-16,00
I	25,74	-0,97	-15,03
J	45,00	0,00	0,00
K	-7,00	-0,03	-0,65
L	7,03	-0,64	-0,69
M	25,36	-0,99	-1,49
N	0,43	-1,03	-8,30
O	7,90	1,23	-8,56
P	24,91	0,46	-9,17
Q	0,86	-0,07	-16,43
R	7,34	-0,51	-16,70
S	24,60	-1,23	-16,72

Figure F.2: Location of nodes and stress points for OP1

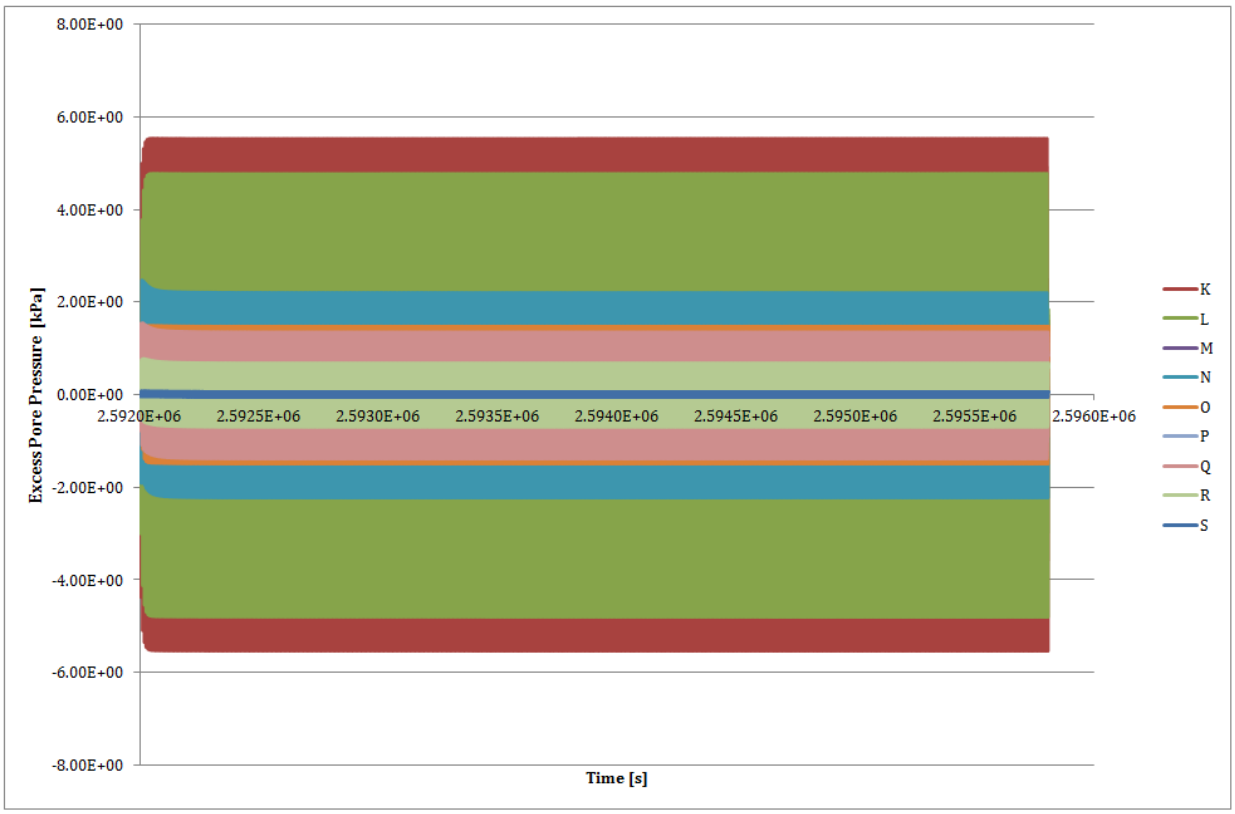

Figure F.3: Excess pore pressure from OP1

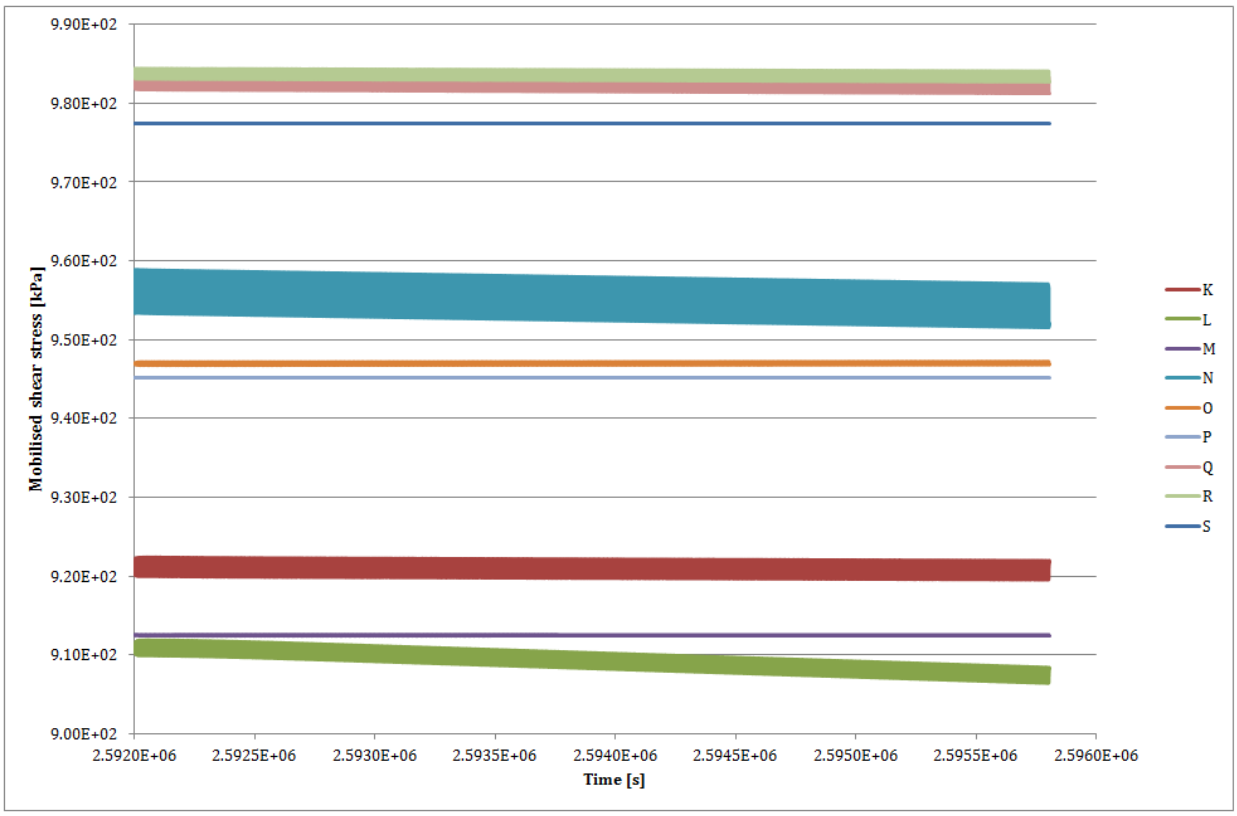

Figure F.4: Mobilised shear strength from OP1

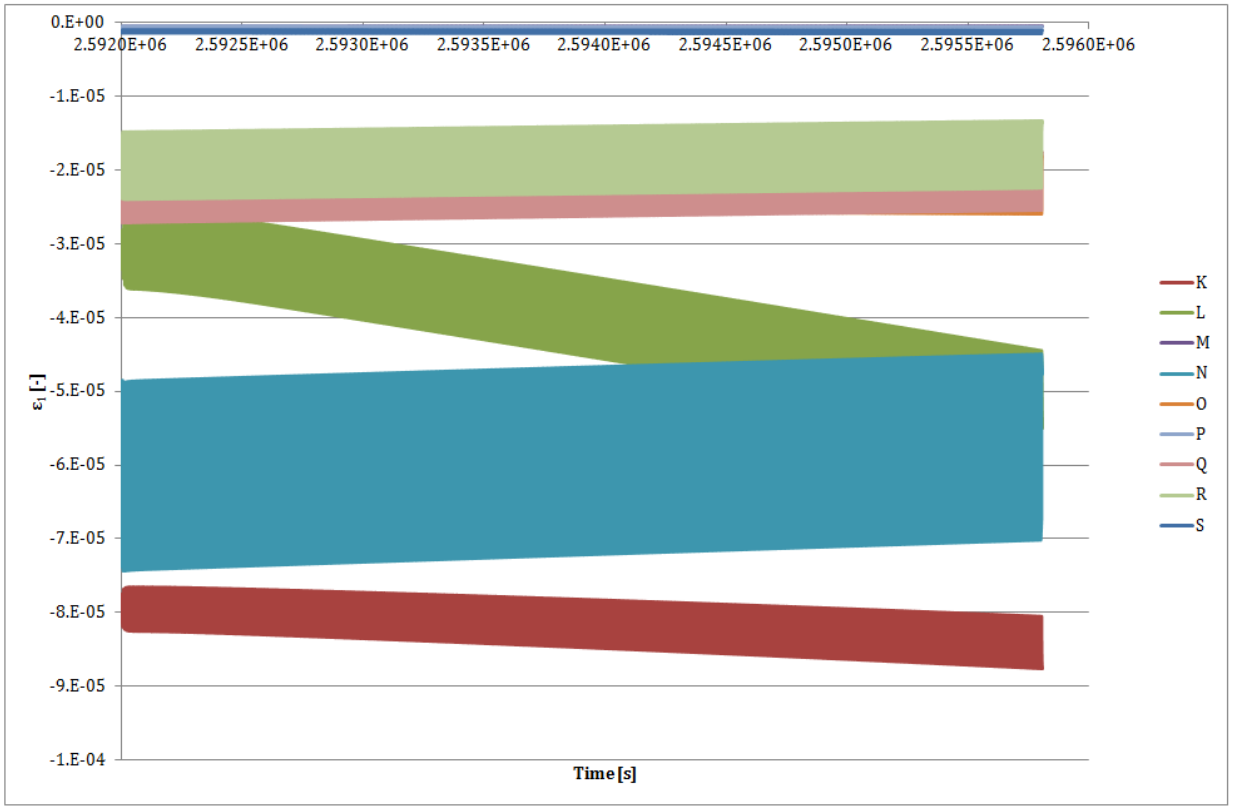

Figure F.5: Axial strain from OP1

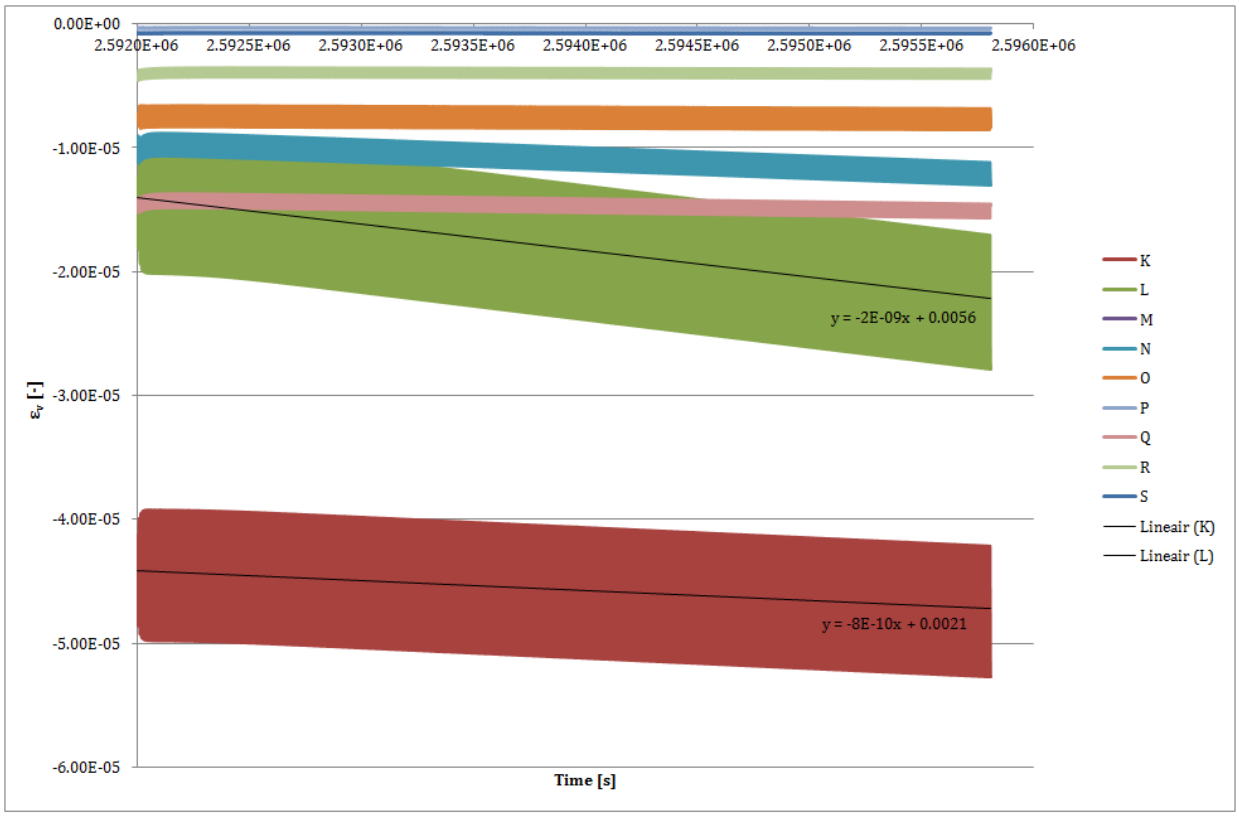

Figure F.6: Volumetric strain from OP1

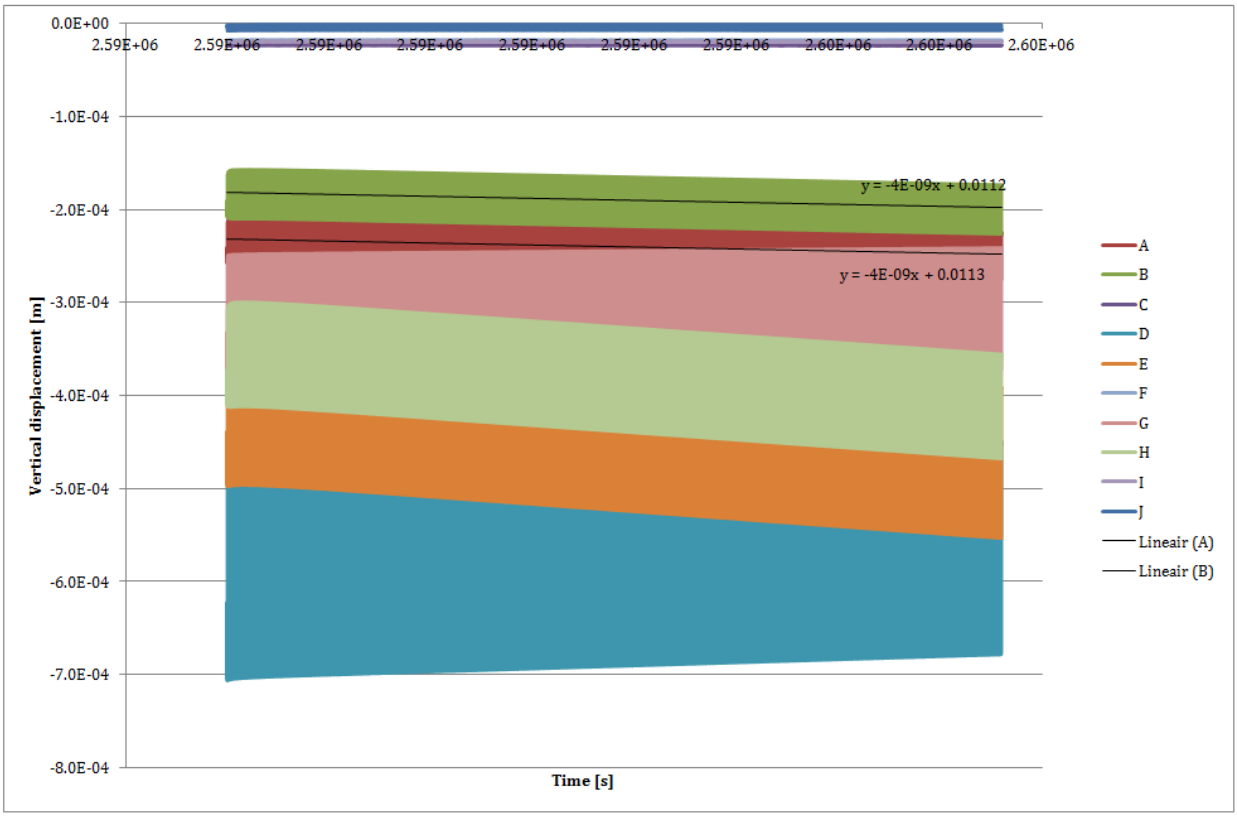

Figure F.7: Vertical displacements from OP1

F.2 CASE OP2

Name	X	Y	Z
A	-7,44	0,94	0,00
B	7,50	0,00	0,00
C	25,21	0,58	0,00
D	-1,04	0,13	-8,18
E	7,50	0,00	-7,71
F	26,92	0,47	-8,36
G	-0,60	0,08	-16,00
H	7,50	0,00	-16,00
I	25,74	-0,97	-15,03
J	45,00	0,00	0,00
K	-7,00	-0,03	-0,65
L	7,03	-0,64	-0,69
M	25,36	-0,99	-1,49
N	0,43	-1,03	-8,30
O	7,90	1,23	-8,56
P	24,91	0,46	-9,17
Q	0,86	-0,07	-16,43
R	7,34	-0,51	-16,70
S	25,75	0,09	-16,88

Figure F.8: Location of nodes and stress points for OP2

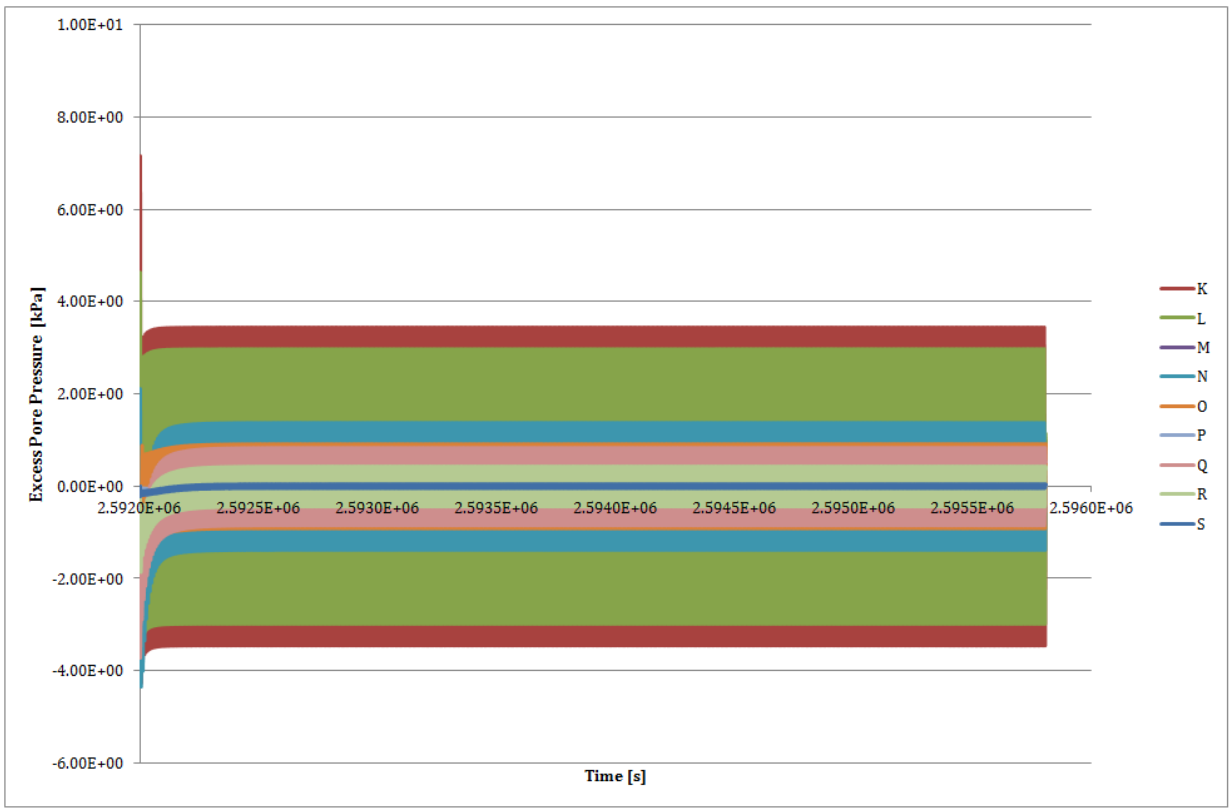

Figure F.9: Excess pore pressure from OP2

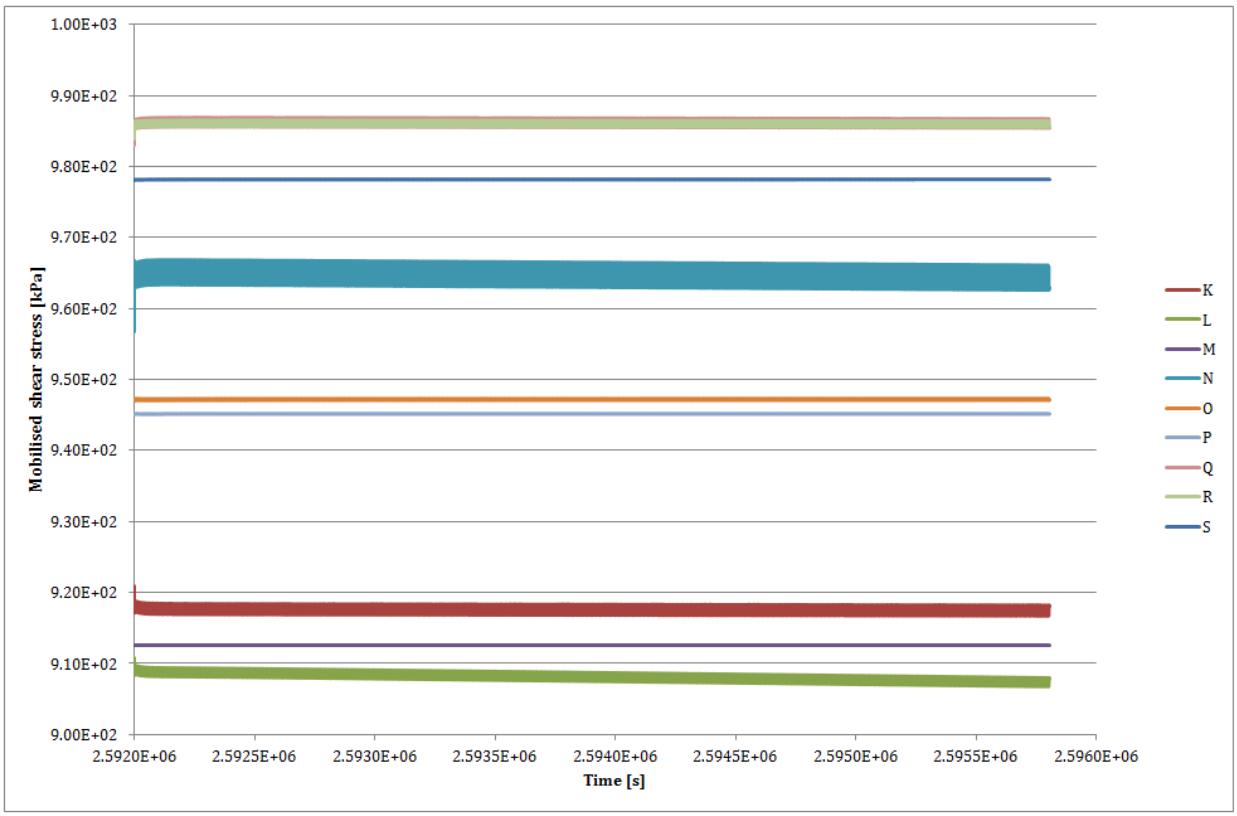

Figure F.10: Mobilised shear strength from OP2

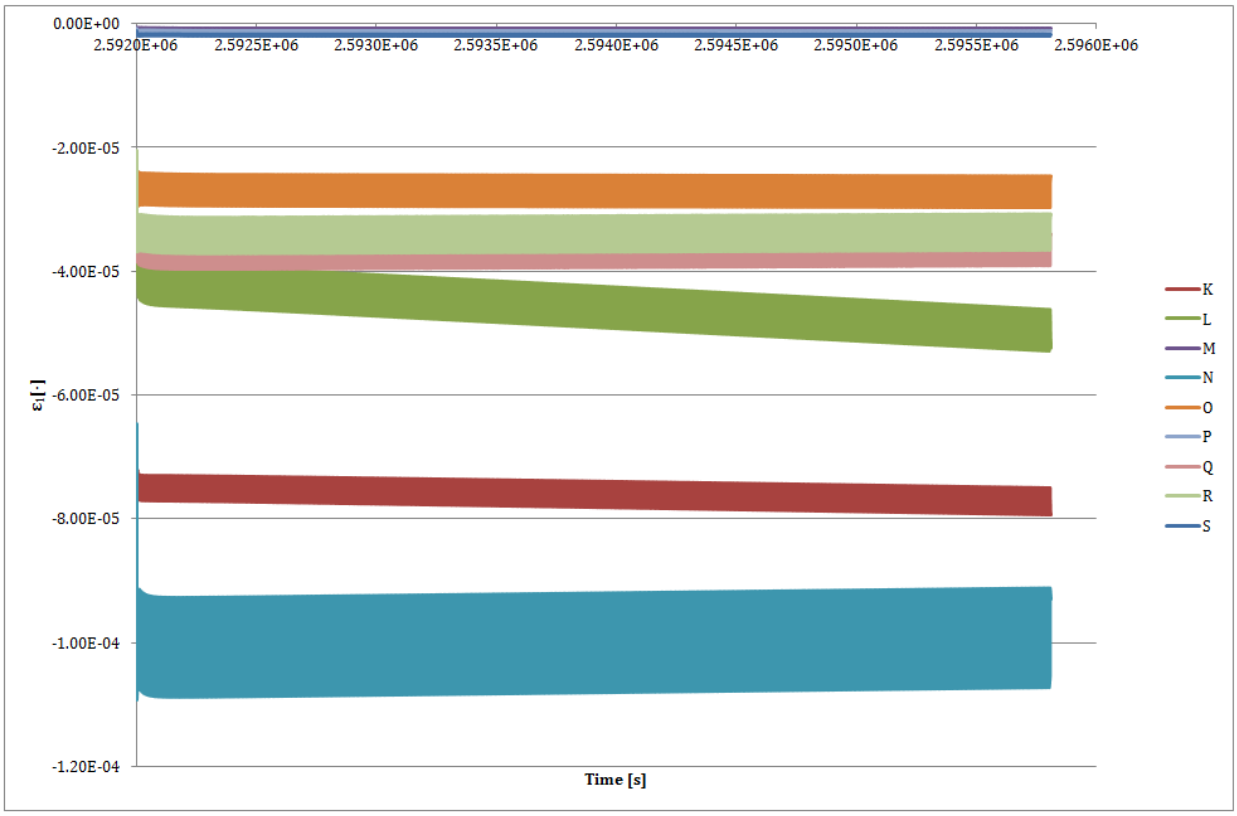

Figure F.11: Axial strain from OP2

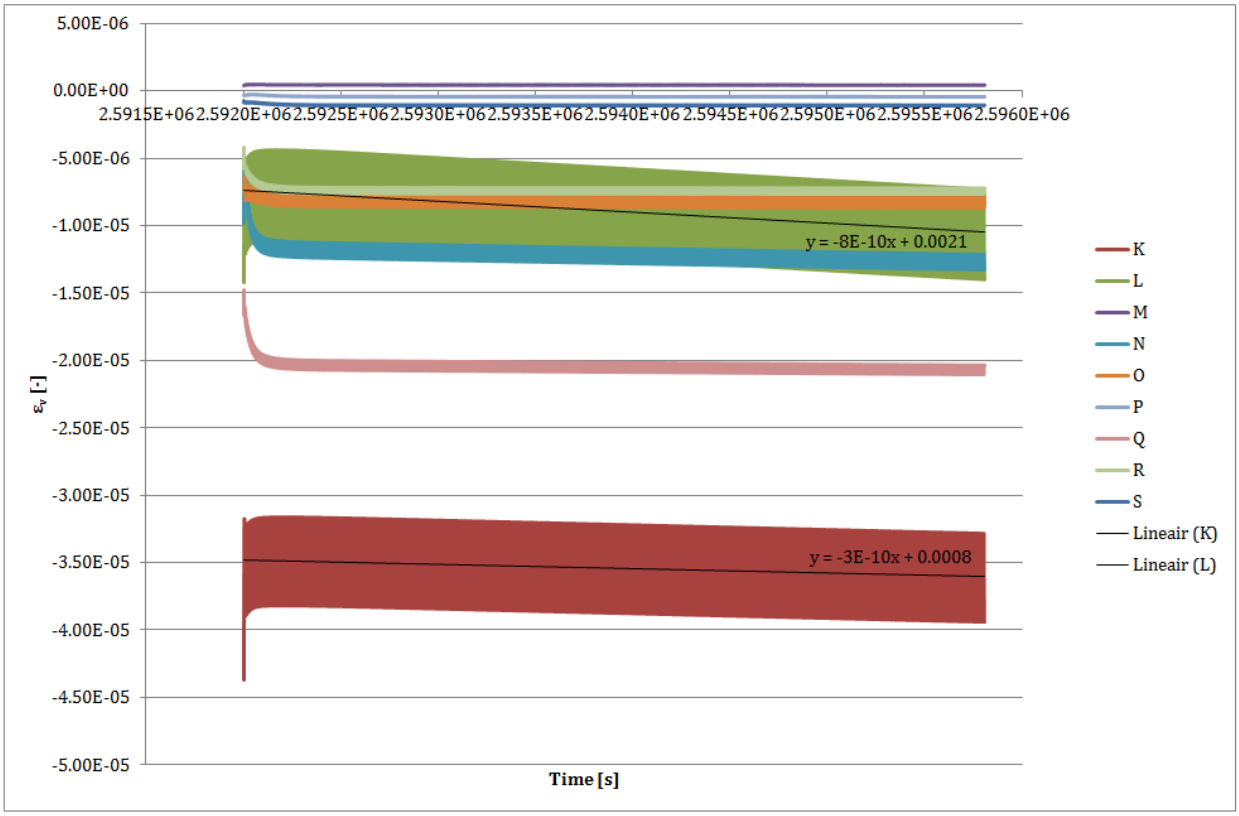

Figure F.12: Volumetric strain from OP2

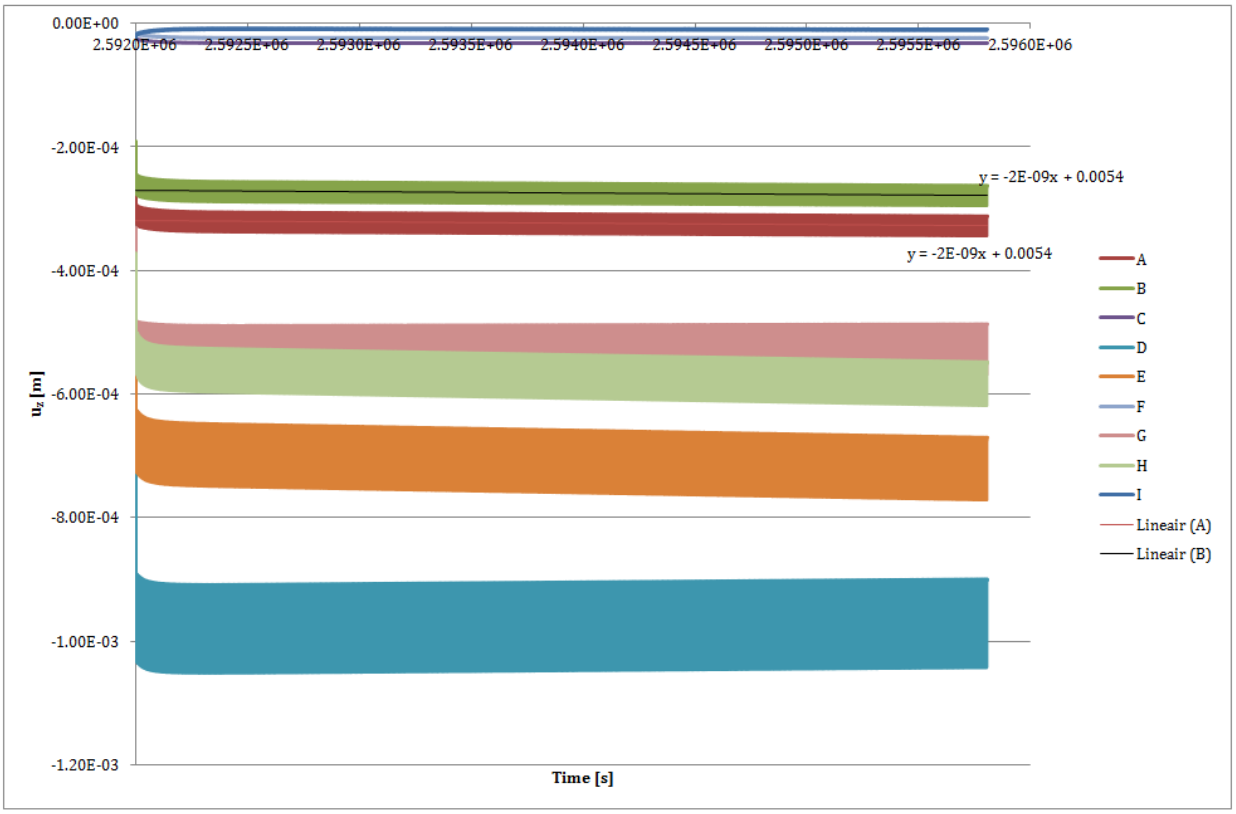

Figure F.13: Vertical displacements from OP2

F.3 CASE OP3

Name	X	Y	Z
A	-7,44	0,94	0,00
B	7,50	0,00	0,00
C	25,21	0,58	0,00
D	0,12	0,03	-6,97
E	7,50	0,00	-8,00
F	23,68	2,40	-8,09
G	-0,60	0,08	-16,00
H	7,50	0,00	-16,00
I	23,92	0,20	-16,53
J	45,00	0,00	0,00
K	-6,99	0,49	-0,44
L	7,04	0,50	-0,44
M	25,34	-0,99	-1,44
N	-0,13	-0,67	-7,68
O	7,91	0,60	-7,11
P	24,69	0,39	-8,75
Q	0,83	-0,12	-16,47
R	7,84	-0,43	-15,51
S	25,99	-0,47	-16,57

Figure F.14: Location of nodes and stress points for OP3

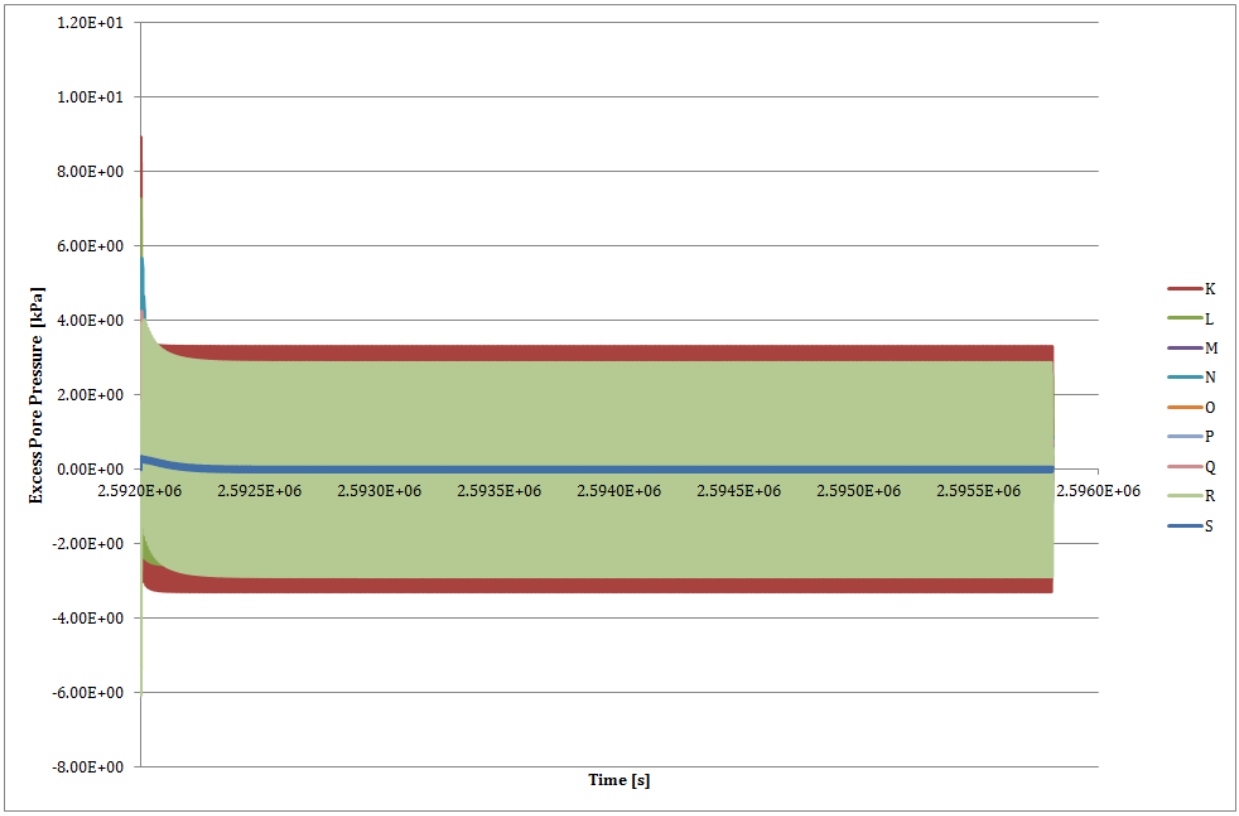

Figure F.15: Excess pore pressure from OP3

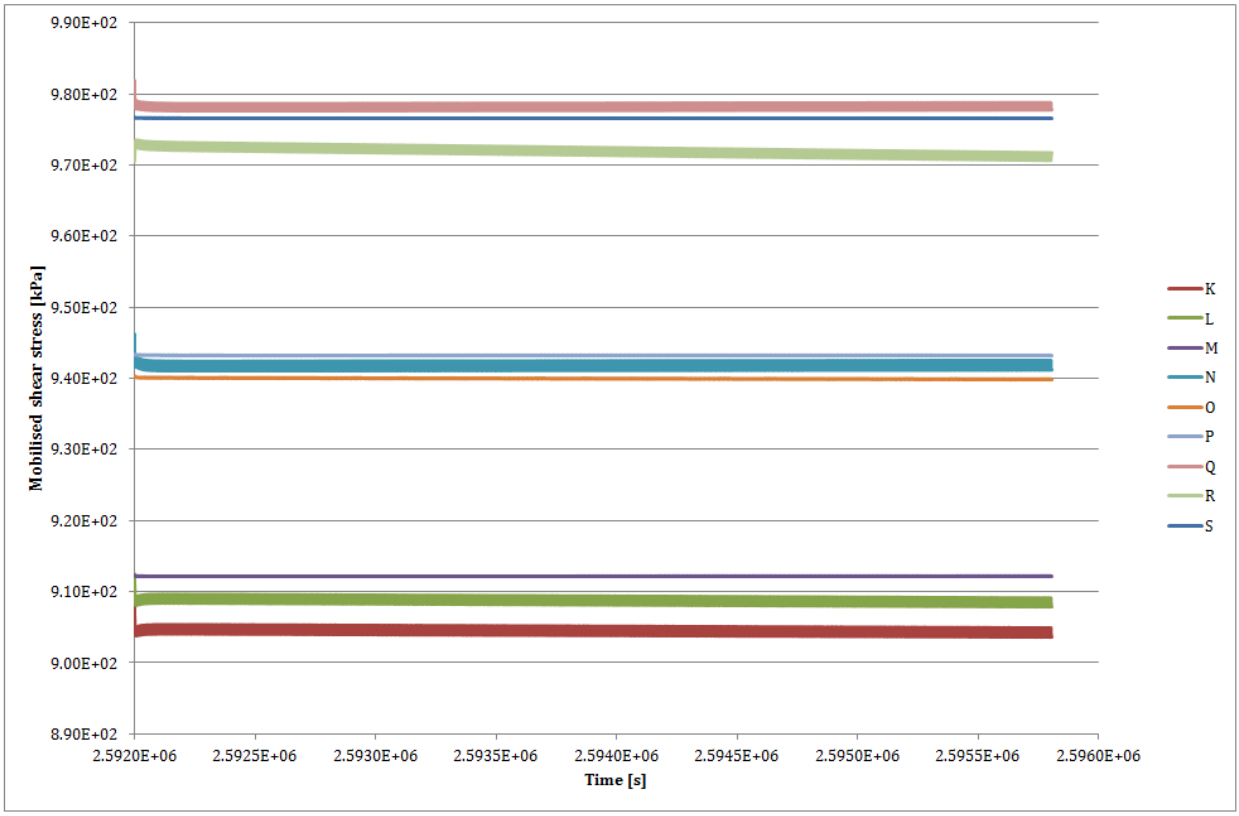

Figure F.16: Mobilised shear strength from OP3

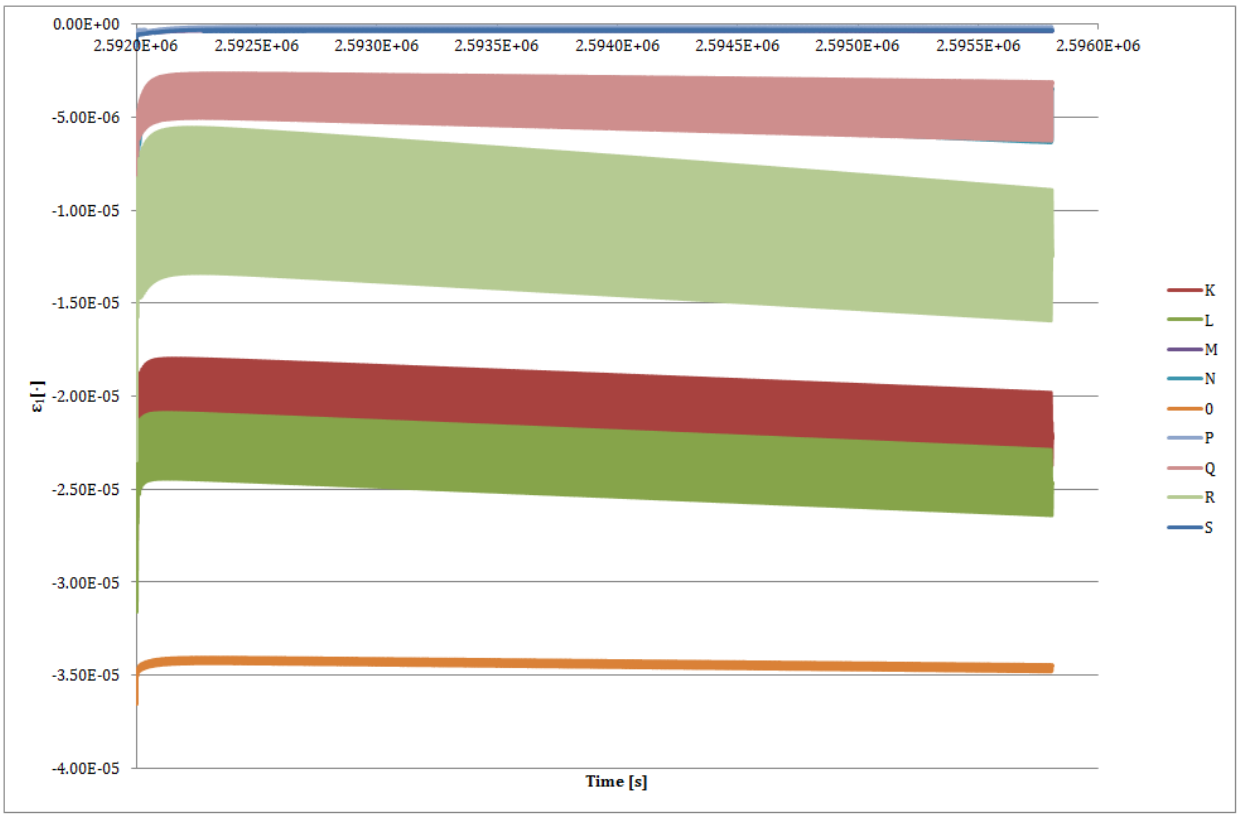

Figure F.17: Axial strain from OP3

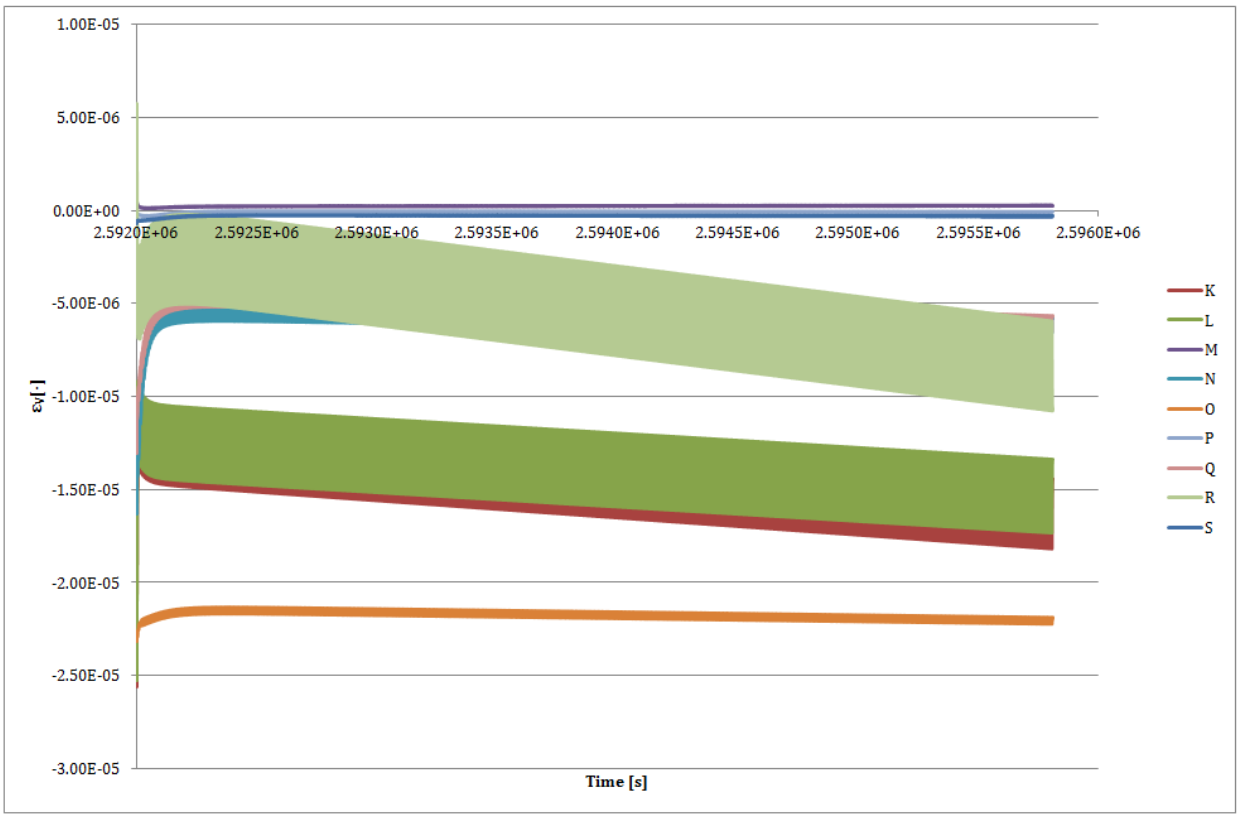

Figure F.18: Volumetric strain from OP3

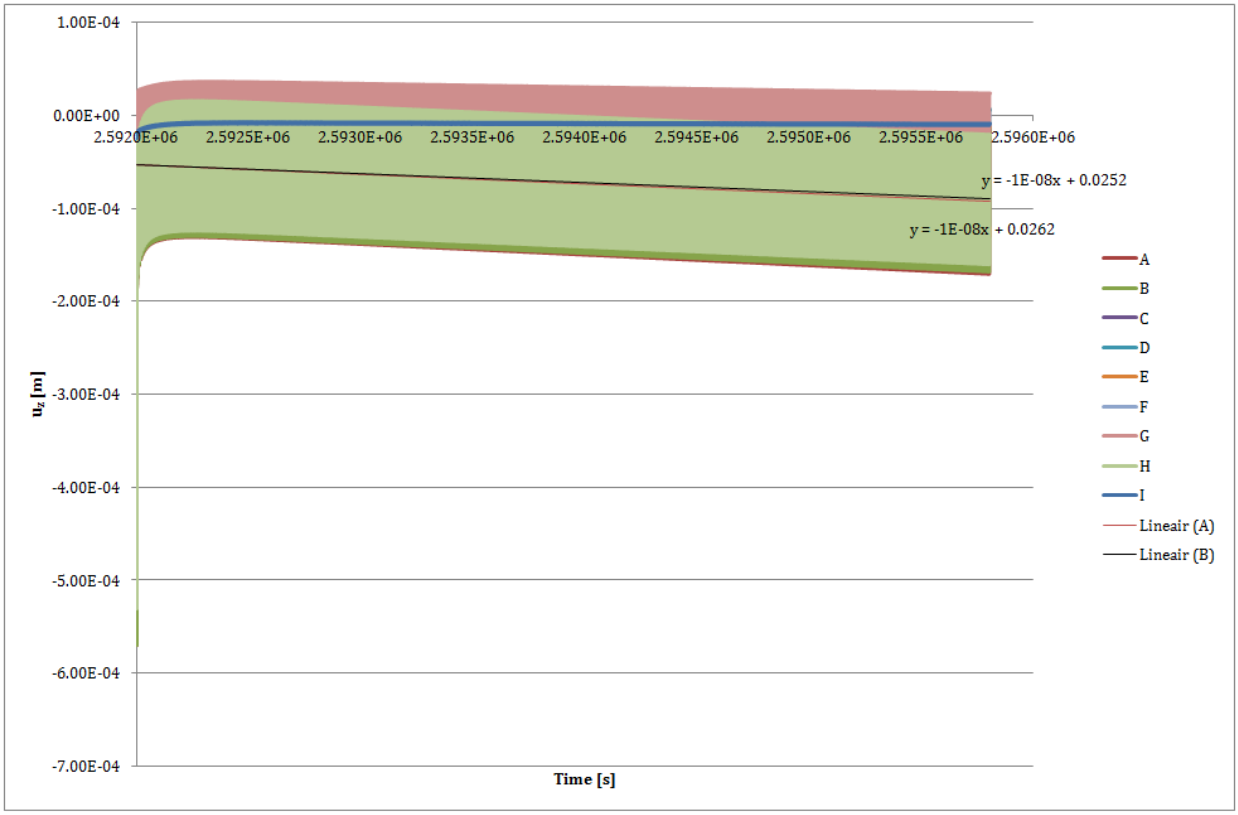

Figure F.19: Vertical displacements from OP3

Appendix G

RESULTS OF EXTREME CONDITIONS

The current appendix presents the results obtained from applying the operational load cases as defined in Figure G.1. The locations of the stress points and nodes can be seen in Figure G.2.

Extreme cases					Mean/	Max/
Case	Period	Caisson	Mean Load	Amplitude	Capacity	Capacity
[-]	[s]	[-]	[kN]	[kN]	[%]	[%]
EX 1	7.32	1 or 2	-35189	8797	50.0%	62.5%
				17595		75.0%
				35189		100.0%
EX 2	7.32	1 or 2	-24600	500	35%	35.7%
				5000		42.1%
				1500		37.1%
EX 3	7.32	3	20200	500	40.7%	41.7%
				5000		50.8%
				10000		60.9%

Figure G.1: Characteristics of extreme load scenarios (negative values represent compressive forces and positive values represent tensile forces)

G.1 CASE EX 1 i

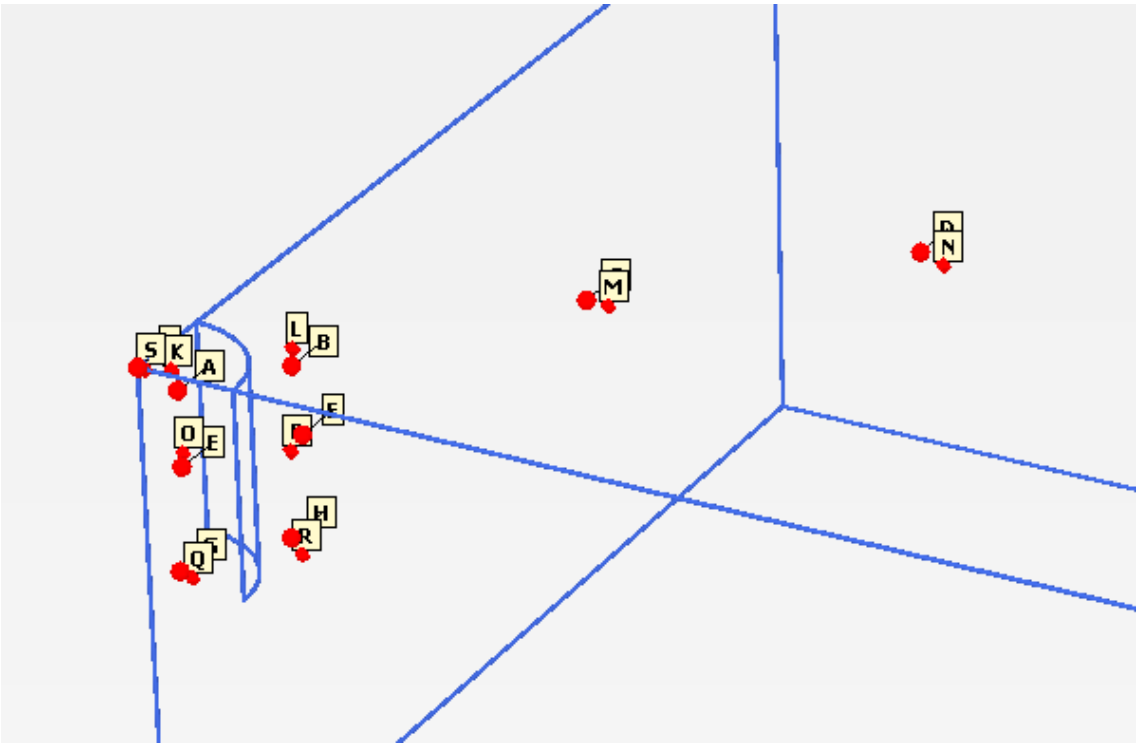

Figure G.2: Location of nodes and stress points for extreme cases EX 1i and 1ii]

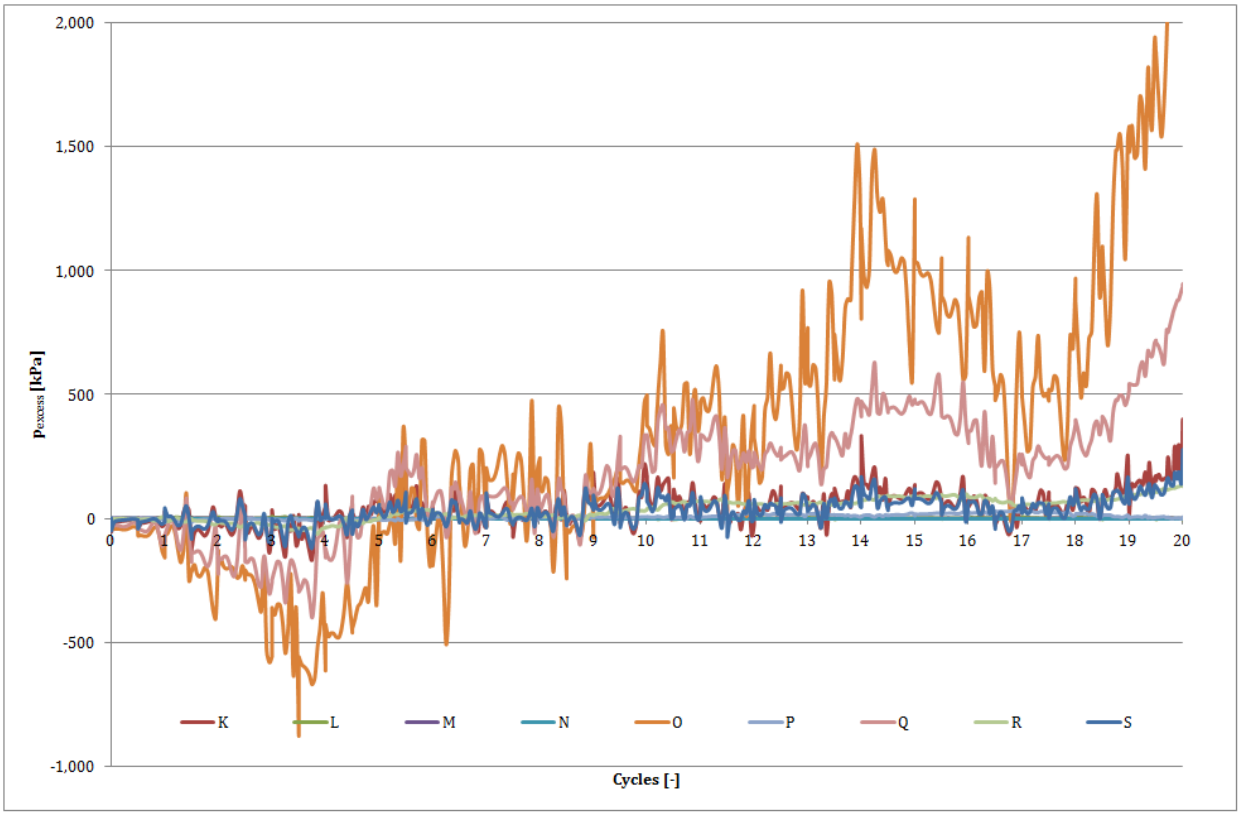

Figure G.3: Excess pore pressure development for EX 1 i

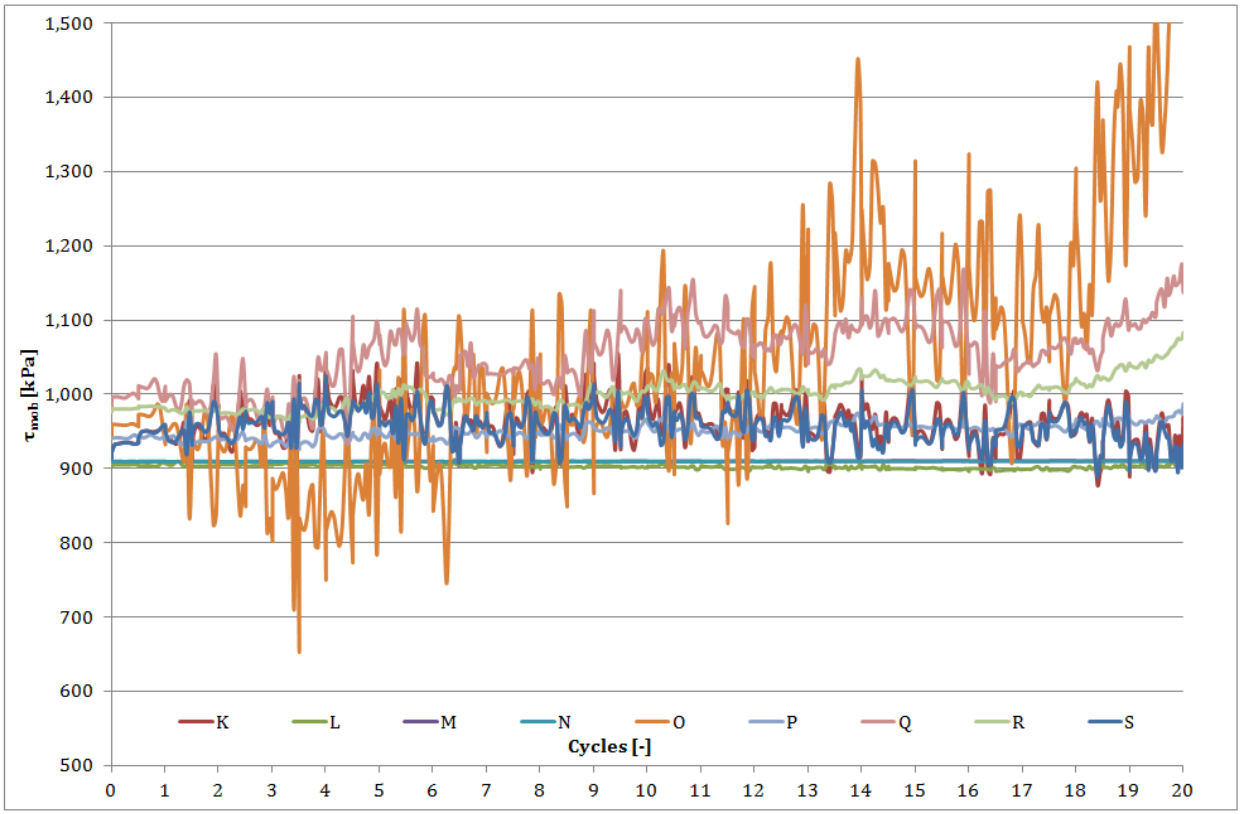

Figure G.4: Mobilised shear strength from EX 1 i

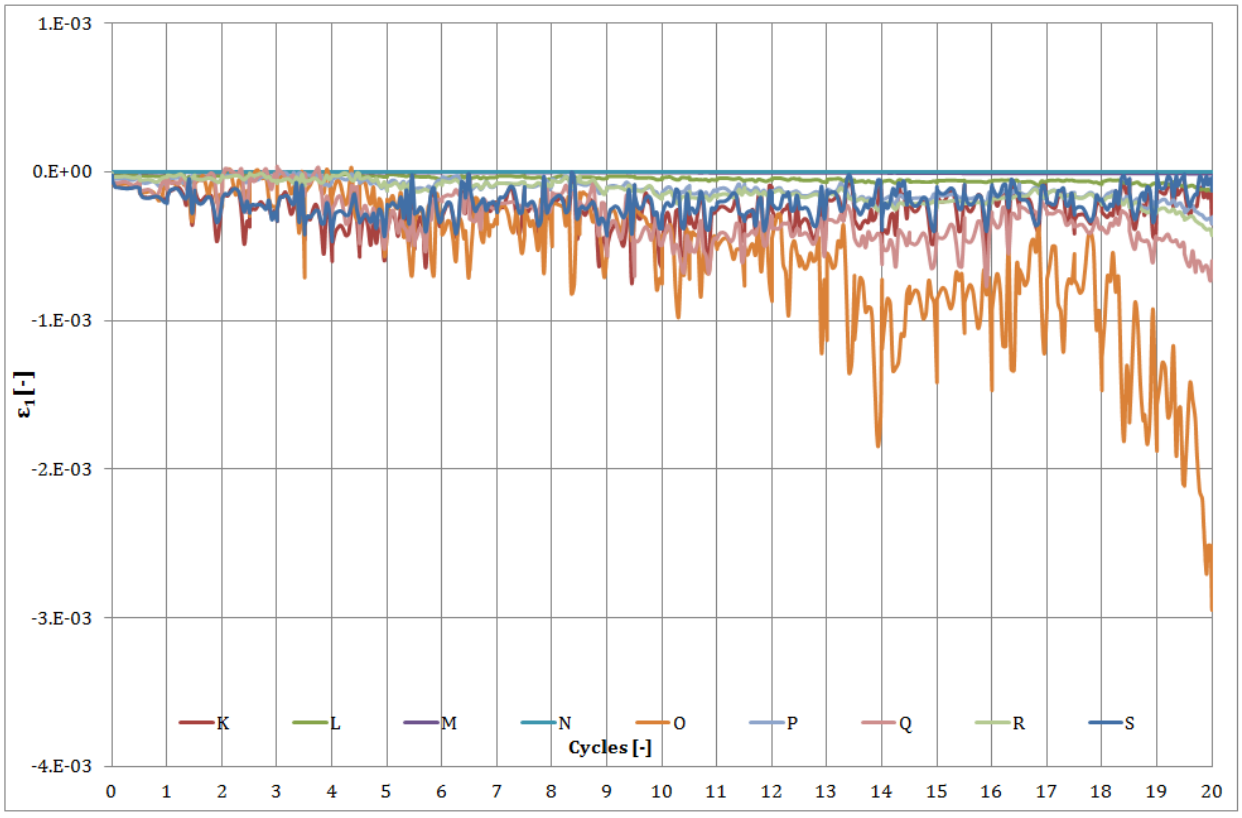

Figure G.5: Axial strain from EX 1 i

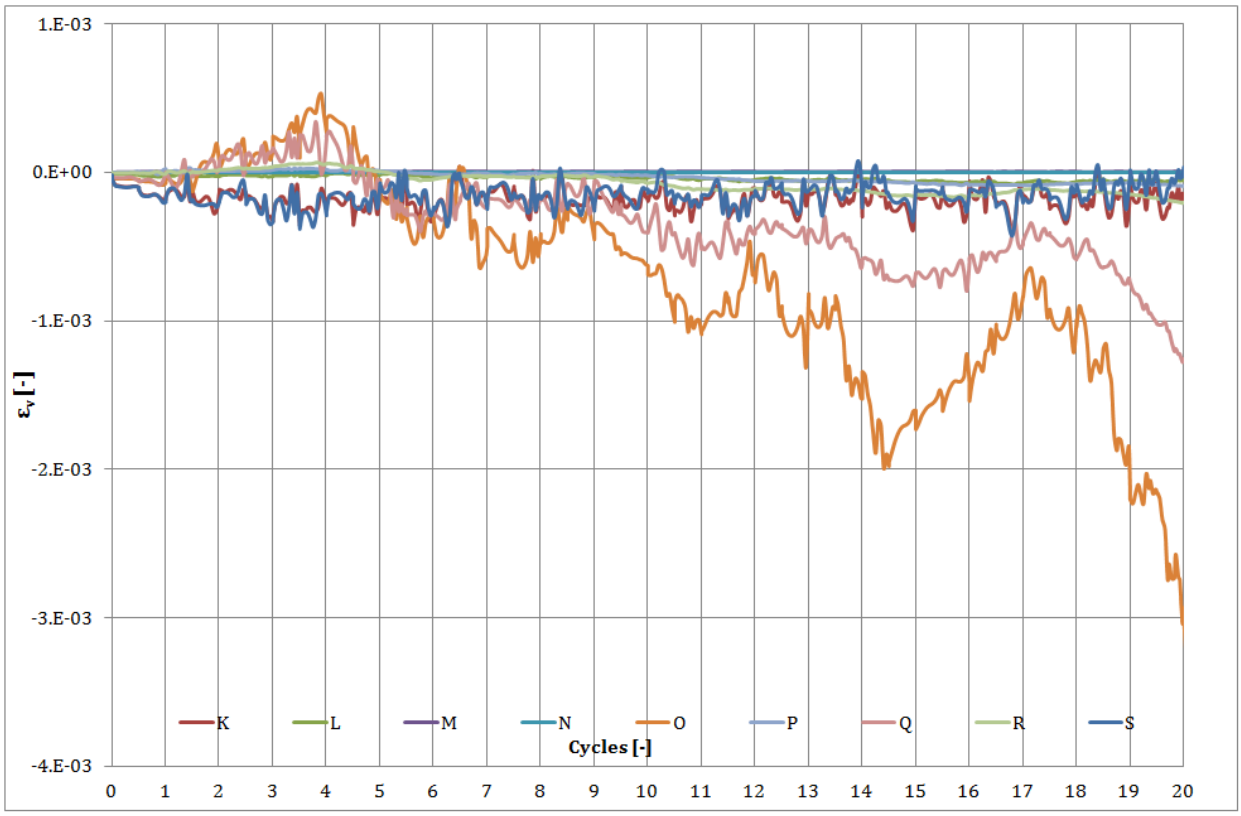

Figure G.6: Volumetric strain in time for EX 1 i

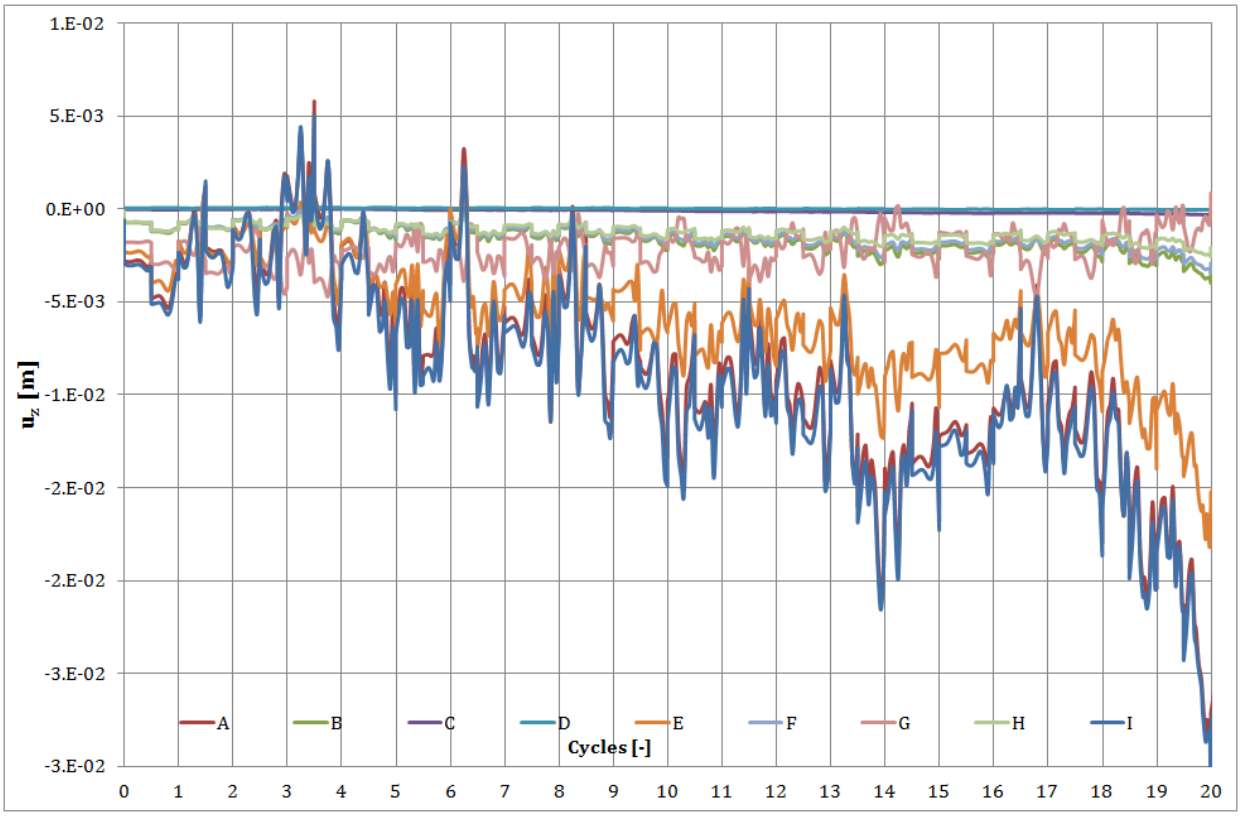

Figure G.7: Vertical displacements from EX 1 i

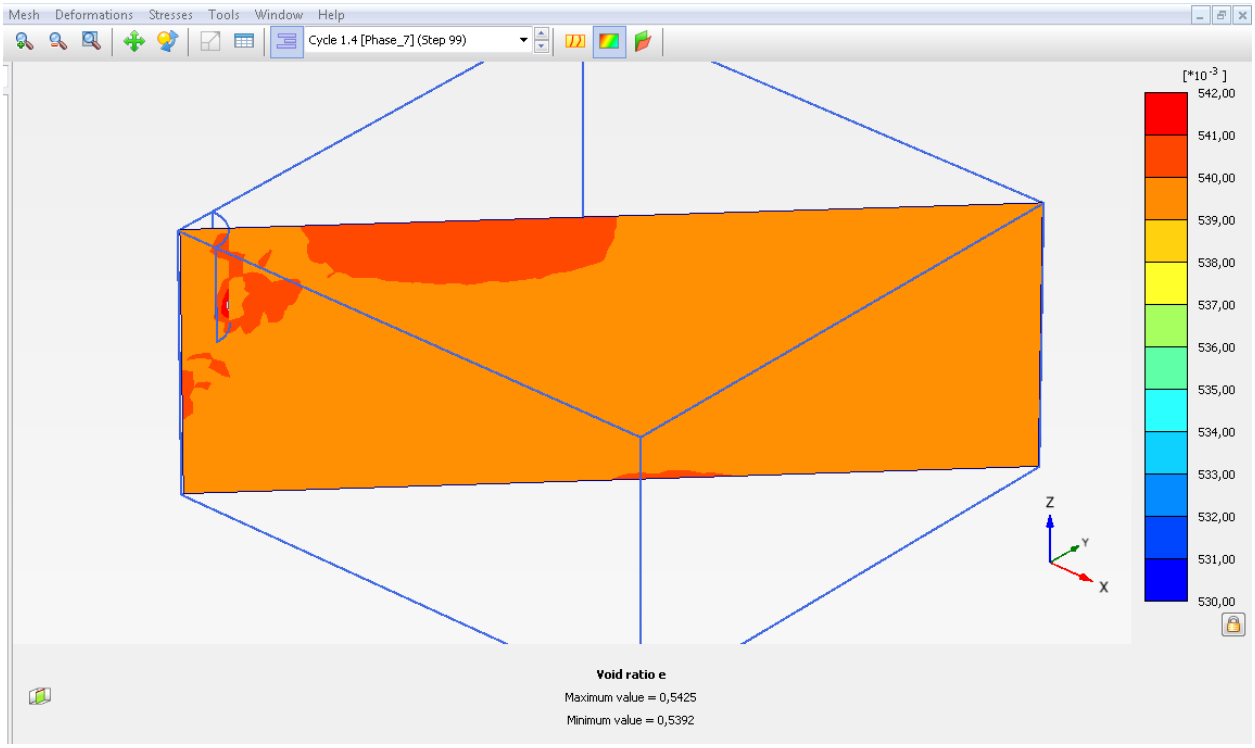

Figure G.8: Changes void ratio from EX 1 i, 1^{st} cycle

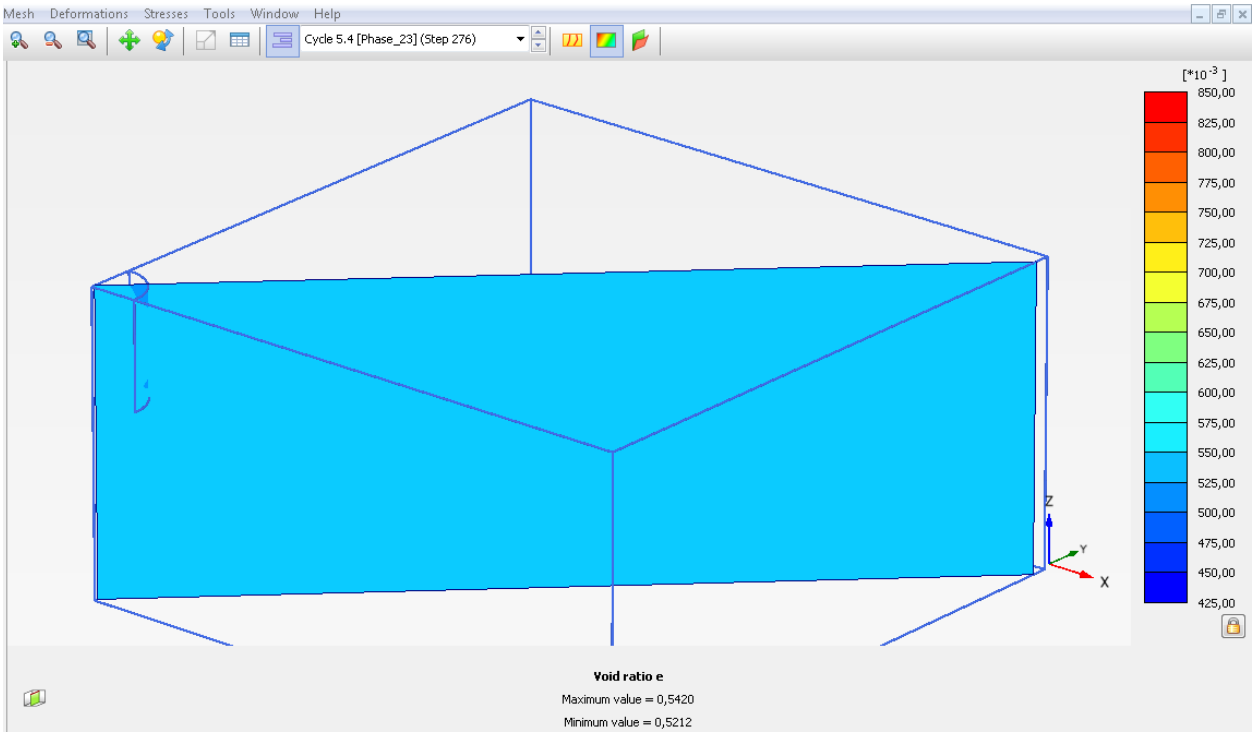

Figure G.9: Changes void ratio from EX 1 i, 5^{th} cycle

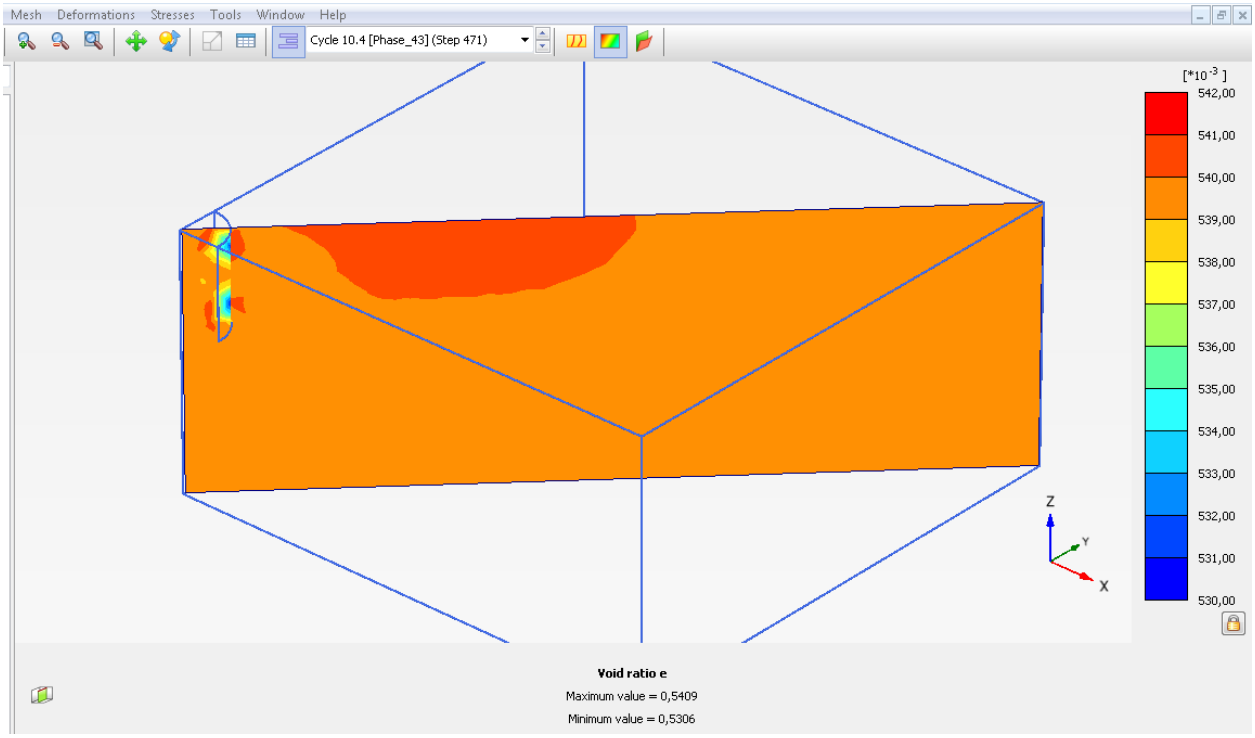

Figure G.10: Changes void ratio from EX 1 i, 10^{th} cycle

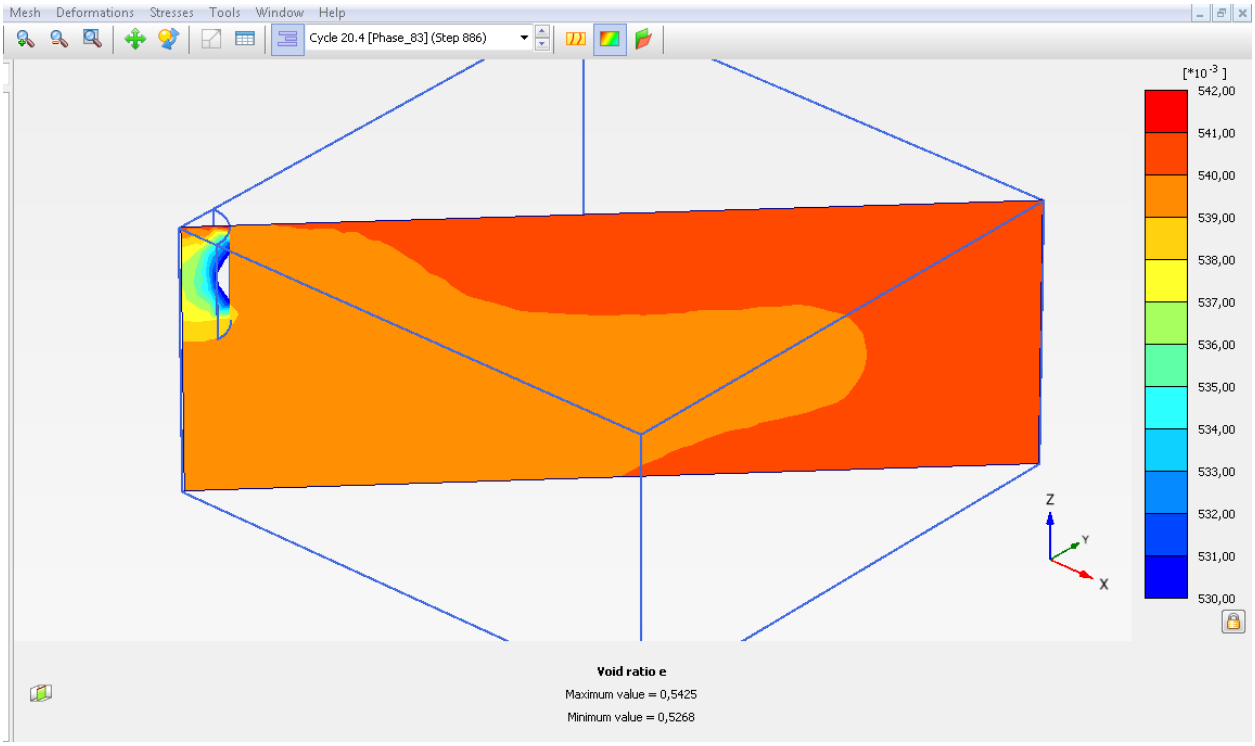

Figure G.11: Changes void ratio from EX 1 i, 20^{th} cycle

G.2 CASE EX 1 ii

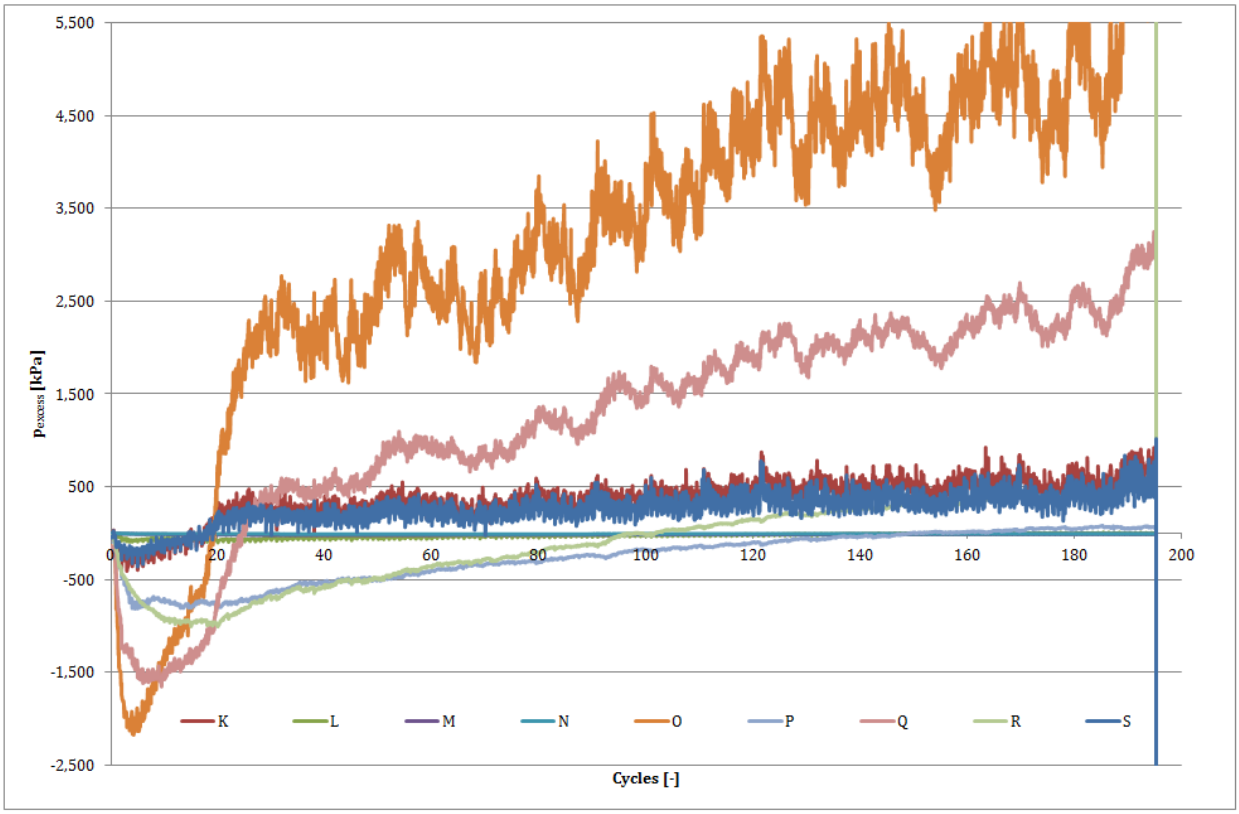

Figure G.12: Excess pore pressure in time for EX 1 ii

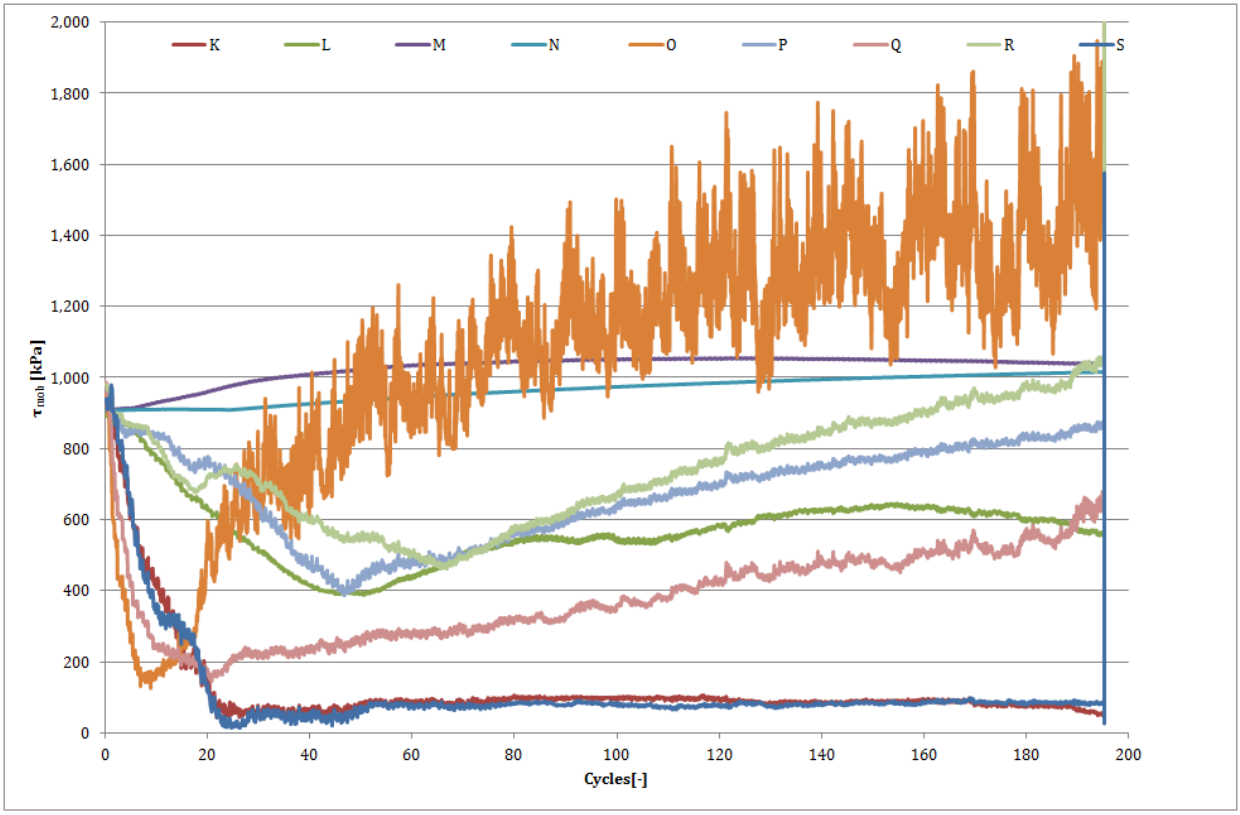

Figure G.13: Mobilised shear strength from EX 1 ii

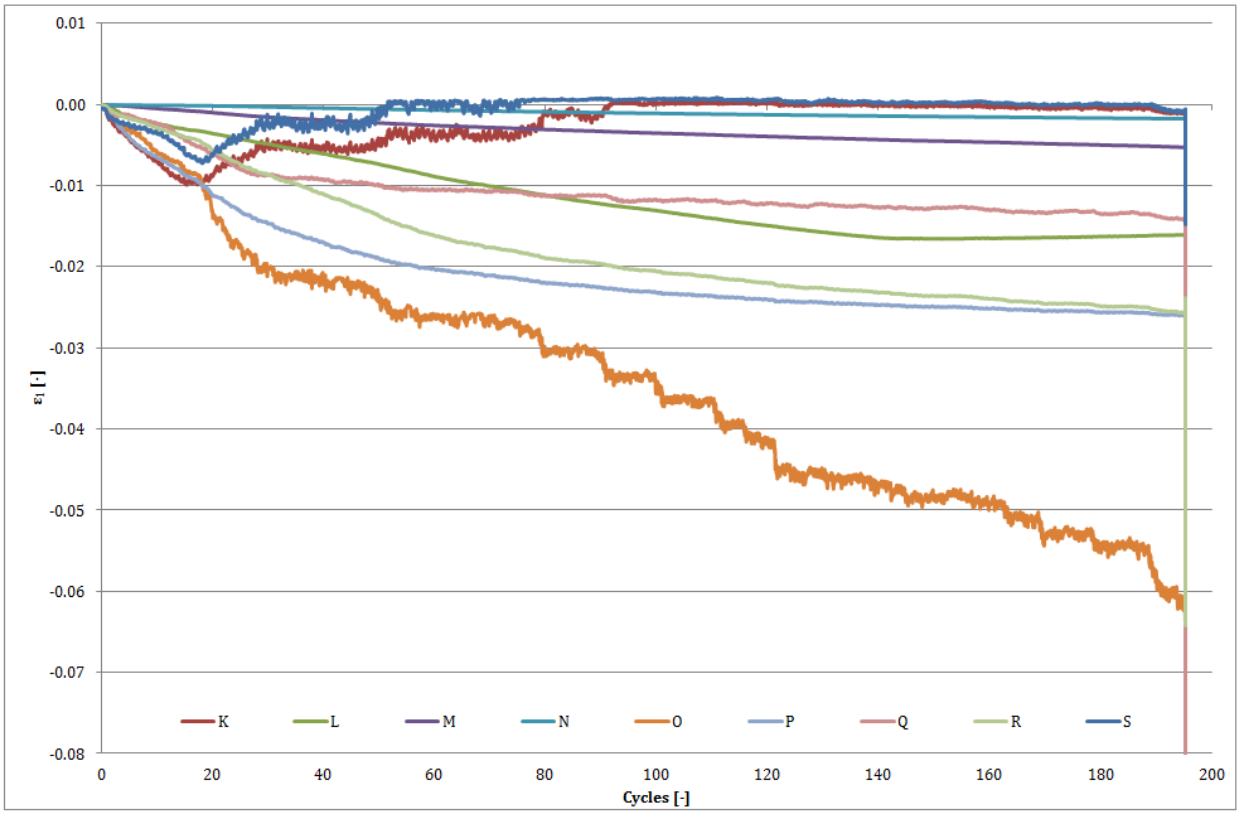

Figure G.14: Axial strain from EX 1 ii

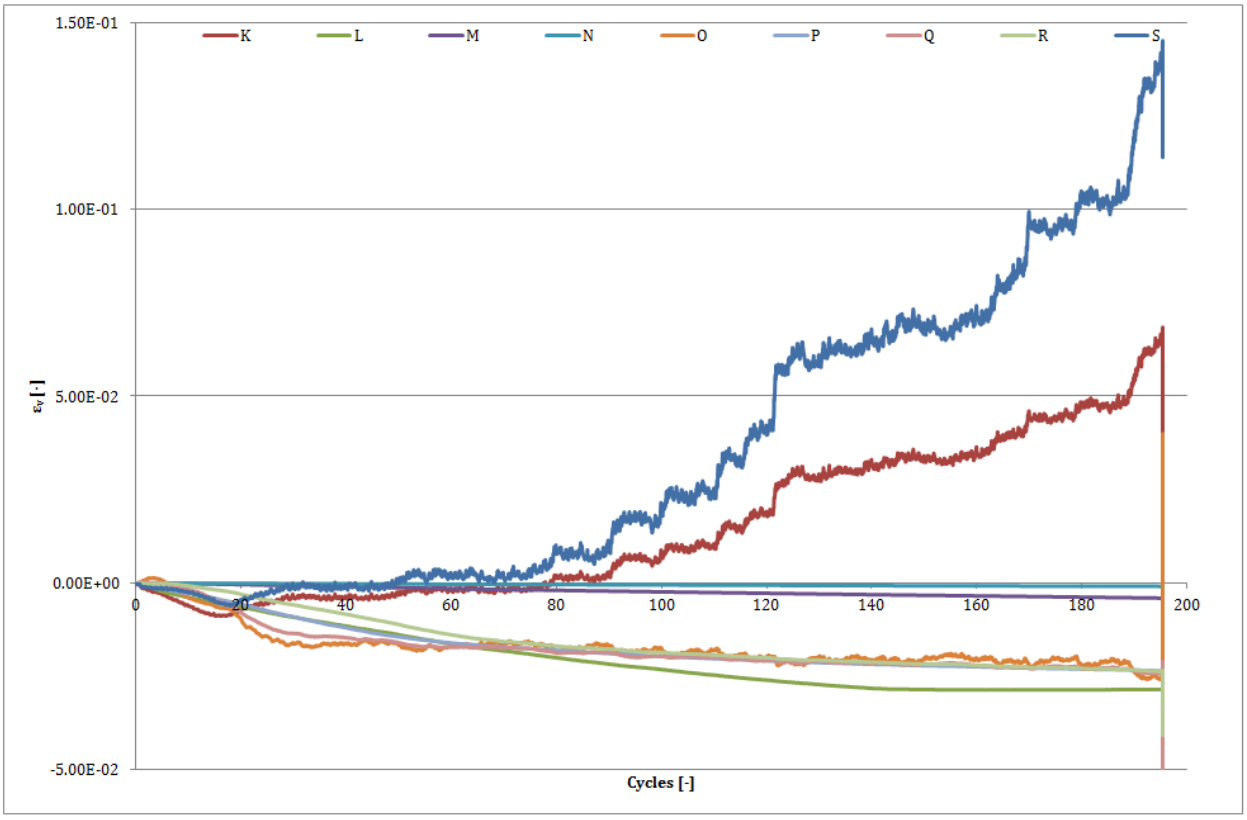

Figure G.15: Volumetric strain in time for EX 1 ii

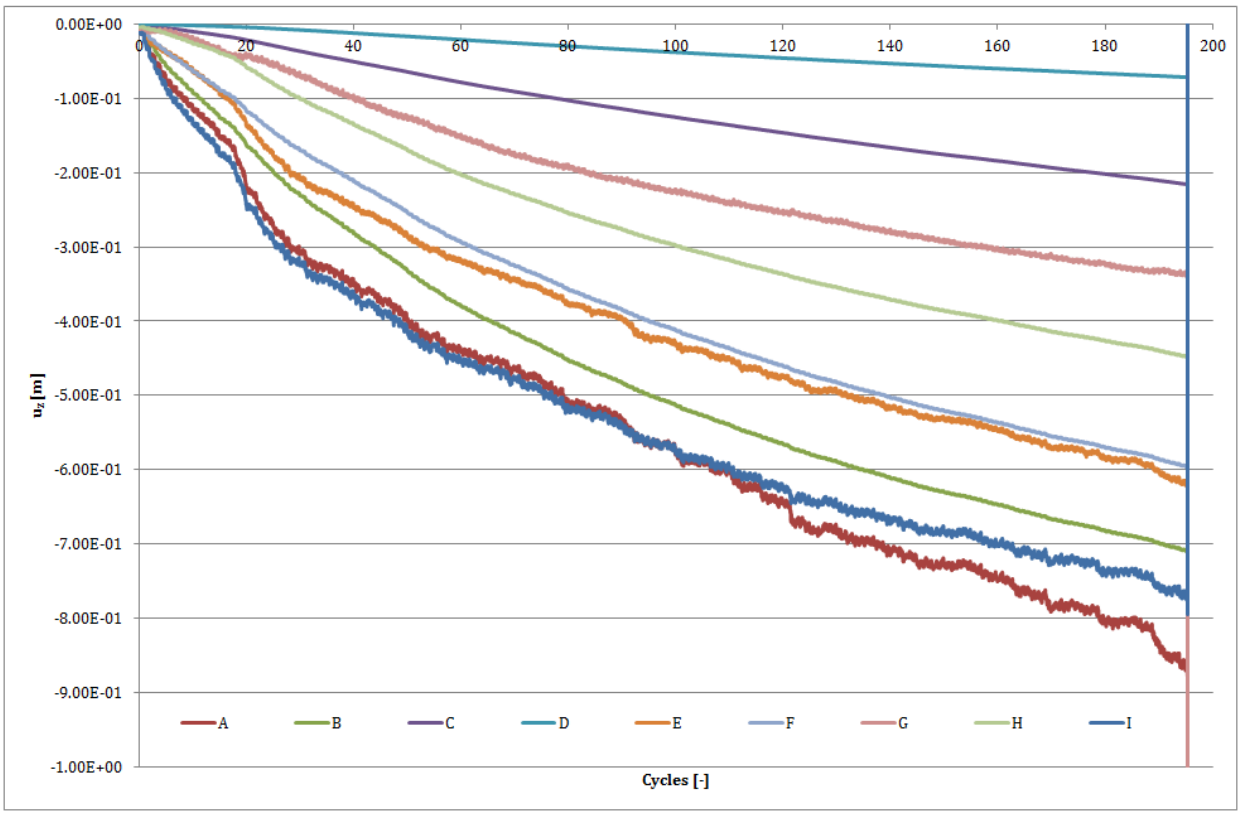

Figure G.16: Vertical displacements from EX 1 ii

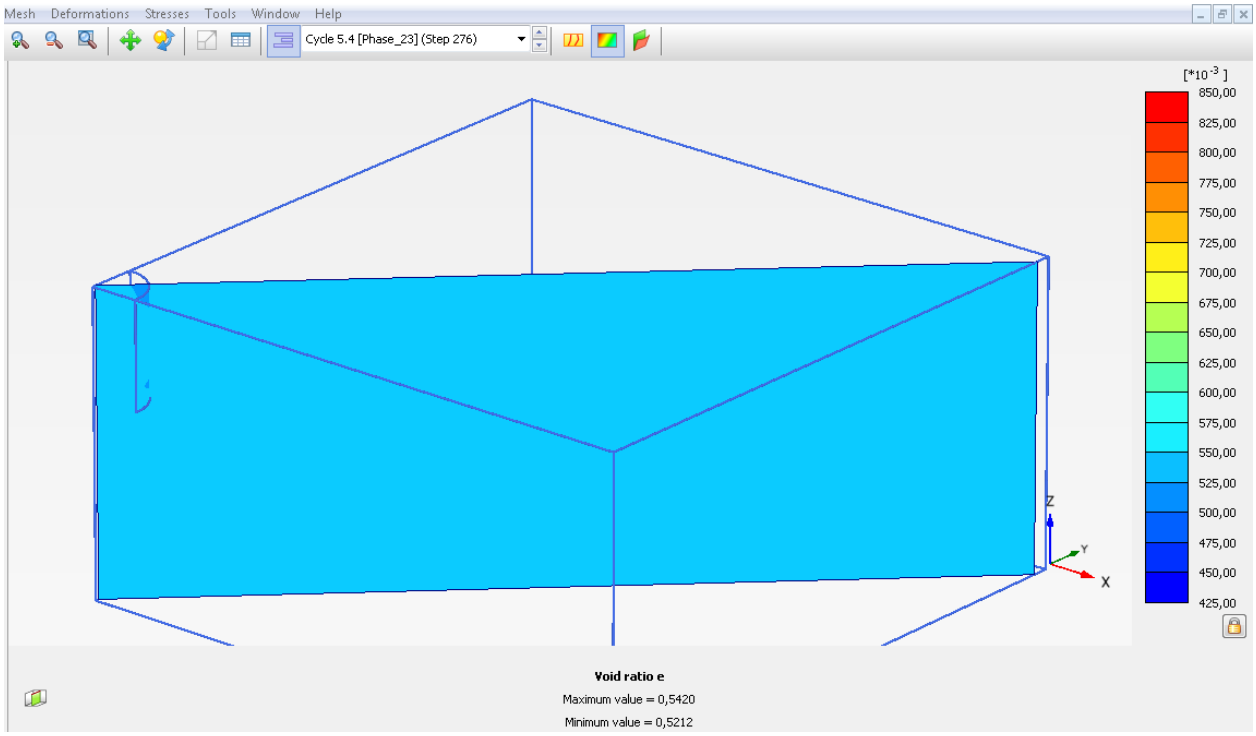

Figure G.17: Changes void ratio from EX 1 ii, 5^{th} cycle

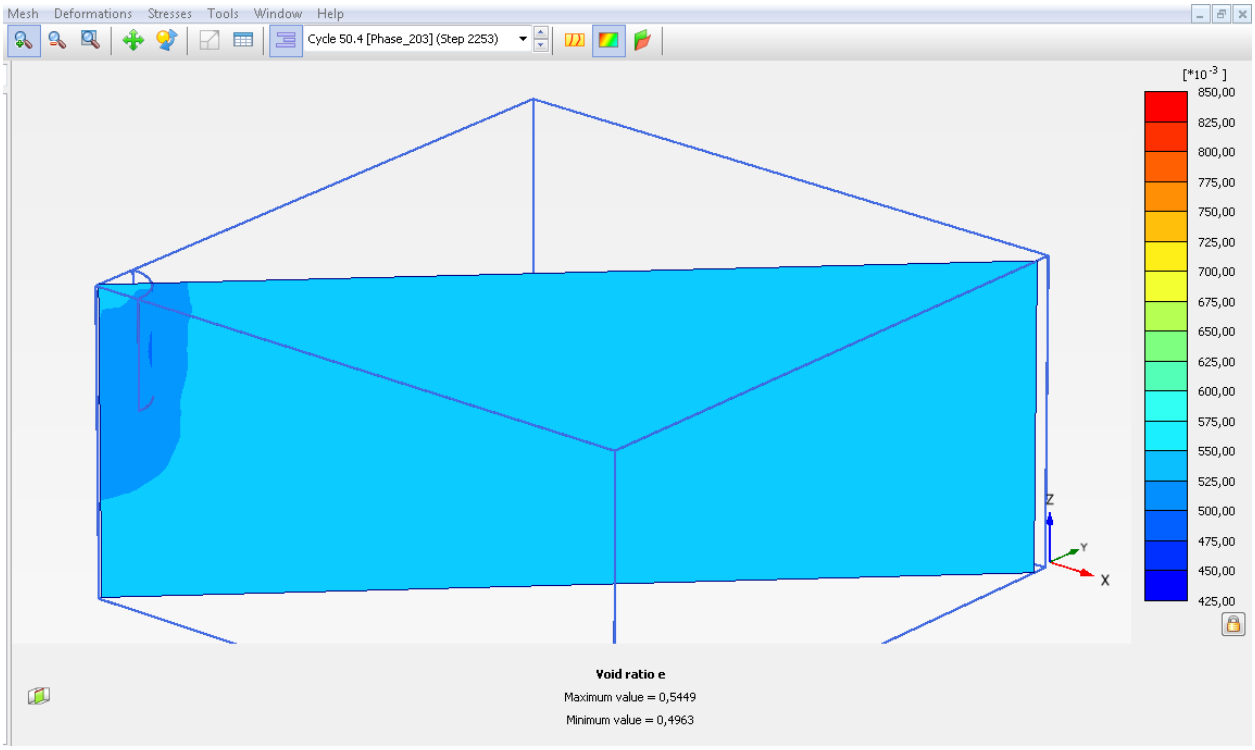

Figure G.18: Changes void ratio from EX 1 ii, 50^{th} cycle

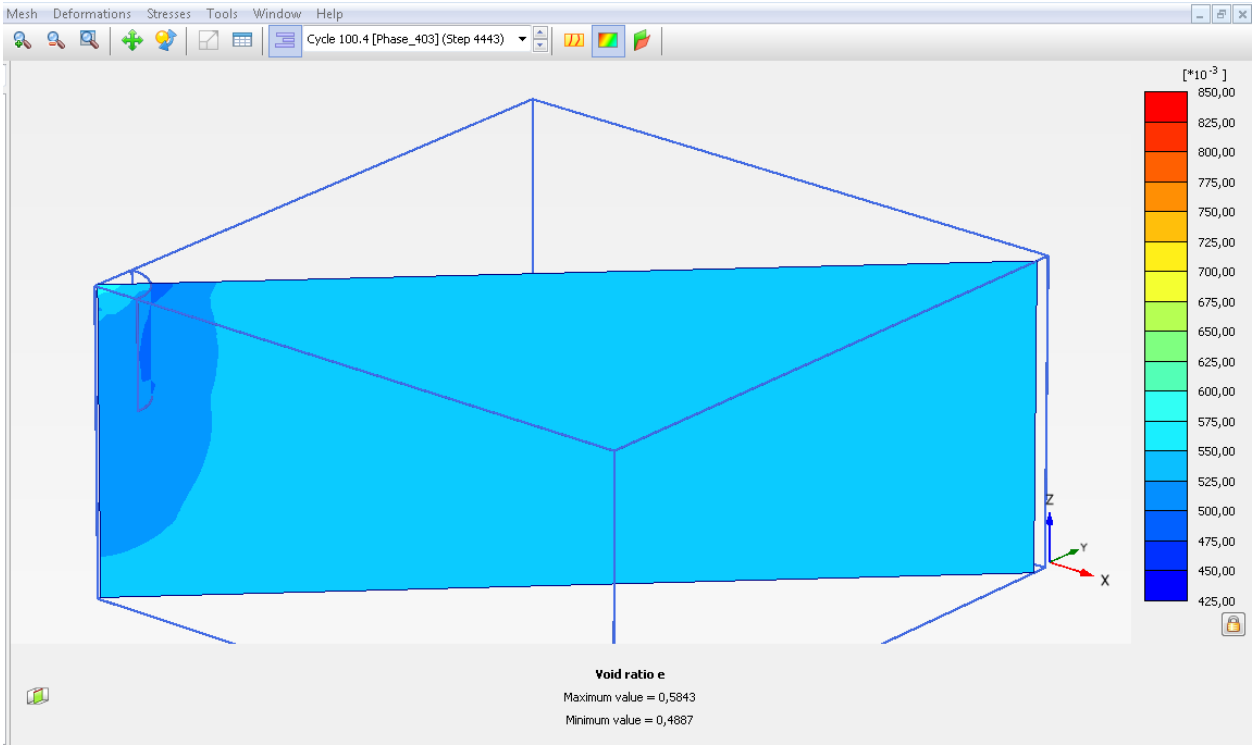

Figure G.19: Changes void ratio from EX 1 ii, 100^{th} cycle

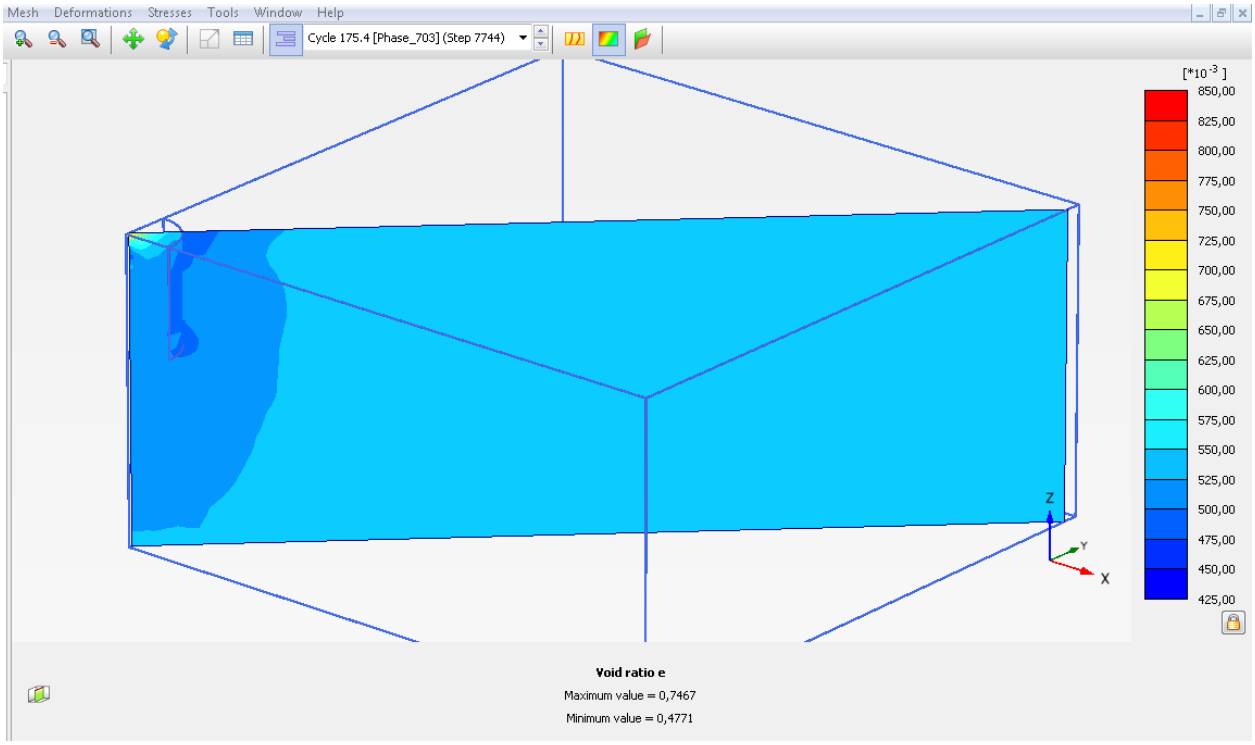

Figure G.20: Changes void ratio from EX 1 ii, 175^{th} cycle

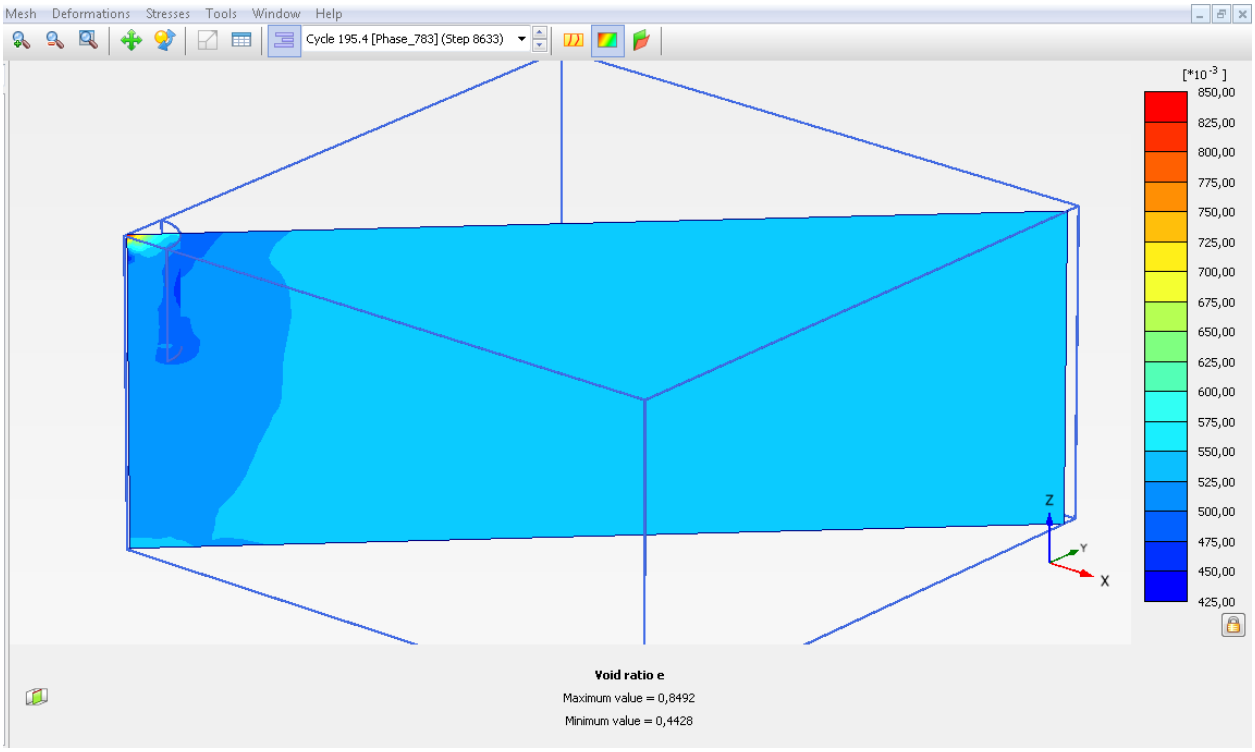

Figure G.21: Changes void ratio from EX 1 ii, 195^{th} cycle

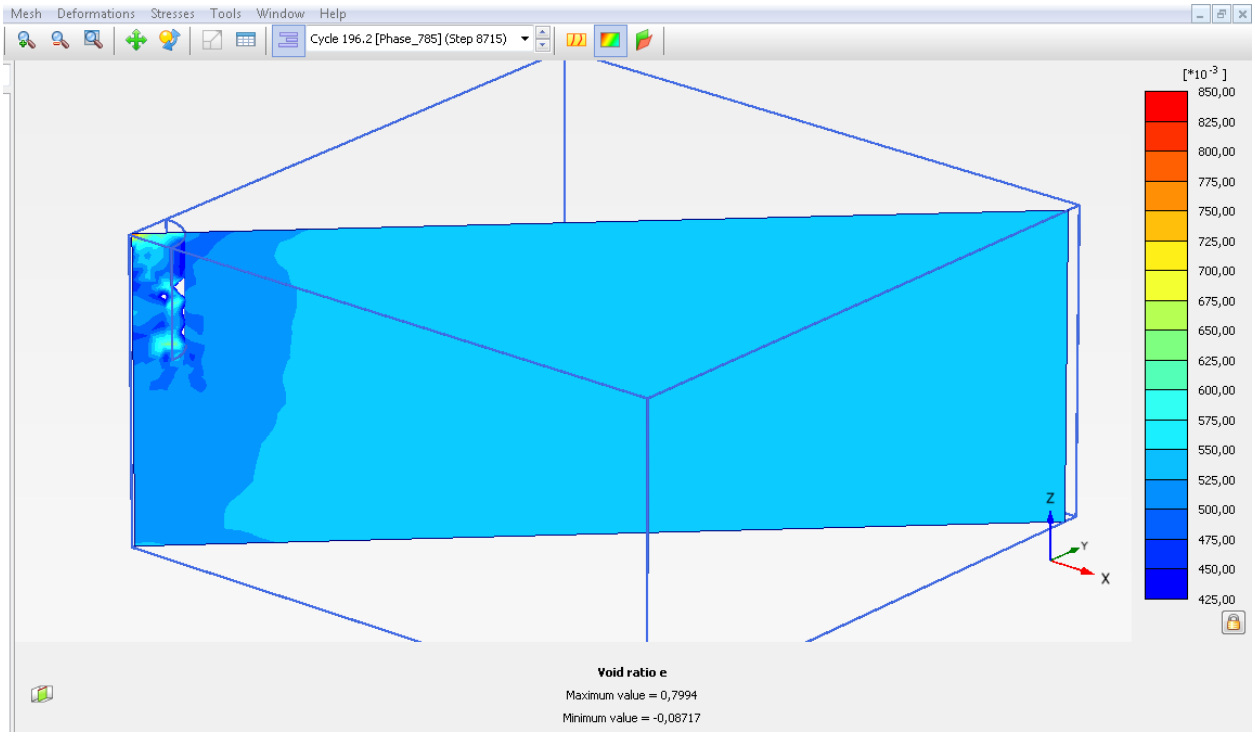

Figure G.22: Changes void ratio from EX 1 ii, 196^{th} cycle

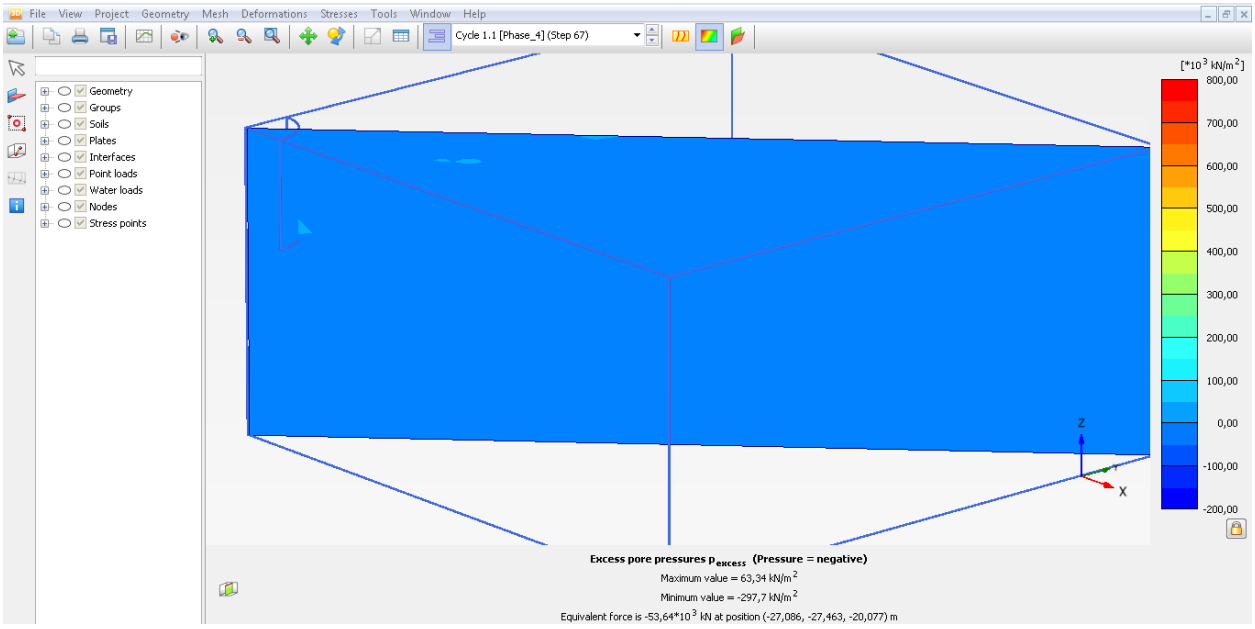

Figure G.23: Pore pressure distribution in the first phase of the first cycle for axisymmetry case EX 1ii

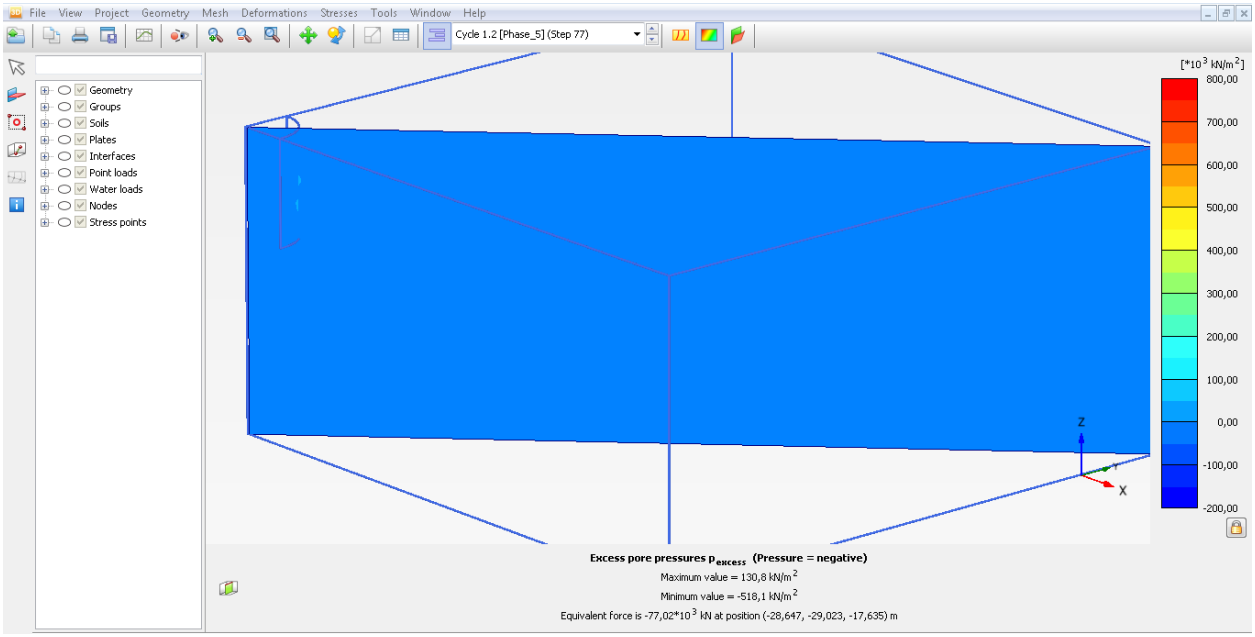

Figure G.24: Pore pressure distribution in the second phase of the first cycle for axisymmetry case EX 1ii

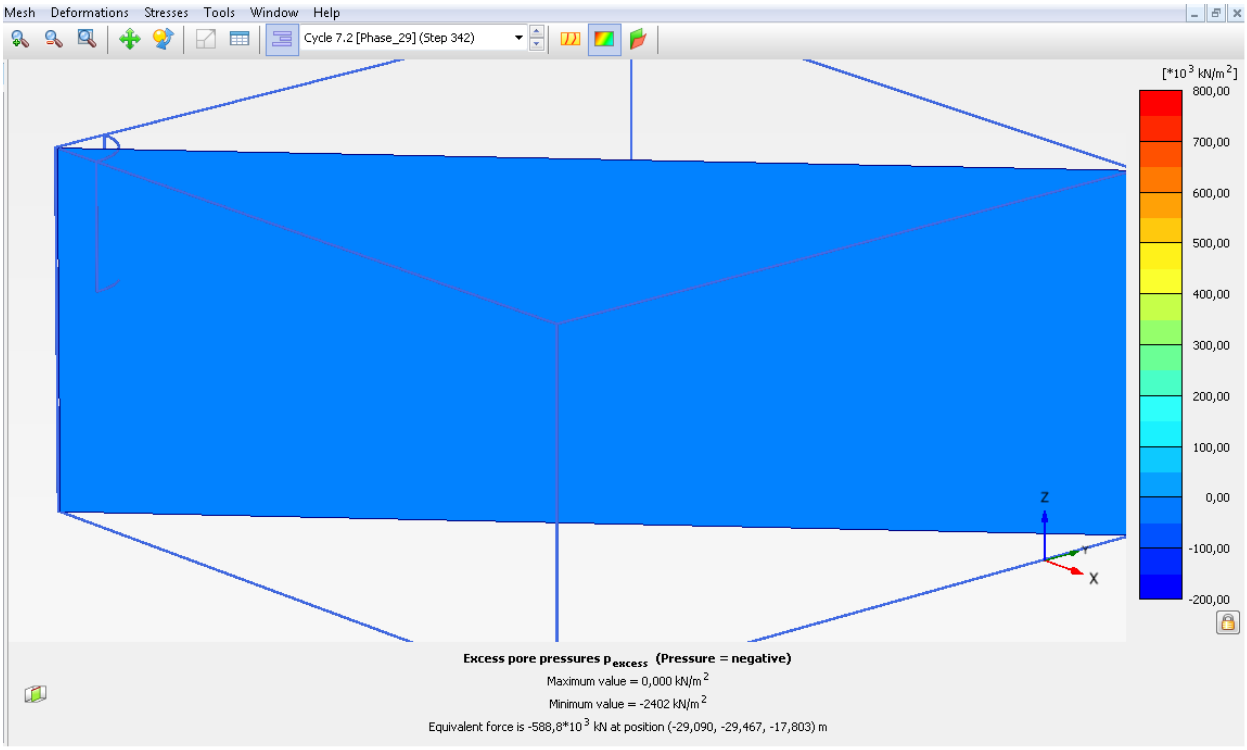

Figure G.25: Pore pressure distribution in the second phase of the seventh cycle for axisymmetry case EX 1ii

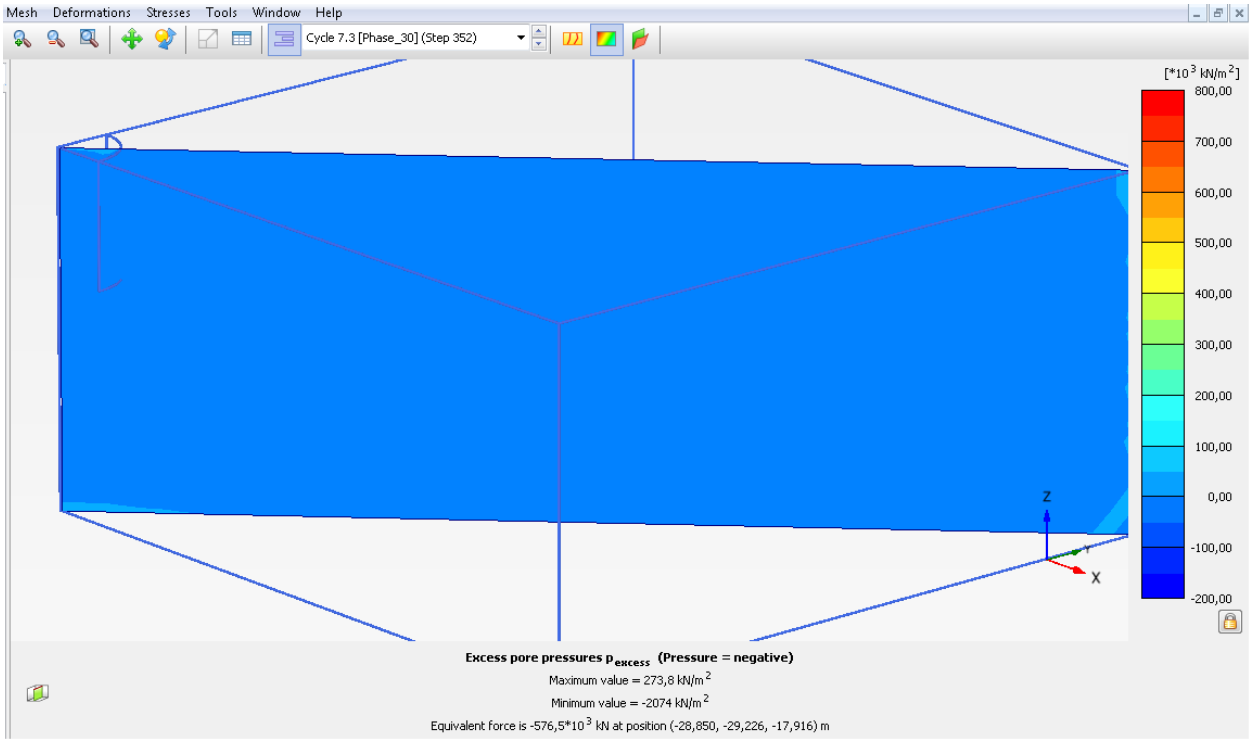

Figure G.26: Pore pressure distribution in the second phase of the seventh cycle for axisymmetry case EX 1ii—before maximum pore pressure is reached

G.3 CASE EX 2 i

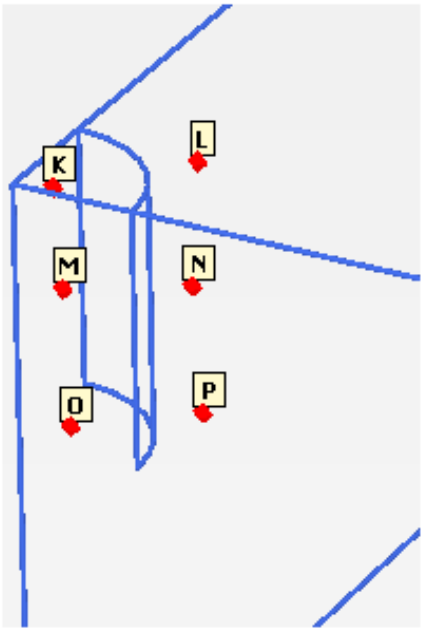

Figure G.27: Location of stress points for case EX 2 i

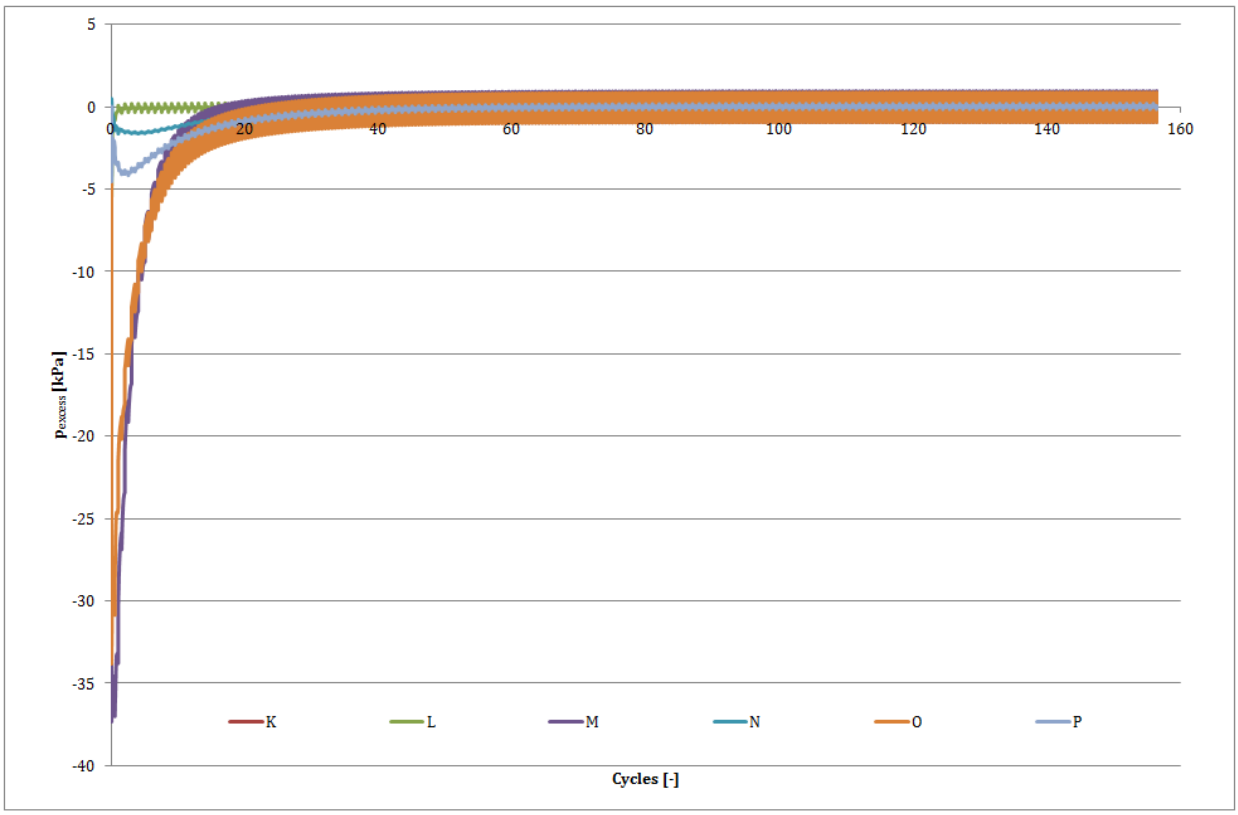

Figure G.28: Excess pore pressure in time for EX 2 i

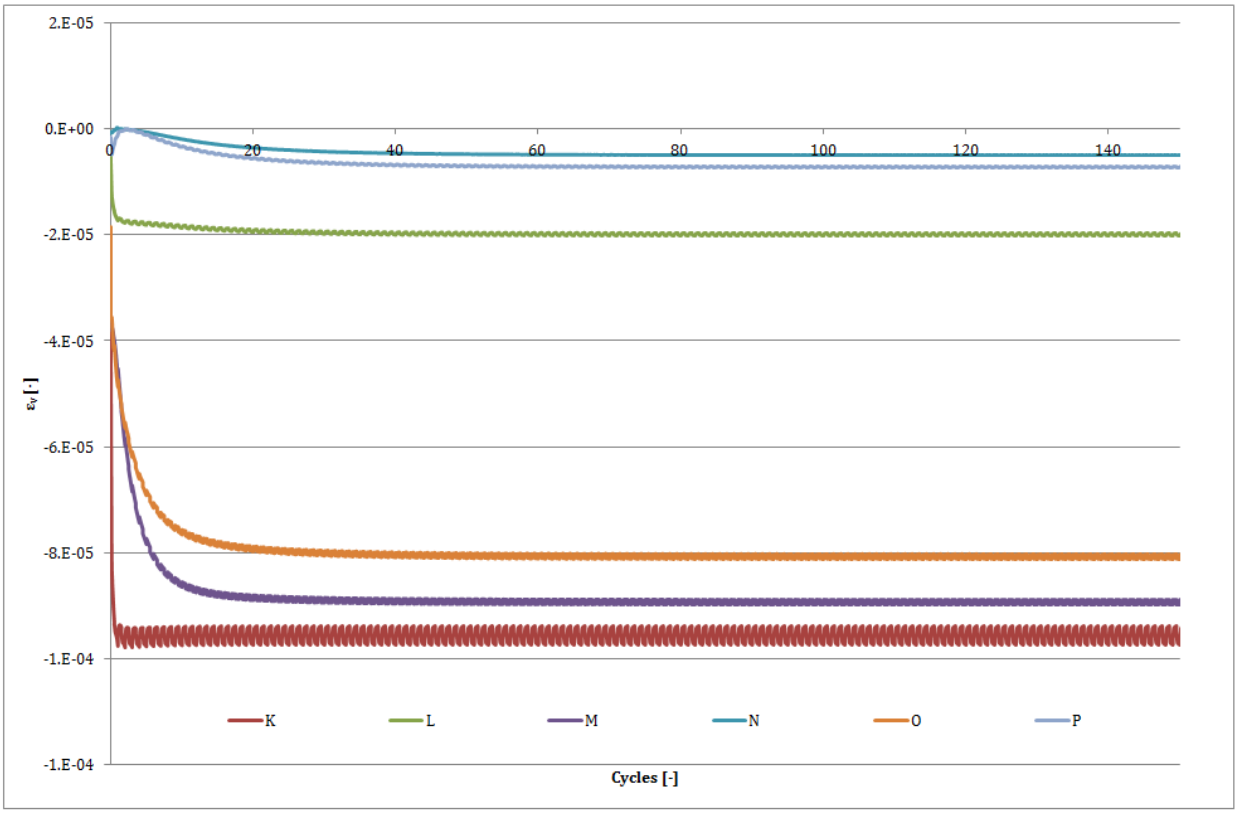

Figure G.29: Volumetric strain from EX 2 i

G.4 CASE EX 3 i

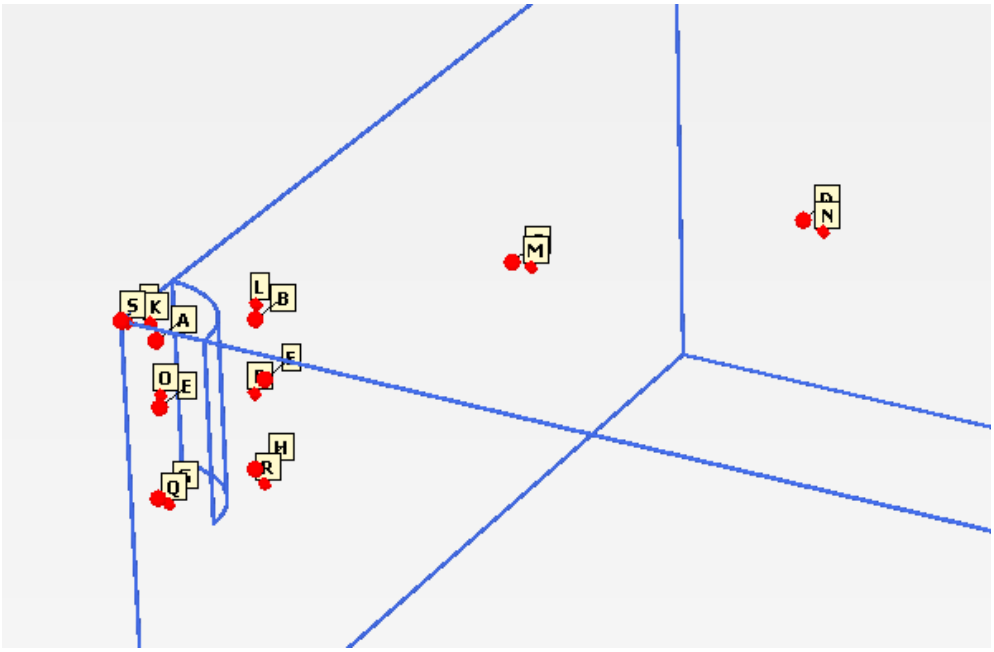

Figure G.30: Location of stress points for case EX 3 i

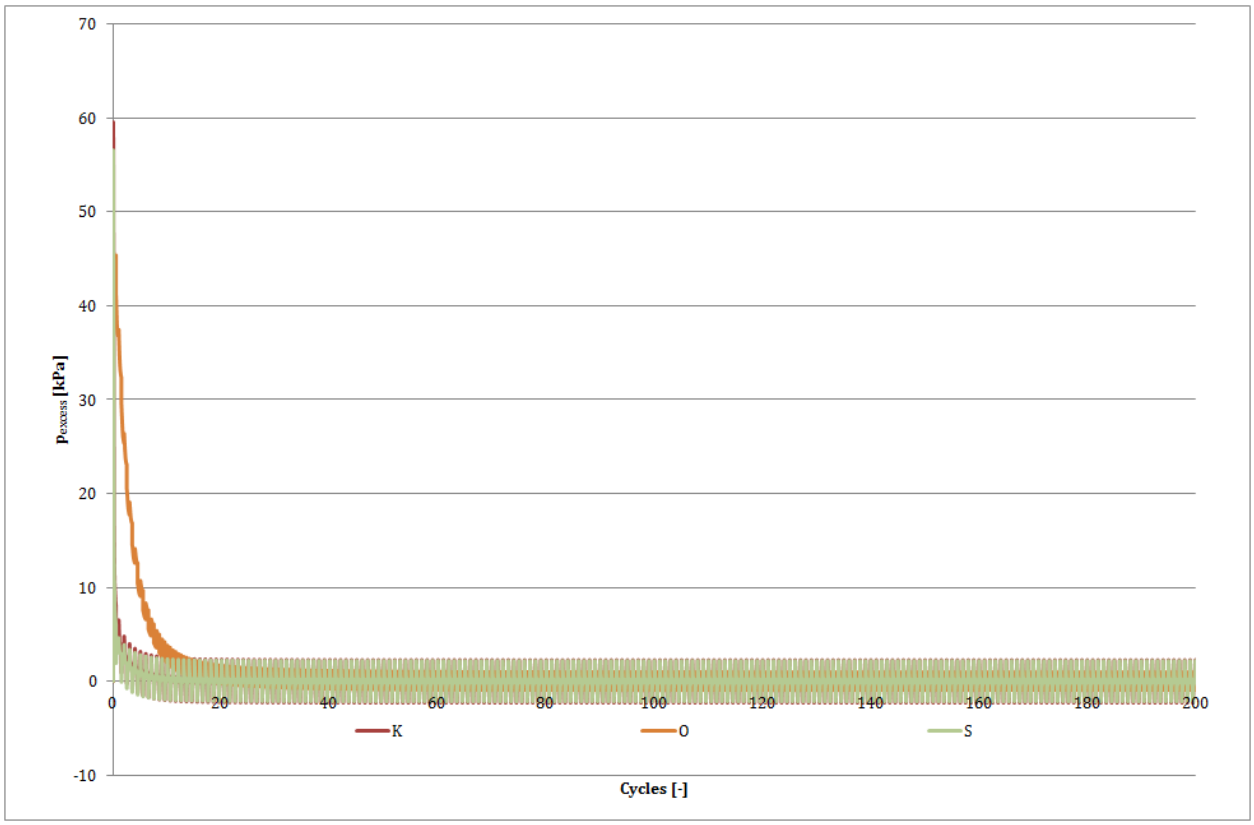

Figure G.31: Excess pore pressure in time for EX 3 i

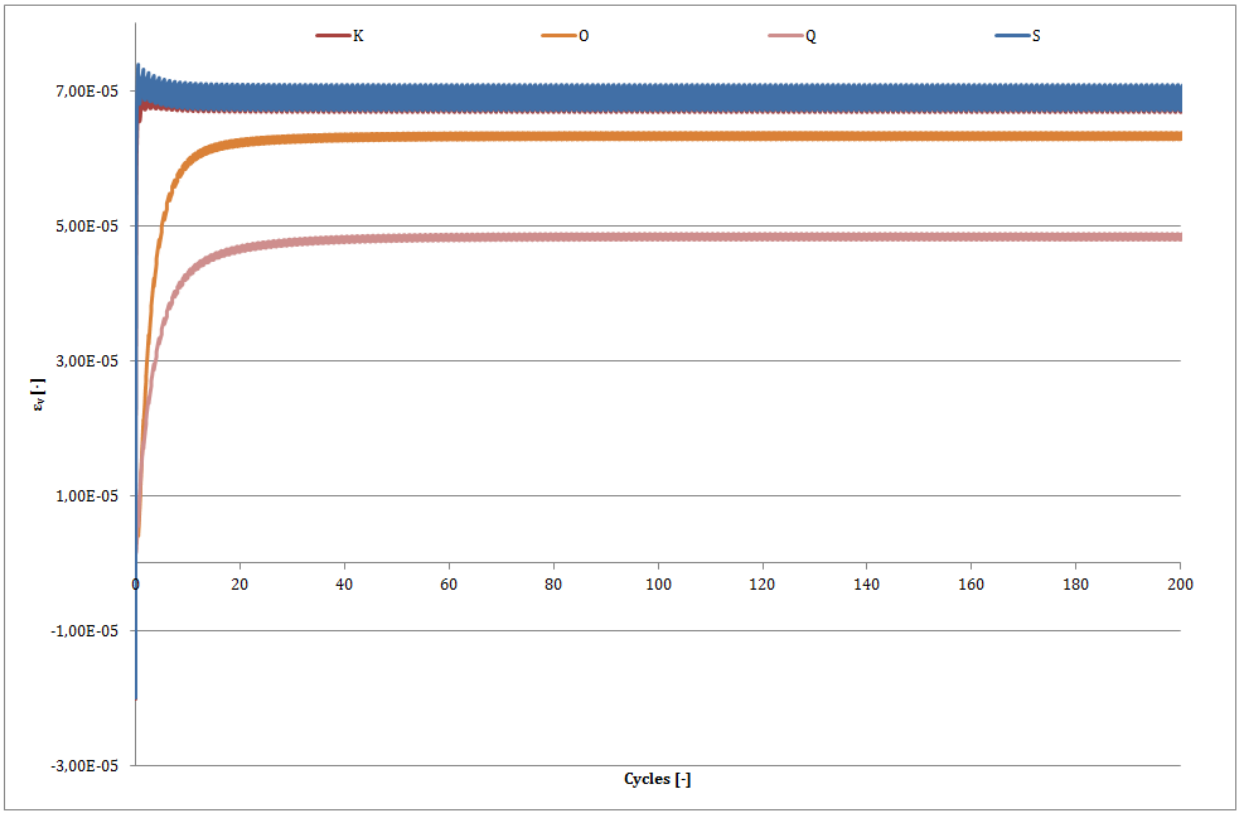

Figure G.32: Volumetric strain from EX 3 i

G.5 CASE EX 3 ii

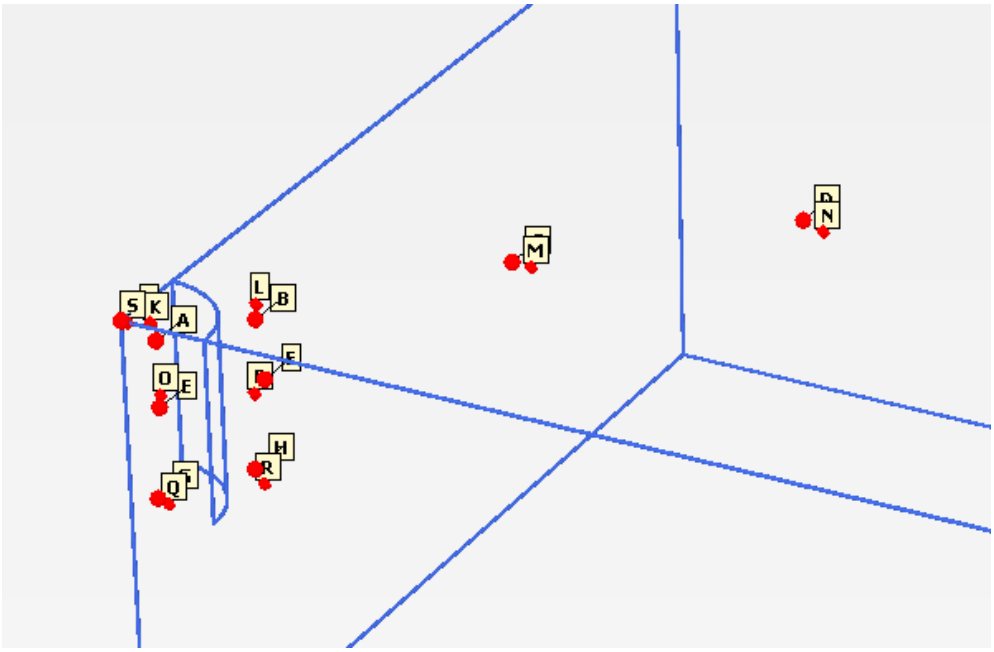

Figure G.33: Location of stress points for case EX 3 ii

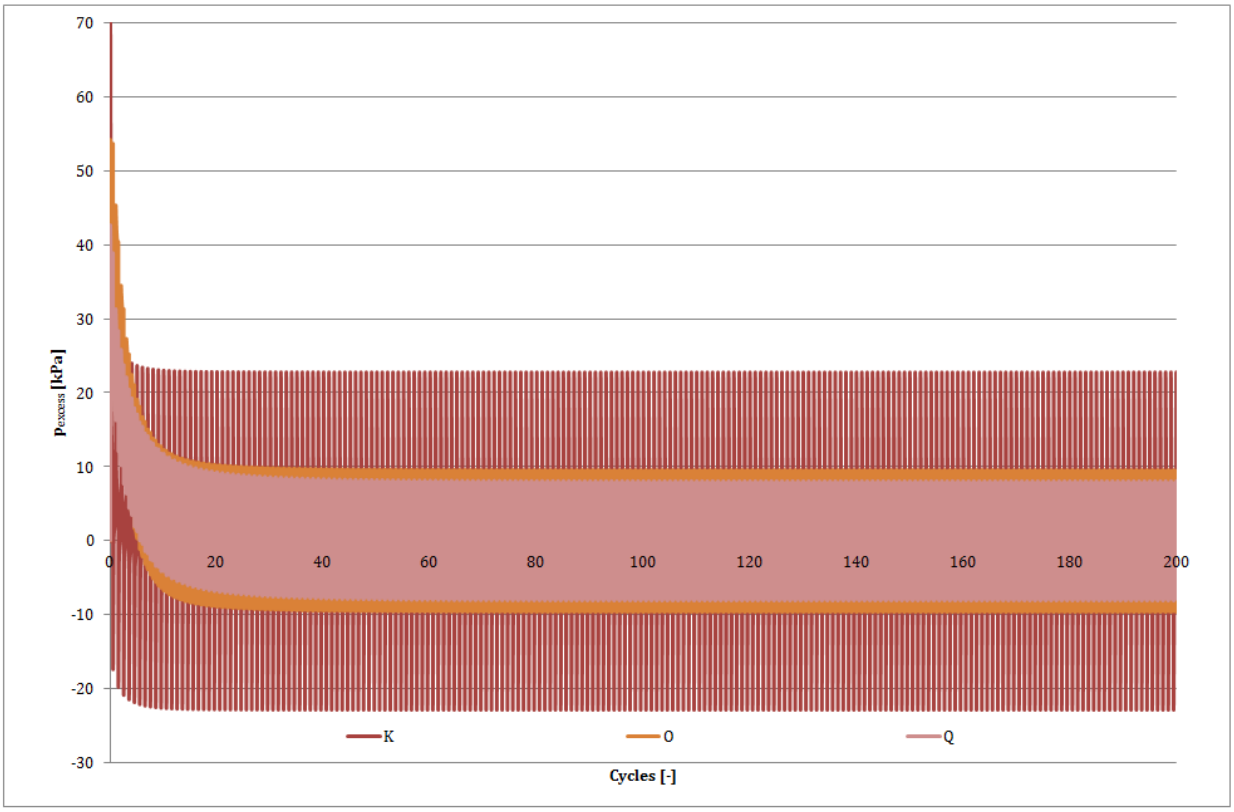

Figure G.34: Excess pore pressure in time for EX 3 ii

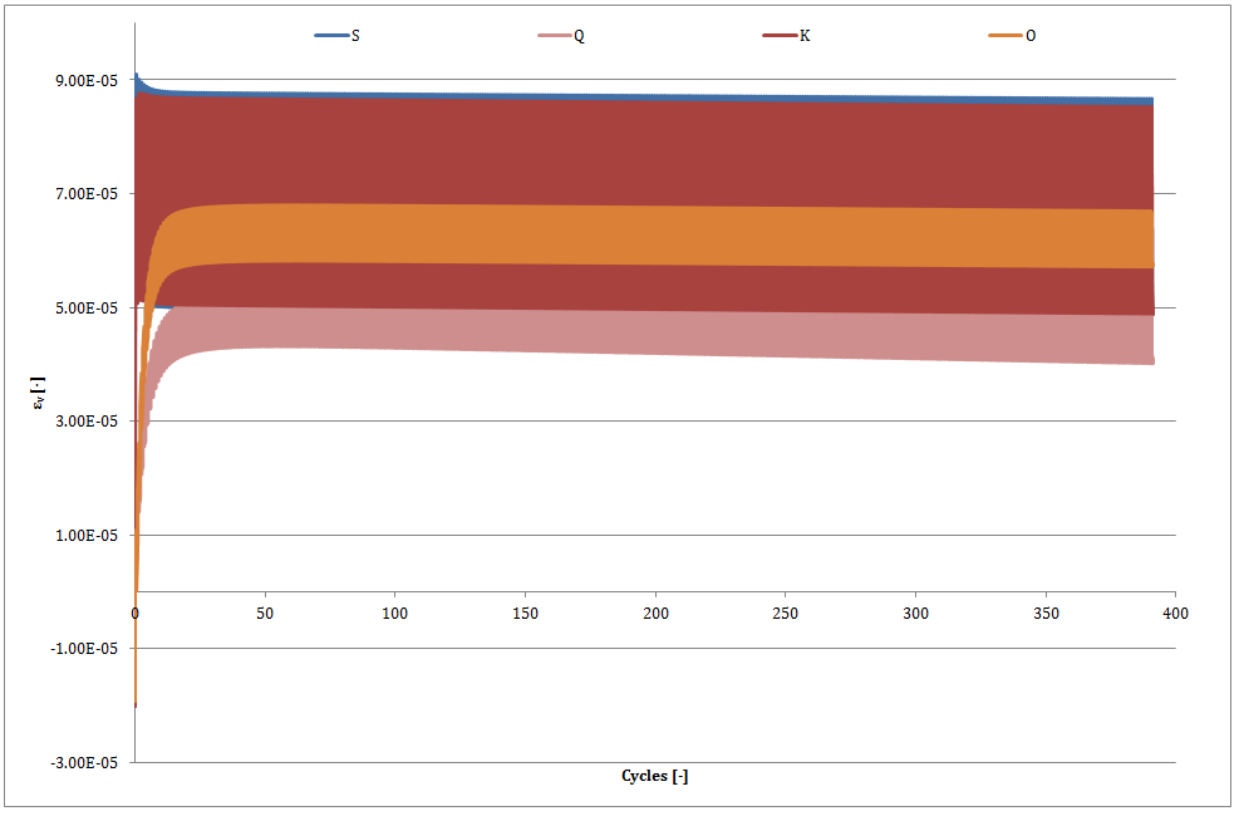

Figure G.35: Volumetric strain from EX 3 ii

Appendix H

MODEL VALIDATION RESULTS

This appendix will present the results of the three analyses carried out in order to validate the proposed model. The geometry of the problem and location of points can be found in Figure H.1. Additionally, in all cases the load is no longer applied as point loads, but as surface load. All analyses were stopped once the maximum pore pressure exceeded the vertical effective stress.

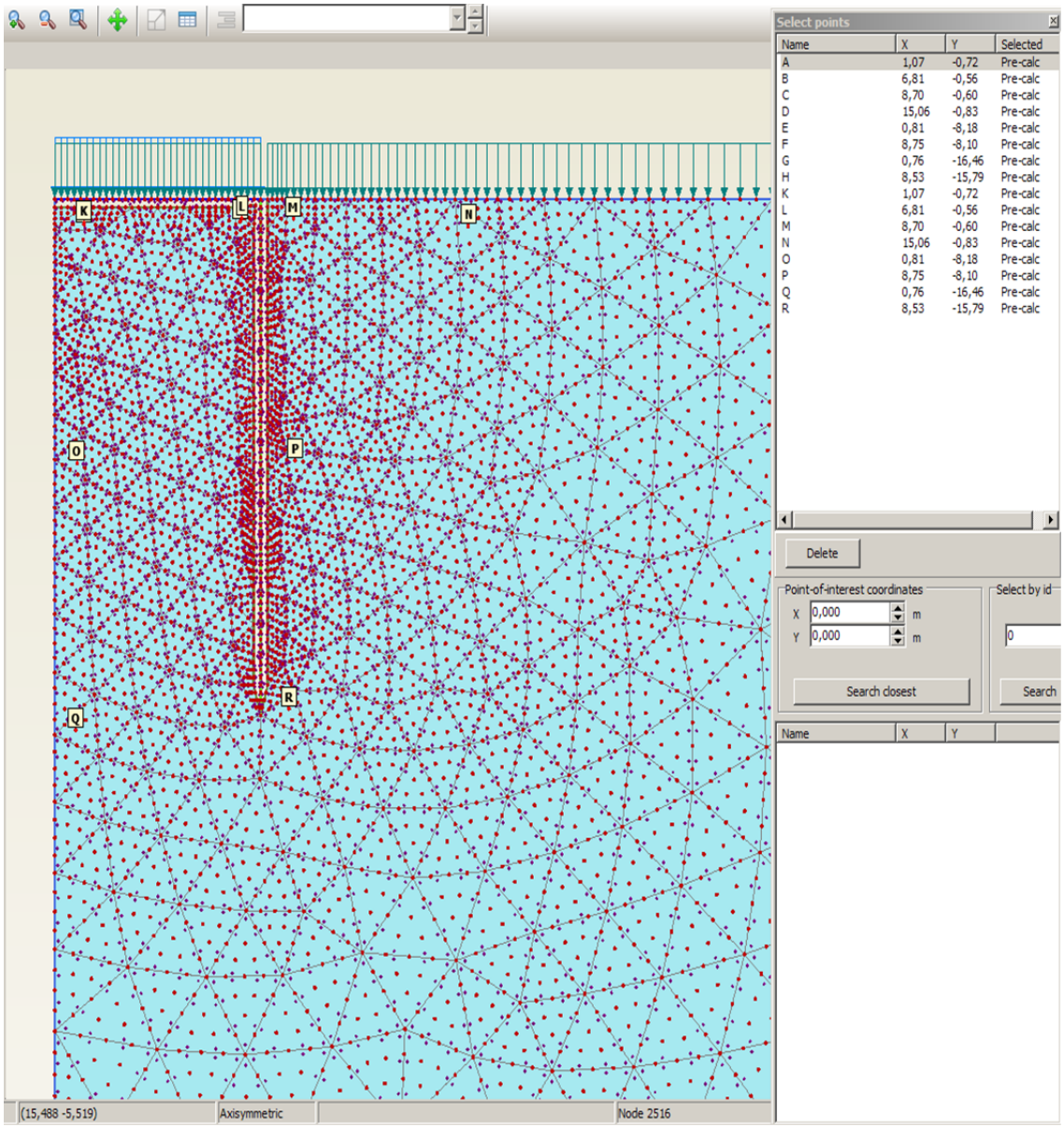

Figure H.1: Geometry and locus of stress points for the axisymmetric cases

H.1 CASE A

In case A the load was applied using 4 consolidation phases, basically the 2 plastic phases as defined in the three dimensional environment were replaced by 2 consolidation phases with a duration of 0.1 s. The test was carried out for 7 cycles until the maximum pore pressure exceeded the vertical effective stress.

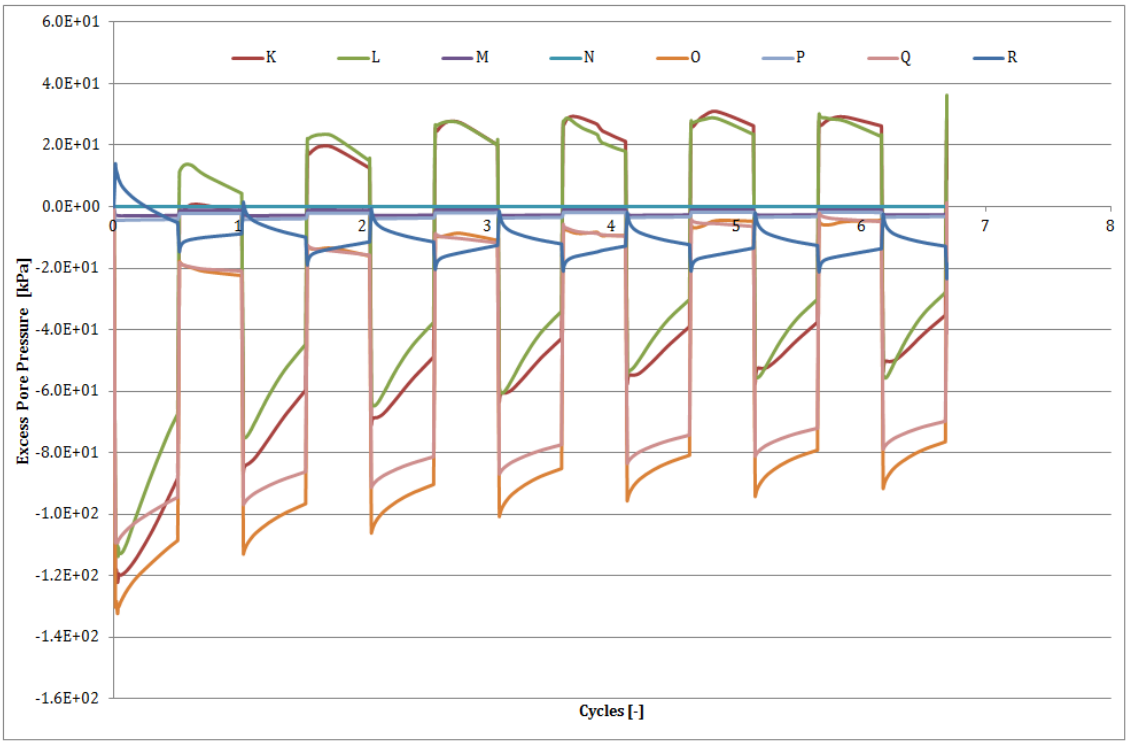

Figure H.2: Excess pore pressure with respect to the number of cycles for axisymmetry case A

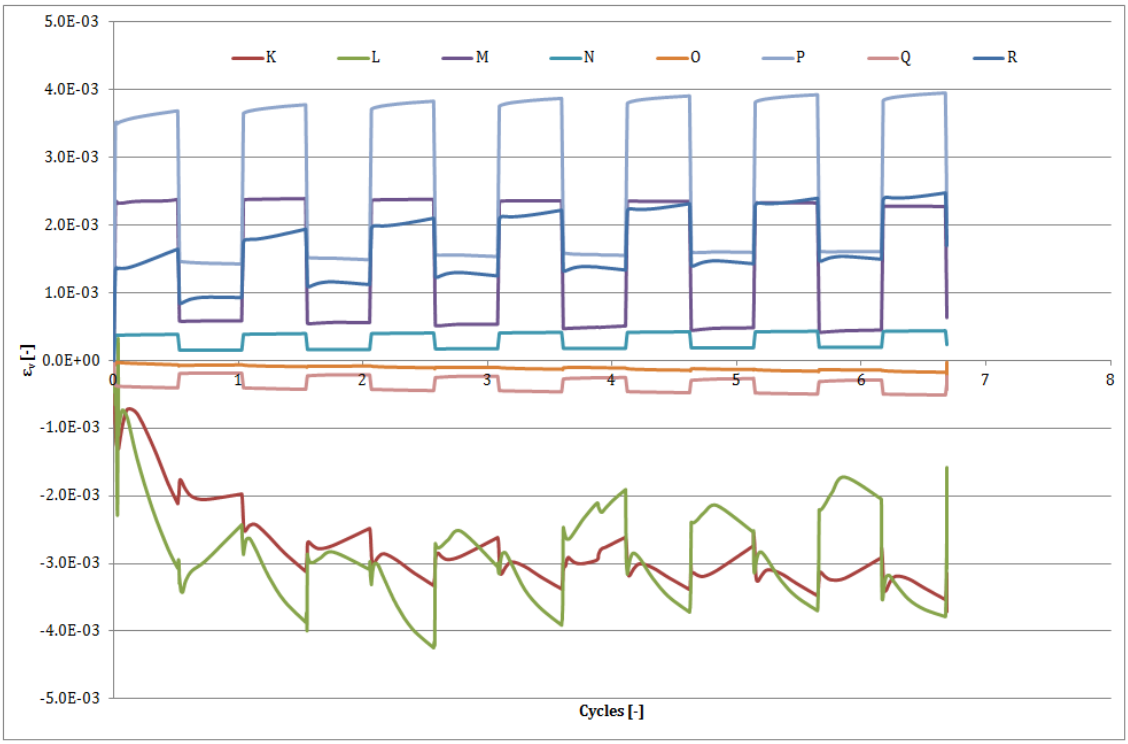

Figure H.3: Volumetric strain with respect to the number of cycles for axisymmetry case A

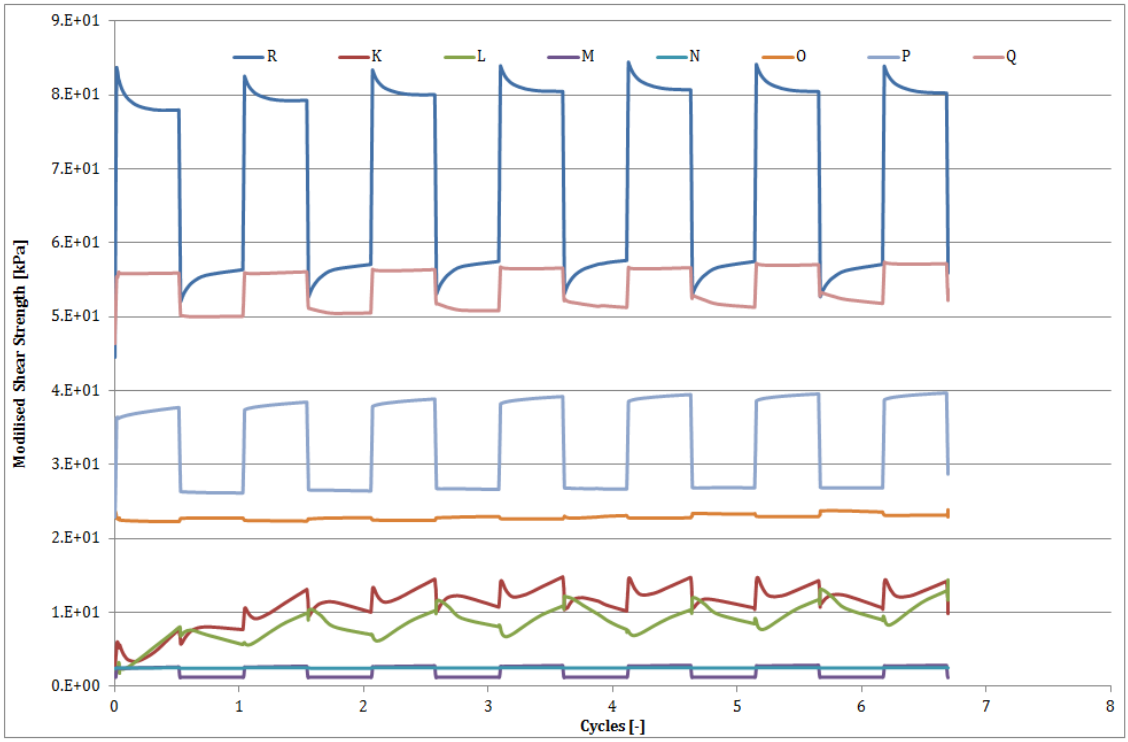

Figure H.4: Mobilised shear strength with respect to the number of cycles for axisymmetry case A

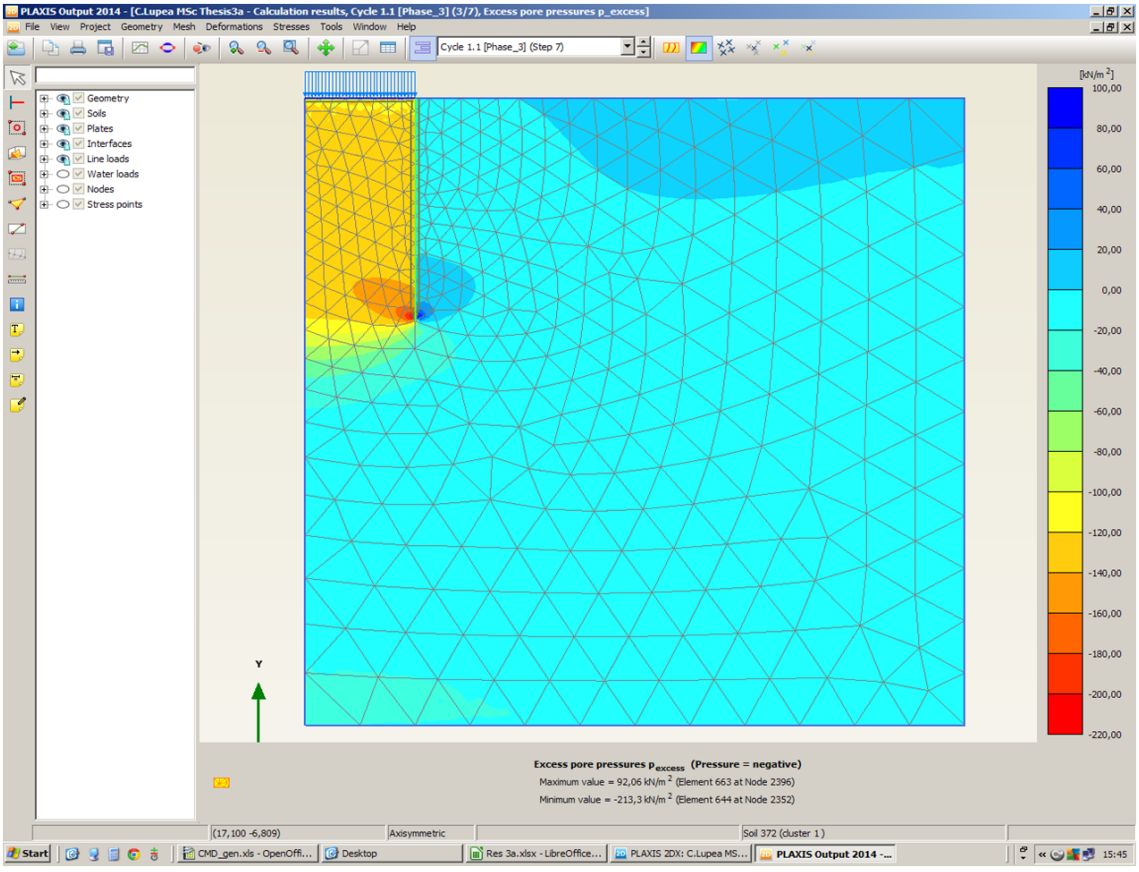

Figure H.5: Pore pressure distribution in the first phase of the first cycle for axisymmetry case A

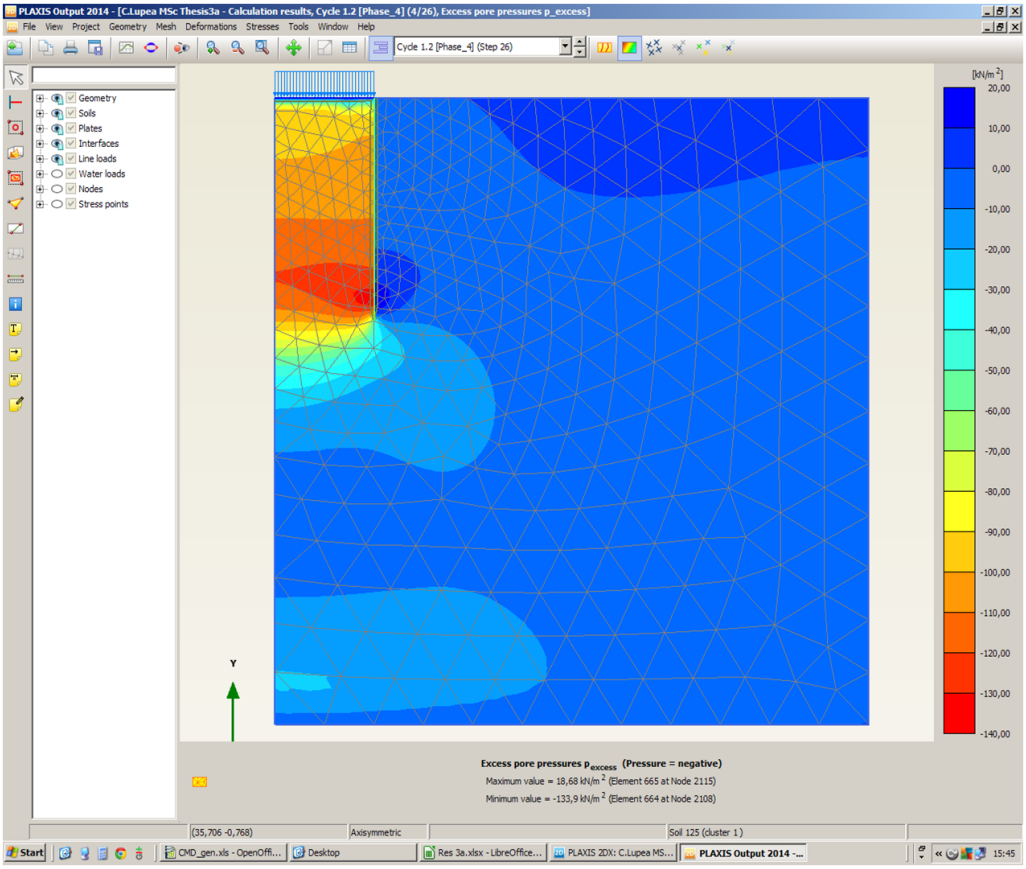

Figure H.6: Pore pressure distribution in the second phase of the first cycle for axisymmetry case A

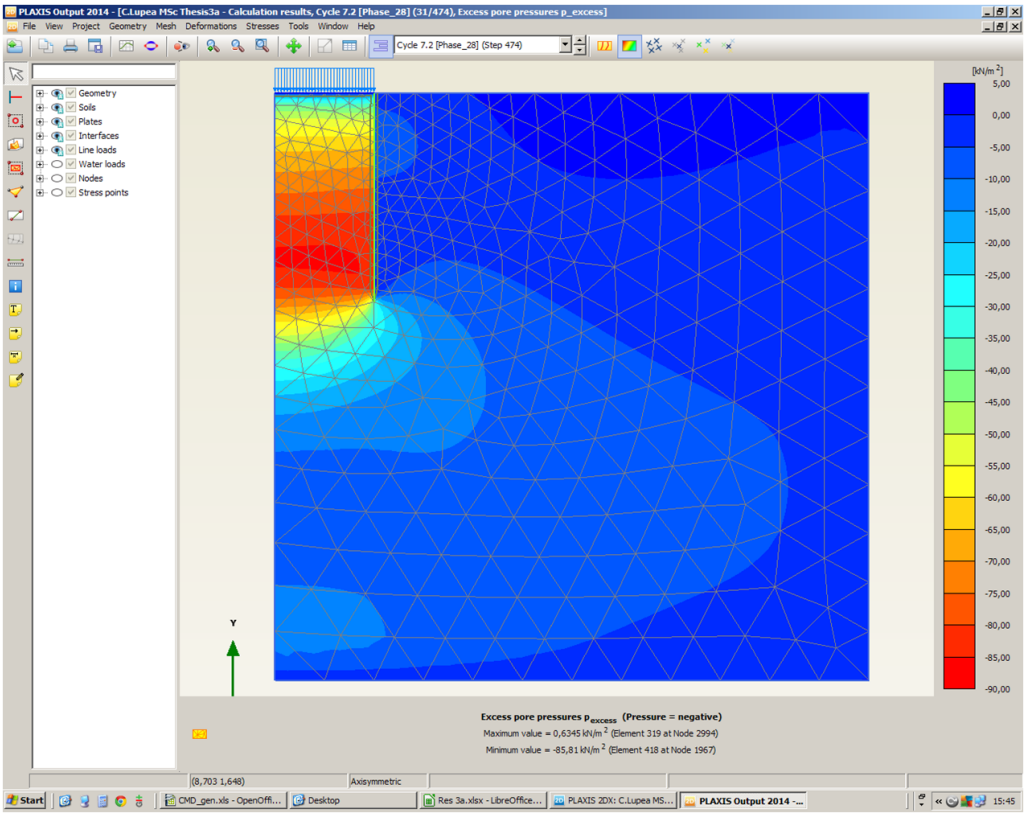

Figure H.7: Pore pressure distribution in the second phase of the seventh cycle for axisymmetry case A

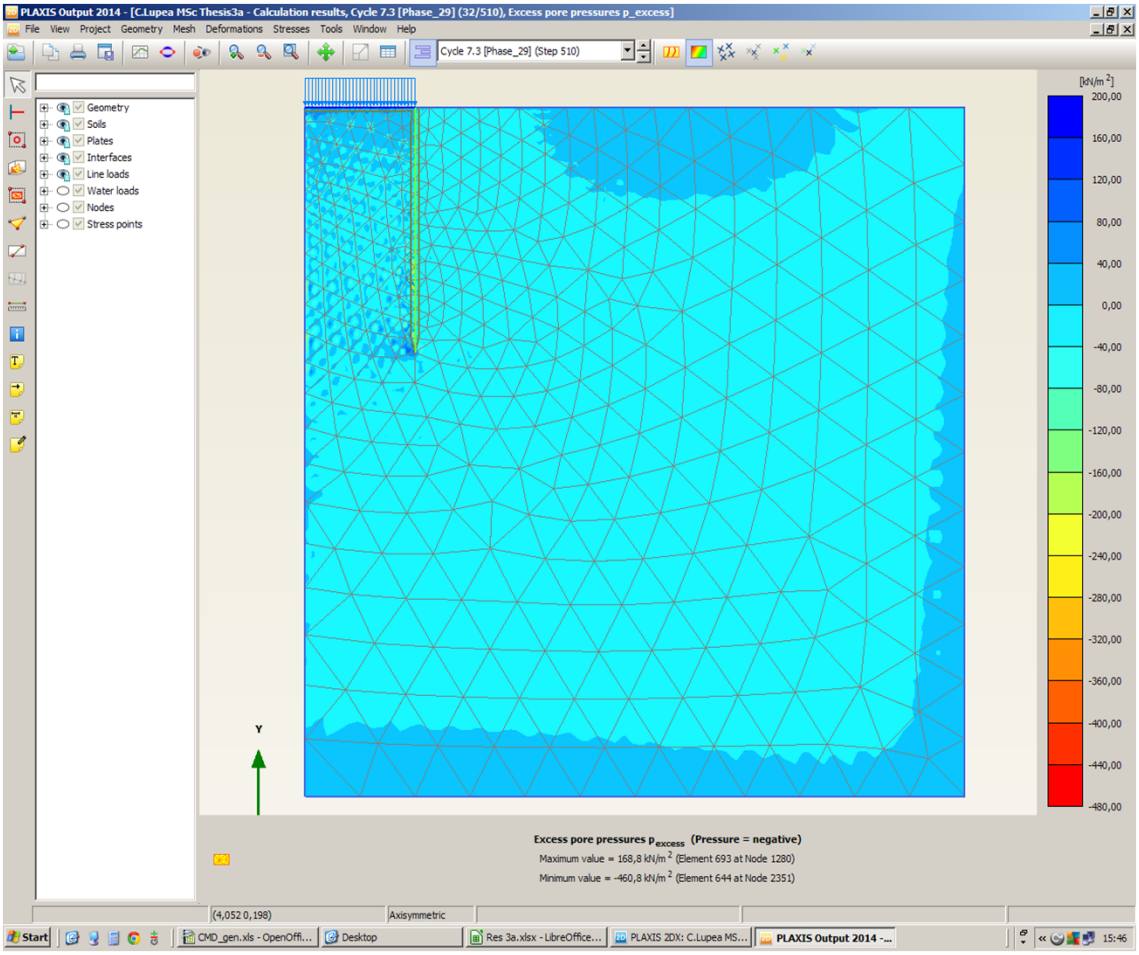

Figure H.8: Pore pressure distribution in the second phase of the seventh cycle for axisymmetry case A—before maximum pore pressure is reached

H.2 CASE B

In case B the load was applied in 4 phases as described in subsection 5.2.4, 2 plastic phases on instantaneous loading each followed by a very short consolidation phase. The test was carried out for the first cycle when the maximum pore pressure exceeded the vertical effective stress.

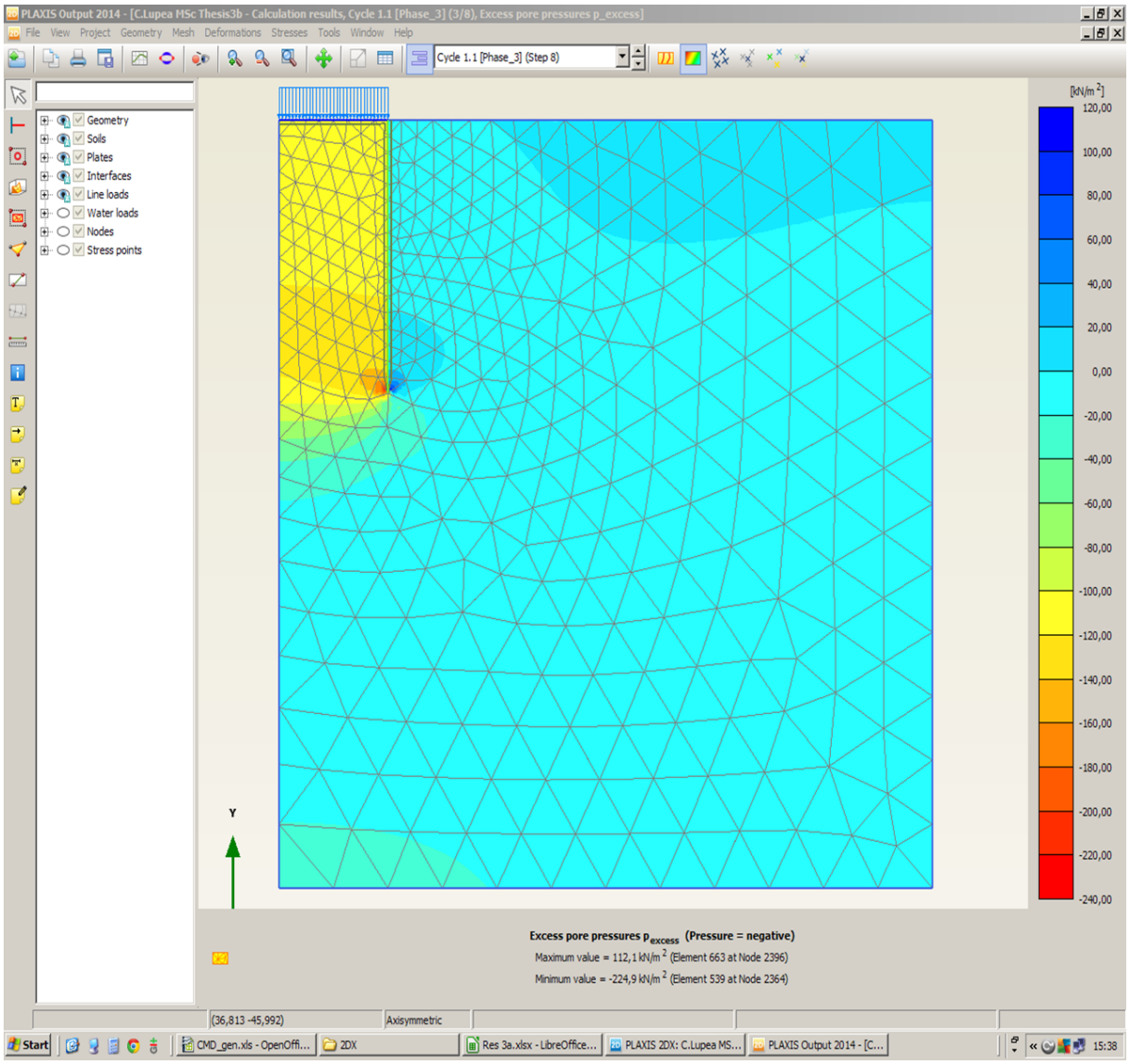

Figure H.9: Pore pressure distribution in the first phase of the first cycle for axisymmetry case B

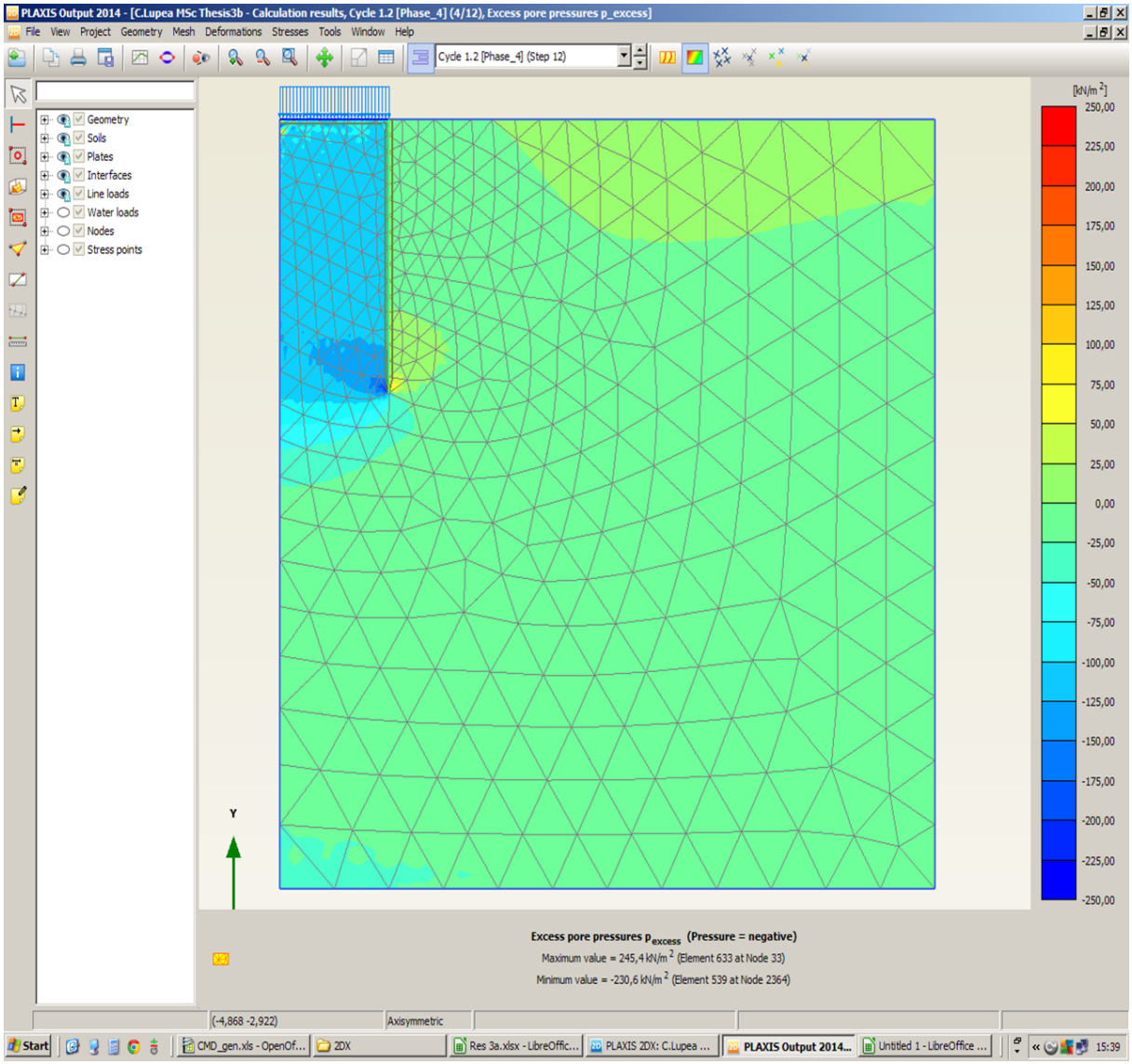

Figure H.10: Pore pressure distribution in the second phase of the first cycle for axisymmetry case B—before maximum pore pressure is reached

H.3 CASE C

In case C the load was applied using 4 consolidation phases, basically the 2 plastic phases as defined in the three dimensional environment were replaced by 2 consolidation phases with a duration of 0.01 s. The test was carried out for 1 cycle until the maximum pore pressure exceeded the vertical effective stress.

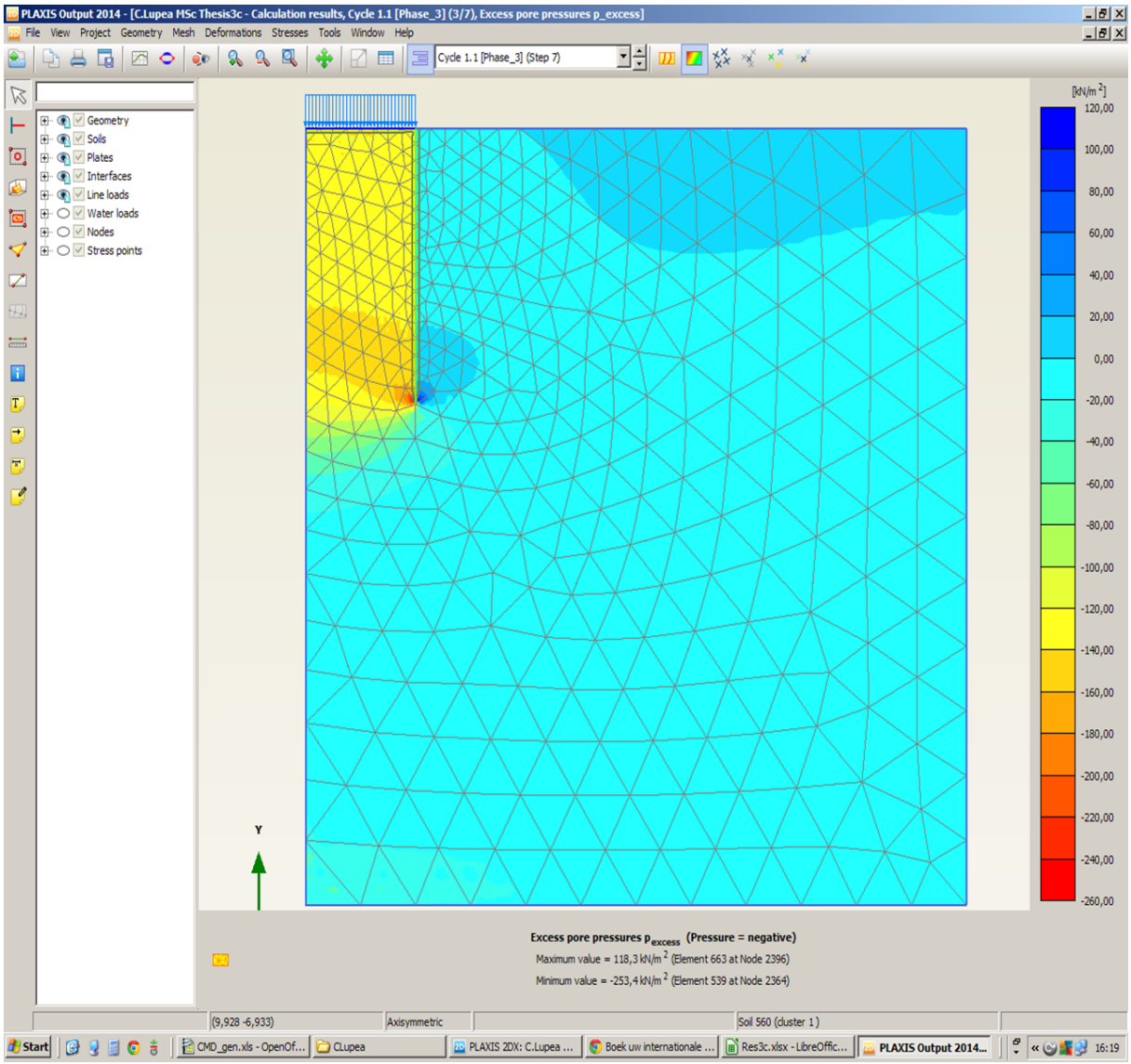

Figure H.11: Pore pressure distribution in the first phase of the first cycle for axisymmetry case C

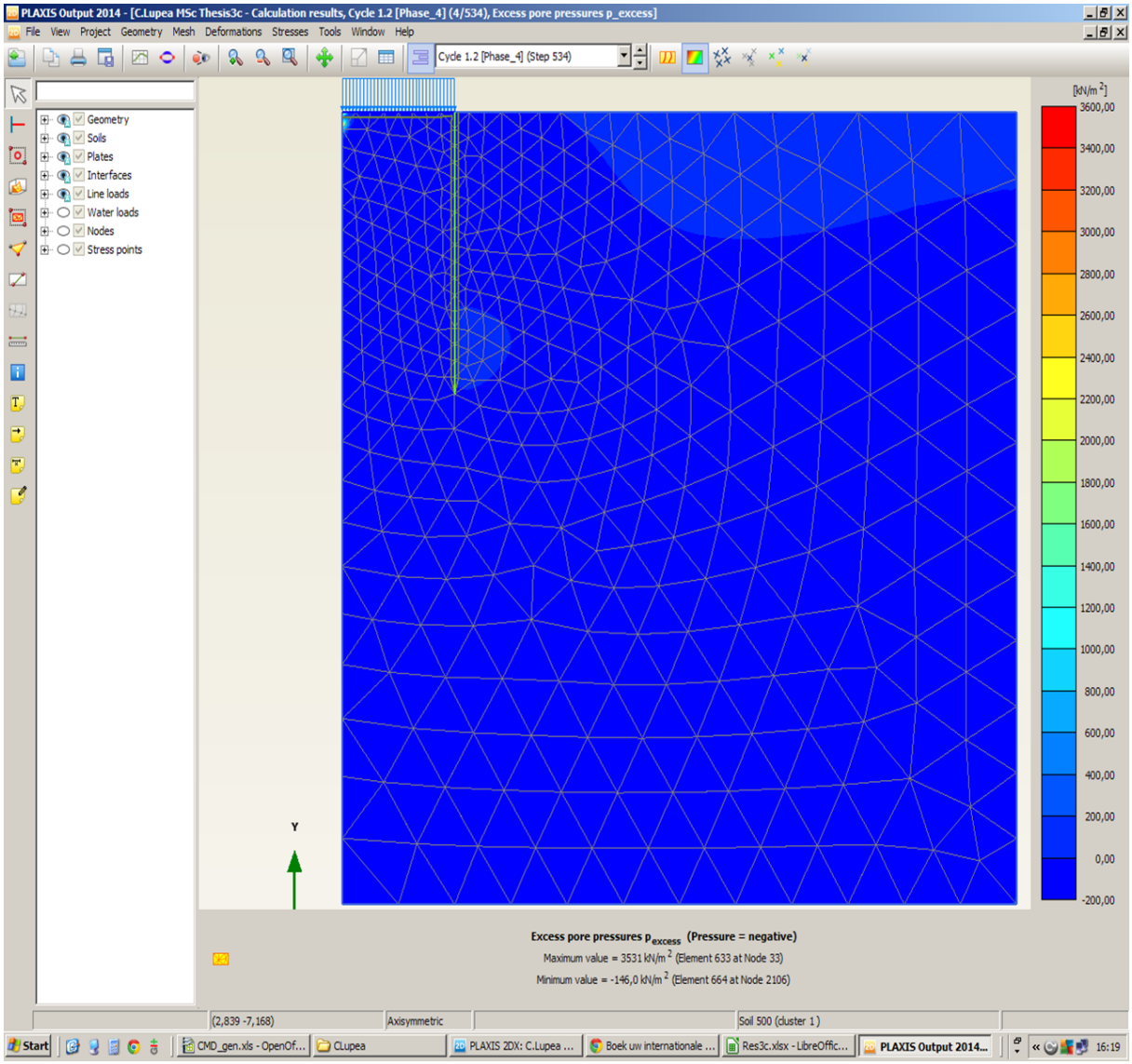

Figure H.12: Pore pressure distribution in the second phase of the first cycle for axisymmetry case C—before maximum pore pressure is reached

H.4 CASE D

In case D the load was applied using 4 consolidation phases, basically the 2 plastic phases as defined in the three dimensional environment were replaced by 2 consolidation phases with a duration of 0.05 s. The test was carried out for 1 cycle until the maximum pore pressure exceeded the vertical effective stress.

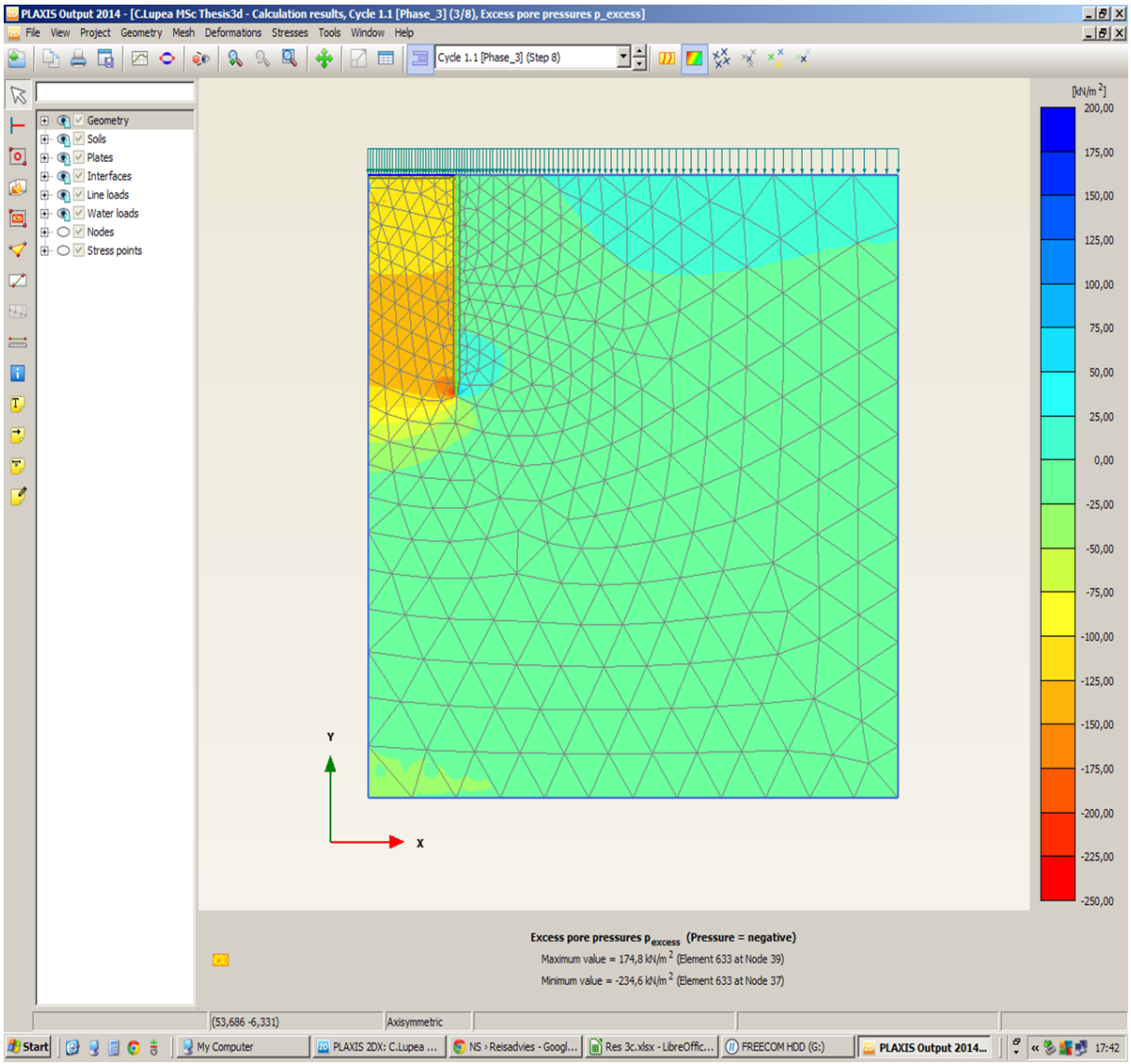

Figure H.13: Pore pressure distribution in the first phase of the first cycle for axisymmetry case D

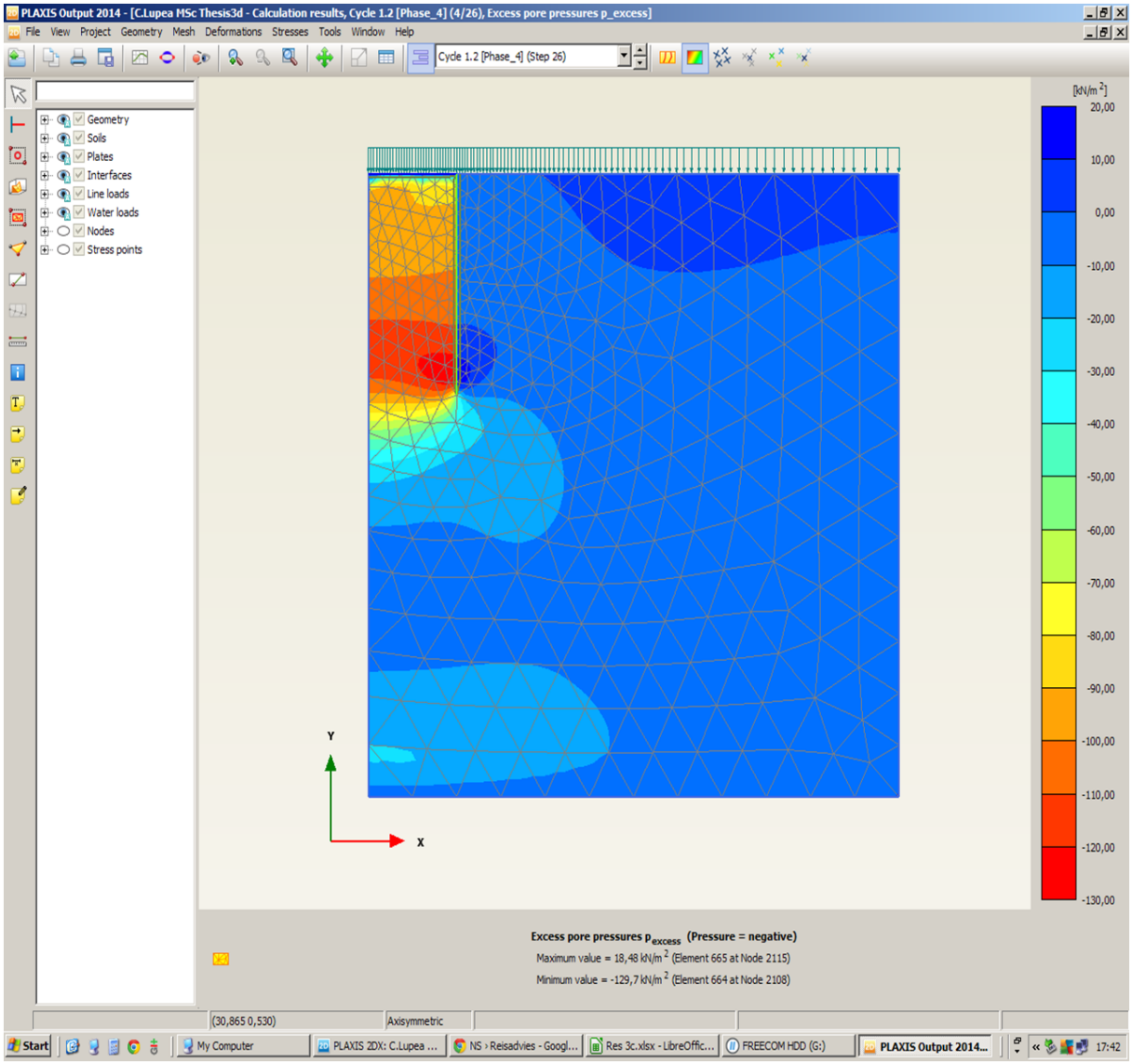

Figure H.14: Pore pressure distribution in the second phase of the first cycle for axisymmetry case D

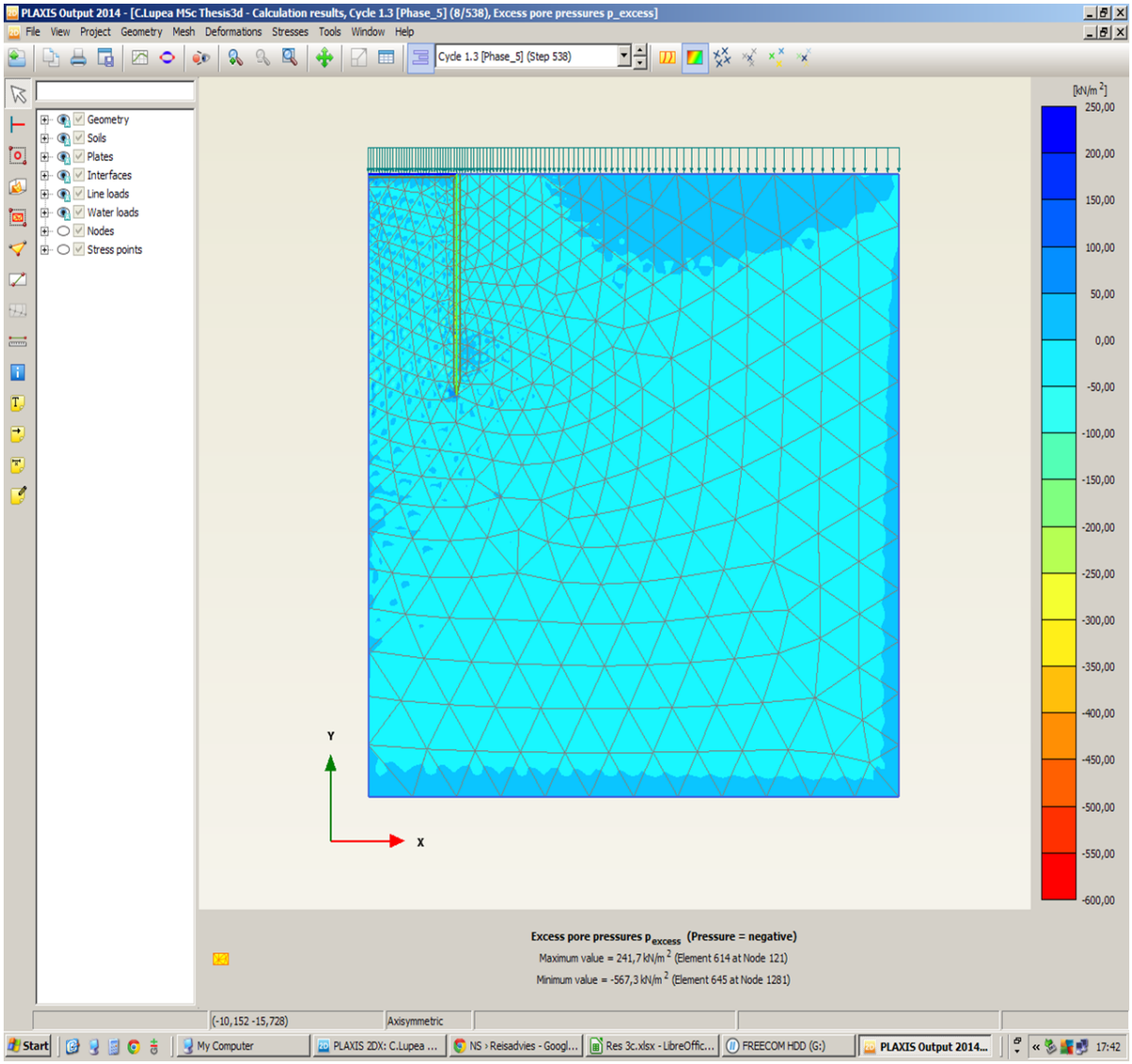

Figure H.15: Pore pressure distribution in the third phase of the first cycle for axisymmetry case D—before maximum pore pressure is reached

Appendix I

RESULTS OF LOAD IMPACT ANALYSIS

This appendix presents the summary of the results of the analyses carried out in order to determine the impact of the applied load in determining the dominantly hypoelastic or dominantly hypoplastic behaviour of the foundation (Figure 6.6). The choice between the dominance of one of the two behaviours was based on the potential change in void ratio over 10^6 cycles, assuming a linear accumulation of the volumetric strain.

Case ID	Mean Load	Amplitude	Hypo-behaviour assessment								
			Cycle(s) - N	ε_v	$\Delta\varepsilon_v$	$\Delta\varepsilon_v/N$	e	N	$\Delta\varepsilon_v$	e_{1e6}	
H1	-17595	4399	N/A					1.00E+06			Hypo-plastic
H2	-17595	3519	0	-7.17E-05							
			91	-7.25E-05	-8.00E-07	-8.7E-09	0.539999		-8.7E-03	0.527	Hypo-elastic
H3	-6600	1700	0	-3.50E-05							
			120	-3.55E-05	-5.00E-07	-4.1E-09	0.539999		-4.1E-03	0.534	Hypo-elastic
H4	-6600	3519	0	-2.77E-05							
			200	-2.90E-05	-1.30E-06	-6.5E-09	0.539998		-6.5E-03	0.530	Hypo-elastic
H5	-6600	17595	0	-3.00E-05							
			299	-1.70E-04	-1.40E-04	-4.7E-07	0.539784		-4.7E-01	0.179	Hypo-plastic
H6	-35189	500	0	-1.06E-04							
			165	-1.06E-04	-3.00E-07	-1.8E-09	0.540000		-1.8E-03	0.537	Hypo-elastic
H7	-35189	2500	0	-1.06E-04							
			253	-1.07E-04	-1.00E-06	-3.9E-09	0.539998		-3.9E-03	0.534	Hypo-elastic
H8	-35189	3519	0	-1.04E-04							
			186	-1.07E-04	-2.50E-06	-1.34E-08	0.539996		-1.3E-02	0.519	Hypo-plastic
H9	-6600	3167	0	-7.53E-05							
			185	-7.72E-05	-1.90E-06	-1.0E-08	0.539997		-1.0E-02	0.524	Hypo-elastic
H10	-6600	9853	0	-3.00E-05							
			200	-5.30E-05	-2.30E-05	-1.1E-07	0.539965		-1.1E-01	0.364	Hypo-plastic
H11	-6600	12668	0	-3.50E-05							
			200	-7.50E-05	-4.00E-05	-2.0E-07	0.539938		-2.0E-01	0.234	Hypo-plastic
H12.13	0	24791	0	-3.00E-05							
			200	-2.00E-04	-1.70E-04	-8.5E-07	0.539738		-8.5E-01	0.762	Hypo-plastic
H14.15	0	17353	0	-1.00E-05							
			200	-9.00E-05	-8.00E-05	-4.0E-07	0.539877		-4.0E-01	0.073	Hypo-plastic
H16	-45746	500	0	-1.68E-04							
			173	-1.67E-04	2.00E-07	1.1E-09	0.540000		1.1E-03	0.542	Hypo-elastic
H17	-45746	1500	0	-1.33E-04							
			173	-1.36E-04	-2.80E-06	-1.6E-08	0.539996		-1.6E-02	0.515	Hypo-plastic
H18	-45746	3000	0	-1.34E-04							
			172	-1.37E-04	-2.50E-06	-1.4E-08	0.539996		-1.4E-02	0.518	Hypo-plastic
H19	-52784	1500	0	-1.53E-04							
			173	-1.55E-04	-2.00E-06	-1.15E-08	0.539997		-1.1E-02	0.522	Hypo-plastic
H20	-52784	2500	0	-1.53E-04							
			173	-1.56E-04	-2.70E-06	-1.5E-08	0.539996		-1.5E-02	0.516	Hypo-plastic
H21	-63341	500	0	-1.82E-04							
			173	-1.85E-04	-2.70E-06	-1.5E-08	0.539996		-1.5E-02	0.516	Hypo-plastic
H22	-63341	1500	0	-1.82E-04							
			173	-1.85E-04	-2.70E-06	-1.5E-08	0.539996		-1.5E-02	0.516	Hypo-plastic
H23	-52784	500	N/A								Hypo-plastic
H24	-63341	100	0	-1.76E-04							
			110	-1.84E-04	-8.00E-06	-7.2E-08	0.539988		-7.2E-02	0.429	Hypo-plastic
H26.27	0	2479	0	-8.12E-06							
			173	-8.78E-06	-6.58E-07	-3.8E-09	0.539999		-3.8E-03	0.534	Hypo-elastic
H28.29	0	4223	0	-2.84E-05							
			193	-3.66E-05	-8.22E-06	-4.2E-08	0.539987		-4.2E-02	0.475	Hypo-plastic
H30.31	0	7038	0	-1.22E-05							
			253	-2.50E-05	-1.28E-05	-5.0E-08	0.539980		-5.0E-02	0.462	Hypo-plastic
H32.33	0	4958	0	-7.50E-06							
			253	-2.00E-05	-1.25E-05	-4.9E-08	0.539981		-4.9E-02	0.464	Hypo-plastic
H34	4958	4958	0	6.00E-06							
			253	-3.00E-06	-9.00E-06	-3.5E-08	0.539986		-3.5E-02	0.485	Hypo-plastic
H35	4958	3471	0	5.00E-06							
			193	0.00E+00	-5.00E-06	-2.6E-08	0.539992		-2.6E-02	0.500	Hypo-plastic
H36	9916	3471	0	2.25E-05							
			193	1.75E-05	-5.00E-06	-2.6E-08	0.539992		-2.6E-02	0.500	Hypo-plastic
H37	9916	2479	0	3.10E-05							
			193	2.84E-05	-2.59E-06	-1.3E-08	0.539996		-1.3E-02	0.519	Hypo-plastic
H38	14874	2479	0	2.98E-05							
			193	2.70E-05	-2.76E-06	-1.4E-08	0.539996		-1.4E-02	0.518	Hypo-plastic
H39	14874	1735	0	2.42E-05							
			193	2.26E-05	-1.60E-06	-8.2E-09	0.539998		-8.2E-03	0.527	Hypo-elastic
H40	4958	2479	0	-4.90E-06							
			184	-6.75E-06	-1.85E-06	-1.0E-08	0.539997		-1.0E-02	0.525	Hypo-elastic
H41	9916	1735	0	2.81E-05							
			186	2.67E-05	-1.40E-06	-7.5E-09	0.539998		-7.5E-03	0.528	Hypo-elastic
H42	20200	1000	0	4.26E-05							
			186	4.19E-05	-6.70E-07	-3.6E-09	0.539999		-3.6E-03	0.534	Hypo-elastic

Figure I.1: Characteristics of load impact scenarios and obtained results (extrapolation of volumetric strain was done using equation 5.6)

Bibliography

K. H. Andersen (2009). Bearing capacity under cyclic loading -offshore, along the coast, and on land. the 21st bjerrum lecture presented in oslo, 23 november 2007. *Canadian Geotechnical Journal*, 46(5):513–535.

API (2011). *Geotechnical and Foundation Design Considerations*. American Petroleum Institute, 1st edition.

API & ISO19901-4 (2000). *Recommended practice for planning, designing and constructing fixed offshore platforms—Working Stress Design*. American Petroleum Institute, 21st edition.

J. H. Atkinson, D. Richardson & S. E. Stallebrass (1990). Effect of recent stress history on the stiffness of overconsolidated soil. *Gèotechnique*, 40(4):531–540.

S. Bang, K. Jones, K. Kim, Y. Kim & Y. Cho (2011). Inclined loading capacity of suction piles in sand. *Ocean Engineering*, 38(7):915 – 924. ISSN 0029-8018. URL `http://www.sciencedirect.com/science/article/pii/S002980181000243X`. ¡ce:title¿Offshore Geotechnics¡/ce:title¿.

E. Bauer (1996). Calibration of a comprehensive constitutive equation for granular materials. *Soils and Foundations*, 36(1):13–26.

F. Bianchi, H. d. Battista & R. Mantz (2007). *Wind Turbine Control Systems. Principles, Modelling and Gain Schedulling Design*. Advances in Industrial Control. Springer.

L. Bjerrum (1973). Geotechnical problems involved in froundations of structures in the north sea. *Gèotechnique*, 23(3):319–358.

M. D. Bolton (1986). Strength and dilatancy of sands. *Gèotechnique*, 36(1):65–78.

A. J. Bond & R. J. Jardine (1990). Instruments for measuring the effective stresses acting on a pile jacked into overconsolidated clay. *Geotechnical instrumentation in practice.Proc.conference, Nottingham, 1989*, pp. 583–605.

J.-L. Briaud & G. Y. Felio (1986a). Cyclic axial loads on piles: analysis of existing data. *Canadian geotechnical journal*, 23(3):362–371.

J.-L. Briaud & G. Y. Felio (1986b). Cyclic axial loads on piles: Analysis of existing data. *Canadian geotechnical journal*, 23(3):362–371.

B. Byrne, G. Houlsby, C. Martin & P. Fish (2002). Suction caisson foundations for offshore wind turbines. *Wind Engineering*, 26(3):145–155.

B. W. Byrne & G. T. Houlsby (2000). Experimental investigations of the cyclic response of suction caissons in sand. In *Proceedings of the Annual Offshore Technology Conference*, volume 1, pp. 787–795.

B. W. Byrne & G. T. Houlsby (2002). Experimental investigations of response of suction caissons to transient vertical loading. *Journal of Geotechnical and Geoenvironmental Engineering*, 128(11):926–939.

B. W. Byrne & G. T. Houlsby (2003). Foundations for offshore wind turbines. *Philosophical Transactions of the Royal Society A: Mathematical, Physical and Engineering Sciences*, 361(1813):2909–2930.

B. W. Byrne & G. T. Houlsby (2004). Experimental investigations of the response of suction caissons to transient combined loading. *Journal of Geotechnical and Geoenvironmental Engineering*, 130(3):240–253.

M. J. Cassidy & B. Bienen (2002). Three-dimensional numerical analysis of jack-up structures on sand. In *Proceedings of the International Offshore and Polar Engineering Conference*, volume 12, pp. 807–814.

M. J. Cassidy & G. T. Houlsby (1999). On the modelling of foundations for jack-up units on sand. *Proceedings of the Annual Offshore Technology Conference*, 1:783–795.

M. J. Cassidy, C. M. Martin & G. T. Houlsby (2004). Development and application of force resultant models describing jack-up foundation behaviour. *Marine Structures*, 17(3-4):165–193.

CEN-ISO/TS17892-11 (2004). *Geotechnical Investigation and Testing—Laboratory Testing of Soil—Part 11: Determination of Permeability by Constant and Falling Head, Technical Specification.* European Committee for Standardization. ISBN CEN ISO/TS 17892-11.

CEN-ISO/TS17892-9 (2004). *Geotechnical Investigation and Testing—Laboratory Testing of Soil—Part 9: Consolidated Triaxial Tests on Water Saturated Soil.* European Committee for Standardization. ISBN CEN ISO/TS 17892-9.

CUR (2001). *Ontwerpregels voor trekpalen (Design rules for tension piles).* Civieltechnisch Centrum Uitvoering Research en Regelgeving (CUR).

F. Darve, R. Nova, G. Servant, I. Vardoulakis & C. Lambert (2004). *Development of elastic plastic strain hardening models of soil behaviour.* Wien [u.a.] : Springer.

M. B. de Groot, M. D. Bolton, P. Foray, P. Meijers, A. C. Palmer, R. Sandven, A. Sawicki & T. C. Teh (2006). Physics of liquefaction phenomena around marine structures. *Journal of Waterway, Port, Coastal and Ocean Engineering*, 132(4):227–243.

DNV (1992). *Foundations, Classification Notes No. 30.4.* Det Norske Veritas.

DNV (2004). *Guidelines for design of Wind Turbines.* Det Norske Veritas, 2nd edition.

J. P. Doherty & A. J. Deeks (2006). Stiffness of a flexible circular footing embedded in an elastic half-space. *International Journal of Geomechanics*, 6(1):46–54.

J. P. Doherty, G. T. Houlsby & A. J. Deeks (2005). Stiffness of flexible caisson foundations embedded in nonhomogeneous elastic soil. *Journal of Geotechnical and Geoenvironmental Engineering*, 131(12):1498–1508.

DTI (2001). *Monitoring & Evaluation of Blyth Offshore Wind Farm.* Department of Trade and Industry.

P. Eecen, L. A. H. Machielse & A. P. W. M. Curvers (2006). Meteorological measurements owez—half year report 01-07-2006–31-12-2006. Technical report, ECN.

S. Emeis (2010). Meteorological explanation of wake clouds at horns rev wind farm. *DEWI Magazin*, 37:52–55.

EWEA (2011). Wind in our sails - the coming of europe's offshore wind energy industry.

EWEA (2012). European offshore statistics 2012.

T. Feld (2004). State-of-the-art design standard specific developed and applicable for offshore wind turbine structures. In *Proceedings of the European Wind Energy Conference (EWEC).*

W. D. L. Finn, C. H. Maartman & R. Lo (1978). Cyclic pore pressure under anisotropic conditions. *Earthquake Engineering and Soil Dynamics - Proc. of the ASCE Geotechnical Engineering Division Specialty Conference, Pasadena*, pp. 458–470.

G. Gudehus (1996). A comprehensive constitutive equation for granular materials. *Soils and Foundations*, 36(1):1–12.

I. Herle & G. Gudehus (1999). Determination of parameters of a hypoplastic constitutive model from properties of grain assemblies. *Mechanics of Cohesive-Frictional Materials*, 4:461–486.

G. T. Houlsby (2003). Modelling of shallow foundations for offshore structures. In *BGA International Conference on Foundations, Innovations, Observations, Design and Practice*, pp. 11–26.

G. T. Houlsby & B. W. Byrne (2005). Design procedures for installation of suction caissons in sand. *Proceedings of the Institution of Civil Engineers: Geotechnical Engineering*, 158(3):135–144.

G. T. Houlsby, L. B. Ibsen & B. W. Byrne (2005a). Suction caissons for wind turbines. In *Frontiers in Offshore Geotechnics, ISFOG 2005 - Proceedings of the 1st International Symposium on Frontiers in Offshore Geotechnics*, pp. 75–93.

G. T. Houlsby, R. B. Kelly & B. W. Byrne (2005b). The tensile capacity of suction caissons in sand under rapid loading. In *Frontiers in Offshore Geotechnics, ISFOG 2005 - Proceedings of the 1st International Symposium on Frontiers in Offshore Geotechnics*, pp. 405–410.

G. T. Houlsby, R. B. Kelly, J. Huxtable & B. W. Byrne (2006). Field trials of suction caissons in sand for offshore wind turbine foundations. *Geotechnique*, 56(1):3–10.

IEC61400-3 (2005). *Wind Turbines, Part 3: Design Requirements for Offshore Wind Turbines*. International Electrotechnical Commission(IEC).

K. Ishihara (1996). *Soil Behaviour in Earthquake Engineering*. Oxford science publications. Clarendon Press-New York. ISBN 9780198562245. URL `http://books.google.nl/books?id=OXNxQgAACAAJ`.

R. Jardine, A. Puech & K. Andersen (2012). Keynote paper. cyclic loading of offshore piles: potential effects and practical design. In *7th International Conference on Offshore Site Investigations and Geotechnics, London*, pp. 59–100. Society for Underwater Technology.

H. P. Jostad, K. H. Andersen & T. I. Tjelta (1997). Analyses of skirted foundations and anchors in sand subjected to cyclic loading. *Publikasjon - Norges Geotekniske Institutt*, 199:149–162.

J. Journée & W. Massie (2001). *Offshore Hydromechanics–First Edition*. Delft University of Technology.

J. C. Kaimal (1972). Spectral characteristics of surface layer turbulence. *Quarterly Journal of the Royal Meteorological Society*, 98:563–589.

K. Karlsrud, C. J. F. Clausen & P. M. Aas (2005). Bearing capacity of driven piles in clay, the ngi approach. In *Frontiers in Offshore Geotechnics, ISFOG 2005 - Proceedings of the 1st International Symposium on Frontiers in Offshore Geotechnics*, pp. 775–782.

T. V. Kármán & C. Lin (1951). On the statistical theory of isotropic turbulence. In R. V. Mises & T. V. Kármán, editors, *Advances in Applied Mechanics*, volume 2, pp. 1–19. Elsevier.

S. Kay & E. Palix (2011). Caisson capacity in clay: Vhm resistance envelope - part 2: Vhm envelope equation and design procedures. In *Frontiers in Offshore Geotechnics II - Proceedings of the 2nd International Symposium on Frontiers in Offshore Geotechnics*, pp. 741–746.

R. Kelly, G. Houlsby & B. Byrne (2006a). Tensile loading of model caisson foundations for structures in sand. *Gèotechnique*, 56(10):665–675.

R. B. Kelly, G. T. Houlsby & B. W. Byrne (2006b). A comparison of field and laboratory tests of caisson foundations in sand and clay. *Geotechnique*, 56(9):617–626.

R. B. Kelly, G. T. Houlsby & B. W. Byrne (2006c). Transient vertical loading of model suction caissons in a pressure chamber. *Geotechnique*, 56(10):665–675.

D. Kolymbas (2000). *Constitutive Modelling of Granular Materials*. Engineering Online Library. Springer-Verlag. ISBN 9783540669197. URL `http://books.google.nl/books?id=WQDXM5pgx-AC`.

C. LeBlanc, G. T. Houlsby & B. W. Byrne (2010). Response of stiff piles in sand to long-term cyclic lateral loading. *Geotechnique*, 60(2):79–90.

M. Liingaard (2006). *Dynamic behaviour of suction caissons*. Ph.D. thesis, Aalborg University.

S. Maïolino & M. P. Luong (2009). Measuring discrepencies between coulomb and other geotechnical criteria: Drucker-prager and matsuoka-nakai. In *7th EUROMECH Solid Mechanics Conference*.

T. Marcher, P. Vermeer & P.-A. von Wolffersdorff (1999). Hypoplastic and elasto-plastic modelling - a comparison with test data. In S.-V. B. H. N. York, editor, *Proc. III Euroconference on Constitutive Modelling of Granular Materials*, pp. 353–374.

D. Mašín (2012). *PLAXIS Implementation of Hypoplasticity*. Charles University of Prague.

W. H. Michel (1968). Sea spectra simplified. *Marine Technology*, 5(1):17–30.

K. Miura, K. Maeda & S. Toki (1997). Method of measurement for the angle of repose of sands. *Soils and Foundations (Japanese Geotechnical Society)*, 37(2):89–96.

N. National Environment Research Council (2013). Planet earth—spring 2013.

A. Niemunis (2003). Extended hypoplastic models for soils. *Schriftenreihe des Instituts für Grundbau und Bodenmechanik der Ruhr-Universität Bochum*.

A. Niemunis & I. Herle (1997). Hypoplastic model for cohesionless soils with elastic strain range. *Mechanics of Cohesive-Frictional Materials*, 2:279–299.

NORSOK (2002). *Guidelines for design of Wind Turbines*. Standards Norway.

F. Nowacki, K. Karlsrud & P. Sparrevik (1993). Comparison of recent tests on oc clay and implications for design. *Large-scale pile tests in clay.Proc.conference, London, 1992*, pp. 511–537.

S. M. Olson (2001). *Liquefaction analysis of level and slopping ground using filed case histories and penetration resistance*. Ph.D. thesis, University of Illinois.

S. M. Olson & T. D. Stark (2003). Yield strength ratio and liquefaction analysis of slopes and embankments. *Journal of Geotechnical and Geoenvironmental Engineering*, 129(8):727–737.

J. M. Pestana, G. Biscontin, F. Nadim & K. Andersen (2000). Modeling cyclic behavior of lightly overconsolidated clays in simple shear. *Soil Dynamics and Earthquake Engineering*, 19(7):501–519.

E. Petersen, N. Mortensen, L. Landberg, J. Hojstrup & H. Frank (1998). Wind power meteorology. part 1: climate and tu. *Wind Energy*, 1:25–45.

M. Poblete, T. Wichtmann, A. Niemunis & T. Triantafyllidis (2011). Accumulation of residual deformations due to cyclic loading with multidimensional strain loops. In *Proceedings of the 5th International Conference on Earthquake Geotechnical Engineering*, pp. 1–12.

M. F. Randolph & C. P. Wroth (1978). Analysis of deformation of vertically loaded piles. *ASCE J Geotech Eng Div*, 104(12):1465–1488. URL `www.scopus.com`. Cited By (since 1996):277.

D. Richardson (1988). *PhD Thesis: Investigations of Treshold Effects in Soil Deformation*. City University London.

S. Safinus, G. Sedlacek & U. Hartwig (2011). Cyclic response of granular subsoil under a gravity base foundation for offshore wind turbines. In *Proceedings of the International Conference on Offshore Mechanics and Arctic Engineering - OMAE*, volume 7, pp. 875–882.

H. B. Seed & M. S. Rahman (1978). Wave-induced pore pressure in relation to ocean floor stability of cohesionless soils. *Mar Geotechnol*, 3(2):123–150.

M. Senders (2005). Tripods with suction caissons as foundations for offshore wind turbines on sand. In *Frontiers in Offshore Geotechnics, ISFOG 2005 - Proceedings of the 1st International Symposium on Frontiers in Offshore Geotechnics*, pp. 397–403.

M. Senders (2008). *Suction Caissons in Sand as Tripod Foundations for Offshore Wind Turbines*. Ph.D. thesis, The University of Western Australia—School of Civil and Resource Engineering.

M. L. Silver & H. B. Seed (1971). Volume changes in sand due to cyclic loading. *ASCE Journal*, 97(9):1171–1182.

N. J. Smith (2011). Chapter 2 - the genesis of the north sea oil and gas industry. In N. J. Smith, editor, *The Sea of Lost Opportunity: North Sea Oil and Gas, British Industry and the Offshore Supplies Office*, volume 7 of *Handbook of Petroleum Exploration and Production*, pp. 23–59. Elsevier. URL `http://www.sciencedirect.com/science/article/pii/B9780444536457000025`.

E. X. Song (1990). *Elasto-Plastic Consolidation under Steady and Cyclic Loads*. Ph.D. thesis, Delft University of Technology.

R. Soulsby (1997). *Dynamics of marine sands: a manual for practical applications*. Thomas Telford Publications.

M. Srbulov (2008). *Geotechnical earthquake engineering - Simplified analyses with case studies and examples*. Springer Science+Business Media B.V.

T. D. Stark & G. Mesri (1992). Undrained shear strength of liquefied sands for stability analysis. *Journal of Geotechnical Engineering*, 118(11):1727–1747.

C. Supachawarote, M. Randolph & S. Gourvenec (2004). Inclined pull-out capacity of suction caissons. In *Proceedings of the International Offshore and Polar Engineering Conference*, pp. 500–506. URL `www.scopus.com`. Cited By (since 1996):20.

R. Thijssen, E. Alderlieste & T. Visser (2011). Cyclic loading of suction caissons. *Plaxis Bulletin*, 32:16–21.

Y. P. Vaird & J. C. Chern (1983). Effect of static shear on resistance to liquefaction. *Soils and Foundations*, 23(1):47–60.

J.-F. Vanden Berghe (2001). *Sand strength degradation within the framework of vibratory pile driving*. Ph.D. thesis, Université Catholique de Louvain.

P. von Wolffersdorff (1996). A hypoplastic relation for granular materials with a predifined limit state surface. *Mechanics of Cohesive-Frictional Materials*, 1:251–271.

T. Wichtmann, A. Niemunis & T. Triantafyllidis (2005). Fe prediction of the settlement of shallow foundations on sand under cyclic loading. *Bautechnik*, 82(12):902–911.

T. Wichtmann, A. Niemunis & T. Triantafyllidis (2011). Towards the finite element prediction of permanent deformations of offshore wind power plant foundations using a high-cycle accumulation model. In *Frontiers in Offshore Geotechnics II - Proceedings of the 2nd International Symposium on Frontiers in Offshore Geotechnics*, pp. 635–640.

A. J. Wortman (1983). *Introduction to wind turbine engineering*. Butterworth.

M. Yoshimine & K. Ishihara (1998). Flow potential of sand during liquefaction. *Soils and Foundations*, 38(3):187–196.

L. Youd (2011). A look inside the debate over eeri monograph mno 12. In *The California Geotechnical Engineering Association (CalGeo), 2011 Annual Conference*, pp. 1–63.

T. L. Youd (1972). Compaction of sands by repeated straining. *ASCE Journal*, 98(7):709–725.

O. Zienkiewicz, C. Chang & P. Bettess (1980). Drained, undrained, consolidating and dynamic behaviour assumptions in soils. *Gèotechnique*, 30(4):385–395.